Development of Novel Phosphine- and Copper-Catalyzed Alkyne Functionalization Methods

Nicklas W. Buchbinder

Dissertation submitted to the faculty of the Virginia Polytechnic Institute and State University in partial fulfillment of the requirements for the degree of

Doctor of Philosophy
In
Chemistry

Webster L. Santos, Committee Chair

James M. Tanko

Emily C. Gentry

Ming Chen

April 2nd, 2026
Blacksburg, Virginia

Keywords: alkyne • hydroboration • methodology • hydroamidation

Development of Novel Phosphine- and Copper-Catalyzed Alkyne Functionalization Methods

Nicklas W. Buchbinder

Abstract

Organoboron compounds find immense application in organic synthesis and medicinal chemistry. The activation of boron-carbon bonds has enabled the formation of carbon-nitrogen, carbon-oxygen, carbon-sulfur, carbon-hydrogen, and carbon-carbon bonds, making them highly valuable precursors to complex molecules. Unlike many other organometallic reagents used in cross-coupling reactions, organoboron compounds display notable stability and low toxicity, further cementing their value in pharmaceutical science and agrochemical production. Furthermore, medicinal chemists have leveraged the electrophilic character of boron for the development of reversible covalent inhibitors. Five of these compounds have received approval for clinical usage by the Food and Drug Administration (FDA) for various indications. These applications underpin the value of novel reactions that selectively forge carbon-boron bonds.

1,3-Enynes are highly unsaturated substrates that present significant challenges for selective functionalization. Herein, we describe a synthetic protocol for installing a boronic ester (Bpin) into 1,3-enynes with excellent chemo-, regio-, and stereoselectivity. Utilizing a copper catalyst and pinacolborane (HBpin), the boronic ester was delivered to the internal alkyne carbon, a selectivity which had only been previously achieved with the use of directing groups. Both (*Z*)- and (*E*)-1,3-enynes are tolerated without isomerization of the alkene, highlighting that (*Z*,*Z*)- and (*Z*,*E*)-2-boryl-1,3-dienes are accessible with our methodology. The 2-boryl-1,3-diene products were further derivatized into useful functional groups, highlighting their synthetic utility.

In a follow-up study, the mechanistic intricacies of the previously disclosed hydroboration reaction were investigated. A kinetic analysis revealed that the 1,3-enyne has first-order kinetics, HBpin has zeroth-order kinetics, and the catalyst (CuOAc and Xantphos) has a positive fractional rate order. These results indicate that hydrocupration (copper-hydride insertion into the alkyne) is rate-limiting and important for governing the observed selectivity. A positive fractional rate order in the catalyst suggests that the copper-hydride catalyst is in rapid equilibrium with an off-cycle complex that is catalytically incompetent. ^{11}B NMR studies involving copper(I) acetate, Xantphos, and HBpin revealed a new peak in the ^{11}B NMR spectra (8.9 ppm), which may be the off-cycle complex. DFT calculations indicate that a cyclic CuHBpinOAc species serves as the off-cycle complex, which is consistent with our experimental data. DFT calculations also corroborated that hydrocupration was rate-limiting and that the transition state leading to internal alkyne borylation was the most energetically accessible.

Finally, we developed a mild and convenient approach for the synthesis of α,β-dehydroamino acids using an inexpensive trialkyl phosphine catalyst. α,β-dehydroamino acids are non-canonical amino acids that contain unsaturation between the α- and β-sidechain carbons. This motif appears in many bioactive natural products and the FDA-approved dehydropeptidase inhibitor Cilastatin. The synthesis of α,β-dehydroamino acids has been heavily explored, but most previously established syntheses result in N-protected dehydroamino acids, which have very limited application in the synthesis of complex α,β-dehydroamino acids. The problem arises when attempting to deprotect the N-terminus, resulting in a primary enamine which tautomerizes into the corresponding imine before hydrolyzing into the α-keto ester. To circumvent this issue, we report a straightforward synthetic method that couples complex amides to alkynoates directly, negating any requirement for N-terminal deprotection at the unsaturated amino acid. The reaction

relies on a substoichiometric amount of *n*-tributylphosphine, an inexpensive commodity. Several dehydroamino acid-containing dipeptides were accessed using our method, without epimerization of the chiral center. The α,β-dehydroamino acids were chemically modified into two natural products, one of which (scutianene M) had never been synthesized before.

Development of Novel Phosphine- and Copper-Catalyzed Alkyne Functionalization Methods

Nicklas W. Buchbinder

General Audience Abstract

The synthesis of complex molecules (pharmaceutical agents, agrochemicals, precursors to materials, etc.) often requires sequential chemical reactions that together make up a synthetic route. Designing new chemical reactions changes the landscape of synthetic chemistry, making more synthetic routes possible, thus enabling the synthesis of a greater number of complex molecules for application studies. The focus of this dissertation is on developing new chemical reactions and understanding how they operate. Organoboron compounds are particularly important as boronic esters can be converted into numerous functional groups and therefore can be used in a greater number of synthetic routes. We developed a chemical reaction that resulted in 2-boryl-1,3-dienes (despite the opportunity for many other products to form) and proved that the boronic ester can be modified without affecting the skeletal structure (1,3-diene). In chapter two, we studied the mechanism of the previously mentioned borylation reaction, using kinetic experiments and advanced computational models, which revealed that the reaction pathway leading to 2-borlyl-1,3-dienes occurs faster than opposing reaction pathways. In chapter three, we developed a chemical reaction that affords α,β-dehydroamino acids, which are structural analogs of amino acids (the building blocks of proteins). Our reaction tolerates a much broader scope of substrates compared to previous syntheses, which streamlines the synthesis of complex molecules with the α,β-dehydroamino acid motif. Notably, our reaction was applied to the synthesis of a compound that had only previously been isolated from nature and has been shown to inhibit bacterial cell growth.

Acknowledgements

I would first like to acknowledge Prof. Webster Santos for his endless guidance throughout graduate school. His kind and friendly demeanor has created a rich environment for growth and development. Despite juggling businesses, family, teaching, mentoring, and running a research program, Prof. Santos always offered support and advice when it was required. He has served as a source of inspiration for how to be a scientist and a mentor. I will try to emulate Prof. Santos' passion for science, work ethic, and kindness as my career develops. I am especially impressed by Prof. Santos' ability to personalize the graduate school experience for each student's needs and career goals. I have benefited greatly from this.

Each of my committee members (Prof. James Tanko, Prof. Emily Gentry, and Prof. Ming Chen) provided guidance and encouragement that I am grateful for. The encouraging words of Prof. Tanko and Prof. Gentry after my original research proposal presentation will stay with me throughout my career. Prof. Ming Chen has also offered numerous suggestions that I found to be very insightful and helpful with my research. Although she did not serve as a committee member, I am grateful to Prof. Emily Mevers for offering career support and teaching me about the amazing world of natural products.

I am very thankful for the love, patience, and support provided by my wonderful girlfriend Kalee Shahayda. I greatly appreciated our journeys searching for wildlife, which afforded much-needed reprieve from the rigors of research. Without her technical support, I may have succumbed to malnutrition during graduate school. I would also like to thank my parents (James Buchbinder and Val Buchbinder) for always encouraging me to continue my studies and for taking me on many bird-watching adventures on Smith Mountain Lake. Both of my parents have been role models throughout my life, exemplifying work ethic, sacrifice, and compromise. My siblings (Matthew

Buchbinder, Andrew Buchbinder, Danielle Buchbinder, and Mike Buchbinder) have always been a source of inspiration, which has been helpful for my academic endeavors.

I have been fortunate to call many talented scientists my colleagues. Dr. Andrew Bage catalyzed a profound period of growth during my academic career; without his guidance, I would not have become the scientist I am today. Dr. Connor Swetkowski was my first mentor and taught me not to take life too seriously. Matthew Dupuis has become a close friend, offering ample support both emotional and technical throughout the later years of graduate school. I suspect we will be friends for life. Dr. Ramkrishna Laha has taught me a lot about chemistry (especially photochemistry) and life. His carefree attitude is one that I have tried to emulate. Justin Rodgers has always been good for a laugh and controversial opinion, which provoked many interesting conversations in the lab. I am grateful to Carolyn Curley, who joined the lab in my fifth year, as she reintroduced me to ice hockey and is always pleasant to work with. I have had the good fortune of working with several undergraduate students during my PhD. Long Nguyen, Owen Beck, David Burgo, and Kaamia Harris are all brilliant in their own way. I am excited to watch their careers develop.

Table of Contents

Abstract i

General Audience Abstract iv

Acknowledgements v

Table of Contents vii

List of Figures ix

List of Schemes xii

List of Tables xv

Chapter 1: Chemo-, Regio-, and Stereoselective *cis*-Hydroboration of 1,3-Enynes: Copper-catalyzed Access to (*Z,Z*)- and (*Z,E*)-2-Boryl-1,3-dienes 1

1.1. Contributions 1

1.2. Abstract 2

1.3. Applications of Organoboron Compounds in Synthesis and Medicinal Chemistry 3

1.4. 1,3-Enyne Hydroboration Reactions 8

1.5. Results and Discussion 17

1.6. Applications 22

1.7. Conclusions 23

1.8. References 24

Chapter 2: Experimental and Theoretical Investigations of Copper-Catalyzed Chemo-, Regio-, and Stereoselective *cis*-Hydroboration of 1,3-Enynes 28

2.1. Contributions 28

2.2. Abstract 29

2.3. 1,3-Enyne Hydroboration Mechanisms 30

2.4. Results and Discussion 39
2.5. Conclusions 48
2.6. References 49
Chapter 3: Phosphine-Catalyzed Regio- and Stereoselective Umpolung Addition of Amides to Alkynoates: Access to Complex α,β-Dehydroamino Acid Derivatives 51
3.1. Contributions 51
3.2. Abstract 52
3.3. α,β-Dehydroamino Acid Derivatives in Drug Discovery and Synthesis 53
3.4. Synthetic Methods for Accessing α,β-Dehydroamino Acids 56
3.5. Results and Discussion 60
3.6. Conclusions 68
3.7. References 68
Chapter 4: Experimental Procedures and Characterization Data 71
4.1. General Experimental Methods 71
4.2. Instrumentation 71
4.3. Synthetic Procedures and Characterization of Compounds for Chapter 1 72
4.4. X-Ray Crystallography for Chapter 1 99
4.5. Synthetic Procedures for Chapter 2 103
4.6. X-Ray Crystallography for Chapter 2 125
4.7. Synthetic Procedures and Characterization of Compounds for Chapter 3 128
4.8. X-Ray Crystallography for Chapter 3 163
4.9. References 167
Appendix A 171

List of Figures

Figure 1.1: Structures of boron-containing FDA approved drugs. 4

Figure 2.1: a) Bonding HOMO-LUMO interaction (coordination). b) Back donation HOMO-LUMO interactions. c) Orbital population analysis via DFT calculations (B3LYP/6-31G(d,p)). d) Proposed catalytic cycle for the regiodivergent hydroboration of 1,3-enynes. 30

Figure 2.2: a) Proposed catalytic cycle for the palladium-catalyzed *trans*-3,4-hydroboration of 1,3-enynes. b) Experimental evidence to support the proposed catalytic cycle. 32

Figure 2.3: a) proposed mechanism for the copper-catalyzed 1,4-hydroboration of 1,3-enynes. b) mechanistic experiments to understand epimerization mechanisms. 35

Figure 2.4: Kinetic analysis of Cu(I)-catalyzed hydroboration of 1,3-enyne **2.25** using VTNA. 39

Figure 2.5: ^{11}B NMR (^{1}H coupled) experiments for elucidation of the off-cycle species. a) Stoichiometric reaction in the absence of substrate. b) Stoichiometric reaction in the absence of substrate and ligand (Xantphos)..... 40

Figure 2.6: a) Calculated free energy profile for transformation of the pre-catalyst **2.27** to the Cu-H or Cu-Bpin complex. The blue values represent the length of selective bonds in Å. b) Calculated relative free energies for dimeric species in equilibrium with the copper hydride complex Cu-H. Relative Gibbs free energies and relative electronic energies (in parenthesis) are given in kcal/mol..... 43

Figure 2.7: a) Calculated free energy profile for the borylation of substrate S. The pink values represent the length of selective bonds in Å. The green values represent the NBO charge of selected atoms. Relative Gibbs free energies and relative electronic energies (in parenthesis) are given in kcal/mol. b) Comparison of the energies of **2.26'** and **2.29**. Relative Gibbs free energy is given in kcal/mol..... 45

Figure 3.1: Representative natural products and synthetic compounds which feature the α,β-dehydroamino acid motif 54

Figure 3.2: Retrosynthetic analysis of α,β-dehydroamino acids. PG = protecting group, LG = leaving group 57

Figure 4.1: ORTEP diagram of **1.59b** with thermal ellipsoids at 50% probability level..... 100

Figure 4.2: [**2.26**] (M) vs. Time (Min)..... 106

Figure 4.3: [**2.26**] (M) vs. Σ[**2.25**]$^{0}\Delta$t..... 108

Figure 4.4: [**2.26**] (M) vs. Σ[**2.25**]$^{1}\Delta$t..... 108

Figure 4.5: [**2.26**] (M) vs. Σ[**2.25**]$^{2}\Delta$t..... 109

Figure 4.6: [**2.26**] M vs. t[CuOAc+Xantphos]^{0} 111

Figure 4.7: [**2.26**] M vs. t[CuOAc+Xantphos]$^{0.7}$ 111

Figure 4.8: [**2.26**] (M) vs. t[CuOAc+Xantphos]^{1}..... 112

Figure 4.9: [**2.26**] (M) vs. t[CuOAc+Xantphos]^{2}..... 112

Figure 4.10: Initial Rate (M/min) vs. [CuOAc+Xantphos]$_{0}$ (M) 114

Figure 4.11: [**2.26**] M vs. Σ[HBpin]$^{0}\Delta$t..... 117

Figure 4.12: [**2.26**] M vs. Σ[HBpin]$^{1}\Delta$t..... 117

Figure 4.13: [**2.26**] M vs. Σ[HBpin]$^{2}\Delta$t..... 118

Figure 4.14: [**2.26**] M vs. Σ[CuOAc+Xantphos]^{1}[**2.25**]^{1}[HBpin]$^{0}\Delta$t..... 119

Figure 4.15: [**2.26**] M vs. Σ[CuOAc+Xantphos]$^{0.7}$[**2.25**]^{1}[HBpin]$^{0}\Delta$t..... 120

Figure 4.16: Solid-state molecular structures for [Cu(Xantphos)(OAc)] (**2.27**), (with anisotropic displacement ellipsoids at 50% probability level. Color scheme: Cu, green; P, pink; O, red C, gray. Hydrogens and solvent molecules are omitted for clarity. 127

Figure 4.17: ^{1}H NMR spectra for mechanistic study ($CDCl_3$, 400 MHz). 155

Figure 4.18: ^{1}H NMR spectra for mechanistic study including benzamide ($CDCl_3$, 400 MHz). 156

Figure 4.19: Crude ^{1}H NMR spectra for Mosher's amide synthesis ($CDCl_3$, 400 MHz). 159

Figure 4.20: Crude ^{19}F NMR spectra for Mosher's amide synthesis ($CDCl_3$, 376 MHz). 160

Figure 4.21: Crude ^{1}H NMR spectra for Mosher's amide synthesis stacked against authentic sample **3.49**. ($CDCl_3$, 400 MHz). 161

Figure 4.22: Zoomed in crude ^{1}H NMR spectra for Mosher's amide synthesis stacked against authentic sample **3.49**. ($CDCl_3$, 400 MHz). 162

Figure 4.23: Crude ^{19}F NMR spectra for Mosher's amide synthesis stacked against authentic sample **3.49**. ($CDCl_3$, 376 MHz). 163

Figure 4.24: Solid-state molecular structure of compound **3.47b** with anisotropic displacement ellipsoids at 50% probability level ;Color scheme: O, red; N,blue; C,gray; H, white. 165

List of Schemes

Scheme 1.1: Phenylboronic acid coordination with sodium hydroxide. 3

Scheme 1.2: Representative transformations using organoboron compounds. a: oxidation, b: Chan-Evans-Lam coupling, c: Suzuki-Miyaura cross-coupling, d: carbonylative Suzuki-Miyaura cross-coupling, e-h: halogenation, i: trifluoromethylation, j: Matteson-homologation, k: Petasis reaction, l: protodeboronation. m: thioetherification, n: phosphination 5

Scheme 1.3: Matteson-Homologation of pinacol boronic esters..... 7

Scheme 1.4: Basic reaction pathways of 1,3-enynes hydroboration reactions. Regio- and stereoisomers omitted for clarity. 8

Scheme 1.5: Non-catalyzed 1,3-enyne hydroboration reactions using 9-BBN or HBcat. 9

Scheme 1.6: Early examples of transition metal catalyzed 1,3-enyne hydroboration reactions using HBcat..... 10

Scheme 1.7: Copper-catalyzed hydroboration reactions of 1,3-enyens with diboron reagents. .. 11

Scheme 1.8: Palladium-catalyzed trans-3,4-hydroboration of 1,3-enynes..... 12

Scheme 1.9: Copper-catalyzed 1,4-hydroboration reactions of 1,3-enynes. 13

Scheme 1.10: Recent reports of earth abundant 3,4-hydroborations of 1,3-enynes..... 14

Scheme 1.11: Outlook on 1,3-enyne hydroboration reactions after 58 years of research. 16

Scheme 1.12: Hidden borane catalysis control experiment..... 18

Scheme 1.13: Substrate scope of (*Z*)-1,3-enynes. Isolated yields are reported. >99:1 *Z*:*E* determined by ^{1}H NMR. [a]1.2 equiv HBpin, 4 h. [b] 1.6 mmol scale. 20

Scheme 1.14: Substrate Scope of (*E*)-1,3-enynes. Isolated yields are reported. >99:1 *Z*:*E* determined by ^{1}H NMR. 21

Scheme 1.15: Synthetic applications of 2-boryl-1,3-dienes. Isolated yields are reported. Z:E determined by ^{1}H NMR. a: KHF_2 (3.0 equiv), acetic acid (0.5 mL). b: $Pd_2(dba)_3$ (4 mol%), SPhos (5 mol%), 4-iodobenzonitrile (1.5 equiv), THF/3 M NaOH (3:1), 70 °C. c: H_2O_2 (30 equiv), 3 M NaOH (30 equiv), THF (0.5 mL). d: nBuLi (3.0 equiv), dibromomethane (4.0 equiv), THF (1.0 mL) −78 - 25 °C, 4 h then H_2O_2 (5.0 equiv), 3 M NaOH (5.0 equiv). 23

Scheme 2.1: Outlook on 1,3-enyne hydroboration mechanisms. 38

Scheme 2.2: a) Crystal structure of **2.27**, ([(Xantphos)Cu(OAc)]. b) Control experiments towards understanding the role of acetate in the reaction. 41

Scheme 2.3: Proposed mechanism of 1,3-enyne hydroboration based on experimental and computations studies. 47

Scheme 3.1: Synthetic applications of α,β-dehydroamino acids..... 55

Scheme 3.2: Motivation for the described research. PG = protecting group 58

Scheme 3.3: Amide substrate scope. Yields refer to isolated yields. >99:1 *Z*:*E* selectivity unless otherwise noted, based on isolated yield of each isomer. 0.25 mmol **3.45a**, 0.025 mmol PBu_3, 0.30 mmol **3.46**, 0.25 M in toluene. [a]70 °C. [b]20 mol% PBu_3. [c]20 mol% K_2CO_3. 61

Scheme 3.4: Alkynoate substrate scope. Yields refer to isolated yields. >99:1 *Z*:*E* selectivity unless otherwise noted, based on isolated yield of each isomer. 0.25 mmol **3.45**, 0.025 mmol PBu_3, 0.30 mmol **3.46a**, 0.25 M in toluene. [a]70 °C. [b]20 mol% PBu_3. [c]20 mol% K_2CO_3. 63

Scheme 3.5: Wide array of biologically relevant substrates. Yields refer to isolated yields. >99:1 *Z*:*E* selectivity unless otherwise noted, based on isolated yield of each isomer. 0.25 mmol **3.45**, 0.025 mmol PBu_3, 0.30 mmol **3.46**, 0.25 M in toluene. [a]90 °C. 64

Scheme 3.6: Epimerization study using Mosher's acid chloride. 65

Scheme 3.7: Synthetic applications of α,β-dehydroamino acids. 66

Scheme 3.8: Proposed mechanism. 67

Scheme 4.1: Semi-reduction for synthesis of 1,3-enyne starting material**.** 72

Scheme 4.2: Sonogashira cross-coupling for the synthesis of 1,3-enyne starting material. 73

Scheme 4.3: Kumada cross-coupling for the synthesis of 1,3-enyne starting material. 74

Scheme 4.4: DCC esterification for the synthesis of alkyne starting material. 74

Scheme 4.5: Williamson ether synthesis 75

Scheme 4.6: Sonogashira-Cross coupling with trimethylsilyacetylene (TMSA). 75

Scheme 4.7: Trimethylsilyl alkyne deprotection 76

Scheme 4.8: The chemo-, regio-, and stereoselective *cis*-hydroboration of 1,3-enynes. 82

Scheme 4.9: Protodeboration of 2-boryl-1,3-diene **1.59f**. 95

Scheme 4.10: Basic peroxide oxidation of 2-boryl-1,3-diene **5**. 96

Scheme 4.11: Homologation-oxidation of 2-boryl-1,3-diene **1.59f**. 97

Scheme 4.12: Suzuki-Miyaura cross-coupling of 2-boryl-1,3-diene **1.59f** and 4-iodobenzonitrile. 98

Scheme 4.13: Acetate mechanistic studies. 122

Scheme 4.14: Acylation of terminal alkynes. 128

Scheme 4.15: CDI coupling of carboxylic acids and ammonium hydroxide. 128

Scheme 4.16: Synthesis of substrate **3.45m**. 129

Scheme 4.17: Bestmann-Ohira to synthesize terminal alkyne **4.84**. 132

Scheme 4.18: Synthesis of α,β-dehydroamino acids. 136

Scheme 4.19: Photocatalyzed isomerization of α,β-dehydroamino acid **3.47a.** 152

Scheme 4.20: Boc-deprotection of substrate **3.47u**. 157

Scheme 4.21: Synthesis of Mosher's amide from **3.48**. 158

List of Tables

Table 1.1: Optimization of Reaction Conditions[a] 17

Table 3.1: Reaction optimization 60

Table 4.1: References for 1,3-enyne and alkyne starting materials. 77

Table 4.2: Crystal data and structure refinement for cs3055 (1.59b). 101

Table 4.3: Concentration Data for Standard Conditions Reaction Progress Profile 105

Table 4.4: Concentration Data for Excess (0.350 M) **2.25** Conditions 107

Table 4.5: Concentration Data for Excess (0.0250 M) CuOAc+Xantphos Conditions 110

Table 4.6: Initial Rate Data for CuOAc+Xantphos. Rate Order Determination 114

Table 4.7: Concentration Values Determined by ^{1}H NMR for Initial Rates 114

Table 4.8: Concentration Data for Excess (0.675 M) HBpin Conditions 116

Table 4.9: Concentration Data for K_{obs} Graph 121

Table 4.10: X-ray diffraction experimental details 125

Table 4.11: References for alkyne, alkynoate, and amide starting materials. 132

Table 4.12: X-ray diffraction experimental details. 165

Chapter 1: Chemo-, Regio-, and Stereoselective *cis*-Hydroboration of 1,3-Enynes: Copper-catalyzed Access to (*Z*,*Z*)- and (*Z*,*E*)-2-Boryl-1,3-dienes

1.1. Contributions

Nicklas Buchbinder discovered the transformation, completed the optimization studies, synthesized substrates **1.58a-158k, 1.58p-1.58x**, synthesized products **1.59a-159k, 1.59p-1.59x**, **1.61, 1.63** and grew the crystals for X-ray crystallography analysis. Long Ngyuen synthesized substrates **1.58l** – **1.58o**, synthesized products **1.59l** – **1.59o** and performed the scale up of substrate **1.59b**. Owen Beck synthesized **1.60** and **1.62**. Andrew Bage advised throughout the project and contributed to the preparation and editing of the final manuscript. Dr. Carla Slebodnick was responsible for crystallographic experiments and analysis. Prof. Webster Santos advised throughout the project and contributed to the preparation and editing of the final manuscript. The final manuscript was prepared in collaboration with Nicklas Buchbinder, Andrew Bage, and Prof. Webster Santos. This work has been published in *Organic Letters* and is available online. Reprint (adapted) with permission from (Buchbinder, N. W.; Nguyen, L. H.; Beck, O. N.; Bage, A. D.; Slebodnick, C.; Santos, W. L. Chemo-, Regio-, and Stereoselective cis-Hydroboration of 1,3-Enynes: Copper-Catalyzed Access to (*Z*,*Z*)- and (*Z*,*E*)-2-Boryl-1,3-dienes. *Org. Lett.* **2024**, *26* (29), 6136–6141.) Copyright (**2024**) American Chemical Society.

1.2. Abstract

A copper-catalyzed alkyne-selective hydroboration of 1,3-enynes is disclosed providing access to the previously elusive 2-boryl-1,3-dienes. Using CuOAc, Xantphos, and HBpin, the boryl group was installed on the internal carbon of a series of symmetric and nonsymmetric 1,3-enynes affording products with excellent *Z*:*E* selectivity. A broad scope of substrates was tolerated including electron-donating groups, electron-withdrawing groups, halides, and heterocycles. The utility of the 2-boryl-1,3-diene products was demonstrated by transformation to useful functional groups.

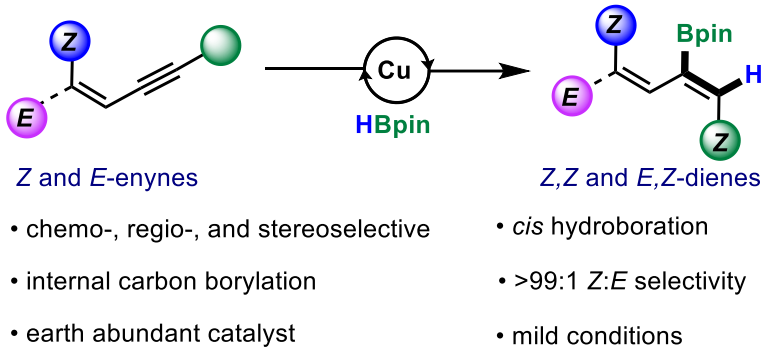

1.3. Applications of Organoboron Compounds in Synthesis and Medicinal Chemistry

Organoboron compounds have abundant and diverse applications within organic chemistry. The adoption of organoboron compounds in organic synthesis and medicinal chemistry is largely attributed to their unique ability to remain relatively unreactive until activated. Under neutral conditions, organoboron compounds generally feature a trivalent, sp^2-hybridized boron atom which contains an empty p-orbital. The empty p-orbital allows for Lewis base coordination that results in a tetravalent, anionic, sp^3-hybridized boronate complex that is reactive compared to the neutral form.[1] For instance, the reaction between phenylboronic acid (**1.1)** and sodium hydroxide reversibly forms the boronate complex **1.2** (Scheme 1.1).[2] This process has been leveraged extensively in organic synthesis and medicinal chemistry.

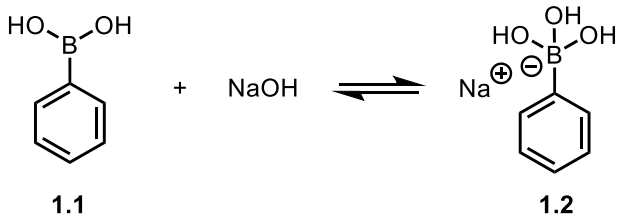

1.1 **1.2**

Scheme 1.1: Phenylboronic acid coordination with sodium hydroxide.

In medicinal chemistry, boron has recently been labeled a magic element which implies that it has unique properties that influence the pharmacological effects of a compound.[3] To date, five boron-containing small molecules have been approved by the Food and Drug Administration (FDA) (Figure 1.1). Bortezomib (Velcade®, **1.3**) was the first boron-containing compound to reach approval and is used clinically to treat multiple myeloma and mantel cell lymphoma. Mechanistically, bortezomib reversibly binds to the catalytic site of the 26S proteasome preventing protein degradation and thus protein turnover, resulting in cytotoxicity.[4] Malignant cells have increased proteasomal activity compared to healthy cells which results in selective toxicity towards malignant cells, however; off-target side effects are commonly reported with clinical usage of

bortezomib. Bortezomib lacks oral bioavailability and requires intravenous injection, thus ixazomib (Ninlaro®, **1.4**) was discovered as an orally bioavailable alternative for the treatment of multiple myeloma and maintains the same mechanism of action as bortezomib.[5] In 2014, tavaborole (Kerydin®, **1.5**) received FDA approval for the treatment of onychomycosis, a fungal infection of the toe nail bed. Instead of a boronic acid, tavaborole features an oxaborole which is the pharmacophore of the drug. Tavaborole inhibits protein synthesis by reversibly binding to leucyl-tRNA synthetase, preventing cell growth and ultimately inducing fungal cell death.[6] Crisaborole (Eucrisa®, **1.6**) is another oxaborole-based FDA drug, used for the treatment of atopic dermatitis (eczema). The mechanism of action for crisaborole involves the inhibition of phosphodiesterase-4 (primarily phosphodiesterase-4B), which is implicated in the release of various cytokines. Thus, inhibition of phosphodiesterase-4B results in lower cytokine migration and reduced inflammation.[7] The final boron-containing small molecule to receive FDA approval was vaborbactam (Vabormere®, **1.7**) in 2017. Vaborbactam is a β-lactamase inhibitor, co-

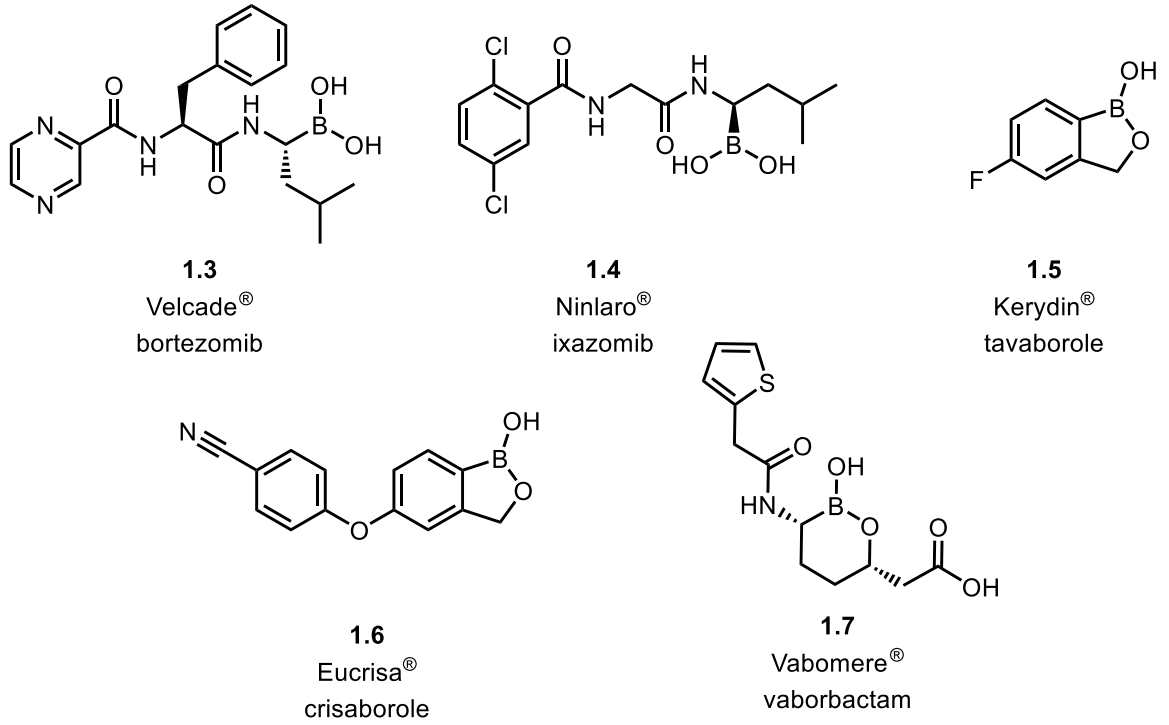

Figure 1.1: Structures of boron-containing FDA approved drugs.

administered with meropenem for the treatment of gram-negative bacterial infections. As with all the previously mentioned drugs, boron's empty p-orbital is essential for inhibition as the β-lactamase active site serine forms a covalent bond with the oxaborole in vaborbactam.[8]

The advent of organoboron drugs marks a new age for both drug discovery and organoboron chemistry. In addition to the five FDA approved organoboron drugs, many more (hundreds) boron-containing compounds are currently being explored for their application in drug discovery.[9] The usage of organoboron compounds in drug discovery underpins the value of exploring novel synthetic methods for making boron-carbon bonds. Specifically, the ability to precisely add a boronic ester into carbon frameworks stands to aid in the development of new boron-containing small molecules for applications in drug discovery.

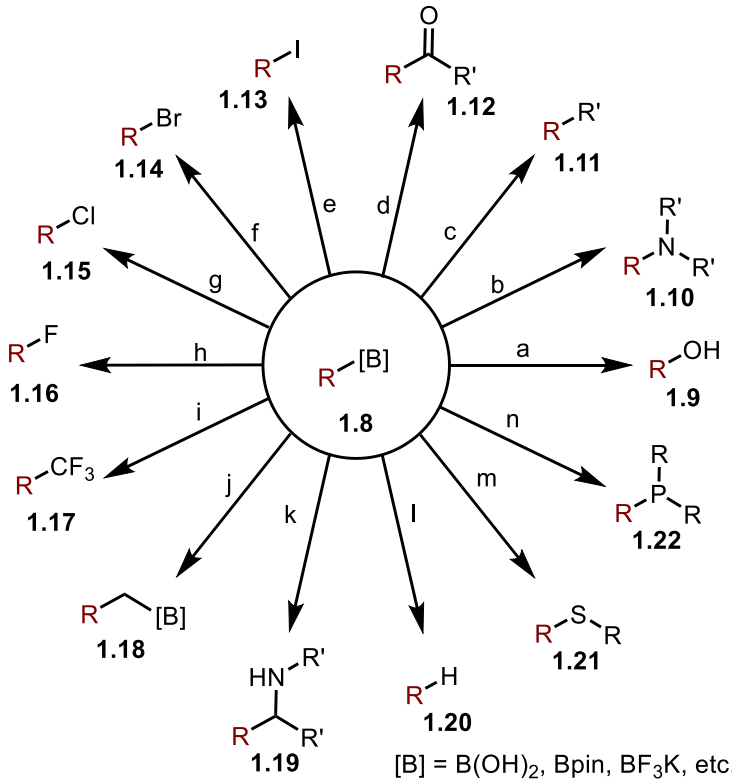

Scheme 1.2: Representative transformations using organoboron compounds. a: oxidation, b: Chan-Evans-Lam coupling, c: Suzuki-Miyaura cross-coupling, d: carbonylative Suzuki-Miyaura cross-coupling, e-h: halogenation, i: trifluoromethylation, j: Matteson-homologation, k: Petasis reaction, l: protodeboronation. m: thioetherification, n: phosphination

The activation of boron-carbon bonds has powered myriads of valuable transformations in organic synthesis (Scheme 1.2). For example, the one-pot hydroboration-oxidation of alkenes results in formal anti-Markovnikov alkene hydration which would be inaccessible through traditional olefin hydration methods (**1.9**).[10] Professor Herbert Brown was later awarded the Nobel Prize for his discovery of this reaction.[11] Early examples of the hydroboration-oxidation operated through trialkylboron intermediates which are notoriously challenging to purify. Contemporary organoboron transformations utilize boronic esters and boronic acids which are more stable and easier to handle.[1] Chan-Evans-Lam coupling offers a convenient approach for making carbon-nitrogen bonds from an organoboron reagent and amine (or other nucleophiles such as alcohols, thiols, amides, etc.). The reaction requires a copper(II) catalyst and oxidant to forge the new carbon-heteroatom bond (**1.10**).[12] The Suzuki-Miyaura cross-coupling (SMC) reaction has become a staple of synthetic chemistry as a method for making carbon-carbon bonds (**1.11**). In the presence of a palladium(0) catalyst and base, aryl halides couple to organoboron reagents, offering mild conditions for the generation of sp^2-sp^3 or sp^2-sp^2 carbon-carbon bonds.[13] Professor Akira Suzuki was awarded one third of the 2010 Nobel Prize the discovery of SMC, which highlights the value of this transformation and organoboron reagents as nucleophiles in organic chemistry.[14] Carbonylative Suzuki-Miyaura cross-coupling has also been developed as a means of accessing ketones from aryl halides and organoboron reagents (**1.12**). Carbon monoxide is inserted into the palladium-aryl bond prior to transmetalation of the boron reagent.[15] Halogenation of organoboron compounds represents a mild way of accessing aryl halides and typically requires a Lewis base or metal catalyst (Ag, Cu or Au) and electrophilic halide (*N*-iodosuccinimide, *N*-bromosuccinimide, *N*-chlorosuccinimide, Selectfluor) (**1.13**, **1.14**, **1.15**, **1.16**).[16-18] Trifluoromethyl groups are commonly found in pharmaceutical agents, making their synthesis of great importance.[19] Qing

reported the first oxidative copper catalyzed trifluoromethylation of aryl and alkenyl boronic acids using Me_3SiCF_3 as the trifluoromethyl source (**1.17**).[20] The Matteson-Homologation is a powerful tool for inserting methylene units into C-B bonds. (**1.18**). The insertion of a methylene unit while maintaining the boronic ester for further functionalization has proven useful in total synthesis.[21] The mechanism of this reaction features a 1,2-metallate shift, which has been repurposed for numerous transformations including transition-metal free C-C bond formation (Scheme 1.3).[22] The Petasis reaction (Boronic Acid Mannich reaction) is a three-component reaction that involves carbonyls, amines and boronic acids. Like the Mannich reaction, imine condensation occurs first, however; instead of enolizable ketones, boronic acids migrate to the imine carbon, converting them into the corresponding amines (**1.19**).[23] Protodeboronation involves the protonation of organoboron compounds, replacing the boryl group with a hydrogen atom. Sequences involving a one-pot hydroboration-protodeboronation have enabled mild and selective reductions of substrates that would be otherwise challenging to reduce. This technology is particularly advantageous when substrates contain several sites of unsaturation and overreduction is likely with traditional reduction conditions such as Pd/C and H_2 (**1.20**).[24, 25] Recently, a method for the stereoretentive thioetherification of enantioenriched boronic esters has been developed using alkyllithium to activate boron and reacting the resulting boronate complex with a sulfonothioate ($RSSO_2R'$) and copper catalyst (**1.21**).[26] In the same report, a method for the stereoretentive phosphination of

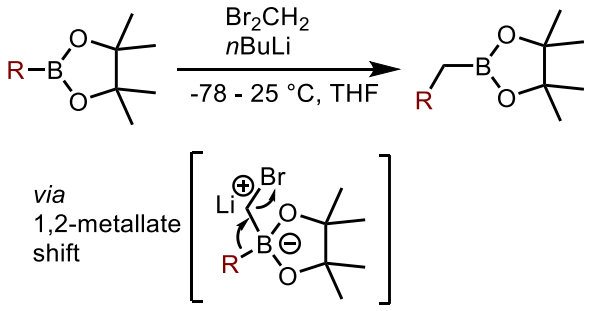

Scheme 1.3: Matteson-Homologation of pinacol boronic esters.

enantioenriched boronic esters was established. Instead of the sulfonothioate, a chlorophoshine was used as the electrophile to afford the enantioenriched phosphines (**1.22**).[26]

The aforementioned transformations provide only a sample of the numerous reactions that rely on organoboron compounds for introducing useful functional groups into carbon frameworks. The ubiquity of organoboron reagents in organic synthesis has fueled the field of research in which the objective is to incorporate boronic esters into new and useful organic substrates. 1,3-Enynes represent an interesting class of substrates for hydroboration reactions because they contain inequivalent sites of unsaturation (alkene and alkyne) that can both participate in the hydroboration reaction. Selective hydroboration reactions on 1,3-enynes leave unsaturated carbon-carbon bonds which can be further derivatized. The next section will discuss borylation reactions that involve 1,3-enynes as substrates.

1.4. 1,3-Enyne Hydroboration Reactions

1,3-Enynes are highly unsaturated substrates that feature an alkene which is conjugated to an alkyne. The extended conjugation makes selective functionalization of this moiety challenging as

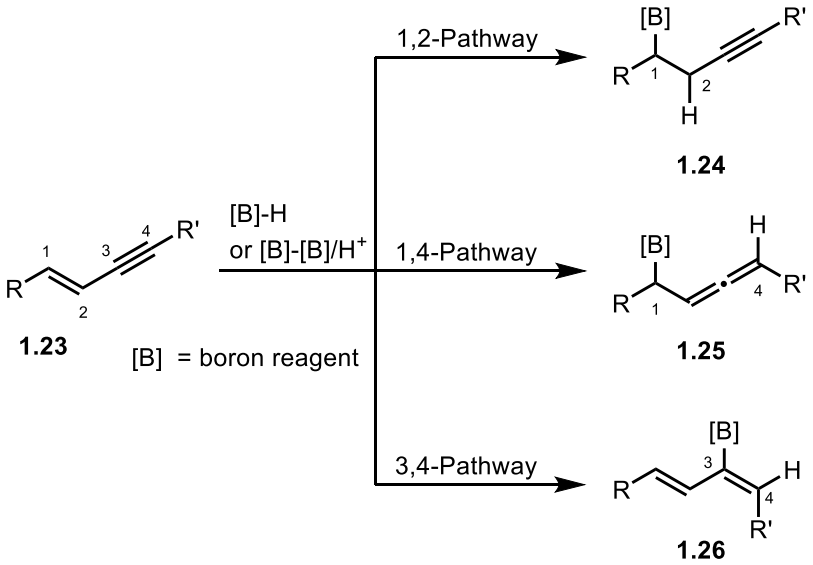

Scheme 1.4: Basic reaction pathways of 1,3-enynes hydroboration reactions. Regio- and stereoisomers omitted for clarity.

three reaction pathways are possible: 1,2-functionalization, 1,4- functionalization and 3,4-functionalization (Scheme 1.4). In the context of hydroboration reactions, both the boryl group and hydrogen atom can behave as nucleophiles or electrophiles depending on the reaction conditions. As such, careful consideration is required when selecting the reaction conditions to favor a desired product. In many cases, a transitionmetal catalyst and ligand are required to achieve appreciable selectivity for 1,3-enyne hydroboration reactions.[27]

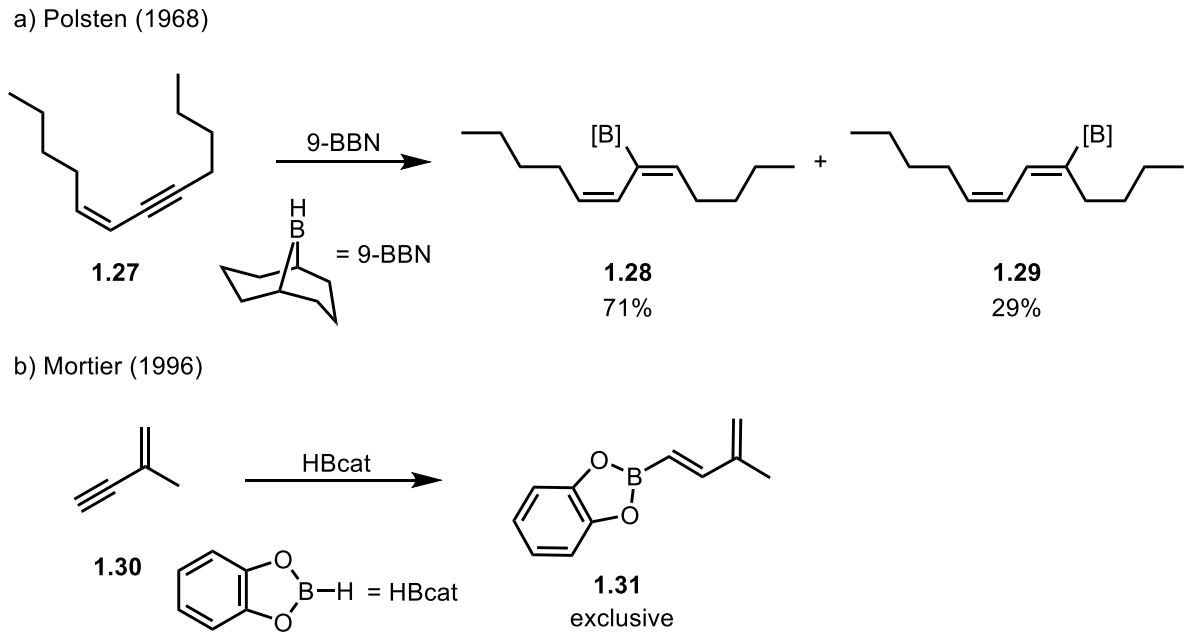

Scheme 1.5: Non-catalyzed 1,3-enyne hydroboration reactions using 9-BBN or HBcat.

The first report of a 1,3-enyne hydroboration reaction was published in 1968. In this study, Polston and coworkers introduced (*Z*)-dodec-5-en-7-yne (**1.27**) to 9-BBN. Surprisingly, the non-catalyzed reaction proceeded in both a chemo- and stereoselective manner, albeit with modest regioselectivity. The regioisomers **1.28** and **1.29** were detected by crude ^{1}H NMR analysis in 71% and 29%, respectively (Scheme 1.5a).[28] The observed chemoselectivity can be rationalized by the presumed thermodynamic cost of breaking conjugation between the unsaturated units, although this was not studied in detail. Non-catalyzed hydroboration reactions often occur in syn-fashion due to a concerted transitions state. While (*Z*)-dodec-5-en-7-yne (**1.27**) was the only 1,3-enyne

evaluated in this study, it set the stage for further optimization studies and established that the hydroboration of 1,3-enynes can be useful tool for accessing boryl-1,3-dienes. Nearly 30 years later, Mortier reported the selective hydroboration of 2-methylbut-1-en-3-yne (**1.30**) using catecholborane (HBcat). The reaction formed a single product (**1.31**) in the absence of a catalyst (Scheme 1.5b).[29] Like Polsten's report, the reaction conditions left the alkene intact and thus the first chemo-, regio- and stereoselective hydroboration of 1,3-enynes was established. Unfortunately, methylbut-1-en-3-yne was the only 1,3-enyne used in the study so the generality of this reaction remains in question.

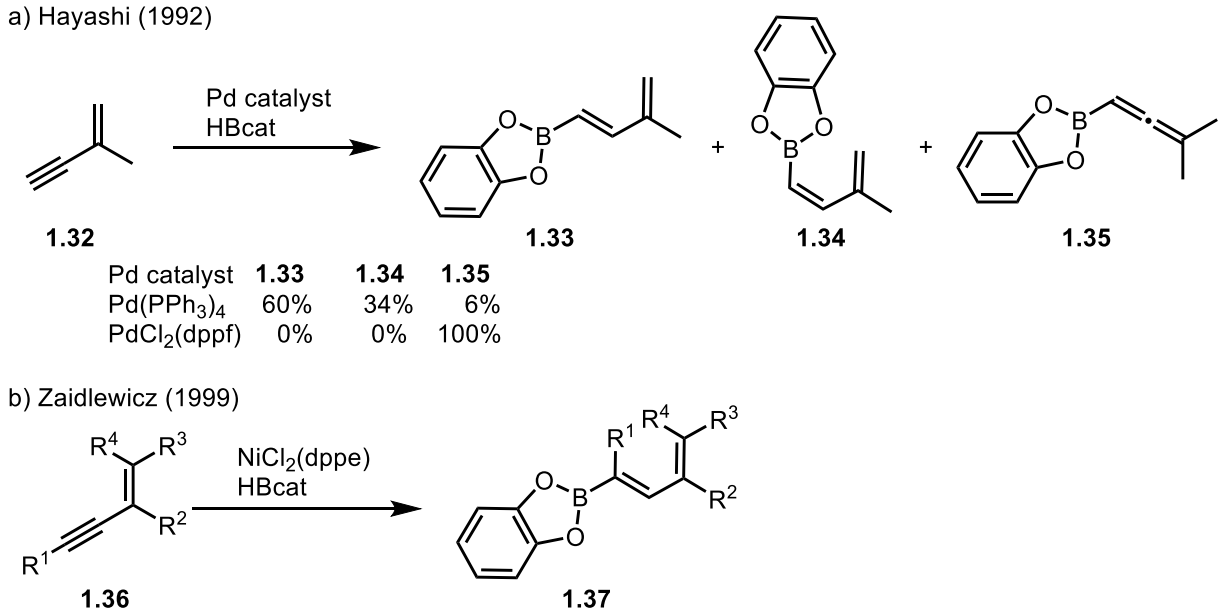

Scheme 1.6: Early examples of transition metal catalyzed 1,3-enyne hydroboration reactions using HBcat.

In 1992, the Hayashi group developed a palladium-catalyzed method for accessing boryl-allenes from 1,3-enynes. Notably, this was the first example of a selective 1,4-hydroboration on 2-methylbut-1-en-3-yne (**1.32**) which complemented the report by Mortier (3,4-hydroboration). Monodentate phosphine ligands such as triphenylphosphine afforded a mixture of hydroboration products (Scheme 1.6a, **1.33**, **1.34** and **1.35)** with the boryl-allene (**1.35)** being formed as a minor product (6%). Conversely, a bidentate phosphine ligand (dppf) afforded boryl-allenes (**1.35)**

exclusively, revealing that minor changes in the catalyst play an important role in governing the selectivity of the reaction.[30] The first and only report of a nickel-catalyzed 1,3-enyne hydroboration was published in 1999 by the Zaidlewicz group (Scheme 1.6b). Dichloro(1,2-bis(diphenylphosphino)ethane)nickel was used as the catalyst and catecholborane as the boron reagent. These reaction conditions resulted in borylation of the external alkyne carbon (**1.37**), like the uncatalyzed method. However, a broader scope of 1,3-enynes were evaluated in this study including internal enynes and cyclic enynes.[31]

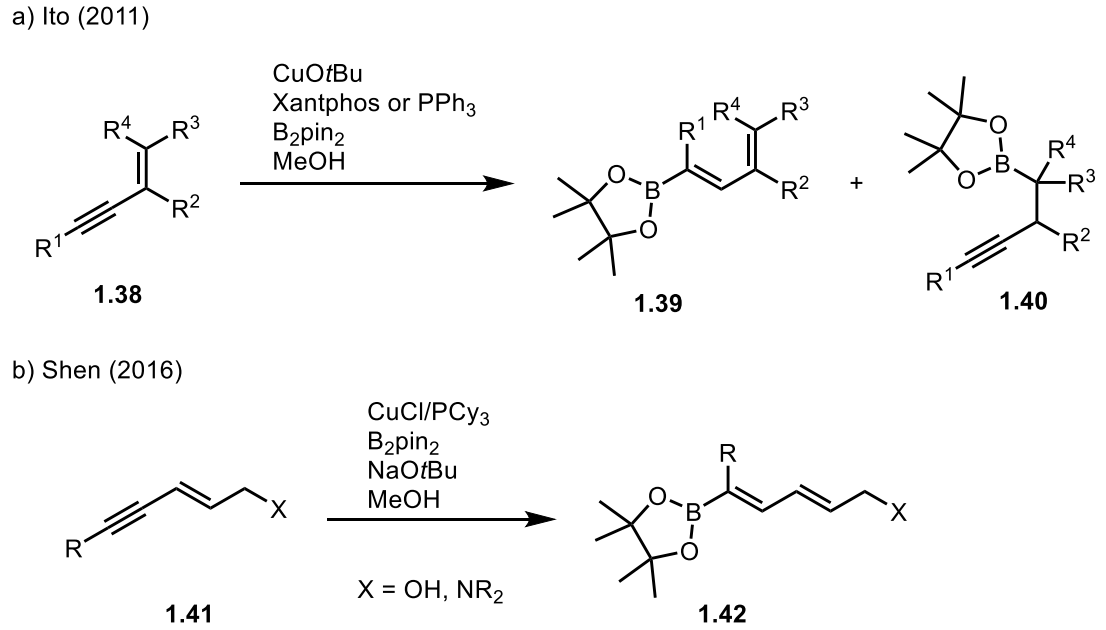

Scheme 1.7: Copper-catalyzed hydroboration reactions of 1,3-enyens with diboron reagents.

In 2011, Ito reported a chemodivergent hydroboration of 1,3-enynes using various copper(I) complexes. Depending on the substrate and ligand, either the alkyne or the alkene reacted to form 1-boryl-1,3-dienes (**1.39**) or alkynylboronates (**1.40**), respectively (Scheme 1.7a). When R^3 and R^4 are small (H), hydroboration occurred at the alkene regardless of whether Xanthos or triphenylphosphine was used as the ligand. When a single methyl was present at positions R^2, R^3 or R^4, hydroboration occurred at either unsaturated bond depending on the ligand. The smaller triphenylphosphine enabled borylcupration at the alkyne, resulting in the formation of the 1-bory-

1,3-diene product (**1.39**) while the larger XantphosCuBpin complex formed the alkynlboronate (**1.40**). Steric hinderance and respective cone angle of the ligand was provided as a justification for the observed chemodivergence. When di- or trisubtituted alkenes were used with either triphenylphosphine or Xantphos, hydroboration occurred at the alkyne and the alkynylboronate (**1.40**) was formed.[32] Ito's report is the first example of a 1,2-hydroboration of 1,3-enynes and the first example of a copper catalyzed 1,3-enyne hydroboration. It also highlights the challenges associated with selective functionalization of 1,3-enynes as minor differences in the substrate and catalyst resulted in unique selectivity. In a similar transformation, the Shen group reported a copper-catalyzed 3,4-hydroboration of 1,3-enynes bearing pennant alcohols and trialkylamines (Scheme 1.7b). The boronic ester was installed in the external alkyne carbon resulting in 1-boryl-1,3-dienes (**1.42**).[33] While the transformation bears similarity to the earlier report by Ito, it is operationally simpler as it utilizes copper chloride which is an air stable precatalyst rather than copper *tert*-butoxide which needs to be generated in a glovebox.

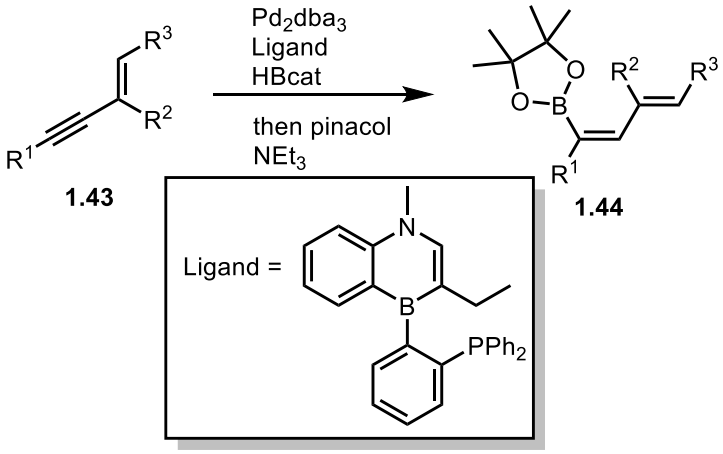

Scheme 1.8: Palladium-catalyzed trans-3,4-hydroboration of 1,3-enynes.

In comparison to *cis*-hydroboration reactions, *trans*-hydroboration reactions are exceptionally less common. In an elegant display of ligand design, the Liu group established a synthetic protocol for achieving the first *trans*-hydroboration of 1,3-enynes (Scheme 1.8). The reaction utilizes a palladium(0) catalyst, a 1,4-azaborine-based phosphine ligand and

catecholborane to deliver the boronic ester into the external alkyne carbon (**1.41**).[34] The 1,3-dienyl catecholboronates were not stable during purification so transesterification with pinacol and triethylamine was required. A thorough mechanistic investigation suggests that an outer-sphere oxidative addition mechanism is responsible for the selectivity, although a more in-depth mechanistic discussion is included in the next chapter.[35]

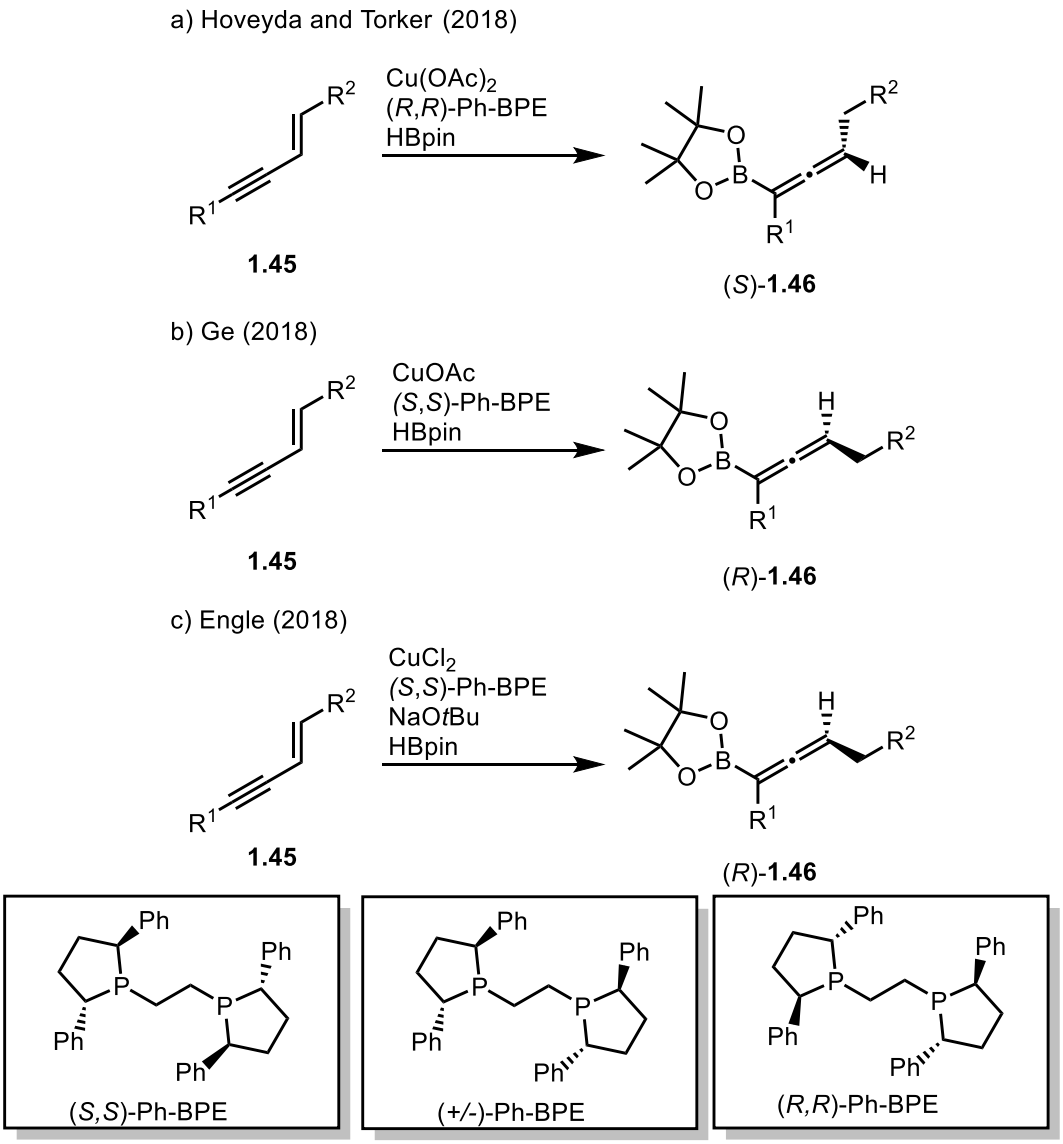

Scheme 1.9: Copper-catalyzed 1,4-hydroboration reactions of 1,3-enynes.

The copper-catalyzed 1,4-hydroboration of 1,3-enynes has been studied extensively. Hoveyda and Torker reported the first example of a copper-catalyzed 1,4-hydroboration of 1,3-

enynes which resulted in enantioenriched boryl-allenes ((*S*)-**1.46**). An enantioenriched, (*R*,*R*)-phenyl-bpe-copper-hydride complex was used to synthesize the axially chiral boryl-allenes (Scheme 1.9a). The proposed mechanism involves hydrocupration of the alkene, rapid rearrangement to an allenylcuprate intermediate which is trapped by HBpin generating the new carbon-boron bond and reforming the copper-hydride catalyst.[36] A few months later, the Ge group published a similar procedure for synthesizing the opposite enantiomer ((*R*)-**1.46**). Copper(I) acetate was used instead of copper(II) acetate suggesting the oxidation state of the precatalyst has little effect on the overall transformation.[37] Within the same year, the Engle group reported the same transformation replacing only the copper(I) acetate precatalyst with a copper(II) chloride and exogenous base (NaO*t*Bu) (Scheme 1.9c).[38] Interestingly, all three groups independently found Ph-BPE to be the optimal ligand for both enantioselectivity and yield.

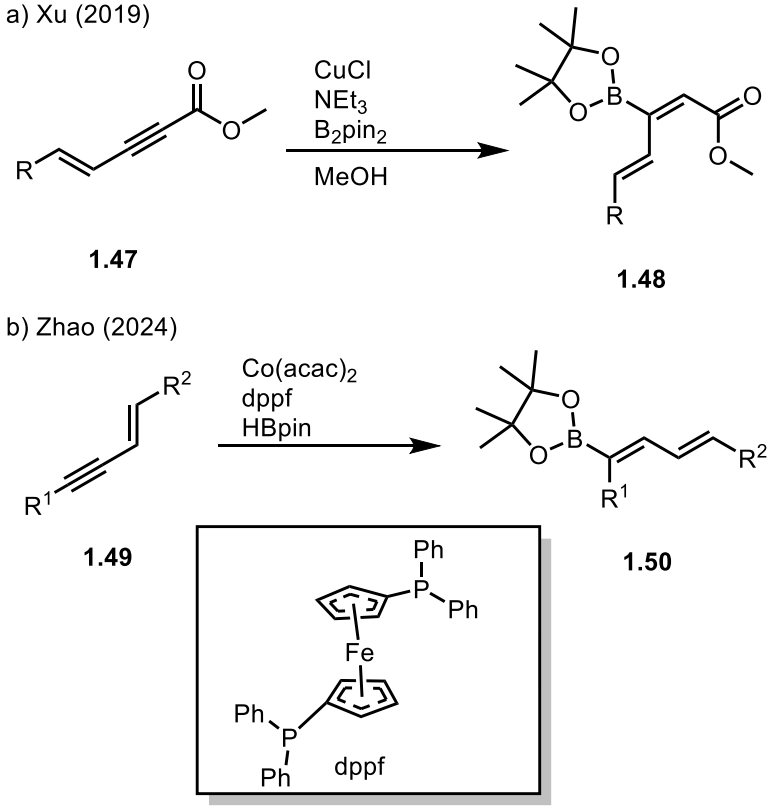

Scheme 1.10: Recent reports of earth abundant 3,4-hydroborations of 1,3-enynes.

In 2019, the Xu group reported the first example of a 3,4-hydroboration that delivered the boronic ester into the internal alkyne carbon (Scheme 1.10a, **1.48**). This was achieved by using a copper-Bpin catalytic system (B_2pin_2, base and copper salt) on polarized 1,3-enynoate substrates (**1.47**). Notably, the electron-withdrawing group was present throughout their study and serves as a directing group in this reaction by making the 3-position of the 1,3-enyne more electrophilic. Surprisingly, the reaction works in the absence of a well-defined ligand perhaps because triethylamine can serve as both a ligand and base (used in 10 mol%). After copper-boron addition to the alkyne, protonation of the resulting organocuprate with methanol (solvent) generates copper-methoxide which reacts with B_2pin_2 to reform the copper-Bpin catalyst.[39]

Recently, the 3,4-hydroboration of 1,3-enynes was achieved using cobalt catalysis (Scheme 1.10b). In this example by the Zhao group, the boronic ester is delivered into the external alkyne carbon resulting in 1-boryl-1,3-dienes (**1.50**).[40] Bidentate phosphine ligands resulted in the highest yield of **1.50** with 1,1'-Bis(diphenylphosphino)ferrocene being the optimal ligand for this transformation. Interestingly, these conditions result in cobalt-hydride rather than cobalt-Bpin and hydrometallation occurs at the alkyne instead of the alkene like the previously discussed copper-hydride reactions (Scheme 1.9). A thorough mechanistic investigation is required to understand the reason for this unusual selectivity.

Despite nearly 60 years of research being conducted on 1,3-enyne hydroboration reactions, several selectivities remain elusive. For instance, the 1,2-hydroboration of 1,3-enynes which results in propargylic boronic esters (Scheme 1.11, **1.53**) has not yet been discovered. While one might anticipate that the propargylic cuprate generated from alkene hydrocupration would be trapped by HBpin resulting in **1.53**, it instead rapidly rearranges into the allenylcuprate resulting in **1.55** (after trapping with HBpin). Similarly, the 1,4-hydroboration of 1,3-enynes resulting in an

alkylboronate adjacent to the allene remains elusive (**1.54**). It is worth noting that these products are accessible through the borylation of propargylic leaving groups with copper or palladium catalysis but not from 1,3-enynes.[41-43] The 3,4-hydroboration of 1,3-enynes which installs the boronic ester in the internal alkyne carbon (**1.56**) has only been achieved with the use of a directing group.[39] Detailed below is our study to address this gap in the literature and provide access to a broader scope of 2-boryl-1,3-dienes that does not require directing groups or prerequisite functionalization.

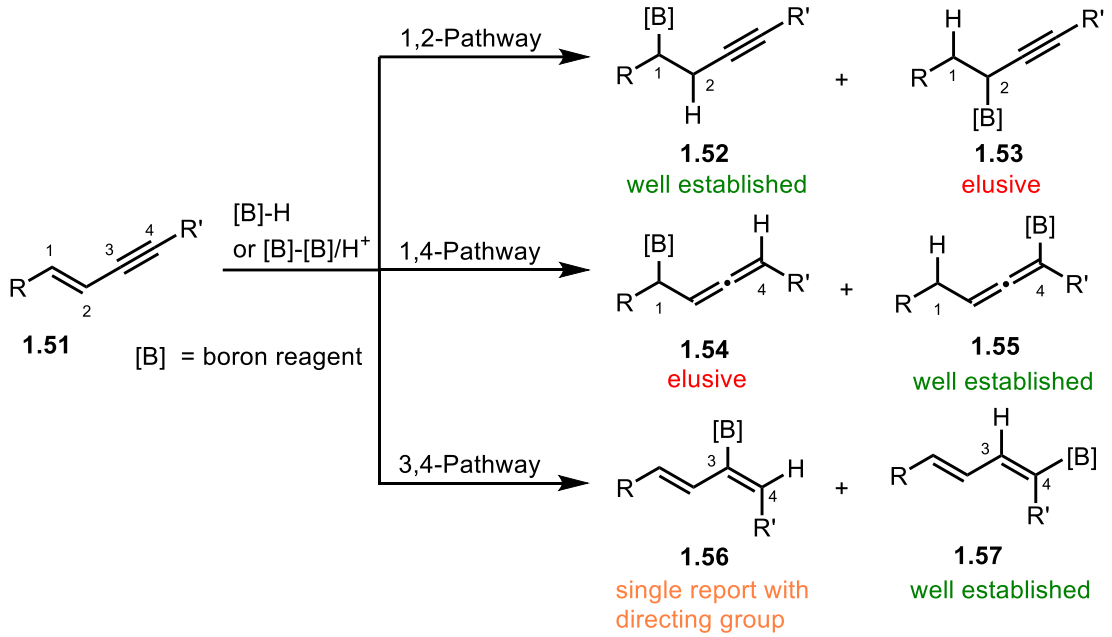

Scheme 1.11: Outlook on 1,3-enyne hydroboration reactions after 58 years of research.

1.5. Results and Discussion

Investigations into selective formation of 2-boryl-1,3-dienes from 1,3-enynes began by treating the model substrate (*Z*)-but-1-en-3-yne-1,4-diyldibenzene (**1.58a**) with CuOAc (10

Table 1.1: Optimization of Reaction Conditions[a]

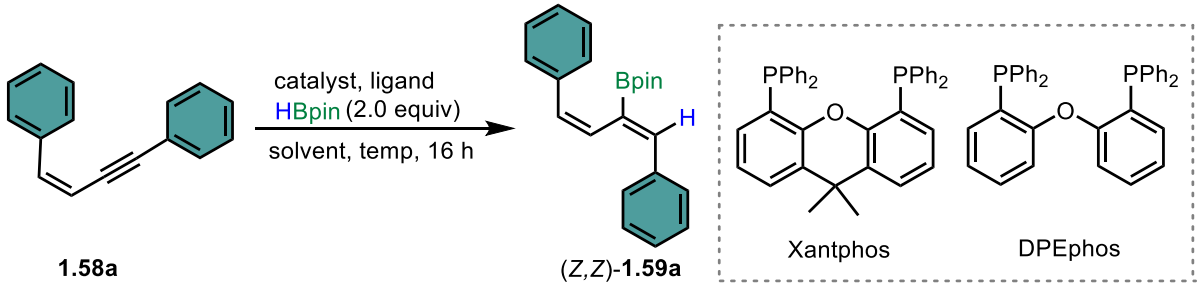

Entry	Catalyst	Ligand	Cat. Loading (mol%)[b]	Solvent	Temp (°C)	Yield (%)	*Z*:*E*[c]
1	CuOAc	Xantphos	10	toluene	50	75	>99:1
2	CuCN	Xantphos	10	toluene	50	8	>99:1
3	CuCl	Xantphos	10	toluene	50	4	>99:1
4	$Cu(OAc)_2$	Xantphos	10	toluene	50	55	>99:1
5	$CuCl_2$	Xantphos	10	toluene	50	4	>99:1
6	CuOAc	PPh_3	10	toluene	50	25	96:4
7	CuOAc	DPEphos	10	toluene	50	13	76:24
8	CuOAc	Xantphos	10	THF	50	53	>99:1
9	CuOAc	Xantphos	10	MeCN	50	13	>99:1
10	CuOAc	Xantphos	10	1,4-dioxane	50	72	>99:1
11	CuOAc	Xantphos	5	toluene	50	80	>99:1
12	CuOAc	Xantphos	5	toluene	60	80	>99:1
13	CuOAc	Xantphos	5	toluene	40	89	>99:1
14	CuOAc	Xantphos	5	toluene	25	80	>99:1
15	-	Xantphos	10	toluene	50	0	-
16	CuOAc	-	10	toluene	50	0	-

[a]Performed under N_2 atmosphere, 0.125 mmol scale, 0.25 M, isolated yield. [b]Refers to copper salt and ligand loading. [c]Determined by GC-MS.

mol%), Xantphos (10 mol%) and HBpin (2.0 equiv) in toluene at 50 °C for 16 hours (Table 1.1, entry 1). Interestingly, hydroboration occurred on the alkyne moiety in a *cis* fashion with Bpin installed on the internal carbon proving access to these elusive conjugated vinyl boronates. Thus, (*Z*,*Z*)-2-boryl-1,3-diene **1.59a** was isolated in 75% yield with >99:1 *Z*:*E* selectivity. Stereochemistry was established by protodeborylation with KHF_2 where the alkene coupling constants of 9.4 Hz were consistent with *Z* geometry. We next tested alternative Cu(I) and Cu(II) salts but these displayed decreased yields of **1.59a** (entries 2-5). The use of the monodentate phosphine ligand triphenylphosphine or bidentate ligand (oxybis(2,1-phenylene))bis(diphenylphosphane) (DPEphos) had a negative impact on the isolated yield and *Z*:*E* ratio (entries 6-7). A survey of solvents such as tetrahydrofuran (THF), 1,4-dioxane or acetonitrile (MeCN) decreased the yield (entries 8-10). Catalyst loading was also evaluated; interestingly, a reduced loading (5 mol%) of the copper precatalyst (CuOAc) and ligand (Xantphos) resulted in an increase in yield of **1.59a** (80%), possibly due to the decreased amount of sacrificial HBpin in formation of the active copper hydride catalyst (entry 11) (*vide infra*). We next investigated the effect of temperature and found that the reaction was optimal when performed at 40 °C (entries 12-14). Control reactions without catalyst or ligand gave no product formation, suggesting that both are essential for reactivity (entries 15-16). To ensure hidden borane catalysis

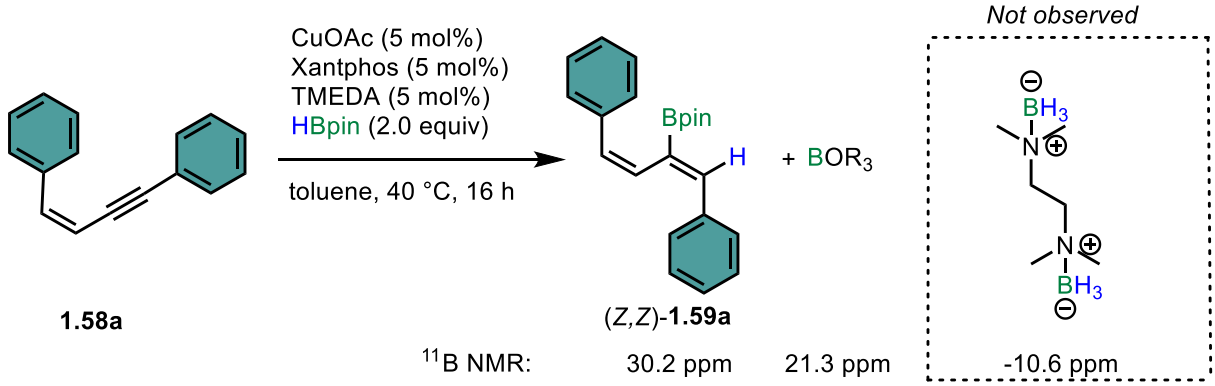

Scheme 1.12: Hidden borane catalysis control experiment.

was not occurring, substoichiometric TMEDA was introduced to the reaction and no borane-TMEDA adduct was observed (Scheme 1.12). The optimized conditions were found to be copper(I) acetate (5 mol%), Xantphos (5 mol%), HBpin (2.0 equiv) in toluene at 40 °C for 16 hours, which provided **1.59a** in an 89% isolated yield and >99:1 *Z*:*E* ratio (entry 13).

With the reaction conditions optimized, our focus turned to probing the selectivity of the transformation by the completion of a substrate scope (Schemes 1.13 and 1.14). The model substrate **1.58a** underwent hydroboration to give **1.59a** in a good yield (73%) (Scheme 1.13). Methyl substitution on the aryl rings was well tolerated in both the *para* (**1.59b**) and *meta* positions (**1.59c**) with 78% and 69% isolated yields, respectively. The (*Z*,*Z*)-configuration of **1.59b** (CCDC 2297662) was unambiguously confirmed by X-ray crystallography. Larger alkyl substitution such as *t*-butyl and *n*-propyl reacted smoothly into their corresponding 2-boryldienes (**1.59d**-**1.59e**) with comparable yields. Likewise, the

presence of methoxy groups in either the *para* (**1.59f**) or *meta* (**1.59g**) positions resulted in excellent yields. Performing the reaction on a 1.6 mmol scale resulted in good yield (65%) of boryldiene **1.59f** without affecting selectivity. A benzyl protected substrate **1.58h** was tolerated under the reaction conditions forming 2-boryl-1,3-diene **1.59h** in good yield (61%) while the thioether 2-boryldiene **1.59i** was successfully prepared in a similar yield (58%). Boryldienes bearing electron withdrawing functionalities such as trifluoromethyl (**1.59j**) and trifluoromethoxy (**1.59k**) were obtained in moderate yields. Halogen containing substrates such as fluoro in the *meta* (**1.59m**) and *para* (**1.59l**) positions served as good substrates while chloro substitution in the *ortho* (**1.59p**), *meta* (**1.59o**) and *para* (**1.59n**) positions resulted in the formation of the corresponding boryldienes in moderate to good yields (34%, 55%, 65%), with increasing yields in the order of

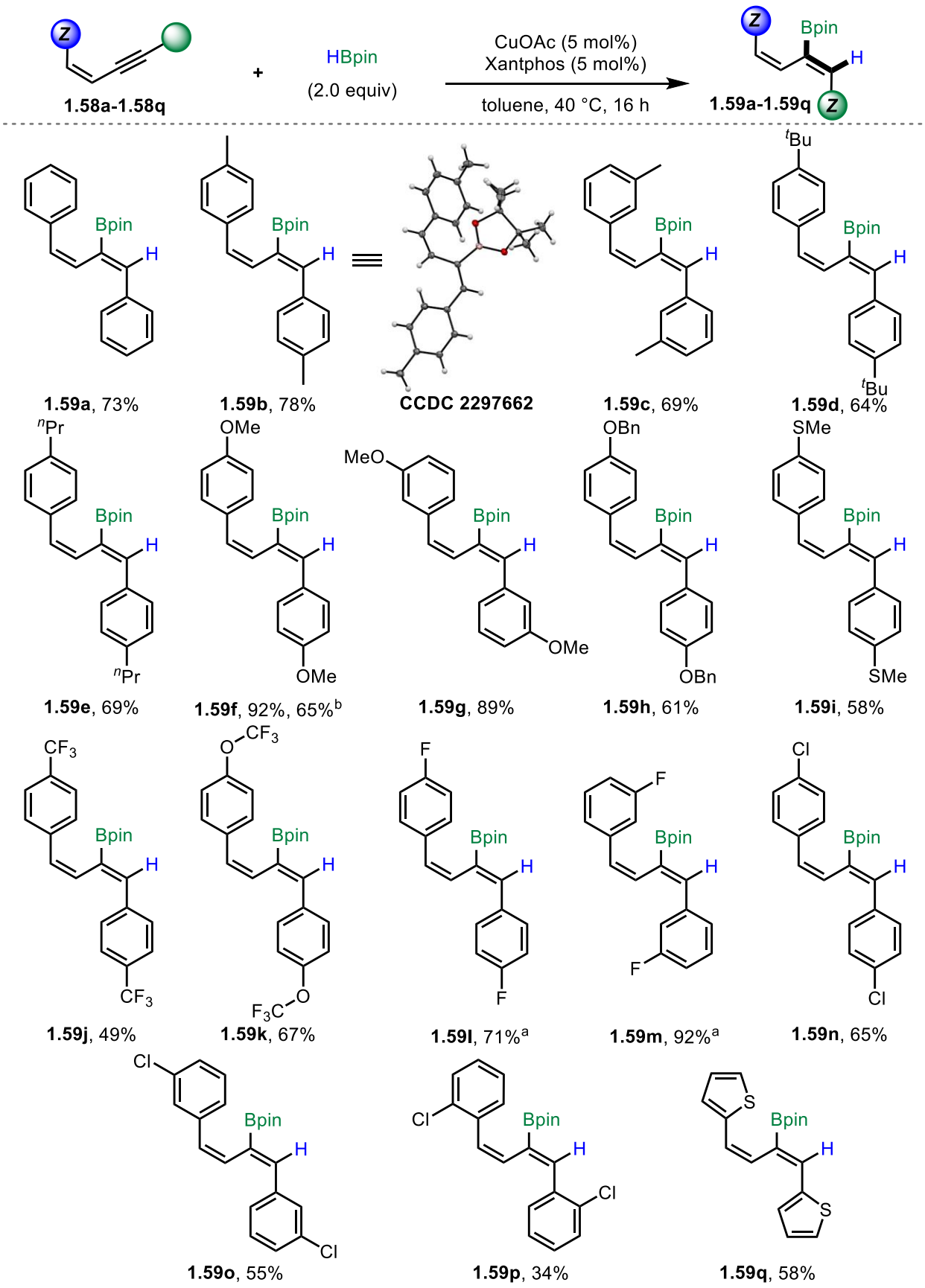

Scheme 1.13: Substrate scope of (*Z*)-1,3-enynes. Isolated yields are reported. >99:1 *Z*:*E* determined by ^{1}H NMR. [a]1.2 equiv HBpin, 4 h. [b] 1.6 mmol scale.

ortho to *meta* and *para*, suggesting steric hindrance at the *ortho* position may affect reactivity. Heterocycles were also tested under the reaction conditions. A boryldiene bearing thiophene moiety (**1.59q**) was obtained in a good yield (58%)

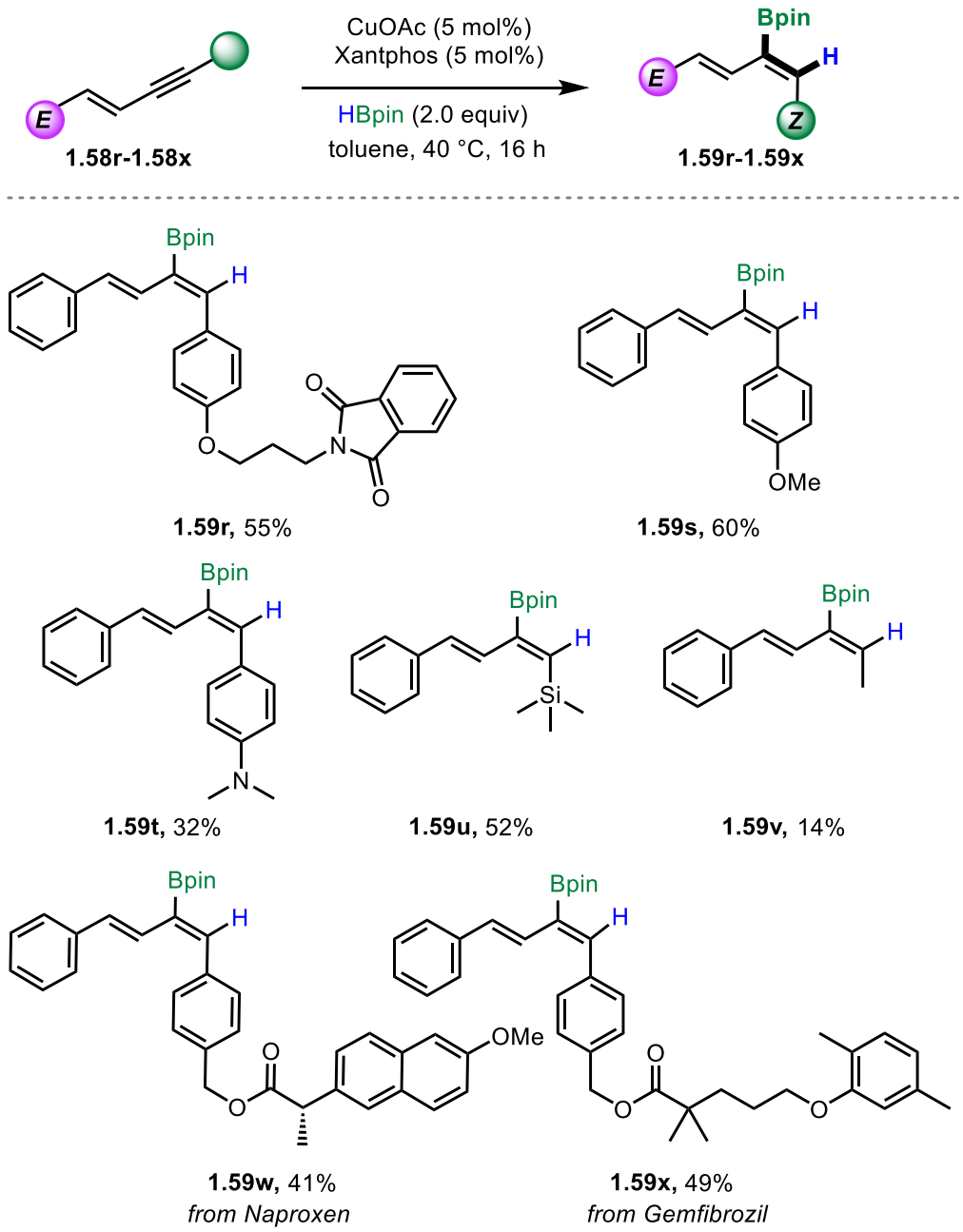

Scheme 1.14: Substrate Scope of (*E*)-1,3-enynes. Isolated yields are reported. >99:1 *Z*:*E* determined by ^{1}H NMR.

With the substrate scope of the (*Z*)-enynes established, we next investigated the complementary (*E*)-enynes as substrates (Scheme 1.14). Thus, we synthesized unsymmetrical enyne **1.58r** bearing phthalimide. To our delight, the corresponding boryldiene **1.59r** was afforded exclusively and the Bpin moiety chemoselectively added to the alkyne unit (55% yield). The anisyl containing boryldiene **1.59s** was isolated in a 60% yield. Likewise, the boryldiene bearing a tertiary aniline **1.59t** was obtained in a 32% yield as a single isomer. Explorations into monoaryl, unsymmetrical substrates showed that a trimethylsilyl capped enyne (**1.58u**) underwent hydroboration to give the corresponding 2-boryldiene in a 52% yield. While most alkyl substrates resulted in a complex mixture of products boryldiene **1.59v** was isolated in a 14% yield as a single isomer. Finally, enyne derivatives of non-steroidal anti-inflammatory drug Naproxen and lipid lowering agent Gemfibrozil were synthesized (**1.58w**, **1.58x**) and subjected to the optimized conditions to give boryldienes **1.59w** and **1.59x** in moderate yields (41%, 49%). These results demonstrate chemoselectivity for the alkyne in substrates bearing carbonyls as no reduction of the amide (**1.59r**) or esters (**1.59w**, **1.59x**) were observed.

1.6. Applications

To demonstrate the synthetic potential of the 2-boryl-1,3-dienes, compound **1.59f** was subjected to various transformations (Scheme 1.15). First, boronic ester **1.59f** underwent protodeboration using KHF_2 and acetic acid to produce the (*Z*,*Z*) disubstituted 1,3-diene, **1.60** with >99:1 *Z*:*E* retention of stereochemistry. Suzuki-Miyaura cross coupling was performed with $Pd_2(dba)_3$ and 4-iodobenzonitrile to afford the trisubstituted-diene **1.61** in 74% yield. Oxidation with hydrogen peroxide afforded α,ß-unsaturated ketone **1.62** in good yield (54%) with concomitant alkene isomerization to the more stable (*E*) geometry. Finally, under Matteson

homologation conditions, 2-boryl-1,3- diene **1.59f** underwent stereoretentive homologation to generate allylic alcohol **1.63**.

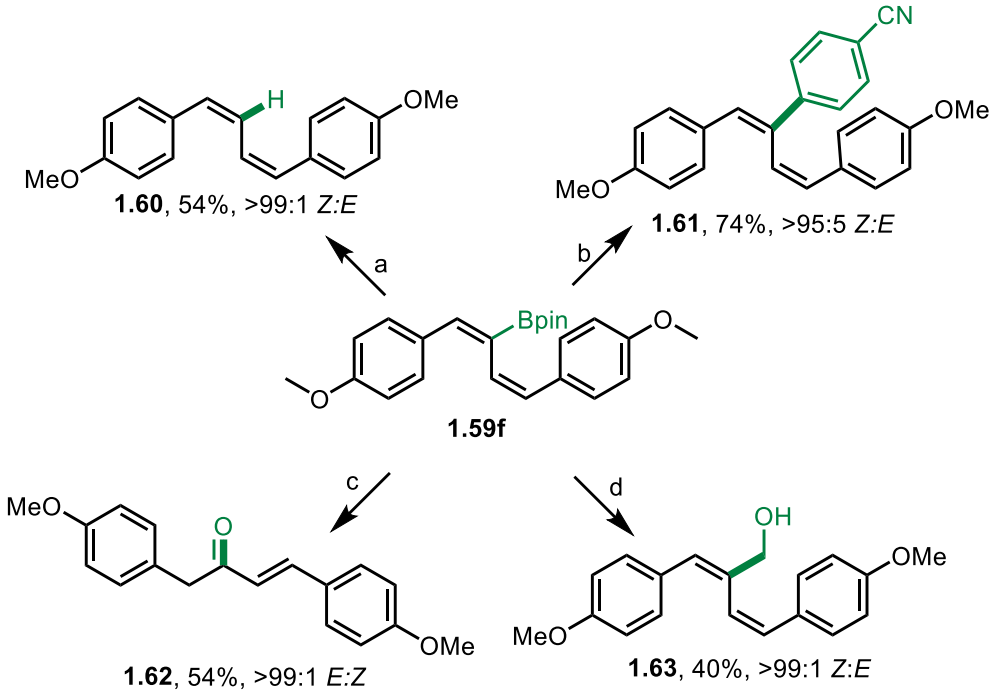

Scheme 1.15: Synthetic applications of 2-boryl-1,3-dienes. Isolated yields are reported. Z:E determined by ^{1}H NMR. a: KHF_2 (3.0 equiv), acetic acid (0.5 mL). b: $Pd_2(dba)_3$ (4 mol%), SPhos (5 mol%), 4-iodobenzonitrile (1.5 equiv), THF/3 M NaOH (3:1), 70 °C. c: H_2O_2 (30 equiv), 3 M NaOH (30 equiv), THF (0.5 mL). d: nBuLi (3.0 equiv), dibromomethane (4.0 equiv), THF (1.0 mL) −78 - 25 °C, 4 h then H_2O_2 (5.0 equiv), 3 M NaOH (5.0 equiv).

1.7. Conclusions

In conclusion, we have developed a copper-catalyzed method for the *cis*-alkyne-hydroboration of 1,3-enynes. Notably, installation of the Bpin group occurred on the internal carbon; a general method for this isomer has not yet been realized. This protocol utilizes commercially available reagents and mild conditions to achieve moderate to excellent yields with excellent chemo-, regio-, and stereoselectivity. Both (*Z*)- and (*E*)-1,3-enynes were successfully converted into their corresponding 2-boryl-1,3-dienes. The synthetic utility of the 2-boryldienes was showcased through further functionalization, undergoing exemplar reactions involving

boronic esters, including oxidation, protodeborylation, homologation, and cross-coupling. Justification for the high level of selectivity and the mechanistic intricacies of this reaction will be disclosed in the next chapter.

1.8. References

1. Hall, D. G. Structure, Properties, and Preparation of Boronic Acid Derivatives. Overview of Their Reactions and Applications. In *Boronic Acids*, 2005; pp 1–99.

2. Lennox, A. J.; Lloyd-Jones, G. C. Selection of boron reagents for Suzuki–Miyaura coupling. *Chem. Soc. Rev.* **2014**, *43* (1), 412–443.

3. Chatterjee, S.; Tripathi, N. M.; Bandyopadhyay, A. The modern role of boron as a 'magic element'in biomedical science: Chemistry perspective. *Chem. Commun.* **2021**, *57* (100), 13629–13640.

4. Piperdi, B.; Ling, Y.-H.; Liebes, L.; Muggia, F.; Perez-Soler, R. Bortezomib: understanding the mechanism of action. *Mol Cancer Ther* **2011**, *10* (11), 2029–2030.

5. Shirley, M. Ixazomib: first global approval. *Drugs* **2016**, *76* (3), 405–411.

6. Jinna, S.; Finch, J. Spotlight on tavaborole for the treatment of onychomycosis. *Drug Des. Devel. Ther.* **2015**, 6185–6190.

7. Paton, D. M. Crisaborole: Phosphodiesterase inhibitor for treatment of atopic dermatitis. *Drugs Today* **2017**, *53* (4), 239–245.

8. Lomovskaya, O.; Sun, D.; Rubio-Aparicio, D.; Nelson, K.; Tsivkovski, R.; Griffith, D. C.; Dudley, M. N. Vaborbactam: spectrum of beta-lactamase inhibition and impact of resistance mechanisms on activity in Enterobacteriaceae. *Antimicrob. Agents. Chemother.* **2017**, *61* (11), 10.1128/aac. 01443–01417.

9. Krinos, E. L.; Gwinn, R. K.; Santos, W. L. Boron: The Rise of a "Magic-Element" in Medicinal Chemistry. In *Burger's Medicinal Chemistry and Drug Discovery*, pp 1–47.

10. Brown, H. C. Hydroboration—a powerful synthetic tool. *Tetrahedron* **1961**, *12* (3), 117–138.

11. Vedejs, E.; Brewster, J. H.; Negishi, E.-I. The 1979 nobel prize for chemistry. *Science* **1980**, *207* (4426), 42–46.

12. Lam, P. Chan–Lam Coupling Reaction: Copper-promoted C–Element Bond Oxidative Coupling Reaction with Boronic Acids. **2016**.

13. Han, F.-S. Transition-metal-catalyzed Suzuki–Miyaura cross-coupling reactions: a remarkable advance from palladium to nickel catalysts. *Chem. Soc. Rev.* **2013**, *42* (12), 5270–5298.

14. Suzuki, A.; Heck, R. F.; Negishi, E.-i. The nobel prize in chemistry 2010. *TRENDS IN THE SCI* **2010**, *16* (5), 10.

15. Bhattacherjee, D.; Rahman, M.; Ghosh, S.; Bagdi, A. K.; Zyryanov, G. V.; Chupakhin, O. N.; Das, P.; Hajra, A. Advances in transition-metal catalyzed carbonylative Suzuki-Miyaura coupling reaction: an update. *Adv. Synth. Catal.* **2021**, *363* (6), 1597–1624.

16. Santarsiere, A.; Galgano, P.; Funicello, M.; Lupattelli, P.; Chiummiento, L. NCS-Mediated Ipso-Halogenation of Arylboronic Acids in Water Using Sodium Halides. *ACS Omega* **2025**, *10* (26), 27856–27860.

17. Molloy, J. J.; O'Rourke, K. M.; Frias, C. P.; Sloan, N. L.; West, M. J.; Pimlott, S. L.; Sutherland, A.; Watson, A. J. B. Mechanism of Cu-Catalyzed Aryl Boronic Acid Halodeboronation Using Electrophilic Halogen: Development of a Base-Catalyzed Iododeboronation for Radiolabeling Applications. *Org. Lett.* **2019**, *21* (7), 2488–2492.

18. Furuya, T.; Ritter, T. Fluorination of Boronic Acids Mediated by Silver(I) Triflate. *Org. Lett.* **2009**, *11* (13), 2860–2863.

19. Nair, A. S.; Singh, A. K.; Kumar, A.; Kumar, S.; Sukumaran, S.; Koyiparambath, V. P.; Pappachen, L. K.; Rangarajan, T. M.; Kim, H.; Mathew, B. FDA-Approved Trifluoromethyl Group-Containing Drugs: A Review of 20 Years. *Processes* **2022**, *10* (10), 2054.

20. Chu, L.; Qing, F.-L. Copper-Mediated Oxidative Trifluoromethylation of Boronic Acids. *Org. Lett.* **2010**, *12* (21), 5060–5063.

21. Andler, O.; Kazmaier, U. Matteson Homologation-Based Total Synthesis of Meliponamycin A. *Org. Lett.* **2024**, *26* (1), 148–152.

22. He, Z.; Song, F.; Sun, H.; Huang, Y. Transition-Metal-Free Suzuki-Type Cross-Coupling Reaction of Benzyl Halides and Boronic Acids via 1,2-Metalate Shift. *J. Am. Chem. Soc.* **2018**, *140* (7), 2693–2699.

23. Saeed, S.; Munawar, S.; Ahmad, S.; Mansha, A.; Zahoor, A. F.; Irfan, A.; Irfan, A.; Kotwica-Mojzych, K.; Soroka, M.; Głowacka, M.; et al. Recent Trends in the Petasis Reaction: A Review of Novel Catalytic Synthetic Approaches with Applications of the Petasis Reaction. *Molecules* **2023**, *28* (24), 8032.

24. Burgio, A. L.; Buchbinder, N. W.; Santos, W. L. Regio- and Stereoselective Copper-Catalyzed Borylation–Protodeboronation of 1,3-Diynes: Access to (Z)-1,3-Enynes. *Org. Lett.* **2023**, *25* (15), 2652–2656.

25. Kuang, Z.; Yang, K.; Zhou, Y.; Song, Q. Base-promoted domino-borylation-protodeboronation strategy. *Chem. Commun.* **2020**, *56* (48), 6469–6479, 10.1039/D0CC00614A.

26. Liang, H.; Berwanger, M. R.; Morken, J. P. Stereospecific Phosphination and Thioetherification of Organoboronic Esters. *J. Am. Chem. Soc.* **2024**, *146* (28), 18873–18878.

27. Mao, L.; Bose, S. K. Hydroboration of Enynes and Mechanistic Insights. *Adv. Synth. Catal.* **2020**, *362* (20), 4174–4188.

28. Zweifel, G.; Polston, N. L. Selective hydroboration of conjugated diynes with dialkylboranes. A convenient route to conjugated cis-enynes, .alpha.,.beta.-acetylenic ketones, and cis,cis-dienes. *J. Am. Chem. Soc.* **1970**, *92* (13), 4068–4071.

29. Garnier, L.; Plunian, B.; Mortier, J.; Vaultier, M. Diels-Alder reactions of 1, 3-dienylborate salts with activated dienophiles. *Tetrahedron Lett.* **1996**, *37* (37), 6699–6700.

30. Matsumoto, Y.; Naito, M.; Hayashi, T. Palladium (0)-catalyzed hydroboration of 1-buten-3-ynes: preparation of allenylboranes. *Organometallics* **1992**, *11* (7), 2732–2734.

31. Zaidlewicz, M.; Meller, J. Syntheses with organoboranes. X. Monohydroboration of conjugated enynes with catecholborane catalyzed by nickel (II) chloride complexes with diphosphines. *Collect. Czechoslov. Chem. Commun.* **1999**, *64* (6), 1049–1056.

32. Sasaki, Y.; Horita, Y.; Zhong, C.; Sawamura, M.; Ito, H. Copper (I)-Catalyzed Regioselective Monoborylation of 1, 3-Enynes with an Internal Triple Bond: Selective Synthesis of 1, 3-Dienylboronates and 3-Alkynylboronates. *Angew. Chem. Int. Ed.* **2011**, *50* (12), 2778–2782.

33. Xu, H.-D.; Wu, H.; Jiang, C.; Chen, P.; Shen, M.-H. Chemo-, regio-, and stereoselective hydroboration of conjugated enyne alcohol/amine: facile synthesis of Z, Z-/Z, E-1, 3-dien-1/2-ylboronic ester bearing hydroxyl/amino group. *Tetrahedron Lett.* **2016**, *57* (26), 2915–2918.

34. Xu, S.; Zhang, Y.; Li, B.; Liu, S.-Y. Site-selective and stereoselective trans-hydroboration of 1, 3-enynes catalyzed by 1, 4-azaborine-based phosphine–Pd complex. *J. Am. Chem. Soc.* **2016**, *138* (44), 14566–14569.

35. Zhang, Y.; Wang, Z.; Lamine, W.; Xu, S.; Li, B.; Chrostowska, A.; Miqueu, K.; Liu, S.-Y. Mechanism of Pd/Senphos-Catalyzed trans-Hydroboration of 1,3-Enynes: Experimental and Computational Evidence in Support of the Unusual Outer-Sphere Oxidative Addition Pathway. *J. Org. Chem.* **2023**, *88* (4), 2415–2424.

36. Huang, Y.; del Pozo, J.; Torker, S.; Hoveyda, A. H. Enantioselective Synthesis of Trisubstituted Allenyl–B(pin) Compounds by Phosphine–Cu-Catalyzed 1,3-Enyne Hydroboration. Insights Regarding Stereochemical Integrity of Cu–Allenyl Intermediates. *J. Am. Chem. Soc.* **2018**, *140* (7), 2643–2655.

37. Sang, H. L.; Yu, S.; Ge, S. Copper-catalyzed asymmetric hydroboration of 1,3-enynes with pinacolborane to access chiral allenylboronates. *Org. Chem. Front.* **2018**, *5* (8), 1284–1287, 10.1039/C8QO00167G.

38. Gao, D.-W.; Xiao, Y.; Liu, M.; Liu, Z.; Karunananda, M. K.; Chen, J. S.; Engle, K. M. Catalytic, Enantioselective Synthesis of Allenyl Boronates. *ACS Catal.* **2018**, *8* (4), 3650–3654.

39. Meng, F.-F.; Xue, Q.-Y.; Jiang, B.; Zhao, M.; Xie, J.-H.; Xu, Y.-H.; Loh, T.-P. Divergent Protosilylation and Protoborylation of Polar Enynes. *Org. Lett.* **2019**, *21* (8), 2932–2936.

40. Jia, Y.; Yang, L.; Wang, X.; Yang, W.; Zhao, W. Cobalt-Catalyzed Selective Hydroboration of 1,3-Enynes with HBpin toward 1,3-Dienylboronate Esters. *Org. Lett.* **2024**, *26* (15), 3258–3262.

41. Ito, H.; Sasaki, Y.; Sawamura, M. Copper(I)-Catalyzed Substitution of Propargylic Carbonates with Diboron: Selective Synthesis of Multisubstituted Allenylboronates. *J. Am. Chem. Soc.* **2008**, *130* (47), 15774–15775.

42. Zhao, T. S. N.; Yang, Y.; Lessing, T.; Szabó, K. J. Borylation of Propargylic Substrates by Bimetallic Catalysis. Synthesis of Allenyl, Propargylic, and Butadienyl Bpin Derivatives. *J. Am. Chem. Soc.* **2014**, *136* (21), 7563–7566.

43. Law, C.; Kativhu, E.; Wang, J.; Morken, J. P. Diastereo- and Enantioselective 1,4-Difunctionalization of Borylenynes by Catalytic Conjunctive Cross-Coupling. *Angew. Chem. Int. Ed.* **2020**, *59* (26), 10311–10315.

Chapter 2: Experimental and Theoretical Investigations of Copper-Catalyzed Chemo-, Regio-, and Stereoselective *cis*-Hydroboration of 1,3-Enynes

2.1. Contributions

Nicklas Buchbinder conducted all chemical synthesis, kinetic experiments, control experiments and grew the crystals for X-ray crystallography analysis. Andrew Bage advised throughout the project and contributed to the preparation and editing of the final manuscript. Dr. Carla Slebodnick and Reilly Gwinn were responsible for crystallographic experiments and analysis. DFT calculations were performed by Dr. Farshad Shiri under the guidance of Prof. Zhenyang Lin at the Hong Kong University of Science and Technology. Prof. Webster Santos advised throughout the project and contributed to the preparation and editing of the final manuscript. The final manuscript was prepared in collaboration with Nicklas Buchbinder, Andrew Bage, Dr. Farshad Shiri, Prof. Zhenyang Lin and Prof. Webster Santos. This work has been published in *European Journal of Organic Chemistry* and is available online. Reprint (adapted) with permission from (Shiri, F.; Buchbinder, N.W.; Bage, A.B.; Gwinn, R; Slebodnick, C.; Santos, W.L.; Lin, Z. *Eur. J. Org. Chem.* **2025**, 28, e202501027.) Reproduced (adapted) with permission from John Wiley and Sons ©2017 Wiley-VCH Verlag GmbH&Co. KGaA,Weinheim].

2.2. Abstract

The mechanistic details of the chemo-, regio-, and stereoselective *cis*-hydroboration of 1,3-enynes were investigated using X-ray crystallography, kinetic analysis and DFT calculations. The kinetic analysis revealed that the reaction is first order in enyne, zeroth order in HBpin and fractional order in the catalyst. Our studies suggest that a cyclic CuHBpinOAc species was determined to be the/an off-cycle species (via DFT analysis) that contributes to the experimentally observed fractional rate order regarding the catalyst. Experimental and computational data suggests that hydrocupration is rate limiting and essential for achieving selectivity.

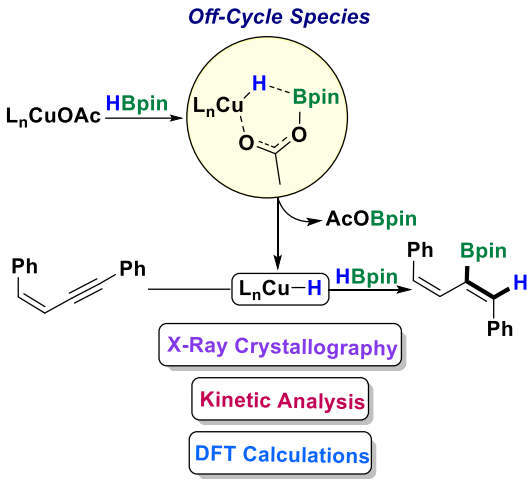

2.3. 1,3-Enyne Hydroboration Mechanisms

Elucidating the mechanistic details of reactions is an important practice to inform further reaction optimization studies and develop analogous reactions. For example, the Buchwald group used kinetic analysis to propose a detailed catalytic cycle for their enantioselective hydroamination of alkenes. This endeavor resulted in insight that enabled a second round of optimization shortening reactions times (18 hours to 10 minutes), lowering temperatures (40 °C to 25 °C), expanding the scope and increasing yields.[1] This is just one example in which mechanistic studies supported practical applications in organic synthesis.

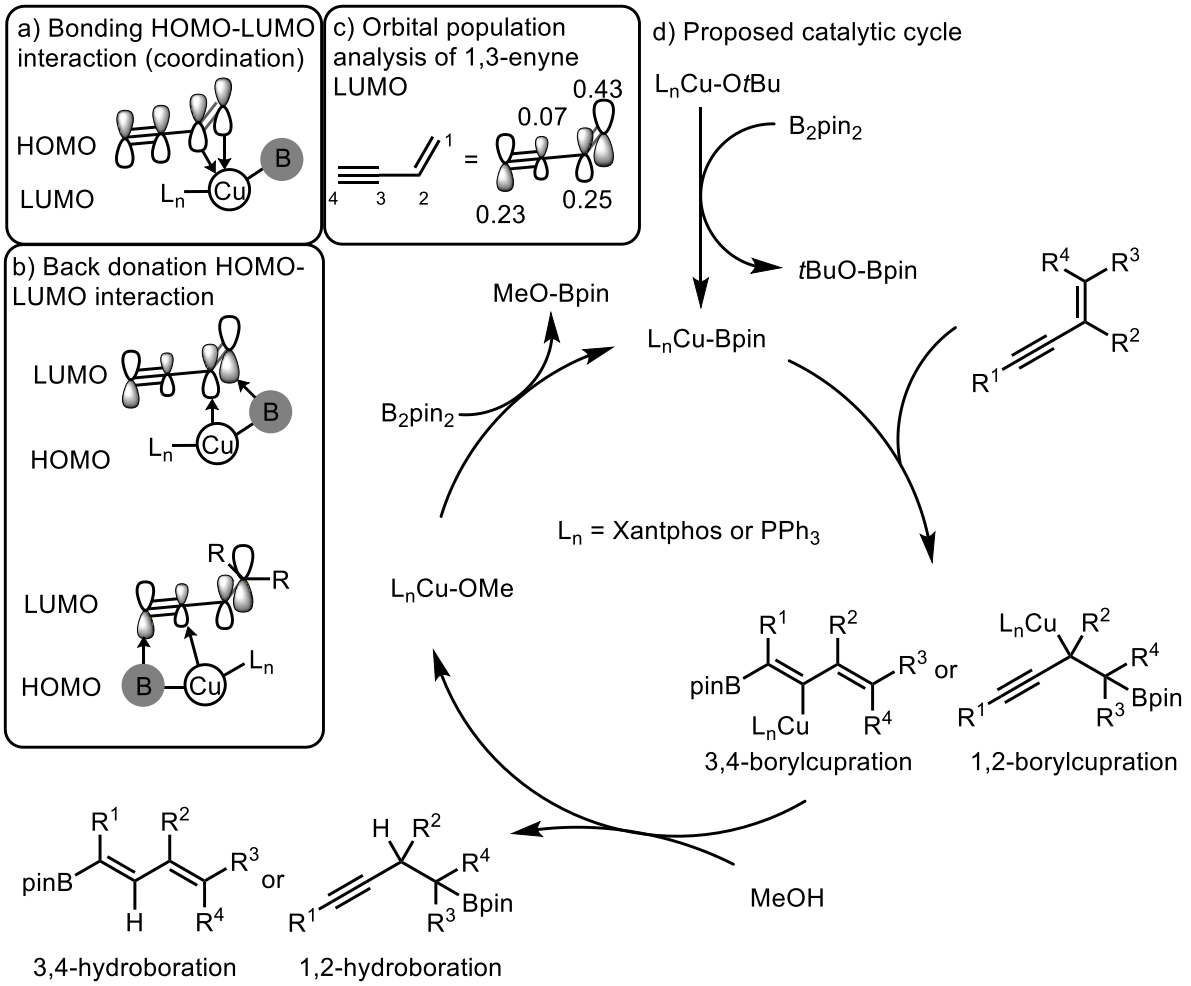

Figure 2.1: a) Bonding HOMO-LUMO interaction (coordination). b) Back donation HOMO-LUMO interactions. c) Orbital population analysis via DFT calculations (B3LYP/6-31G(d,p)). d) Proposed catalytic cycle for the regiodivergent hydroboration of 1,3-enynes.

Considering the breadth of research on 1,3-enyne hydroboration reactions, several of their mechanisms have been studied in detail. Ito's copper-catalyzed regiodivergent hydroboration of 1,3-enynes was the first example of an enyne hydroboration reaction that included a thorough mechanistic study. Marder and coworkers had previously established that copper-boron complexes will engage C-C π-bonds through coordination of the copper catalyst to the π bond and simultaneous back donation from the copper catalyst into the substrate's π* antibonding orbital. The bonding interaction (coordination) involves donation from the π orbital of the substrate (highest occupied molecular orbital, HOMO) into the lowest unoccupied molecular orbital on the copper complex (LUMO) (Figure 2.1a). The back donation involves the donation of the copper center's HOMO (d-orbital) into the π* LUMO of the C-C unsaturated bond (Scheme 2.1b).[2] To evaluate whether the back-donation preferentially occurs at the alkyne or the alkene, DFT calculations (B3LYP/6-31G(d,p), Gaussian 09W) were used to perform an orbital population analysis of but-1-en-3-yne's LUMO. The orbital population analysis revealed that the 2p orbitals of the alkene (C1 = 0.43, C2 = 0.25) contribute more than the alkyne carbons (C3 = 0.07, C4 = 0.23) (Figure 2.1c). The larger contribution of the alkene provides justification for the observed chemoselectivity (1,2-borylcupration and 1,2-hydroboration) in the absence of steric hinderance (Figure 2.1d). However, when moderate steric hindrance on the substrate and a larger ligand (Xantphos) are present in the system, coordination and back donation occur at the alkyne resulting in 3,4-borylcupration and eventually 3,4-hydroboration (Figure 2.1d).[3]

The palladium-catalyzed *trans*-3,4-hydroboration of 1,3-enynes was subjected to a thorough mechanistic analysis including kinetic studies, kinetic isotope experiments, DFT calculations, and double cross-over experiments. The proposed mechanism includes coordination

of the ligated palladium(0) complex to the substrate resulting in intermediate **2.4**. Intermediate **2.5**

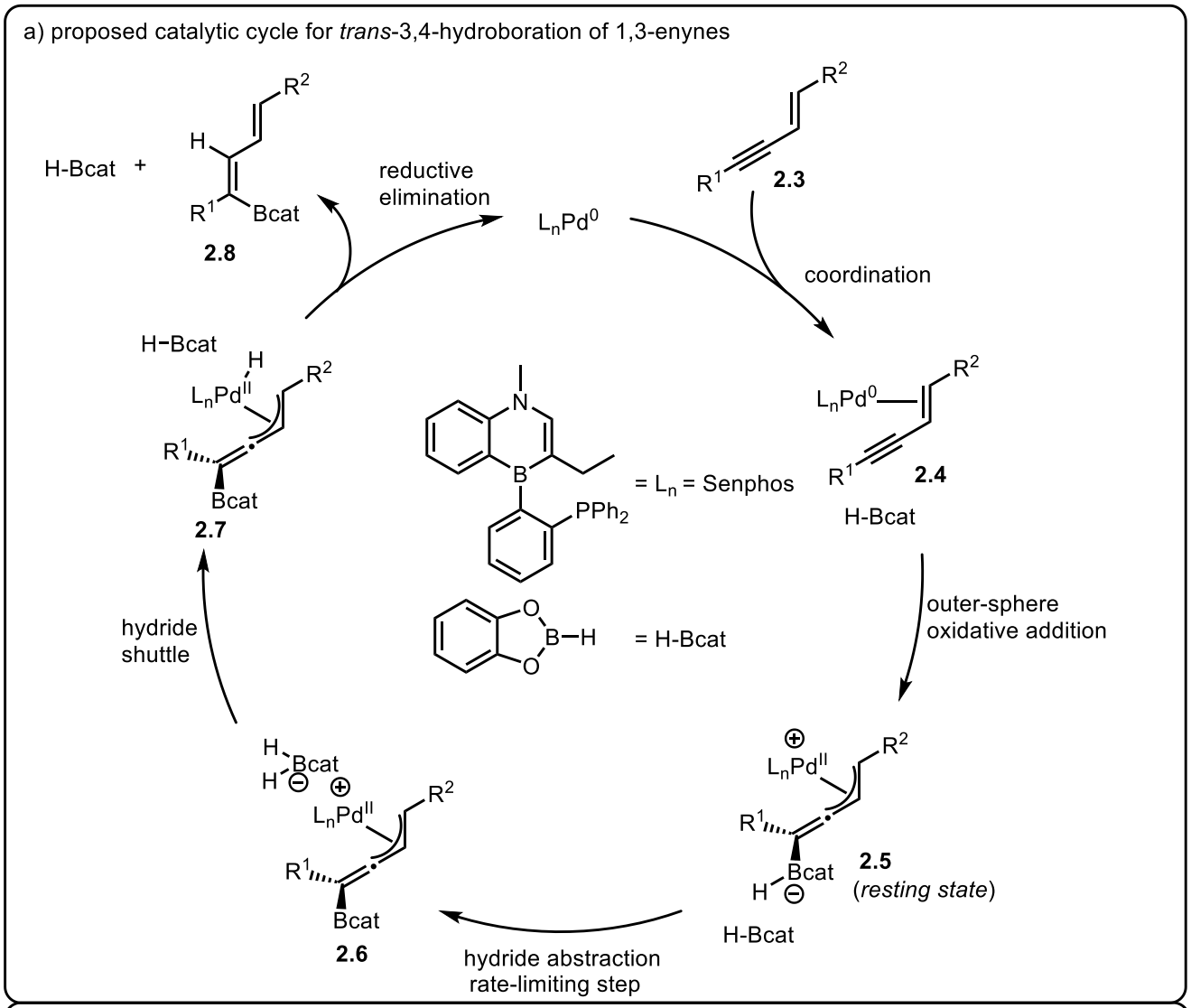

Figure 2.2: a) Proposed catalytic cycle for the palladium-catalyzed *trans*-3,4-hydroboration of 1,3-enynes. b) Experimental evidence to support the proposed catalytic cycle.

is accessed after an outer-sphere oxidative addition and simultaneous boronate formation with HBcat. The boronate bound to the substrate in intermediate **2.5** donates a hydride to another equivalent of HBcat resulting in close ion pair **2.6**, in the rate-limiting step of the mechanism. The hydride is subsequently transferred to the cationic palladium(II) η^3 complex regenerating HBcat and intermediate **2.7**. Finally, reductive elimination affords the 1-boryl-1,3-diene and the palladium(0) catalyst (Figure 2.2a).

To support the proposed mechanism, double cross-over experiments with double isotopically-labeled HBcat (D^{11}Bcat) were performed. The presence of singly isotopically-labeled 1-boryl-1,3-dienes (**2.9a** and **2.9b**) supports the hydride abstraction step of the proposed mechanism (Figure 2.2b). It is worth noting that **2.9a** and **2.9b** are indistinguishable by GC-MS as such the summation of the two was reported as **2.9**. Interestingly, the reduced boranes loading in these experiments enabled the formation of the *cis*-hydroboration product presumably through an intramolecular hydride transfer from intermediate **2.5** to the cationic palladium(II) center and subsequent reductive elimination. Reduced boranes loadings relative to the optimized conditions were used in these experiments to reduce the amount of background scrambling. The relatively small (1.0) ratio of *cis*-**2.9** when 0.11 equivalences of borane was used, indicated that background scrambling was slower than the proposed catalytic cycle. To support that notion, control experiments were performed with even lower borane (0.06 equivalences) which resulted in a lower ratio (0.5) of *cis*-**2.9**. The isotopically-labeled D^{11}Bcat and its non-deuterated, ^{10}B counterpart (HBcat) were premixed for 4 hours, resulting in an increased ratio (1.7) of *cis*-**2.9**. The presence of mono-isotopically labeled 1-boryl-1,3-diene in these experiments indicates that a second equivalence of boranes is involved in the reaction mechanism. In an inner-sphere mechanism, the mono-isotopically labeled 1-boryl-1,3-diene can only be derived from background scrambling of

the boranes. The *cis*-hydroboration product observed in these experiments is derived from an inner-sphere mechanism, so premixing of boranes should result in an increased amount of mono-isotopically-labeled *cis*-hydroboration product (**2.9**-*cis*) and this was the case, with a 3-fold increase in **2.9**-*cis* in the premixing experiment. However, premixing the boranes resulted in a slight decrease in the amount of mono-isotopically-labeled *trans*-hydroboration product which suggests that the mono-isotopically-labeled *trans*-hydroboration product is derived from the proposed outer-sphere mechanism rather than background scrambling. Together, these experiments suggest that the mono-isotopically labeled 1-boryl-1,3-dienes (**2.9**) were derived from the proposed outer-sphere oxidative addition mechanism rather than background scrambling of the isotopically-labeled and non-isotopically-labeled boranes.

DFT analysis suggested that the cationic palladium(II) η^3 boronate complex **2.5** was the resting state species and that hydride abstraction by a second equivalent of HBcat was the rate-limiting step of the transformation (Figure 2.2a). Experimental evidence to support this was obtained in the form of a kinetic study using variable time normalization analysis. The kinetic study revealed that HBcat has first-order kinetics, enyne has zeroth-order kinetics and the palladium/Senphos complex has first-order kinetics. These results are consistent with the proposed catalytic cycle and rate-limiting step as HBcat serves as a hydride acceptor in the rate-limiting step. The observed zeroth-order kinetics in enyne is expected as intermediate **2.5** is derived from both enyne and the palladium/Senphos complex, therefore additional enyne does not result in a higher concentration of **2.5** (saturation kinetics). Conversely, the first-order kinetics in the palladium/Senphos complex is consistent with the proposed mechanism as it is the limiting reagent in the formation of complex **2.5**. Finally, a primary kinetic isotope effect (1.1) was observed when DBcat was used instead of HBcat which also supports that hydride abstraction is rate-limiting. The

authors noted that primary kinetic isotope effects involving B-H/B-D bonds are relatively smaller than those of C-H/C-D bonds.[4, 5]

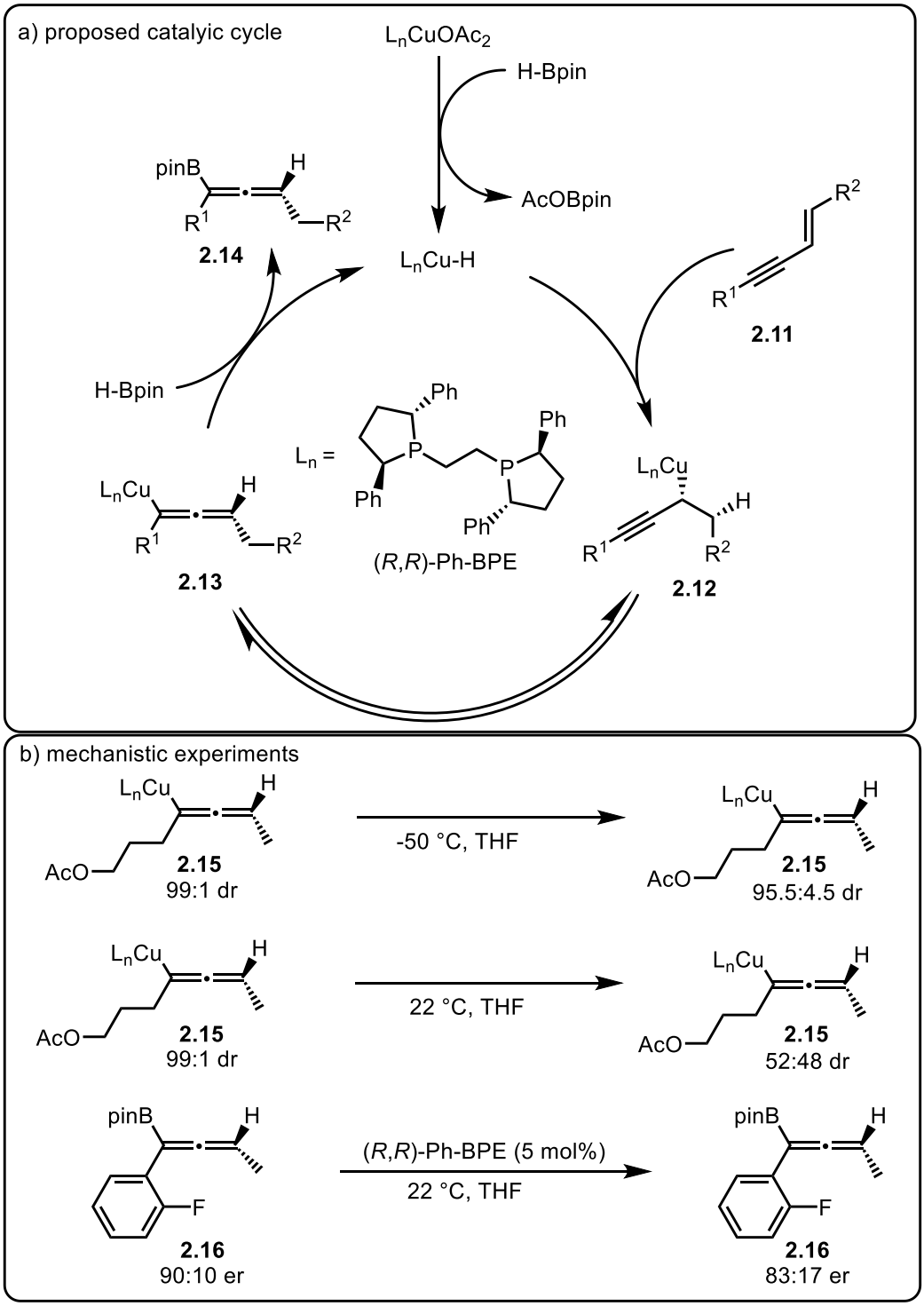

Figure 2.3: a) proposed mechanism for the copper-catalyzed 1,4-hydroboration of 1,3-enynes. b) mechanistic experiments to understand epimerization mechanisms.

The enantioselective 1,4-hydroboration of 1,3-enynes operates through the mechanism shown in Figure 2.3a. $Cu(OAc)_2$ reacts with (*R*,*R*)-phenyl-bpe and HBpin to form an enantioenriched copper-hydride catalyst. Hydrocupration of substrate **2.11** forms propargyl cuprate **2.12,** which rapidly rearranges to the allenynlcuprate **2.13**. Trapping with HBpin regenerates the copper-hydride catalyst and results in the enantioenriched boryl allene **2.14**. While most substrates afforded the boryl allenes in >95:5 er, electron-withdrawing groups in conjugation with enyne resulted in modest enantiomeric ratio (≈80:20 er). This result prompted the authors to study possible mechanisms that could lead to lower enantiomeric ratios.

Possible mechanisms leading to epimerization include isomerization of the allenylcuprate intermediate **2.13**, phosphine catalyzed epimerization of the boryl allene product **2.14** or uncatalyzed epimerization of the boryl allene product **2.14**. To explore these mechanistic possibilities DFT calculations (MN15/Def2TZVPPthf(SMD)// M06L/DF-Def2SVPthf(PCM) level) were performed. The isomerization of the allenylcuprate intermediate **2.13** required 17.0 kcal/mol for electron neutral enynes and 15.8 kcal/mol for electron deficient enynes (*p*-CF_3), which agrees with the experimental findings that electron deficient enynes afforded boryl allenes with lower enantiomeric ratios. The trapping of intermediate **2.13** with HBpin only required 15.7 kcal/mol for electron neutral enynes, indicating that epimerization occurs slower than trapping with HBpin. However, at low concentrations of electrophile (HBpin) epimerization is feasible. Therefore, the authors performed the reaction in reduced loadings of HBpin and indeed saw a lower enantiomeric ratio of the product (96:4 er with 2.0 equiv of HBpin and 91:9 er with 0.5 equiv of HBpin). The phosphine ((*R*,*R*)-phenyl-bpe) catalyzed epimerization of the boryl allene product **2.14** required 26.6 kcal/mol which is considerably higher than the requirement of the isomerization of the allenylcuprate intermediate (17.0 kcal/mol) but not unreasonable considering

hydrocupration of the enyne requires 29.0 kcal/mol. The uncatalyzed epimerization of the boryl allene product **2.14** required a calculated energy requirement of 48.5 kcal/mol which indicates that this mechanism is unlikely.

To gain experimental evidence for whether the phosphine catalyzed isomerization of the boryl allene **2.14** or the isomerization of the allenylcuprate intermediate **2.13** occurs, several control experiments were performed (Figure 2.3b). Firstly, the diasteromerically-pure allenyl cuprate **2.15** was prepared in an NMR tube and a low temperature (-50 °C) ^{31}P NMR experiment was conducted which confirmed that the material was pure (99:1 dr). After 2.75 hours at -50 °C, the dr had eroded to 95.5:4.5 suggesting the isomerization of allenyl cuprate **2.15** was possible even at low temperatures. Increasing the sample's temperature to 22 °C for an undisclosed amount of time resulted in a diastereomeric ratio of 52:48 indicating the isomerization of allenyl cuprate **2.15** occurs in the absence of an electrophile. These experiments, along with the result that reduced HBpin loadings erode enantiomeric ratios highlight that trapping with HBpin is a fast process. This notion agrees with the DFT calculations which revealed that hydrocupration of the enyne is the rate-limiting step of the transformation. However, these findings do not preclude the possibility that free phosphine can epimerize the boryl allene product **2.14** through a nucleophilic addition**,** rotation, elimination sequence. To explore this possibility, boryl allene **2.16** was subjected to a catalytic amount (5 mol%) of (*R*,*R*)-phenyl-bpe in THF at 22 °C for 15 hours (to mimic the reaction conditions) and indeed the enantiomeric ratio dropped a measurable amount (90:10 er to 83:17 er) (Figure 2.3b).[6]

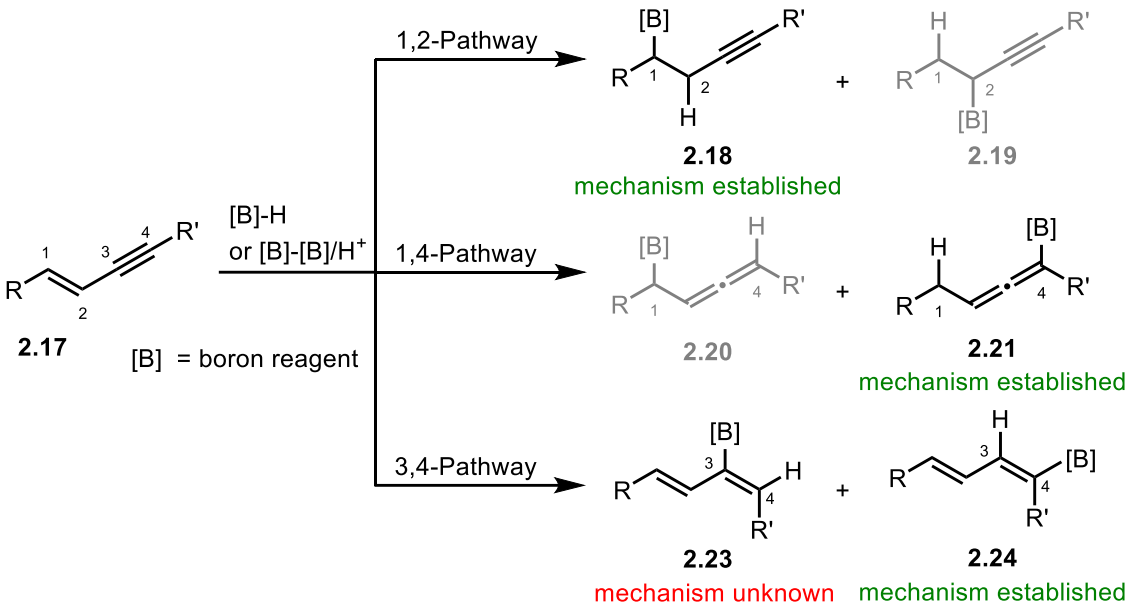

Scheme 2.1: Outlook on 1,3-enyne hydroboration mechanisms.

With mechanisms established for the 1,2-hydroboration (**2.18**), 1,4-hydroboration (**2.21**) and 3,4-hydroboration (**2.24**), we sought to understand the mechanistic intricacies that lead to internal borylation through the 3,4-pathway (**2.23**) (Scheme 2.1). Our mechanistic studies including kinetic analysis, X-ray crystallography, control experiments, ^{11}B NMR spectroscopy and DFT calculations are detailed below.

2.4. Results and Discussion

Our investigation began by using Burés' variable time normalization analysis (VTNA) to determine the reaction orders of each reactant (Figure 2.4).[7] Formation of compound **2.26** was followed by ^{1}H NMR spectroscopy for a series of "different excess" experiments in which the initial concentration of three reagents were varied. Standard reaction conditions are as follows: 0.250 M **2.25**, 0.500 M HBpin and 0.0125 M of CuOAc + Xantphos. Excess conditions evaluated for the kinetic study were 0.350 M **2.25**, 0.675 M HBpin and 0.0250 M CuOAc + Xantphos. The reaction order of **2.25**, catalyst (CuOAc + Xantphos) and HBpin were determined by observing overlap between "[**2.26**] vs. time" plots of standard and excess conditions when the time function

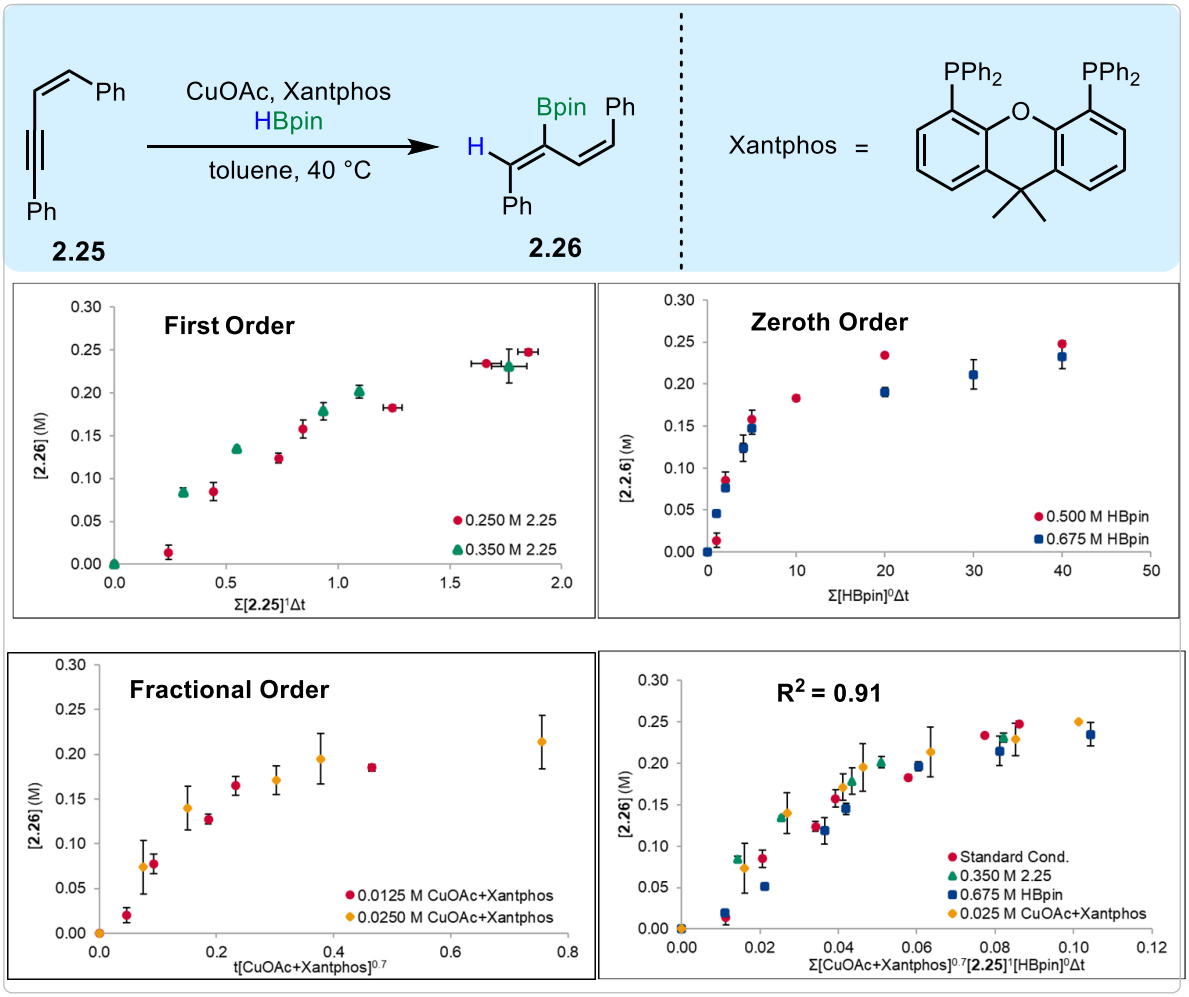

Figure 2.4: Kinetic analysis of Cu(I)-catalyzed hydroboration of 1,3-enyne **2.25** using VTNA.

was normalized with VTNA, and the correct order is used. The reaction was found to be first order in **2.25**, fractional order in CuOAc + Xantphos (0.7) and zeroth order in HBpin. When all "different excess" experiments were plotted together, a K_{obs} graph was generated giving a R^2 of 0.91 (Figure 2.4). The fractional rate order in CuOAc + Xantphos was corroborated by initial rate analysis. The zeroth order in HBpin and fractional order in CuOAc + Xantphos strongly suggests the presence of inactive off-cycle species likely in rapid equilibrium with the active catalyst.[8, 9] This equilibrium reduces the concentration of the active catalyst, resulting in a partial reaction order. Herein, we sought to determine the identity of the off-cycle species.

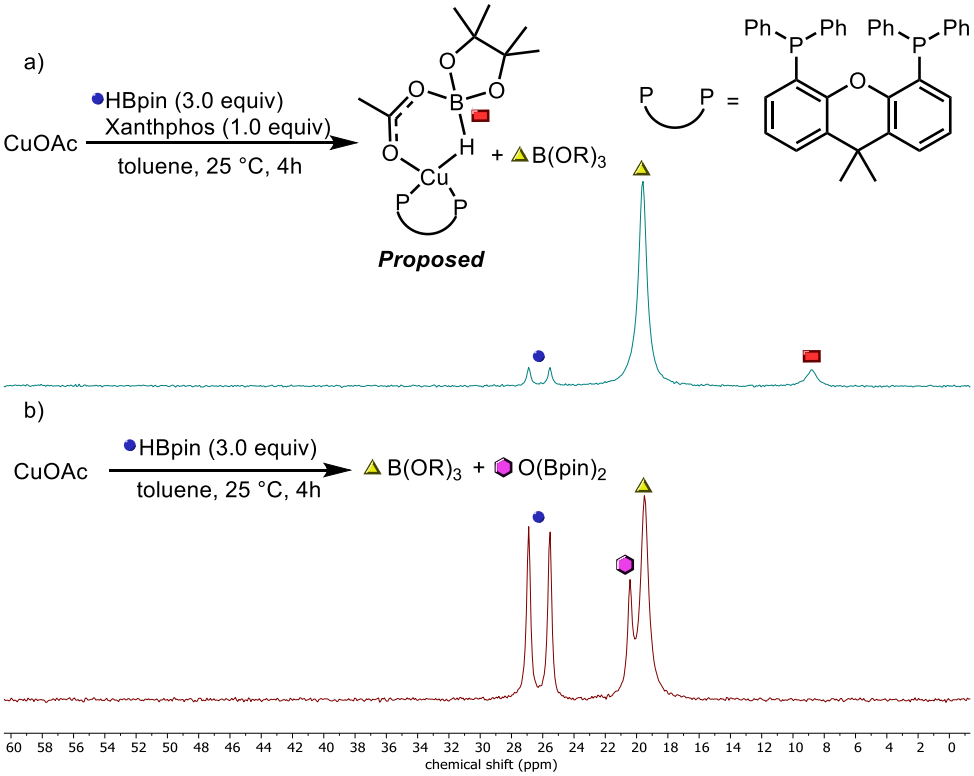

Figure 2.5: ^{11}B NMR (^{1}H coupled) experiments for elucidation of the off-cycle species. a) Stoichiometric reaction in the absence of substrate. b) Stoichiometric reaction in the absence of substrate and ligand (Xantphos).

Copper hydride species are known to oligomerize or form dihydroboronate complexes with HBpin, and could be the possible cause of the observed fractional rate order.[10, 11] Hartwig and co-workers found that a copper dihydroboronate species was the resting-state catalyst in the copper

hydride-catalyzed asymmetric hydroboration of internal alkenes.[12] However, we can rule out this type of complex because of the observed zeroth order in HBpin. Experiments using stoichiometric copper, ligand and excess HBpin revealed an ^{11}B NMR peak at 8.9 ppm, which is consistent with a tetrahedral boron species, possibly the off-cycle complex (Figure 2.5a). When ligand is omitted from the experiment, the peak at 8.9 ppm does not appear, ruling out the possibility that the peak at 8.9 ppm is the acetate pinacolboronate complex with a copper counterion (Figure 2.5b). Interestingly, a second peak in the $B(OR)_3$ region appeared in this experiment, which is consistent with 2,2'-oxybis(4,4,5,5-tetramethyl-1,3,2-dioxaborolane) ($O(Bpin)_2$).[13] This species is reported as a byproduct of the acid reductions by borane reagents into their corresponding boryl ethers.[14]

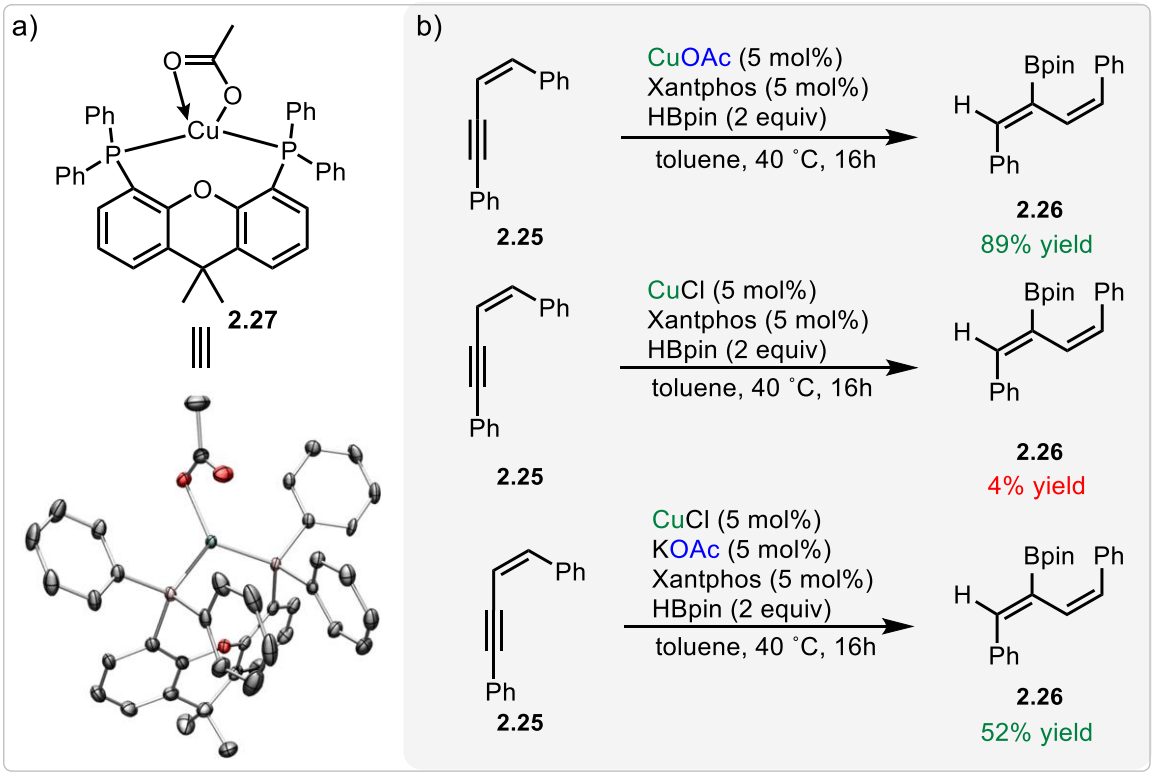

Scheme 2.2: a) Crystal structure of **2.27**, ([(Xantphos)Cu(OAc)]. b) Control experiments towards understanding the role of acetate in the reaction.

Attempts to isolate the copper hydride catalyst species proved unsuccessful. However, we were successful in obtaining a crystal using one equivalent CuOAc, one equivalent of Xantphos

and two equivalents of HBpin in toluene. Singe crystal X-ray diffraction analysis revealed a ligated copper acetate complex **2.27** (Scheme 2.2a).[15] Next, control experiments were performed to investigate and explain the vast difference in yields when various copper pre-catalysts were used. For example, CuOAc and CuCl afforded 89% and 4% yield, respectively (Scheme 2.2b). When CuCl was used in the presence of KOAc (5 mol%) the yield improved to 52%, suggesting that the acetate counterion plays an essential role in the catalytic cycle, probably acting as a Lewis base for activating HBpin to transfer a hydride to the copper pre-catalyst to form the copper hydride complex. Indeed, the role of oxygen-donor Lewis bases for earth-abundant metal catalysis has been studied and is consistent with our experiments.[16] Taken together, our studies suggest that the off-cycle species may include a ligated copper acetate species that is complexed to HBpin.

To further explore this possibility in the reaction mechanism, we employed DFT calculations at the SMD(toluene)/M06D3/def2-TZVP//SMD/M06D3/SDD(toluene)~6-31G(d) level of theory. Our computational analysis was initiated by examining the mechanistic details for the transformation from the pre-catalyst **2.27** [(Xantphos)Cu(OAc)] to either the **Cu-H** or **Cu-Bpin** complex (Figure 2.6a). Two distinct pathways emerge: pathway *red* leads to **Cu-Bpin** while pathway *black* leads to the **Cu-H** complex. Pathway *red* is initiated by the coordination of HBpin to **2.27**, resulting in the formation of **2.30**. The elongation of the B-H bond in the adduct (1.196 Å) from this bond in HBpin (1.187 Å) signifies the donation of the B-H σ-bonding electron pair to the unoccupied p orbital on the copper center in **2.30**. Complex **2.30** then transforms into **Cu-Bpin** with a very high barrier of 26.0 kcal/mol via the deprotonation transition structure $\mathbf{TS_{2.30\text{-}CuBOAc}}$. The very high barrier here is expected since H-Bpin shows hydridic but not protic reactivity. In contrast, pathway *black* also involves HBpin's boron coordinating to the pendant oxygen on the coordinated acetate in **2.27**, resulting in the formation of **2.28.** The B-H bond length in this adduct

(1.193 Å) is slightly longer than that in HBpin, a result related to both the participation of the B-H σ-bonding electron pair in the donation to the vacant p orbital on the copper center and the notable B-O interaction (an O-B bond distance of 2.579 Å).

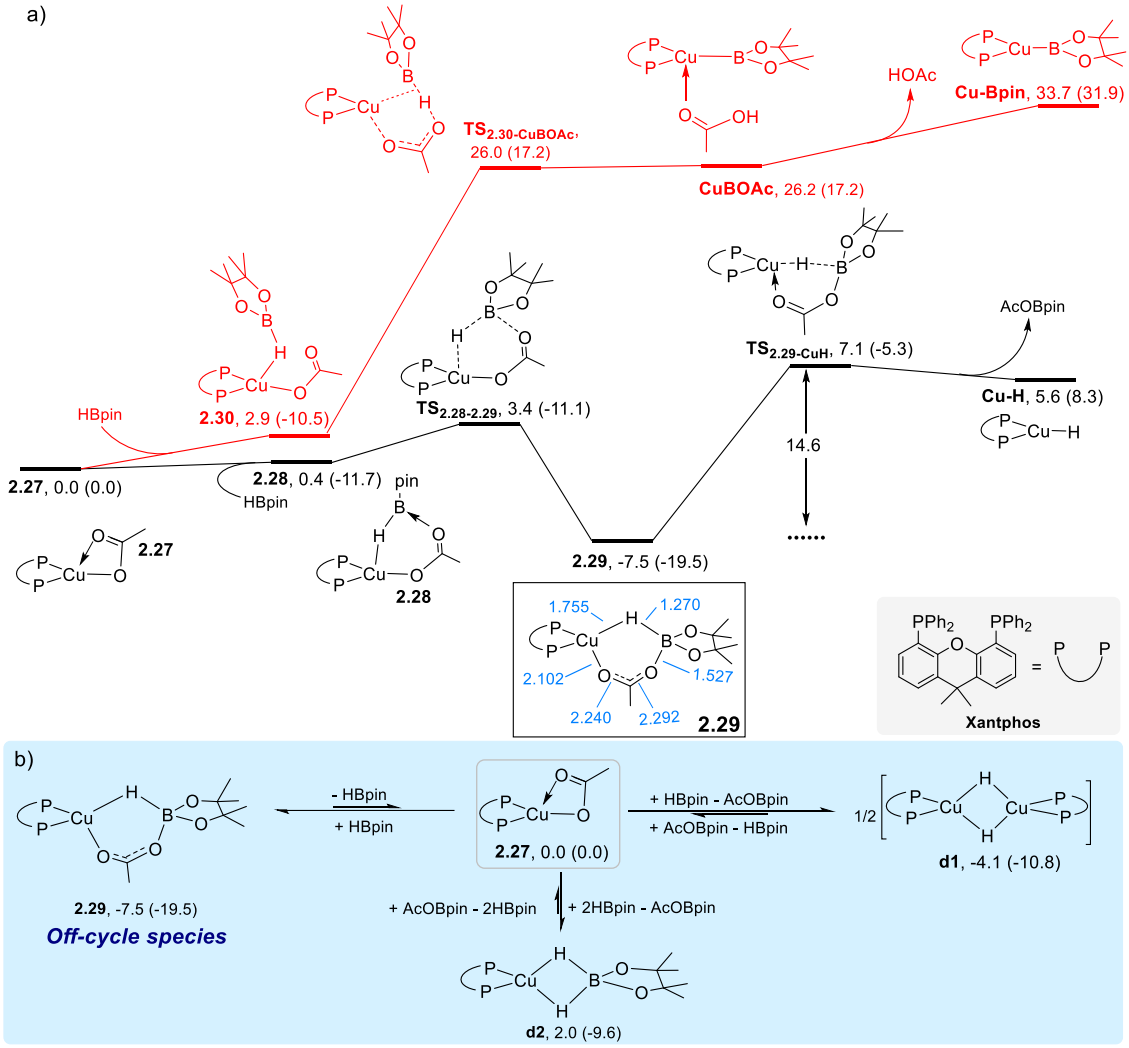

Figure 2.6: a) Calculated free energy profile for transformation of the pre-catalyst **2.27** to the Cu-H or Cu-Bpin complex. The blue values represent the length of selective bonds in Å. b) Calculated relative free energies for dimeric species in equilibrium with the copper hydride complex Cu-H. Relative Gibbs free energies and relative electronic energies (in parenthesis) are given in kcal/mol.

In the presence of HBpin, complex **2.28** converts to intermediate **2.29** through transition structure **TS$_{2.28\text{-}2.29}$**, overcoming a barrier as low as 3.4 kcal/mol. Intermediate **2.29** is the lowest energy complex calculated (-7.5 kcal/mol), which has all of the components of an off-cycle species

suggested by our experimental studies (*vide supra*). The same structure was proposed in a recent computational study performed by the Zhang group.[17] The acetate ligand plays a crucial role in stabilizing this off-cycle species, which bridges the HBpin boron and the copper center. Indeed, the absence of acetate in our experimental work results in decreased yield. The **Cu-H** complex can be generated from **2.29** by releasing **AcOBpin** through the transition structure $\mathbf{TS_{2.29\text{-}CuH}}$. Figure 2.6a clearly shows that generation of the **Cu-H** complex is much more favorable both kinetically and thermodynamically than that of **Cu-Bpin** and that **Cu-Bpin** is energetically inaccessible. We have also examined the scenarios where the formed copper hydride complex **Cu-H** can potentially exist in equilibrium with the dimeric species **d1** and **d2** (Figure 2.6b). Our calculations reveal that both the dimeric species **d1** and **d2** are energetically less stable when compared to **2.29**. Figure 2.7a shows the energy profiles calculated for the reaction starting from **Cu-H**. Upon formation of **Cu–H**, the enyne substrate **2.25** coordinates to the copper center, either through its alkyne or alkene moiety. The alkyne coordination can proceed through two distinct pathways: one leading to structure **2.31** (Figure 2.7a, pathway *black*) and the other leading to structure **2.33** (Figure 2.7a, pathway *gray*). The formation of the alkyne-coordinated species **2.31** is endergonic by 1.2 kcal/mol compared to **Cu-H** (Figure 2.7a, pathway *black*). From **2.31**, hydrocupration, i.e., alkyne insertion into the **Cu-H** bond, occurs on the Cu-coordinated alkyne moiety via the transition structure $\mathbf{TS_{2.31\text{-}2.32}}$, resulting in the formation of the intermediate **2.32**. In the alternative pathway involving alkene coordination followed by insertion into the Cu-H bond, alkene insertion exhibits a substantially higher activation barrier compared to alkyne insertion (Figure 2.7a). The preference for alkyne hydrocupration can be attributed to preservation of the conjugated π-system during alkyne coordination, whereas alkene hydrocupration would disrupt the extended conjugation and be sterically less favorable, resulting in an unfavorable pathway.

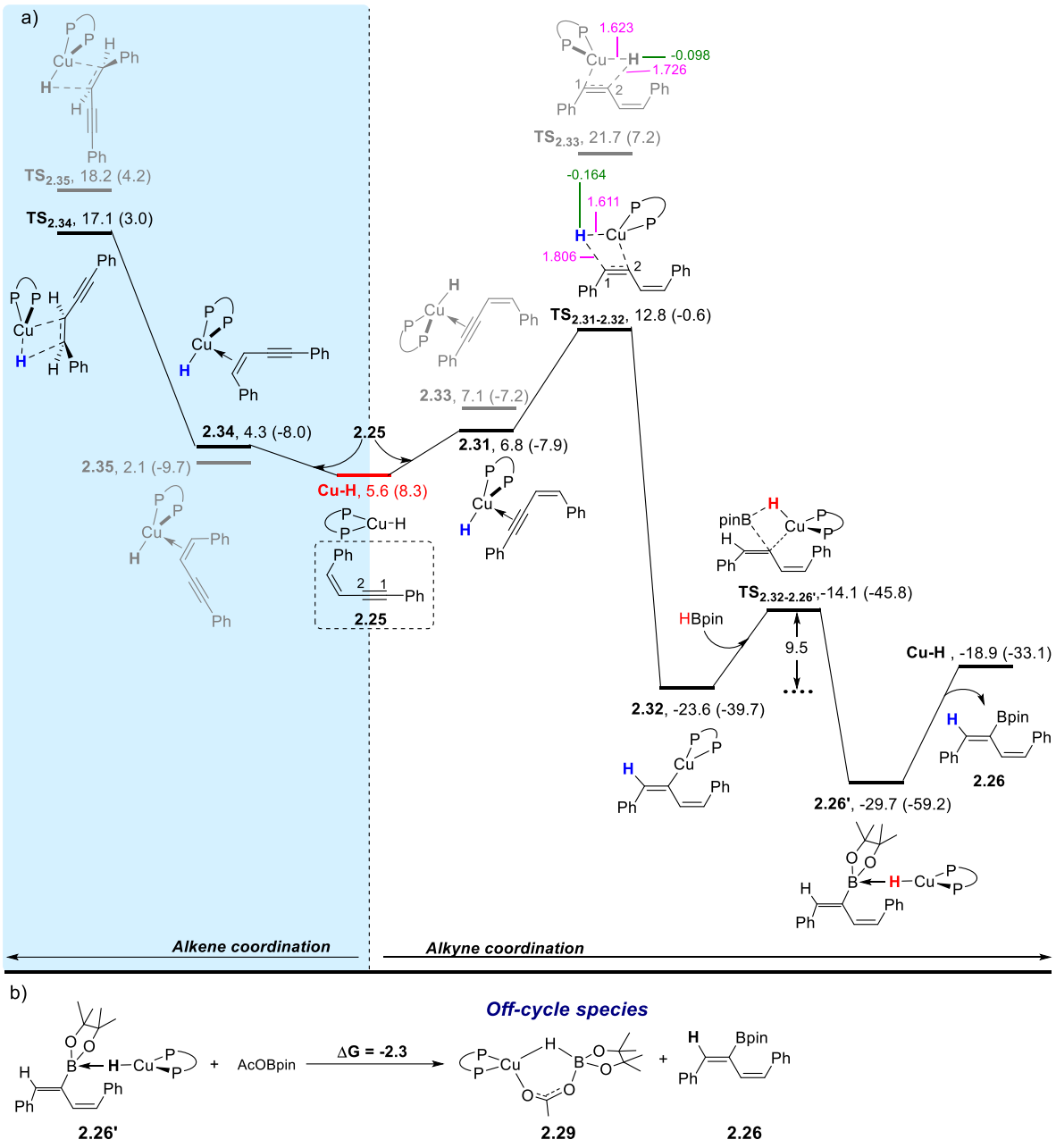

Figure 2.7: a) Calculated free energy profile for the borylation of substrate S. The pink values represent the length of selective bonds in Å. The green values represent the NBO charge of selected atoms. Relative Gibbs free energies and relative electronic energies (in parenthesis) are given in kcal/mol. b) Comparison of the energies of **2.26'** and **2.29**. Relative Gibbs free energy is given in kcal/mol.

Intermediate **2.32** subsequently undergoes metathesis through transition structure **TS2.32-2.26'** with an energy barrier of 9.5 kcal/mol. This leads to the formation of complex **2.26'**, which subsequently dissociates affording the final product **2.26** and regenerate the **Cu-H** complex**.** Figure

2.7a clearly shows that the transition structures **TS$_{2.31\text{-}2.32}$** lies lower in energy than the transition structures **TS$_{2.33}$**, demonstrating the more favorable nature of pathway *black*. NBO analysis reveals that the hydride ligand in **TS$_{2.31\text{-}2.32}$** carries a more negative charge than its counterpart in **TS$_{2.33}$** (Figure 2.7a), indicating a greater nucleophilicity of the hydride in **TS$_{2.31\text{-}2.32}$**. Additionally, the extended π-conjugation present in **TS$_{2.31\text{-}2.32}$** provides a more effective pathway for charge delocalization during hydride migration to C1, whereas the corresponding charge transfer to C2 in **TS$_{2.33}$** occurs through a less conjugated system. Therefore, the hydrocupration step serves as the regioselectivity-determining step of the reaction.

Utilizing the energetic span model and its refinement,[18, 19] Figure 2.7a indicates that **TS$_{2.31\text{-}2.32}$** is the rate-determining transition state and the overall energy barrier for the catalytic reaction is determined to be 18.0 kcal/mol { = (12.8 – 5.6) + [(-18.9) - (-29.7)]}. The rate-determining transition state **TS$_{2.31\text{-}2.32}$** involves the insertion of the alkyne substrate into the active catalyst's **Cu-H** bond, and is not influenced by the reactant HBpin. This finding aligns perfectly with the reaction's rate order, which is first order in **2.25** and zeroth order in HBpin (Figure 2.4). Considering the nature of the rate-determining transition state, one would anticipate that the rate order with respect to the catalyst is also first order. However, the observed fractional rate order of 0.7 concerning the catalyst (Figure 2.4) suggests that the reaction rate is not directly proportional to the catalyst concentration.[20, 21] As shown in Figure 2.6a, we found that intermediate **2.29** exhibits notable stability in relation to the active species **Cu-H**. Moreover, as shown in Figure 2.7b, **2.26′**, a product-coordinated species within the catalytic cycle, can combine with AcOBpin that was produced in catalytic amounts during the generation of the **Cu-H** active species (Figure 2.6a), to give **2.29**, an off-cycle species as previously mentioned. The experimentally observed fractional

rate order regarding the CuOAc + Xantphos (0.7) can be rationalized by the existence of the proposed off-cycle complex.

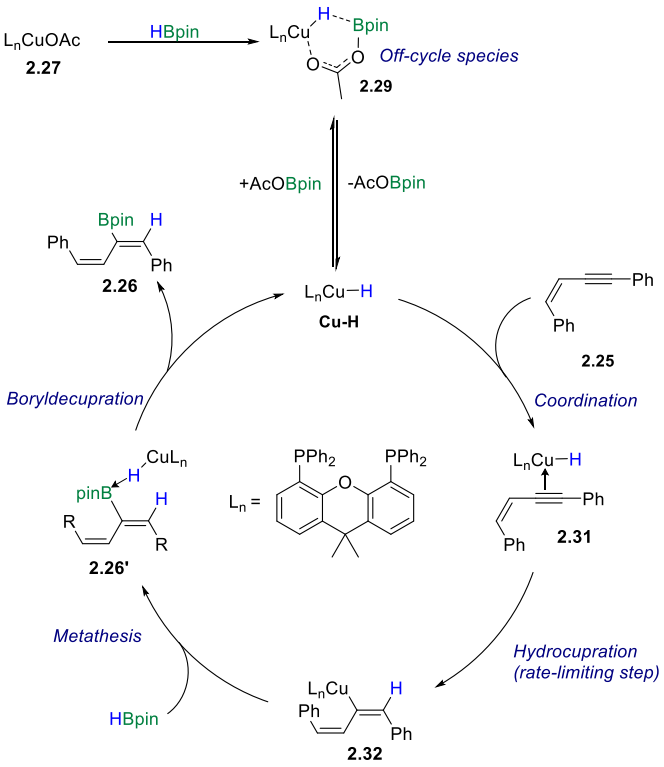

Scheme 2.3: Proposed mechanism of 1,3-enyne hydroboration based on experimental and computations studies.

Based on experimental and computational studies, a catalytic cycle for the (*Z*)-3,4-hydroboration of 1,3-enynes is proposed (Scheme 2.3). In the presence of a ligand and a Lewis base (acetate), the copper pre-catalyst **2.27** reacts with HBpin, forming the active species **Cu-H**. **Cu-H** is derived from intermediate **2.29**, which is an off-cycle species. Coordination of enyne **2.25** with **Cu-H** results in complex **2.31**. Hydrocupration of complex **2.31** forms vinyl cuprate **2.32** as the rate-limiting step of the catalytic cycle. Then, **2.32** undergoes a metathesis reaction to generate complex **2.26′**, which subsequently dissociates to afford final product **2.26** and regenerate the **Cu-H** active species**.**

2.5. Conclusions

In conclusion, the mechanistic complexities of the chemo-, regio-, and stereoselective *cis*-hydroboration of 1,3-enynes were investigated. Kinetic analysis and computational studies suggest that hydrocupration is rate limiting and essential for achieving a high level of selectivity. Experimental studies revealed the importance of acetate for reactivity. Further, kinetic studies suggest a fractional rate order in catalyst and a zeroth order in HBpin. These observations can be rationalized by a more stable off-cycle CuHBpinOAc complex, which is supported by our computational investigation.

2.6. References

1. Bandar, J. S.; Pirnot, M. T.; Buchwald, S. L. Mechanistic Studies Lead to Dramatically Improved Reaction Conditions for the Cu-Catalyzed Asymmetric Hydroamination of Olefins. *J. Am. Chem. Soc.* **2015**, *137* (46), 14812–14818.

2. Dang, L.; Lin, Z.; Marder, T. B. DFT Studies on the Borylation of α,β-Unsaturated Carbonyl Compounds Catalyzed by Phosphine Copper(I) Boryl Complexes and Observations on the Interconversions between O- and C-Bound Enolates of Cu, B, and Si. *Organometallics* **2008**, *27* (17), 4443–4454.

3. Sasaki, Y.; Horita, Y.; Zhong, C.; Sawamura, M.; Ito, H. Copper(I)-Catalyzed Regioselective Monoborylation of 1,3-Enynes with an Internal Triple Bond: Selective Synthesis of 1,3-Dienylboronates and 3-Alkynylboronates. *Angew. Chem. Int. Ed.* **2011**, *50* (12), 2778–2782.

4. Zhang, Y.; Wang, Z.; Lamine, W.; Xu, S.; Li, B.; Chrostowska, A.; Miqueu, K.; Liu, S.-Y. Mechanism of Pd/Senphos-Catalyzed trans-Hydroboration of 1,3-Enynes: Experimental and Computational Evidence in Support of the Unusual Outer-Sphere Oxidative Addition Pathway. *J. Org. Chem.* **2023**, *88* (4), 2415–2424.

5. Hawthorne, M. F.; Lewis, E. S. Amine Boranes. III. Hydrolysis of Pyridine Diphenylborane and the Mechanism of Hydride Transfer Reactions. *J. Am. Chem. Soc.* **1958**, *80* (16), 4296–4299.

6. Huang, Y.; del Pozo, J.; Torker, S.; Hoveyda, A. H. Enantioselective Synthesis of Trisubstituted Allenyl–B(pin) Compounds by Phosphine–Cu-Catalyzed 1,3-Enyne Hydroboration. Insights Regarding Stereochemical Integrity of Cu–Allenyl Intermediates. *J. Am. Chem. Soc.* **2018**, *140* (7), 2643–2655.

7. Burés, J. Variable Time Normalization Analysis: General Graphical Elucidation of Reaction Orders from Concentration Profiles. *Angew. Chem. Int. Ed.* **2016**, *55* (52), 16084–16087.

8. Somerville, R. J.; Hale, L. V.; Gómez-Bengoa, E.; Burés, J.; Martin, R. Intermediacy of Ni–Ni species in sp2 C–O bond cleavage of aryl esters: relevance in catalytic C–Si bond formation. *J. Am. Chem. Soc.* **2018**, *140* (28), 8771–8780.

9. Rosner, T.; Le Bars, J.; Pfaltz, A.; Blackmond, D. G. Kinetic studies of Heck coupling reactions using palladacycle catalysts: experimental and kinetic modeling of the role of dimer species. *J. Am. Chem. Soc.* **2001**, *123* (9), 1848–1855.

10. Kutateladze, D. A.; Mai, B. K.; Dong, Y.; Zhang, Y.; Liu, P.; Buchwald, S. L. Stereoselective synthesis of trisubstituted alkenes via copper hydride-catalyzed alkyne hydroalkylation. *J. Am. Chem. Soc.* **2023**, *145* (32), 17557–17563.

11. Liu, C.-Y.; Yuan, S.-F.; Wang, S.; Guan, Z.-J.; Jiang, D.-e.; Wang, Q.-M. Structural transformation and catalytic hydrogenation activity of amidinate-protected copper hydride clusters. *Nat. Commun.* **2022**, *13* (1), 2082.

12. Xi, Y.; Hartwig, J. F. Mechanistic studies of copper-catalyzed asymmetric hydroboration of alkenes. *J. Am. Chem. Soc.* **2017**, *139* (36), 12758–12772.

13. Bagherzadeh, S.; Mankad, N. P. Catalyst Control of Selectivity in CO2 Reduction Using a Tunable Heterobimetallic Effect. *J. Am. Chem. Soc.* **2015**, *137* (34), 10898–10901.

14. Barman, M. K.; Das, K.; Maji, B. Selective Hydroboration of Carboxylic Acids with a Homogeneous Manganese Catalyst. *J. Org. Chem.* **2019**, *84* (3), 1570–1579.

15. Deposition number 2377607 contains the supplementary crystallographic data for this paper. These data are provided free of charge by the joint Cambridge Crystallographic Data Centre Fachinformationszentrum Karlsruhe Access Structures service www.ccdc.cam.ac.uk/structures.

16. Docherty, J. H.; Peng, J.; Dominey, A. P.; Thomas, S. P. Activation and discovery of earth-abundant metal catalysts using sodium tert-butoxide. *Nat. Chem.* **2017**, *9* (6), 595–600.

17. Zhang, L.; Li, S.; Wen, Y.; Ma, X.; Zhang, J.; Zhou, J.; Meng, X. DFT Study on Copper-Catalyzed Hydroboration of 1, 3-Diynes: Mechanism, Selectivity, and Comparison with Ruthenium. *Asian J. Org. Chem.* **2025**, *14* (1), e202400430.

18. Kozuch, S.; Shaik, S. How to Conceptualize Catalytic Cycles? The Energetic Span Model. *Acc. Chem. Res.* **2011**, *44* (2), 101–110.

19. Li, Y.; Lin, Z. Understanding the reaction mechanisms of Pd-catalysed oxidation of alcohols and domino oxidation–arylation reactions using phenyl chloride as an oxidant. *Org. Chem. Front.* **2014**, *1* (10), 1188–1196.

20. Scott, M.; Sud, A.; Boess, E.; Klussmann, M. Reaction Progress Kinetic Analysis of a Copper-Catalyzed Aerobic Oxidative Coupling Reaction with N-Phenyl Tetrahydroisoquinoline. *J. Org. Chem.* **2014**, *79* (24), 12033–12040.

21. Pistritto, V. A.; Liu, S.; Nicewicz, D. A. Mechanistic Investigations into Amination of Unactivated Arenes via Cation Radical Accelerated Nucleophilic Aromatic Substitution. *J. Am. Chem. Soc.* **2022**, *144* (33), 15118–15131.

Chapter 3: Phosphine-Catalyzed Regio- and Stereoselective Umpolung Addition of Amides to Alkynoates: Access to Complex α,β-Dehydroamino Acid Derivatives

3.1. Contributions

Nicklas Buchbinder discovered the transformation, performed one of each optimization experiment, synthesized substrates **3.45a**, **3.45d** – **3.45m, 3.46e, 3.46o** and **3.46p**, synthesized products **3.47a**, **3.47b**, **3.47e**, **3.47g** – **3.47j**, **3.47n – 3.47ae**, synthesized **3.48** – **3.52**, conducted the epimerization study and conducted the mechanistic study. Kyle Dunnavant synthesized substrates **3.46q** and **3.46r**. Owen Beck synthesized substrates **3.45b - 3.45d** and products **3.47k** – **3.47m**. Kaamia Harris performed one of each optimization experiment and products **3.47c**, **3.47d** and **3.47f**. Andrew Bage advised throughout the project and contributed to the preparation and editing of the final manuscript. Reilly Gwinn performed X-ray crystallography experiments and analyzed the X-ray crystallography data. Prof. Webster Santos advised throughout the project and contributed to the preparation and editing of the final manuscript. The final manuscript was prepared in collaboration with Nicklas Buchbinder, Andrew Bage, and Prof. Webster Santos. This work has been published in *Organic Letters* and is available online. Reprint (adapted) with permission from (Buchbinder, N. W.; Dunnavant, K. L.; Bage, A. D.; Beck, O. N.; Harris, K. R.; Gwinn, R. K.; Santos, W. L. Phosphine-Catalyzed Regio- and Stereoselective Umpolung Addition of Amides to Alkynoates: Access to Complex α,β-Dehydroamino Acid Derivatives. *Org. Lett.* **2026**. *in-press*) Copyright (**2026**) American Chemical Society.

3.2. Abstract

Accessing complex α,β-dehydroamino acids remains challenging due to the instability of the enamine product during N-terminal deprotection. We report a mild, organocatalytic method for the installation of primary amides on the alpha-carbon of alkynoates that avoids N-terminal deprotection. The PBu_3 catalyst is key to umpolung reactivity and affords α,β-dehydroamino acids in good yield with excellent (*Z*)-selectivity. The utility of this reaction was demonstrated in the synthesis of two natural products: a 2,5-diketopiperazine and scutianene M.

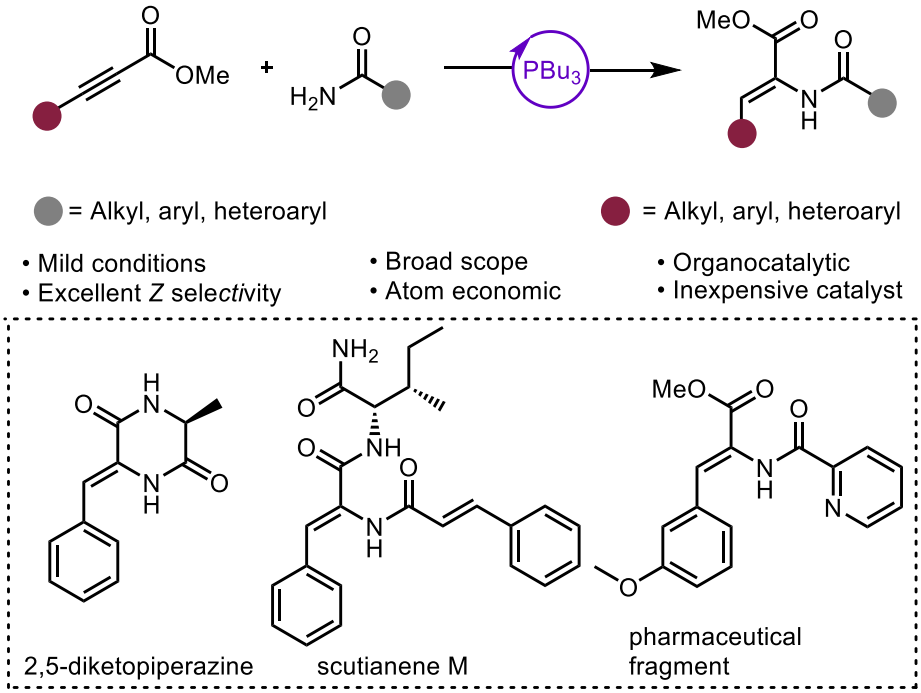

3.3. α,β-Dehydroamino Acid Derivatives in Drug Discovery and Synthesis

α,β-Dehydroamino acid are non-proteogenic amino acids that contain a site of unsaturation between the α and β sidechain carbons. The site of unsaturation changes the chemical properties of the α,β-dehydroamino acid compared to their proteogenic counterparts. For instance, the α- and β-sidechain carbons have decreased bond distance, increased bond angles and increased rigidity. These properties significantly change the three-dimensional structure of proteins and peptides that contain α,β-dehydroamino acids.[1] It has been proposed that the dehydroamino acids increase proteolytic stability of peptides, implicating their utility in increasing the half-life of bioactive compounds.[2] α,β-Dehydroamino acids have also been used as synthons for accessing structurally diverse non-proteogenic amino acids.[3] Therefore, α,β-dehydroamino acids have been studied extensively in drug discovery.

Numerous biologically-active compounds feature the α,β-dehydroamino acid motif including both natural products and synthetic compounds. Natural products containing dehydroamino acids have been isolated from plants, animals, bacteria and fungi (Figure 3.1).[4] The biological activity of such natural products is broad, including but not limited to anticancer, cytotoxic, antibacterial, antifungal and herbicidal. In addition to the natural products which contain α,β-dehydroamino acids in their mature forms, many more natural products are believed to utilize α,β-dehydroamino acids during their biosynthesis.[4] Synthetic compounds with important biological activity also contain the α,β-dehydroamino acid motif. Cilastatin (**3.6**), for example, is an FDA approved dehydropeptidase inhibitor administered with imipenem (β-lactam antibiotic) to prevent degradation of the antibiotic.[5] Several other compounds have been reported with broad activity including hepatitis B virus replication inhibition (**3.7**), COX-2 inhibition (**3.8**), and anticholinesterase activity (**3.9**) (Scheme 3.1).[6-8]

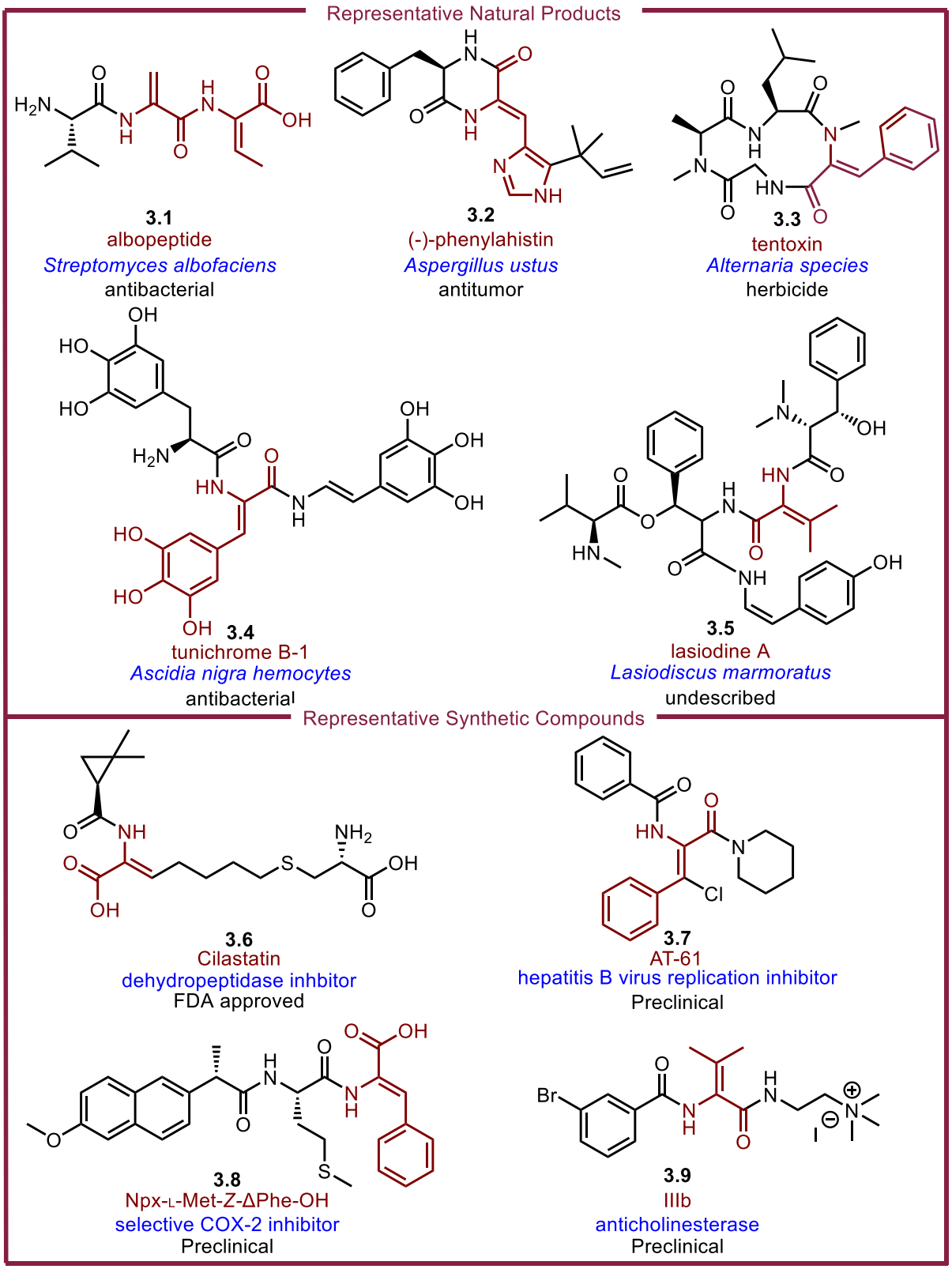

Figure 3.1: Representative natural products and synthetic compounds which feature the α,β-dehydroamino acid motif

The utility of dehydroamino acids is not limited to bioactivity; synthetic chemists have

proven their value as precursors for accessing a broad scope of heterocyclic compounds. The 1,3-oxazole is an important heterocycle in drug discovery as several FDA approved drugs feature this motif. The Zhoa group developed a transition-metal-free oxidative cyclization of α,β-dehydroamino acids (**3.10**) which resulted in 1,3-oxazoles (**3.11**) (Scheme 3.1a). Notably, the reaction was used to access Oxaprozin, a nonsteroidal anti-inflammatory drug (NSAID).[9] A nickel-catalyzed C-H functionalization of α,β-dehydroamino acids (**3.12**) has been reported for the synthesis of isotetronic acid derivatives (**3.13**) (Scheme 3.1b).[10] Both reactions operate through

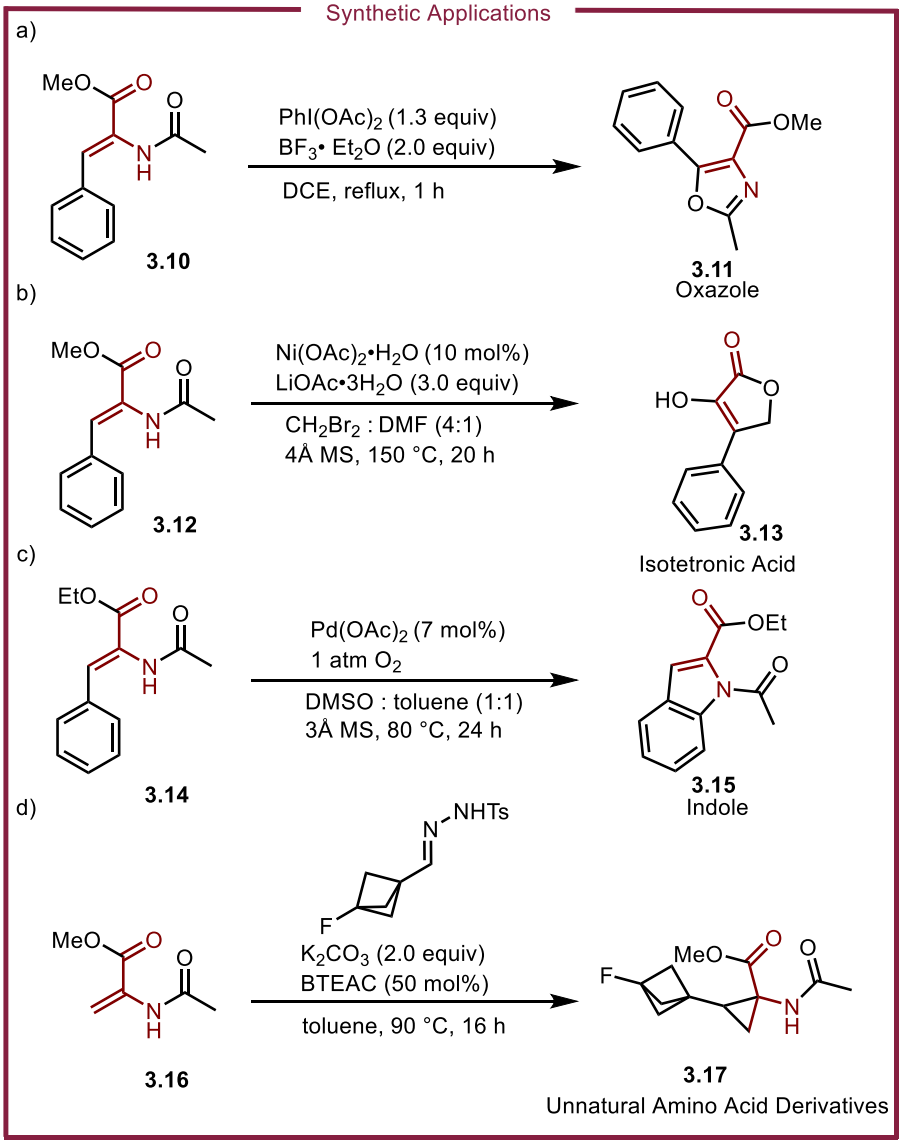

Scheme 3.1: Synthetic applications of α,β-dehydroamino acids

vinylic C-H functionalization which implies that there are opportunities for future reaction development functionalizing the β-carbon of α,β-dehydroamino acids though C-H activation. Conversely, Clagg and coworkers developed a palladium catalyzed aryl C-H functionalization of α,β-dehydroamino acids (**3.14**) which afforded acylated indole derivates (**3.15**) (Scheme 3.1c).[11] The ability to precisely control which C-H bond is activated and subsequently which heterocycle is formed, underpins the value of α,β-dehydroamino acids as important synthetic intermediates. Finally, a recent study revealed carbene insertion to the olefin of α,β-dehydroamino acid (**3.16**) affords unnatural amino acid derivates which might serve as bioisosteres for proteogenic amino acids (**3.17**) (Scheme 3.1d).[12]

3.4. Synthetic Methods for Accessing α,β-Dehydroamino Acids

Considering the broad applications of α,β-dehydroamino acids, the synthesis of these molecules has been heavily explored. Early methodologies such as Erlenmeyer–Plöchl azalactonization utilize excess reagents and elevated temperatures which results in transacylation in some cases (Figure 3.2a).[13] Specialized protecting groups have been developed for preventing transacylation but require additional steps for protection and deprotection, reducing overall efficiency.[14] The Horner-Wadsworth-Emmons (HWE) reaction is commonly used to access α,β-dehydroamino acids but specialized building blocks (**3.22**), stoichiometric reagents and multistep synthesis is generally required (Figure 3.2a).[15] Heck coupling (aryl-halide) and oxidative heck coupling (aryl boronic acids and C-H activation) have also been used to synthesize α,β-dehydroamino acids; however, the terminal olefin (**3.23**) is reported as being prone to polymerization and challenging to purify (Figure 3.2b).[16] Additionally, Heck coupling requires an expensive palladium catalyst and in some cases the oxidative Heck coupling requires stoichiometric palladium.[17] Stoichiometric reactions involving the elimination of a halide or

oxygen based leaving group have been developed, but lack catalytic efficiency (Figure 3.2c).[18,19,20] Ullmann coupling has also be leveraged for accessing α,β-dehydroamino acids but high catalyst loading (60 mol% of copper iodide) and multistep synthesis of the electrophile (**3.27**) reduce the overall efficiency of this approach (Figure 3.2d).[21] α-Keto esters (**3.30**) will undergo condensation with amide nucleophiles (**3.29**) resulting in α,β-dehydroamino acids; however, the use of elevated temperatures to azeotropically remove the water that is generated during the reaction limits broad application of this reaction (Figure 3.2d).[22] Finally, the umpolung addition of nitrogen-pronucleophiles (**3.32**) to alkynoates (**3.31**) has been previously reported (Figure 3.2d). Recently, Zhang developed a phosphine-catalyzed intramolecular cyclization of primary amides (**3.33**) and

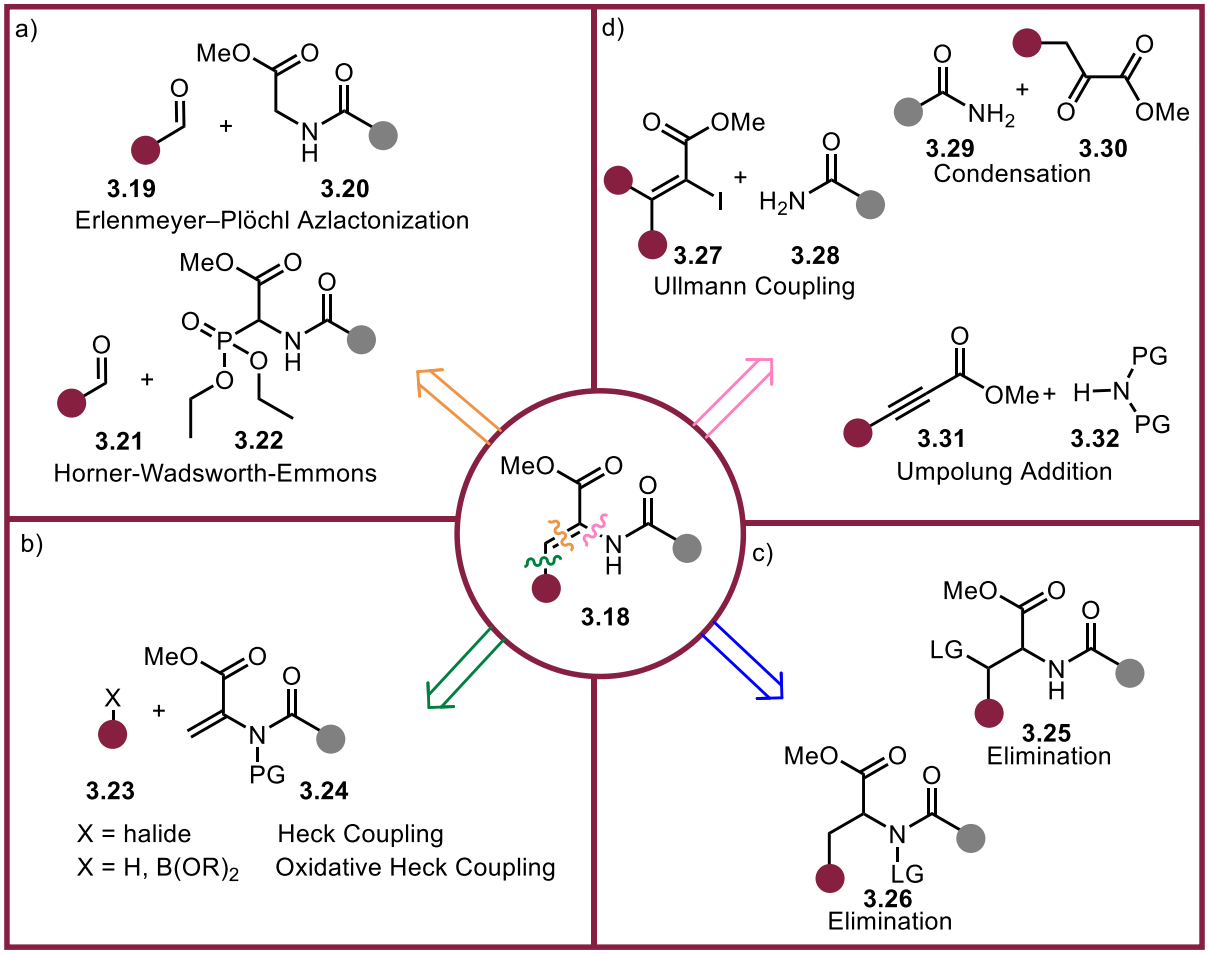

Figure 3.2: Retrosynthetic analysis of α,β-dehydroamino acids. PG = protecting group, LG = leaving group

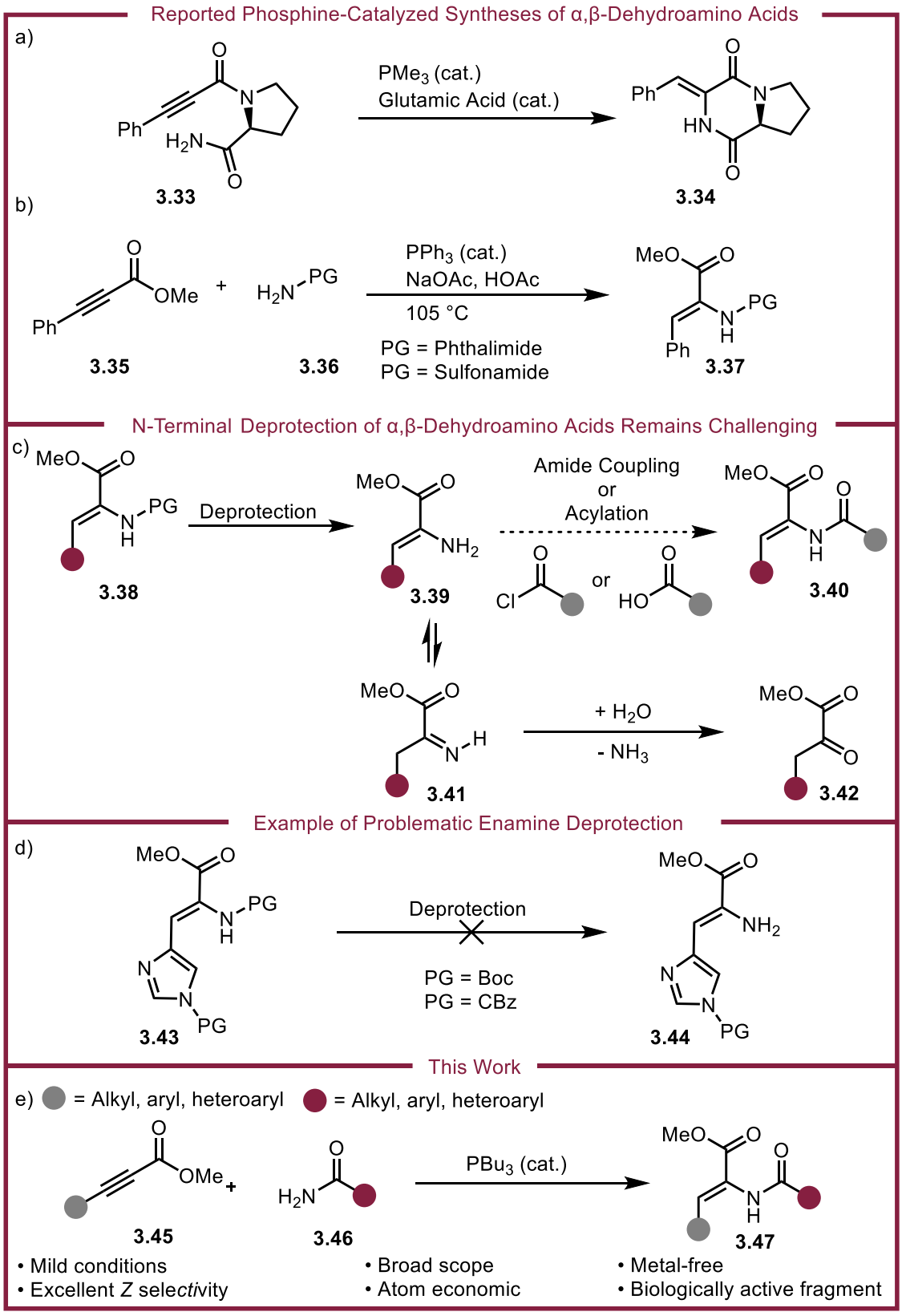

Scheme 3.2: Motivation for the described research. PG = protecting group

employed it towards the synthesis of spirotryprostatins (Scheme 3.2a).[23] However, intermolecular

versions of this reaction remain unexplored. Seminal work from Trost reported a triarylphosphine-catalyzed addition of phthalimides and sulfonamides (**3.36**) to alkynoates (**3.35**) resulting in N-protected α,β-dehydroamino acids (**3.37**); however, the use of elevated temperature, buffered conditions and use of phthalimides/sulfonamides limits broad application (Scheme 3.2b).[24]

Many research efforts have focused on the synthesis of N-protected α,β-dehydroamino acids; however, this approach has limited application towards the synthesis of complex α,β-dehydroamino acids (**3.40**) due to instability of the deprotected enamine (**3.39**), which tautomerizes into the imine (**3.41**) and irreversibly hydrolyze into the α-keto ester (**3.42**) (Scheme 3.2c).[25] Accessing complex dehydroamino acids by deprotection and elongation of the N-terminus has been a long-standing issue in organic synthesis. For example, during the total synthesis of isoroquefortine C, deprotection of the enamine (**3.43**) failed and ultimately a different synthetic route was required (Scheme 3.2d).[26] Despite the limitations of N-protected α,β-dehydroamino acids, many of the synthetic methods that result in α,β-dehydroamino acids have focused on substrates that are protected on the N-terminus. Conversely, we envisioned a method that avoids N-terminus deprotection. Instead, we envision coupling complex amides (**3.46**) (including amino acid derivatives) to alkynoates (**3.45**) directly through an intermolecular phosphine-catalyzed umpolung addition (Scheme 3.2e).

3.5. Results and Discussion

Our investigations on the phosphine-catalyzed hydroamidation of alkynoates began by treating our model substrates methyl-3-phenylpropiolate **3.45a** and benzamide **3.46a** with catalytic tri-*n*-butyl phosphine (PBu_3) in toluene at 40 °C for 1 hour. The α,β-dehydroamino acid derivative (*Z*)-**3.47a** was formed in a 62% yield with >95:5 *Z*:*E* selectivity (Table 3.1**,** entry 1). When $P(NEt_2)_3$, PCy_3 or PPh_3 were used instead of PBu_3 lower efficiency was observed (entries 2-4). Decreasing the temperature to 25 °C resulted in a loss of yield; however, increasing the temperature to 70 °C afforded (*Z*)-**3.47a** in a 68% yield without deterioration of selectivity (entries 6-7). A survey of

Table 3.1: Reaction optimization

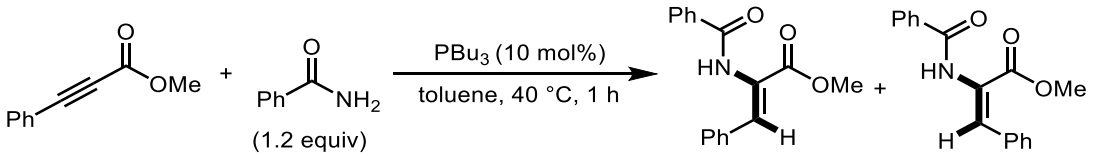

3.45a **3.46a** (*Z*)-**3.47a** (*E*)-**3.47a**

Entry	Variation from above conditions	Yield	*Z*:*E*
1	None	62%	>95:5
2	$P(NEt_2)_3$ instead of PBu_3	3%	>95:5
3	PCy_3 instead of PBu_3	8%	94:6
4	PPh_3 instead of PBu_3	0%	-
5	dppe instead of PBu_3	5%	22:78
6	25 °C instead of 40 °C	44%	92:8
7	70 °C instead of 40 °C	68%	>95:5
8	[a]MeCN instead of toluene	33%	93:6
9	[a]hexanes instead of toluene	45%	96:4
10	[a]DCE instead of toluene	36%	90:10
11	16 hours instead of 1 hour	>95%	>95:5
12	PPh_3, NaOAc/HOAc (1:1), 105 °C	3%	>95:5

0.125 mmol **3.45a**, 0.0125 mmol PBu_3, 0.15 mmol **3.46a**, 0.25 M in toluene. Yield determined using ^1H NMR with mesitylene as the internal standard. All reactions performed in duplicate and averaged. [a]70 °C.

reaction solvents revealed that toluene was optimal for both selectivity and yield (entries 8-10).

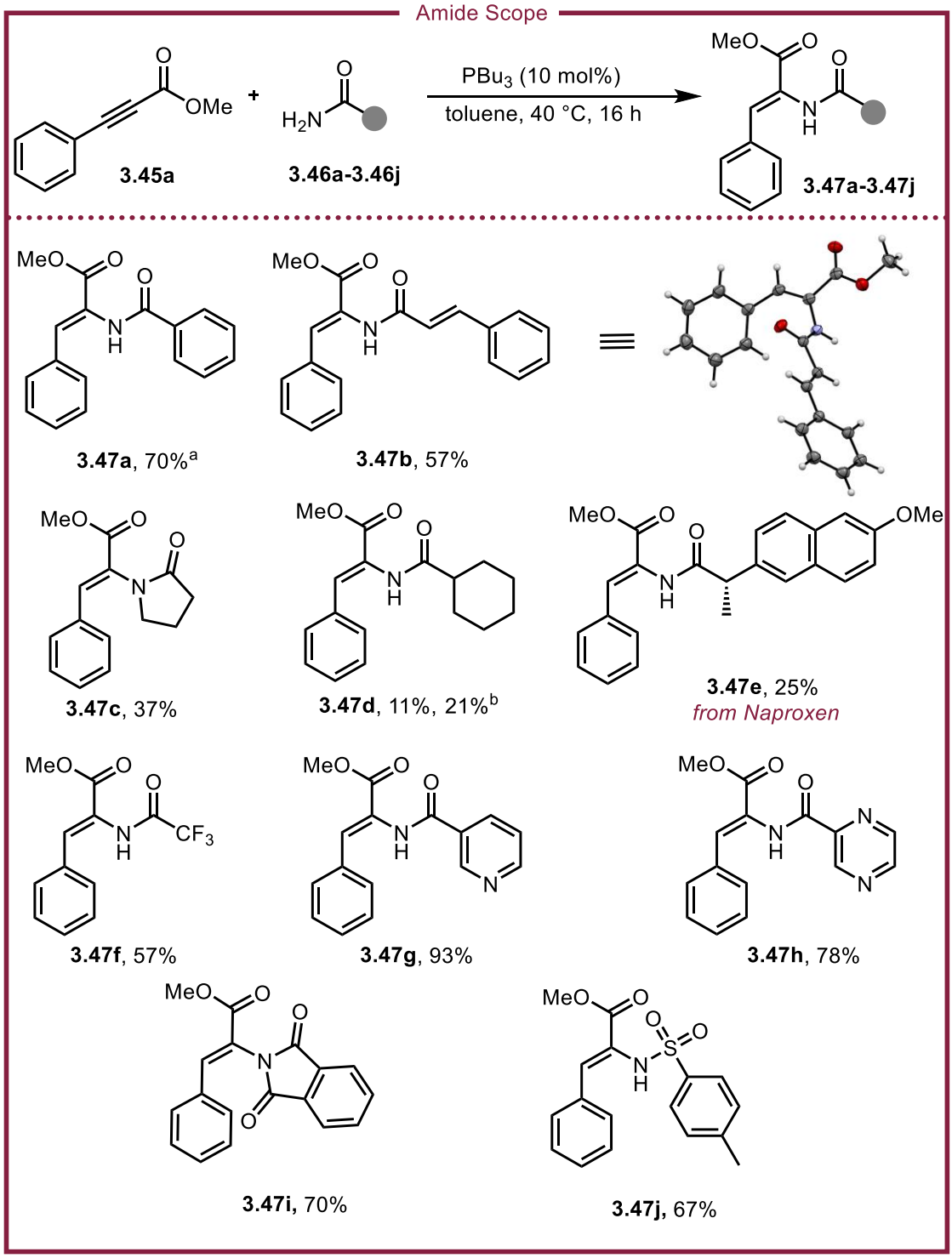

Scheme 3.3: Amide substrate scope. Yields refer to isolated yields. >99:1 *Z*:*E* selectivity unless otherwise noted, based on isolated yield of each isomer. 0.25 mmol **3.45a**, 0.025 mmol PBu_3, 0.30 mmol **3.46**, 0.25 M in toluene. [a]70 °C. [b]20 mol% PBu_3. [c]20 mol% K_2CO_3.

The optimal conditions were found when the reaction time was extended to 16 hours (in toluene at 40 °C), which afforded (*Z*)-**3.47a** in >95% yield (entry 11). Using Trost's optimal conditions only a 3% yield of (*Z*)-**3.47a** was detected (entry 12).

With the optimal conditions in hand, our attention turned to determining the scope and limitations of the reaction. Our model substrate **3.47a** was isolated in a 70% yield (Scheme 3.3). When Cinnamamide was used, α,β-dehydroamino acid derivative **3.47b** was isolated in a 57% yield. Alkyl amides afforded α,β-dehydroamino acid derivatives **3.47c** and **3.47d** in low to modest yields (37% and 21%, respectively). A Naproxen derived amide afforded **3.47e** in a 25% yield. Trifluoroacetamide resulted in a 57% yield of compound **3.47f.** Heterocyclic amides reacted smoothly, resulting in α,β-dehydroamino acid derivatives **3.47g** and **3.47h** in 91% and 78% yields, respectively. Phthalimide and sulfonamide were also found to be competent substrates for this reaction (**3.47i** and **3.47j**).

To evaluate functional group tolerance on the alkynoate, a series of substrates were synthesized (Scheme 3.4). Firstly, *p*-, *m*- and *o*-tolylalkynoates were found to afford α,β-dehydroamino acid derivatives **3.47k**-**3.47m** in low to modest yield with *para*-substitution performing the best. A methoxy derivative, **3.47n**, was synthesized in a 57% yield. Electron deficient alkynoates resulted in low to modest yields of α,β-dehydroamino acid derivatives **3.47o**-**3.47r** (29-47%). When a cyclopropyl substrate **3.45j** (product **3.47s**) was used, low reactivity was observed (21% yield); however, introduction of a sub-stoichiometric amount of base (K_2CO_3) improved the yield to 66% but with diminished selectivity (63:37, *Z*:*E*).

Next, a series of biologically relevant substrates were tested (Scheme 3.5). Firstly, an intermediate used in the synthesis of Atevirdine, an FDA-approved non-nucleoside reverse transcriptase inhibitor, **3.47t** was synthesized in 68% yield with modest selectivity (83:17, *Z*:*E*).[27]

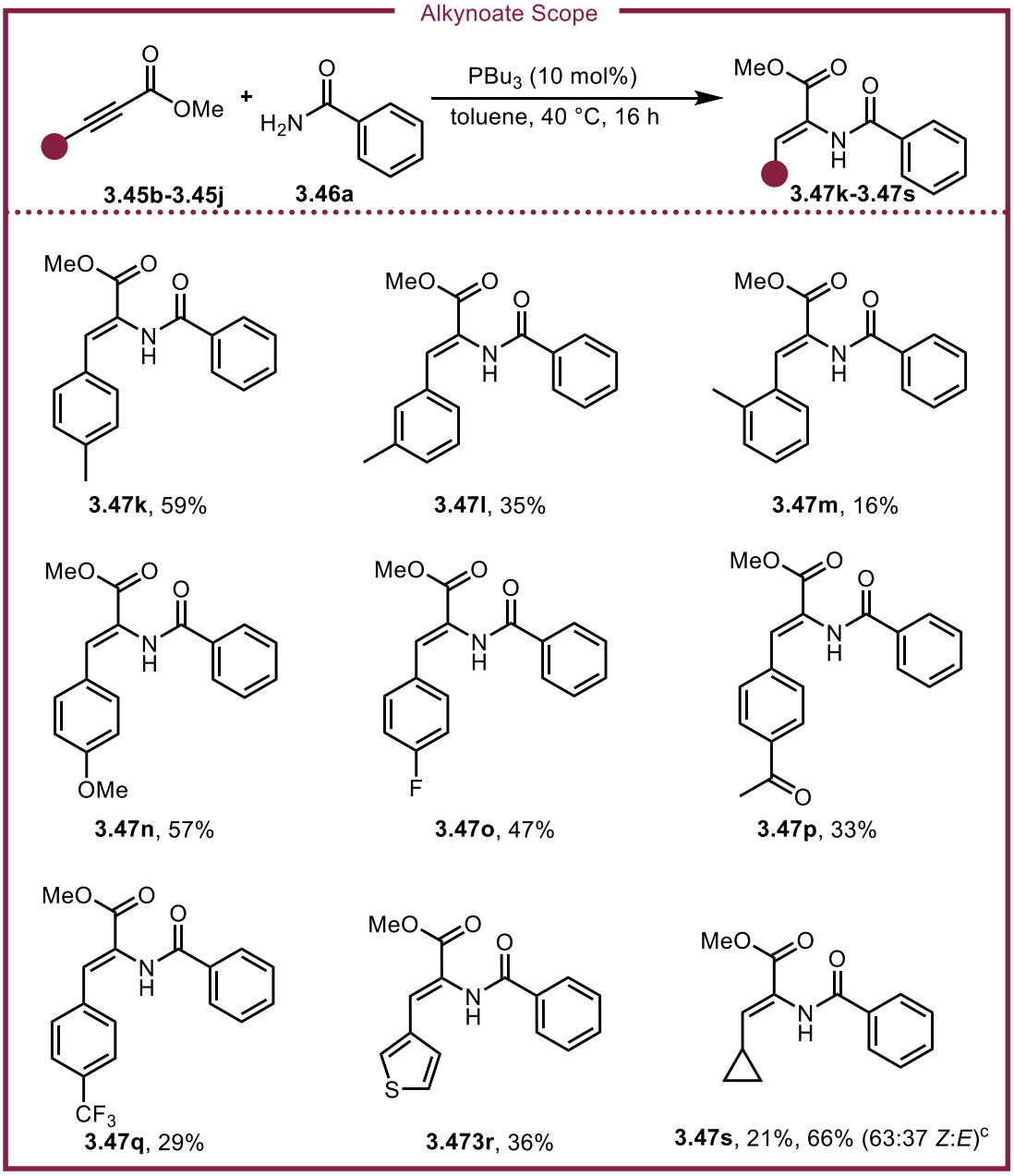

Scheme 3.4: Alkynoate substrate scope. Yields refer to isolated yields. >99:1 *Z*:*E* selectivity unless otherwise noted, based on isolated yield of each isomer. 0.25 mmol **3.45**, 0.025 mmol PBu_3, 0.30 mmol **3.46a**, 0.25 M in toluene. [a]70 °C. [b]20 mol% PBu_3. [c]20 mol% K_2CO_3.

Various protected amino amides were also evaluated to afford α,β-dehydroamino acid containing dipeptides. The reaction displayed good tolerance for *tert*-butyl carbamates (Boc) as the N-terminus protecting group, with compounds **3.47u**-**3.47y** being isolated in good yield (51-66%). Notably, the yield of **3.47u** improved to 58% when the reaction was performed on a 3.0 mmol

scale. A glycine derived Boc-protected amino amide resulted in a 16% yield of compound **3.47y** using the optimal conditions; however, increasing the temperature to 90 °C resulted in a 43% yield of the desired α,β-dehydroamino acid. When 9-fluorenylmethyl carbamates (Fmoc) were used as

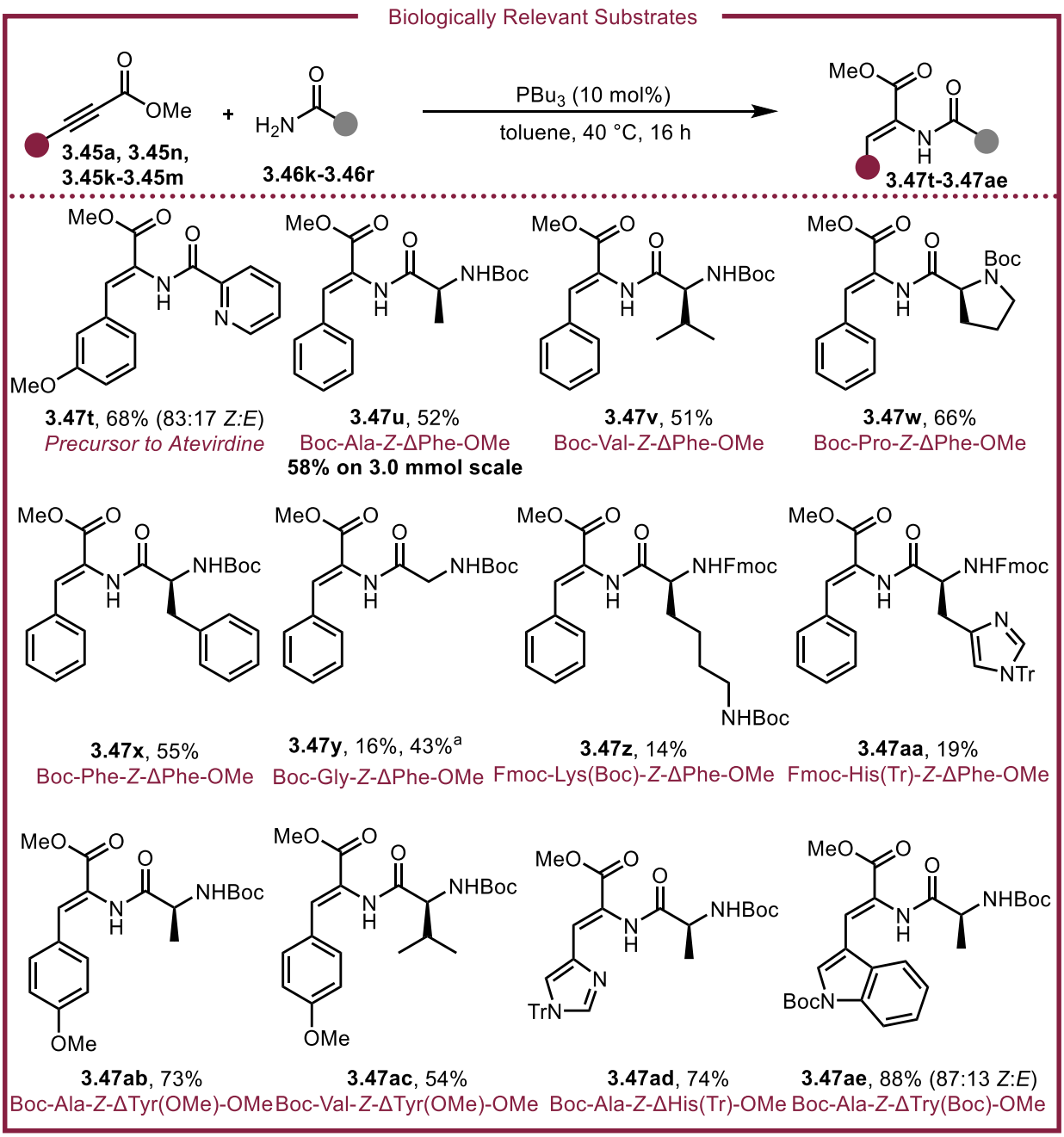

Scheme 3.5: Wide array of biologically relevant substrates. Yields refer to isolated yields. >99:1 *Z*:*E* selectivity unless otherwise noted, based on isolated yield of each isomer. 0.25 mmol **3.45**, 0.025 mmol PBu_3, 0.30 mmol **3.46**, 0.25 M in toluene. [a]90 °C.

the N-terminus protecting group, low yield was achieved (**3.47z**, **3.47aa**), presumably due to phosphine-catalyzed deprotection (14-19%). Methyl protected-tyrosine dehydroamino acid derivatives **3.47ab** and **3.47ac** were afforded in good yields (54-74%). A triphenylmethyl-protected (trityl) dehydro-histidine substrate **3.47ad** was formed in 74% yield revealing that the reaction tolerates trityl protecting groups. Boc-protected dehydro-tryptophan was also synthesized using this method with substrate **3.47ae** being isolated in an 88% yield with 87:13 *Z*:*E* selectivity. To evaluate whether the reaction epimerized the optically pure amino acid fragments, **3.47u** was Boc-deprotected and converted into Mosher's amide (**3.49**). Characterization of **3.49** indicated the presence of a single diastereomer and suggest that that epimerization does not occur under the reaction conditions (Scheme 3.6)

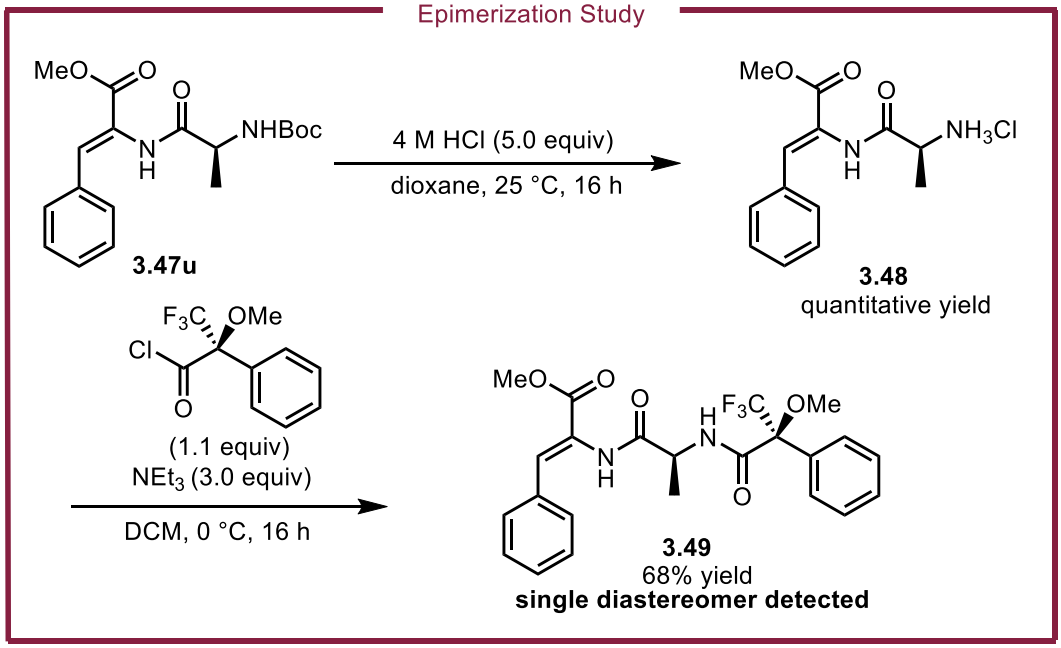

Scheme 3.6: Epimerization study using Mosher's acid chloride.

To demonstrate the utility of this transformation, the α,β-dehydroamino acids were chemically modified. First, α,β-dehydroamino acid **3.47b** was hydrolyzed under basic conditions to afford compound **3.50** in a near quantitative yield without isomerization of the double bond geometry (Scheme 3.7a). Compound **3.50** was then coupled to isoleucinamide (L-H-Ile-NH_2) to

afford scutianene M (**3.51**) in an overall yield of 50% from commercially available starting material. To our knowledge, this is the first reported synthesis of scutianene M, an alkaloid natural product that exhibits a minimum inhibitory concentration (MIC) of 12.5 μg/mL against *Enterococcus spp*.[28] Other structural motifs commonly found in natural products include 2,5-diketopiperazines. Utilizing our standard reaction conditions, we were able to access 2,5-diketopiperazine **3.52** by treating α,β-dehydroamino acid **3.47u** with 4 M HCl in dioxane followed by neutralization with triethylamine (Scheme 3.7b). Compound **3.52** is both a natural product (isolated from *Nocardiopsis alba* SCSIO 03039) and an intermediate in the synthesis of other

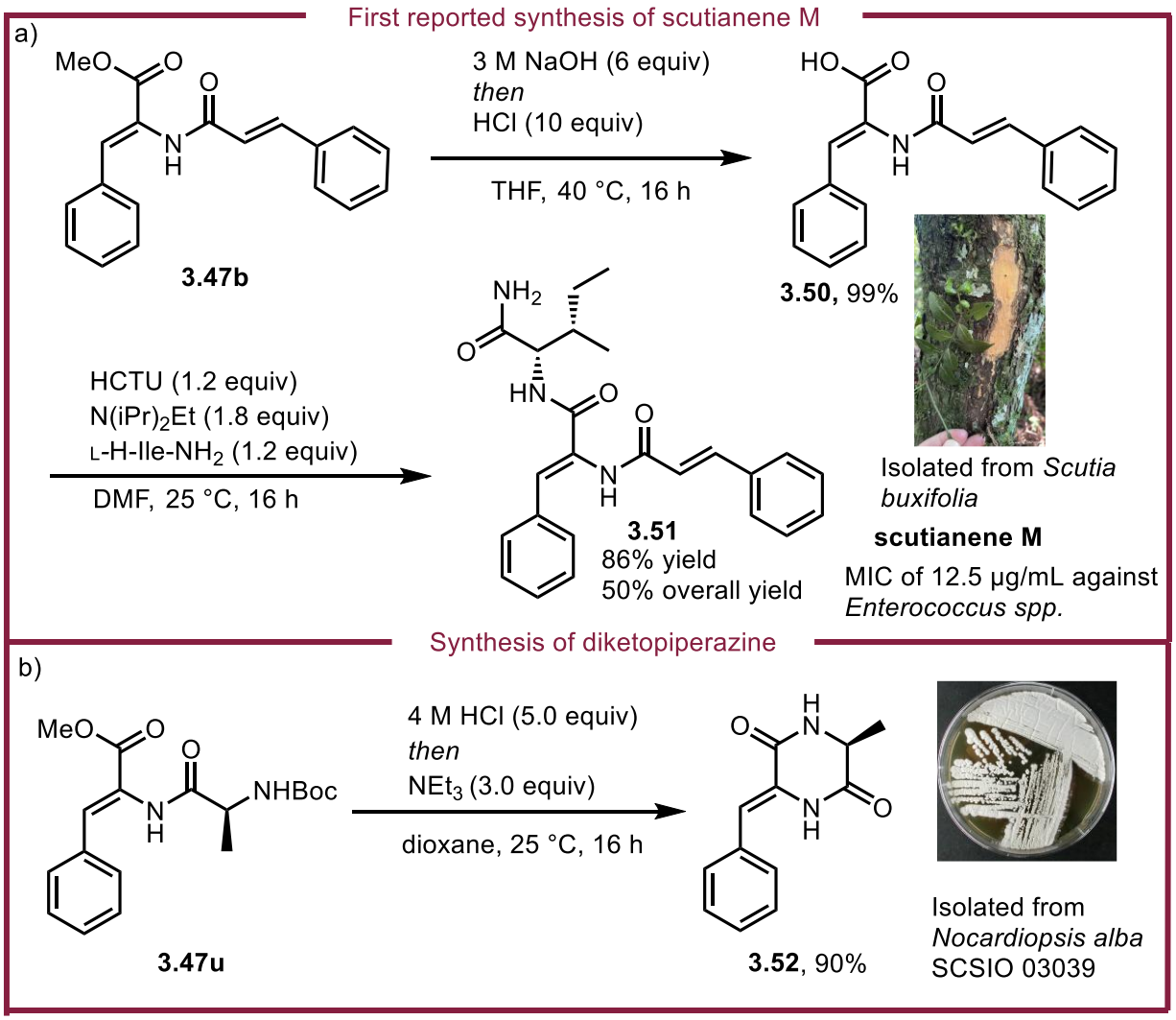

Scheme 3.7: Synthetic applications of α,β-dehydroamino acids.

natural products (puniceloid D). Importantly, the synthesis of **3.52** was previously achieved in a 3% yield over 5 steps; however, using our methodology, compound **3.52** was furnished in a 52% yield over 3 steps.[29]

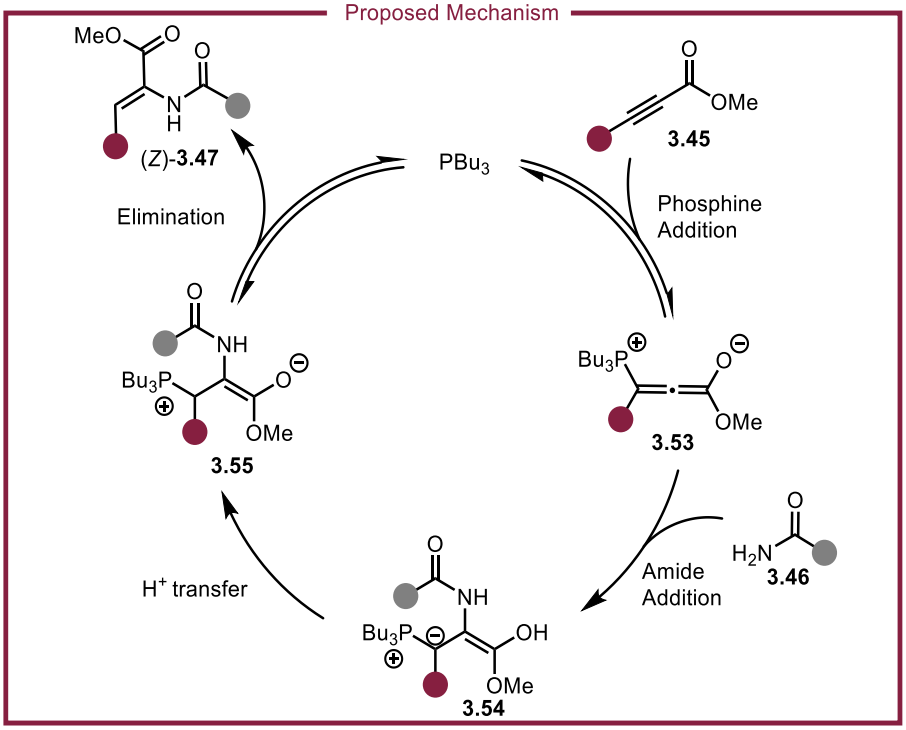

Scheme 3.8: Proposed mechanism.

Based on literature precedence, a plausible mechanism is proposed in Scheme 3.8.[30-32] First, tri-*n*-butylphosphine attacks alkynoate **3.45**, resulting in the zwitterionic phosphonium-allenolate **3.53**. Amide **3.46** undergoes deprotonation and subsequent nucleophilic addition with intermediate **3.53** to form ylide intermediate **3.54**. Proton transfer quenches the ylide furnishing the zwitterion intermediate **3.55**, which collapses the catalyst to generate the (*Z*)-product. While the origin of *Z*-selectivity is unknown, initial mechanistic studies provide a clue. When (*E*)-**3.47a** was subjected to the reaction conditions, crude NMR analysis revealed that the (*E*)-isomer isomerized into a mixture of (*E*)- and (*Z*)-isomers. Conversely, when (*Z*)- **3.47a** was subjected to the same experiment, no isomerization occurred. These experiments suggest that a mixture of (*E*)-

and (*Z*)-isomers may be generated during the catalytic cycle, but the mixture is isomerized into the (*Z*)-isomer.

3.6. Conclusions

In conclusion, a simple and mild method for the synthesis of α,β-dehydroamino acids is disclosed. Alkyl, aryl and heteroaryl substitution on either coupling partner is tolerated. The reaction is void of transition metals and the catalyst is an inexpensive standard commodity. The α,β-dehydroamino acid products can be utilized for the synthesis of scutianene natural products as well as a medicinal chemistry fragment.

3.7. References

1. Siodłak, D. α, β-Dehydroamino acids in naturally occurring peptides. *Amino Acids* **2015**, *47* (1), 1–17.

2. Shimohigashi, Y.; Chen, H.-C.; Stammer, C. H. The enzyme stability of dehydro-enkephalins. *Peptides* **1982**, *3* (6), 985–987.

3. Jones, L. H. Dehydroamino acid chemical biology: an example of functional group interconversion on proteins. *RSC Chemical Biology* **2020**, *1* (5), 298–304.

4. Wang, S.; Wu, K.; Tang, Y.-J.; Deng, H. Dehydroamino acid residues in bioactive natural products. *Nat. Prod. Rep.* **2024**, *41* (2), 273–297, 10.1039/D3NP00041A.

5. Kahan, F. M.; Kropp, H.; Sundelof, J. G.; Birnbaum, J. Thienamycin: development of imipenem-cilastatin. *J. Antimicrob. Chemother.* **1983**, *12* (suppl_D), 1–35.

6. Moreira, R.; Jervis, P. J.; Carvalho, A.; Ferreira, P. M.; Martins, J. A.; Valentão, P.; Andrade, P. B.; Pereira, D. M. Biological evaluation of naproxen–dehydrodipeptide conjugates with self-hydrogelation capacity as dual LOX/COX inhibitors. *Pharmaceutics* **2020**, *12* (2), 122.

7. Perni, R. B.; Conway, S. C.; Ladner, S. K.; Zaifert, K.; Otto, M. J.; King, R. W. Phenylpropenamide derivatives as inhibitors of hepatitis B virus replication. *Bioorg. Med. Chem. Lett.* **2000**, *10* (23), 2687–2690.

8. Topuzyan, V. O.; Alebyan, Z. G.; Paronikyan, R. V. Synthesis, Anticholinesterase, and Antibacterial Activity of N-Aroyl-a-Aminoacrylic Acid Dialkylaminoalkylamides. *Pharm. Chem. J.* **2015**, *49* (5), 304–308.

9. Zheng, Y.; Li, X.; Ren, C.; Zhang-Negrerie, D.; Du, Y.; Zhao, K. Synthesis of Oxazoles from Enamides via Phenyliodine Diacetate-Mediated Intramolecular Oxidative Cyclization. *J. Org. Chem.* **2012**, *77* (22), 10353–10361.

10. Roy, B.; Das, E.; Roy, A.; Mal, D. Ni(ii)-Catalyzed vinylic C–H functionalization of 2-acetamido-3-arylacrylates to access isotetronic acids. *Org. Biomol. Chem.* **2020**, *18* (19), 3697–3706, 10.1039/D0OB00557F.

11. Clagg, K.; Hou, H.; Weinstein, A. B.; Russell, D.; Stahl, S. S.; Koenig, S. G. Synthesis of Indole-2-carboxylate Derivatives via Palladium-Catalyzed Aerobic Amination of Aryl C–H Bonds. *Org. Lett.* **2016**, *18* (15), 3586–3589.

12. Ma, X.; Beard, A. M.; Burgess, S. A.; Darlak, M.; Newman, J. A.; Nogle, L. M.; Pietrafitta, M. J.; Smith, D. A.; Wang, X.; Yue, L. General Synthesis of Conformationally Constrained Noncanonical Amino Acids with C(sp3)-Rich Benzene Bioisosteres. *J. Org. Chem.* **2024**, *89* (7), 5010–5018.

13. Bennett, E. L.; Niemann, C. Transacylation in the Erlenmeyer—Plöchl Reaction. *J. Am. Chem. Soc.* **1950**, *72* (4), 1803–1804.

14. Sawamura, J.; Ieiri, D.; Yazaki, R.; Ohshima, T. α, β-Dehydroamino Acid Synthesis through Proline-Catalyzed Aldol Condensation with a Glycine Schiff Base. *Precis. Chem.* **2023**, *2* (1), 14–20.

15. A Bisceglia, J.; R Orelli, L. Recent progress in the Horner-Wadsworth-Emmons reaction. *Curr. Org. Chem.* **2015**, *19* (9), 744–775.

16. Praquin, C. l. F.; de Koning, P. D.; Peach, P. J.; Howard, R. M.; Spencer, S. L. Development of an Asymmetric Hydrogenation Route to (S)-N-Boc-2, 6-dimethyltyrosine. *Org. Process Res. Dev.* **2011**, *15* (5), 1124–1129.

17. Vinogradov, A. A.; Pan, S.-Y.; Suga, H. Ligand-enabled selective coupling of MIDA boronates to dehydroalanine-containing peptides and proteins. *J. Am. Chem. Soc.* **2025**, *147* (9), 7533–7544.

18. Ferreira, P. T.; Maia, H. S.; Monteiro, L. High yielding synthesis of dehydroamino acid and dehydropeptide derivatives. *J. Chem. Soc., Perkin Trans. 1* **1999**, (24), 3697–3703.

19. Nanjo, T.; Oshita, T.; Matsumoto, A.; Takemoto, Y. Late-Stage Installation of Dehydroamino Acid Motifs into Peptides Enabled by an N-Chloropeptide Strategy. *Chem. Eur. J.* **2022**, *28* (36), e202201120.

20. Gausmann, M.; Kreidt, N.; Christmann, M. Electrosynthesis of Protected Dehydroamino Acids. *Org. Lett.* **2023**, *25* (13), 2228–2232.

21. Kuranaga, T.; Sesoko, Y.; Sakata, K.; Maeda, N.; Hayata, A.; Inoue, M. Total synthesis and complete structural assignment of yaku'amide A. *J. Am. Chem. Soc.* **2013**, *135* (14), 5467–5474.

22. Smełka, L.; Rzeszotarska, B.; Pietrzyński, G.; Kubica, Z. Synthesis of peptides with α, β-dehydroamino acids, VI. Synthesis of N-benzyloxycarbonyl and N-trifluoroacetyl dipeptides of α, β-dehydro-butyrine,-valine,-leucine, and-isoleucine. *Liebigs Ann. Chem.* **1988**, *1988* (5), 485–486.

23. Xi, Y. K.; Zhang, H.; Li, R. X.; Kang, S. Y.; Li, J.; Li, Y. Total synthesis of spirotryprostatins through organomediated intramolecular umpolung cyclization. *Chem. Eur. J.* **2019**, *25* (12), 3005–3009.

24. Trost, B. M.; Dake, G. R. Nucleophilic α-addition to alkynoates. A synthesis of dehydroamino acids. *J. Am. Chem. Soc.* **1997**, *119* (32), 7595–7596.

25. Lu, S.-P.; Lewin, A. H. Enamine/imine tautomerism in α, β-unsaturated-α-amino acids. *Tetrahedron* **1998**, *54* (50), 15097–15104.

26. Schiavi, B. M.; Richard, D. J.; Joullié, M. M. Total synthesis of isoroquefortine C. *J. Org. Chem.* **2002**, *67* (3), 620–624.

27. Cizikovs, A.; Basens, E. E.; Zagorska, P. A.; Kinens, A.; Grigorjeva, L. Indole Synthesis by Cobalt-Catalyzed Intramolecular Amidation via the Oxidatively Induced Reductive Elimination Pathway. *ACS Catal.* **2024**, *14* (3), 1690–1698.

28. Dahmer, J.; Marangon, P.; Adolpho, L. O.; Reis, F. L.; Maldaner, G.; Burrow, R. A.; Mostardeiro, M. A.; Dalcol, I. I.; Morel, A. F. Alkaloids from the stem barks of Scutia buxifolia Reissek (Rhamnaceae): Structures and antimicrobial evaluation. *Phytochemistry* **2022**, *196*, 113071.

29. Jung, Y. J.; Hosseininasab, N.; Park, J.; Hyun, S.; Jung, J.-K.; Kwak, J.-H. Microwave-Promoted Total Synthesis of Puniceloid D for Modulating the Liver X Receptor. *Molecules* **2024**, *29* (2), 416.

30. Fritzemeier, R. G.; Nekvinda, J.; Vogels, C. M.; Rosenblum, C. A.; Slebodnick, C.; Westcott, S. A.; Santos, W. L. Organocatalytic trans Phosphinoboration of Internal Alkynes. *Angew. Chem. Int. Ed.* **2020**, *59* (34), 14358–14362.

31. An, F.; Brossette, J.; Jangra, H.; Wei, Y.; Shi, M.; Zipse, H.; Ofial, A. R. Reactivities of tertiary phosphines towards allenic, acetylenic, and vinylic Michael acceptors. *Chem. Sci.* **2024**, *15* (43), 18111–18126, 10.1039/D4SC04852K.

32. Pierce, B. M.; Simpson, B. F.; Ferguson, K. H.; Whittaker, R. E. Phosphine-mediated partial reduction of alkynes to form both (E)- and (Z)-alkenes. *Org. Biomol. Chem.* **2018**, *16* (36), 6659–6662, 10.1039/C8OB01848K.

Chapter 4: Experimental Procedures and Characterization Data

4.1. General Experimental Methods

Unless otherwise noted, reactions were performed in flame dried glassware (round bottom, 2-dram vial, or 6-dram vials) with Teflon coated stir bars. When Schlenk technique was used, argon or nitrogen was used as the inert gas. THF, toluene, DMF, DCM and MeCN were dried using an Innovative Technology Pure SolvMD solvent purification system. Column chromatography was performed using SiliaFlash P60 40-63 μm, 60 Å on a Teledyne NexGen 300 Automated System. TLC analyses were performed using Silicycle aluminum backed silica gel F-254 plates. Unless otherwise noted, chemicals were purchased from commercial sources. Abbreviations: pinacolborane: HBpin, Boc: *tert*-butyloxycarbonyl, Fmoc: fluorenylmethyloxycarbonyl, Trityl: triphenylmethyl, THF: tetrahydrofuran, DMF: dimethylformamide, DCM: dichloromethane, MeCN: acetonitrile.

4.2. Instrumentation

^{1}H, ^{13}C, ^{11}B, ^{19}F NMR spectroscopic experiments were performed using Agilent 400-MR 400 MHz, Agilent U4-DD2 400 Hz, Bruker Avance II 500 MHz, or Bruker Avance II 600 MHz spectrometers. Chemical shifts are reported in δ ppm, coupling constants, *J*, are reported in Hz (to 1 decimal place). ^{1}H NMR spectra are referenced to the residual protonated solvent signal ($CDCl_3$, 7.26 ppm; CD_3OD, 3.31 ppm; DMSO-d_6, 2.50 ppm; acetone-d_6, 2.05 ppm) and ^{13}C NMR spectra are referenced to the deuterated solvent signal ($CDCl_3$, 77.16 ppm; CD_3OD, 49.00 ppm; DMSO-d_6, 39.52 ppm; acetone-d_6; 29.84 ppm) and are ^{1}H decoupled. Signal multiplicities reported as singlet (s), doublet (d), triplet (t), quartet (q), multiplet (m). Mass spectrometry was performed at

VT-MSI HRMS facility. High resolution mass spectra (HRMS) were recorded on Agilent 6220 using flow injection analysis (FIA). LC flow is 0.1 ml/min with a composition of 25:75 water: acetonitrile with 0.1% formic acid. Run times were 1 minute.

4.3. Synthetic Procedures and Characterization of Compounds for Chapter 1

Synthetic Procedures for 1,3-Enyne Substrates:

1,3-Enyne substrates **1.50a – 1.50q** and **1.58s – 1.58v** were synthesized according with previous literature and references for the spectra of previously known 1,3-enynes are provided in Table 4.1. 1,3-Enynes **1.58r** and **1.58w - 1.58x** were synthesized following the procedures which are listed below.

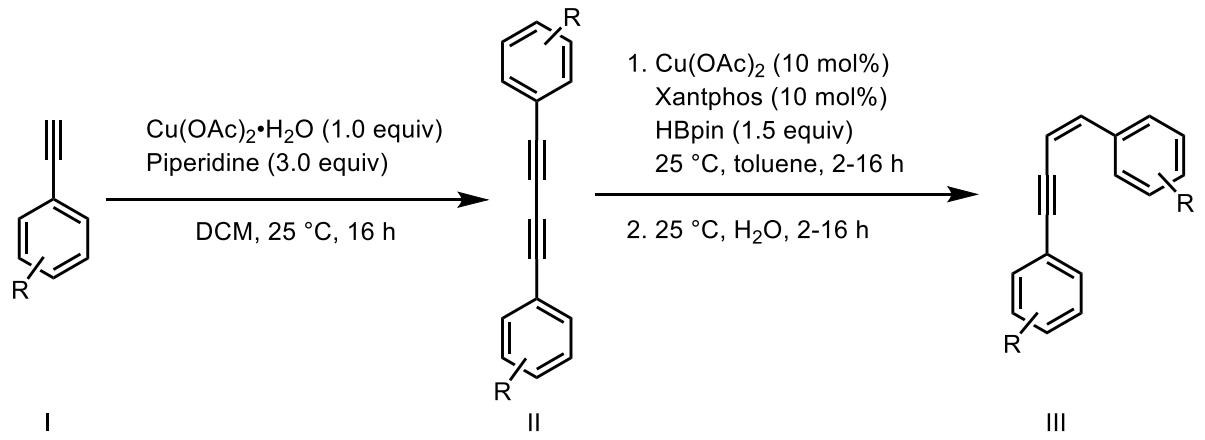

Scheme 4.1: Semi-reduction for synthesis of 1,3-enyne starting material**.**

Procedure 4.1: According to a modified procedure from Burgio *et al.*, to a stirring suspension of $Cu(OAc)_2•H_2O$ (1.0 equiv) in dichloromethane (5 mL) was added acetylene (**I**) (1.0 equiv) and piperidine (3.0 equiv). The reaction was stirred at room temperature overnight. Reaction progress was followed via TLC. Upon completion, the reaction mixture was concentrated *in vacuo* and purified by flash column chromatography to afford the corresponding diyne (**II**).[1] According to a modified procedure from Burgio *et al.*, to a stirring solution of diyne (II) (1.0 equiv), Cu(OAc) (10

mol%) and Xantphos (10 mol%) in toluene (5 mL) was added pinacolborane (1.5 equiv) under a nitrogen atmosphere. The reaction was stirred at room temperature, and reaction progress was followed by TLC. Upon completion, the reaction was quenched with water (5.0 equiv), concentrated *in vacuo,* and purified by flash column chromatography to afford the corresponding enyne.

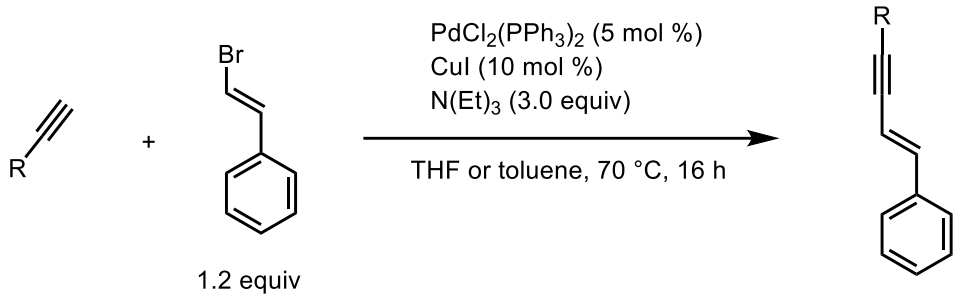

Scheme 4.2: Sonogashira cross-coupling for the synthesis of 1,3-enyne starting material.

Procedure 4.2: According to a modified procedure from Wang *et al*.[2] To a 6-dram vial with screw on septa cap: a stir bar, acetylene (1.0 equiv), $PdCl_2(PPh_3)_2$ (5 mol%) and CuI (10 mol%) were added. The reaction flask was put under inert atmosphere (N_2) using standard *Schlenk* technique. Toluene or THF (5 mL), (*E*)-(2-bromovinyl)benzene (1.2 equiv) and triethylamine (3.0 equiv) were then added to the reaction flask. The reaction was heated to 70 °C and allowed to stir for 16 hours. The reaction mixture was reduced under negative pressure and purified via flash column chromatography to afford the corresponding 1,3-enyne.

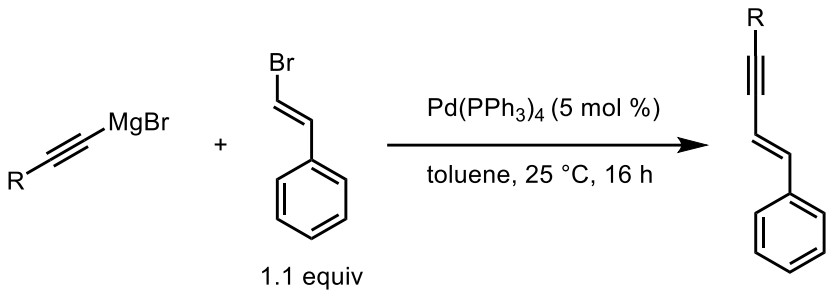

Scheme 4.3: Kumada cross-coupling for the synthesis of 1,3-enyne starting material.

Procedure 4.3: According to a modified procedure from Wang *et al*.[2] To a 6-dram vial with screw on septa cap: a stir bar and $Pd(PPh_3)_4$ (5 mol%) were added. The reaction flask was put under inert atmosphere (N_2) using standard *Schlenk* technique. Toluene (5 mL), (*E*)-(2-bromovinyl)benzene (1.1 equiv) and 1-propynylmagnesium bromide (0.5 M in THF) (1.0 equiv) were then added to the reaction flask. The reaction was allowed to stir for 16 hours. The reaction mixture was reduced under negative pressure and purified via flash column chromatography to afford the corresponding 1,3-enyne.

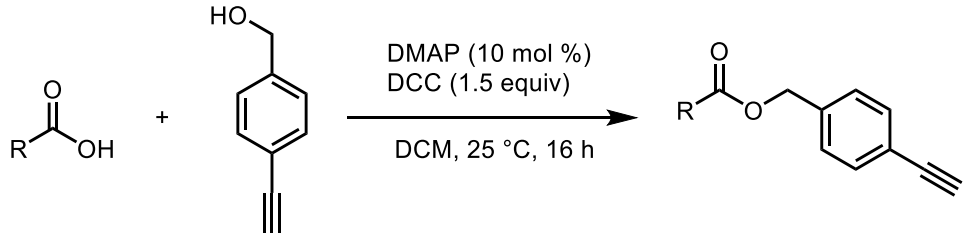

Scheme 4.4: DCC esterification for the synthesis of alkyne starting material.

Procedure 4.4: To a solution of carboxylic acid (1.0 equiv) in DCM (5 mL), 4-iodobenzyl alcohol (1.0 equiv), dicyclohexylcarbodiimide (DCC) (1.5 equiv), dimethylaminopyridine (4-DMAP) (10 mol%) was added. The reaction was stirred at room temperature until the reaction was complete. Upon completion, the mixture was concentrated under negative pressure and purified flash column chromatography to afford the desired ester.

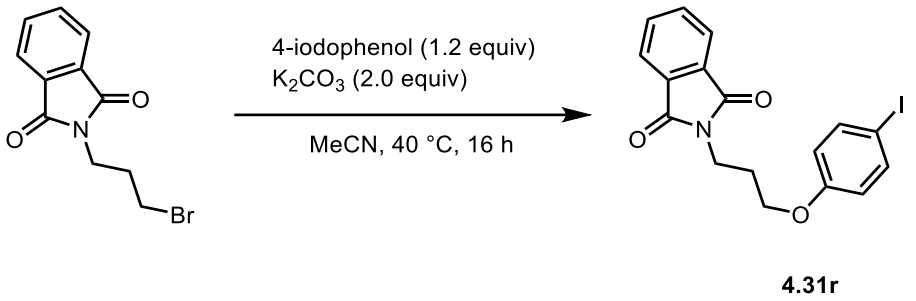

Scheme 4.5: Williamson ether synthesis

Procedure 4.5: To a 6-dram vial: 2-(3-bromopropyl)isoindoline-1,3-dione (2.27 mmol), 4-iodophenol (2.73 mmol), potassium carbonate (4.55 mmol) and MeCN (5 mL) were added. The vial was heated to 40 °C for 16 hours. Water (5 mL) and EtOAc (5 mL) were added. Two additional aliquots of EtOAc were added and extracted, then washed with brine. The organic phase was reduced under negative pressure and the aryl iodide was then purified via column chromatography. afford 2-(3-(4-iodophenoxy)propyl)isoindoline-1,3-dione **4.31r** (923 mg, 2.27 mmol, 87%) as a white amorphous solid. **^{1}H NMR** (400 MHz, $CDCl_3$) δ 7.84 (dd, *J* = 5.5, 3.0 Hz, 2H), 7.72 (dd, *J* = 5.5, 3.0 Hz, 2H), 7.50 (d, *J* = 9.0 Hz, 2H), 6.57 (d, *J* = 9.1 Hz, 2H), 3.98 (t, *J* = 6.0 Hz, 2H), 3.90 (t, *J* = 6.8 Hz, 2H), 2.22 – 2.12 (m, 2H). **^{13}C NMR** (101 MHz, $CDCl_3$) δ 168.3, 158.6, 138.1, 134.0, 132.1, 123.3, 116.8, 82.9, 65.8, 35.4, 28.2. HRMS calcd for $C_{17}H_{14}INNaO_3^+$ $[M+Na]^+$ 429.9911 m/z, found 429.9891 m/z. Δ -4.6513.

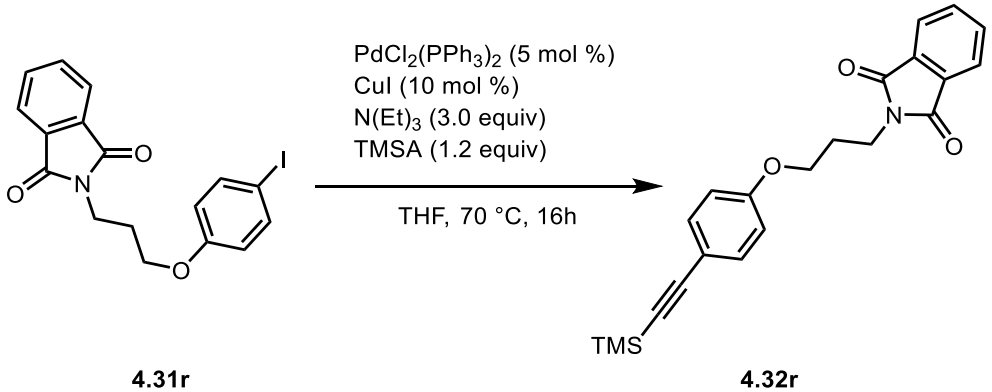

Scheme 4.6: Sonogashira-Cross coupling with trimethylsilyacetylene (TMSA).

Procedure 4.6: To a 6-dram vial with screw on septa cap: a stir bar, 2-(3-(4-iodophenoxy)propyl)isoindoline-1,3-dione **4.31r** (1.11 mmol), $PdCl_2(PPh_3)_2$ (55.3 μmol) and CuI (111 μmol) were added. The reaction flask was put under inert atmosphere (N_2) using standard *Schlenk* technique. THF (5 mL), TMSA (1.33 mmol) and triethylamine (3.32 mmol) were then added to the reaction flask. The reaction was heated to 70 °C and allowed to stir for 16 hours. Water (5 mL) and EtOAc (5 mL) were added. Two additional aliquots of EtOAc were added and extracted, then washed with brine. The organic phase was reduced under negative pressure and the column chromatography was used to purify 2-(3-(4-((trimethylsilyl)ethynyl)phenoxy)propyl)isoindoline-1,3-dione **4.32r** (298.1 mg, 790.4 μmol, 71%) as a white amorphous. **^{1}H NMR** (400 MHz, $CDCl_3$) δ 7.84 (dd, *J* = 5.5, 2.9 Hz, 2H), 7.71 (dd, *J* = 5.5, 3.1 Hz, 2H), 7.34 (d, *J* = 8.9 Hz, 2H), 6.70 (d, *J* = 8.9 Hz, 2H), 4.02 (t, *J* = 6.0 Hz, 2H), 3.90 (t, *J* = 6.8 Hz, 2H), 2.22 – 2.14 (m, 2H), 0.23 (s, 9H). **^{13}C NMR** (101 MHz, $CDCl_3$) δ 168.5, 159.0, 138.3, 134.1, 133.6, 123.4, 117.0, 114.4, 105.4, 92.6, 65.8, 35.6, 28.4, 0.2. HRMS calcd for $C_{22}H_{24}NO_3Si^+$ $[M+H]^+$ 378.1525 m/z, found 378.1529 m/z. Δ 1.0578.

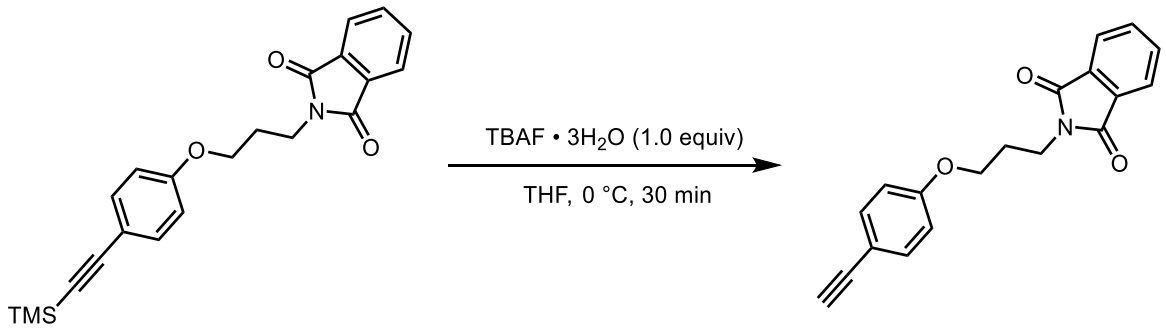

Scheme 4.7: Trimethylsilyl alkyne deprotection

Procedure 4.7: To a 6 dram vial, 2-(3-(4-((trimethylsilyl)ethynyl)phenoxy)propyl)isoindoline-1,3-dione **4.33r** (609 μmol) was dissolved in THF (6 mL). Then, TBAF trihydrate (731 μmol) was added slowly at 0 °C. The reaction was stirred at 0 °C until TLC analysis showed the complete

consumption of **4.32r** (about 0.5 h). The solution was quenched with NH_4Cl (aq) (10 mL). Then Water (5 mL) and EtOAc (5 mL) were added. Two additional aliquots of EtOAc were added and extracted, then washed with brine. The organic phase was reduced under negative pressure and purified via column chromatography to afford afford 2-(3-(4-ethynylphenoxy)propyl)isoindoline-1,3-dione **4.33r** (167.23 mg, 548.1 μmol, 90%) as a white amorphous solid. **^{1}H NMR** (400 MHz, $CDCl_3$) δ 7.84 (dd, *J* = 5.5, 3.1 Hz, 2H), 7.72 (dd, *J* = 5.5, 3.0 Hz, 2H), 7.37 (d, *J* = 8.9 Hz, 2H), 6.73 (d, *J* = 8.9 Hz, 2H), 4.03 (t, *J* = 6.1 Hz, 2H), 3.91 (t, *J* = 6.8 Hz, 2H), 2.98 (s, 1H), 2.22 – 2.15 (m, 2H). **^{13}C NMR** (101 MHz, CDCl3) δ 168.5, 159.2, 134.1, 133.7, 132.3, 123.4, 114.6, 114.4, 83.8, 75.9, 65.9, 35.6, 28.4. HRMS calcd for $C_{19}H_{15}NNaO_3^+$ $[M+Na]^+$ 328.0944 m/z, found 328.0959 m/z. Δ 4.5719.

Characterization of 1,3-Enynes:

Table 4.1: References for 1,3-enyne and alkyne starting materials.

Compound	Structure	Procedure	Reference
1.58a[1]	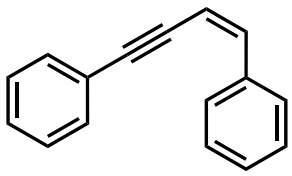	**4.1**	*Org. Lett.* **2023**, *25* (15), 2652–2656.
1.58b[1]	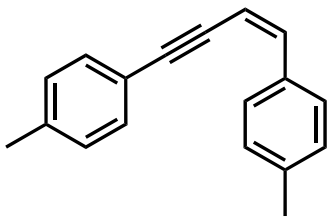	**4.1**	*Org. Lett.* **2023**, *25* (15), 2652–2656.
1.58c[1]	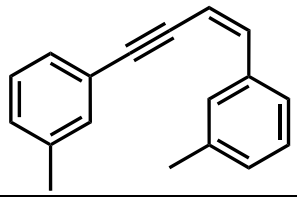	**4.1**	*Org. Lett.* **2023**, *25* (15), 2652–2656.

1.58d[1]	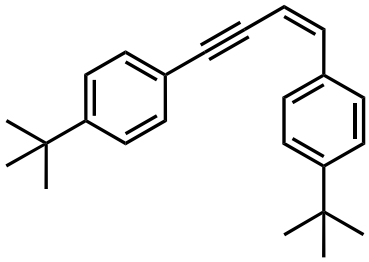	**4.1**	*Org. Lett.* **2023**, *25* (15), 2652–2656.
1.58e[1]	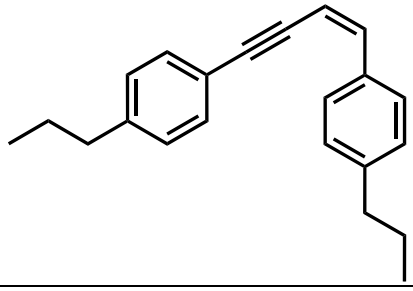	**4.1**	*Org. Lett.* **2023**, *25* (15), 2652–2656.
1.58f[1]	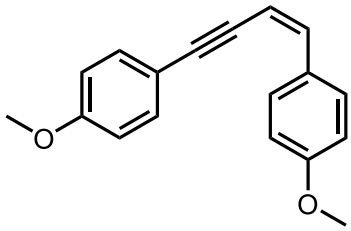	**4.1**	*Org. Lett.* **2023**, *25* (15), 2652–2656.
1.58g[1]	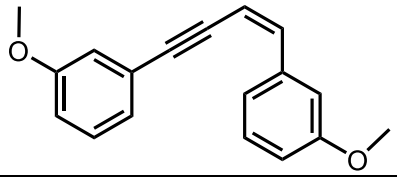	**4.1**	*Org. Lett.* **2023**, *25* (15), 2652–2656.
1.58h[1]	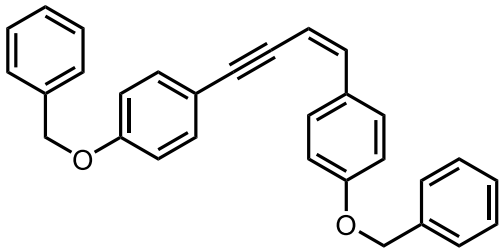	**4.1**	*Org. Lett.* **2023**, *25* (15), 2652–2656.
1.58i[1]	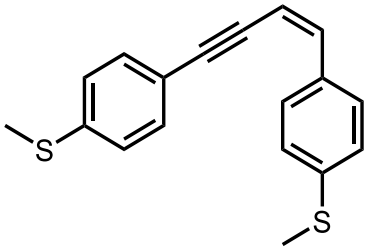	**4.1**	*Org. Lett.* **2023**, *25* (15), 2652–2656.

1.58j[1]	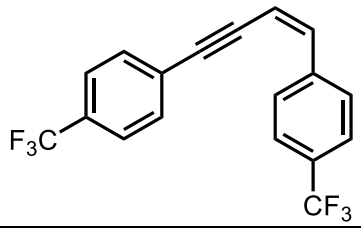	**4.1**	*Org. Lett.* **2023**, *25* (15), 2652–2656.
1.58k[1]	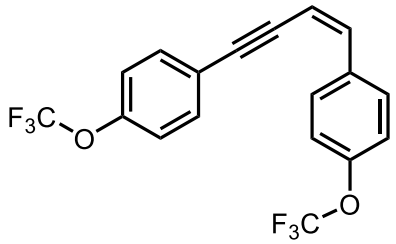	**4.1**	*Org. Lett.* **2023**, *25* (15), 2652–2656.
1.58l[1]	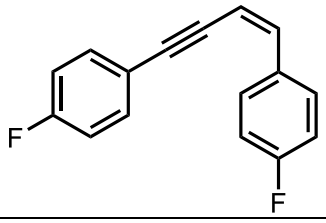	**4.1**	*Org. Lett.* **2023**, *25* (15), 2652–2656.
1.58m[1]	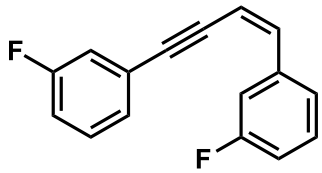	**4.1**	*Org. Lett.* **2023**, *25* (15), 2652–2656.
1.58n[1]	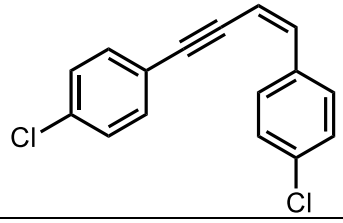	**4.1**	*Org. Lett.* **2023**, *25* (15), 2652–2656.
1.58o[1]	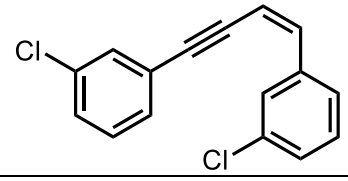	**4.1**	*Org. Lett.* **2023**, *25* (15), 2652–2656.
1.58p[1]	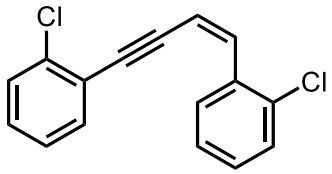	**4.1**	*Org. Lett.* **2023**, *25* (15), 2652–2656.
1.58q[1]	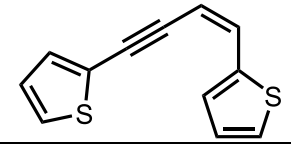	**4.1**	*Org. Lett.* **2023**, *25* (15), 2652–2656.

1.58s[3]	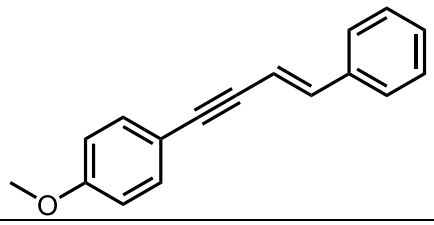	**4.2**	*Org. Lett.* **2022**, *24* (29), 5486–5490.
1.58t[3]	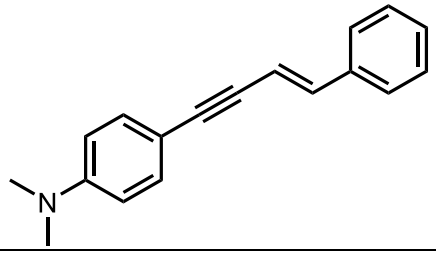	**4.2**	*Org. Lett.* **2022**, *24* (29), 5486–5490.
1.58u[4]	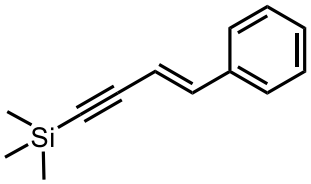	**4.2**	*Org. Lett.* **2011**, *13* (23), 6192–6195.
1.58v[5]	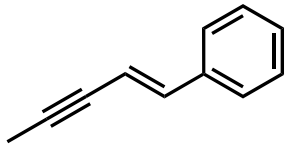	**4.3**	*J. Am. Chem. Soc.* **2016**, *138* (44), 14566–14569.
4.33w[6]	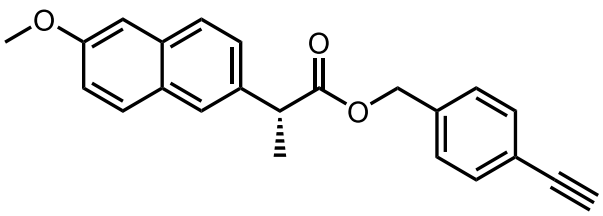	**4.4**	*Org. Lett.* **2022**, *24* (37), 6794–6799.

4-ethynylbenzyl 5-(2,4-dimethylphenoxy)-2,2-dimethylpentanoate (4.33x) Following general procedure **4.4**, compound **4.33x** (1.41 mmol) was isolated using 5-(2,5-dimethylphenoxy)-2,2-dimethylpentanoic acid (1.51 mmol) by flash column chromatography, 0-25% EtOAc:Hex in an 93% yield. White solid. **^{1}H NMR** (400 MHz, $CDCl_3$) δ 7.46 (d, *J* = 8.5 Hz, 2H), 7.28 (dd, *J* = 7.9, 0.7 Hz, 2H), 6.97 (d, *J* = 0.9 Hz, 1H), 6.64 (d, *J* = 7.5

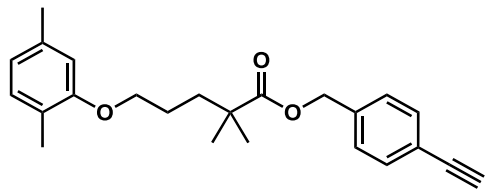

Hz, 1H), 6.58 (s, 1H), 5.08 (s, 2H), 3.87 (t, *J* = 5.7 Hz, 2H), 3.07 (s, 1H), 2.29 (s, 3H), 2.14 (s, 3H), 1.73 – 1.70 (m, 4H), 1.23 (s, 6H). **^{13}C NMR** (101 MHz, $CDCl_3$) δ 177.6, 157.0, 137.1, 136.5, 132.4, 130.4, 127.8, 123.7, 121.9, 120.9, 120.8, 112.0, 83.4, 77.6, 67.9, 65.7, 42.3, 37.2, 24.8, 21.5, 15.8. HRMS calcd for $C_{24}H_{29}O_3^+$ $[M+H]^+$ 365.2117 m/z, found 365.2130 m/z. Δ 3.5596.

***(E)*-2-(3-(4-(4-phenylbut-3-en-1-yn-1-yl)phenoxy)propyl)isoindoline-1,3-dione (1.58r)** (107 mg, 263 μmol, 50%)) Following **Procedure 4.2**, compound **1.58r** was isolated by flash chromatography as a white amorphous solid. **^{1}H NMR** (400 MHz, $CDCl_3$) δ 7.83 (dd, *J* = 6.0, 3.2 Hz, 2H), 7.71 (dd, *J* = 5.6, 2.9 Hz, 2H), 7.40 f(d, *J* = 7.4 Hz, 2H), 7.38 – 7.26 (m, 5H), 6.98 (d, *J* = 16.2 Hz, 1H), 6.74 (d, *J* = 8.3 Hz, 2H), 6.36 (d, *J* = 16.2 Hz, 1H), 4.03 (t, *J* = 6.1 Hz, 2H), 3.90 (t, *J* = 6.8 Hz, 2H), 2.18 (p, *J* = 6.5 Hz, 2H). **^{13}C NMR** (101 MHz, $CDCl_3$) δ 168.5, 158.9, 140.6, 136.7, 134.1, 133.1, 132.3, 130.9, 128.9, 128.6, 126.4, 123.4, 114.7, 108.6, 92.0, 90.0, 65.9, 35.6, 28.4. HRMS calcd for $C_{27}H_{22}NO_3^+$ $[M+H]^+$ 408.1600 m/z, found 408.1607 m/z. Δ 1.7150.

(*E*)-4-(4-phenylbut-3-en-1-yn-1-yl)benzyl (*R*)-2-(6-methoxynaphthalen-2-yl)propanoate (1.58w) Following **Procedure 4.2**, compound **1.58w** (360 μmol) was isolated using **4.33w** (581 μmol) by flash column chromatography, 0-20% EtOAc:Hex in a 62% yield. Colorless oil.**^{1}H NMR** (400 MHz, $CDCl_3$) δ 7.69 (dd, *J* = 8.6, 5.5 Hz, 2H), 7.65 – 7.64 (m, 1H), 7.44 – 7.39 (m, 3H), 7.39 – 7.34 (m, 4H), 7.33 – 7.29 (m, 1H), 7.19 (d, *J* = 0.6 Hz, 1H), 7.18 – 7.10 (m, 3H), 7.04 (d, *J* = 16.3 Hz, 1H), 6.37 (d, *J* = 16.2 Hz, 1H), 5.13 (d, *J* = 12.8 Hz, 1H), 5.08 (d, *J* = 12.8 Hz,

1H), 3.92 (s, 3H), 3.90 (q, J = 7.1 Hz, 1H), 1.60 (d, J = 7.2 Hz, 3H). **^{13}C NMR** (101 MHz, $CDCl_3$) δ 174.4, 147.0, 141.4, 136.0, 133.7, 131.5, 129.3, 128.9, 128.7, 128.7, 128.3, 127.8, 127.2, 126.3, 126.2, 126.0, 123.9, 123.1, 119.0, 108.0, 105.6, 91.3, 77.2, 66.0, 55.3, 45.4, 18.5. HRMS calcd for $C_{31}H_{27}O_3^+$ $[M+H]^+$ 447.1960 m/z, found 447.1974 m/z. Δ 3.1306.

(*E*)-4-(4-phenylbut-3-en-1-yn-1-yl)benzyl-5-(2,4-dimethylphenoxy)-2,2-dimethylpentanoate

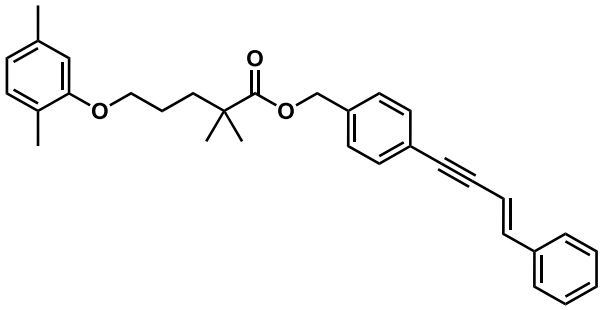

(1.58x) Following **Procedure 4.2**, compound **1.58x** (222 µmol) was isolated using **4.33x** (617 µmol) by flash column chromatography, 0-20% EtOAc:Hex in a 36% yield. Colorless oil. **^{1}H NMR** (400 MHz, $CDCl_3$) δ 7.47 – 7.41 (m, 4H), 7.38 – 7.33 (m, 2H), 7.32 – 7.28 (m, 3H), 7.05 (d, J = 16.2 Hz, 1H), 7.00 (dd, J = 7.4, 0.9 Hz, 1H), 6.68 – 6.64 (m, 1H), 6.60 (d, J = 16.2 Hz, 1H), 6.38 (d, J = 16.2 Hz, 1H), 5.11 (s, 2H), 3.89 (t, J = 5.6 Hz, 2H), 2.31 (s, 3H), 2.16 (s, 3H), 1.75 – 1.72 (m, 4H), 1.25 (s, 6H). **^{13}C NMR** (101 MHz, $CDCl_3$) δ 177.7, 157.1, 141.6, 136.6, 136.5, 136.5, 131.8, 130.4, 128.8, 128.0, 126.5, 123.8, 123.3, 120.9, 112.1, 108.2, 91.5, 89.4, 68.0, 65.9, 43.7, 42.3, 37.3, 25.3, 24.7, 21.5, 15.9. HRMS calcd for $C_{32}H_{35}O_3^+$ $[M+H]^+$ 467.2586 m/z, found 467.2589 m/z. Δ 0.6420.

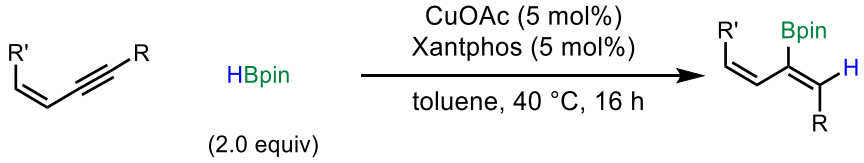

Scheme 4.8: The chemo-, regio-, and stereoselective *cis*-hydroboration of 1,3-enynes.

General Procedure 4.8: To a flame dried 2-dram vial with a septa lid: a stir bar, corresponding enyne (0.250 mmol), copper(I)acetate (0.013 mmol) and Xantphos (0.013 mmol) were added. The reaction vial was put under inert atmosphere (N_2 or Ar) using standard *Schlenk* technique. Then, toluene (1 mL) was added, and the mixture was allowed to complex at 40 °C. Once the mixture became a homogenous green solution, pinacolborane (0.500 mmol) was added. The reaction was

allowed to stir for 16 hours. Upon completion, volatile solvents were removed by rotary evaporator and the desired 2-boryl-1,3-diene was purified via flash column chromatography.

Characterization of 2-Boryl-1,3-Dienes:

2-((1*Z*,3*Z*)-1,4-diphenylbuta-1,3-dien-2-yl)-4,4,5,5-tetrayl-1,3,2-dioxaborolane (1.59a).

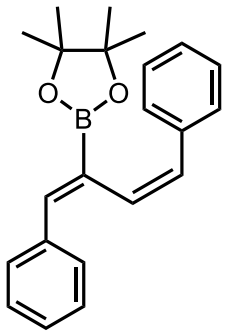

Synthesized according to **Procedure 4.8**. Isolated in 0-5% EtOAc:Hex as a yellow oil in 73% yield (60.8 mg, 0.183 mmol). **^{1}H NMR** (400 MHz, $CDCl_3$) δ 7.64 – 7.57 (m, 2H), 7.44 – 7.40 (m, 2H), 7.39 – 7.33 (m, 2H), 7.32 – 7.27 (m, 3H), 7.25 – 7.23 (m, 1H), 7.23 – 7.17 (m, 1H), 6.72 (d, *J* = 11.6 Hz, 1H), 6.61 (dd, *J* = 11.7, 2.0 Hz, 1H), 0.99 (s, 12H). **^{13}C NMR** (101 MHz, $CDCl_3$) δ 143.4, 139.1, 138.0, 131.6, 130.6, 129.7, 128.9, 128.4, 128.3, 128.3, 127.1, 83.6, 24.6, (C-B not observed). **^{11}B NMR** (128 MHz, $CDCl_3$) δ 30.3. HRMS calcd for $C_{22}H_{26}BO_2^+$ $[M+H]^+$ 333.2026 m/z, found 333.2026 m/z. Δ 0.0000.

2-((1*Z*,3*Z*)-1,4-di-p-tolylbuta-1,3-dien-2-yl)-4,4,5,5-tetramethyl-1,3,2-dioxaborolane (1.59b)

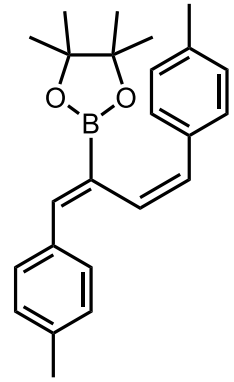

Synthesized according to **Procedure 4.8**. Isolated in 0-5% EtOAc:Hex as a yellow oil in 78% yield (70.2 mg, 0.195 mmol). **^{1}H NMR** (400 MHz, $CDCl_3$) δ 7.51 (d, *J* = 8.4 Hz, 2H), 7.30 (d, *J* = 8.3 Hz, 2H), 7.19 – 7.14 (m, 3H), 7.10 (d, *J* = 0.9 Hz, 2H), 6.67 (d, *J* = 11.6 Hz, 1H), 6.56 (dd, *J* = 11.6, 2.0 Hz, 1H), 2.36 (s, 3H), 2.31 (s, 3H), 0.99 (s, 12H). **^{13}C NMR** (101 MHz, $CDCl_3$) δ 142.7, 137.9, 136.5, 136.0, 135.0, 131.0, 129.7, 129.4, 128.7, 128.7, 128.5, 24.3, 21.2, 21.0, (*C*-B not observed). **^{11}B NMR** (128 MHz, $CDCl_3$) δ 30.7. HRMS calcd for $C_{24}H_{30}BO_2^+$ $[M+H]^+$ 361.2339 m/z, found 361.2338 m/z. Δ 0.2768.

2-((1*Z*,3*Z*)-1,4-di-m-tolylbuta-1,3-dien-2-yl)-4,4,5,5-tetramethyl-1,3,2-dioxaborolane (1.59c).

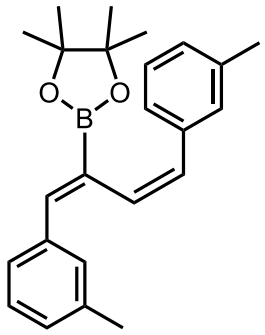

Synthesized according to **Procedure 4.8**. Isolated in 0-5% EtOAc:Hex as a yellow oil in 69% yield (44.3 mg, 0.123 mmol). **^{1}H NMR** (400 MHz, $CDCl_3$) δ 7.46 – 7.38 (m, 2H), 7.25 – 7.22 (m, 2H), 7.21 – 7.14 (m, 3H), 7.11 (d, *J* = 7.6 Hz, 1H), 7.01 (dt, *J* = 7.2, 2.0 Hz, 1H), 6.70 – 6.65 (m, 1H), 6.59 (dd, *J* = 11.6, 2.0 Hz, 1H), 2.36 (s, 3H), 2.32 (s, 3H), 0.98 (s, 12H). **^{13}C NMR** (101 MHz, $CDCl_3$) δ 142.9, 138.8, 137.7, 137.6, 137.5, 131.2, 130.2, 130.1, 129.2, 128.7, 128.1, 127.9, 127.6, 126.6, 125.8, 83.2, 24.3, 21.3, 21.2, (*C*-B not observed). **^{11}B NMR** (128 MHz, $CDCl_3$) δ 31.5. HRMS calcd for $C_{24}H_{30}BO_2^+$ $[M+H]^+$ 361.2339 m/z, found 361.2345 m/z. Δ 1.6610.

2-((1*Z*,3*Z*)-1,4-bis(4-(tert-butyl)phenyl)buta-1,3-dien-2-yl)-4,4,5,5-tetramethyl-1,3,2-dioxaborolane (1.59d). Synthesized according to **Procedure 4.8**. Isolated in 0-5% EtOAc:Hex as a yellow oil in 64% yield (71.0 mg, 0.160 mmol). **^{1}H NMR** (400 MHz, $CDCl_3$) δ 7.62 – 7.51 (m, 2H), 7.39 – 7.35 (m, 2H), 7.35 – 7.29 (m, 4H), 7.17 (s, 1H), 6.69 (d, *J* = 11.3 Hz, 1H), 6.60 (dd, *J* = 11.5, 2.0 Hz, 1H), 1.33 (s, 9H), 1.29 (s, 9H), 0.96 (s, 12H). **^{13}C NMR** (101 MHz, $CDCl_3$) δ 151.3, 150.1, 142.9, 136.5, 135.4, 131.2, 130.4, 129.5, 128.6, 125.3, 125.2, 83.5, 34.8, 34.7, 31.4, 31.4, 24.6, (*C*-B not observed). **^{11}B NMR** (128 MHz, $CDCl_3$) δ 31.3. HRMS calcd for $C_{30}H_{41}BO_2^+$ $[M+H]^+$ 445.3278 m/z, found 445.3269 m/z. Δ 2.0210.

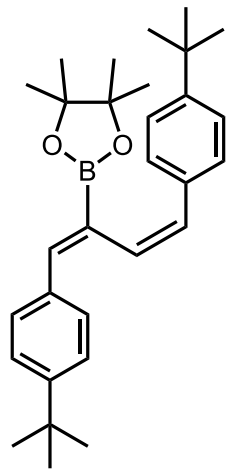

2-((1*Z*,3*Z*)-1,4-bis(4-propylphenyl)buta-1,3-dien-2-yl)-4,4,5,5-tetramethyl-1,3,2-

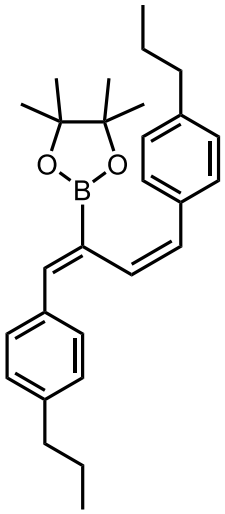

dioxaborolane (1.59e). Synthesized according to **Procedure 4.8**. Isolated in 0-5% EtOAc:Hex as a yellow oil in 69% yield (72.0 mg, 0.173 mmol). **^{1}H NMR** (400 MHz, $CDCl_3$) δ 7.54 – 7.51 (m, 2H), 7.32 (dd, *J* = 7.9, 0.5 Hz, 2H), 7.19 – 7.14 (m, 3H), 7.09 (d, *J* = 8.0 Hz, 2H), 6.67 (d, *J* = 11.8 Hz, 1H), 6.57 (dd, *J* = 11.5, 2.1 Hz, 1H), 2.56 (dt, *J* = 19.8, 7.9 Hz, 4H), 1.70 – 1.55 (m, 4H), 0.98 (s, 12H), 0.97 – 0.91 (m, 6H). **^{13}C NMR** (126 MHz, $CDCl_3$) δ 143.0, 143.0, 141.8, 136.7, 135.6, 131.3, 130.1, 129.7, 128.8, 128.5, 128.4, 83.5, 38.1, 38.0, 24.9, 24.6, 24. 6, 14.0, 14.0, (*C*-B not observed). **^{11}B NMR** (128 MHz, $CDCl_3$) δ 30.5. HRMS calcd for $C_{28}H_{38}BO_2^+$ $[M+H]^+$ 417.2965 m/z, found 417.2974 m/z. Δ 2.1567.

2-((1*Z*,3*Z*)-1,4-bis(4-methoxyphenyl)buta-1,3-dien-2-yl)-4,4,5,5-tetramethyl-1,3,2-

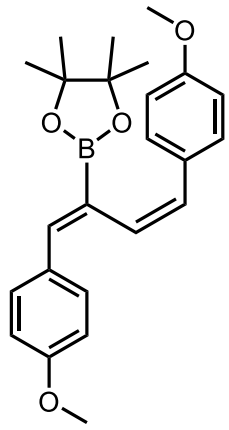

dioxaborolane (1.59f), Synthesized according to **Procedure 4.8**. Isolated from 0-10% EtOAc:Hex as a yellow oil in 92% yield (90.2 mg, 0.230 mmol), **^{1}H NMR** (400 MHz, $CDCl_3$) δ 7.58 (d, *J* = 8.8 Hz, 2H), 7.35 (d, *J* = 8.8 Hz, 2H), 7.15 (d, *J* = 1.5 Hz, 1H), 6.88 (d, *J* = 8.8 Hz, 2H), 6.83 (d, *J* = 8.7 Hz, 2H), 6.64 (d, *J* = 11.5 Hz, 1H), 6.51 (dd, *J* = 11.5, 2.0 Hz, 1H), 3.82 (s, 3H), 3.78 (s, 3H), 1.01 (s, 12H). **^{13}C NMR** (101 MHz, $CDCl_3$) δ 159.6, 158.9, 142.6, 132.1, 131.2, 131.0, 130.6, 130.1, 129.3, 113.8, 113.7, 83.5, 55.5, 55.4, 24.7, (*C*-B not observed). **^{11}B NMR** (128 MHz, $CDCl_3$) δ 29. 8. HRMS calcd for $C_{24}H_{30}BO_4^+$ $[M+K]^+$ 431.1796 m/z, found 431.1788 m/z. Δ 1.8554.

2-((1*Z*,3*Z*)-1,4-bis(3-methoxyphenyl)buta-1,3-dien-2-yl)-4,4,5,5-tetramethyl-1,3,2-

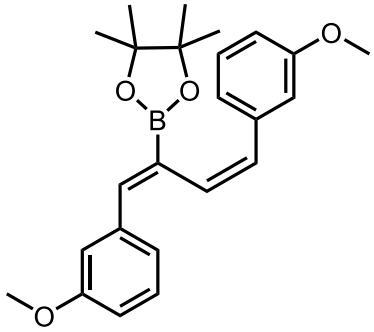

dioxaborolane (1.59g), Synthesized according to **Procedure 4.8**. Isolated from 0-10% EtOAc:Hex as a yellow oil in 89% yield (87.3 mg, 0.223 mmol). **^{1}H NMR** (400 MHz, $CDCl_3$) δ 7.30 – 7.23 (m, 1H), 7.22 – 7.14 (m, 4H), 7.02 – 6.95 (m, 2H), 6.89 – 6.81 (m, 1H), 6.80 – 6.72 (m, 1H), 6.69 (d, *J* = 11.7 Hz, 1H), 6.63 (dd, *J* = 11.7, 1.5 Hz, 1H), 3.80 (s, 3H), 3.78 (s, 3H), 1.00 (s, 12H).**^{13}C NMR** (101 MHz, $CDCl_3$) δ 159.7, 159.5, 142.9, 140.4, 139.3, 131.4, 130.9, 129.5, 129.3, 122.4, 121.6, 114.8, 114.1, 113.7, 113.4, 83.6, 55.4, 55.2, 24.6, (*C*-B not observed). **^{11}B NMR** (128 MHz, $CDCl_3$) δ 30.2. HRMS calcd for $C_{24}H_{30}BO_4^+$ $[M+H]^+$ 393.2237 m/z, found 393.2243 m/z. Δ 1.5259.

2-((1*Z*,3*Z*)-1,4-bis(4-(benzyloxy)phenyl)buta-1,3-dien-2-yl)-4,4,5,5-tetramethyl-1,3,2-

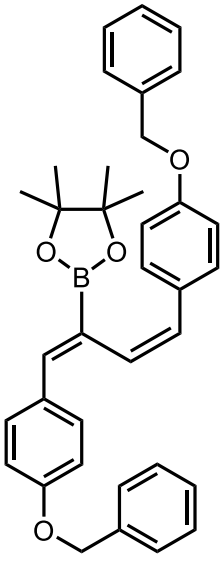

dioxaborolane (1.59h) - Synthesized according to **Procedure 4.8.** Isolated from 0-10% EtOAc:Hex as a yellow oil in 61% yield (83.0 mg, 0.153 mmol). **^{1}H NMR** (400 MHz, $CDCl_3$) δ 7.57 (d, *J* = 8.8 Hz, 2H), 7.47 – 7.29 (m, 12H), 7.14 (d, *J* = 1.7 Hz, 1H), 6.95 (d, *J* = 8.8 Hz, 2H), 6.89 (d, *J* = 8.7 Hz, 2H), 6.63 (d, *J* = 11.6 Hz, 1H), 6.51 (dd, *J* = 11.6, 2.1 Hz, 1H), 5.08 (s, 2H), 5.06 (s, 2H), 0.99 (s, 12H). **^{13}C NMR** (101 MHz, $CDCl_3$) δ 158.9, 158.0, 142.6, 137.0, 132.3, 131.3, 131.2, 130.7, 130.1, 129.3, 128.9, 128.8, 128.7, 128.2, 128.0, 127.6, 127.4, 114.9, 114.6, 83.5, 70.1, 24.7, (*C*-B not observed). **^{11}B NMR** (128 MHz, $CDCl_3$) δ 28.1. HRMS calcd for $C_{36}H_{38}BO_4^+$ $[M+H]^+$ 545.2863 m/z**,** found 545.2864 m/z. Δ 0.1834.

2-((1*Z*,3*Z*)-1,4-bis(4-(methylthio)phenyl)buta-1,3-dien-2-yl)-4,4,5,5-tetramethyl-1,3,2-

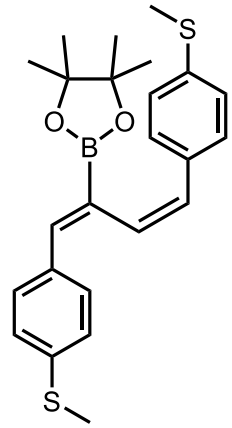

dioxaborolane (1.59i), Synthesized according to **Procedure 4.8**. Isolated from 0-10% EtOAc:Hex as a yellow oil in 58% yield (61.7 mg, 0.145 mmol)**.** ^{1}H NMR (400 MHz, $CDCl_3$) δ 7.56 – 7.48 (m, 2H), 7.36 – 7.29 (m, 2H), 7.23 – 7.17 (m, 4H), 7.16 (d, *J* = 1.6 Hz, 1H), 6.65 (d, *J* = 11.6 Hz, 1H), 6.56 (dd, *J* = 11.6, 2.0 Hz, 1H), 2.49 (s, 3H), 2.45 (s, 3H), 1.01 (s, 12H). ^{13}C NMR (101 MHz, $CDCl_3$) δ 142.8, 139.0, 137.2, 136.3, 134.7, 130.9, 130.4, 130.1, 129.3, 126.9, 125.9, 83.7, 24.6, 16.3, 15.6 (*C*-B not observed).^{11}B NMR (128 MHz, $CDCl_3$) δ 31.7. HRMS calcd for $C_{24}H_{30}BO_2S_2^+$ $[M+H]^+$ 425.1780 m/z, found 425.1768 m/z. Δ 2.8224.

2-((1*Z*,3*Z*)-1,4-bis(4-(trifluoromethyl)phenyl)buta-1,3-dien-2-yl)-4,4,5,5-tetramethyl-1,3,2-

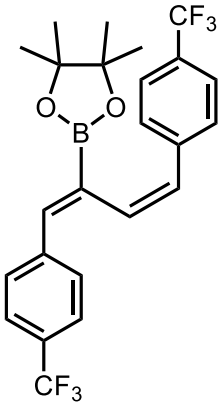

dioxaborolane (1.59j), Synthesized according to **Procedure 4.8**. Isolated from 0-10% EtOAc:Hex as a yellow solid in 49% yield (57.6 mg, 0.123 mmol). **^{1}H NMR** (400 MHz, $CDCl_3$) δ 7.67 (d, *J* = 8.2 Hz, 2H), 7.61 (d, *J* = 8.2 Hz, 2H), 7.56 (d, *J* = 8.2 Hz, 2H), 7.48 (d, *J* = 8.2 Hz, 2H), 7.29 (s, 1H), 6.76 (d, *J* = 11.7 Hz, 1H), 6.65 (dd, *J* = 11.8, 2.0 Hz, 1H), 0.99 (s, 12H). **^{13}C NMR** (126 MHz, $CDCl_3$) δ 142.7, 140.8, 136.5, 131.9, 130.9, 130.1, 129.6, 128.8, 127.1, 125.3 (q, *J* = 5.4 Hz), 125.2 (q, *J* = 5.6 Hz), 123.1 (q, *J* = 271.4 Hz), 123.0 (q, *J* = 271.4 Hz), 83.8, 24.4 (*C*-B not observed).**^{11}B NMR** (128 MHz, $CDCl_3$) δ 30.0. **^{19}F NMR** (376 MHz, $CDCl_3$) δ -62.53, -62.54. HRMS calcd for $C_{24}H_{24}BF_6O_2^+$ $[M+NH_4]^+$ 486.2039 m/z, found 486.2020 m/z. Δ 3.9078.

2-((1*Z*,3*Z*)-1,4-bis(4-(trifluoromethoxy)phenyl)buta-1,3-dien-2-yl)-4,4,5,5-tetramethyl-1,3,2-dioxaborolane (1.59k), Synthesized according to **Procedure 4.8**. Isolated from 0-10% EtOAc:Hex as a yellow oil in 67% yield (82.8 mg, 0.168 mmol). **^{1}H NMR** (400 MHz, $CDCl_3$) δ 7.60 (d, *J* = 8.7 Hz, 2H), 7.40 (d, *J* = 8.6 Hz, 2H), 7.21 (s, 1H), 7.19 (d, *J* = 7.9 Hz, 2H), 7.15 (d, *J* = 7.8 Hz, 2H), 6.69 (d, *J* = 11.7 Hz, 1H), 6.58 (dd, *J* = 11.7, 2.0 Hz, 1H), 1.00 (s, 12H). **^{13}C NMR** (126 MHz, $CDCl_3$) δ 148.9, 148.2, 142.3, 137.6, 136.2, 130.9, 130.8, 130.5, 130.0, 121.5 (q, *J* = 256.7 Hz), 121.1, 120.6, 119.4 (q, *J* = 257.6 Hz), 83.7, 24.4(*C*-B not observed). **^{11}B NMR** (128 MHz, $CDCl_3$) δ 28.4. **^{19}F NMR** (376 MHz, $CDCl_3$) δ -57.7, -58.0. HRMS calcd for $C_{24}H_{24}BF_6O_4^+$ $[M+NH_4]^+$, 518.1937 m/z found 518.1950 m/z. Δ 2.5087.

2-((1*Z*,3*Z*)-1,4-bis(4-fluorophenyl)buta-1,3-dien-2-yl)-4,4,5,5-tetramethyl-1,3,2-dioxaborolane (1.59l) – Modified from **Procedure 4.8**: 1.2 equivalence pinacolborane, reaction time 1 hour. Isolated from 0-10% EtOAc:Hex as a yellow oil in 71% yield (65.3 mg, 0.178 mmol). **^{1}H NMR** (500 MHz, $CDCl_3$) δ 7.57 (dd, *J* = 8.7, 5.6 Hz, 2H), 7.36 (dd, *J* = 8.6, 5.6 Hz, 2H), 7.19 (d, *J* = 1.6 Hz, 1H), 7.04 (dd, *J* = 9.1, 8.7 Hz, 2H), 6.98 (dd, *J* = 9.0, 8.8 Hz, 2H), 6.66 (d, *J* = 11.6 Hz, 1H), 6.53 (dd, *J* = 11.6, 2.1 Hz, 1H), 1.02 (s, 12H). **^{13}C NMR** (126 MHz, $CDCl_3$) δ 162.6 (d, *J* = 248.9 Hz),162.1 (d, *J* = 246.6 Hz), 142.6, 135.1 (d, *J* = 3.2 Hz), 134.0 (d, *J* = 3.4 Hz), 131.4 (d, *J* = 8.1 Hz), 130.6, 130.4 (d, *J* = 7.8 Hz), 130.1 (d, *J* = 1.6 Hz), 115.4 (d, *J* = 9.5 Hz), 115.2 (d, *J* = 9.5 Hz), 83.7, 24.6, (*C*-B not observed). **^{11}B NMR** (128 MHz, $CDCl_3$) δ 30.3. **^{19}F NMR** (376 MHz, $CDCl_3$) δ -112.62, -114.97. HRMS calcd for $C_{22}H_{24}BF_2O_2^+$ $[M+ H]^+$ 369.1837 m/z**,** found 369.1825 m/z. Δ 3.2504.

2-((1*Z*,3*Z*)-1,4-bis(3-fluorophenyl)buta-1,3-dien-2-yl)-4,4,5,5-tetramethyl-1,3,2-

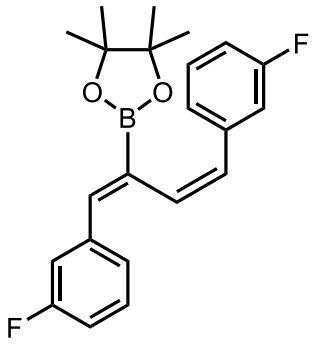

dioxaborolane (1.59m) – Modified from **Procedure 4.8**: 1.2 equivalence pinacolborane, reaction time 1 hour. Isolated from 0-10% EtOAc:Hex as a yellow oil in 92% yield (84.6 mg, 0.230 mmol). **^{1}H NMR** (400 MHz, $CDCl_3$) δ 7.36 – 7.27 (m, 3H), 7.25 – 7.22 (m, 1H), 7.21 (d, *J* = 2.9 Hz, 1H), 7.16 (dt, *J* = 7.9, 1.5 Hz, 1H), 7.09 (ddd, *J* = 10.3, 2.6, 1.6 Hz, 1H), 7.03 – 6.96 (m, 1H), 6.91 (tdd, *J* = 8.4, 2.6, 1.1 Hz, 1H), 6.68 (d, *J* = 11.8 Hz, 1H), 6.60 (dd, *J* = 11.8, 2.0 Hz, 1H), 1.02 (s, 12H). **^{13}C NMR** (101 MHz, $CDCl_3$) δ 163.1 (d, *J* = 245.2 Hz), 162.8 (d, *J* = 245.1 Hz), 142.6 (d, *J* = 2.5 Hz), 141.1 (d, *J* = 7.7 Hz), 139.9 (d, *J* = 7.7 Hz), 131.2, 130.9 (d, *J* = 2.4 Hz), 129.9 (d, *J* = 8.2 Hz), 129.8 (d, *J* = 8.3 Hz) , 125.6 (d, *J* = 2.8 Hz), 124. 7 (d, *J* = 2.8 Hz), 116.1 (d, *J* = 21.7 Hz), 115.5 (d, *J* = 21.6 Hz), 115.3 (d, *J* = 21.4 Hz), 114.1 (d, *J* = 21.2 Hz), 83.8, 24.6, (*C*-B not observed). **^{11}B NMR** (128 MHz, $CDCl_3$) δ 29.35. **^{19}F NMR** (376 MHz, $CDCl_3$) δ -113.27, -113.68. HRMS calcd for $C_{22}H_{24}BF_2O_2^+$ $[M+H]^+$ 369.1837 m/z**,** found 369.1841 m/z. Δ 1.0835.

2-((1*Z*,3*Z*)-1,4-bis(4-chlorophenyl)buta-1,3-dien-2-yl)-4,4,5,5-tetramethyl-1,3,2-

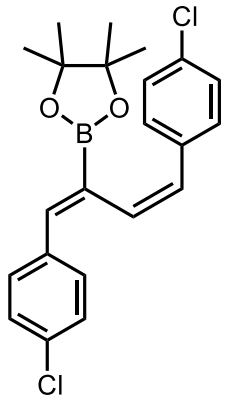

dioxaborolane (1.59n), Synthesized according to **Procedure 4.8**. Isolated from 0-10% EtOAc:Hex as a yellow oil in 65% yield (65.0 mg, 0.163 mmol). **^{1}H NMR** (400 MHz, $CDCl_3$) δ 7.51 (d, *J* = 8.5 Hz, 2H), 7.31 (d, *J* = 9.2 Hz, 4H), 7.28 – 7.23 (m, 2H), 7.18 (d, *J* = 2.0 Hz, 1H), 6.65 (d, *J* = 11.7 Hz, 1H), 6.55 (dd, *J* = 11.7, 2.0 Hz, 1H), 1.02 (s, 12H). **^{13}C NMR** (101 MHz, $CDCl_3$) δ 142.6, 137.4, 136.2, 134.2, 133.0, 130.9, 130.7, 130.7, 130.1, 128.6, 128.6, 83.8, 24.6, (*C*-B not observed). **^{11}B NMR** (128 MHz, $CDCl_3$) δ

29.9. HRMS calcd for $C_{22}H_{24}BCl_2O_2^+$ $[M+CH_3OH+H]^+$ 433.1509 m/z, found 433.1491 m/z. Δ 4.1556.

2-((1*Z*,3*Z*)-1,4-bis(3-chlorophenyl)buta-1,3-dien-2-yl)-4,4,5,5-tetramethyl-1,3,2-

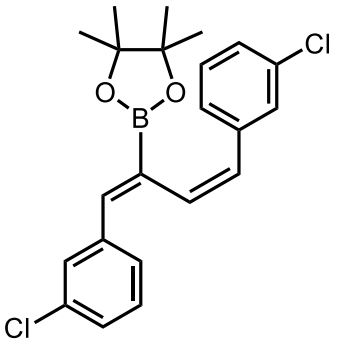

dioxaborolane (1.59o), Synthesized according to **Procedure 4.8**. Isolated from 0-10% EtOAc:Hex as a yellow oil in 55**%** yield. (55.0 mg, 0.138 mmol) **, ^{1}H NMR** (400 MHz, $CDCl_3$) δ 7.56 (s, 1H), 7.45 – 7.42 (m, 1H), 7.37 (s, 1H), 7.29 – 7.27 (m, 2H), 7.25 – 7.24 (m, 1H), 7.22 (s, 1H), 7.20 – 7.17 (m, 2H), 6.66 (d, *J* = 11.8 Hz, 1H), 6.59 (dd, *J* = 11.7, 2.0 Hz, 1H), 1.02 (s, 12H). **^{13}C NMR** (101 MHz, $CDCl_3$) δ 142.5, 140.7, 139.4, 134.5, 134.3, 131.2, 130.8, 129.7, 129.6, 129.4, 128.7, 128.4, 127.9, 127.3, 127.1, 83.9, 24.6, (*C*-B not observed). **^{11}B NMR** (128 MHz, $CDCl_3$) δ 30.2. HRMS calcd for $C_{45}H_{51}B_2Cl_4O_5^+$ $[2M+MeOH+H]^+$ 833.2671 m/z, found 833.2650 m/z. Δ 2.5202.

2-((1*Z*,3*Z*)-1,4-bis(2-chlorophenyl)buta-1,3-dien-2-yl)-4,4,5,5-tetramethyl-1,3,2-

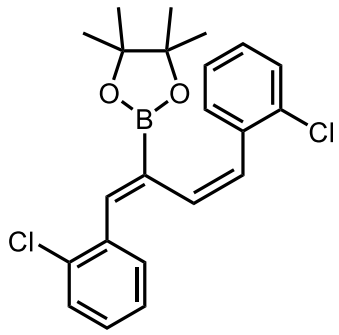

dioxaborolane (1.59p), Synthesized according to **Procedure 4.8**. Isolated from 0-10% EtOAc:Hex as a yellow oil in 34**%** yield (34.1 mg ,0.085 mmol). **^{1}H NMR** (400 MHz, $CDCl_3$) δ 7.71 – 7.62 (m, 1H), 7.45 – 7.34 (m, 4H), 7.25 – 7.22 (m, 2H), 7.20 – 7.16 (m, 2H), 6.78 (d, *J* = 11.4 Hz, 1H), 6.54 (dd, *J* = 11.6, 1.9 Hz, 1H), 0.97 (s, 12H). **^{13}C NMR** (101 MHz, $CDCl_3$) δ 140.3, 137.4, 135.7, 134.0, 131.2, 130.9, 130.6, 129.7, 129.6, 129.5, 129.4, 128.6, 126.7, 126.3, 83.7, 24.6, (*C*-B not observed). **^{11}B NMR** (128 MHz, $CDCl_3$) δ 30.1. HRMS calcd for $C_{22}H_{23}BCl_2NaO_2^+$ $[M+Na]^+$ 423.1066 m/z, found 423.1053 m/z. Δ -3.0725.

2-((1*Z*,3*Z*)-1,4-di(thiophen-2-yl)buta-1,3-dien-2-yl)-4,4,5,5-tetramethyl-1,3,2-dioxaborolane

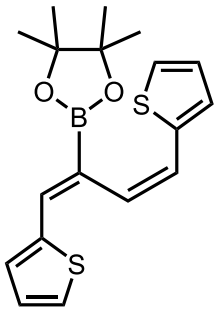

(1.59q), Synthesized according to **Procedure 4.8**. Isolated from 0-10% EtOAc:Hex as a yellow oil in 76% yield (65.4 mg, 0.190 mmol). **^{1}H NMR** (400 MHz, $CDCl_3$) δ 7.50 (dd, *J* = 2.2, 1.0 Hz, 1H), 7.34 (d, *J* = 5.1 Hz, 1H), 7.25 – 7.23 (m, 1H), 7.17 (dd, *J* = 5.1, 1.2 Hz, 1H), 7.06 – 7.01 (m, 2H), 6.95 (dd, *J* = 5.1, 3.6 Hz, 1H), 6.89 – 6.85 (m, 1H), 6.52 (dd, *J* = 11.4, 2.2 Hz, 1H), 1.15 (s, 12H). **^{13}C NMR** (101 MHz, $CDCl_3$) δ 141.6, 141.4, 137.3, 130.0, 128.6, 128.4, 127.5, 127.1, 127.1, 125.9, 125.2, 83.8, 24.8, (*C*-B not observed). **^{11}B NMR** (128 MHz, $CDCl_3$) δ 30.1. HRMS calcd for $C_{18}H_{22}BO_2S_2^+$ $[M+H]^+$ 345.1154 m/z, found 345.1158 m/z. Δ 1.1590.

2-(3-(4-((1*Z*,3*E*)-4-phenyl-2-(4,4,5,5-tetramethyl-1,3,2-dioxaborolan-2-yl)buta-1,3-dien-1-yl)phenoxy)propyl)isoindoline-1,3-dione (1.59r) –

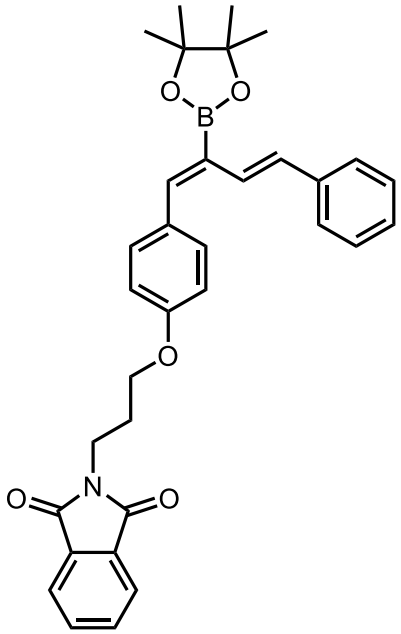

Synthesized according to **Procedure 4.8**. Isolated from 5-30% EtOAc:Hex as a white solid in 55% yield (73.6 mg, 0.138 mmol). **^{1}H NMR** (400 MHz, $CDCl_3$) δ 7.81 (dd, *J* = 5.5, 3.0 Hz, 2H), 7.69 (dd, *J* = 5.5, 3.0 Hz, 2H), 7.38 (d, *J* = 7.2 Hz, 2H), 7.37 – 7.25 (m, 5H), 7.25 (d, *J* = 7.1 Hz, 1H), 6.96 (d, *J* = 16.2 Hz, 1H), 6.72 (d, *J* = 8.7 Hz, 2H), 6.34 (d, *J* = 16.2 Hz, 1H), 4.01 (t, *J* = 6.0 Hz, 2H), 3.88 (t, *J* = 6.8 Hz, 2H), 2.16 (p, *J* = 6.4 Hz, 2H), 1.24 (s, 12H). **^{13}C NMR** (101 MHz, $CDCl_3$) δ 168.5, 158.8, 140.5, 136.6, 134.1, 133.0, 132.2, 128.8, 128.5, 126.3, 115.7, 114.6, 108.5, 92.0, 87.7, 65.8, 35.5, 28.3, 24.6, 24.2, (*C*-B not observed). **^{11}B NMR** (128 MHz, $CDCl_3$) δ 22.4. HRMS calcd for $C_{33}H_{35}BNO_5^+$ $[M+H]^+$ 536.2608 m/z, found 536.2617 m/z. Δ 1.6783.

2-((1*Z*,3*E*)-1-(4-methoxyphenyl)-4-phenylbuta-1,3-dien-2-yl)-4,4,5,5-tetramethyl-1,3,2-dioxaborolane (1.59s) – Synthesized according **Procedure 4.8**. Isolated from 0-15% EtOAc:Hex as a white solid in 60% yield (54.3 mg, 0.150 mmol). **^{1}H NMR** (400 MHz, $CDCl_3$) δ 7.45 – 7.27 (m, 8H), 7.24 – 7.17 (m, 2H), 6.91 (d, *J* = 8.8 Hz, 2H), 3.84 (s, 3H), 1.37 (s, 12H). **^{13}C NMR** (101 MHz, $CDCl_3$) δ 159.3, 143.3, 138.7, 133.1, 131.5, 130.6, 128.6, 128.1, 127.2, 126.6, 113.8, 83.7, 55.4, 25.0. (*C*-B not observed). **^{11}B NMR** (128 MHz, $CDCl_3$) δ 30.9. HRMS calcd for $C_{23}H_{28}BO_3^+$ $[M+H]^+$ 363.2131 m/z**,** found 363.2132 m/z. Δ 0.2753.

N,N-dimethyl-4-((1*Z*,3*E*)-4-phenyl-2-(4,4,5,5-tetramethyl-1,3,2-dioxaborolan-2-yl)buta-1,3-dien-1-yl)aniline (1.59t) – Synthesized according to **Procedure 4.8**. Isolated from 0-15% EtOAc:Hex as a yellow solid in 32% yield (30.0 mg, 0.080 mmol). **^{1}H NMR** (400 MHz, $CDCl_3$) δ 7.45 – 7.34 (m, 5H), 7.32 – 7.27 (m, 2H), 7.25 – 7.19 (m, 2H), 7.19 – 7.14 (m, 1H), 6.71 (d, *J* = 8.8 Hz, 2H), 3.00 (s, 6H), 1.36 (s, 12H). **^{13}C NMR** (101 MHz, $CDCl_3$) δ 150.0, 144.3, 139.0, 132.1, 131.6, 128.9, 128.6, 126.9, 126.5, 123.5, 111.8, 83.5, 40.4, 25.0, (*C*-B not observed). **^{11}B NMR** (128 MHz, $CDCl_3$) δ 30.7. HRMS calcd for $C_{24}H_{31}BNO_2^+$ $[M+H]^+$ 376.2448 m/z**,** found 376.2447 m/z. Δ 0.2658.

trimethyl((1*Z*,3*E*)-4-phenyl-2-(4,4,5,5-tetramethyl-1,3,2-dioxaborolan-2-yl)buta-1,3-dien-1-yl)silane (1.59u) – Synthesized according to **Procedure 4.8**. Isolated from 0-5% EtOAc:Hex as a colorless oil in 52% yield (42.6 mg, 0.130 mmol). **^{1}H NMR** (400 MHz, $CDCl_3$) δ 7.60 (d, *J* = 10.8 Hz, 1H), 7.43 (d, *J* = 7.7 Hz, 2H), 7.40 – 7.32 (m, 2H), 7.28 (d, *J* = 7.3 Hz, 1H), 7.24

– 7.16 (m, 1H), 6.74 (d, *J* = 15.2 Hz, 1H), 1.30 (s, 12H), 0.30 (s, 9H). **^{13}C NMR** (101 MHz, $CDCl_3$) δ 156.1, 137.9, 137.2, 129.7, 128.8, 128.3, 127.0, 83.1, 24.9, 1.5, (*C*-B not observed). **^{11}B NMR** (128 MHz, $CDCl_3$) δ 31.6. HRMS calcd for $C_{19}H_{30}BO_2Si^+$ $[M+H]^+$ 329.2108 m/z**,** found 329.2116 m/z. Δ 2.4301.

4,4,5,5-tetramethyl-2-((1*E*,3*Z*)-1-phenylpenta-1,3-dien-3-yl)-1,3,2-dioxaborolane (1.59v) –

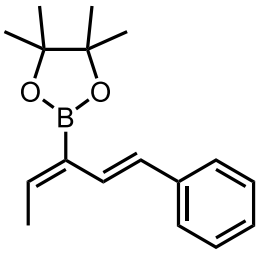

Synthesized according to **Procedure 4.8**. Isolated from 0-10% EtOAc:Hex as a colorless oil in 14% yield (9.45 mg, 0.035 mmol). **^{1}H NMR** (400 MHz, $CDCl_3$) δ 7.45 (d, *J* = 6.8 Hz, 2H), 7.31 (t, *J* = 7.5 Hz, 2H), 7.22 (d, *J* = 13.7 Hz, 1H), 7.18 (d, *J* = 12.3 Hz, 1H), 7.14 (d, *J* = 6.7 Hz, 1H), 6.51 (q, *J* = 7.2 Hz, 1H), 1.94 (d, *J* = 7.1 Hz, 3H), 1.32 (s, 12H). **^{13}C NMR** (101 MHz, $CDCl_3$) δ 142.7, 138.7, 132.1, 128.6, 127.2, 126.5, 126.2, 83.4, 25.0, 14.9. (*C*-B not observed). **^{11}B NMR** (128 MHz, $CDCl_3$) δ 30.5. HRMS calcd for $C_{17}H_{24}BO_2^+$ $[M+H]^+$ 271.1869 m/z**,** found 271.1873 m/z. Δ 1.4750.

4-((1*Z*,3*E*)-4-phenyl-2-(4,4,5,5-tetramethyl-1,3,2-dioxaborolan-2-yl)buta-1,3-dien-1-yl)benzyl (R)-2-(6-methoxynaphthalen-2-yl)propanoate (1.59w) – Synthesized according **Procedure 4.8**. Isolated from 0-20% EtOAc:Hex as a yellow oil in 41% yield (58.8 mg, 0.103 mmol). **^{1}H NMR** (400 MHz, $CDCl_3$) δ 7.71 – 7.65 (m, 3H), 7.41 (d, *J* = 1.9 Hz, 1H), 7.39 (dt, *J* = 6.6, 1.3 Hz, 2H), 7.32 (d, *J* = 8.0 Hz, 2H), 7.28 (d, *J* = 8.0 Hz, 2H), 7.29 – 7.17 (m, 6H), 7.12 (dd, *J* = 8.8, 2.5 Hz, 1H), 7.09 (d, *J* = 2.5 Hz, 1H), 5.16 (d, *J* = 12.7 Hz, 1H), 5.10 (d, *J* = 12.7 Hz, 1H), 3.93 (q, *J* = 7.5 Hz, 1H), 3.89 (s, 3H), 1.61 (d, *J* = 7.1 Hz, 3H), 1.37 (s, 12H). **^{13}C NMR** (101 MHz,

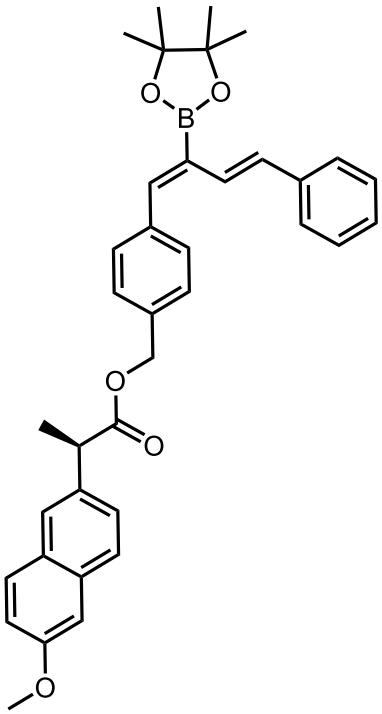

$CDCl_3$) δ 174.6, 157.8, 142.8, 138.4, 137.7, 135.7, 135.4, 134.0, 133.9, 130.0, 129.4, 129.1, 128.6, 127.6, 127.4, 127.3, 126.7, 126.4, 126.2, 119.1, 105.7, 83.8, 66.3, 60.5, 45.6, 25.0, 18.7, 14.3, (*C*-B not observed). **^{11}B NMR** (128 MHz, $CDCl_3$) δ 28.2. HRMS calcd for $C_{37}H_{39}BNaO_5^+$ $[M+Na]^+$ 597.2788 m/z**,** found 597.2792 m/z. Δ 0.6697.

4-((1*Z*,3*E*)-4-phenyl-2-(4,4,5,5-tetramethyl-1,3,2-dioxaborolan-2-yl)buta-1,3-dien-1-yl)benzyl 5-(2,5-dimethylphenoxy)-2,2-dimethylpentanoate (1.59x) – Synthesized according to **Procedure 4.8**. Isolated from 0-20% EtOAc:Hex as a yellow oil in 49% yield (72.8 mg, 0.123 mmol). **^{1}H NMR** (400 MHz, $CDCl_3$) δ 7.41 (d, *J* = 2.2 Hz, 2H), 7.39 (d, *J* = 3.4 Hz, 2H), 7.35 (s, 1H), 7.33 (d, *J* = 6.5 Hz, 2H), 7.29 (dd, *J* = 6.3, 1.9 Hz, 4H), 7.23 (d, *J* = 7.2 Hz, 1H), 7.20 (d, *J* = 7.3 Hz, 1H), 6.65 (d, *J* = 7.4 Hz, 1H), 6.60 (s, 1H), 5.14 (s, 2H), 3.90 (t, *J* = 5.5 Hz, 2H), 2.30 (s, 3H), 2.16 (s, 3H), 1.76 (m, 4H), 1.39 (s, 12H), 1.28 (s, 6H). **^{13}C NMR** (101 MHz, $CDCl_3$) δ 177.8, 157.1, 142.8, 138.4, 137.7, 136.6, 135.8, 134.0, 130.4, 130.0, 128.6, 127.7, 127.6, 127.4, 126.7, 123.7, 120.8, 112.1, 83.8, 68.0, 66.0, 42.3, 37.3, 25.3, 25.0, 24.9, 21.5, 15.9, (*C*-B not observed). **^{11}B NMR** (128 MHz, $CDCl_3$) δ 29.2. HRMS calcd for $C_{38}H_{48}BO_5^+$ $[M+H]^+$ 595.3595 m/z**,** found 595.3584 m/z. Δ 1.8476.

Procedures and Characterization of 2-Boryl-1,3-Diene Applications:

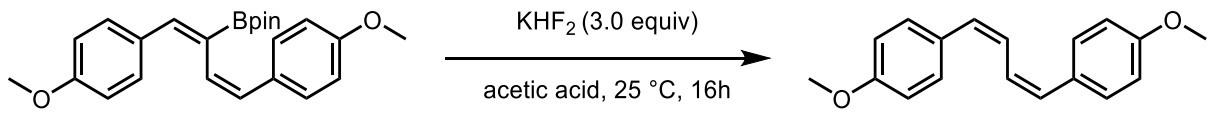

1.59f **1.60**

Scheme 4.9: Protodeboration of 2-boryl-1,3-diene **1.59f**.

Procedure 4.9: To a two-dram vial: a stir bar, 2-((1*Z*,3*Z*)-1,4-bis(4-methoxyphenyl)buta-1,3-dien-2-yl)-4,4,5,5-tetramethyl-1,3,2-dioxaborolane, **1.59f** (0.125 mmol, 1.0 equiv, 49.0 mg), KHF_2 (0.375 mmol, 3.0 equiv, 29.3 mg) and 0.50 mL of acetic acids were added. The reaction was allowed to stir overnight. The reaction was quenched with sodium carbonate and extracted with ethyl acetate (5.0 mL x 3). The organic layer was reduced under vacuum and compound (1*Z*,3*Z*)-1,4-bis(4-methoxyphenyl)buta-1,3-diene **1.60** was isolated via flash chromatography (0-10% EtOAc:Hex) as a white solid in 54% yield (18.0 mg). **^{1}H NMR** (400 MHz, $CDCl_3$) δ 7.37 (dd, *J* = 8.8, 2.1 Hz, 4H), 6.90 (dd, *J* = 8.7, 2.3 Hz, 4H), 6.62 (ddd, *J* = 10.5, 1.7, 0.59 Hz, 2H), 6.49 (ddd, *J* = 10.1, 8.0, 2.0 Hz, 2H), 3.84 (s, 6H). **^{13}C NMR** (101 MHz, $CDCl_3$) δ 158.9, 131.1, 130.6, 125.4, 122.3, 113.8, 55.5. HRMS calcd for $C_{18}H_{19}O_2^+$ $[M+H]^+$ 267.1385 m/z, found 267.1377 m/z. Δ -2.9947.

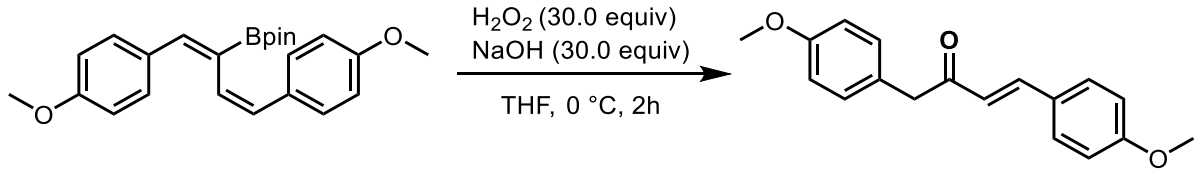

1.59f
>99:1 (*Z*:*E*)

1.61
1:>99 (*Z*:*E*)

Scheme 4.10: Basic peroxide oxidation of 2-boryl-1,3-diene **5**.

Procedure 4.10: To a two-dram vial: a stir bar, 2-((1*Z*,3*Z*)-1,4-bis(4-methoxyphenyl)buta-1,3-dien-2-yl)-4,4,5,5-tetramethyl-1,3,2-dioxaborolane **1.50f** (0.125 mmol, 1.0 equiv, 49.0 mg) and THF (0.5 mL) were added. The reaction vial was put into an ice bath and allowed to cool to 0 °C. Then, 35 wt% hydrogen peroxide (3.75 mmol, 30.0 equiv, 0.25 mL) and 3M NaOH (3.75 mmol, 30.0 equiv, 1.25 mL) were added. The reaction was allowed to stir for 2 hours. Upon completion the reaction was quenched with saturated hydrogen sulfide (5.0 mL x 3) and extracted with ethyl acetate (5.0 mL x 3). The organic layer was reduced under vacuum and compound (*E*)-1,4-bis(4-methoxyphenyl)but-3-en-2-one, **1.61** was isolated via flash chromatography (0-30% EtOAc:Hex)

as a white solid in 54% yield (15.0 mg). **^{1}H NMR** (400 MHz, $CDCl_3$) δ 7.59 (d, *J* = 16.1 Hz, 1H), 7.47 (dd, *J* = 8.8, 1.3 Hz, 2H), 7.18 (d, *J* = 8.6 Hz, 2H), 6.89 (dd, *J* = 8.8, 5.4 Hz, 4H), 6.66 (d, *J* = 16.0 Hz, 1H), 3.85 (s, 2H), 3.84 (s, 3H), 3.80 (s, 3H). **^{13}C NMR** (126 MHz, $CDCl_3$) δ 197.8, 161.8, 158.7, 143.2, 130.6, 130.2, 127.3, 126.8, 123.1, 114.5, 114.3, 55.5, 55.4, 47.6. HRMS calcd for $C_{18}H_{19}O_3^+$ $[M+H]^+$ 283.1334 m/z, found 283.1332 m/z. Δ -0.7064.

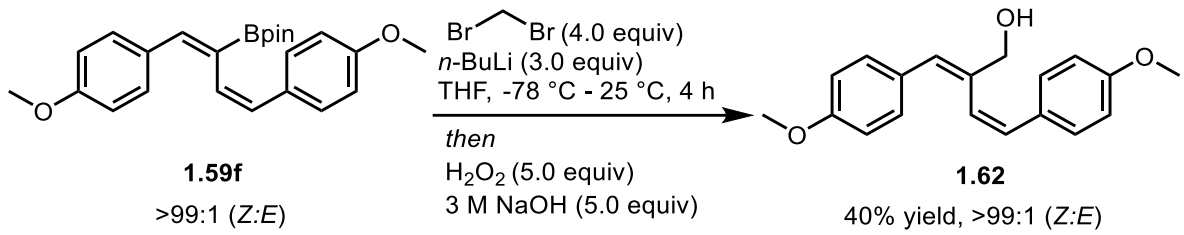

Scheme 4.11: Homologation-oxidation of 2-boryl-1,3-diene **1.59f**.

Procedure 4.11: This procedure was modified from literature. To a flame dried two-dram vial: a stir bar, dibromomethane (0.50 mmol, 4.0 equiv, 86.9 mg) and anhydrous THF (1 mL) were added. The vial was put under inert atmosphere using standard *Schlenk* technique. The reaction was put into a dry ice/acetone bath and allowed to cool to -78 °C. Then, 2.5 M *n*-BuLi in hexanes (0.375 mmol, 3.0 equiv, 150.0 µL) was added and the reaction was allowed to stir for 30 minutes. Then, 2-((1*Z*,3*Z*)-1,4-bis(4-methoxyphenyl)buta-1,3-dien-2-yl)-4,4,5,5-tetramethyl-1,3,2-dioxaborolane **1.59f** (0.125 mmol, 1.0 equiv, 49.0 mg) was added and the reaction was allowed to react for 1 hour. The reaction vessel was removed from the dry ice/acetone bath and allowed to stir at room temperature for 3 hours. After that, 35 wt% hydrogen peroxide (0.625 mmol, 5.0 equiv, 63.8 µL) and 3M NaOH (0.625 mmol, 5.0 equiv, 208.0 µL) were added and the reaction was allowed to stir at room temperature, overnight. Upon completion the reaction was quenched with saturated hydrogen sulfide (5.0 mL x 3) and extracted with ethyl acetate (5.0 mL x 3). The organic layer was reduced under vacuum and compound (*Z*)-2-((*E*)-4-methoxybenzylidene)-4-(4-methoxyphenyl)but-3-en-1-ol **1.62** was isolated via flash chromatography (0-25% EtOAc:Hex) as a yellow oil in 40% yield (14.8 mg). **^{1}H NMR** (500 MHz, $CDCl_3$) δ 7.72 (d, *J* = 8.8 Hz, 2H), 7.12

(d, J = 8.6 Hz, 2H), 6.89 – 6.84 (m, 5H), 6.72 (d, J = 12.8 Hz, 1H), 6.13 (d, J = 12.8 Hz, 1H), 3.83 (s, 3H), 3.79 (s, 3H), 3.73 (s, 2H). **^{13}C NMR** (126 MHz, $CDCl_3$) δ 199.7, 161.2, 159.0, 142.1, 132.8, 130.9, 130.5, 128.1, 127.0, 124.9, 114.5, 113.9, 55.7, 55.6, 50.5. HRMS calcd for $C_{38}H_{41}O_6^+$ $[2M+H]^+$ 593.2898 m/z, found 593.2889 m/z. Δ -1.5170.

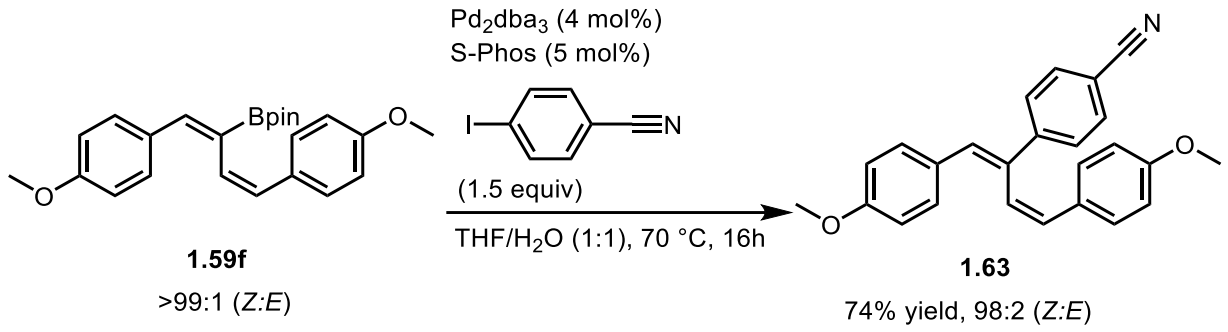

Scheme 4.12: Suzuki-Miyaura cross-coupling of 2-boryl-1,3-diene **1.59f** and 4-iodobenzonitrile.

Procedure 4.12: To a two-dram vial: a stir bar, 2-((1*Z*,3*Z*)-1,4-bis(4-methoxyphenyl)buta-1,3-dien-2-yl)-4,4,5,5-tetramethyl-1,3,2-dioxaborolane **1.59f** (0.125 mmol, 1.0 equiv, 49.0 mg), Pd_2dba_3 (5.28 μmol, 4 mol%, 2.17 mg), S-Phos (4.22 μmol, 5 mol%, 3.87 mg) and 4-iodobenzonitrile (0.158 mmol, 1.5 equiv, 36.3 mg) were added. The vial was sealed and put under inert atmosphere using standard *Schlenk* technique. Then THF : 3M NaOH (2.4 mL : 0.8 mL) were added and the reaction was heated to 60°C and allowed to react overnight. Ethyl acetate (5.0 mL x 3) was added to the mixture followed by extraction, treatment with sodium sulfate and concentration under vacuum. 4-((1*E*,3*Z*)-1,4-bis(4-methoxyphenyl)buta-1,3-dien-2-yl)benzonitrile **1.63** was isolated via flash chromatography (0-15% EtOAc:Hex) as a yellow solid in 74% yield (28.8 mg). **^{1}H NMR** (500 MHz, $CDCl_3$) δ 7.56 (d, J = 8.8 Hz, 2H), 7.49 (d, J = 8.0 Hz, 2H), 7.40 (d, J = 8.2 Hz, 2H), 7.08 (d, J = 8.7 Hz, 2H), 6.90 (d, J = 8.8 Hz, 2H), 6.86 (s, 1H), 6.75 (d, J = 12.0 Hz, 1H), 6.58 (d, J = 8.8 Hz, 2H), 6.49 (dd, J = 11.9, 1.9 Hz, 1H), 3.84 (s, 3H), 3.70 (s, 3H). **^{13}C NMR** (126 MHz, $CDCl_3$) δ 159.6, 159.0, 146.3, 135.6, 133.6, 133.1, 131.9, 131.3,

130.0, 129.4, 127.8, 126.0, 119.3, 113.9, 113.3, 110.0, 103.5, 55.5, 55.3. HRMS calcd for $C_{50}H_{42}N_2NaO_4^+$ $[2M+Na]^+$ 757.3037 m/z, found 757.3039 m/z. Δ 0.2641.

4.4. X-Ray Crystallography for Chapter 1

A large colorless prism was cut (0.24 × 0.38 × 0.45 mm^3) and centered on the goniometer of a Rigaku Oxford Diffraction Synergy-S diffractometer equipped with a HyPix6000HE detector and operating with MoKα radiation. The data collection routine, unit cell refinement, and data processing were carried out with the program CrysAlisPro.[7] The Laue symmetry and systematic absences were consistent with the monoclinic space group $P2_1/n$. The structure was solved using SHELXT[8] and refined using SHELXL[9] via Olex2.[10] The final refinement model involved anisotropic displacement parameters for non-hydrogen atoms and a riding model for all hydrogen atoms. Mercury[11] was used for molecular graphics generation.

Crystal Growth Procedure: Compound **1.59b** (yellow oil) was left in the freezer (0 °C) for approximately 3 months. During which time large colorless crystals formed which were sufficient for X-ray crystallography.

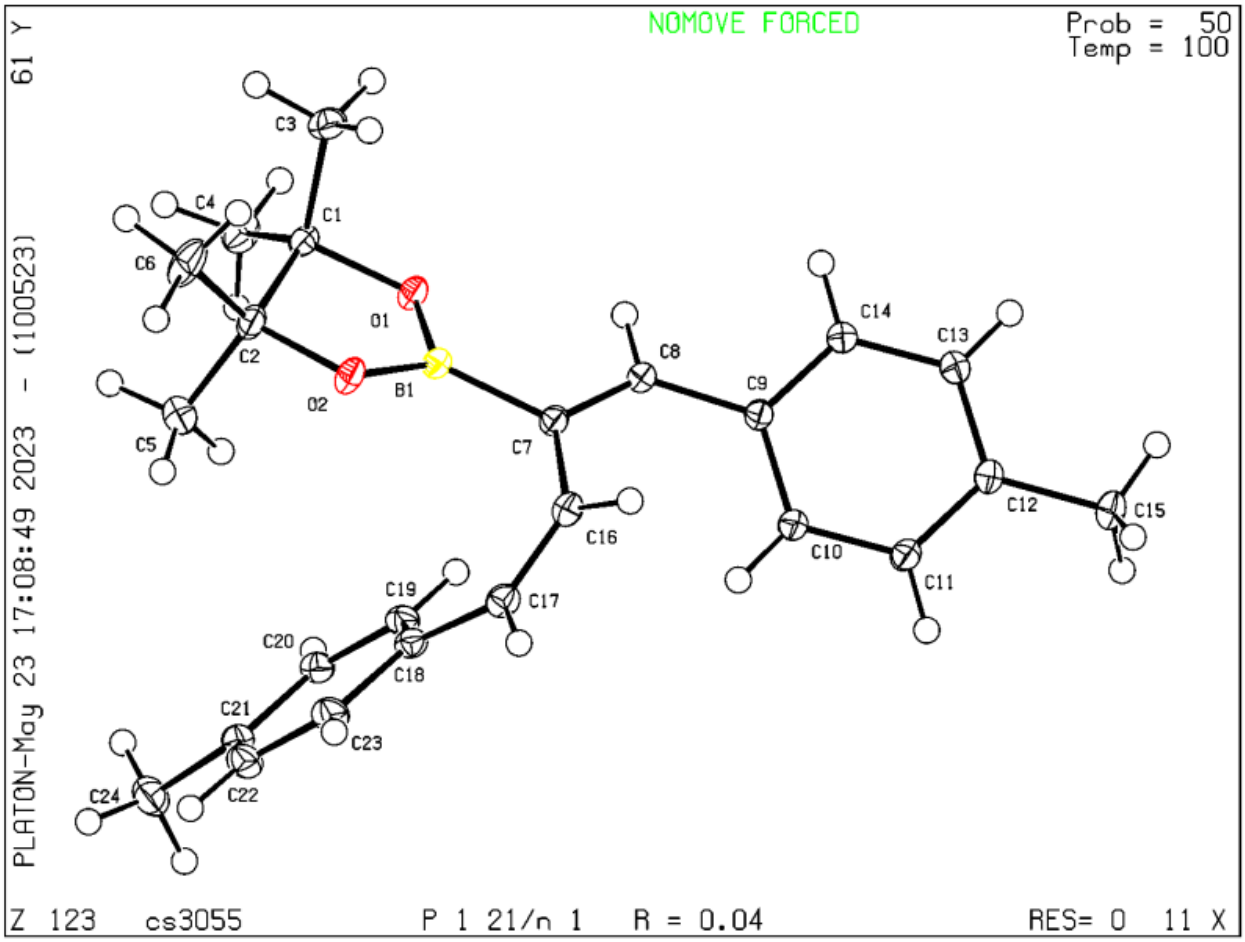

Figure 4.1: ORTEP diagram of **1.59b** with thermal ellipsoids at 50% probability level.

Table 4.2: Crystal data and structure refinement for cs3055 (1.59b).

Identification code	cs3055
Empirical formula	$C_{24}H_{29}BO_2$
Formula weight	360.28
Temperature/K	100
Crystal system	monoclinic
Space group	$P2_1/n$
a/Å	10.3788(2)
b/Å	16.4472(2)
c/Å	12.6082(2)
α/°	90
β/°	108.355(2)
γ/°	90
Volume/Å^3	2042.75(6)
Z	4
ρ_{calc}g/cm^3	1.171
μ/mm^{-1}	0.072
F(000)	776.0
Crystal size/mm^3	0.45 × 0.38 × 0.24
Radiation	Mo Kα (λ = 0.71073)
2Θ range for data collection/°	6.454 to 76.528
Index ranges	-17 ≤ h ≤ 17, -28 ≤ k ≤ 28, -21 ≤ l ≤ 21
Reflections collected	93612
Independent reflections	10844 [R_{int} = 0.0379, R_{sigma} = 0.0214]
Data/restraints/parameters	10844/0/250
Goodness-of-fit on F^2	1.047
Final R indexes [I>=2σ (I)]	R_1 = 0.0408, wR_2 = 0.1171
Final R indexes [all data]	R_1 = 0.0498, wR_2 = 0.1220
Largest diff. peak/hole / e Å^{-3}	0.58/-0.32

Crystal data as a footnote:
Crystal Data for cs3055 (1.59b). $C_{24}H_{29}BO_2$ (*M* =360.28 g/mol): monoclinic, space group $P2_1/n$ (no. 14), *a* = 10.3788(2) Å, *b* = 16.4472(2) Å, *c* = 12.6082(2) Å, *β* = 108.355(2)°, *V* = 2042.75(6) Å^3, *Z* = 4, *T* = 100 K, μ(Mo Kα) = 0.072 mm^{-1}, *Dcalc* = 1.171 g/cm^3, 93612 reflections measured (6.454° ≤ 2Θ ≤ 76.528°), 10844 unique (R_{int} = 0.0379, R_{sigma} = 0.0214) which were used in all calculations. The final R_1 was 0.0408 (I > 2σ(I)) and wR_2 was 0.1220 (all data).

Table 4.4b Bond Lengths for cs3055 (1.59b)

Atom	Atom	Length/Å	Atom	Atom	Length/Å
B1	O1	1.3723(7)	C10	C11	1.3913(8)
B1	O2	1.3651(7)	C11	C12	1.3980(8)
B1	C7	1.5616(8)	C12	C13	1.3937(8)
O1	C1	1.4617(7)	C12	C15	1.5073(8)
O2	C2	1.4602(7)	C13	C14	1.3918(8)
C1	C2	1.5666(8)	C16	C17	1.3470(8)
C1	C3	1.5224(8)	C17	C18	1.4677(8)
C1	C4	1.5202(8)	C18	C19	1.4025(8)
C2	C5	1.5225(9)	C18	C23	1.4030(8)
C2	C6	1.5170(9)	C19	C20	1.3898(8)
C7	C8	1.3590(8)	C20	C21	1.3977(8)
C7	C16	1.4772(8)	C21	C22	1.3960(9)
C8	C9	1.4667(7)	C21	C24	1.5044(9)
C9	C10	1.4025(8)	C22	C23	1.3924(9)
C9	C14	1.4012(8)			

Table 4.4c Bond Angles for cs3055 (1.59b)

Atom	Atom	Atom	Angle/°	Atom	Atom	Atom	Angle/°
O1	B1	C7	122.95(5)	C14	C9	C8	118.65(5)
O2	B1	O1	113.34(5)	C14	C9	C10	117.53(5)
O2	B1	C7	123.68(5)	C11	C10	C9	120.88(5)
B1	O1	C1	107.55(4)	C10	C11	C12	121.37(5)
B1	O2	C2	107.79(4)	C11	C12	C15	120.72(5)
O1	C1	C2	102.78(4)	C13	C12	C11	117.79(5)
O1	C1	C3	106.88(5)	C13	C12	C15	121.48(5)
O1	C1	C4	107.94(5)	C14	C13	C12	121.11(5)
C3	C1	C2	112.85(5)	C13	C14	C9	121.24(5)
C4	C1	C2	115.35(5)	C17	C16	C7	128.04(5)
C4	C1	C3	110.32(5)	C16	C17	C18	128.19(5)
O2	C2	C1	102.70(4)	C19	C18	C17	122.95(5)
O2	C2	C5	107.18(5)	C19	C18	C23	117.56(5)
O2	C2	C6	108.09(5)	C23	C18	C17	119.40(5)
C5	C2	C1	113.71(5)	C20	C19	C18	121.08(5)
C6	C2	C1	114.33(5)	C19	C20	C21	121.15(5)
C6	C2	C5	110.17(6)	C20	C21	C24	120.70(6)
C8	C7	B1	117.46(5)	C22	C21	C20	118.07(5)
C8	C7	C16	122.62(5)	C22	C21	C24	121.17(5)
C16	C7	B1	119.58(5)	C23	C22	C21	120.92(5)
C7	C8	C9	128.62(5)	C22	C23	C18	121.20(5)
C10	C9	C8	123.77(5)				

Table 4.4d Torsion Angles for cs3055 (1.59b).

A	B	C	D	Angle/°	A	B	C	D	Angle/°
B1	O1	C1	C2	-19.47(6)	C7	C8	C9	C14	-156.71(6)
B1	O1	C1	C3	99.54(5)	C7	C16	C17	C18	8.44(10)
B1	O1	C1	C4	-141.80(5)	C8	C7	C16	C17	-137.59(6)
B1	O2	C2	C1	-20.05(6)	C8	C9	C10	C11	179.79(5)
B1	O2	C2	C5	100.03(6)	C8	C9	C14	C13	179.09(5)
B1	O2	C2	C6	-141.24(6)	C9	C10	C11	C12	0.30(9)
B1	C7	C8	C9	-179.83(5)	C10	C9	C14	C13	-3.14(9)
B1	C7	C16	C17	49.24(8)	C10	C11	C12	C13	-1.80(9)
O1	B1	O2	C2	8.77(7)	C10	C11	C12	C15	179.46(6)
O1	B1	C7	C8	16.53(8)	C11	C12	C13	C14	0.81(9)
O1	B1	C7	C16	-169.95(5)	C12	C13	C14	C9	1.70(9)
O1	C1	C2	O2	23.70(5)	C14	C9	C10	C11	2.15(9)
O1	C1	C2	C5	-91.75(5)	C15	C12	C13	C14	179.54(5)
O1	C1	C2	C6	140.52(5)	C16	C7	C8	C9	6.86(9)
O2	B1	O1	C1	7.79(6)	C16	C17	C18	C19	24.64(9)
O2	B1	C7	C8	-161.53(5)	C16	C17	C18	C23	-158.85(6)
O2	B1	C7	C16	11.99(8)	C17	C18	C19	C20	176.44(5)
C3	C1	C2	O2	-91.04(5)	C17	C18	C23	C22	-176.98(6)
C3	C1	C2	C5	153.50(5)	C18	C19	C20	C21	-0.40(9)
C3	C1	C2	C6	25.78(7)	C19	C18	C23	C22	-0.28(9)
C4	C1	C2	O2	140.89(5)	C19	C20	C21	C22	1.32(9)
C4	C1	C2	C5	25.43(7)	C19	C20	C21	C24	-175.82(6)
C4	C1	C2	C6	-102.30(6)	C20	C21	C22	C23	-1.73(9)
C7	B1	O1	C1	-170.46(5)	C21	C22	C23	C18	1.24(10)
C7	B1	O2	C2	-173.00(5)	C23	C18	C19	C20	-0.13(8)
C7	C8	C9	C10	25.67(9)	C24	C21	C22	C23	175.39(6)

This report has been created with Olex2, compiled on 2023.03.06 svn.rbb2c1857 for OlexSys.

4.5. Synthetic Procedures for Chapter 2

Introduction to Variable Time Normalization Analysis

Variable time normalization analysis (VTNA) is a very convenient way of elucidating the reaction orders of various reagents without measuring rates directly. Instead of measuring rates, the concentration of the substrate or product is measured. In this study, ^{1}H NMR was used to determine the concentration of product (**2.26**) at specific time points. In VTNA, plots are generated using concentration of **2.26** (x-axis) vs. the normalized time function (y-axis). The time function is normalized using the equation shown below.

$$\int_{t=0}^{t=n} [A]^x \, dt = \sum_{i=1}^{n} \left(\frac{[A]_i + [A]_{i-1}}{2} \right)^x (t_i - t_{i-1})$$

The equation shows the integrated rate law approximated using the trapezoid rule. Time is easily measured by indicating at which time point a concentration data point was collected. Concentration data is obtained, either directly through NMR analysis or inferred using stoichiometry ($[A]_t = [A]_0 - [\mathbf{2.26}]_t$). Therefore, the rate order "x" is the only unknown variable. To circumvent the necessity of experimentally determining the rate to solve for the rate order, two data sets are plotted on the same graph, one consists of the standard reaction conditions, and one consists of "excess" reaction conditions where the reagent which is being evaluated is used in excess. The rate order (x) is then systematically varied until the two datasets overlap with each other. The time normalization function removes the kinetic effect of the reagent from the reaction profile. Thus, when the appropriate rate order is substituted for "x" the two data sets converge. When all data sets are plotted together, the time normalization function is applied to each data set, and the correct rate orders are added, the datasets will converge and the slope corresponds to K_{obs} for the reaction.

VTNA has several advantages when compared to standard methods for measuring reaction kinetics, firstly, less experiments are required to determine the reaction orders. In our case, reaction progress profiles (non-time normalized plots using [**2.26**] vs. time) for standard reaction condition, excess HBpin, excess substrate **2.25**, and excess catalyst (CuOAc+Xantphos) were generated. Each of these experiments was duplicate and averaged. The reaction progress profile generated for the standard conditions are then compared to the three excess conditions individually and the time normalization function is applied. Including duplicates, only eight reactions were required to determine the reaction orders of three reagents. Another advantage of VTNA is that it allows for analysis of the reaction from start to finish rather than just the initial

part of the reaction like the initial rate method. However, it is important to note that visual analysis of reaction progress profiles is subject to human bias which is a limitation of this methodology.[12]

Procedure 4.13: Each experiment was run in duplicate and averaged. To a flame dried and sealed 2-dram vial: a stir bar, 250 µl of a 0.025 M solution of CuOAc (0.05 equiv, 6.25 µmol) and Xantphos (0.05 equiv, 6.25 µmol) in dichloromethane (DCM) was added. The DCM was removed under vacuum and the vial was put under inert atmosphere using standard *Schlenk* technique. Then, 500 µl of a 0.250 M solution of enyne **2.25** (1.0 equiv, 0.125) and 0.125 M solution of 1,2,4,5-tetramethylbenzene (internal standard, 0.50 equiv, 0.0625 mmol) in toluene was added. Finally, pinacolborane (2.0 equiv, 0.250 mmol) was added and a timer was started. Aliquots (10 µl) of the reaction were removed at recorded times, exposed to air, and diluted in $CDCl_3$. Formation of 2-boryl-1,3-diene **2.26** was tracked via ^1H NMR with 1,2,4,5-tetramethylbenzene as an internal standard.

Table 4.3: Concentration Data for Standard Conditions Reaction Progress Profile

Standard Conditions				
	Trial A	Trial B		
t (min)	[**2.26**] (M)	[**2.26**] (M)	Average [**2.26**] (M)	STD
0	0.000	0.000	0.000	0.000
1	0.008	0.020	0.014	0.006
2	0.093	0.078	0.085	0.008
4	0.120	0.128	0.124	0.004
5	0.150	0.165	0.158	0.008
10	0.180	0.185	0.183	0.003
20	0.233	0.235	0.234	0.001
40	0.250	0.245	0.248	0.003

Figure 4.2: [**2.26**] (M) vs. Time (Min)

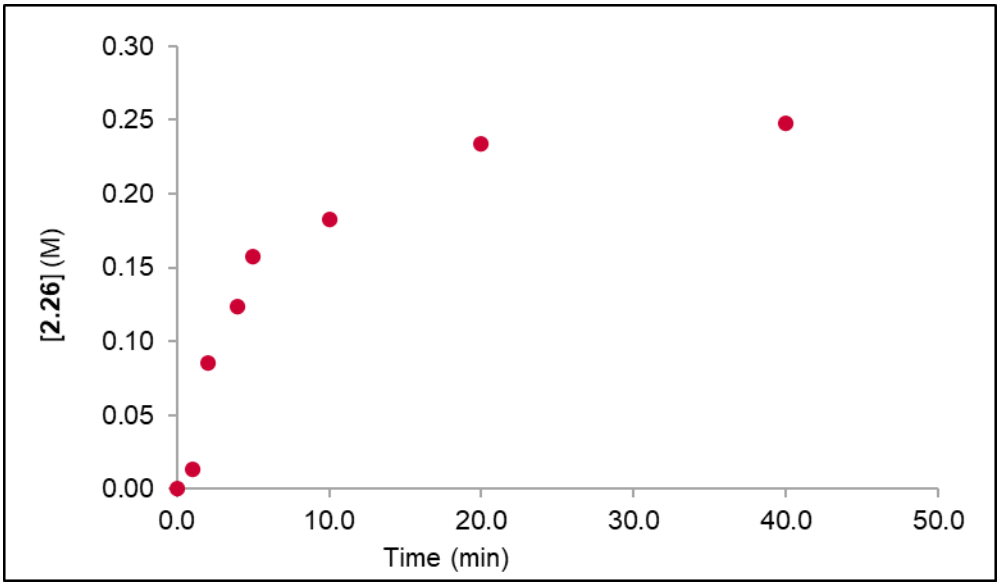

Figure 4.2: Reaction progress profile of standard conditions. Initial concentrations: [**2.25**] = 0.250 M, [HBpin] = 0.500 M, [CuOAc+Xantphos] = 0.0125 M.

Determination of Reaction Order in Enyne 2.25 via VTNA[12]

Procedure 4.14: Each experiment was run in duplicate and averaged. To a flame dried and sealed 2-dram vial: a stir bar, 250 µl of a 0.025 M solution of CuOAc (0.05 equiv, 6.25 µmol) and Xantphos (0.05 equiv, 6.25 µmol) in dichloromethane (DCM) was added. The DCM was removed under vacuum and the vial was put under inert atmosphere using standard *Schlenk* technique. Then, 500 µl of a 0.250-0.260 M solution of enyne **2.25** (1.0 equiv, 0.125-0.130 mmol) and 0.125 M solution of 1,2,4,5-tetramethylbenzene (internal standard, 0.50 equiv, 0.0625 mmol) in toluene was added. Finally, pinacolborane (2.0 equiv, 0.250 mmol) was added and a timer was started. Aliquots (10 µl) of the reaction were removed at recorded times, exposed to air, and diluted in $CDCl_3$. Formation of 2-boryl-1,3-diene **2.26** was tracked via ^1H NMR with 1,2,4,5-tetramethylbenzene as an internal standard. Using visual analysis (observing overlap between the standard excess condition plots), first order kinetics were observed for enyne **2.26**.

Table 4.4: Concentration Data for Excess (0.350 M) **2.25** Conditions

Excess **2.25** Conditions				
	Trial A	Trial B		
t (min)	[**2.26**] (M)	[**2.26**] (M)	Average [**2.26**] (M)	STD
0	0.000	0.000	0.000	0.000
1	0.088	0.081	0.084	0.004
2	0.137	0.133	0.135	0.002
4	0.172	0.186	0.179	0.007
5	0.196	0.207	0.201	0.005
10	0.217	0.245	0.231	0.014

Figure 4.3: [**2.26**] (M) vs. Σ[**2.25**]$^{0}\Delta$t

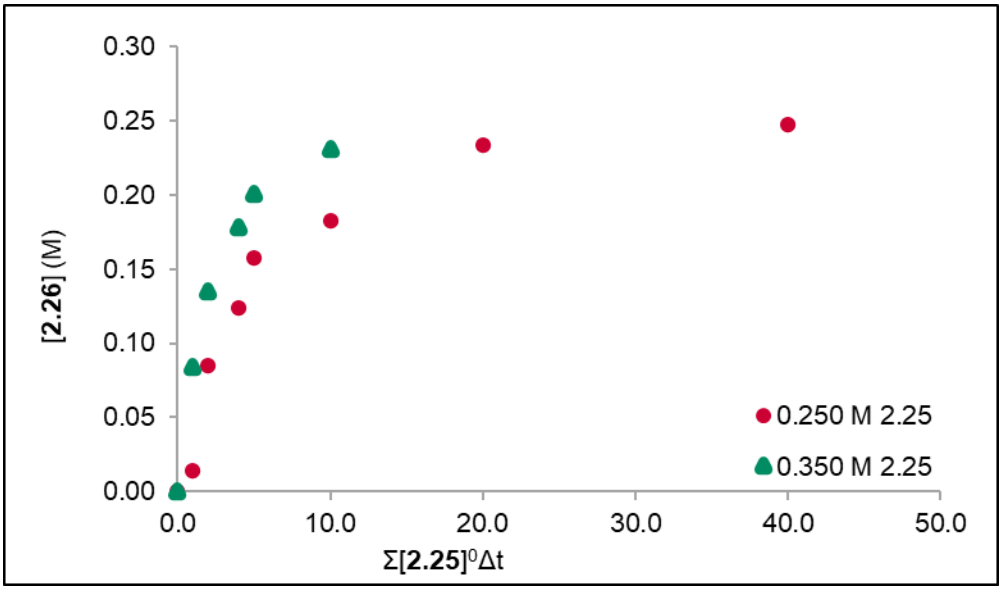

Figure 4.3: Time normalized reaction progress profile of excess **2.25** (0.350 M). Initial concentrations for excess conditions: [**2.25**] = 0.350 M, [HBpin] = 0.500 M, [CuOAc+Xantphos] = 0.0125 M.

Figure 4.4: [**2.26**] (M) vs. Σ[**2.25**]$^{1}\Delta$t

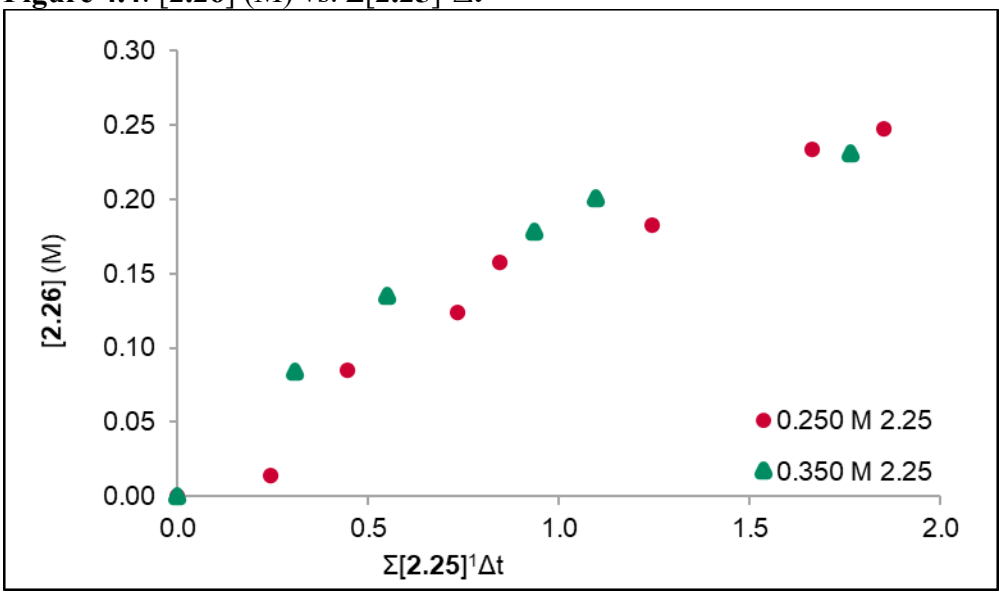

Figure 4.4: Time normalized reaction progress profile of excess **2.25** (0.350 M). Initial concentrations for excess conditions: [**2.25**] = 0.350 M, [HBpin] = 0.500 M, [CuOAc+Xantphos] = 0.0125 M.

Figure 4.5: [**2.26**] (M) vs. Σ[**2.25**]$^2\Delta$t

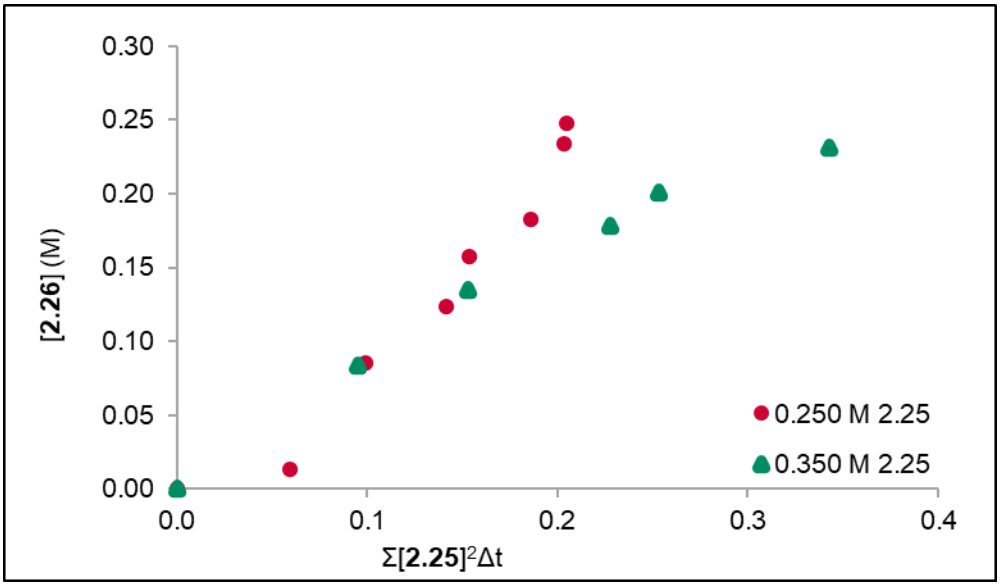

Figure 4.5: Time normalized reaction progress profile of excess **2.25** (0.350 M). Initial concentrations for excess conditions: [**2.25**] = 0.350 M, [HBpin] = 0.500 M, [CuOAc+Xantphos] = 0.0125 M.

Determination of Reaction Order in CuOAc+Xantphos via VTNA

Procedure 4.53: Each experiment was duplicated and averaged. To a flame dried and sealed 2-dram vial: a stir bar, 500 µl of a 0.025 M solution of CuOAc (0.10 equiv, 12.5 µmol) and Xantphos (0.10 equiv, 12.5 µmol) in dichloromethane (DCM) was added. The DCM was removed under vacuum and the vial was put under inert atmosphere using standard *Schlenk* technique. Then, 500 µl of a 0.250 M solution of enyne **2.25** (1.0 equiv, 0.125) and 0.125 M solution of 1,2,4,5-tetramethylbenzene (internal standard, 0.50 equiv, 0.0625 mmol) in toluene was added. Finally, pinacolborane (2.0 equiv, 0.250 mmol) was added and a timer was started. Aliquots (10 µl) of the reaction were removed at recorded times, exposed to air, and diluted in $CDCl_3$. Formation of 2-boryl-1,3-diene **2.26** was tracked via ^1H NMR with 1,2,4,5-tetramethylbenzene as an internal standard. Using visual analysis (observing overlap between the standard excess condition plots), fractional order kinetics were observed for CuOAc+Xantphos.

Table 4.5: Concentration Data for Excess (0.0250 M) CuOAc+Xantphos Conditions

Excess CuOAc+Xantphos				
	Trial A	Trial B		
t (min)	[**2.26**] (M)	[**2.26**] (M)	Average [**2.26**] (M)	STD
0	0	0	0	0
1	0.0525	0.095	0.0738	0.0301
2	0.1225	0.1575	0.14	0.0247
4	0.16	0.1825	0.171	0.0159
5	0.175	0.215	0.195	0.0283
10	0.1925	0.235	0.214	0.0300
20	0.215	0.2425	0.229	0.0194
40	0.25	0.25	0.25	0

Figure 4.6: [**2.26**] M vs. t[CuOAc+Xantphos]^{0}

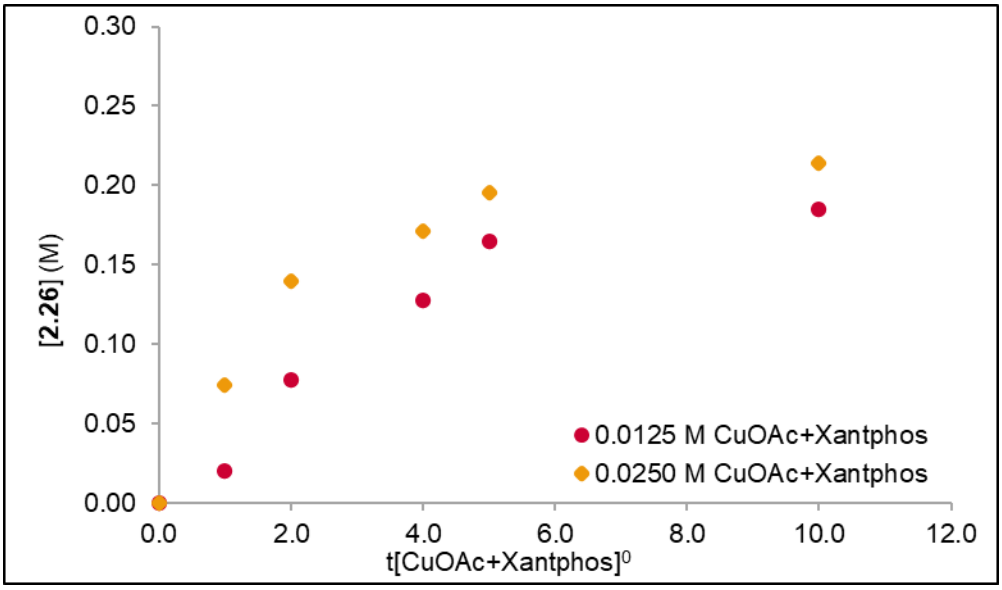

Figure 4.6: Time normalized reaction progress profile of excess CuOAc+Xantphos (0.025 M). Initial concentrations for excess conditions: [**2.26**] = 0.250 M, [HBpin] = 0.500 M, [CuOAc+Xantphos] = 0.0250 M.

Figure 4.7: [**2.26**] M vs. t[CuOAc+Xantphos]$^{0.7}$

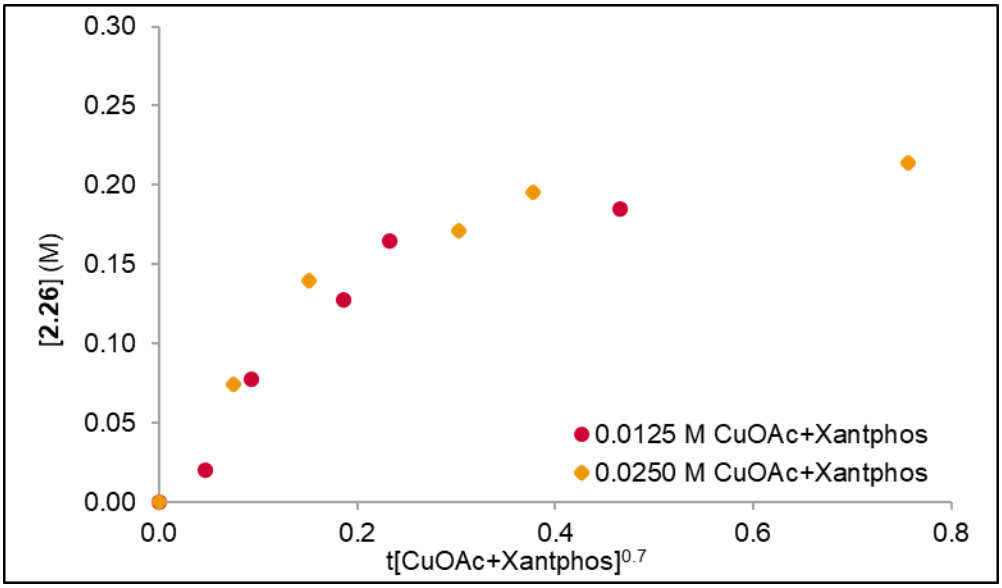

Figure 4.7: Time normalized reaction progress profile of excess CuOAc+Xantphos (0.025 M). Initial concentrations for excess conditions: [**2.25**] = 0.250 M, [HBpin] = 0.500 M, [CuOAc+Xantphos] = 0.0250 M.

Figure 4.8: [**2.26**] (M) vs. t[CuOAc+Xantphos]^{1}

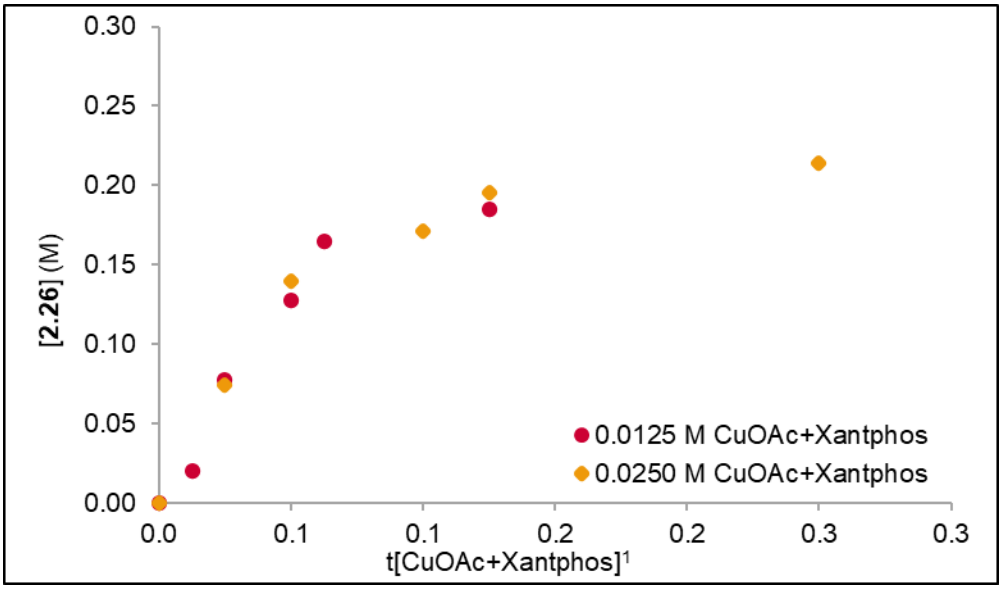

Figure 4.8: Time normalized reaction progress profile of excess CuOAc+Xantphos (0.025 M). Initial concentrations for excess conditions: [**2.25**] = 0.250 M, [HBpin] = 0.500 M, [CuOAc+Xantphos] = 0.0250 M.

Figure 4.9: [**2.26**] (M) vs. t[CuOAc+Xantphos]^{2}

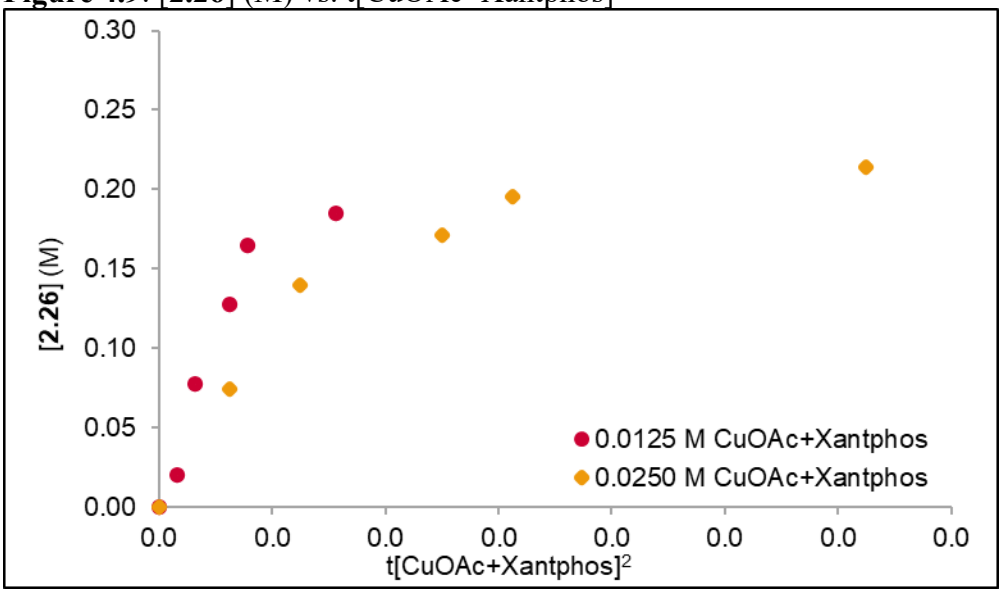

Figure 4.9: Time normalized reaction progress profile of excess CuOAc+Xantphos (0.025 M). Initial concentrations for excess conditions: [**2.25**] = 0.250 M, [HBpin] = 0.500 M, [CuOAc+Xantphos] = 0.0250 M.

Determination of Reaction Order in CuOAc+Xantphos via Initial Rates.
To corroborate the fractional order in CuOAc+Xantphos, initial rate analysis was used.

While VTNA is a very useful tool for determining the rate order of various reagents, it is susceptible to error because analysis is performed qualitatively by observing overlap. This makes determination of fractional rate orders (especially those close to 1) less reliable. To determine whether the fractional rate order in CuOAc+Xantphos was an artifact of the collected data, or a result of true off-cycle process we conducted initial rate studies. **Table 4.6** details the collected data for the initial rate vs. $[CuOAc+Xantphos]_0$ plot. The non-linear nature of the graph in **Figure 4.10** is suggestive that a fractional rate order was observed.

Procedure 4.15: Each experiment was run in duplicate and averaged. To a flame dried and sealed 2-dram vial: a stir bar, 125-1,250 µl (5 initial concentrations were tested) of a 0.025 M solution of CuOAc (0.05-0.25 equiv, 6.25-31.3 µmol) and Xantphos (0.05-0.25 equiv, 6.25-31.3 µmol) in dichloromethane (DCM) was added. The DCM was removed under vacuum and the vial was put under inert atmosphere using standard *Schlenk* technique. Then, 500 µl of a 0.250 M solution of enyne **2.25** (1.0 equiv, 0.125 mmol) and 0.125 M solution of 1,2,4,5-tetramethylbenzene (internal standard, 0.50 equiv, 0.0625 mmol) in toluene was added. Finally, pinacolborane (2.0 equiv, 0.250 mmol) was added and a timer was started. Aliquots (10 µl) of the reaction were removed at recorded times, exposed to air, and diluted in $CDCl_3$. Formation of 2-boryl-1,3-diene **2.26** was tracked via ^1H NMR with 1,2,4,5-tetramethylbenzene as an internal standard at t = 1 min, 2 min, 3 min, 4 min and 5 min (or 8 min). The initial rate (mol/L•min) was determined by finding the slope between [**2.26**] M vs. time (min). A plot of initial rate (mol/L•min) vs. $[CuOAc+Xantphos]_0$ M was then generated.

Table 4.6: Initial Rate Data for CuOAc+Xantphos. Rate Order Determination

$[CuOAc+Xantphos]_0$	Initial rate	STD
0.0625	0.0324	0.00211
0.025	0.0304	0.00035
0.0188	0.0266	0.00083
0.0125	0.0209	0.00091
0.006	0.0142	0.00061
0	0	0

Figure 4.10: Initial Rate (M/min) vs. $[CuOAc+Xantphos]_0$ (M)

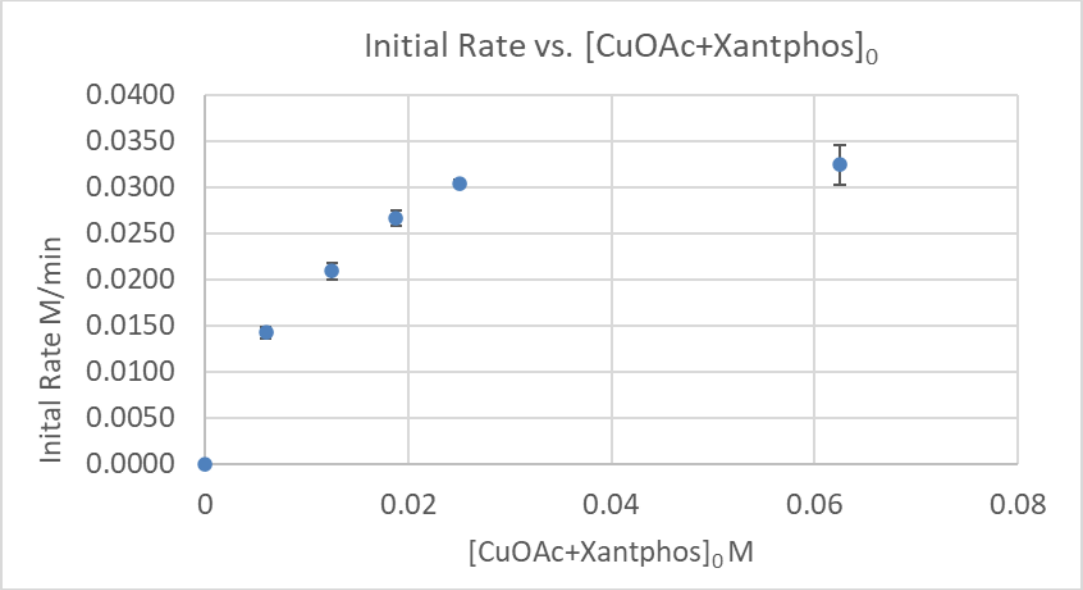

Figure 4.10: Initial Rate vs. $[CuOAc+Xantphos]_0$. Initial Concentrations: [**2.25**] = 0.250 M, [HBpin] = 0.500 M, [CuOAc+Xantphos] = 0.000 M, 0.006 M, 0.0125 M, 0.0188 M, 0.0250 M, 0.0625 M.

Table 4.7: Concentration Values Determined by ^1H NMR for Initial Rates

$[CuOAc+Xantphos.]_0$	0.0625 M				
a		b			
t (min)	[**2.26**] (M)	t (min)	[**2.26**] (M)		Slope (initial rate)
0	0	0	0	a	0.0299
1	0.043	1	0.0425	b	0.03475
2	0.065	2	0.085	ave.	0.03234
3	0.100	3	0.12	std	0.00241
4	0.118	4	0.135		

5	0.158	5	0.16		
$[CuOAc+Xantphos.]_0$	0.0250 M				
a		b			
t (min)	[**2.26**] (M)	t (min)	[**2.26**] (M)		Slope (initial rate)
0	0	0	0	a	0.0308
1	0.0875	1	0.0925	b	0.0301
2	0.125	2	0.1275	ave.	0.0304
4	0.1625	4	0.16	std	0.000349
5	0.17	5	0.17		
$[CuOAc+Xantphos.]_0$	0.0188 M				
a		b			
t (min)	[**2.26**] (M)	t (min)	[**2.26**] (M)		Slope (initial rate)
0	0.025	0	0.0075	a	0.0258
1	0.123	1	0.128	b	0.0274
2	0.15	2	0.14	ave.	0.0266
4	0.163	4	0.16	std	0.000349
5	0.183	5	0.18		
$[CuOAc+Xantphos.]_0$	0.0125 M				
a		b			
t (min)	[**2.26**] (M)	t (min)	[**2.26**] (M)		Slope (initial rate)
0	0	0	0	a	0.0191
1	0.0075	1	0.02	b	0.0209
2	0.0925	2	0.0775	ave.	0.02
4	0.12	4	0.1275	std	0.000906
8	0.15	8	0.165		
$[CuOAc+Xantphos.]_0$	0.006 M				
a		b			
t (min)	[**2.26**] (M)	t (min)	[**2.26**] (M)		Slope (initial rate)
0	0	0	0	a	0.0136
1	0.025	1	0.025	b	0.0148
2	0.04	2	0.0525	ave.	0.0142
3	0.0475	3	0.06	std	0.000607
4	0.06	4	0.07		
5	0.0725	5	0.075		

Determination of Reaction Order in HBpin

Procedure 4.16: Each experiment was run in duplicate and averaged. To a flame dried and sealed 2-dram vial: a stir bar, 250 µl of a 0.025 M solution of CuOAc (0.05 equiv, 6.25 µmol) and

Xantphos (0.05 equiv, 6.25 µmol) in dichloromethane (DCM) was added. The DCM was removed under vacuum and the vial was put under inert atmosphere using standard *Schlenk* technique. Then, 500 µl of a 0.250 M solution of enyne **2.25** (1.0 equiv, 0.125) and 0.125 M solution of 1,2,4,5-tetramethylbenzene (internal standard, 0.50 equiv, 0.0625 mmol) in toluene was added. Finally, pinacolborane (2.0-3.0 equiv, 0.250-0.375 mmol) was added and a timer was started. Aliquots (10 µl) of the reaction were removed at recorded times, exposed to air, and diluted in $CDCl_3$. Formation of 2-boryl-1,3-diene **2.26** was tracked via ^1H NMR with 1,2,4,5-tetramethylbenzene as an internal standard. Using visual analysis (observing overlap between the standard excess condition plots), zeroth order kinetics were observed for HBpin.

Table 4.8: Concentration Data for Excess (0.675 M) HBpin Conditions

Excess HBpin				
	Trial A	Trial B		
t (min)	[**2.26**] (M)	[**2.26**] (M)	Average [**2.26**] (M)	STD
0	0	0	0	0
1	0.0225	0.0175	0.020	0.00354
2	0.0525	0.05	0.051	0.00177
4	0.13	0.108	0.119	0.0159
5	0.15	0.14	0.145	0.00707
10	0.2	0.193	0.196	0.00530
20	0.228	0.203	0.215	0.0177
40	0.245	0.225	0.235	0.0141

Figure 4.11: [**2.26**] M vs. $\Sigma[HBpin]^0\Delta t$

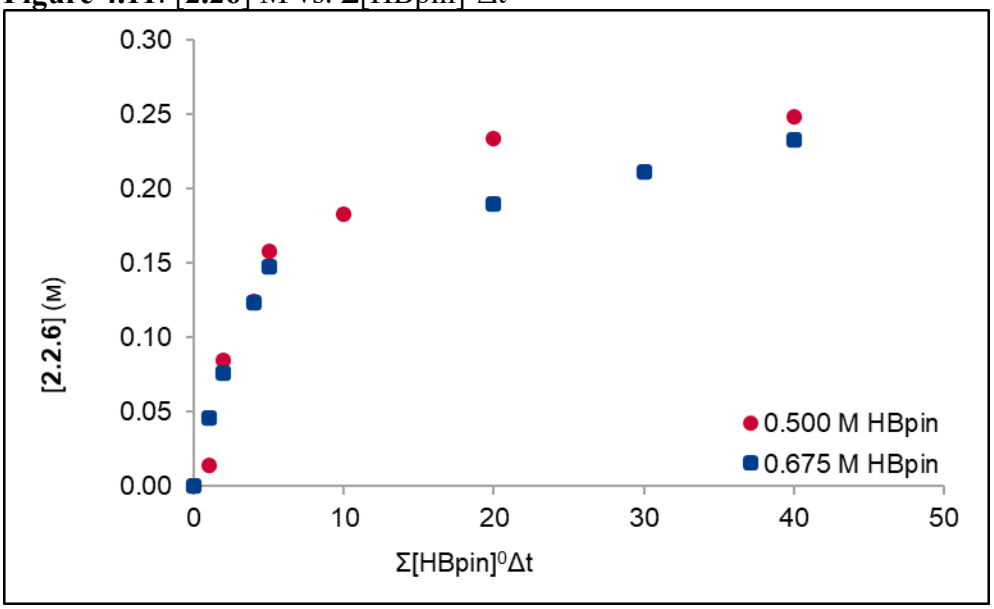

Figure 4.11: Time normalized reaction progress profile of excess HBpin (0.675 M). Initial concentrations for excess conditions: [**2.25**] = 0.250 M, [HBpin] = 0.675 M, [CuOAc+Xantphos] = 0.0250 M.

Figure 4.12: [**2.26**] M vs. $\Sigma[HBpin]^1\Delta t$

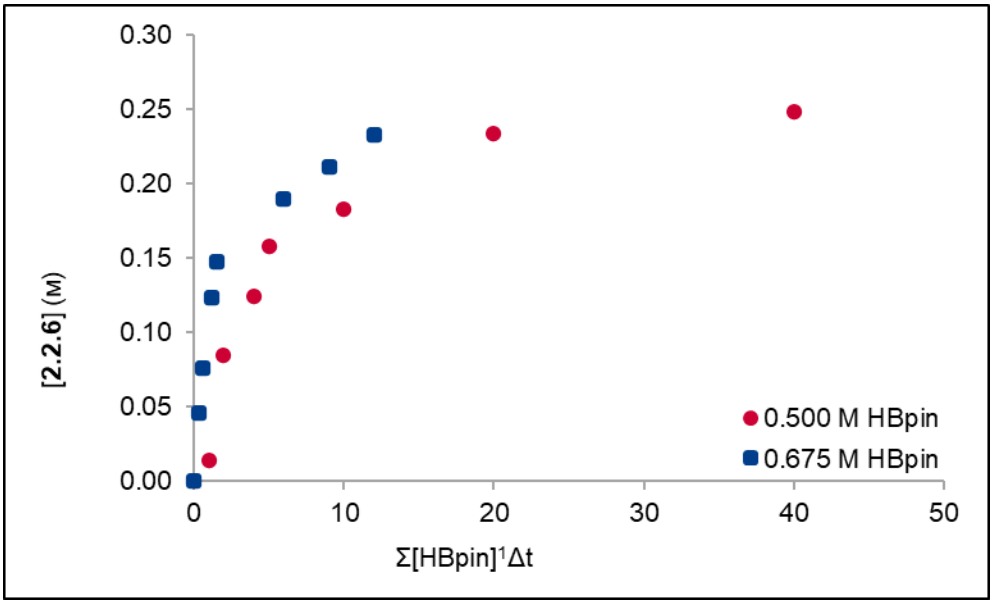

Figure 4.12: Time normalized reaction progress profile of excess HBpin (0.675 M). Initial concentrations for excess conditions: [**2.25**] = 0.250 M, [HBpin] = 0.675 M, [CuOAc+Xantphos] = 0.0250 M.

Figure 4.13: [**2.26**] M vs. $\Sigma[HBpin]^2\Delta t$

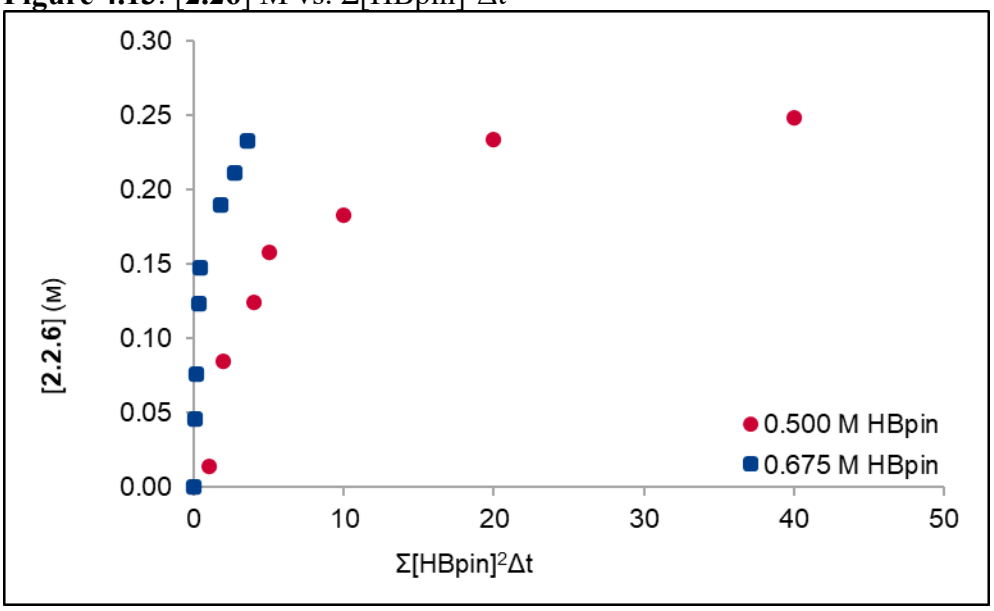

Figure 4.13: Time normalized reaction progress profile of excess HBpin (0.675 M). Initial concentrations for excess conditions: [**2.26**] = 0.250 M, [HBpin] = 0.675 M, [CuOAc+Xantphos] = 0.0250 M.

K_{obs} Graph

Figure 4.14: [**2.26**] M vs. Σ[CuOAc+Xantphos]^1[**2.25**]^1[HBpin]^{0}Δt

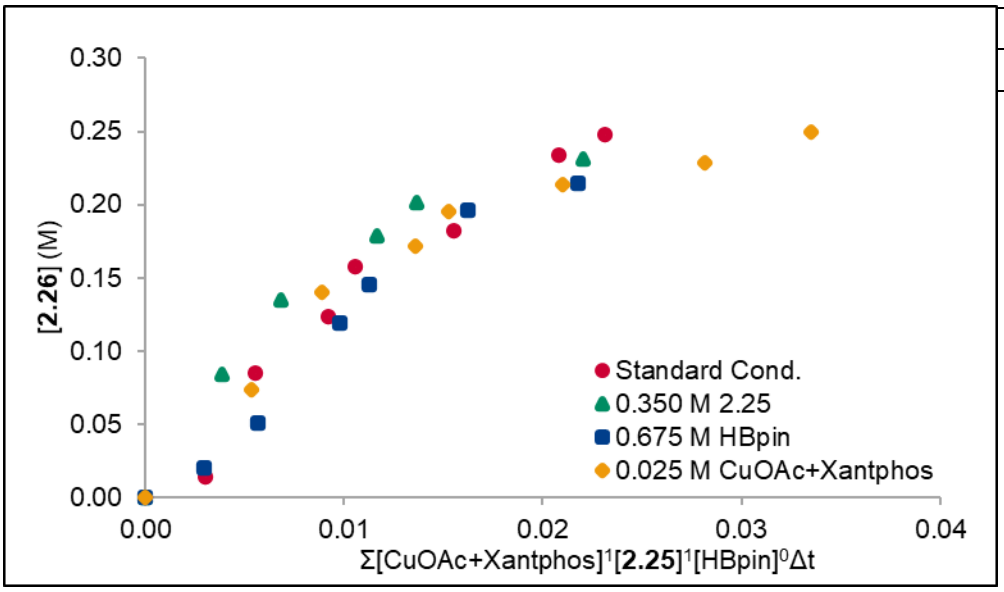

Slope	9.4
R^2	0.900

Figure 4.14: K_{obs} Plot. Initial concentrations: Red: [**2.25**] = 0.250 M, [HBpin] = 0.500 M, [CuOAc+Xantphos] = 0.0125 M. Green [**S**] = 0.350 M, [HBpin] = 0.500 M, [CuOAc+Xantphos] = 0.0125 M. Blue [**2.25**] = 0.250 M, [HBpin] = 0.675 M, [CuOAc+Xantphos] = 0.0125 M. Yellow [**2.25**] = 0.250 M, [HBpin] = 0.500 M, [CuOAc+Xantphos] = 0.0250 M.

Figure 4.15: [**2.26**] M vs. Σ[CuOAc+Xantphos]$^{0.7}$[**2.25**]^{1}[HBpin]^{0}Δt

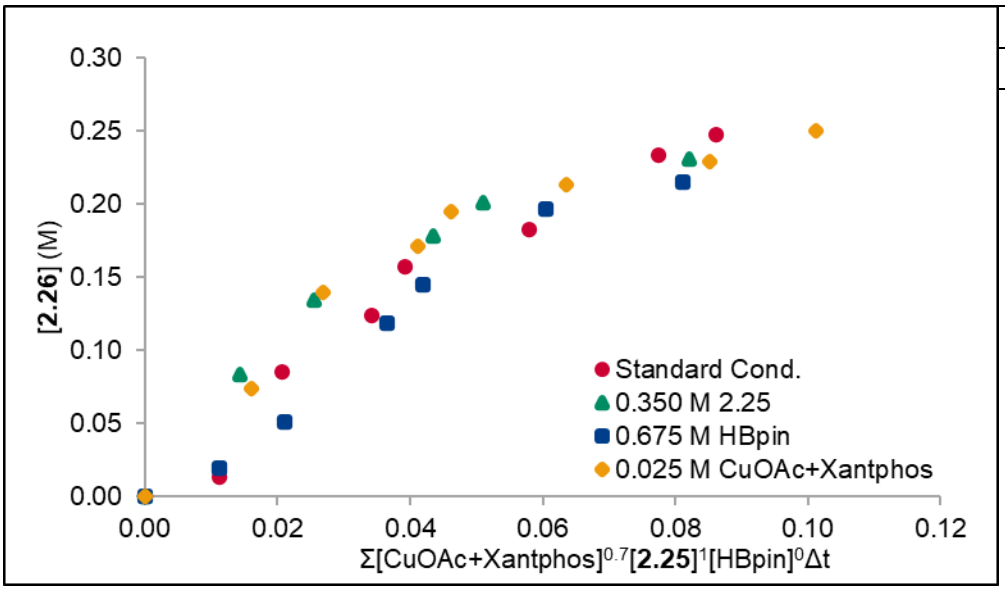

Slope	2.8
R^2	0.914

Figure 4.15: K_{obs} Plot. Initial concentrations: Red: [**2.25**] = 0.250 M, [HBpin] = 0.500 M, [CuOAc+Xantphos] = 0.0125 M. Green [**S**] = 0.350 M, [HBpin] = 0.500 M, [CuOAc+Xantphos] = 0.0125 M. Blue [**2.25**] = 0.250 M, [HBpin] = 0.675 M, [CuOAc+Xantphos] = 0.0125 M. Yellow [**2.25**] = 0.250 M, [HBpin] = 0.500 M, [CuOAc+Xantphos] = 0.0250 M.

Table 4.9: Concentration Data for K_{obs} Graph

Standard Conditions		Excess **2.25** (0.350 M)	
t(min)	[**2.26**] M	t(min)	[**2.26**] M
0.00	0.000	0.00	0.000
1.00	0.014	1.00	0.084
2.00	0.085	2.00	0.135
4.00	0.124	4.00	0.179
5.00	0.158	5.00	0.201
10.00	0.183	10.00	0.231
20.00	0.234		
40.00	0.248		
Excess HBpin (0.675 M)		Excess CuOAc+Xantphos (0.025 M)	
t(min)	[**2.26**] M	t(min)	[**2.26**] M
0	0.000	0	0.000
1	0.020	1	0.0738
2	0.051	2	0.14
4	0.119	4	0.1713
5	0.145	5	0.195
10	0.196	10	0.2138
20	0.215	20	0.229
40.00	0.235	40	0.25

Note: K_{obs} function in VTNA spreadsheet prompts the user to include the concentration of remaining substrate. This was calculated by subtracting the concentration of initial substrate by the concentration of the product.

Control Experiments

Procedure 4.17: To a flame dried 2 dram vial: a stir bar, 25.5 mg of **2.25** (1.0 equiv, 0.125 mmol), 1.53 mg of CuOAc or 1.24 mg of CuCl (0.05 equiv, 12.5 µmol) and 7.26 mg of Xantphos (0.05 equiv, 12.5 µmol) were added (in the case of reaction Scheme 4.51c: 0.61 mg of KOAc (0.05 equiv, 12.5 µmol) was also added). The vial was put under inert atmosphere using standard *Schlenk* technique. Next, toluene (500 µl, 0.25 M) was added. Finally, 36.6 µl of pinacolborane (2.0 equiv, 0.250 mmol) was added. The reaction was put into an oil bath set to 40 °C. After 16 hours, celite was added to the reaction, volatiles were removed under vacuum and **2.26** was purified using flash chromatography. Characterization for compound **2.26** matches literature.[11]

a) Lewis Base (acetate) Activation

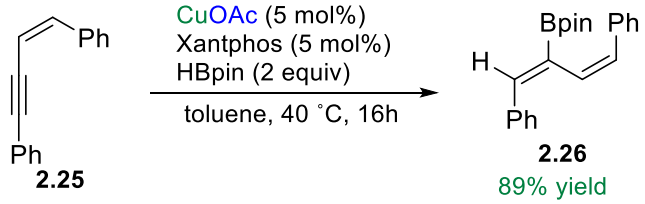

b) Weak Lewis Base (chloride) Activation

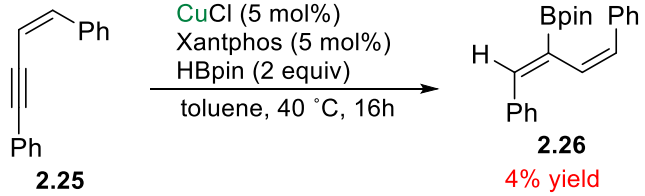

c) Lewis Base Additive (acetate) Activation

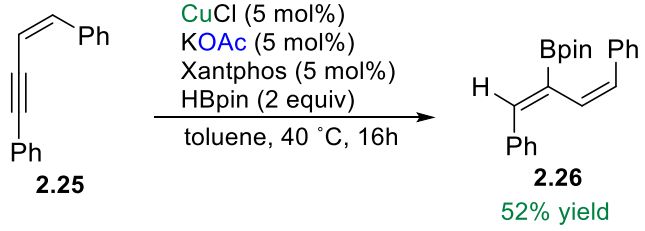

Scheme 4.13: Acetate mechanistic studies.

Stoichiometric Control Experiments (Off-Cycle Equilibrium Species Elucidation)

Procedure 4.18: CuOAc (1.0 equiv, 7.6 mg, 62.5 μmol), Xantphos (1.0 equiv, 36.2 mg, 62.5 μmol) and a stir bar were added to a 2-dram vial. The reaction flask was put under inert atmosphere using standard *Schlenk* technique. Then 2.5 mL of anhydrous toluene was added. The reaction was allowed to stir for approximately 10 minutes until a green, homogeneous mixture was observed. Pinacolborane (3.0 equiv, 27.2 μL, 188 μmol) was then added and the reaction was allowed to stir for 4 hours. A quartz NMR tube was fixed with a septa lid and put under inert atmosphere using standard *Schlenk* technique. The reaction mixture was transferred via cannula to the quartz NMR tube and the following ^{11}B NMR spectra were collected.

^{11}B NMR for stoichiometric CuOAc and Xantphos reaction with excess pinacolborane. Pinacolborane appears as a doublet because this is a ^{1}H coupled ^{11}B NMR experiment.

4.6 Computational Details for Chapter 2

All the structures discussed in this paper were fully optimized using Gaussian 16. [13] The optimization was done at the level of theory of the M06 functional, developed by Truhlar and Zhao. [14] Additionally, Grimme's empirical dispersion was incorporated with the D3 term during the optimization calculations.[15] For all of the calculations, solvent effects were considered using the SMD solvation model of Truhlar and workers[16] with toluene as the solvent. The SDD basis set with effective core potential (ECP) was chosen to describe Cu and 6-31G(d) basis set was employed for all other atoms.[17-19] This basis set combination is referred to as **BS1**. Frequency calculations were carried out at the same level of theory as those for structural optimization. Transition structures were located using the Berny algorithm.[20] Intrinsic reaction coordinate (IRC) calculations were used to confirm the connectivity between transition structures and minima.[21] To further refine the energies obtained from the SMD/ M06-D3/SDD,6-31G(d) calculations, we

carried out single-point energy calculations using the M06 functional method for all of the structures with a larger basis set def2-TZVP (**BS2**).[22] Grimme empirical dispersion was added with the D3 term on all the single-point energy calculations.[15] A tight convergence criterion and ultrafine integral grid were also employed to increase the accuracy of the calculations.

XYZ file

Please refer to the xyz file for the total potential energy (E), enthalpy (H), and Gibbs free energy (G) of all structures optimized at the SMD/M06D3//**BS1** level of theory. The total potential energies calculated by SMD/M06D3/**BS2**//SMD/M06D3/**BS1** are also included.

Here are the basis sets used:

BS1: 6-31G(d) for all atoms except Cu, where SDD is employed.

BS2: def2-TZVP for all atoms.

4.6. X-Ray Crystallography for Chapter 2

[Cu(Xantphos)(OAc)] (**2.27**): A colorless prism shaped crystal (0.06 x 0.12 x 0.21 mm3) was centered on the goniometer of a Rigaku Oxford Diffraction Synergy-S diffractometer equipped with a HyPix6000HE detector and operating with MoKα radiation. The data collection routine, unit cell refinement, and data processing were carried out with the program CrysAlisPro.[23] The trigonal space group R-3 was assigned. The structure was solved using SHELXT[9] and refined using SHELXL[9] via Olex2[10]. PovRay[24] and ORTEP[25] applications were used to generate structure graphics. The final refinement model involved anisotropic displacement parameters for non-hydrogen atoms and a riding model for all hydrogen atoms. The toluene solvent molecule exhibited disorder that was resolved by modeling the solvent in the asymmetric unit via the FragmentDB tool.

Note: The data showed streaks of diffuse scattering indicating a disorder that cannot be modeled exclusively through Bragg reflections. Although this negatively impacts the statistics for the structure model and leaves unsatisfactorily large difference electron density peaks, the structure model does confirm the desired compound was synthesized.

Crystal Growth Procedure: Compound **2.27** (colorless solid) was prepared in an NMR tube. 1 equivalent of CuOAc (1.52 mg, 12.5 μmol) and 1 equivalent of Xantphos (7.24 mg, 12.5 μmol) was put into an NMR tube with a septa lid. Then the NMR tube was put under inert atmosphere. 500 μl of toluene was then added. Finally, 20 equivalents of HBpin (36 μl, 250 μmol) was added via a syringe. The NMR tube was shaken vigorously and allowed to rest for 2 days. During which time large colorless crystals formed which were sufficient for X-ray crystallography.

(Deposition #: 2377607)

Table 4.10: X-ray diffraction experimental details

	[Cu(Xantphos)(OAc)] (**2.27**)
Empirical Formula	$2[C_{41}H_{35}CuO_3P_2]$ $1[C_7H_8]$
Formula Weight	1494.47
Temp. (K)	100.15
Radiation	Cu
Crystal System	Monoclinic
Space Group	P21/n
a (Å)	8.61421(8)
b (Å)	22.3632(3)
c (Å)	19.42325(18)
α (◦)	90
β (◦)	91.8316(8)
γ (◦)	90
Volume (Å3)	3739.81(7)
Z	2
ρcalc (g/cm3)	1.327
μ (mm-1)	1.943
F(000)	1556.0
Crystal size (mm3)	0.21 x 0.12 x 0.06
2Θ range for data collection (°)	6.028 to 154.878
Index Ranges	$-9 \leq h \leq 10$, $-28 \leq k \leq 27$, $-24 \leq l \leq 2$
Reflections Collected	66447
Independent Reflections	7917
Data/Restraints/Parameters	7917/102/483
GOF	1.074
Final R indexes [I>=2σ (I)]	R1 = 0.0723, wR2 = 0.1998
Final R indexes [all data]	R1 = 0.0736, wR2 = 0.2012
Largest diff. peak/hole/e (Å-3)	3.31/-0.67

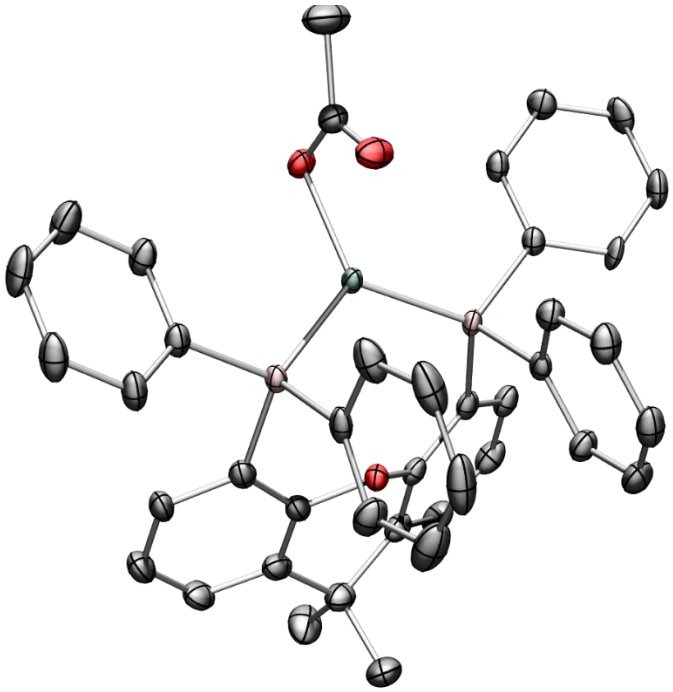

Figure 4.16: Solid-state molecular structures for [Cu(Xantphos)(OAc)] (**2.27**), (with anisotropic displacement ellipsoids at 50% probability level. Color scheme: Cu, green; P, pink; O, red C, gray. Hydrogens and solvent molecules are omitted for clarity.

4.7. Synthetic Procedures and Characterization of Compounds for Chapter 3

Synthetic Procedures for Alkynoates (3.45) and Amides (3.46):

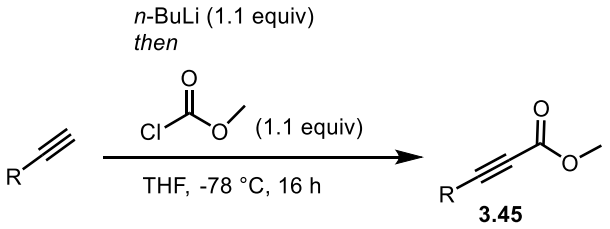

3.45

Scheme 4.14: Acylation of terminal alkynes.

Procedure 4.19: A round bottom flask was charged with a stir bar, flame dried and put under an inert atmosphere using standard *Schlenk* technique. Dry THF (7.83 mL, 0.25 M) and terminal alkyne (1.96 mmol, 1.0 equiv) were added. The reaction flask was added to a dry ice/acetone bath. Then, *n*-BuLi (2.15 mmol, 1.1 equiv) was added dropwise, and the reaction was allowed to stir for 30 minutes. Next, methyl-chloroformate (2.15 mmol, 1.1 equiv) was added dropwise (add slowly to prevent ketone formation). The reaction was allowed to stir overnight and come to room temperature. Upon completion, the reaction was quenched with water and extracted thrice with ethyl acetate, dried over sodium sulfate and concentrated under vacuum. The desired alkynoates were purified using flash chromatography (0-20% EtOAc:Hex gradient).

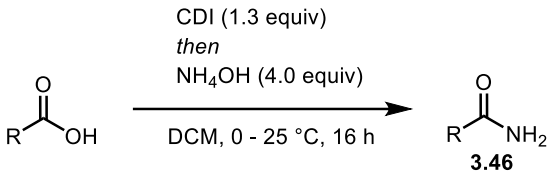

3.46

Scheme 4.15: CDI coupling of carboxylic acids and ammonium hydroxide.

Procedure 4.20: Modified from literature procedure.[26] A round bottom flask was charged with a stir bar and flame dried. Carboxylic acid (0.500 mmol, 1.0 equiv) and carbonyldiimidazole (0.650 mmol, 1.3 equiv) were added. The round bottom was sealed and put under an inert atmosphere using standard *Schlenk* technique. Dry DCM (5.0 mL, 0.25 M) was added, and the reaction flask was added to an ice bath. The reaction was allowed to stir until the evolution of CO_2 gas stopped

(roughly 30 minutes). 25 wt% ammonium hydroxide (2.00 mmol, 4.0 equiv) was then added using a syringe and the reaction was allowed to stir at room temperature for 16 hours. Upon completion, the reaction was quenched with water and extracted thrice with DCM, dried over sodium sulfate and concentrated under vacuum. The desired amides were purified using flash chromatography (0-10% MeOH:DCM gradient).

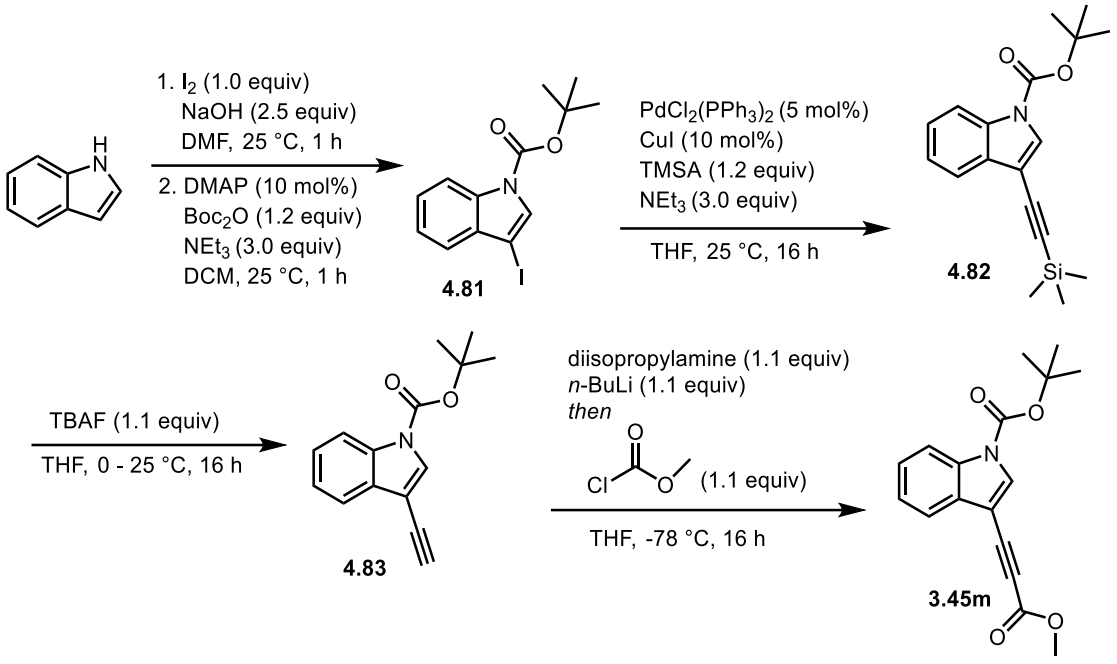

Scheme 4.16: Synthesis of substrate **3.45m**.

Procedure 4..21 *tert*-butyl 3-iodo-1*H*-indole-1-carboxylate (**4.81**) was synthesized using a modified literature procedure.[27] A round bottom flask was charged with a stir bar and flame dried. A solution of 1*H*-indole (500.0 mg, 4.27 mmol, 1.0 equiv) in DMF (15 mL, 28 M) was added to the round bottom. Then, NaOH (426.9 mg, 10.7 mmol, 2.5 equiv) was added and the solution was allowed to stir for 30 minutes. Finally, iodine (1.083 g, 4.27 mmol, 1.0 equiv,) was added and the reaction was allowed to stir for an additional hour. Upon consumption of the starting material via TLC the reaction was quenched with an aqueous solution of lithium bromide and extracted thrice with ethyl acetate. The organic layers were combined and dried over sodium sulfate. Crude

material was concentrated under vacuum. To the crude material 4-dimethylaminopyridine (52.5 mg, 0.43 mmol, 10 mol%,), di-*tert*-butyl-dicarbonate (1.176 mL, 5.12 mmol, 1.2 equiv,), triethylamine (1.784 mL, 12.8 mmol, 3.0 equiv) and DCM (40 mL, 0.11 M) were added at 25 °C. The reaction was allowed to stir for 1 hour. The desired *tert*-butyl 3-iodo-1*H*-indole-1-carboxylate (**4.81**) was purified using flash chromatography (0-5% EtOAc:Hex gradient) as a colorless oil in 81% (1.183 g, 3.45 mmol) yield across two steps. Characterization matched previous reports.[27]

General procedure 4.22: *tert*-butyl 3-((trimethylsilyl)ethynyl)-1*H*-indole-1-carboxylate (**4.81**) was synthesized using a modified literature procedure.[28] A round bottom flask was charged with a stir bar and flame dried. *tert*-butyl 3-iodo-1*H*-indole-1-carboxylate (**4.82**) (350.0 mg, 1.02 mmol, 1.0 equiv), bis(triphenylphosphine)palladium dichloride (35.8 mg, 0.05 mmol, 5 mol%) and copper iodide (19.4 mg, 0.10 mmol, 10 mol%) were added next. The round bottom was sealed and put under an inert atmosphere using standard *Schlenk* technique. Finally, dry THF (5 mL, 0.2 M), triethylamine (426 μL, 3.06 mmol, 3.0 equiv) and trimethylsilyl acetylene (174 μL, 1.22 mmol, 1.2 equiv) were added. The reaction was allowed to stir for 16 hours. Upon completion the reaction was quenched with brine and extracted with DCM thrice. The organic layers were combined and dried over sodium sulfate. Crude material was concentrated under vacuum. *tert*-butyl 3-((trimethylsilyl)ethynyl)-1*H*-indole-1-carboxylate (**4.82**) was purified using flash chromatography (isocratic hexanes) as a brown oil in 82% (263 mg, 838.0 μmol) yield. Characterization matched previous reports.[28]

General procedure 4.23: *tert*-butyl 3-ethynyl-1*H*-indole-1-carboxylate **(4.83)** was synthesized using a modified literature procedure.[29] A round bottom flask was charged with a stir bar and flame dried. The flask was charged with *tert*-butyl 3-((trimethylsilyl)ethynyl)-1*H*-indole-1-carboxylate (**4.82**) (149.4 mg, 477 μmol, 1.0 equiv), of dry THF (1.8 mL, 0.27 M) and added to an ice bath (0

°C). A 1 M solution of tetrabutylammonium fluoride (0.524 mL, 524 μmol, 1.1 equiv) was then added to the round bottom flask dropwise. The reaction was allowed to stir for 1 hour. Upon completion the reaction was quenched with brine and extracted with DCM thrice. The organic layers were combined and dried over sodium sulfate. Crude material was concentrated under vacuum. *tert*-butyl 3-ethynyl-1*H*-indole-1-carboxylate (**4.83**) was purified using flash chromatography (0-5% EtOAc:Hex gradient) as a yellow oil in 86% (91.1 mg, 378 μmol) yield. Characterization matched previous reports.[30]

General procedure 4.24: *tert*-butyl 3-(3-methoxy-3-oxoprop-1-yn-1-yl)-1*H*-indole-1-carboxylate (**3.45m**) was synthesized using a modified general procedure 1. A round bottom flask was charged with a stir bar and flame dried. The round bottom was sealed and put under an inert atmosphere using standard *Schlenk* technique. The round bottom was added to a dry ice/acetone bath. Dry THF (3.0 mL), diisopropylamine (95.9 μL, 684 μmol, 1.1 equiv) and 2.5 M *n*-BuLi in hexanes (274 μL, 684 μmol, 1.1 equiv) were added. A 2.5 M solution of *tert*-butyl 3-ethynyl-1*H*-indole-1-carboxylate (**4.83**) in THF (60.0 μL, 622 μmol, 1.0 equiv) was added dropwise. After 1 hour, methyl-chloroformate (57.8 μL, 746 μmol, 1.2 equiv) was added dropwise (add slowly to prevent ketone formation). The reaction was allowed to stir for 16 hours. Upon completion the reaction was quenched with brine and extracted with DCM thrice. The organic layers were combined and dried over sodium sulfate. Crude material was concentrated under vacuum. *tert*-butyl 3-(3-methoxy-3-oxoprop-1-yn-1-yl)-1*H*-indole-1-carboxylate (**3.45m**) was purified using flash chromatography (0-10% EtOAc:Hex gradient) as a yellow oil in a 43% (80.1 mg, 622 μmol) yield. Characterization matched previous reports.[31]

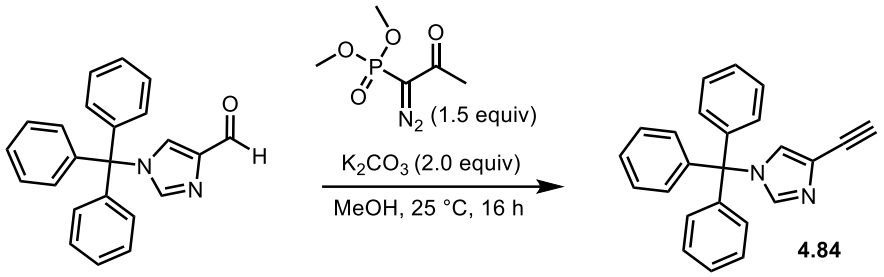

Scheme 4.17: Bestmann-Ohira to synthesize terminal alkyne **4.84**.

General Procedure 4.25: 4-ethynyl-1-trityl-*1H*-imidazole (**4.84**) was synthesized using a modified literature procedure.[32] A round bottom flask was charged with a stir bar and flame dried. 1-trityl-*1H*-imidazole-4-carbaldehyde (501 mg, 1.48 mmol, 1.0 equiv) and potassium carbonate (409 mg, 2.96 mmol, 2.0 equiv) were added to the round bottom flask. The reaction vessel was sealed and put under an inert atmosphere using standard *Schlenk* technique. 10% Dimethyl (1-diazo-2-oxopropyl)phosphonate solution in MeCN (5.17 mL, 2.22 mmol, 1.5 equiv) and MeOH (6 mL, 0.25 M) were then added. The reaction was allowed to stir for 16 hours. Upon completion the reaction was quenched with brine and extracted with DCM thrice. The organic layers were combined and dried over sodium sulfate. Crude material was concentrated under vacuum to afford 4-ethynyl-1-trityl-*1H*-imidazole (**4.84**) (490 mg, 1.47 mmol, 99% yield) as a white solid. Characterization matched previous reports.[33]

Table 4.11: References for alkyne, alkynoate, and amide starting materials.

Code	Structure	Reference	Procedure
3.45a[34]	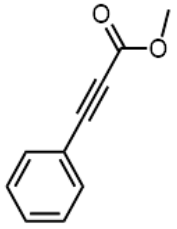	*Angew. Chem. Int. Ed.* **2020,** *59* (34), 14358-14362.	**4.19**

3.45b[35]	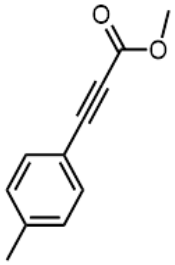	*J. Org. Chem.* **2018,** *83* (17), 10436-10444.	**4.19**
3.45c[35]	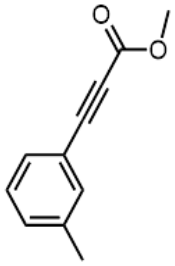	*J. Org. Chem.* **2018,** *83* (17), 10436-10444.	**4.19**
3.45d[34]	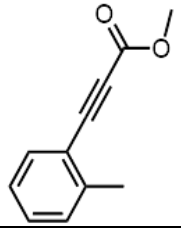	*Angew. Chem. Int. Ed.* **2020,** *59* (34), 14358-14362.	**4.19**
3.45e[34]	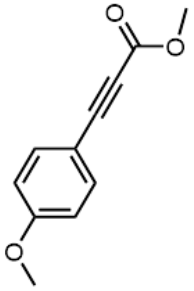	*Angew. Chem. Int. Ed.* **2020,** *59* (34), 14358-14362.	**4.19**
3.45f[34]	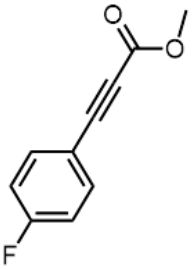	*Angew. Chem. Int. Ed.* **2020,** *59* (34), 14358-14362.	**4.19**
3.45g[34]	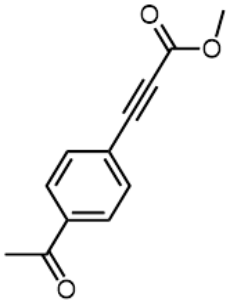	*Angew. Chem. Int. Ed.* **2020,** *59* (34), 14358-14362.	**4.19**

3.45h[35]	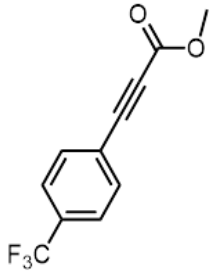	*J. Org. Chem.* **2018,** *83* (17), 10436-10444.	**4.19**
3.45i[36]	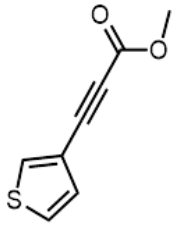	*J. Am. Chem. Soc.* **2021,** *143* (44), 18394-18399.	**4.19**
3.45j[34]	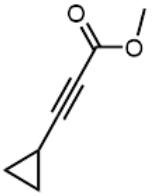	*Angew. Chem. Int. Ed.* **2020,** *59* (34), 14358-14362.	**4.19**
3.45k[34]	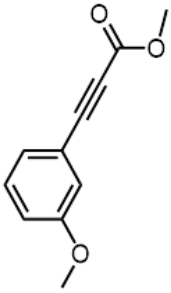	*Angew. Chem. Int. Ed.* **2020,** *59* (34), 14358-14362.	**4.19**
4.84[33]	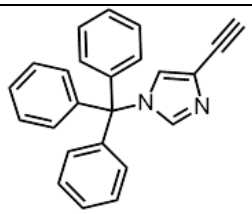	*J. Fluor. Chem.* **2003**, *124*, 105-110.	**4.25**
3.45l[33]	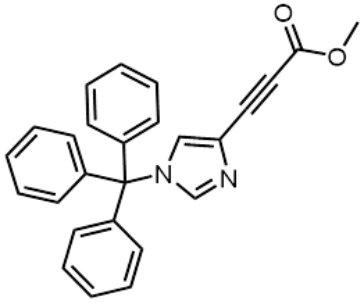	*J. Fluor. Chem.* **2003**, *124*, 105-110.	**4.19**

4.81[37]	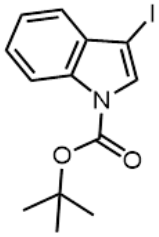	*J. Org. Chem.* **2008,** *73* (17), 6706-6710.	**4.21**
4.82[28]	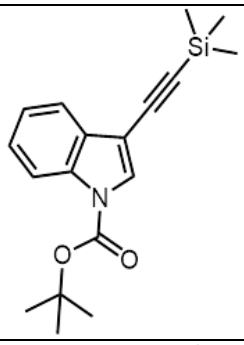	*J. Am. Chem. Soc.* **2011,** *133* (22), 8482-8485.	**4.22**
4.83[30]	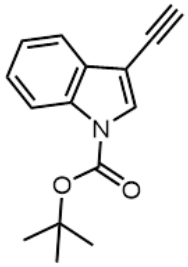	*J. Am. Chem. Soc.* **2021,** *143* (29), 11141-11151.	**4.23**
3.45m[31]	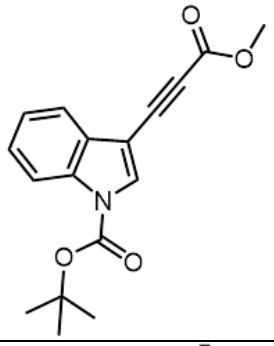	Michaelides, I. N.; Darses, B.; Dixon, D. J., *Org. Lett.* **2011,** *13* (4), 664-667.	**4.24**
3.46e[38]	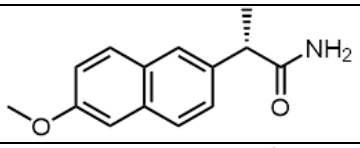	*Chem. Asian J.* **2023,** *18* (22), e202300672.	**4.15**
3.46o[39]	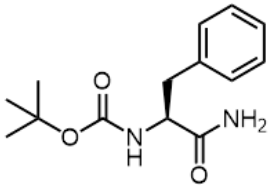	*Org. Lett.* **2017,** *19* (13), 3454-3457.	**4.15**
3.46p[40]	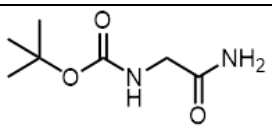	*J. Am. Chem. Soc.* **2002,** *124* (38), 11272-11273.	**4.15**

3.46q[41]	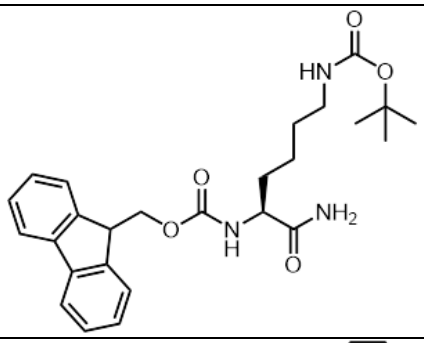	*J. Am. Chem. Soc.* **2001,** *123* (2), 333-334.	**4.15**
3.46r[42]	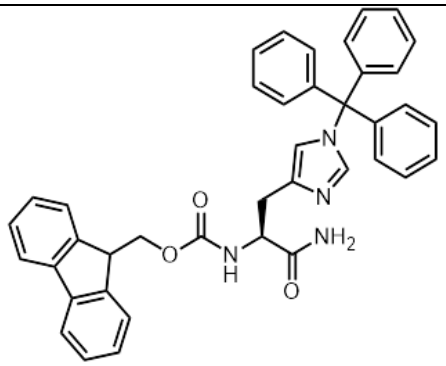	*ACS Med. Chem. Lett.* **2021,** *12* (6), 899-906.	**4.15**
3.46s[43]	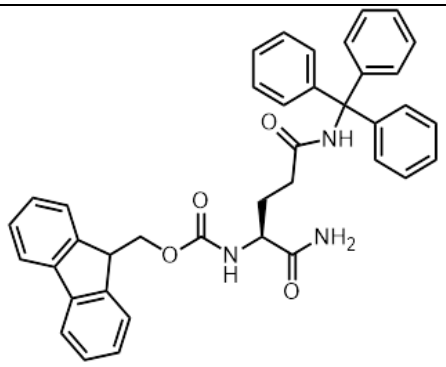	*J. Med. Chem.* **2023,** *66* (17), 12237-12248.	**4.15**

Synthetic Procedure for α,β-dehydroamino acids:

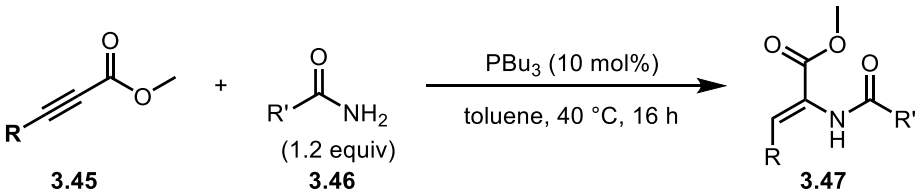

Scheme 4.18: Synthesis of α,β-dehydroamino acids.

Procedure 4.26: To a flame dried 2-dram vial: a stir bar, alkynoate **3.45** (0.250 mmol, 1.0 equiv) and amide **3.46** (0.300 mmol, 1.2 equiv) were added. The vial was sealed with a septa lid and put under an inert atmosphere using standard *Schlenk* technique. Then, toluene (1 mL, 0.25 M) and

tri-*n*-butylphosine (6.2 µL, 0.025 mmol, 10 mol%) were added. The vial was added to a preheated oil bath at 40 °C. The reaction was allowed to stir for 16 hours. The reaction was then opened and 2 mL of EtOAc was added. TLC analysis was conducted using 40% EtOAc:Hex. The α,β-dehydroamino acids generally have an Rf of 0.25 under these conditions. To the mixture, celite was added and volatiles were removed under vacuum. The α,β-dehydroamino acids **3.47** were purified using flash chromatography (0-60% EtOAc:Hex gradient). The *E*:*Z* isomers were separable if both isomers formed.

Characterization of α,β-dehydroamino acids

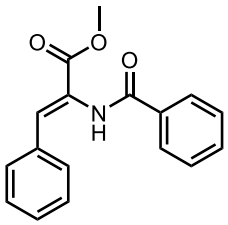

Modified from **procedure 4.26**, methyl (*Z*)-2-benzamido-3-phenylacrylate (**3.47a**) was isolated using flash chromatography (0-60% EtOAc:Hex gradient) as a white solid (49.2 mg, 0.175 mmol, 70% yield) using 70 °C instead of 40 °C. **^{1}H NMR** (400 MHz, $CDCl_3$) δ 7.87 (d, *J* = 7.4 Hz, 2H), 7.80 (br s, 1H), 7.55 (t, *J* = 7.4 Hz, 1H), 7.52 - 7.48 (m, 5H), 7.33 (m, 3H), 3.85 (s, 3H). **^{13}C NMR** (101 MHz, $CDCl_3$) δ 166.0, 134.0, 133.7, 132.3, 132.0, 129.8, 129.6, 128.9, 128.7, 127.6, 124.4, 52.9. One carbon is missing due to overlapping. This data agrees with literature reports.[44]

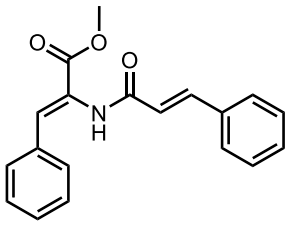

Following **procedure 4.26**, methyl (*Z*)-2-cinnamamido-3-phenylacrylate (**3.47b**) was isolated using flash chromatography (0-60% EtOAc:Hex gradient) as a white solid (43.9 mg, 0.143 mmol, 57% yield). **^{1}H NMR** (600 MHz, $CDCl_3$) δ 7.69 (d, *J* = 15.6 Hz, 1H), 7.56 – 7.45 (m, 4H), 7.43 (br s, 1H), 7.42 – 7.28 (m, 6H), 6.56 (d, *J* = 15.6 Hz, 1H), 3.87 (s, 3H). **^{13}C NMR** (151 MHz, $CDCl_3$) δ 166.0, 164.3, 143.4, 134.6, 134.0, 131.8, 130.3, 129.9, 129.6, 129.0, 128.8, 128.2, 124.1, 119.6, 53.0. **HRMS** (ESI) m/z $[M+H]^+$ calcd for $C_{19}H_{18}NO_3^+$ 308.1281; Found 308.1279, Δ 0.6491 ppm.

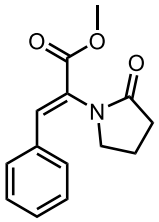

Following **procedure 4.26**, methyl (*Z*)-2-(2-oxopyrrolidin-1-yl)-3-phenylacrylate (**3.47c**) was isolated using flash chromatography (0-60% EtOAc:Hex gradient) as a colorless solid (22.3 mg, 0.093 mmol, 37% yield). **^{1}H NMR** (500 MHz, $CDCl_3$) δ 7.68 (s, 2H), 7.53 – 7.45 (m, 2H), 7.40 – 7.35 (m, 3H), 3.84 (s, 3H), 3.48 (t, *J* = 7.0 Hz, 2H), 2.51 (t, *J* = 8.1 Hz, 2H), 2.16 (tt, *J* = 7.7 Hz, 7.4 Hz, 2H). **^{13}C NMR** (126 MHz, $CDCl_3$) δ 176.6, 164.8, 138.9, 133.0, 130.3, 129.7, 129.0, 127.0, 52.8, 48.1, 30.8, 19.5. This data agrees with literature reports.[45]

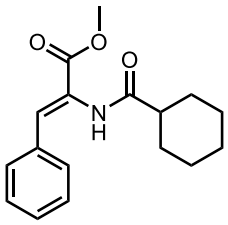

Modified from **procedure 4.26**, methyl (*Z*)-2-(cyclohexanecarboxamido)-3-phenylacrylate (**3.47d**) was isolated using flash chromatography (0-60% EtOAc:Hex gradient) as a white solid (15.2 mg, 0.053 mmol, 21% yield) using 20 mol% PBu_3 instead of 10 mol% PBu_3. **^{1}H NMR** (500 MHz, $CDCl_3$) δ 7.45 – 7.42 (m, 2H), 7.38 – 7.29 (m, 4H), 7.01 (s, 1H), 3.84 (s, 3H), 2.27 (tt, *J* = 11.7, 3.6 Hz, 1H), 1.96 (d, *J* = 12.9 Hz, 2H), 1.82 (d, *J* = 12.3 Hz, 2H), 1.69 (d, *J* = 11.2 Hz, 2H), 1.50 (qd, *J* = 12.2, 3.2 Hz, 2H), 1.37 – 1.28 (m, 2H). **^{13}C NMR** (126 MHz, $CDCl_3$) δ 174.3, 166.0, 134.2, 131.6, 129.7, 129.4, 128.6, 124.4, 52.8, 45.7, 29.9, 29.4, 25.8, 25.7. This data agrees with literature reports.[46]

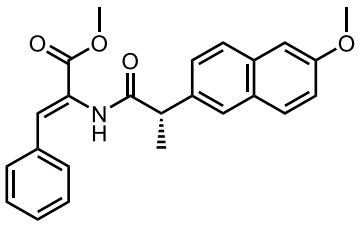

Following **procedure 4.26**, methyl (*S*,*Z*)-2-(2-(6-methoxynaphthalen-2-yl)propanamido)-3-phenylacrylate (**3.47e**) was isolated using flash chromatography (0-60% EtOAc:Hex gradient) as a white solid (24.5 mg, 0.063 mmol, 25% yield). **^{1}H NMR** (600 MHz, $CDCl_3$) δ 7.79 (d, *J* = 8.4 Hz, 1H), 7.75 – 7.70 (m, 2H), 7.44 (d, *J* = 8.3 Hz, 1H), 7.22 – 7.11 (m, 4H), 7.05 (d, *J* = 7.6 Hz, 2H), 6.95 (t, *J* = 7.3 Hz, 3H), 3.94 (s, 3H), 3.87 (q, *J* = 7.0 Hz, 1H), 3.80 (s, 3H), 1.63 (d, *J* = 7.1 Hz, 3H). **^{13}C NMR** (151 MHz, $CDCl_3$) δ 172.3, 165.7, 157.9, 135.4, 134.0, 133.5, 131.2,

129.5, 129.4, 129.3, 129.1, 128.4, 127.9, 126.5, 126.4, 124.6, 119.5, 105.7, 55.5, 52.7, 47.2, 17.9. **HRMS** (ESI) m/z $[M+H]^+$ calcd for $C_{24}H_{23}NO_4^+$ 390.1700; Found 390.1694, Δ 1.5378 ppm.

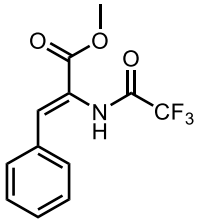

Following **procedure 4.26**, methyl (*Z*)-3-phenyl-2-(2,2,2-trifluoroacetamido)acrylate (**3.47f**) was isolated using flash chromatography (0-60% EtOAc:Hex gradient) as a colorless solid (39.0 mg, 0.143 mmol, 57% yield). **^{1}H NMR** (400 MHz, $CDCl_3$) δ 7.76 (s, 1H), 7.63 (s, 1H), 7.44 – 7.37 (m, 5H), 3.89 (s, 3H). **^{13}C NMR** (126 MHz, $CDCl_3$) δ 164.5, 155.1 (q, *J* = 37.9 Hz), 135.7, 132.8, 130.5, 129.7, 129.0, 121.2, 115.7 (q, *J* = 288.3 Hz), 53.2. **^{19}F NMR** (376 MHz, $CDCl_3$) δ -75.7. **HRMS** (ESI) $[M+H]^+$ calcd for $C_{12}H_{11}F_3NO_3^+$ 274.0686; found 274.0695, Δ 3.2839 ppm.

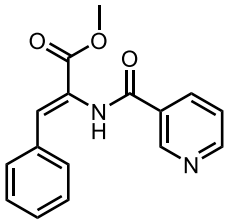

Following **procedure 4.26**, methyl (*Z*)-2-(nicotinamido)-3-phenylacrylate (**3.47g**) was isolated using flash chromatography (0-60% EtOAc:Hex gradient) as a white solid (65.7 mg, 0.233 mmol, 93% yield). ^{1}H NMR (400 MHz, $CDCl_3$) δ 9.05 (s, 1H), 8.75 (dd, *J* = 4.9, 1.7 Hz, 1H), 8.20 – 8.14 (m, 1H), 7.92 (s, 1H), 7.52 (s, 1H), 7.48 (dd, *J* = 7.6, 2.1 Hz, 2H), 7.40 (dd, *J* = 8.0, 4.9 Hz, 1H), 7.37 – 7.28 (m, 3H), 3.87 (s, 3H). **^{13}C NMR** (126 MHz, CDCl3) δ 165.7, 164.1, 152.9, 148.4, 135.8, 133.7, 132.9, 129.9, 129.7, 129.5, 128.9, 123.9, 123.8, 53.0. HRMS (ESI) $[M+H]^+$calcd for $C_{16}H_{15}N_2O_3^+$ 283.1083; found 283.1080, Δ 1.0597 ppm.

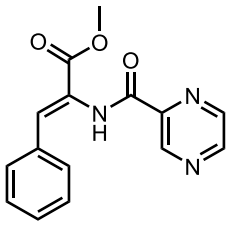

Following **procedure 4.26**, methyl (*Z*)-3-phenyl-2-(pyrazine-2-carboxamido)acrylate (**3.47h**) was isolated using flash chromatography (0-60% EtOAc:Hex gradient) as a white solid (55.2 mg, 0.195 mmol, 78% yield). **^{1}H NMR** (400 MHz, $CDCl_3$) δ 9.44 – 9.38 (m, 2H), 8.79 (d, *J* = 2.4 Hz, 1H), 8.58 (dd, *J* = 2.3, 1.5 Hz, 1H), 7.53 – 7.47 (m, 3H), 7.37 – 7.30 (m, 3H), 3.87 (s, 3H). **^{13}C NMR** (101 MHz, $CDCl_3$) δ 165.4, 161.4, 147.8, 144.9, 143.9, 142.8, 133.7, 132.9, 129.8, 129.7, 128.8,

123.6, 52.9. **HRMS** (ESI) m/z $[M+H]^+$ calcd for $C_{15}H_{14}N_3O_3^+$ 284.1030; Found 284.1034. Δ 1.4079 ppm.

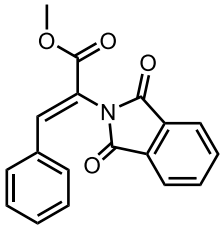

Following **procedure 4.26**, methyl (*Z*)-2-(1,3-dioxoisoindolin-2-yl)-3-phenylacrylate (**3.47i)** was isolated using flash chromatography (0-60% EtOAc:Hex gradient) as a white solid (53.4 mg, 0.174 mmol, 70% yield). **^{1}H NMR** (400 MHz, $CDCl_3$) δ 8.12 (s, 1H), 7.91 (dd, *J* = 5.4, 3.1 Hz, 2H), 7.78 (dd, *J* = 5.5, 3.2 Hz, 2H), 7.44 – 7.36 (m, 2H), 7.29 (q, *J* = 6.8 Hz, 3H), 3.82 (s, 3H). **^{13}C NMR** (151 MHz, $CDCl_3$) δ 166.9, 164.0, 143.1, 134.6, 132.4, 132.2, 130.7, 129.5, 129.0, 124.1, 120.1, 52.9. **HRMS** (ESI) m/z $[M+H]^+$ calcd for $C_{18}H_{14}NO_4^+$ 308.0917; found 308.0931, Δ 4.5441 ppm.

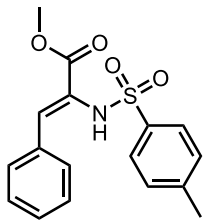

Following **procedure 4.26**, methyl (*Z*)-2-((4-methylphenyl)sulfonamido)-3-phenylacrylate (**3.47j)** was isolated using flash chromatography (0-40% EtOAc:Hex gradient) as a yellow solid (55.5 mg, 0.168 mmol, 67% yield). **^{1}H NMR** (600 MHz, $CDCl_3$) δ 7.89 – 7.76 (m, 2H), 7.66 (d, *J* = 8.1 Hz, 2H), 7.52 (s, 1H), 7.39 – 7.33 (m, 3H), 7.23 (d, *J* = 8.0 Hz, 2H), 6.19 (s, 1H), 3.53 (s, 3H), 2.39 (s, 3H). **^{13}C NMR** (151 MHz, $CDCl_3$) δ 165.5, 144.0, 137.8, 136.5, 132.9, 131.2, 130.5, 129.5, 128.6, 127.7, 122.9, 52.7, 21.7. **HRMS** (ESI) m/z $[M+H]^+$ calcd for $C_{17}H_{18}NO_4S^+$ 332.0951; found 332.0950, Δ 0.30112 ppm.

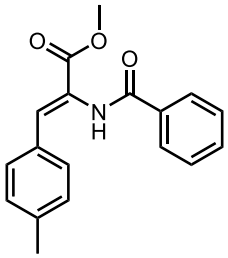

Following **procedure 4.26**, methyl (*Z*)-2-benzamido-3-(*p*-tolyl)acrylate (**3.47k**) was isolated using flash chromatography (0-60% EtOAc:Hex gradient) as a white solid (43.7 mg, 0.148 mmol, 59% yield). **^{1}H NMR** (400 MHz, $CDCl_3$) δ 7.87 (d, *J* = 7.5 Hz, 2H), 7.81 (s, 1H), 7.59 – 7.51 (m, 1H), 7.49 – 7.43 (m, 3H), 7.40 (d, *J* = 8.0 Hz, 2H), 7.13 (d, *J* = 7.8 Hz, 2H), 3.84 (s, 3H), 2.32 (s, 3H). **^{13}C**

NMR (101 MHz, $CDCl_3$) δ 166.1, 165.8, 140.0, 133.8, 132.4, 132.2, 131.1, 129.9, 129.5, 128.8, 127.6, 123.5, 52.8, 21.5. This data agrees with literature reports.[47]

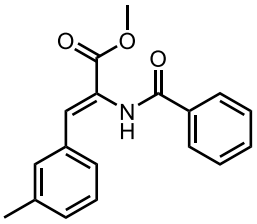

Following **procedure 4.26**, methyl (*Z*)-2-benzamido-3-(*m*-tolyl)acrylate (**3.47l**) was isolated using flash chromatography (0-60% EtOAc:Hex gradient) as a white solid (26.0 mg, 0.088 mmol, 35% yield). **^{1}H NMR** (400 MHz, $CDCl_3$) δ 7.86 (d, *J* = 7.0 Hz, 2H), 7.73 (s, 1H), 7.55 (dd, *J* = 6.5, 1.3 Hz, 1H), 7.52 – 7.41 (m, 3H), 7.32 (d, *J* = 7.3 Hz, 2H), 7.22 (t, *J* = 7.6 Hz, 1H), 7.12 (d, *J* = 7.6 Hz, 1H), 3.85 (s, 3H), 2.29 (s, 3H). **^{13}C NMR** (101 MHz, $CDCl_3$) δ 166.0, 138.3, 133.9, 133.8, 132.3, 132.1, 130.7, 130.5, 128.9, 128.7, 127.6, 126.7, 124.3, 52.9, 21.5. One carbon is missing due to overlapping. **HRMS** (ESI) m/z $[M+H]^+$ calcd $C_{18}H_{17}NNaO_3^+$ 318.1101; Found 318.1106. Δ 1.5718 ppm.

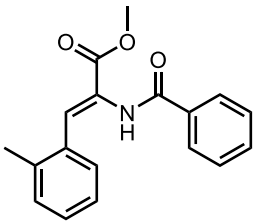

Following **procedure 4.26**, methyl (*Z*)-2-benzamido-3-(*o*-tolyl)acrylate (**3.47m**) was isolated using flash chromatography (0-60% EtOAc:Hex gradient) as a white solid (11.8 mg, 0.040 mmol, 16% yield). ^{1}H NMR (400 MHz, CDCl3) δ 7.78 (d, *J* = 7.8 Hz, 2H), 7.59 (s, 1H), 7.56 – 7.50 (m, 1H), 7.48 (s, 1H), 7.46 – 7.38 (m, 3H), 7.25 – 7.17 (m, 2H), 7.14 – 7.08 (m, 1H), 3.89 (s, 3H), 2.38 (s, 3H). **^{13}C NMR** (126 MHz, $CDCl_3$) δ 165.8, 137.5, 133.7, 133.2, 132.3, 130.7, 129.2, 129.2, 128.8, 127.9, 127.6, 126.1, 125.9, 52.9, 20.2. One carbon is missing due to overlapping. This data agrees with literature reports.[47]

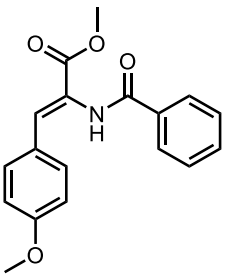

Following **procedure 4.26**, methyl (*Z*)-2-benzamido-3-(4-methoxyphenyl)acrylate (**3.47n**) was isolated using flash chromatography (0-60% EtOAc:Hex gradient) as a white solid (44.5 mg, 0.143 mmol, 57% yield). **^{1}H NMR** (400 MHz, $CDCl_3$) δ 7.88 (d, *J* = 7.6 Hz, 2H), 7.81 (bs, 1H), 7.55 (t,

J = 7.4 Hz, 1H), 7.52 – 7.39 (m, 5H), 6.83 (d, *J* = 8.8 Hz, 2H), 3.82 (s, 3H), 3.78 (s, 3H). **^{13}C NMR** (101 MHz, $CDCl_3$) δ 166.2, 165.5, 160.7, 133.8, 132.7, 132.2, 131.9, 128.8, 127.6, 126.5, 122.0, 114.2, 55.4, 52.7. This data agrees with literature reports.[47]

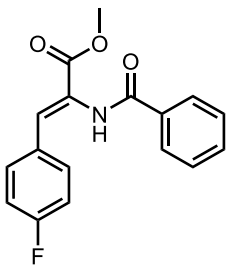

Following **procedure 4.26**, methyl (*Z*)-2-benzamido-3-(4-fluorophenyl)acrylate (**3.47o**) was isolated using flash chromatography (0-60% EtOAc:Hex gradient) as a off-white solid (35.3 mg, 0.118 mmol, 47% yield). **^{1}H NMR** (400 MHz, $CDCl_3$) δ 7.87 (d, *J* = 7.8 Hz, 2H), 7.80 (s, 1H), 7.57 (t, *J* = 7.0 Hz, 1H), 7.53 – 7.44 (m, 5H), 7.01 (t, *J* = 8.6 Hz, 2H), 3.87 (s, 3H). **^{13}C NMR** (126 MHz, $CDCl_3$) δ 166.0, 165.6, 163.1 (d, *J* = 251.3 Hz), 133.7, 132.5, 131.9 (d, *J* = 8.4 Hz), 130.8, 130.3 (d, *J* = 3.4 Hz), 129.0, 127.6, 123.5, 115.9 (d, *J* = 21.7 Hz), 53.0.. **^{19}F NMR** (376 MHz, $CDCl_3$) δ -110.0. This data agrees with literature reports.[47]

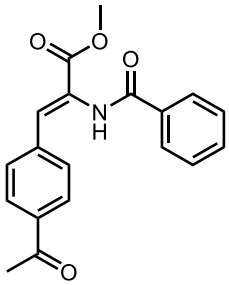

Following **procedure 4.26**, methyl (*Z*)-3-(4-acetylphenyl)-2-benzamidoacrylate (**3.47p**) was isolated using flash chromatography (0-60% EtOAc:Hex gradient) as a off-white solid (26.8 mg, 0.083 mmol, 33% yield). **^{1}H NMR** (400 MHz, $CDCl_3$) δ 7.96 (s, 1H), 7.90 (d, *J* = 8.1 Hz, 2H), 7.86 (d, *J* = 7.7 Hz, 2H), 7.60 – 7.53 (m, 3H), 7.52 – 7.45 (m, 3H), 3.90 (s, 3H), 2.56 (s, 3H). **^{13}C NMR** (126 MHz, $CDCl_3$) δ 197.6, 165.8, 165.2, 139.1, 137.0, 133.5, 132.6, 129.7, 129.1, 129.0, 128.6, 127.6, 125.2, 53.2, 26.8. **HRMS** (ESI) m/z $[M+Na]^+$ calcd for $C_{19}H_{17}NNaO_4^+$ 346.1050; found 346.1050. Δ 0.0000 ppm.

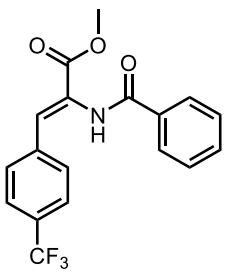

Following **procedure 4.26**, methyl (*Z*)-2-benzamido-3-(4-(trifluoromethyl)phenyl)acrylate (**3.47q**) was isolated using flash chromatography (0-60% EtOAc:Hex gradient) as a yellow solid (25.5 mg, 0.073 mmol, 29% yield). **^{1}H NMR** (400 MHz, $CDCl_3$) δ 7.94 (s, 1H), 7.85 (d,

J = 7.5 Hz, 2H), 7.63 – 7.54 (m, 5H), 7.53 – 7.43 (m, 3H), 3.90 (s, 3H).**^{13}C NMR** (126 MHz, $CDCl_3$) δ 165.7, 165.3, 137.9, 133.5, 132.6, 130.8 (q, *J* = 32.7 Hz), 129.8, 129.1, 129.0, 127.6, 125.5 (d, *J* = 3.8 Hz), 125.3, 122.9 (q, *J* = 272.2 Hz), 53.2. **^{19}F NMR** (376 MHz, $CDCl_3$) δ -62.9 (s, 3F). **HRMS** (ESI) m/z $[M+H]^+$ calcd for $C_{18}H_{15}F_3NO_3^+$ 350.0999; found 350.1010, Δ 3.1420 ppm.

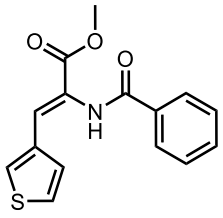

Following **procedure 4.26**, methyl (*Z*)-2-benzamido-3-(thiophen-3-yl)acrylate (**3.47r**) was isolated using flash chromatography (0-60% EtOAc:Hex gradient) as a yellow solid (25.8 mg, 0.090 mmol, 36% yield). **^{1}H NMR** (400 MHz, $CDCl_3$) δ 7.90 (d, *J* = 7.6 Hz, 2H), 7.72 (s, 1H), 7.61 – 7.53 (m, 3H), 7.48 (t, *J* = 7.6 Hz, 2H), 7.28 – 7.25 (m, 2H), 3.83 (s, 3H). **^{13}C NMR** (126 MHz, $CDCl_3$) δ 166.1, 166.1, 135.3, 133.7, 132.4, 129.6, 128.9, 128.0, 127.7, 127.6, 126.3, 122.6, 52.8. **HRMS** (ESI) m/z $[M+H]^+$ calcd for $C_{15}H_{14}NO_3S^+$ 288.0689; found 288.0690, Δ 0.3471 ppm.

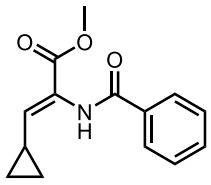

Modified from **procedure 4.26**, methyl (*Z*)-2-benzamido-3-cyclopropylacrylate (**3.47s**) was isolated using flash chromatography (0-60% EtOAc:Hex gradient) as a colorless solid (40.4 mg, 0.165 mmol, 66% yield) using 20 mol% of K_2CO_3 as an additive. **^{1}H NMR** (500 MHz, $CDCl_3$) δ 7.89 (d, *J* = 7.4 Hz, 2H), 7.60 – 7.42 (m, 4H), 6.23 (d, *J* = 10.8 Hz, 1H), 3.77 (s, 3H), 1.75 – 1.54 (m, 1H), 1.06 (td, *J* = 6.8, 4.4 Hz, 2H), 0.73 (dt, *J* = 6.7, 4.4 Hz, 2H). **^{13}C NMR** (126 MHz, $CDCl_3$) δ 166.0, 165.2, 144.3, 134.3, 132.1, 128.8, 127.5, 52.5, 31.2, 12.7, 9.1. **HRMS** (ESI) m/z $[M+H]^+$ calcd for $C_{14}H_{16}NO_3$ 246.1125; found 246.1128, Δ 1.2190 ppm.

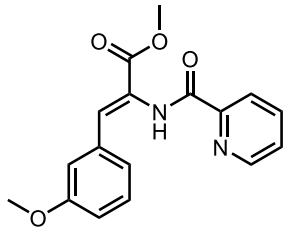

Following **procedure 4.26**, methyl (*Z*)-3-(3-methoxyphenyl)-2-(picolinamido)acrylate (**3.47t**) was isolated using flash chromatography (0-60% EtOAc:Hex gradient) as a colorless oil (53.1 mg, 0.170 mmol,

68% yield). **^{1}H NMR** (400 MHz, $CDCl_3$) δ 9.74 (s, 1H), 8.63 (d, *J* = 4.6 Hz, 1H), 8.24 (d, *J* = 7.8 Hz, 1H), 7.90 (td, *J* = 7.7, 1.7 Hz, 1H), 7.50 (ddd, *J* = 7.6, 4.8, 1.1 Hz, 1H), 7.43 (s, 1H), 7.30 – 7.27 (m, 1H), 7.19 – 7.11 (m, 2H), 6.90 (dd, *J* = 7.9, 2.2 Hz, 1H), 3.90 (s, 3H), 3.72 (s, 3H). **^{13}C NMR** (126 MHz, $CDCl_3$) δ 165.6, 162.7, 159.6, 149.1, 148.4, 137.7, 135.0, 131.6, 129.7, 126.8, 124.6, 122.8, 122.6, 115.8, 114.4, 55.2, 52.8. This data agrees with literature reports.[48]

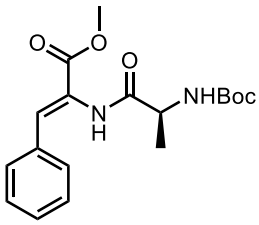

Following **procedure 4.26**, methyl (S,*Z*)-2-(2-((*tert*-butoxycarbonyl)amino)propanamido)-3-phenylacrylate (**3.47u**) was isolated using flash chromatography (0-60% EtOAc:Hex gradient) as a white solid (46.3 mg, 0.133 mmol, 53% yield). **^{1}H NMR** (400 MHz, $CDCl_3$) δ 7.70 (s, 1H), 7.48 (d, *J* = 7.1 Hz, 2H), 7.43 (s, 1H), 7.39 – 7.29 (m, 3H), 4.97 (s, 1H), 4.36 – 4.24 (m, 1H), 3.84 (s, 3H), 1.46 (s, 9H), 1.42 (d, *J* = 7.1 Hz, 3H). **^{13}C NMR** (126 MHz, $CDCl_3$) δ 171.5, 165.6, 155.8, 133.7, 133.2, 129.9, 129.6, 128.7, 123.9, 80.4, 52.8, 50.5, 28.4, 17.9. This data agrees with literature reports.[49]

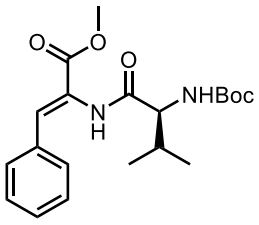

Following **procedure 4.26**, methyl (*S*,*Z*)-2-(2-((*tert*-butoxycarbonyl)amino)-3-methylbutanamido)-3-phenylacrylate (**3.47v**) was isolated using flash chromatography (0-60% EtOAc:Hex gradient) as a white solid (48.2 mg, 0.128 mmol, 51% yield). **^{1}H NMR** (400 MHz, $CDCl_3$) δ 7.72 (s, 1H), 7.46 (d, *J* = 7.2 Hz, 2H), 7.37 (s, 1H), 7.32 (m, 3H), 5.08 (d, *J* = 8.9 Hz, 1H), 4.10 (t, *J* = 7.3 Hz, 1H), 3.81 (s, 3H), 2.23 (h, *J* = 6.7 Hz, 1H), 1.44 (s, 9H), 0.99 (dd, *J* = 22.1, 6.8 Hz, 6H). **^{13}C NMR** (101 MHz, $CDCl_3$) δ 170.8, 165.6, 156.2, 133.7, 132.8, 129.9, 129.6, 128.7, 124.1, 80.3, 60.3, 52.7, 30.6, 28.4, 19.4, 17.7. This data agrees with literature reports.[49]

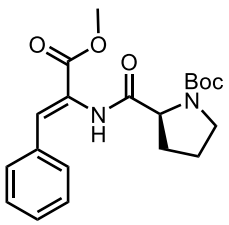

Following **procedure 4.26**, *tert*-butyl (*S*,*Z*)-2-((3-methoxy-3-oxo-1-phenylprop-1-en-2-yl)carbamoyl)pyrrolidine-1-carboxylate (**3.47w**) was isolated using flash chromatography (0-60% EtOAc:Hex gradient) as a white solid (61.7 mg, 0.165 mmol, 66% yield). **^{1}H NMR** (400 MHz, CD_3OD) δ 7.70 (d, *J* = 6.0 Hz, 1H), 7.58 (s, 1H), 7.45 (d, *J* = 6.4 Hz, 1H), 7.38 (d, *J* = 7.3 Hz, 2H), 4.38 (t, *J* = 7.9 Hz, 1H), 3.80 (s, 3H), 3.53 (s, 1H), 3.46 – 3.35 (m, 1H), 2.35 – 2.18 (m, 1H), 2.17 – 2.09 (m, 1H), 2.04 – 1.84 (m, 2H), 1.47 (appd, *J* = 18.2 Hz, 9H). ^{13}C NMR (101 MHz, CD_3OD) δ 175.8*, 167.0, 166.8, 136.1,* 131.6,* 130.9,* 130.8,* 129.7, 126.6,* 81.7, 81.3, 47.9, 32.2,* 31.1,* 28.8,* 25.3.* **HRMS** (ESI) m/z $[M+H]^+$ calcd for $C_{20}H_{26}N_2NaO_5^+$ 397.1734; found 397.1734, Δ 0.0000 ppm. *Note:* This compound exists as a mixture of rotamers. In $CDCl_3$ all ^{1}H NMR peaks are broadened and some ^{13}C NMR peaks are broadened. In CD_3OD two distinct rotamers are observed. "*" indicates a ^{13}C NMR peak that has an observed rotamer peak present in the spectra.

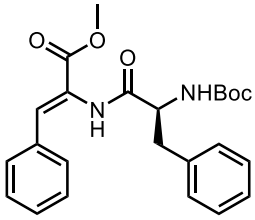

Following **procedure 4.26**, methyl (*S*,*Z*)-2-(2-((*tert*-butoxycarbonyl)amino)-3-phenylpropanamido)-3-phenylacrylate (**3.47x**) was isolated using flash chromatography (0-60% EtOAc:Hex gradient) as a white solid (58.5 mg, 0.138 mmol, 55% yield). **^{1}H NMR** (500 MHz, $CDCl_3$) δ 7.60 (s, 1H), 7.37 (m, 3H), 7.34 – 7.29 (m, 5H), 7.27 (s, 1H), 7.24 (s, 1H), 4.93 (s, 1H), 4.50 (q, *J* = 7.7 Hz, 1H), 3.20 (dd, *J* = 14.0, 6.6 Hz, 1H), 3.08 (dd, *J* = 14.2, 7.2 Hz, 1H), 1.41 (s, 9H). **^{13}C NMR** (126 MHz, $CDCl_3$) δ 170.2, 165.5, 155.8, 136.5, 133.6, 132.7, 129.8, 129.6, 129.5, 128.9, 128.8, 127.2, 123.9, 80.7, 52.8, 37.5, 28.4. This data agrees with literature reports.[49]

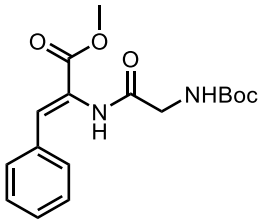

Modified from **procedure 4.26**, methyl (*Z*)-2-(2-((*tert*-butoxycarbonyl)amino)acetamido)-3-phenylacrylate (**3.47y**) was isolated using flash chromatography (0-60% EtOAc:Hex gradient) as a colorless oil

(36.1 mg, 0.108 mmol, 43% yield) using 90 °C instead of 40 °C. **^{1}H NMR** (400 MHz, $CDCl_3$) δ 7.77 (s, 1H), 7.53 – 7.28 (m, 6H), 5.28 (s, 1H), 3.92 (s, 2H), 3.83 (s, 3H), 1.44 (s, 9H). **^{13}C NMR** (151 MHz, $CDCl_3$) δ 168.6, 165.6, 156.3, 133.5, 133.3, 129.9, 129.8, 128.8, 123.6, 80.6, 52.9, 44.9, 28.4. ^{13}C NMR (151 MHz, $CDCl_3$) δ 168.6, 165.6, 156.3, 133.5, 133.3, 129.9, 129.8, 128.8, 123.6, 80.6, 52.9, 44.9, 28.4. This data agrees with literature reports.[49]

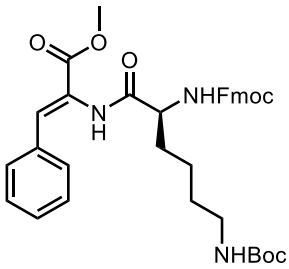

Following **procedure 4.26**, methyl (*S*,*Z*)-2-(2-((((9H-fluoren-9-yl)methoxy)carbonyl)amino)-6-((*tert*-butoxycarbonyl)amino)hexanamido)-3-phenylacrylate (**3.47z**) was isolated using flash chromatography (20-100% EtOAc:Hex gradient) as a white solid (22.0 mg, 0.035 mmol, 14% yield). **^{1}H NMR** (400 MHz, CD_3OD) δ 7.79 (d, *J* = 7.6 Hz, 2H), 7.68 (d, *J* = 7.4 Hz, 2H), 7.61 (d, *J* = 6.7 Hz, 2H), 7.45 (s, 1H), 7.43 – 7.20 (m, 9H), 6.55 (bs, 1H), 4.48 – 4.37 (m, 2H), 4.23 (m, 2H), 3.79 (s, 3H), 3.06 (t, *J* = 5.8 Hz, 2H), 1.94 – 1.80 (m, 1H), 1.77 – 1.64 (m, 1H), 1.55 – 1.46 (m, 4H), 1.42 (s, 9H). **^{13}C NMR** (126 MHz, $CDCl_3$) δ 170.6, 165.4, 156.5, 156.3, 143.7, 143.7, 141.3, 133.4, 133.2, 129.7, 128.6, 127.8, 127.1, 125.1, 123.8, 120.0, 79.2, 67.2, 55.0, 52.7, 47.1, 39.7, 31.4, 29.6, 28.4, 22.2. **HRMS** (ESI) m/z $[M+H]^+$ calcd for $C_{36}H_{42}N_3O_7^+$ 628.3017; found 628.3039, Δ 3.5015 ppm.

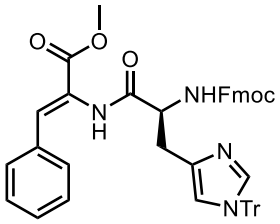

Following **procedure 4.26**, methyl (*S*,*Z*)-2-(2-((((9H-fluoren-9-yl)methoxy)carbonyl)amino)-3-(1-trityl-*1H*-imidazol-4-yl)propanamido)-3-phenylacrylate (**3.47aa**) was isolated using flash chromatography (20-100% EtOAc:Hex gradient) as a white solid (37.0 mg, 0.0475 mmol, 19% yield). **^{1}H NMR** (400 MHz, MeOD) δ 7.78 (d, *J* = 7.3 Hz, 2H), 7.65 – 7.55 (m, 3H), 7.45 (s, 1H), 7.41 – 7.16 (m, 20H), 7.08 (dd, *J* = 6.5, 2.9 Hz, 6H), 6.85 (d, *J* = 4.6 Hz, 1H), 4.56 (dd, *J* = 9.1, 4.8 Hz, 1H), 4.31 (t, *J* = 7.4 Hz, 2H), 4.14 (t, *J* = 6.7 Hz, 1H), 3.71 (s, 3H), 3.13 (dd, *J* = 14.7, 4.6

Hz, 1H), 2.91 (dd, *J* = 14.4, 9.7 Hz, 1H).**^{13}C NMR** (126 MHz, MeOD) δ 173.9, 166.9, 158.4, 145.2, 143.6, 142.6, 139.4, 137.6, 135.6, 134.6, 131.3, 130.9, 130.8, 129.8, 129.3, 129.2, 128.8, 128.2, 126.3, 120.9, 76.9, 68.2, 56.6, 52.9, 37.6, 31.4. **HRMS** (ESI) m/z $[M+H]^+$ calcd for $C_{50}H_{43}N_4O_5^+$ 779.3228; found 779.3229, Δ 0.1283 ppm.

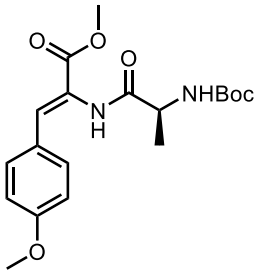

Following **procedure 4.26**, methyl (*S*,*Z*)-2-(2-((*tert*-butoxycarbonyl)amino)propanamido)-3-(4-methoxyphenyl)acrylate (**3.47ab**) was isolated using flash chromatography (0-60% EtOAc:Hex gradient) as a white solid (69.2 mg, 0.183 mmol, 73% yield). **^{1}H NMR** (500 MHz, $CDCl_3$) δ 7.92 (s, 1H), 7.45 (d, *J* = 8.4 Hz, 2H), 7.39 (s, 1H), 6.83 (d, *J* = 8.6 Hz, 2H), 5.27 (d, *J* = 7.3 Hz, 1H), 4.43 – 4.33 (m, 1H), 3.77 (s, 3H), 3.76 (s, 3H), 1.51 – 1.33 (m, 12H).**^{13}C NMR** (126 MHz, $CDCl_3$) δ 171.8, 165.9, 160.7, 155.8, 134.0, 132.0, 126.1, 121.6, 114.1, 80.3, 55.3, 52.6, 50.4, 28.4, 18.1. **HRMS** (ESI) m/z $[M+H]^+$ calcd $C_{19}H_{27}N_2O_6^+$ for 379.1864; found 379.1857, Δ 1.8461 ppm.

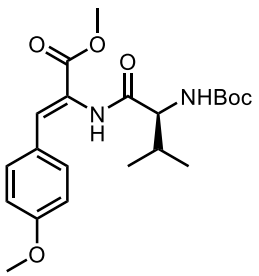

Following **procedure 4.26**, methyl (*S*,*Z*)-2-(2-((*tert*-butoxycarbonyl)amino)-3-methylbutanamido)-3-(4-methoxyphenyl)acrylate (**3.47ac**) was isolated using flash chromatography (0-60% EtOAc:Hex gradient) as a white solid (54.8 mg, 0.135 mmol, 54% yield). **^{1}H NMR** (400 MHz, $CDCl_3$) δ 7.69 (s, 1H), 7.45 (d, *J* = 8.4 Hz, 2H), 7.38 (s, 1H), 6.83 (d, *J* = 8.8 Hz, 2H), 5.11 (d, *J* = 8.8 Hz, 1H), 4.18 – 4.10 (m, 1H), 3.79 – 3.78 (appd, 6H), 2.25 (h, *J* = 5.8 Hz, 1H), 1.44 (s, 9H), 1.01 (dd, *J* = 22.3, 6.8 Hz, 6H). **^{13}C NMR** (101 MHz, $CDCl_3$) δ 170.9, 165.8, 160.8, 156.2, 133.6, 132.0, 126.1, 121.8, 114.2, 80.3, 60.3, 55.4, 52.5, 30.7, 28.5, 19.5. **HRMS** (ESI) m/z $[M+H]^+$ calcd for $C_{21}H_{31}N_2O_6^+$ 407.2177; found 407.2180, Δ 0.7367 ppm.

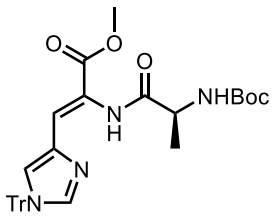

Following **procedure 4.26**, methyl (*S*,*Z*)-2-(2-((*tert*-butoxycarbonyl)amino)propanamido)-3-(1-trityl-*1H*-imidazol-4-yl)acrylate (**3.47ad**) was isolated using flash chromatography (0-60% EtOAc:Hex gradient) as a white solid (107.4 mg, 0.185 mmol, 74% yield). **^{1}H NMR** (400 MHz, $CDCl_3$) δ 10.67 (s, 1H), 7.47 (s, 1H), 7.39 – 7.33 (m, 9H), 7.11 (dd, *J* = 6.3, 2.9 Hz, 6H), 6.91 (s, 1H), 6.49 (s, 1H), 5.30 (s, 1H), 4.40 (s, 1H), 3.80 (s, 3H), 1.45 (d, *J* = 6.9 Hz, 3H), 1.39 (d, *J* = 1.3 Hz, 9H). **^{13}C NMR** (126 MHz, $CDCl_3$) δ 171.3, 165.6, 155.3, 141.9, 139.0, 136.8, 129.8, 128.5, 128.4, 127.0, 123.4, 113.4, 79.6, 75.9, 52.4 50.4, 28.5, 19.5. **HRMS** (ESI) m/z $[M\text{-Boc}+2H]^+$ calcd for $C_{29}H_{29}N_4O_3^+$ 481.2234; found 481.2233, Δ 0.2078 ppm.

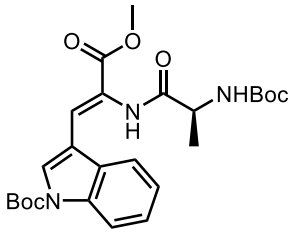

Following **procedure 4.26**, *tert*-butyl (*S*,*Z*)-3-(2-(2-((*tert*-butoxycarbonyl)amino)propanamido)-3-methoxy-3-oxoprop-1-en-1-yl)-*1H*-indole-1-carboxylate (**3.47ae**) was isolated using flash chromatography (0-60% EtOAc:Hex gradient) as a colorless solid (107.2 mg, 0.220 mmol, 88% yield). **^{1}H NMR** (400 MHz, $CDCl_3$) δ 8.13 (d, *J* = 8.1 Hz, 1H), 7.90 (s, 1H), 7.85 (s, 1H), 7.73 (s, 1H), 4.38 (apt, *J* = 6.4 Hz, 1H), 7.38 – 7.27 (m, 2H), 5.08 (s, 1H), 4.38 (d, *J* = 6.5 Hz, 1H), 3.85 (s, 3H), 1.67 (s, 9H), 1.47 (d, *J* = 6.7 Hz, 3H), 1.44 (s, 9H). **^{13}C NMR** (101 MHz, $CDCl_3$) δ 171.3, 171.0, 165.5, 155.8, 149.4, 135.0, 129.6, 127.9, 125.2, 123.3, 122.8, 119.0, 115.5, 114.1, 84.7, 60.5, 52.7, 28.4, 28.3, 21.2, 14.3. **HRMS** (ESI) m/z $[M+H]^+$ calcd for $C_{25}H_{34}N_3O_7^+$ 488.2391; found 488.2391, Δ 0.0000 ppm.

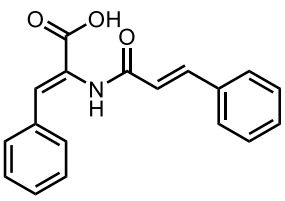

Procedure 4.27: To a 0.25 M solution of **3.47b** (0.411 mmol, 126.0 mg, 1.0 equiv) in THF, powdered sodium hydroxide (2.47 mmol, 59.1 mg, 6.0 equiv) was added. One drop of water was also added to solubilize the sodium hydroxide. The reaction was allowed to stir at 40 °C, overnight. Then, 1 M aqueous HCl

(4.11 mmol, 4.11 mL, 10.0 equiv) was added and a white precipitate formed. Compound **3.50** was extracted with ethyl acetate three times, dried over Na_2SO_4 and dried under vacuum. Upon removal of solvent a white solid remained (118 mg, 0.407 mmol, 99% yield). (*Z*)-2-cinnamamido-3-phenylacrylic acid (**3.50**) **^{1}H NMR** (400 MHz, DMSO-d_6) δ 12.71 (s, 1H), 9.74 (s, 1H), 7.62 (d, *J* = 7.0 Hz, 4H), 7.52 (d, *J* = 15.8 Hz, 1H), 7.41 (m, 6H), 7.28 (s, 1H), 6.86 (d, *J* = 15.8 Hz, 1H). **^{13}C NMR** (101 MHz, DMSO-d_6) δ 166.3, 164.5, 140.4, 134.6, 133.8, 131.1, 129.8, 129.7, 129.2, 129.0, 128.6, 127.8, 127.1, 121.1. **HRMS** (ESI) m/z $[M-H]^-$ calcd for $C_{18}H_{14}NO_3^-$ 292.0979; found 292.0978, Δ 0.3424 ppm.

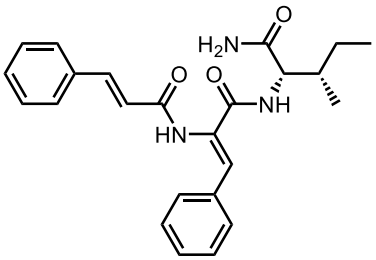

Procedure 4.28: To a 0.25 M solution of compound **3.50** in DMF, O-(1H-6-Chlorobenzotriazole-1-yl)-1,1,3,3-tetramethyluronium hexafluorophosphate(HCTU) (0.150 mmol, 62.1 mg, 1.2 equiv) and *N*,*N*-diispropylethylamine (0.225 mmol, 39.2 μL, 1.8 equiv) were added. The mixture was allowed to stir at room temperature for 1 hour. Then, *L*-isoleucinamide (0.150 mmol, 19.5 mg, 1.2 equiv) was added and the reaction was allowed to stir overnight. Next, the reaction mixture was extracted with aqueous lithium bromide and ethyl acetate, three times each. The organic layer was dried over Na_2SO_4 and filtered. Celite was added and volatiles were removed under vacuum. The crude reaction was purified using flash chromatography with EtOAc:Hex (20-100%) gradient to afford Scutiamine M (**3.51**) as a white solid (43.6 mg, 0.108 mmol, 86% yield). **^{1}H NMR** (400 MHz, DMSO-d_6) δ 9.85 (s, 1H), 7.71 (d, *J* = 8.6 Hz, 1H), 7.63 (d, *J* = 6.6 Hz, 2H), 7.57 (d, *J* = 7.7 Hz, 2H), 7.53 (d, *J* = 16.0 Hz, 1H), 7.48 – 7.29 (m, 7H), 7.12 (s, 1H), 7.01 (s, 1H), 6.90 (d, *J* = 15.8 Hz, 1H), 4.22 (dd, *J* = 8.5, 6.6 Hz, 1H), 1.88 – 1.78 (m, 1H), 1.50 – 1.41 (m, 1H), 1.18 – 1.03 (m, 1H), 0.88 (d, *J* = 6.8 Hz, 3H), 0.83 (t, *J*

= 7.3 Hz, 3H). **^{13}C NMR** (126 MHz, DMSO) δ 173.0, 165.0, 164.9, 140.5, 134.6, 134.1, 130.1, 130.0, 129.5, 129.1, 128.7, 127.9, 127.6, 127.0, 121.0, 57.4, 36.6, 24.4, 15.7, 11.4. **HRMS** (ESI) m/z $[M+H]^+$ calcd for $C_{24}H_{28}N_3O_3^+$ 406.2125; found 406.2105, Δ 4.9235 ppm. $[\alpha]^{27}_D$ -55 (*c* = 0.46, MeOH).

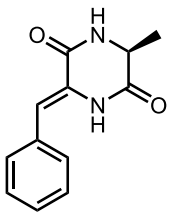

Procedure 4.29: To a 0.25 M solution of **3.47u** in DCM, 4.0 M HCl in 1,3-dioxane (0.625 mmol, 208 μL, 5.0 equiv) was added and the reaction was allowed to stir at room temperature until TLC indicated consumption of **3.47u** (4 hours). Then, triethylamine (0.375 mmol, 52.3 μL, 3.0 equiv) was added and a white precipitate formed immediately. The reaction was allowed to stir overnight. Next, celite was added and volatiles were removed under vacuum. (S,Z)-3-benzylidene-6-methylpiperazine-2,5-dione (**3.52**) was isolated using flash chromatography with MeOH:DCM (10%) as the eluent, as a white solid (24.3 mg, 0.113 mmol, 90% yield). **^{1}H NMR** (600 MHz, DMSO-d_6) δ 9.93 (s, 1H), 8.48 (s, 1H), 7.49 (d, *J* = 7.7 Hz, 2H), 7.40 (t, *J* = 7.7 Hz, 2H), 7.30 (t, *J* = 7.3 Hz, 1H), 6.67 (s, 1H), 4.14 (qd, *J* = 7.1, 1.7 Hz, 1H), 1.34 (d, *J* = 6.9 Hz, 3H). **^{13}C NMR** (151 MHz, DMSO) δ 167.7, 160.4, 133.5, 129.3, 128.7, 128.0, 127.0, 114.1, 50.3, 19.3. **HRMS** (ESI) m/z $[M+H]^+$ calcd for $C_{12}H_{13}N_2O_2^+$ 217.0972; found 217.0980, Δ 3.6850 ppm. $[\alpha]^{27}_D$ +4 (*c* = 1.9, DMSO).

To evaluate whether the tri-*n*-butyl phosphine catalyst could isomerize the α,β-dehydroamino acid products both isomers were required. To gain access to the (*E*)-isomer, a photocatalyzed isomerization reaction was utilized.

Photocatalyzed isomerization of α,β-dehydroamino acid 3.47a

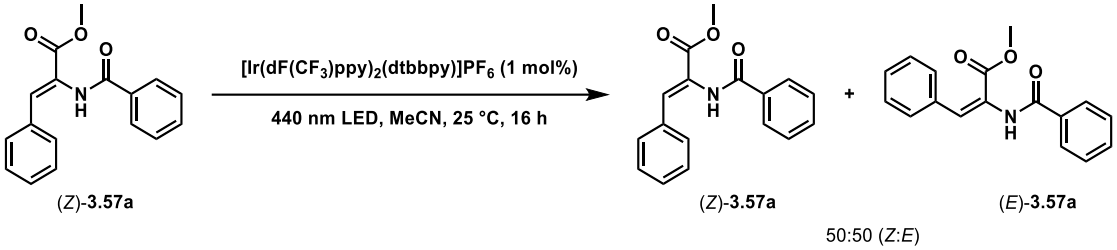

Scheme 4.19: Photocatalyzed isomerization of α,β-dehydroamino acid **3.47a.**

Procedure 4.30: To a flame dried 2 dram vial, a stir bar, [4,4′-*Bis*(1,1-dimethylethyl)-2,2′-bipyridine-*N*1,*N*1′]*bis*[3,5-difluoro-2-[5-(trifluoromethyl)-2-pyridinyl-*N*]phenyl-C]Iridium(III) hexafluorophosphate (3.4 mg, 0.003 mmol, 1 mol%) and (*Z*)-**3.47a** (93.1 mg, 331 mmol, 1.0 equiv) were added. The vial was put under inert atmosphere using standard *Schlenk* technique. Then dry MeCN (9.9 mL, 0.33 M) was added, and the vial was put in a Kessel photochemical reactor (PR160 Rig w/ Fan Kit) with a stir plate. The reactor includes four 440nm (max 45W) LED light fixtures (approximately 5 cm from reaction vial). The mixture was irradiated for 16 hours. After 16 hours, the reaction was diluted with 2 mL of EtOAc and TLC analysis was performed. (*Z*)-**3.47a** and (*E*)-**3.47a** were separated using flash chromatography (0-40% EtOAc:Hex gradient). (*Z*)-**3.47a** was obtained in a 23% yield (21.0 mg, 0.331 mmol) as a white solid. (*E*)-**3.47a** was obtained in a 23% yield (21.0 mg, 0.331 mmol) as a white solid.

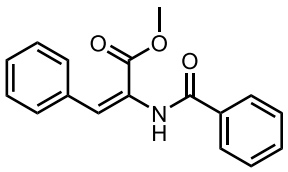

methyl (*E*)-2-benzamido-3-phenylacrylate ((*E*)-**3.47a**). **^{1}H NMR** (400 MHz, $CDCl_3$) δ 8.34 (s, 1H), 8.15 (s, 1H), 7.92 – 7.82 (m, 2H), 7.60 – 7.51 (m, 1H), 7.48 (dd, *J* = 8.2, 6.6 Hz, 2H), 7.31 (m, 5H), 3.68 (s, 3H). **^{13}C NMR** (126 MHz, CDCl3) δ 165.9, 165.6, 135.5, 134.4, 132.2, 129.0, 128.9, 128.0, 127.8, 127.2, 126.6, 126.0, 52.5. This data agrees with literature reports.[25]

Isomerization Study

Procedure 4.31: To a flame dried 2-dram vial: a stir bar and (*Z*)-**3.47a** (30.0 mg, 0.107 mmol, 1.0 equiv) were added. The vial was sealed with a septa lid and put under an inert atmosphere using standard *Schlenk* technique. Then, toluene (427 μL, 0.25 M) and tri-*n*-butylphosine (2.7 μL, 0.011 mmol,10 mol%) were added. The vial was added to a preheated oil bath at 40 °C. The reaction was allowed to stir for 16 hours. The reaction was then opened, and volatiles were removed under vacuum. Crude NMR was analysis was then conducted.

Procedure 4.32: To a flame dried 2-dram vial: a stir bar and (*E*)- **3.47a** (16.0 mg, 0.057 mmol, 1.0 equiv) were added. The vial was sealed with a septa lid and put under an inert atmosphere using standard *Schlenk* technique. Then, toluene (288 μL, 0.25 M) and tri-*n*-butylphosine (1.0 μL, 0.006 mmol, 10 mol%) were added. The vial was added to a preheated oil bath at 40 °C. The reaction was allowed to stir for 16 hours. The reaction was then opened, and volatiles were removed under vacuum. Crude NMR was analysis was then conducted.

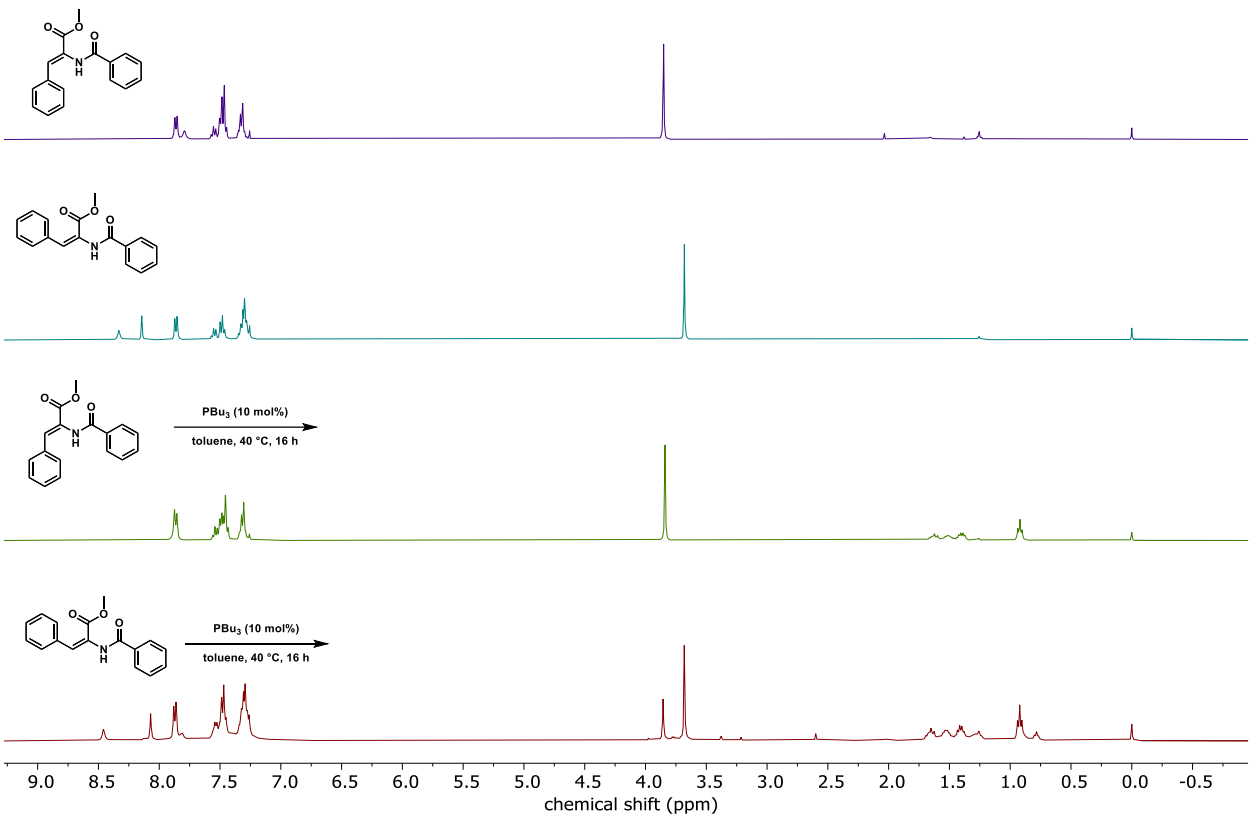

Figure 4.17: ^{1}H NMR spectra for mechanistic study ($CDCl_3$, 400 MHz).

Procedure 4.33: To consider whether the presence of benzamide affected the isomerization of (*E*)- **3.47a**, the sample containing a mixture of (*E*)- and (*Z*)-isomers was dried down and benzamide was added (5.22 mg, 0.043 mmol, 1.2 equiv) and the reaction was put under inert atmosphere using standard *Schlenk* technique. Then, toluene (288 µL, 0.25 M) and tri-*n*-butylphosine (1.0 µL, 0.006 mmol, 10 mol%) were added. The vial was added to a preheated oil bath at 40 °C. The vial was added to a preheated oil bath at 40 °C. After 3.5 hours, an aliquot of the reaction was removed via syringe and volatiles were removed under vacuum. Crude NMR was analysis was then conducted.

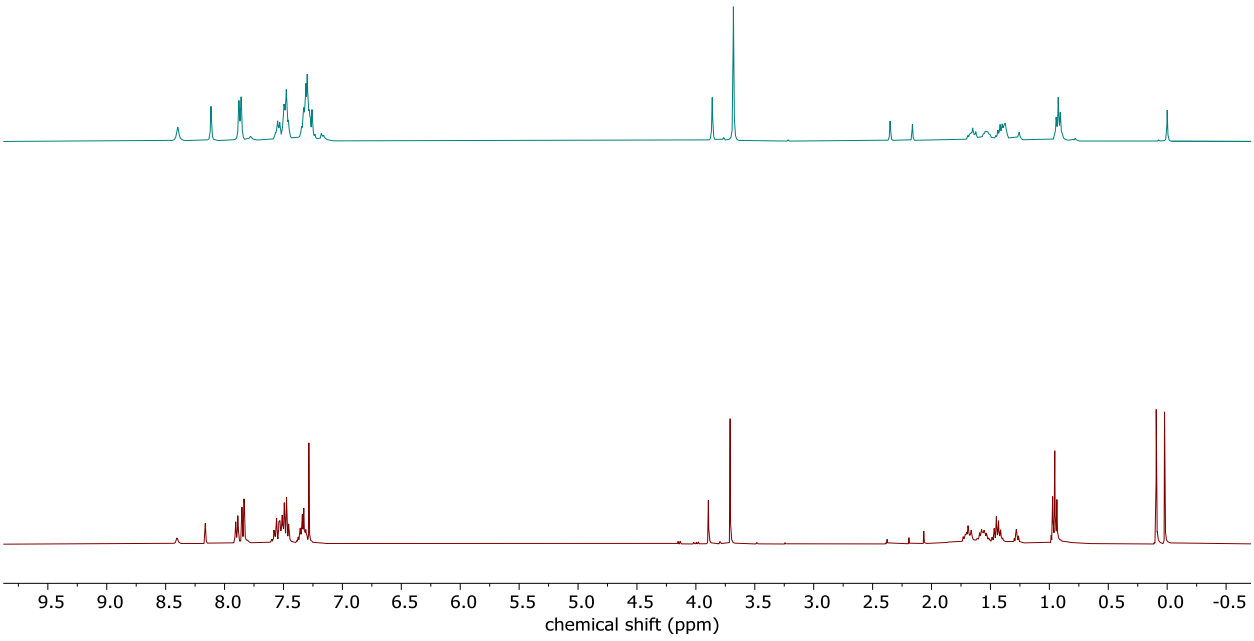

Figure 4.18: ^{1}H NMR spectra for mechanistic study including benzamide ($CDCl_3$, 400 MHz).

Epimerization Study

The goal of this study was to determine whether the amino amides were epimerized during the phosphine-catalyzed umpolung addition to alkynoates. Substrate **3.47u** was deprotected on the N-terminus (Boc-deprotection) and reacted with (*R*)-Mosher's acid chloride. If the amino amide was epimerized, diastereomers would be evident in the crude NMR.

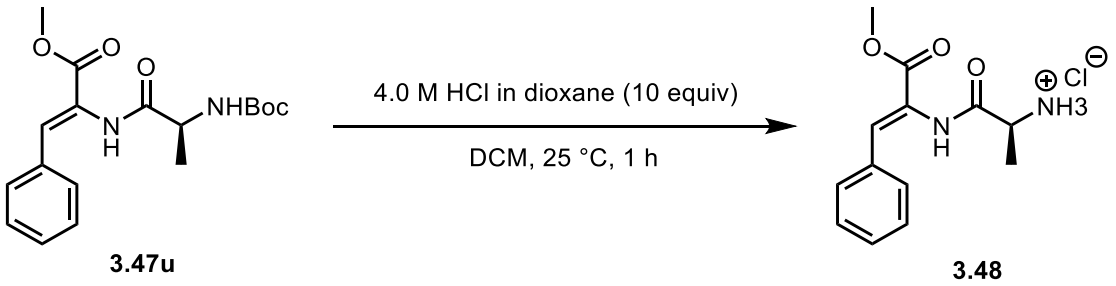

Scheme 4.20: Boc-deprotection of substrate **3.47u**.

Procedure 4.34: To a 6-dram vial: a stir bar and **3.47u** (75.0 mg, 0.215 mmol, 1.0 equiv) were added. Dry DCM (861 µL, 0.25 M) and 4.0 M HCl in dioxane (538 µL, 2.15 mmol, 10 equiv) were added. The reaction was allowed to stir for 1 hour. Upon completion of the reaction as indicated by TLC analysis, volatiles were removed under vacuum. Then **3.48** was triturated with hexanes and dried under vacuum to afford **3.48** as a colorless solid (50.0 mg, 0.215 mmol, quant. yield). **^{1}H NMR** (400 MHz, DMSO-d_6) δ 10.18 (s, 1H), 8.28 (s, 3H), 7.70 – 7.64 (m, 2H), 7.47 – 7.40 (m, 3H), 7.39 (s, 1H), 4.05 (m, 1H), 3.73 (s, 3H), 1.47 (d, J = 7.0 Hz, 3H). **^{13}C NMR** (126 MHz, DMSO-d_6) δ 169.6, 164.9, 133.3, 132.9, 130.1, 129.8, 128.7, 125.0, 52.4, 48.3, 16.7. **HRMS** (ESI) m/z $[M\text{-}Cl]^+$ calcd for $C_{13}H_{17}N_2O_3^+$ 249.1234; found 249.1243.

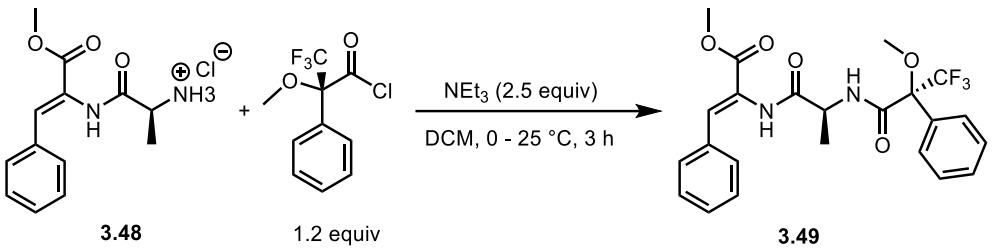

Scheme 4.21: Synthesis of Mosher's amide from **3.48**.

Procedure 4.35: To a flame dried 2-dram vial: a stir bar, (*R*)-3,3,3-trifluoro-2-methoxy-2-phenylpropanoyl chloride (45.7 mg, 0.181 mmol, 1.2 equiv) and **3.48** (35.0 mg, 0.151 mmol, 1.0 equiv) were added and the vial was added to an ice-bath. Dry DCM (603 μL, 0.25 M) and triethylamine (53 μL, 0.377 mmol, 2.5 equiv) were then added. The reaction was allowed to stir for 3 hours. The reaction was aliquoted and dried under vacuum for crude NMR. After crude analysis, celite was added and volatiles were removed under vacuum. Then **3.49** was isolated using flash chromatography using a 0-60% EtOAc:Hex gradient. (47.9 mg, 0.103 mmol, 68% yield). **^{1}H NMR** (400 MHz, $CDCl_3$) δ 8.00 (s, 1H), 7.54 – 7.42 (m, 6H), 7.42 – 7.27 (m, 6H), 4.79 (dt, *J* = 7.2, 6.9 Hz, 1H), 3.79 (s, 3H), 3.39 (s, 3H), 1.42 (d, *J* = 7.0 Hz, 3H). **^{13}C NMR** (151 MHz, $CDCl_3$) δ 170.4, 166.7, 165.4, 134.0, 133.5, 132.6, 129.8, 129.7, 129.7, 128.7, 128.6, 127.4, 123.7 (q, *J* = 290.2 Hz), 123.6, 83.9 (q, *J* = 26.2 Hz), 55.2, 52.7, 49.1, 18.0. **^{19}F NMR** (376 MHz, $CDCl_3$) δ -68.6 (s, 3F). **HRMS** (ESI) m/z $[M+H]^+$ calcd for $C_{23}H_{24}F_3N_2O_5^+$ 465.1632; found 465.1639.

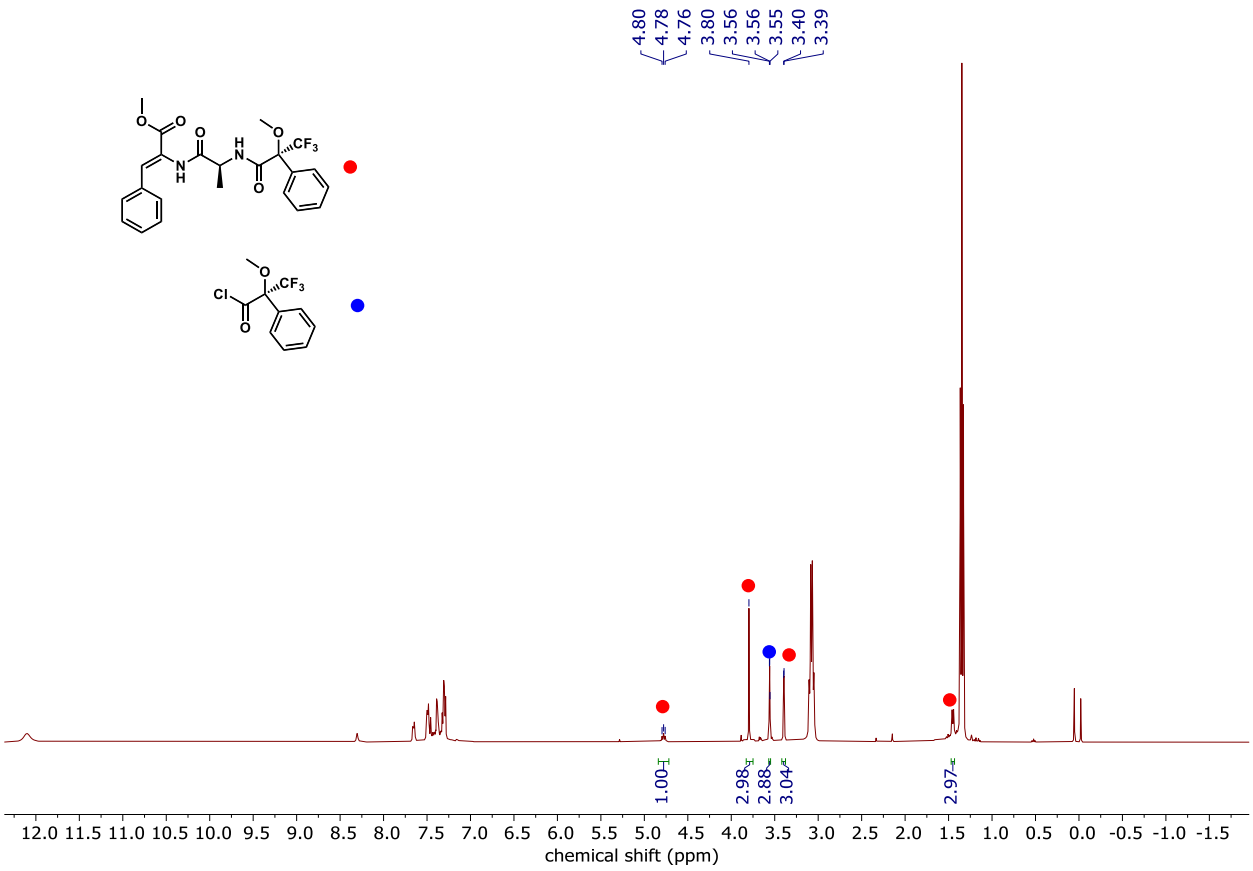

Figure 4.19: Crude ^{1}H NMR spectra for Mosher's amide synthesis ($CDCl_3$, 400 MHz).

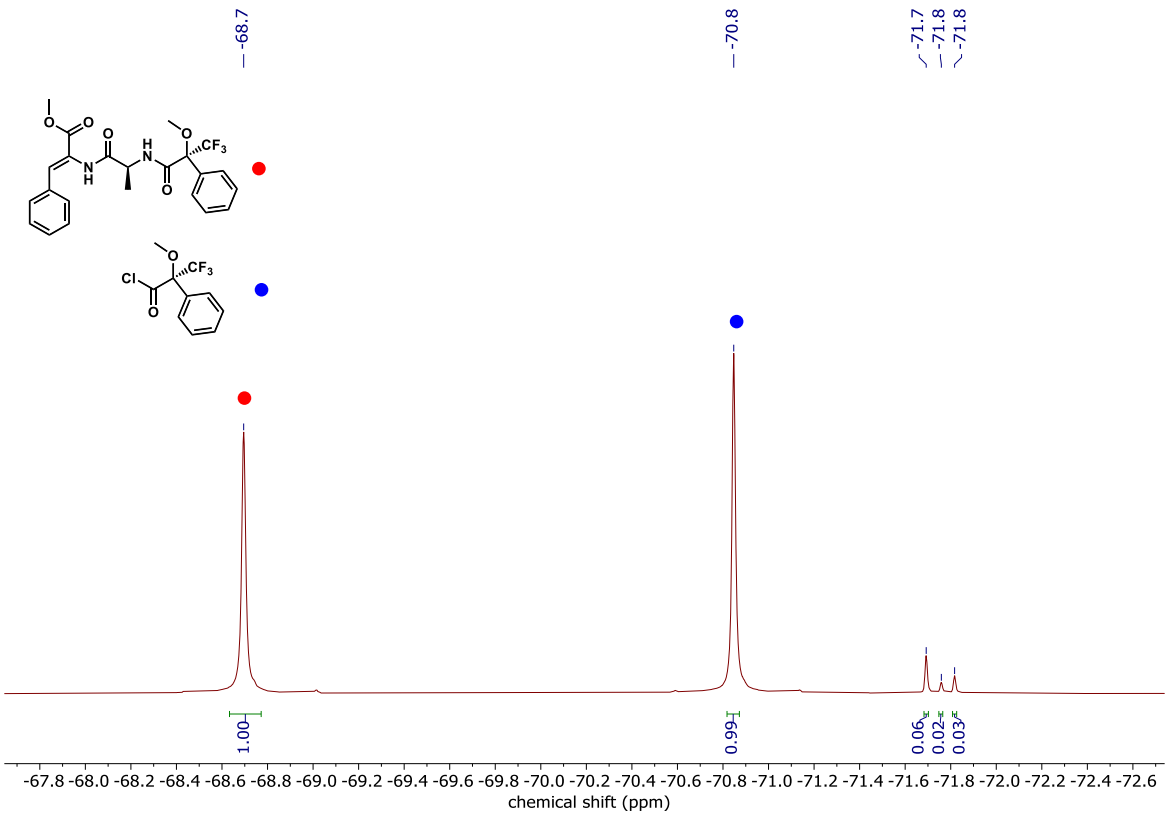

Figure 4.20: Crude ^{19}F NMR spectra for Mosher's amide synthesis ($CDCl_3$, 376 MHz).

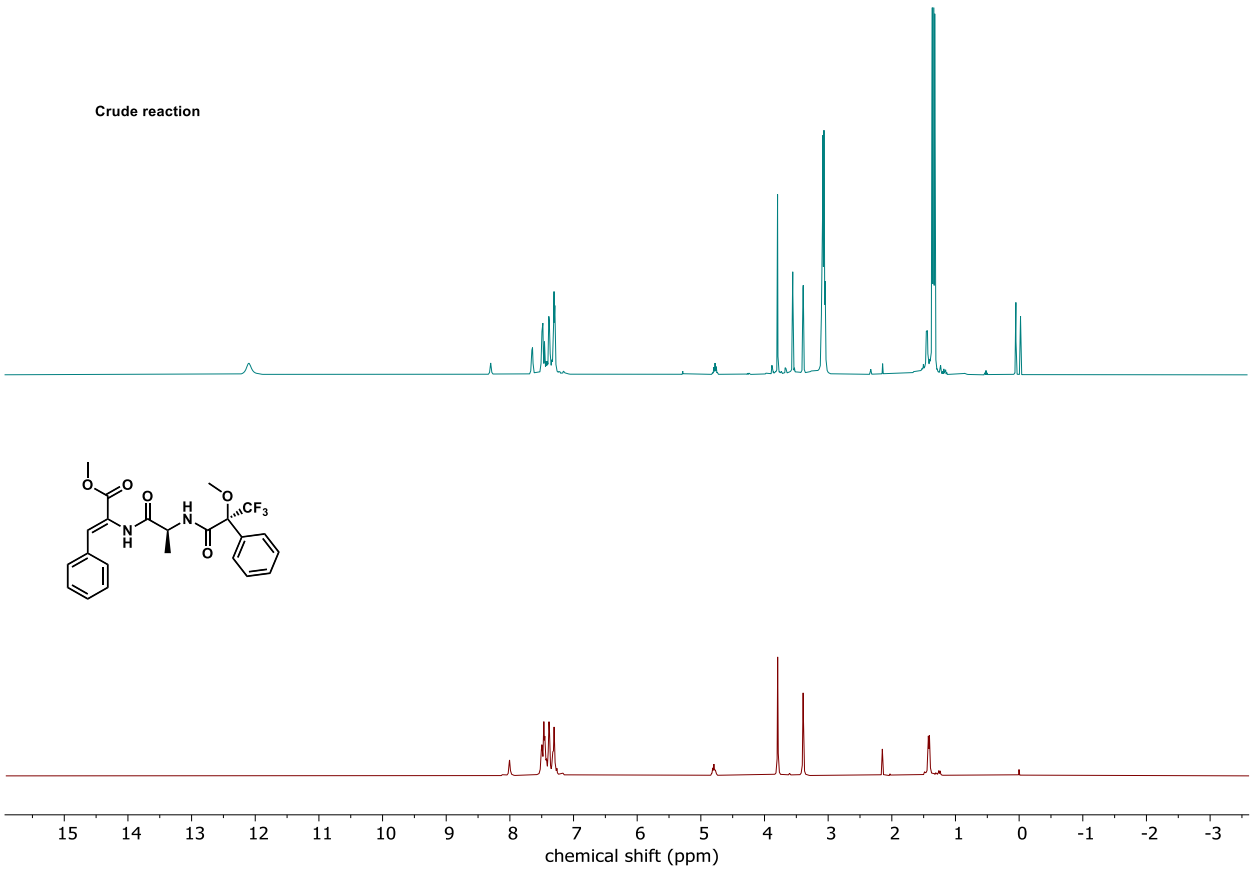

Figure 4.21: Crude ^{1}H NMR spectra for Mosher's amide synthesis stacked against authentic sample **3.49**. ($CDCl_3$, 400 MHz).

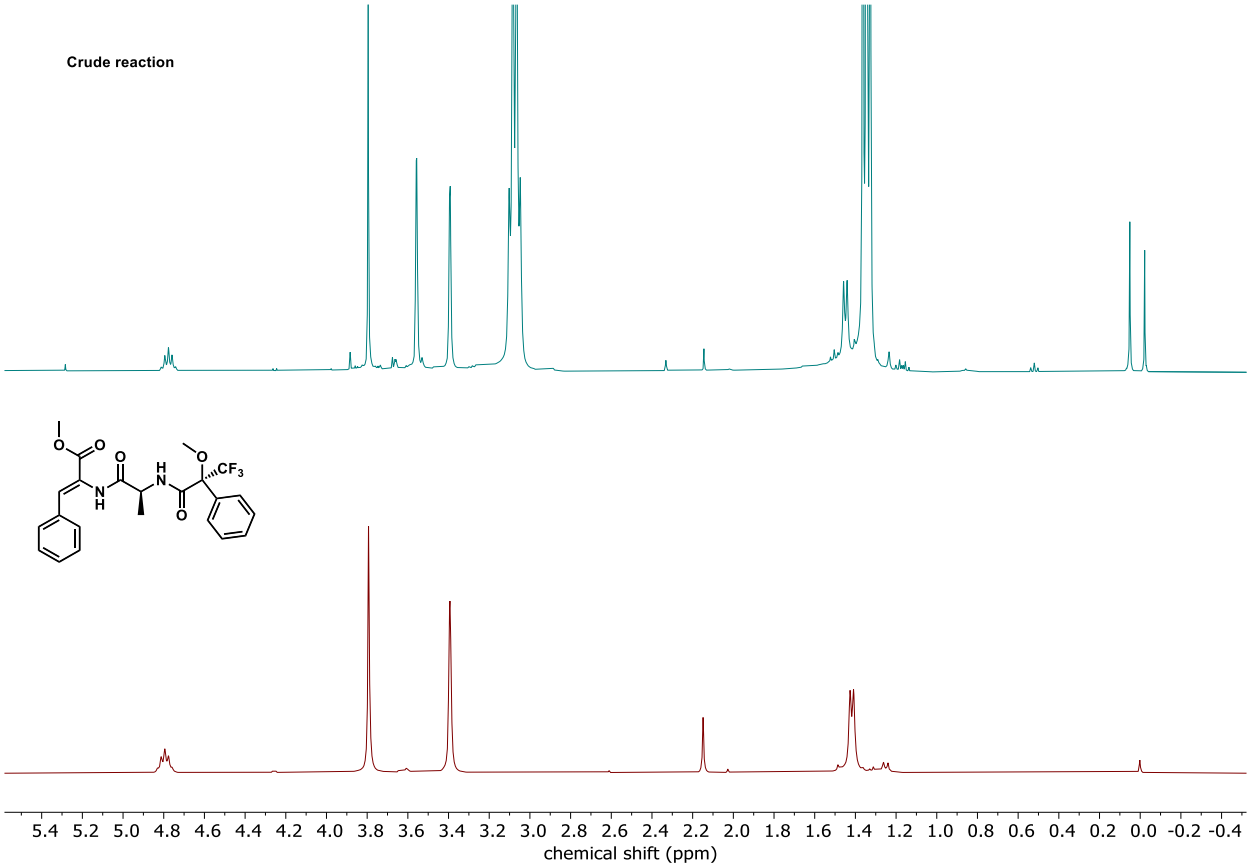

Figure 4.22: Zoomed in crude ^{1}H NMR spectra for Mosher's amide synthesis stacked against authentic sample **3.49**. ($CDCl_3$, 400 MHz).

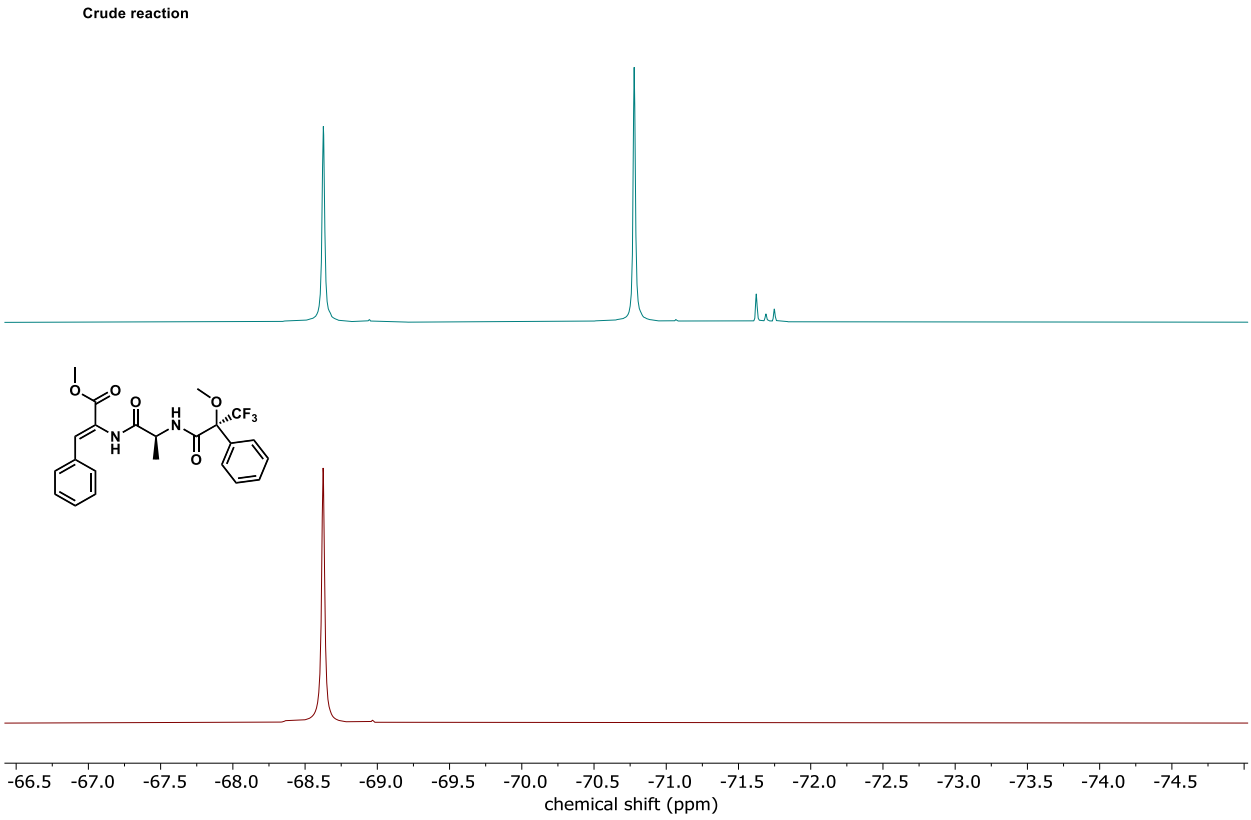

Figure 4.23: Crude ^{19}F NMR spectra for Mosher's amide synthesis stacked against authentic sample **3.49**. ($CDCl_3$, 376 MHz).

4.8. X-Ray Crystallography for Chapter 3

X-Ray Diffraction Techniques. All structures were collected on a Rigaku Oxford Diffraction Synergy-S diffractometer equipped with a HyPix6000HE detector and operating with CuKα radiation source. Data collection, unit cell refinement, and data processing were carried out with CrysAlisPro,[23] while structures were solved utilizing SHELXS[50] and refined using SHELXL[51] via Olex2.[52] Olex2, PovRay,[24] and ORTEP[53] applications were used to generate structure graphics. Crystals were mounted on a cryoloop or glass fiber pin using Paratone N oil. Structures were collected at 100 K. All non-hydrogen atoms were refined anisotropically. Hydrogen atoms were placed at idealized positions and refined using a riding model. The isotropic displacement parameters of all hydrogen atoms were fixed to 1.2 times the atoms they are linked to (1.5 times for methyl groups). Further details on particular structures are noted below.

[$C_{19}H_{17}N_3O$] (**3.47b**) Crystals were grown via slow diffusion in EtOAc at room temperature. The structure was solved in the orthorhombic space group *Pna2₁* with 4 molecules per unit cell. The final refinement model involved anisotropic displacement parameters for non-hydrogen atoms. A riding model was used for the C-H hydrogen atoms. The N-H and O-H hydrogen atoms were located from the difference electron density map, and the positions and isotropic displacement parameters were refined independently.

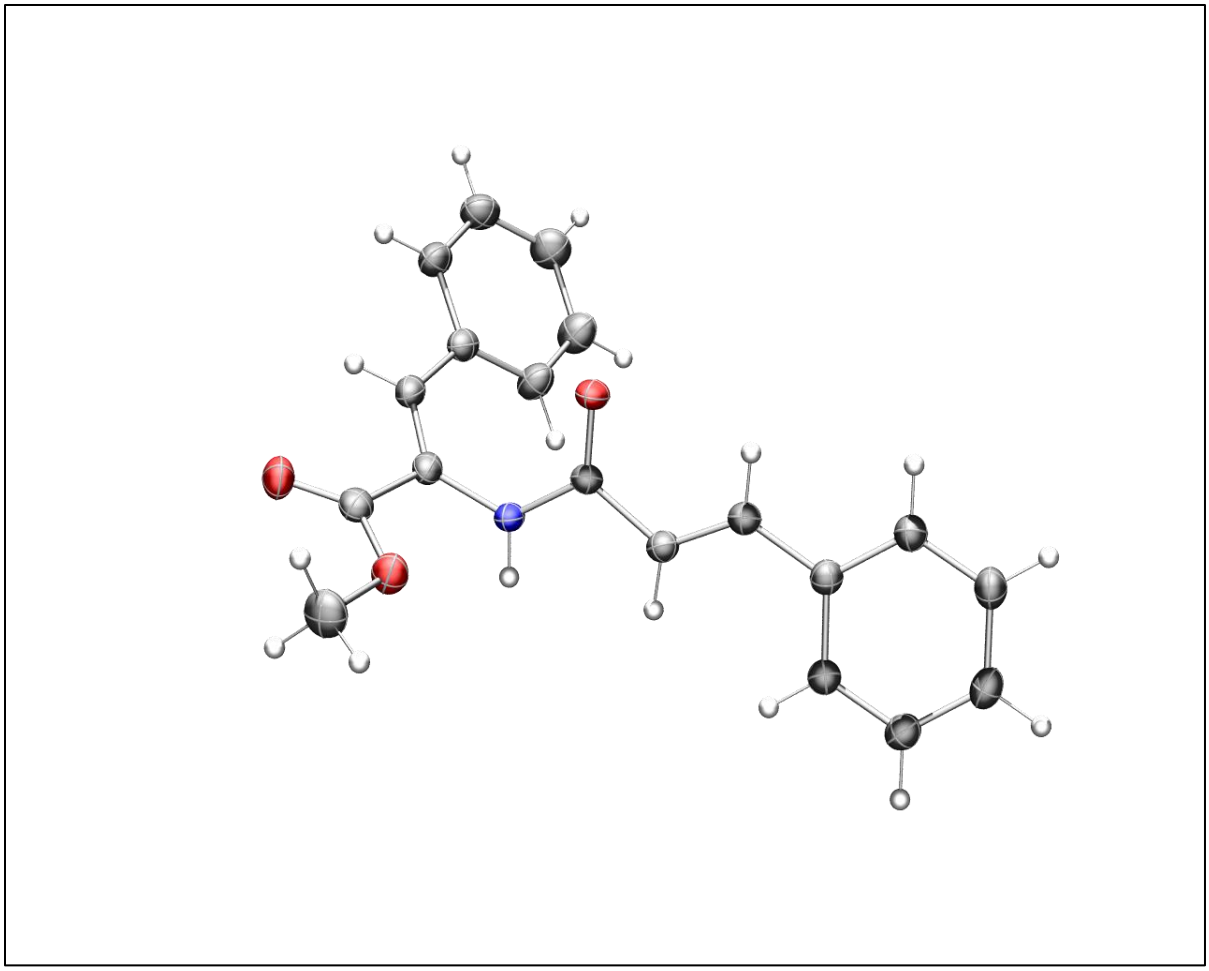

Figure 4.24: Solid-state molecular structure of compound **3.47b** with anisotropic displacement ellipsoids at 50% probability level ;Color scheme: O, red; N,blue; C,gray; H, white.

Table 4.12: X-ray diffraction experimental details.

	$[C_{19}H_{17}N_3O]$ (**3.47b**)
Empirical Formula	$C_{19}H_{17}N_3O$
Formula Weight	307.33
Temp. (K)	100
Radiation	Cu Kα (λ = 1.54184)
Crystal System	Orthorhombic
Space Group	Pna21
a (Å)	9.65680(10)

b (Å)	19.8800(2)
c (Å)	8.24520(10)
α (°)	90
β (°)	90
γ (°)	90
Volume ($Å^3$)	1582.89(3)
Z	4
ρ_{calc} (g/cm^3)	1.290
μ (mm^{-1})	0.709
F(000)	648.0
Crystal size (mm^3)	0.6 × 0.39 × 0.03
2Θ range for data collection (°)	8.896 to 154.894
Index Ranges	$-9 \leq h \leq 12$, $-25 \leq k \leq 25$, $-10 \leq l \leq 10$
Reflections Collected	51679
Independent Reflections	3338
Data/Restraints/Parameters	3338/1/277
GOF	1.068
Final R indexes [I>=2σ (I)]	R1 = 0.0370, wR2 = 0.0976
Final R indexes [all data]	R1 = 0.0373, wR2 = 0.0978
Largest diff. peak/hole/e ($Å^{-3}$)	0.21/-0.20
Flack Parameter	0.2(2)

4.9. References

1. Burgio, A. L.; Buchbinder, N. W.; Santos, W. L. Regio- and Stereoselective Copper-Catalyzed Borylation–Protodeboronation of 1,3-Diynes: Access to (Z)-1,3-Enynes. *Org. Lett.* **2023**, *25* (15), 2652–2656.

2. Wang, Z.; Zhang, C.; Wu, J.; Li, B.; Chrostowska, A.; Karamanis, P.; Liu, S.-Y. trans-Hydroalkynylation of Internal 1,3-Enynes Enabled by Cooperative Catalysis. *J. Am. Chem. Soc.* **2023**, *145* (10), 5624–5630.

3. Huang, F.; Huang, Z.; Liu, G.; Huang, Z. Iridium-Catalyzed Selective trans-Semihydrogenation of 1,3-Enynes with Ethanol: Access to (E,E)-1,4-Diarylbutadienes. *Org. Lett.* **2022**, *24* (29), 5486–5490.

4. Kinoshita, H.; Ishikawa, T.; Miura, K. Dialkylaluminum Hydride-Promoted Cyclodimerization of Silylated 1,3-Enynes via Skeletal Rearrangement. *Org. Lett.* **2011**, *13* (23), 6192–6195.

5. Xu, S.; Zhang, Y.; Li, B.; Liu, S.-Y. Site-Selective and Stereoselective trans-Hydroboration of 1,3-Enynes Catalyzed by 1,4-Azaborine-Based Phosphine–Pd Complex. *J. Am. Chem. Soc.* **2016**, *138* (44), 14566–14569.

6. Zhang, Y.; Liu, W.; Xu, Y.; Liu, Y.; Peng, J.; Wang, M.; Bai, Y.; Lu, H.; Shi, Z.; Shao, X. S-(Methyl-d3) Arylsulfonothioates: A Family of Robust, Shelf-Stable, and Easily Scalable Reagents for Direct Trideuteromethylthiolation. *Org. Lett.* **2022**, *24* (37), 6794–6799.

7. CrysAlisPro Software System, v1.171.42.xx, Rigaku Oxford Diffraction. **2022**, Rigaku Corporation, Oxford, UK.

8. Sheldrick, G. M. "SHELXT – Integrated space-group and crystal structure determination.". *Acta Cryst.* **2015**, A71, 73–78.

9. Sheldrick, G. M. Crystal structure refinement with SHELXL. *Acta Cryst.* **2015**, *71* (1), 3–8.

10. Dolomanov, O. V. B., L. J.; Gildea, R. J.; Howard, J. A. K.; Puschmann, H. . *J. Appl. Cryst.* **2009**, *42*, 339–341.

11. Macrae, C. F.; Sovago, I.; Cottrell, S. J.; Galek, P. T.; McCabe, P.; Pidcock, E.; Platings, M.; Shields, G. P.; Stevens, J. S.; Towler, M. Mercury 4.0: From visualization to analysis, design and prediction. *J. Appl. Cryst.* **2020**, *53* (1), 226–235.

12. Burés, J. Variable Time Normalization Analysis: General Graphical Elucidation of Reaction Orders from Concentration Profiles. *Angew. Chem. Int. Ed.* **2016**, *55* (52), 16084–16087.

13. *Gaussian 16 Rev. C.01*; Wallingford, CT, 2016.

14. Zhao, Y.; Truhlar, D. G. The M06 suite of density functionals for main group thermochemistry, thermochemical kinetics, noncovalent interactions, excited states, and transition elements: two new functionals and systematic testing of four M06-class functionals and 12 other functionals. *Theor. Chem. Acc.* **2008**, *120*, 215–241.

15. Lin, Y.-S.; Li, G.-D.; Mao, S.-P.; Chai, J.-D. Long-range corrected hybrid density functionals with improved dispersion corrections. *J. Chem. Theory Comput.* **2013**, *9* (1), 263–272.

16. Marenich, A. V.; Cramer, C. J.; Truhlar, D. G. Generalized born solvation model SM12. *J. Chem. Theory Comput.* **2013**, *9* (1), 609–620.

17. Bergner, A.; Dolg, M.; Küchle, W.; Stoll, H.; Preuß, H. Ab initio energy-adjusted pseudopotentials for elements of groups 13–17. *Mol. Phys.* **1993**, *80* (6), 1431–1441.

18. Dolg, M.; Wedig, U.; Stoll, H.; Preuss, H. Energy-adjusted ab initio pseudopotentials for the first row transition elements. *J. Chem. Phys.* **1987**, *86* (2), 866–872.

19. Hariharan, P. C.; Pople, J. A. The influence of polarization functions on molecular orbital hydrogenation energies. *Theor. Chim. Acta* **1973**, *28*, 213–222.

20. Li, X.; Frisch, M. J. Energy-represented direct inversion in the iterative subspace within a hybrid geometry optimization method. *J. Chem. Theory Comput.* **2006**, *2* (3), 835–839.

21. Fukui, K. The path of chemical reactions-the IRC approach. *Acc. Chem. Res.* **1981**, *14* (12), 363–368.

22. Weigend, F.; Furche, F.; Ahlrichs, R. Gaussian basis sets of quadruple zeta valence quality for atoms H–Kr. *J. Chem. Phys.* **2003**, *119* (24), 12753–12762.

23. Diffraction, R. O. CrysAlisPro Software system, version 1.171. 41.113 a, Rigaku Corporation. Oxford, UK (compound (BDI) MgNa/SrN ″2 (2);(BDI) MgNa/MgN: 2021.

24. Persistence of Vision (TM) Raytracer; Persistence of Vision Pty. Ltd.: Williamstown, Victoria, Australia, **2004**. http://www.povray.org/.

25. Farrugia, L. J. *J. Appl. Crystallogr.* **2012**, *45*, 849–854.

26. Smyrnov, O. K.; Melnykov, K. P.; Pashenko, O. Y.; Volochnyuk, D. M.; Ryabukhin, S. V. Stellane at the forefront: derivatization and reactivity studies of a promising saturated bioisostere of ortho-substituted benzenes. *Org. Lett.* **2024**, *26* (22), 4808–4812.

27. Trotta, A. H. Total synthesis of oridamycins A and B. *Org. Lett.* **2015**, *17* (13), 3358–3361.

28. He, W.; Li, C.; Zhang, L. An efficient [2+ 2+ 1] synthesis of 2, 5-disubstituted oxazoles via gold-catalyzed intermolecular alkyne oxidation. *J. Am. Chem. Soc.* **2011**, *133* (22), 8482–8485.

29. Wang, W.; Zhou, S.; Li, L.; He, Y.; Dong, X.; Gao, L.; Wang, Q.; Song, Z. 3-Silaazetidine: an unexplored yet versatile organosilane species for ring expansion toward silaazacycles. *J. Am. Chem. Soc.* **2021**, *143* (29), 11141–11151.

30. Wang, W.; Zhou, S.; Li, L.; He, Y.; Dong, X.; Gao, L.; Wang, Q.; Song, Z. 3-Silaazetidine: an unexplored yet versatile organosilane species for ring expansion toward silaazacycles. *J. Am. Chem. Soc.* **2021**, *143* (29), 11141–11151.

31. Michaelides, I. N.; Darses, B.; Dixon, D. J. Acid-catalyzed synthesis of bicyclo [3. n. 1] alkenediones. *Org. Lett.* **2011**, *13* (4), 664–667.

32. Varongchayakul, C.; Danheiser, R. L. One-pot Synthesis of Alkynes from Esters via a Tandem Reduction-Ohira-Bestmann Reaction. *Org. Synth.* **2024**, *101*.

33. Dolensky, B.; Kirk, K. L. New approaches to side-chain fluorinated bioimidazoles: 4-alkynylimidazoles as substrates for fluorination. *J. Fluorine Chem.* **2003**, *124* (1), 105–110.

34. Fritzemeier, R. G.; Nekvinda, J.; Vogels, C. M.; Rosenblum, C. A.; Slebodnick, C.; Westcott, S. A.; Santos, W. L. Organocatalytic trans phosphinoboration of internal alkynes. *Angew. Chem. Int. Ed.* **2020**, *59* (34), 14358–14362.

35. Fritzemeier, R.; Gates, A.; Guo, X.; Lin, Z.; Santos, W. L. Transition metal-free trans hydroboration of alkynoic acid derivatives: Experimental and theoretical studies. *J. Org. Chem.* **2018**, *83* (17), 10436–10444.

36. Fujimoto, H.; Kusano, M.; Kodama, T.; Tobisu, M. Three-component coupling of acyl fluorides, silyl enol ethers, and alkynes by P (III)/P (V) catalysis. *J. Am. Chem. Soc.* **2021**, *143* (44), 18394–18399.

37. Mothes, C.; Lavielle, S.; Karoyan, P. Amino-zinc-ene-enolate cyclization: A short access to cis-3-substituted prolino-homotryptophane derivatives. *J. Org. Chem.* **2008**, *73* (17), 6706–6710.

38. Patel, M. A.; Kapdi, A. R. Ambient-Temperature, Metal-Free, CDI-Mediated Ex-Situ Conversion of Acids to Amides: A Useful Late-Stage Strategy. *Chem. Asian J.* **2023**, *18* (22), e202300672.

39. Inman, M.; Dexter, H. L.; Moody, C. J. Total synthesis of the cyclic dodecapeptides wewakazole and wewakazole B. *Org. Lett.* **2017**, *19* (13), 3454–3457.

40. Schneider, T. L.; Walsh, C. T.; O'Connor, S. E. Utilization of alternate substrates by the first three modules of the epothilone synthetase assembly line. *J. Am. Chem. Soc.* **2002**, *124* (38), 11272–11273.

41. Singh, Y.; Sokolenko, N.; Kelso, M. J.; Gahan, L. R.; Abbenante, G.; Fairlie, D. P. Novel cylindrical, conical, and macrocyclic peptides from the cyclooligomerization of functionalized thiazole amino acids. *J. Am. Chem. Soc.* **2001**, *123* (2), 333–334.

42. Maucort, C.; Vo, D. D.; Aouad, S.; Charrat, C.; Azoulay, S.; Di Giorgio, A.; Duca, M. Design and implementation of synthetic RNA binders for the inhibition of miR-21 biogenesis. *ACS Med. Chem. Lett.* **2021**, *12* (6), 899–906.

43. Ngo, C.; Fried, W.; Aliyari, S.; Feng, J.; Qin, C.; Zhang, S.; Yang, H.; Shanaa, J.; Feng, P.; Cheng, G. Alkyne as a latent warhead to covalently target SARS-CoV-2 main protease. *J. Med. Chem.* **2023**, *66* (17), 12237–12248.

44. Zheng, Y.; Li, X.; Ren, C.; Zhang-Negrerie, D.; Du, Y.; Zhao, K. Synthesis of oxazoles from enamides via phenyliodine diacetate-mediated intramolecular oxidative cyclization. *J. Org. Chem.* **2012**, *77* (22), 10353–10361.

45. Bartoccini, F.; Cannas, D. M.; Fini, F.; Piersanti, G. Palladium (II)-catalyzed cross-dehydrogenative coupling (CDC) of N-phthaloyl dehydroalanine esters with simple arenes: stereoselective synthesis of Z-dehydrophenylalanine derivatives. *Org. Lett.* **2016**, *18* (11), 2762–2765.

46. Almaraz-Girón, M. A.; Vázquez, A. Synthesis of 4-benzylidene-oxazol-5 (4H)-imines, structural analogs of PK11195, under Bischler-Napieralski conditions. *Tetrahedron Lett.* **2017**, *58* (8), 785–788.

47. Shinde, R. S.; Narnawre, A. R.; Karade, N. N. Metal-free intramolecular oxidative cyclization of (Z)-2-benzamido-3-arylacrylates using I2/DMSO: Synthesis of 2, 4, 5-trisubstituted oxazoles. *Tetrahedron Lett.* **2023**, *117*, 154370.

48. Lukasevics, L.; Cizikovs, A.; Grigorjeva, L. Cobalt-catalyzed C (sp 2)–H bond imination of phenylalanine derivatives. *Chem. Commun.* **2022**, *58* (70), 9754–9757.

49. Vilaça, H.; Pereira, G.; Castro, T.; Hermenegildo, B.; Shi, J.; Faria, T.; Micaêlo, N.; Brito, R.; Xu, B.; Castanheira, E. New self-assembled supramolecular hydrogels based on dehydropeptides. *J. Mater. Chem. B* **2015**, *3* (30), 6355–6367.

50. Sheldrick, G. Crystal structure refinement with SHELXL. *Acta. Crystallogr. C* **2015**, *71* (1), 3–8.

51. Sheldrick, G. M. Crystal structure refinement with SHELXL. *Acta. Cryst.* **2015**, *71* (1), 3–8.

52. Dolomanov, O. V.; Bourhis, L. J.; Gildea, R. J.; Howard, J. A. K.; Puschmann, H. OLEX2: a complete structure solution, refinement and analysis program. *J. Appl. Crystallogr.* **2009**, *42* (2), 339–341.

53. Farrugia, L. J. WinGX and ORTEP for Windows: an update. *Appl. Crystallogr.* **2012**, *45* (4), 849–854.

Appendix A

NMR Spectra for 1,3-Enynes for Chapter 1

^{1}H NMR of **4.31r** (400 MHz, $CDCl_3$)

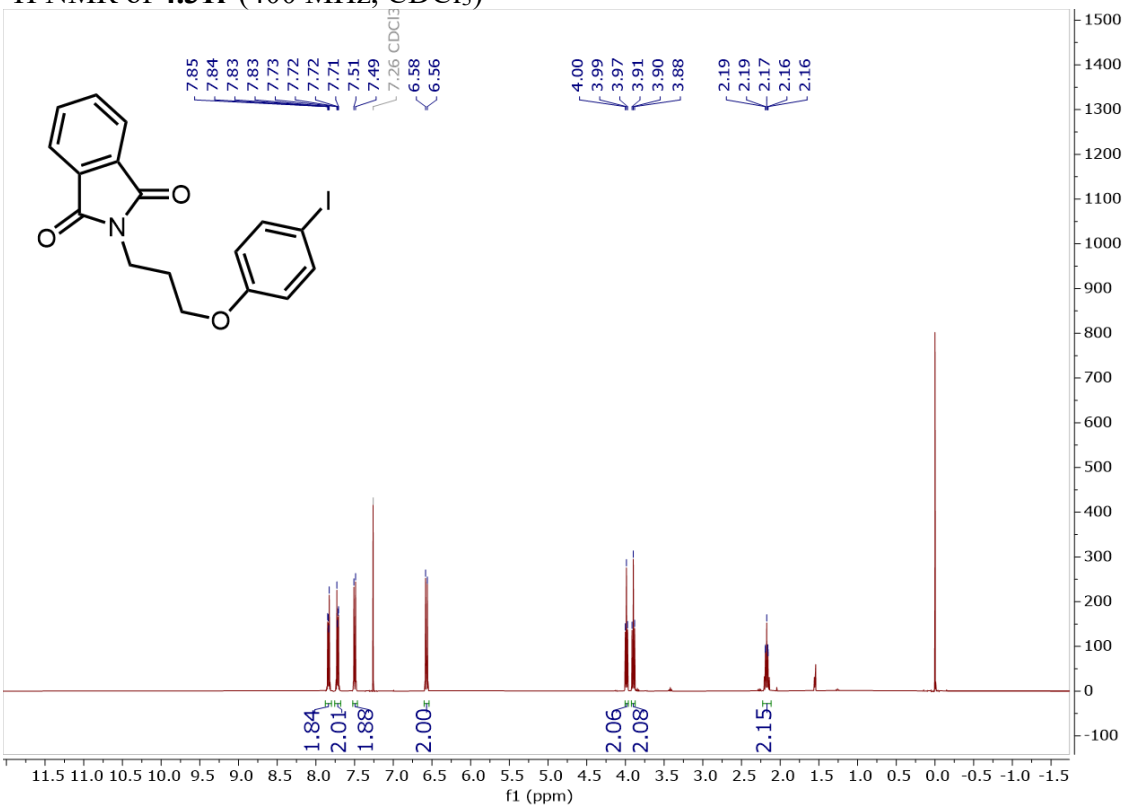

^{13}C NMR of **4.31r** (101 MHz, $CDCl_3$)

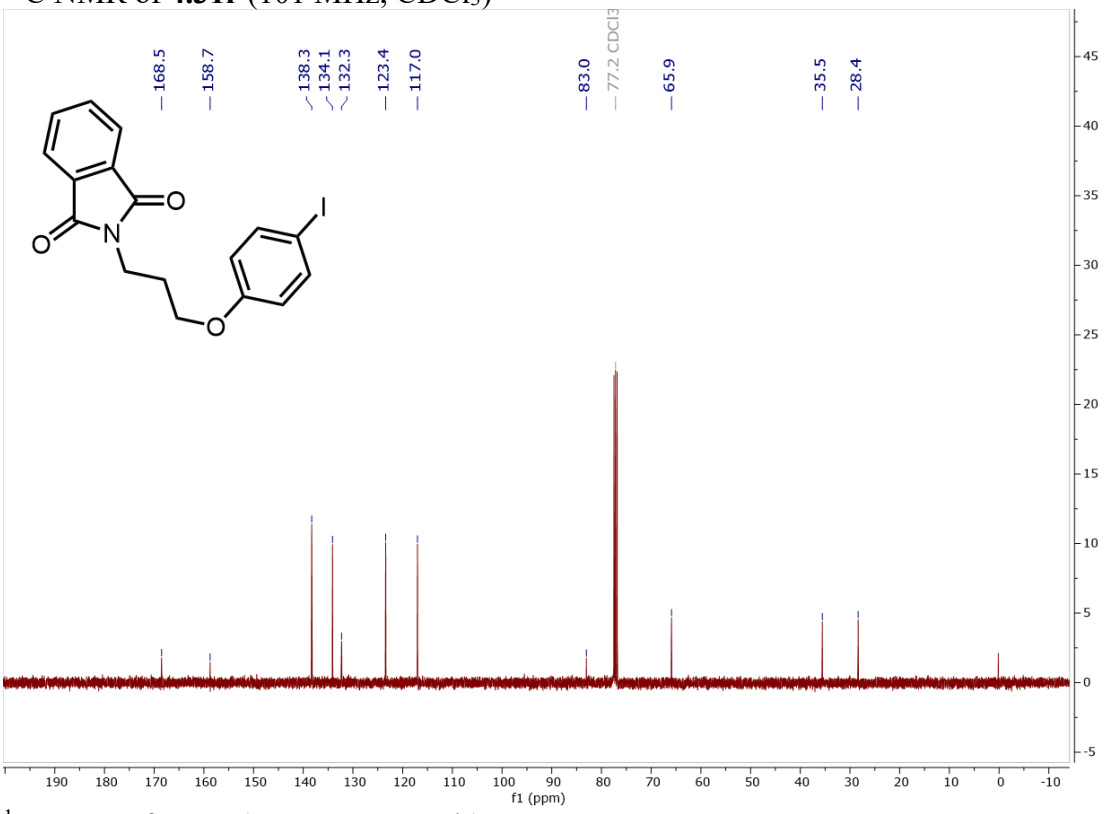

^{1}H NMR of **4.32r** (400 MHz, $CDCl_3$)

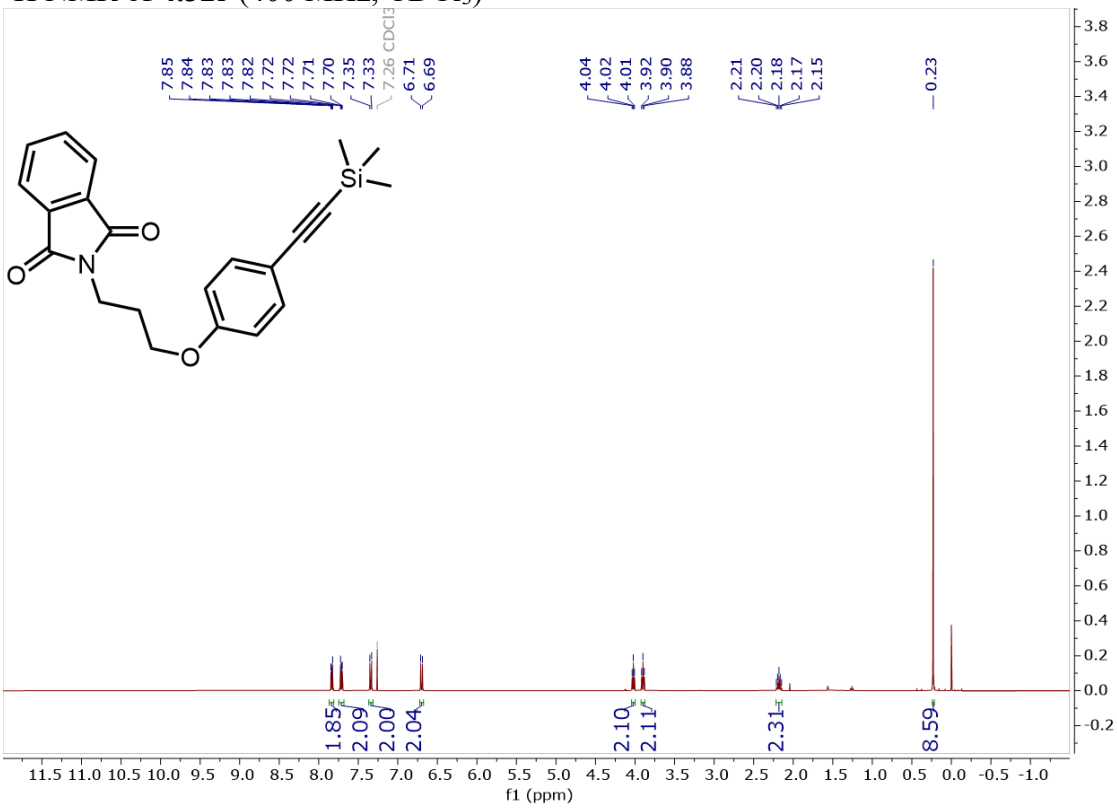

^{13}C NMR of **4.32r** (101 MHz, $CDCl_3$)

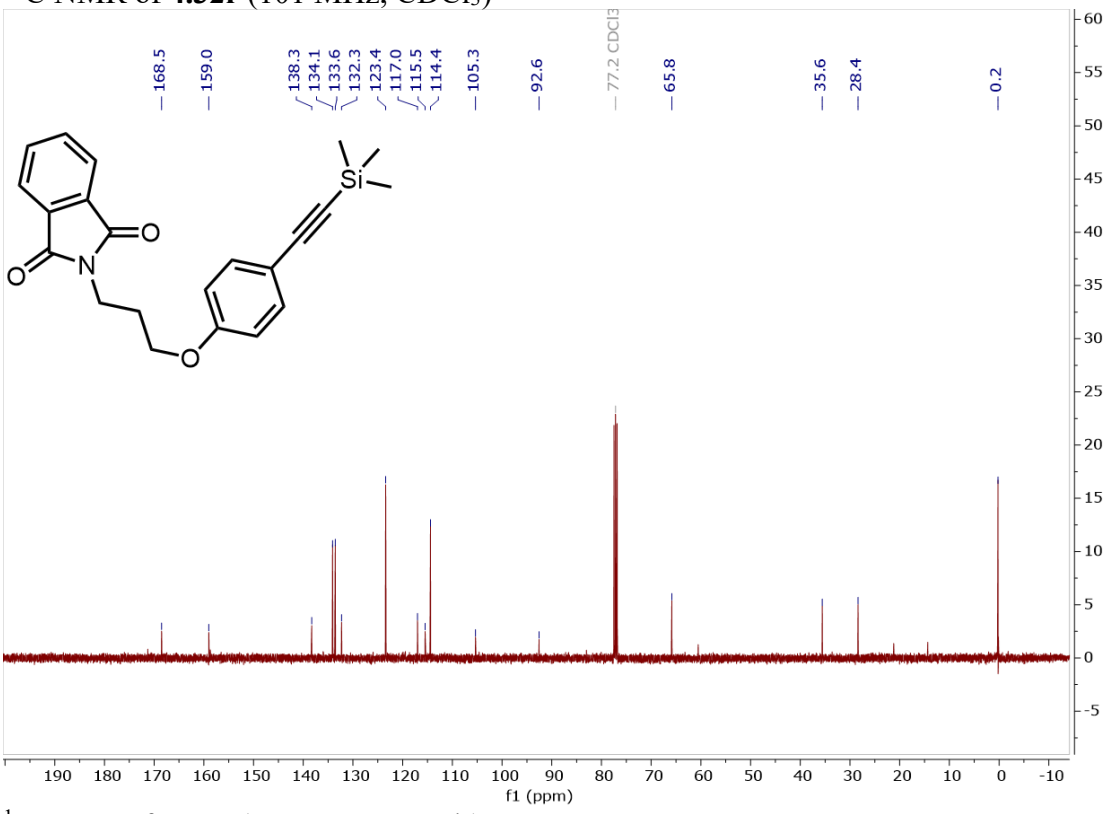

^{1}H NMR of **4.33r** (400 MHz, $CDCl_3$)

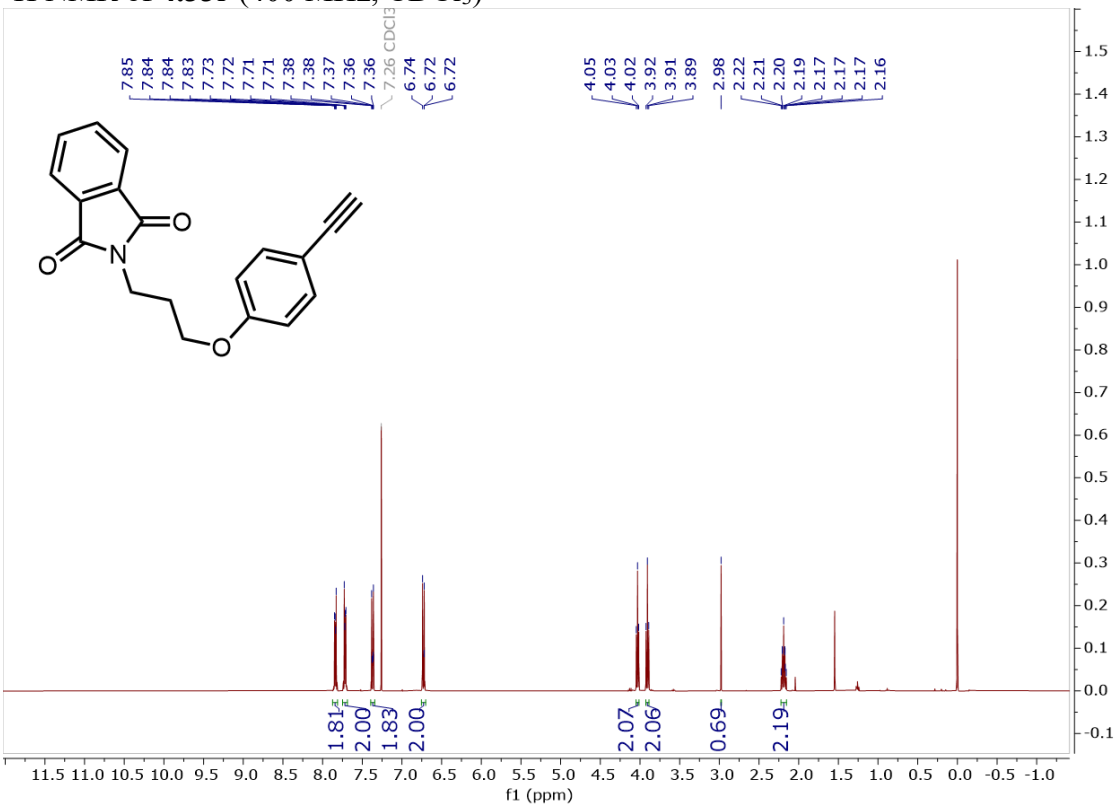

^{13}C NMR of **4.33r** (101 MHz, $CDCl_3$)

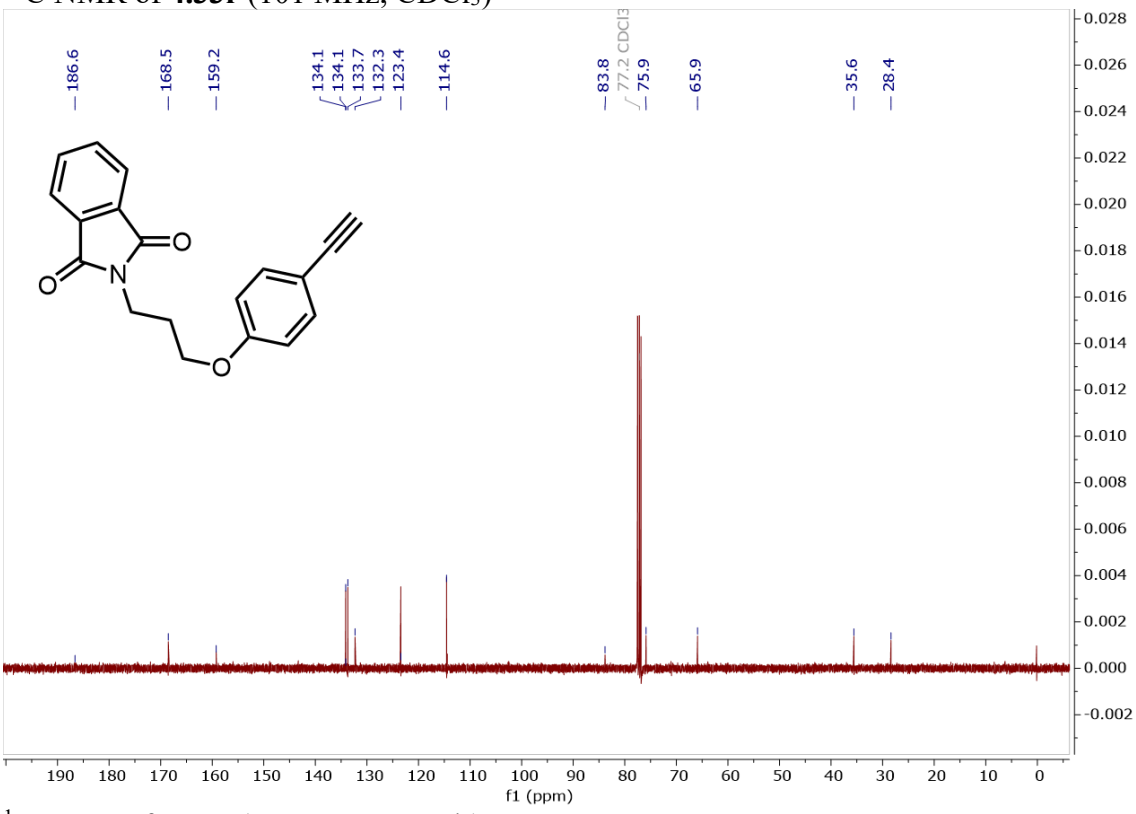

^{1}H NMR of **1.58r** (400 MHz, $CDCl_3$)

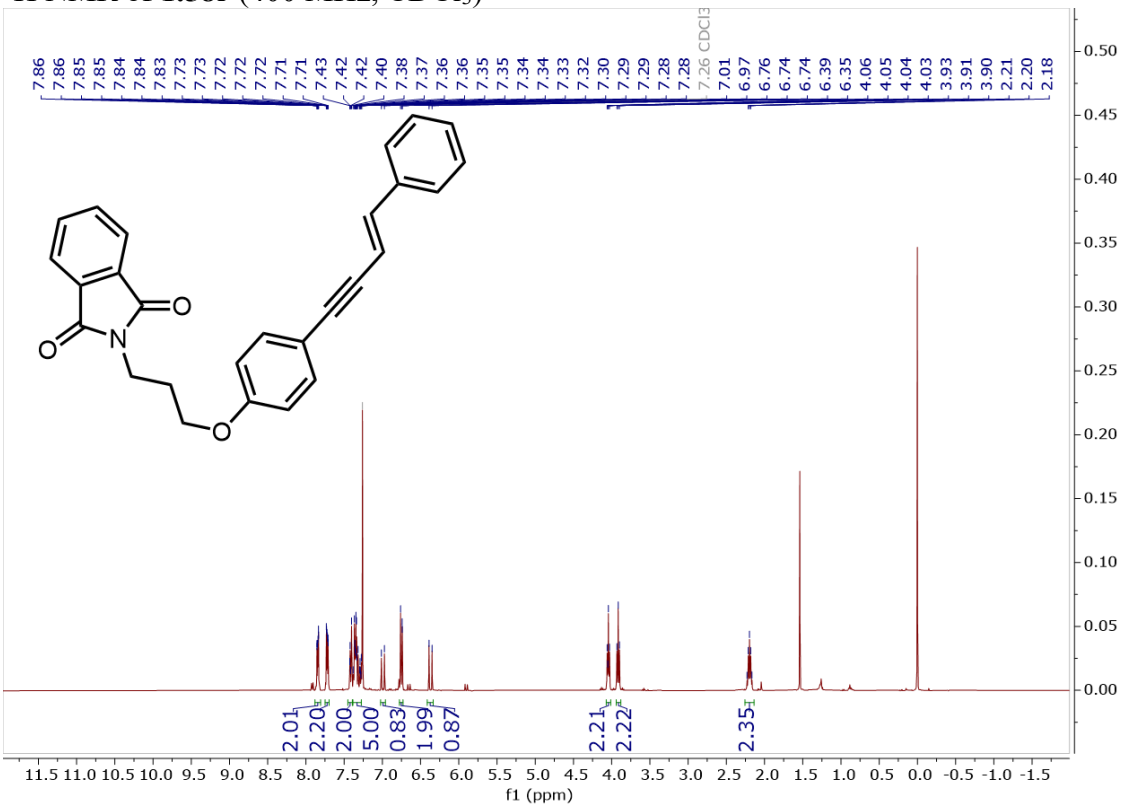

^{13}C NMR of **1.58r** (101 MHz, $CDCl_3$)

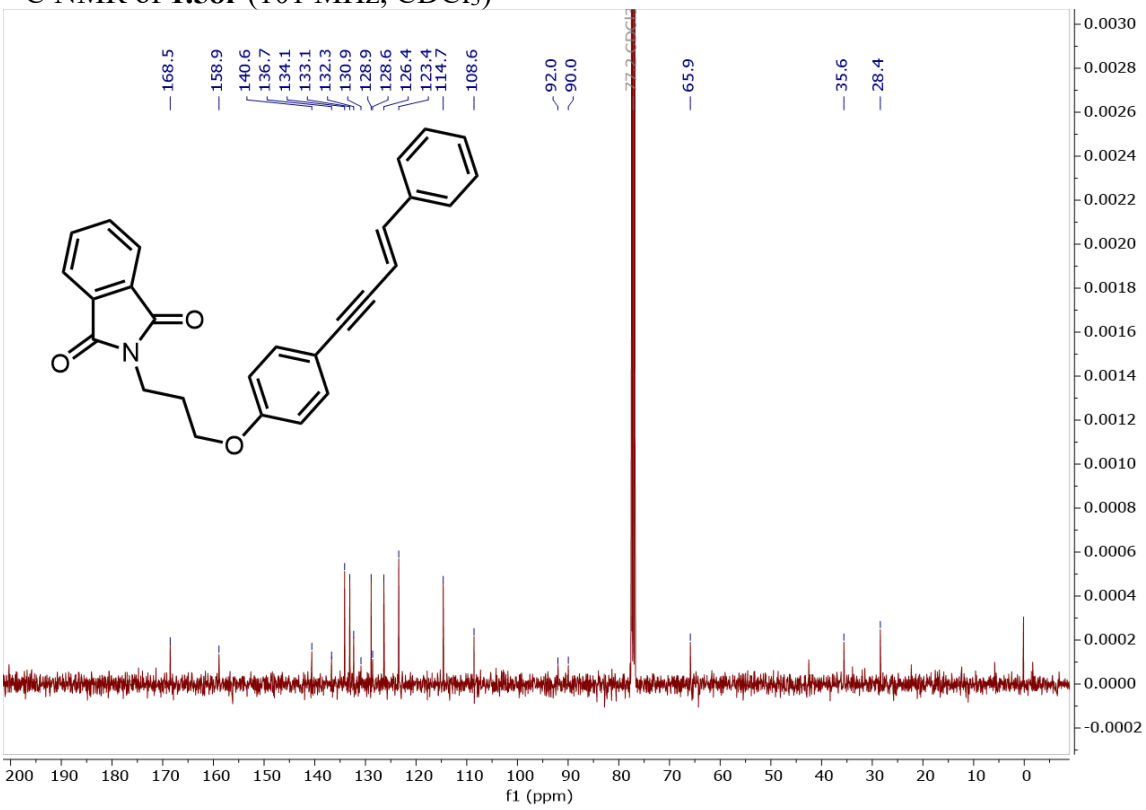

^{1}H NMR of **4.33x** (400 MHz, $CDCl_3$) (isolated with dicyclohexylurea as an impurity).

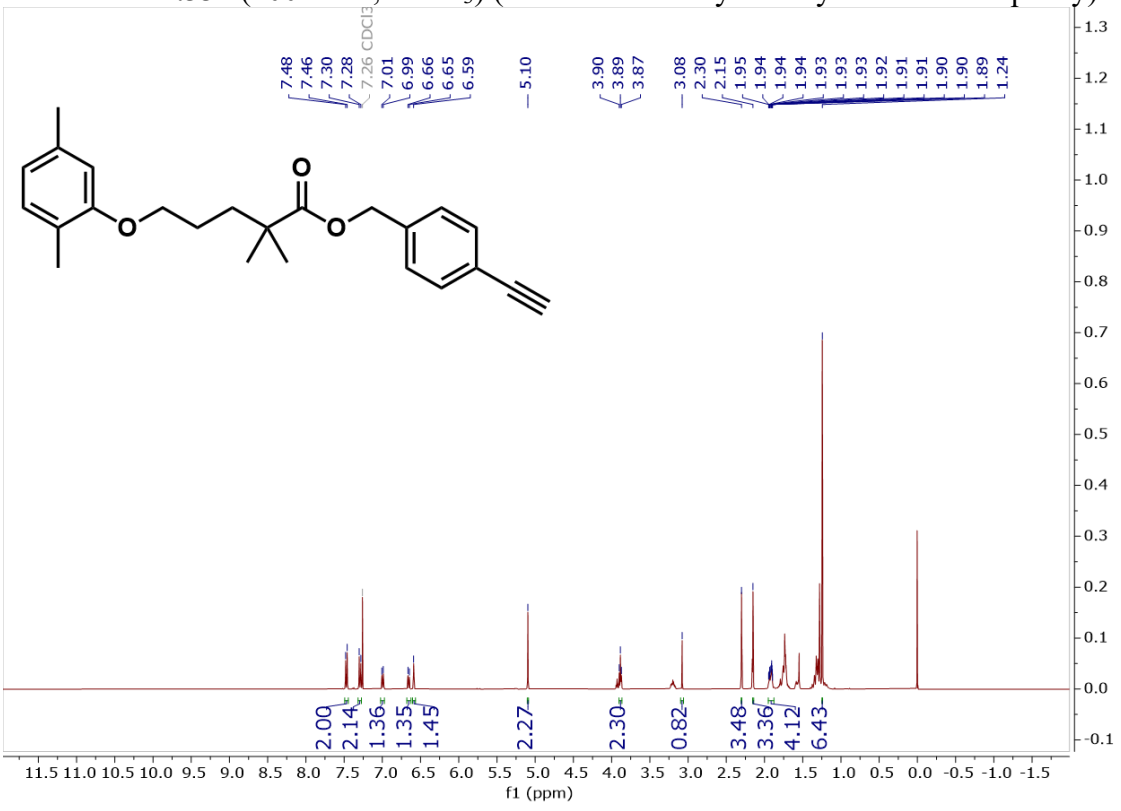

^{13}C NMR of **4.33x** (101 MHz, $CDCl_3$) in (DCU indicates a dicyclohexylurea impurity peak).

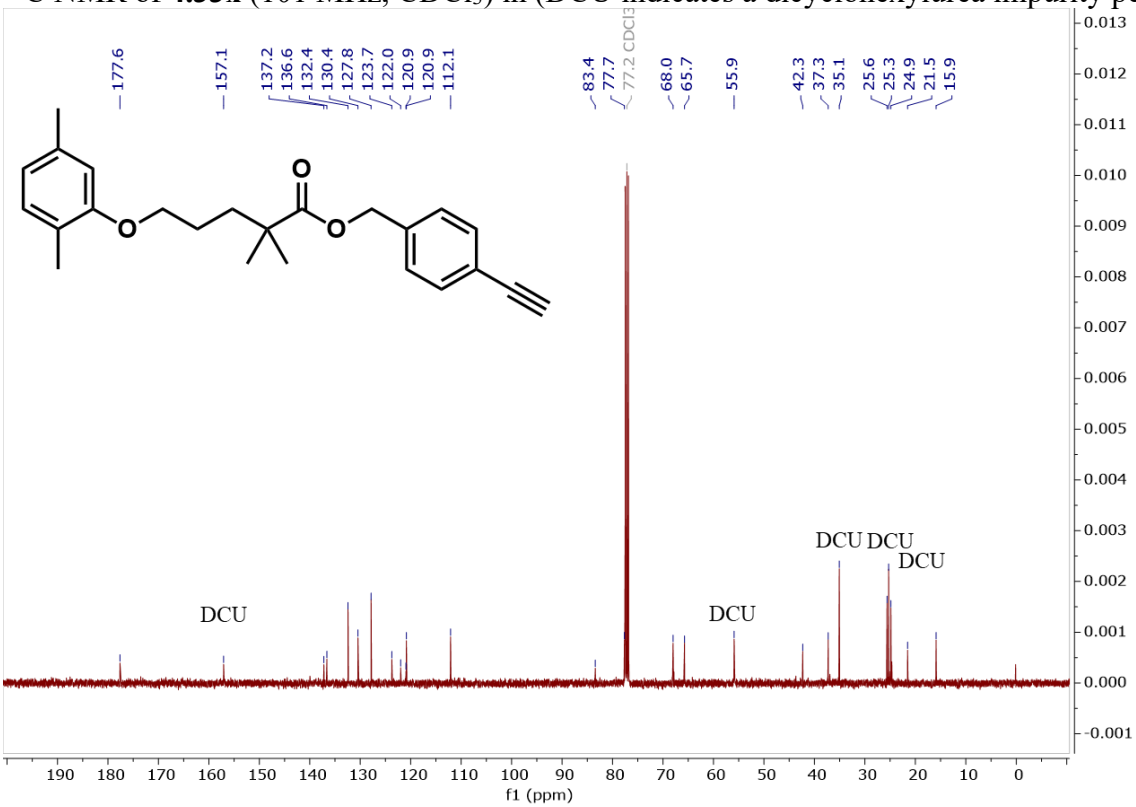

^{1}H NMR of **1.58x** (400 MHz, $CDCl_3$)

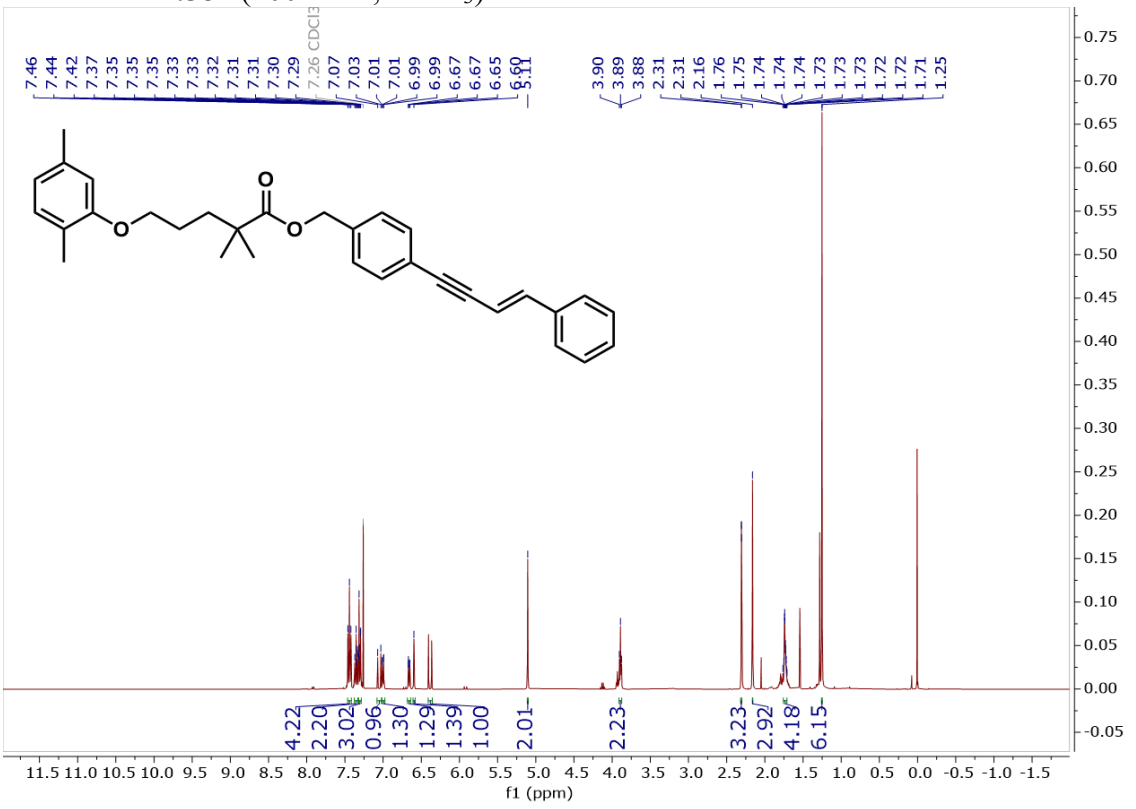

^{13}C NMR of **1.58x** (101 MHz, $CDCl_3$)

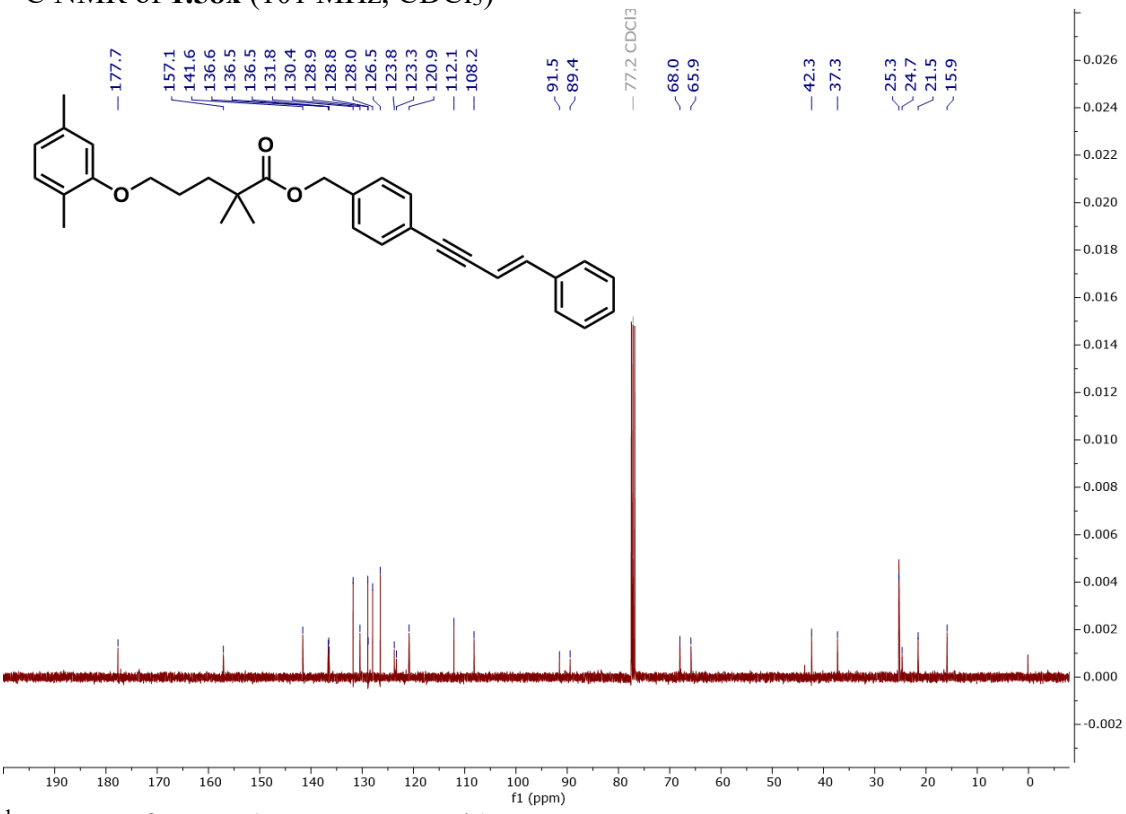

^{1}H NMR of **1.58w** (400 MHz, $CDCl_3$)

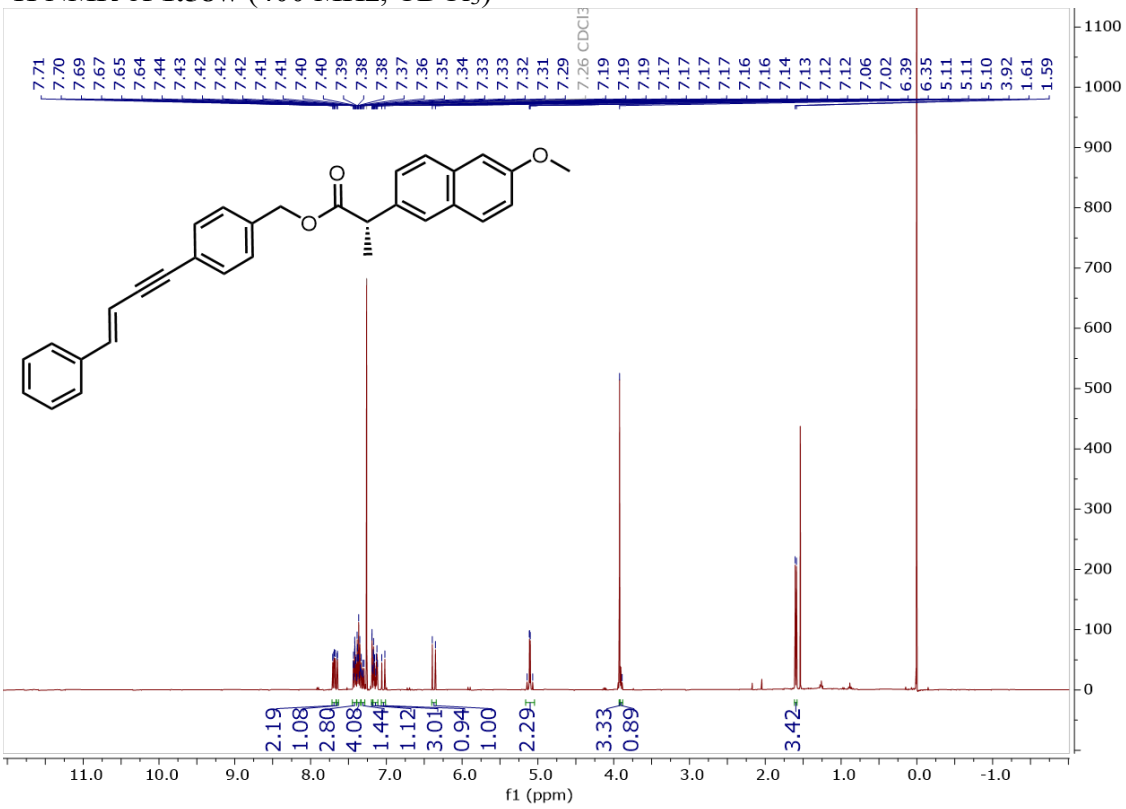

^{13}C NMR of **1.58w** (101MHz, $CDCl_3$)

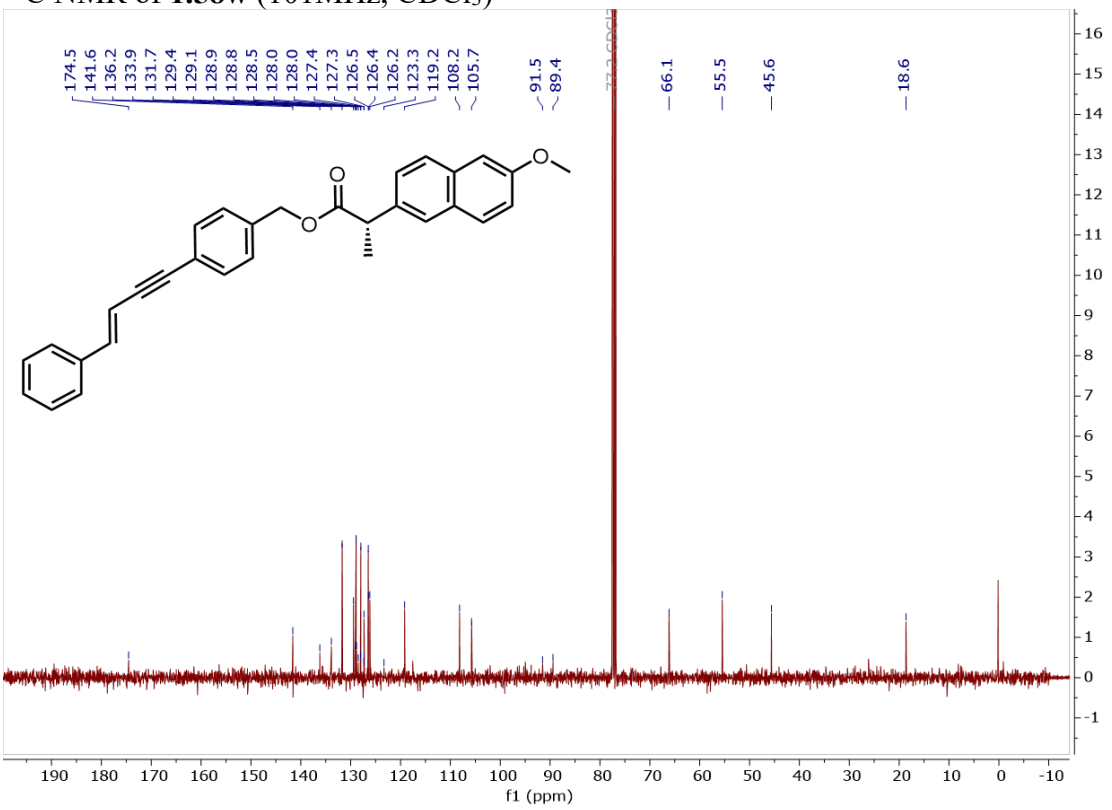

NMR Spectra for 2-boryl-1,3-dienes for Chapter 1

^{1}H NMR of **1.59a** ($CDCl_3$, 400 MHz)

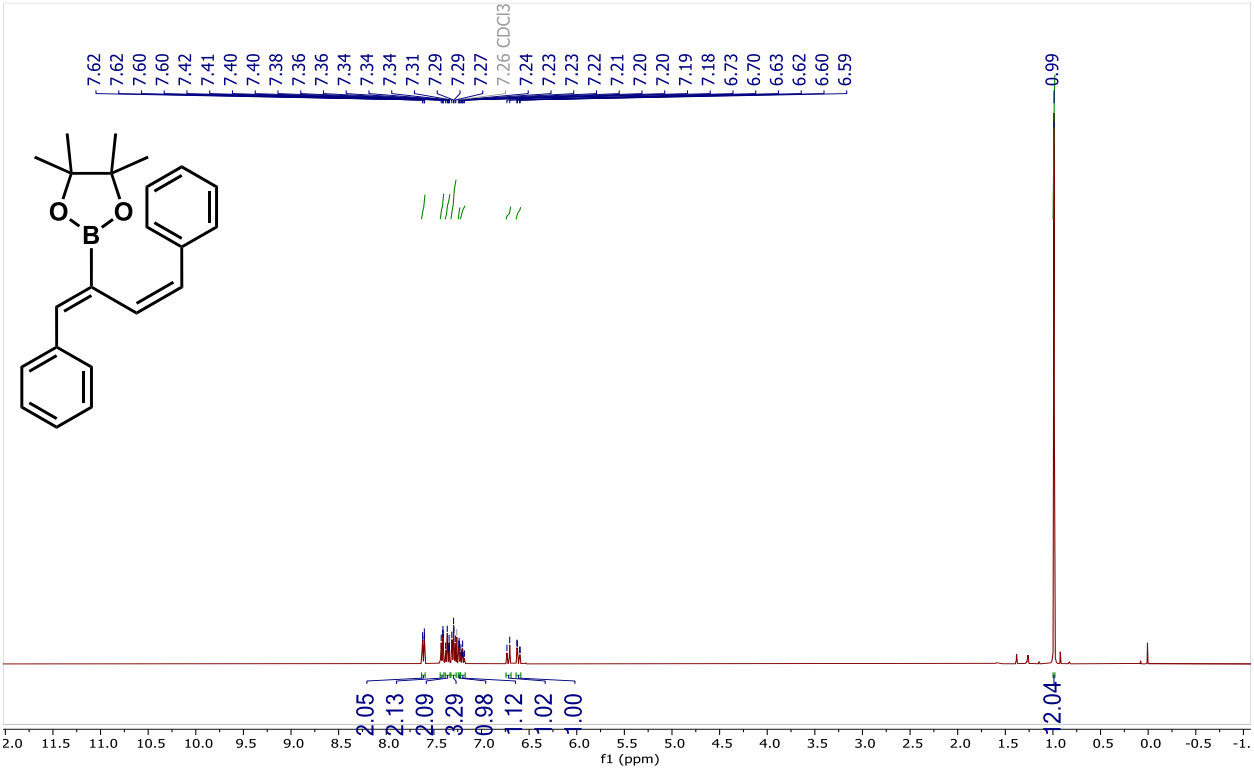

^{13}C NMR of **1.59a** ($CDCl_3$, 101 MHz)

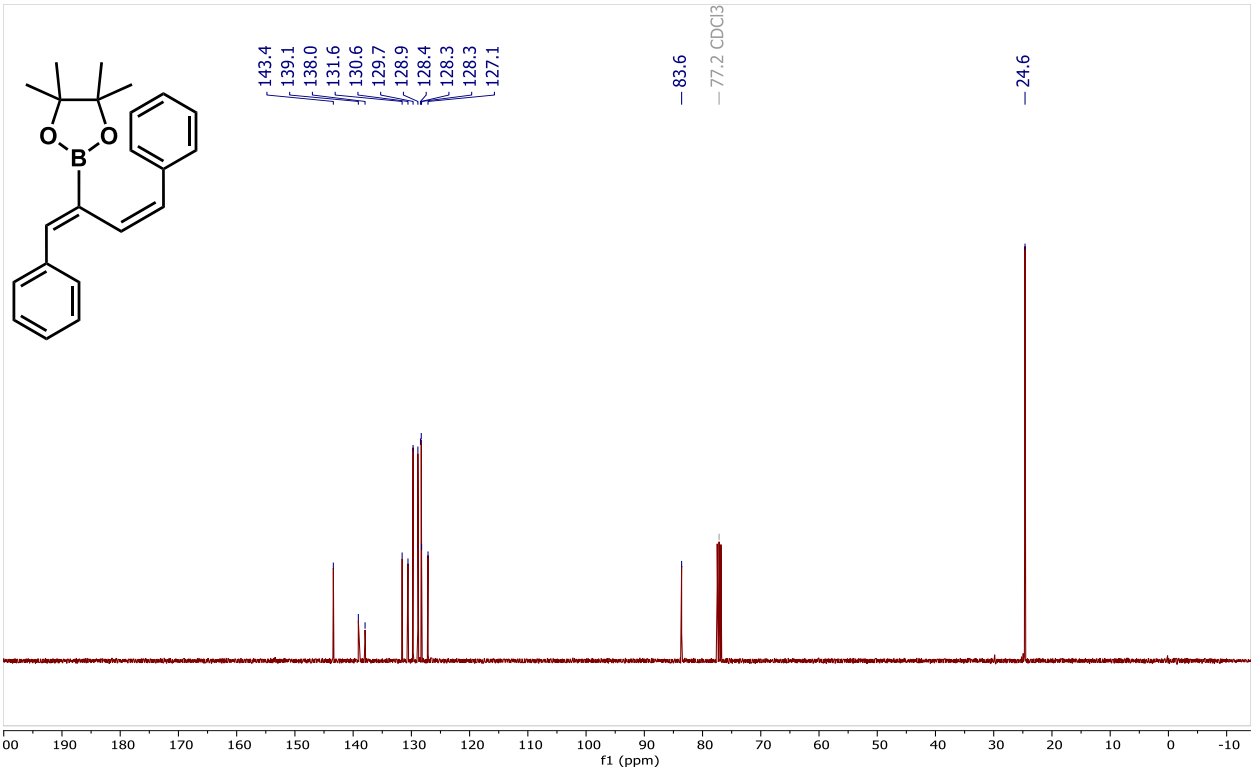

^{11}B NMR of **1.59a** ($CDCl_3$, 128 MHz)

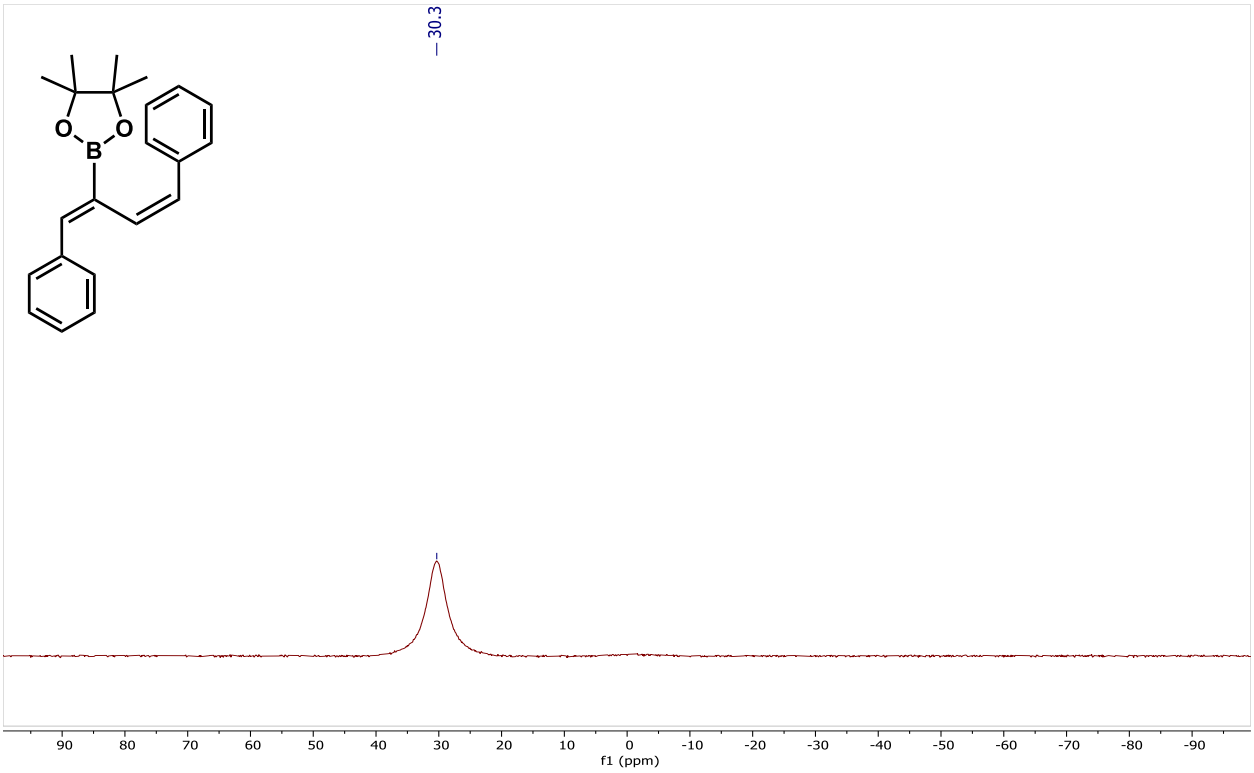

^{1}H NMR of **1.59b** ($CDCl_3$, 400 MHz)

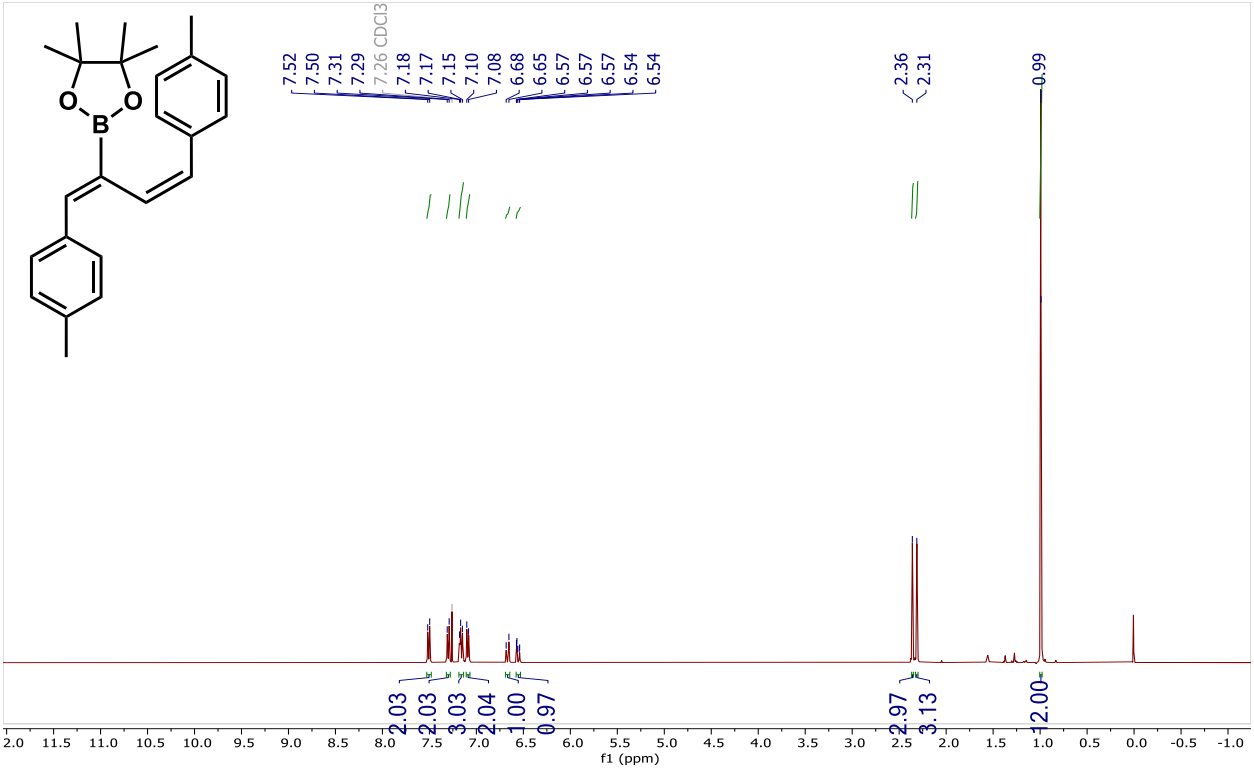

^{13}C NMR of **1.59b** ($CDCl_3$, 101 MHz)

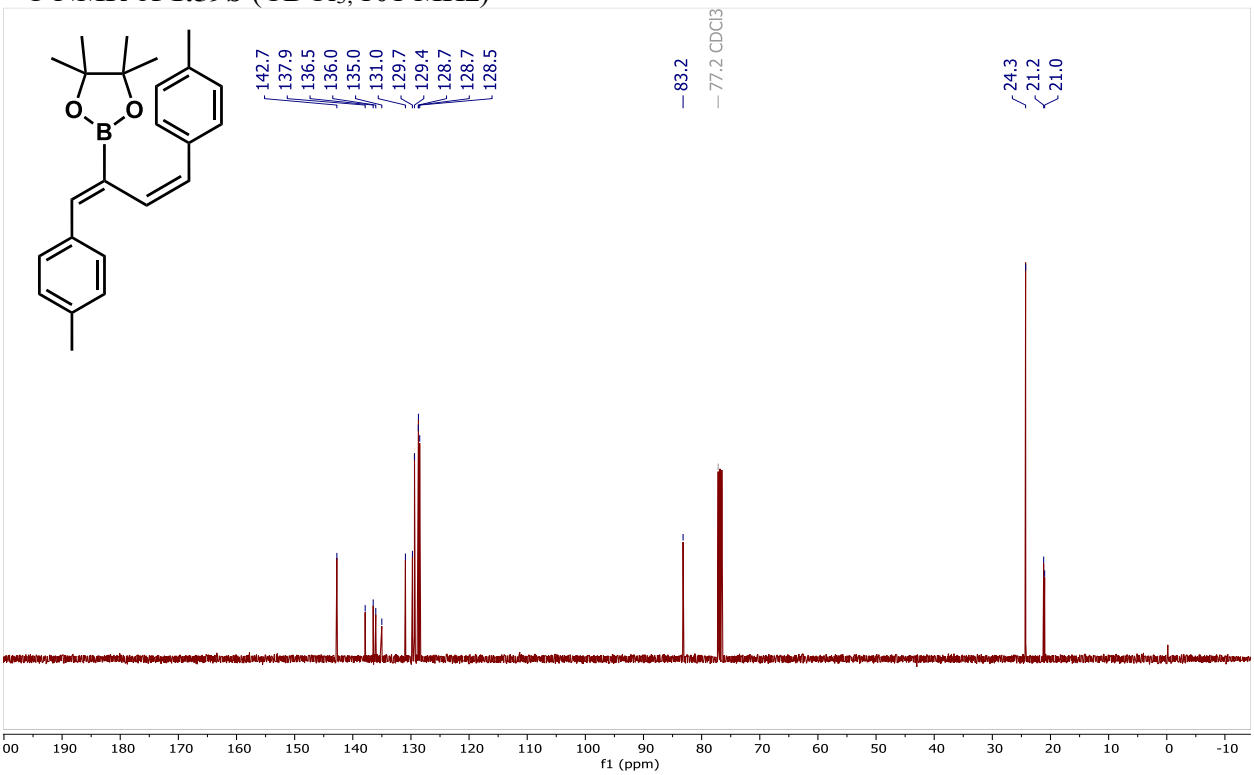

^{11}B NMR of **1.59b** ($CDCl_3$, 128 MHz)

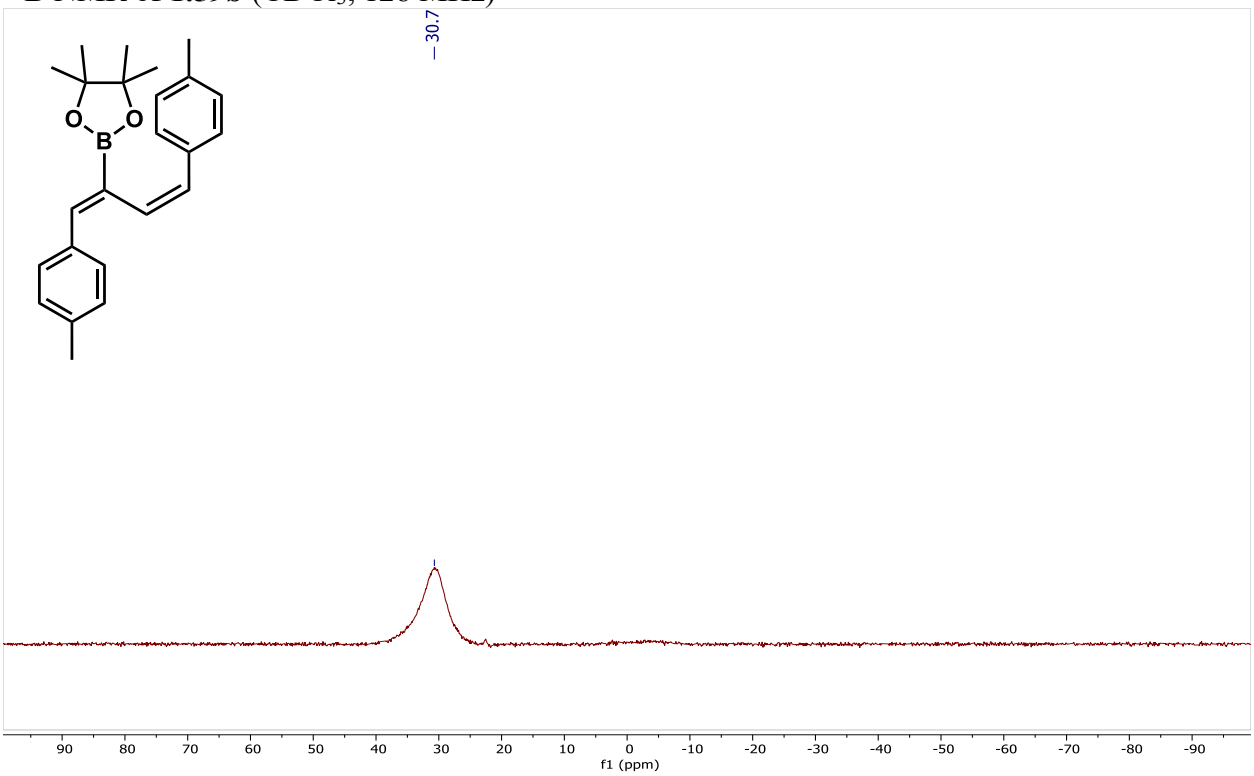

^{1}H NMR of **1.59c** ($CDCl_3$, 400 MHz)

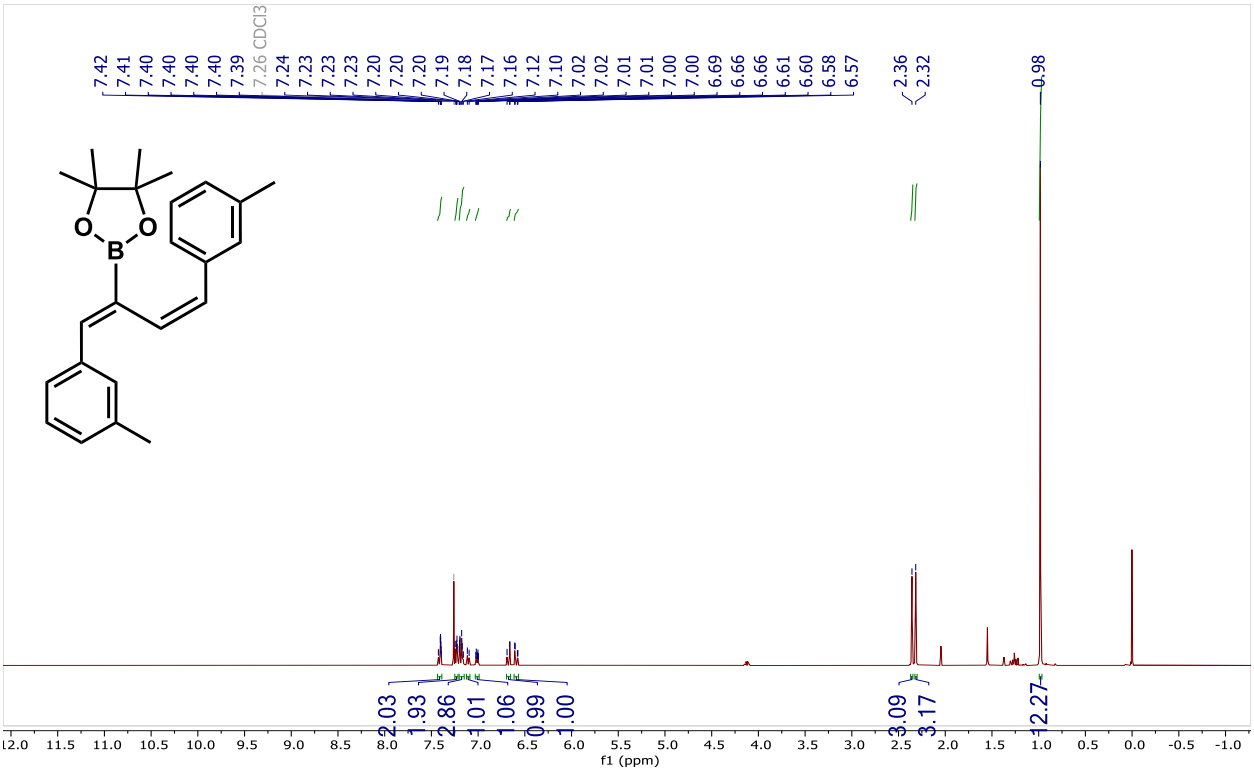

^{13}C NMR of **1.59c** ($CDCl_3$, 101 MHz)

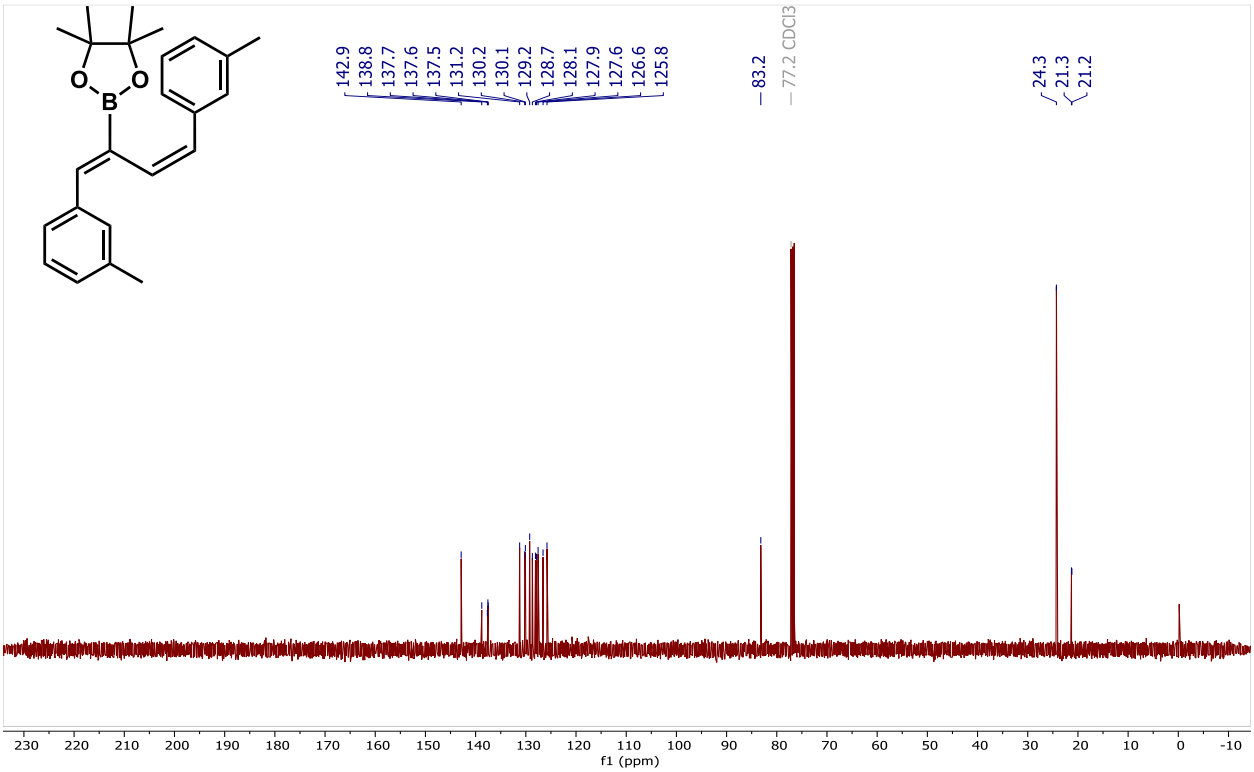

^{11}B NMR of **1.59c** ($CDCl_3$, 128 MHz)

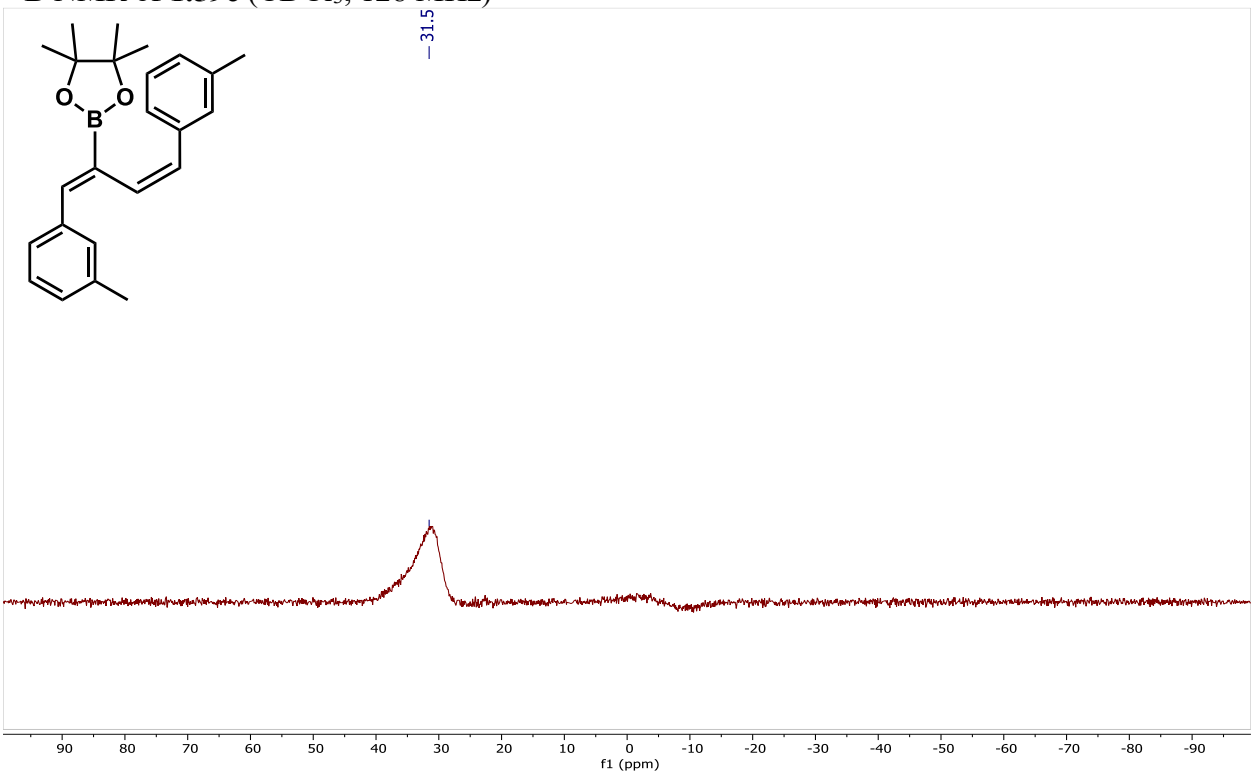

^{1}H NMR of **1.59d** ($CDCl_3$, 400 MHz)

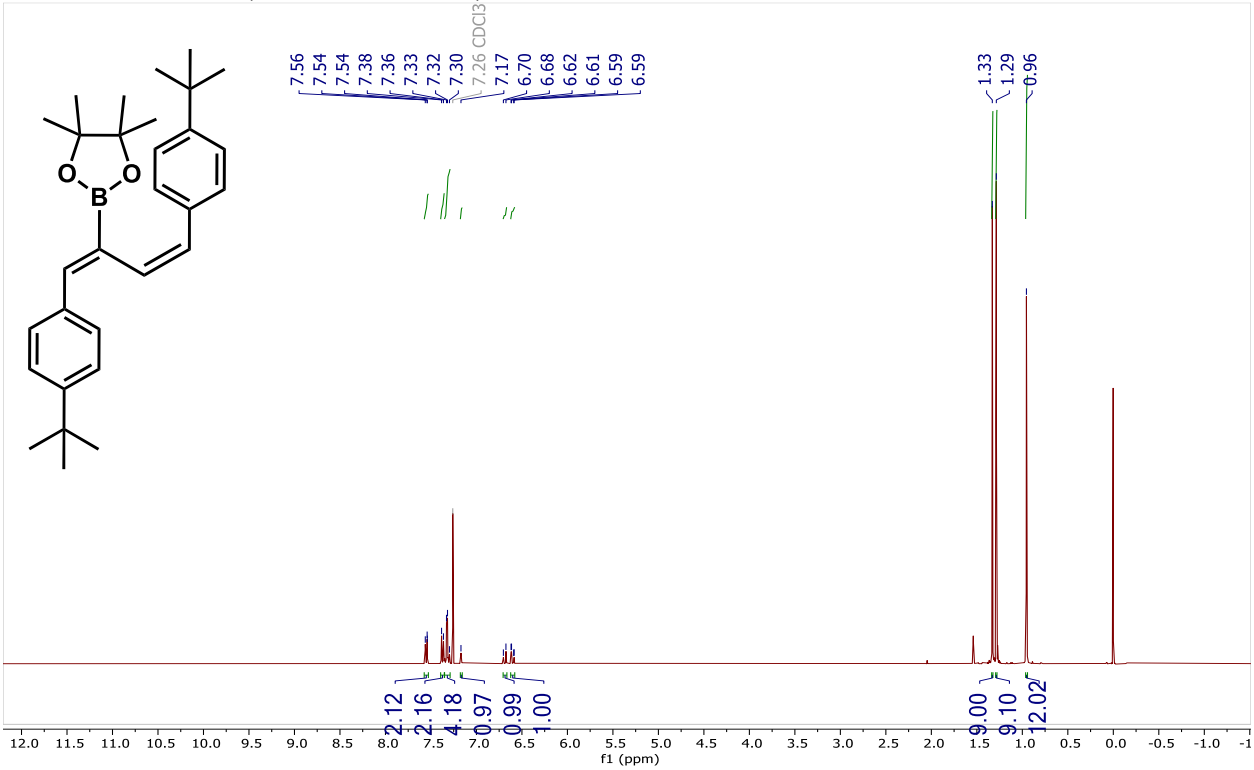

^{13}C NMR of **1.59d** ($CDCl_3$, 101 MHz)

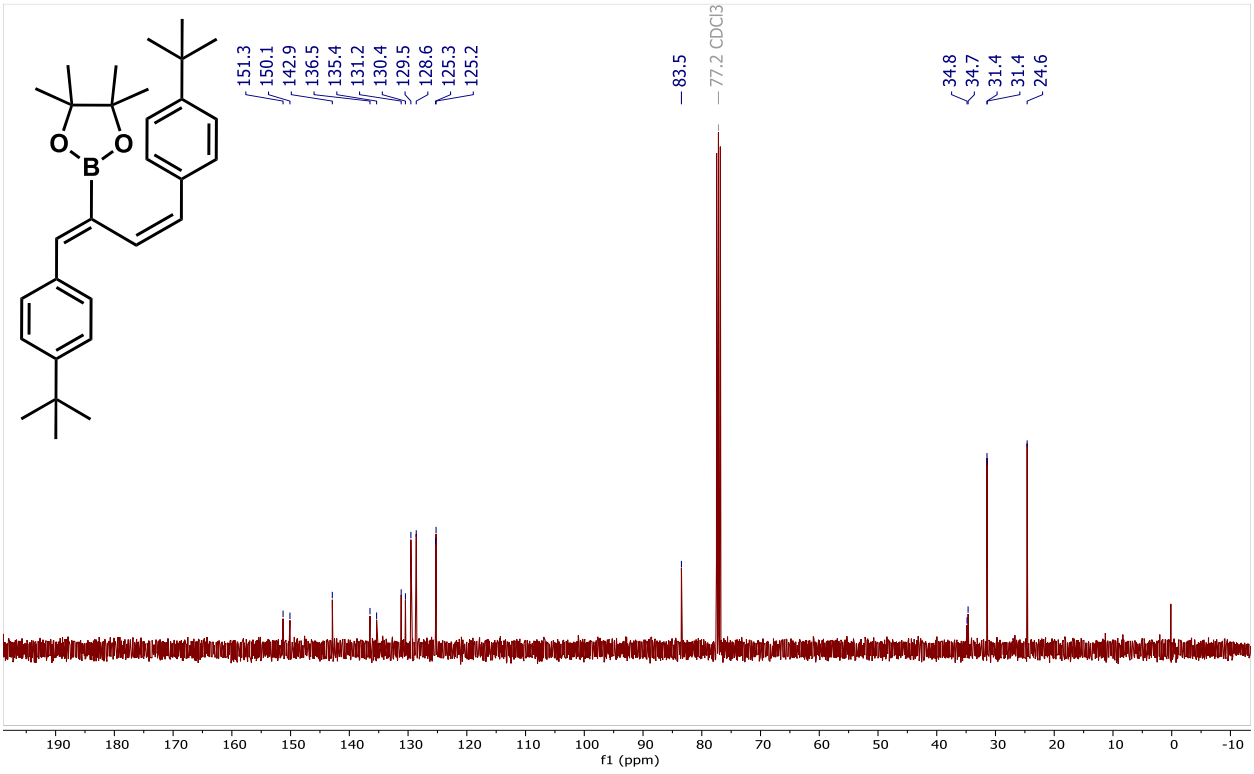

^{11}B NMR of **1.59d** ($CDCl_3$, 128 MHz)

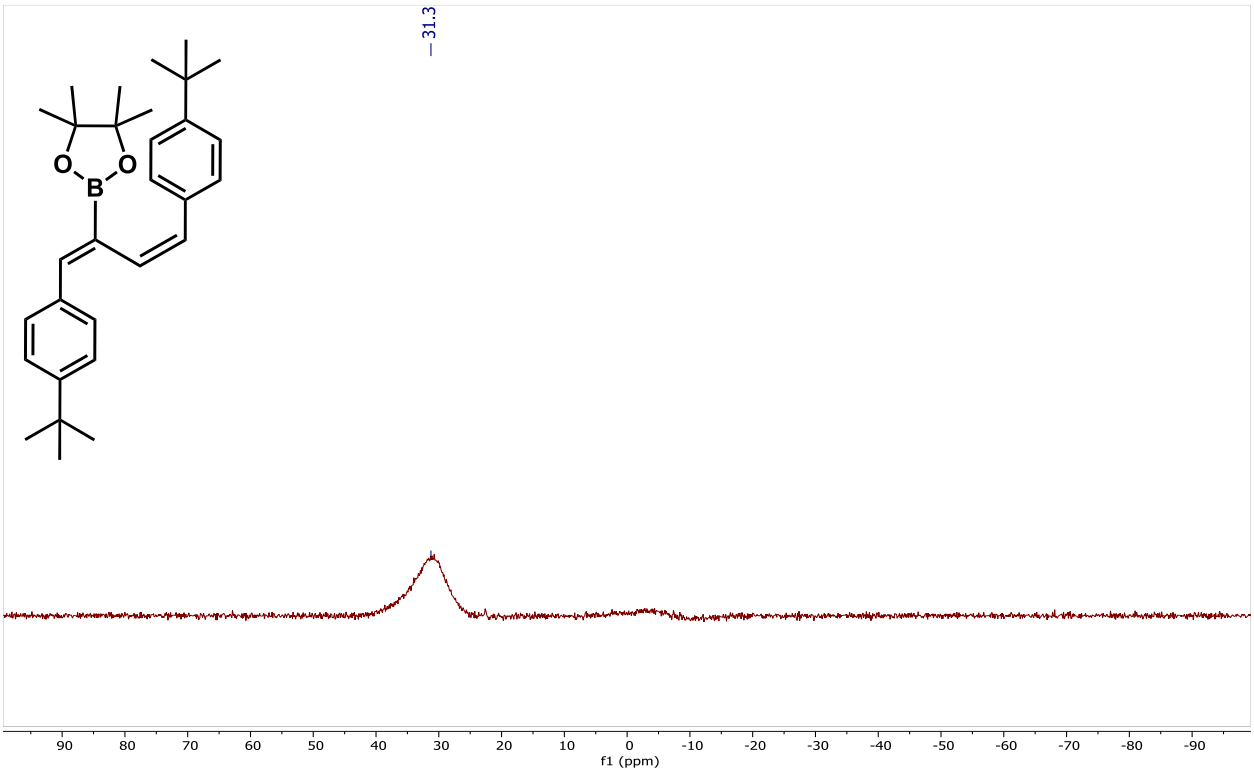

^{1}H NMR of **1.59e** ($CDCl_3$, 400 MHz)

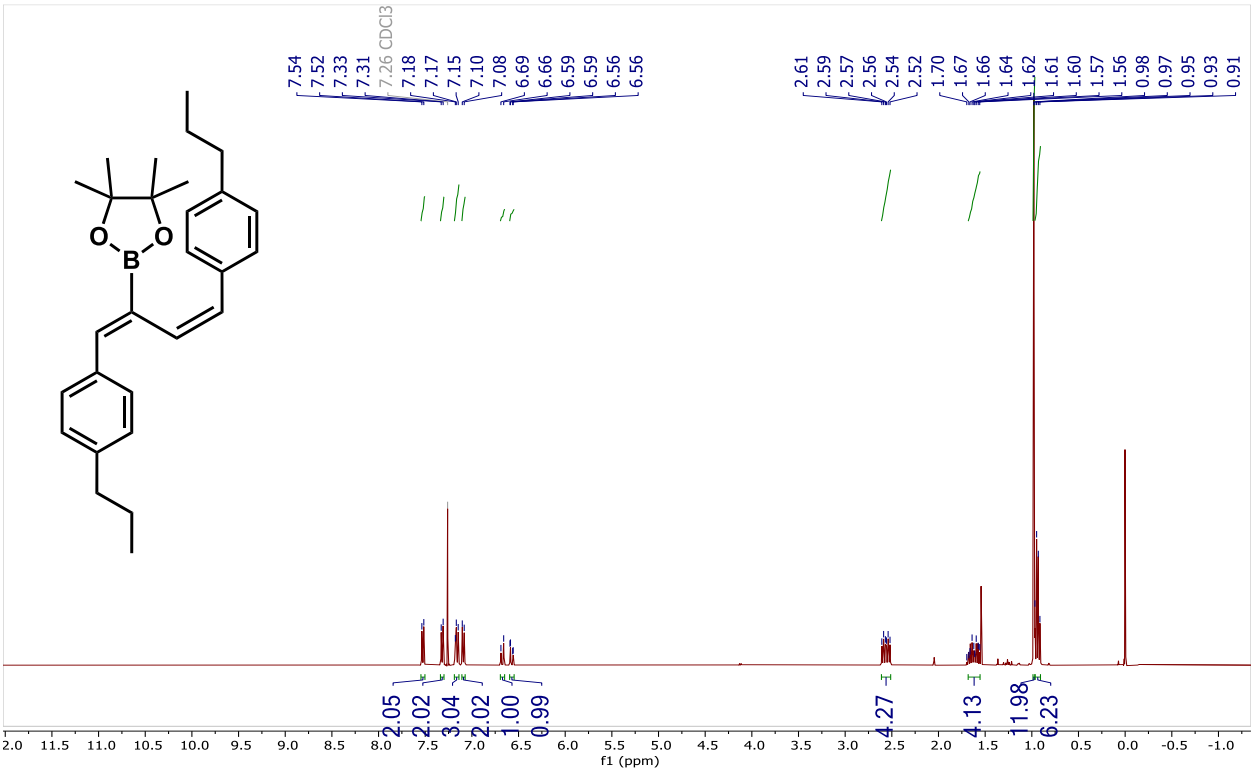

^{13}C NMR of **1.59e** ($CDCl_3$, 101 MHz)

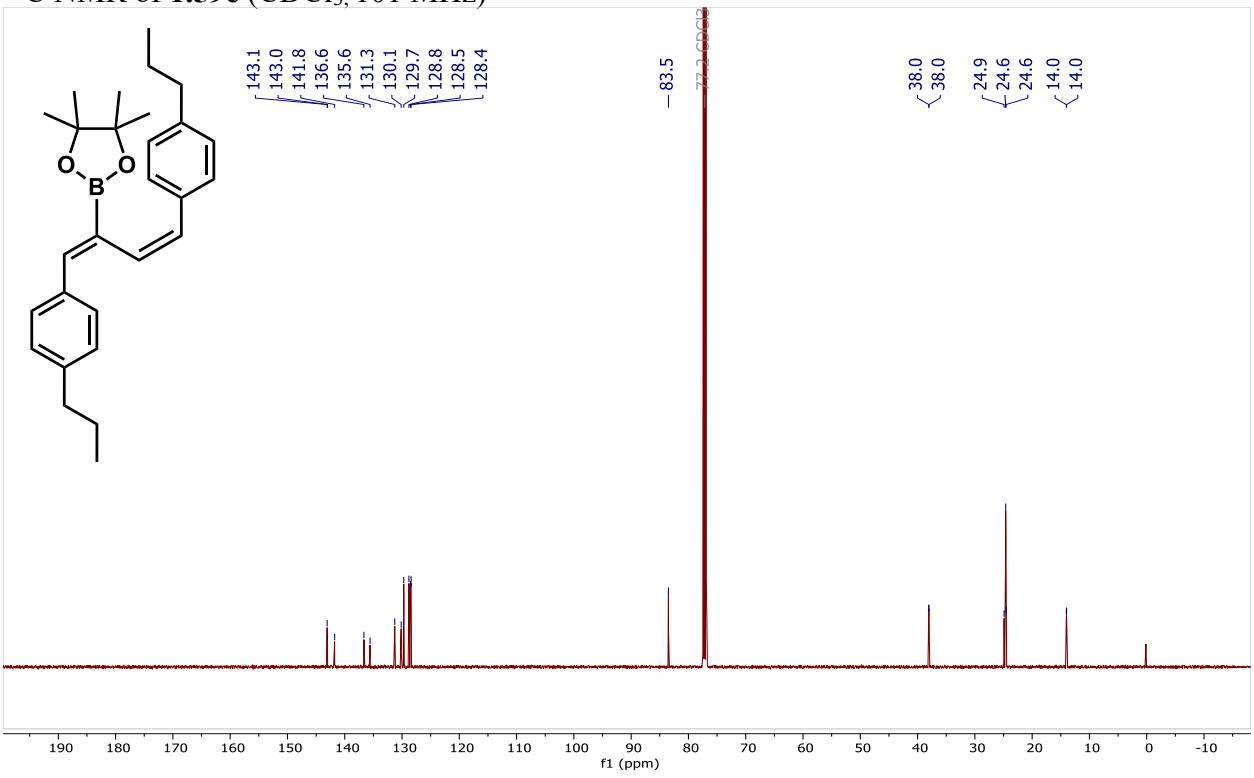

^{11}B NMR of **1.59e** ($CDCl_3$, 128 MHz)

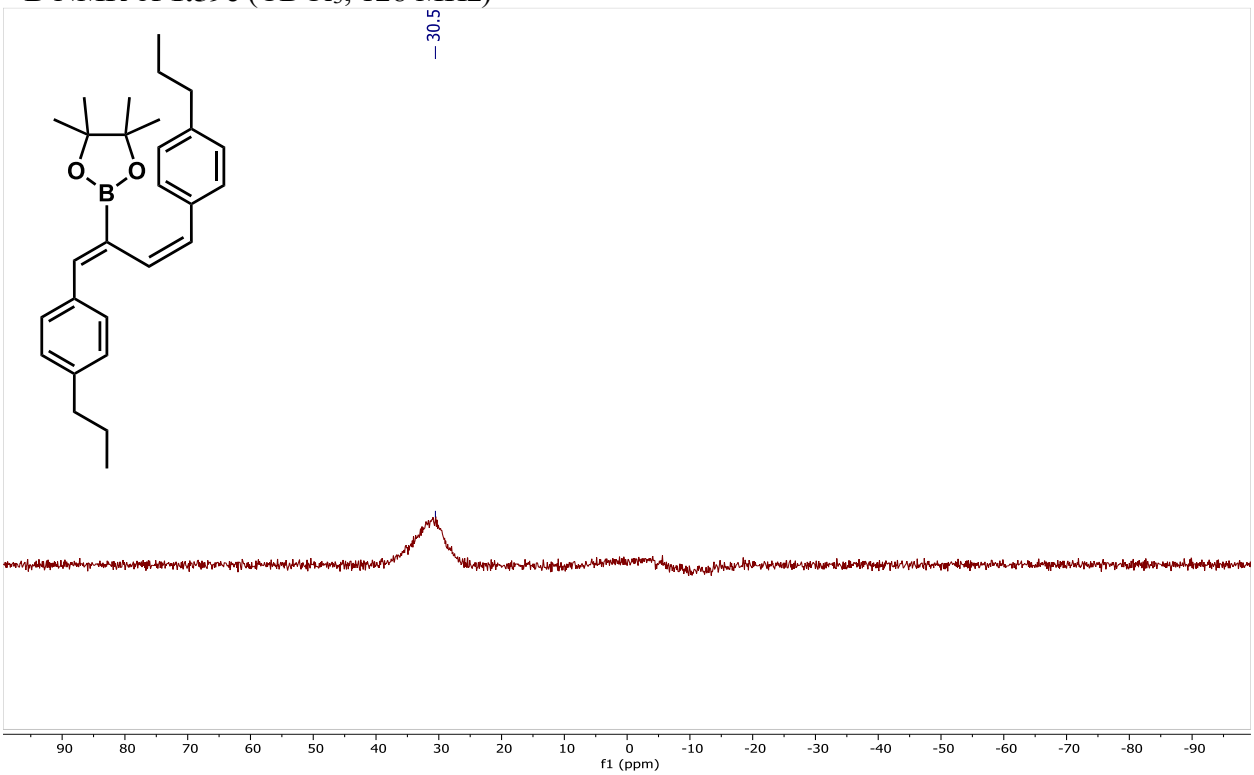

^{1}H NMR of **1.59f** ($CDCl_3$, 400 MHz)

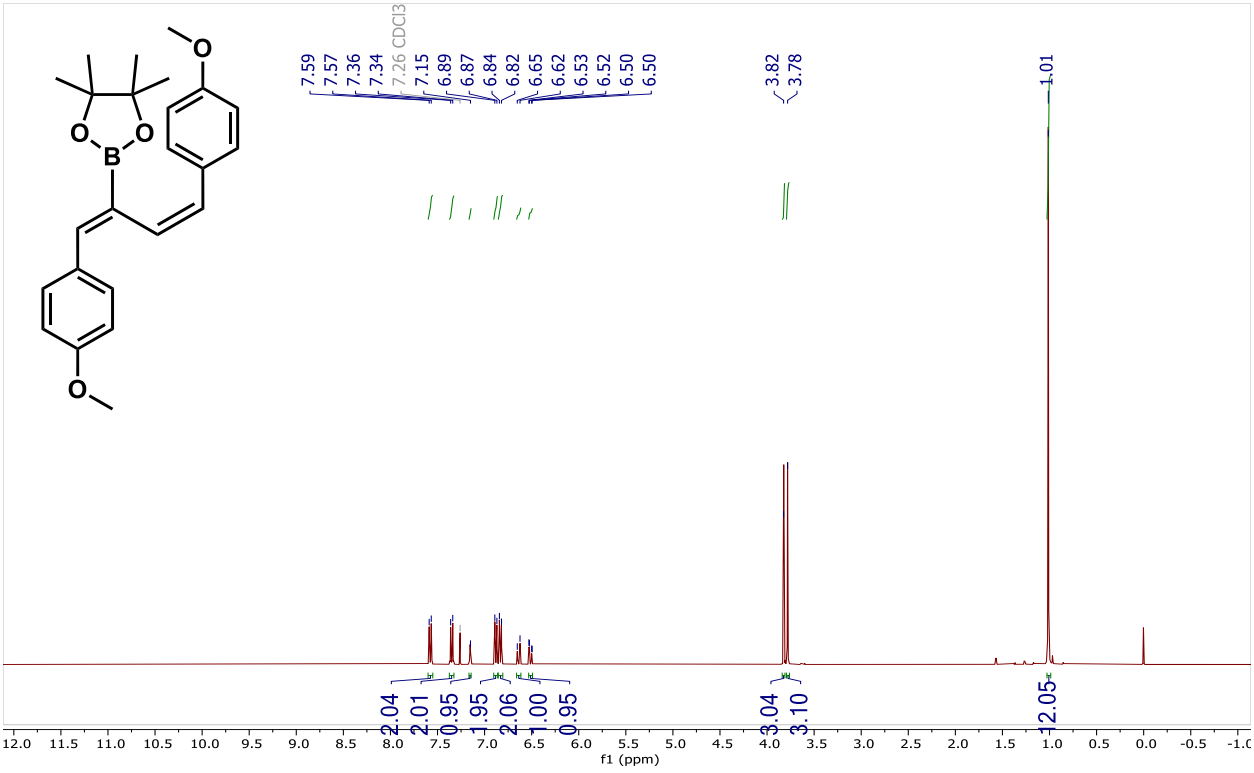

^{13}C NMR of **1.59f** ($CDCl_3$, 101 MHz)

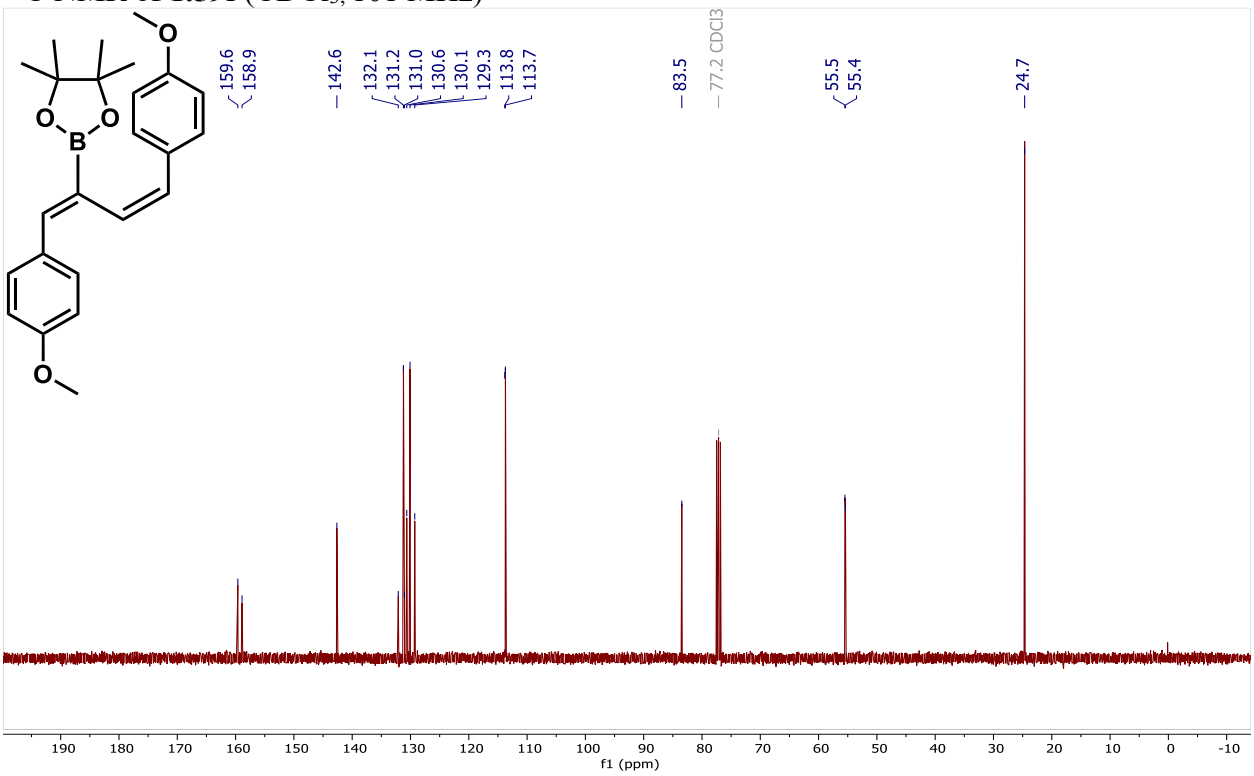

^{11}B NMR of **1.59f** ($CDCl_3$, 128 MHz)

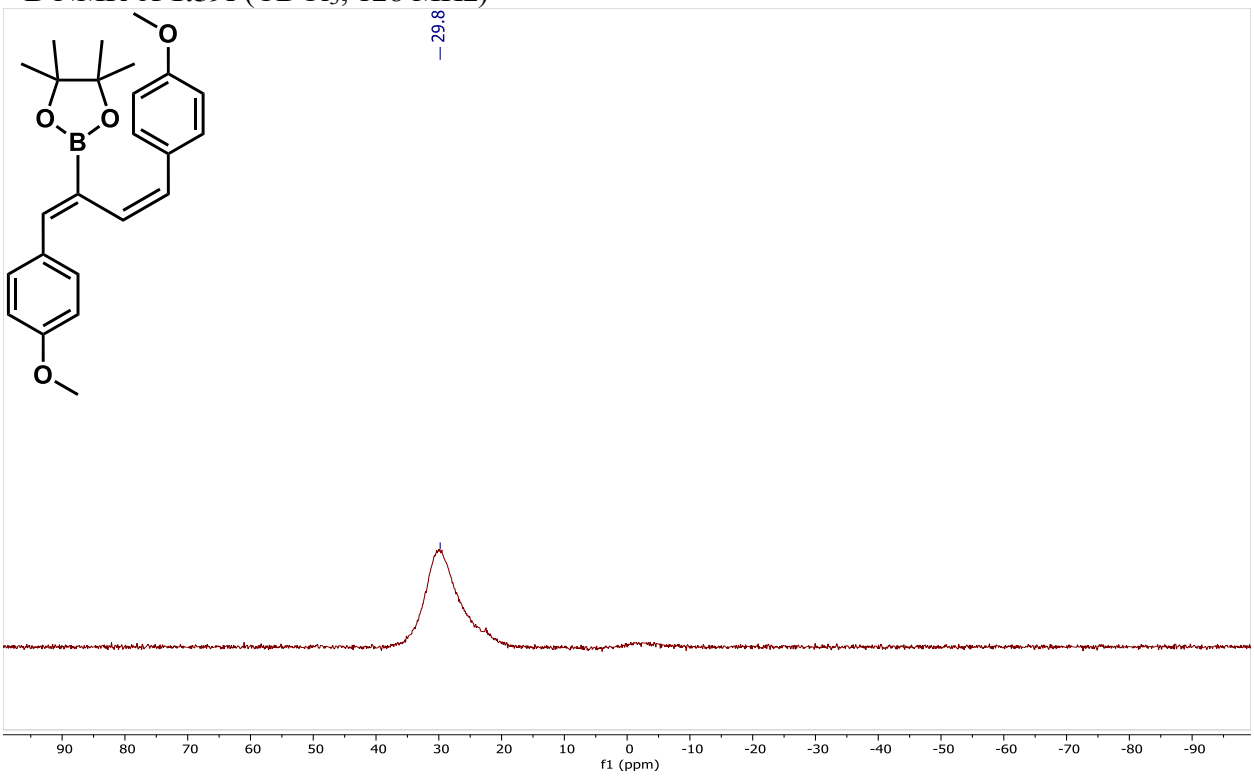

^{1}H NMR of **1.59g** ($CDCl_3$, 400 MHz)

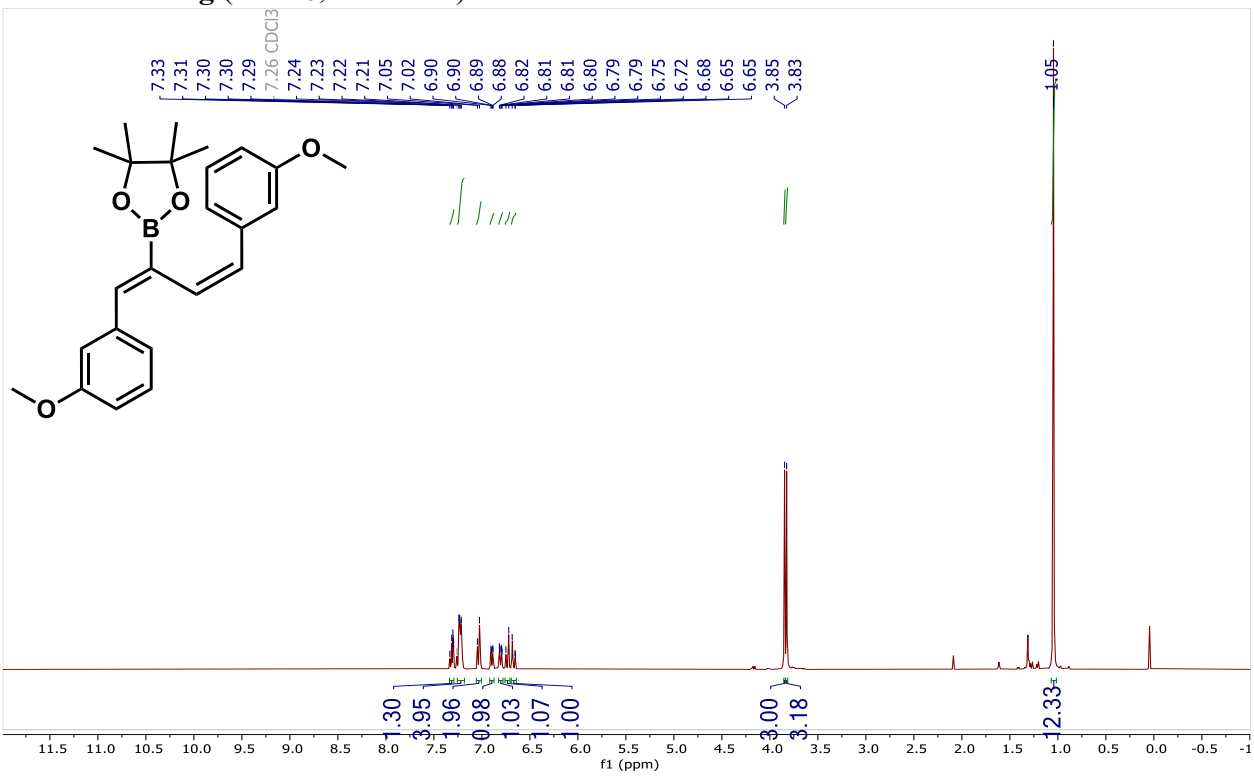

^{13}C NMR of **1.59g** ($CDCl_3$, 101 MHz)

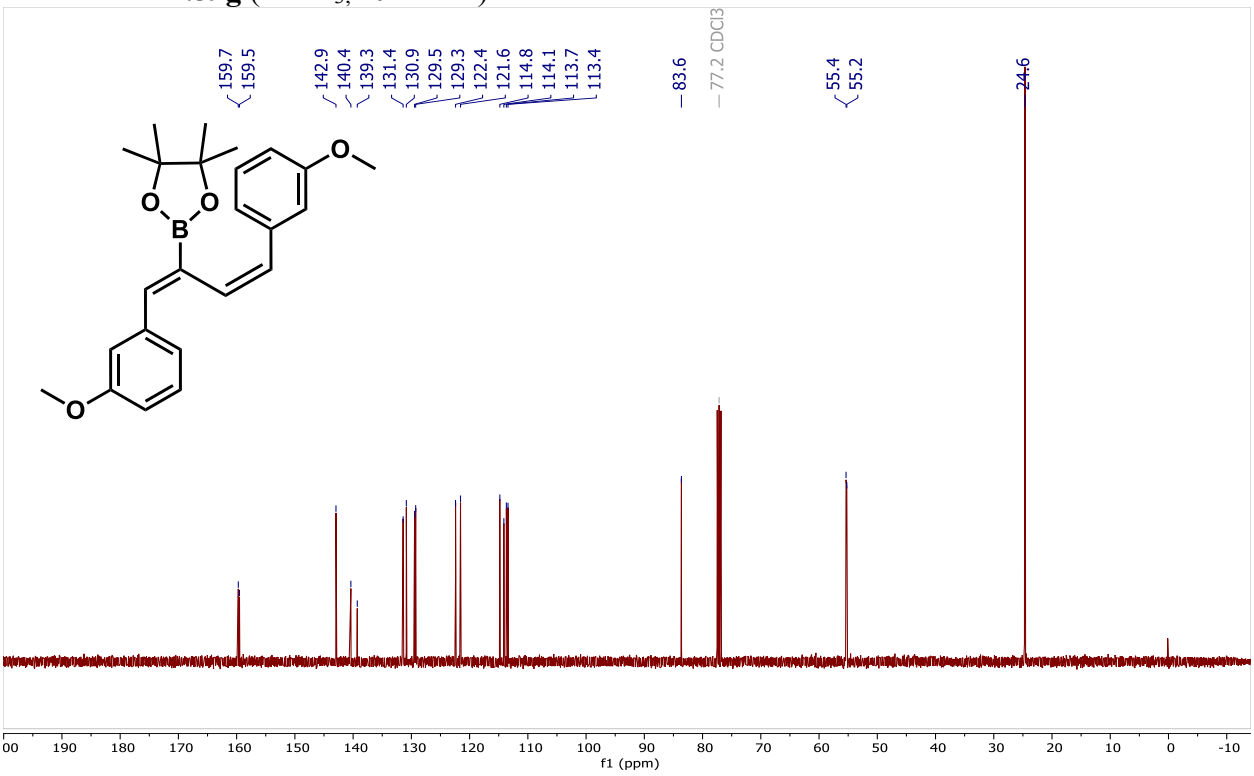

^{11}B NMR of **1.59g** ($CDCl_3$, 128 MHz)

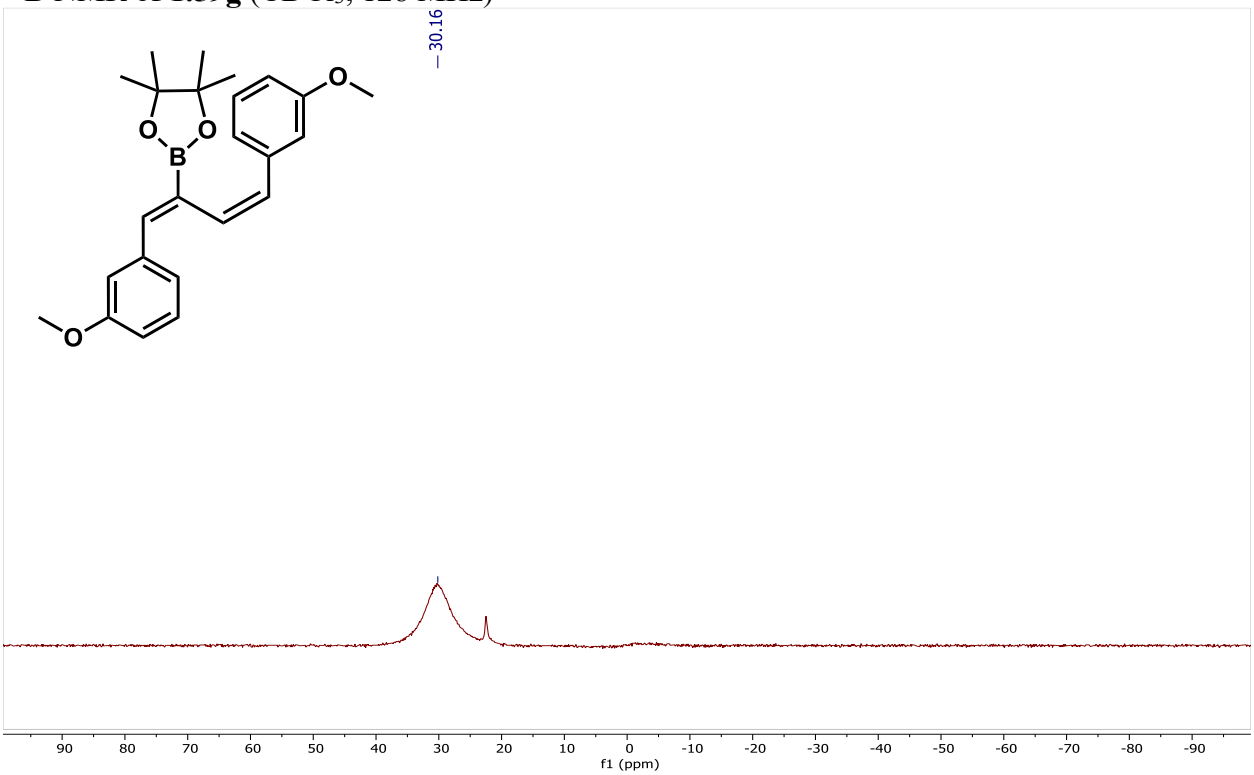

^{1}H NMR of **1.59h** ($CDCl_3$, 400 MHz)

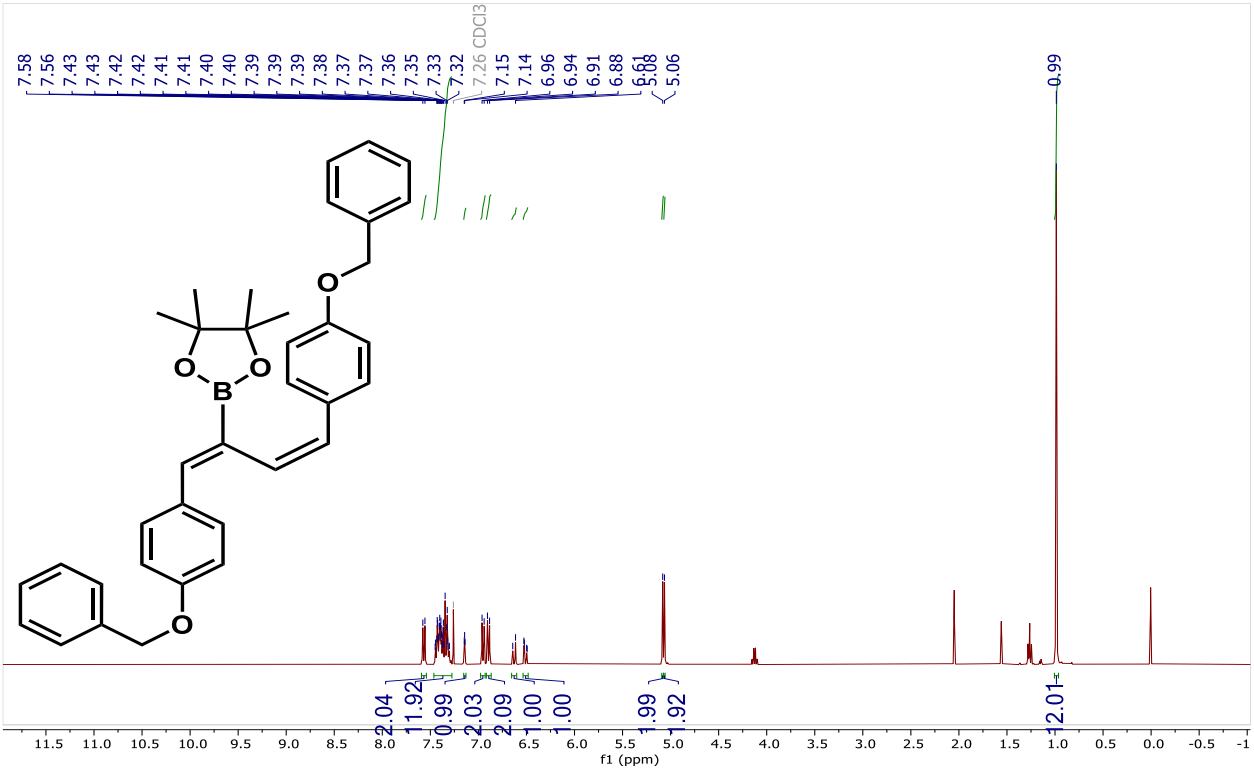

^{13}C NMR of **1.59h** ($CDCl_3$, 101 MHz)

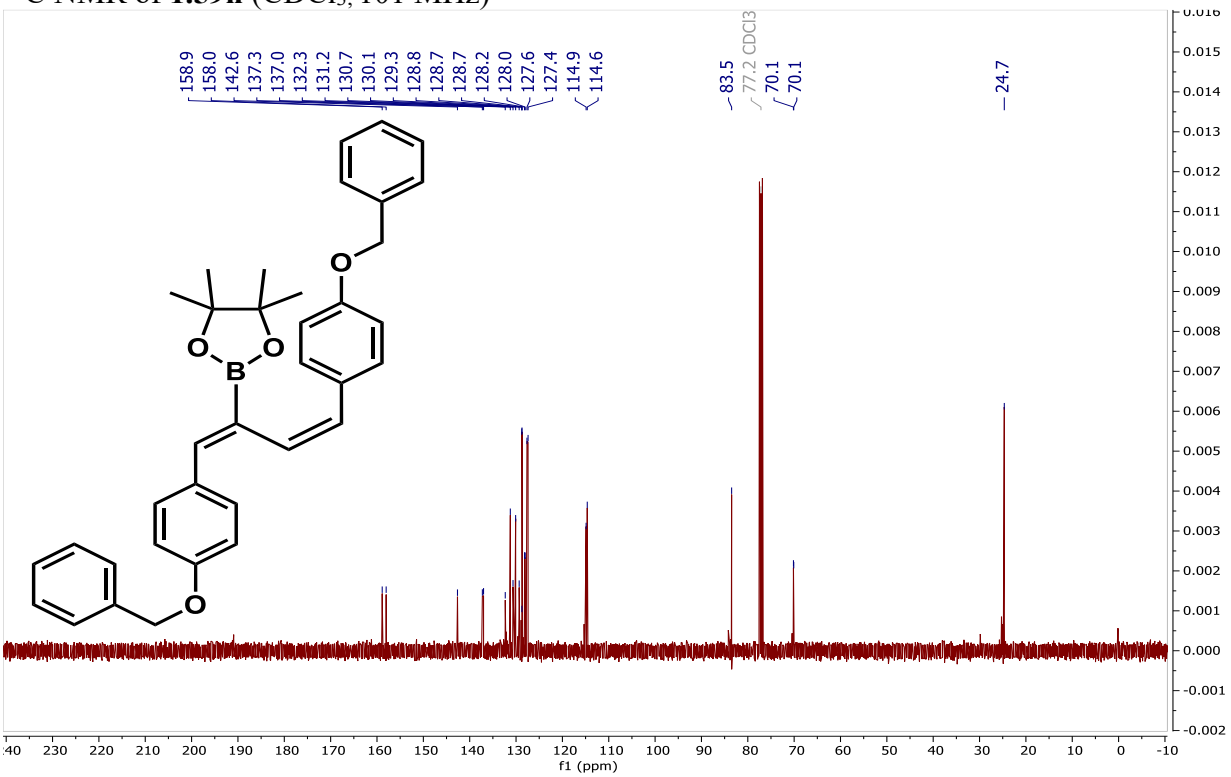

^{11}B NMR of **1.59h** ($CDCl_3$, 128 MHz)

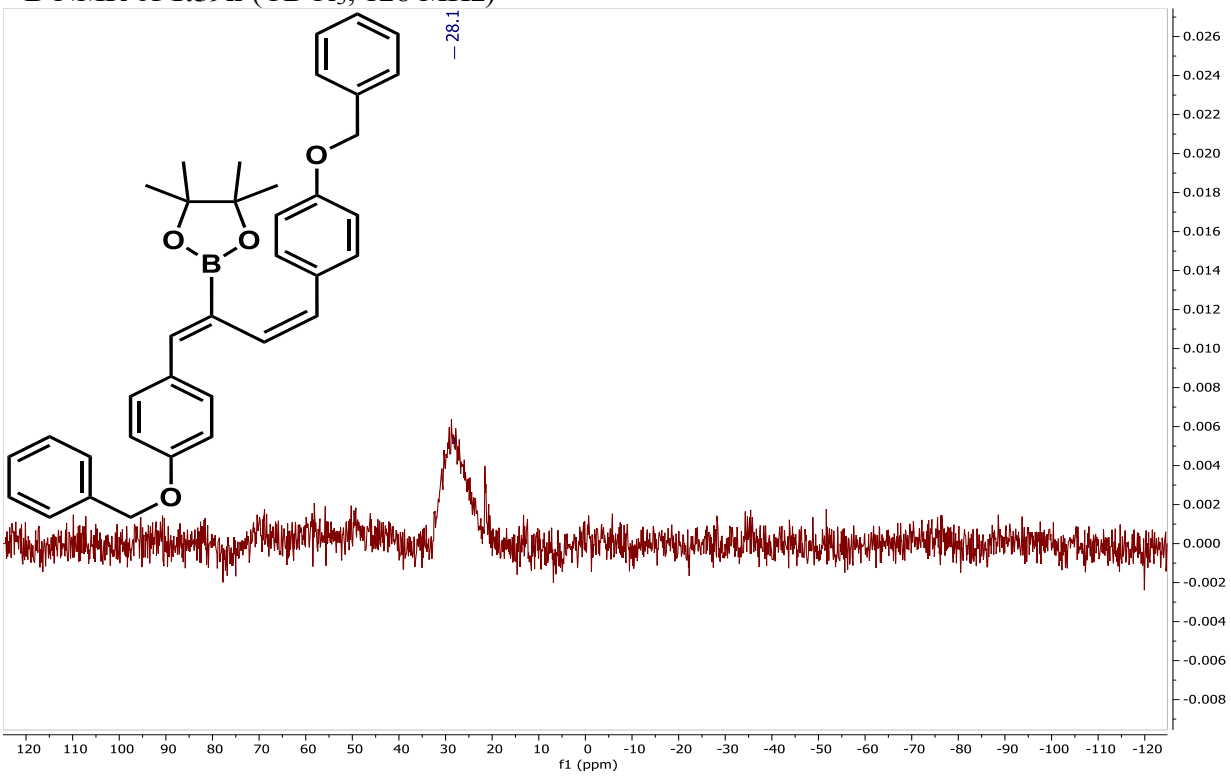

^{1}H NMR of **1.59i** ($CDCl_3$, 400 MHz)

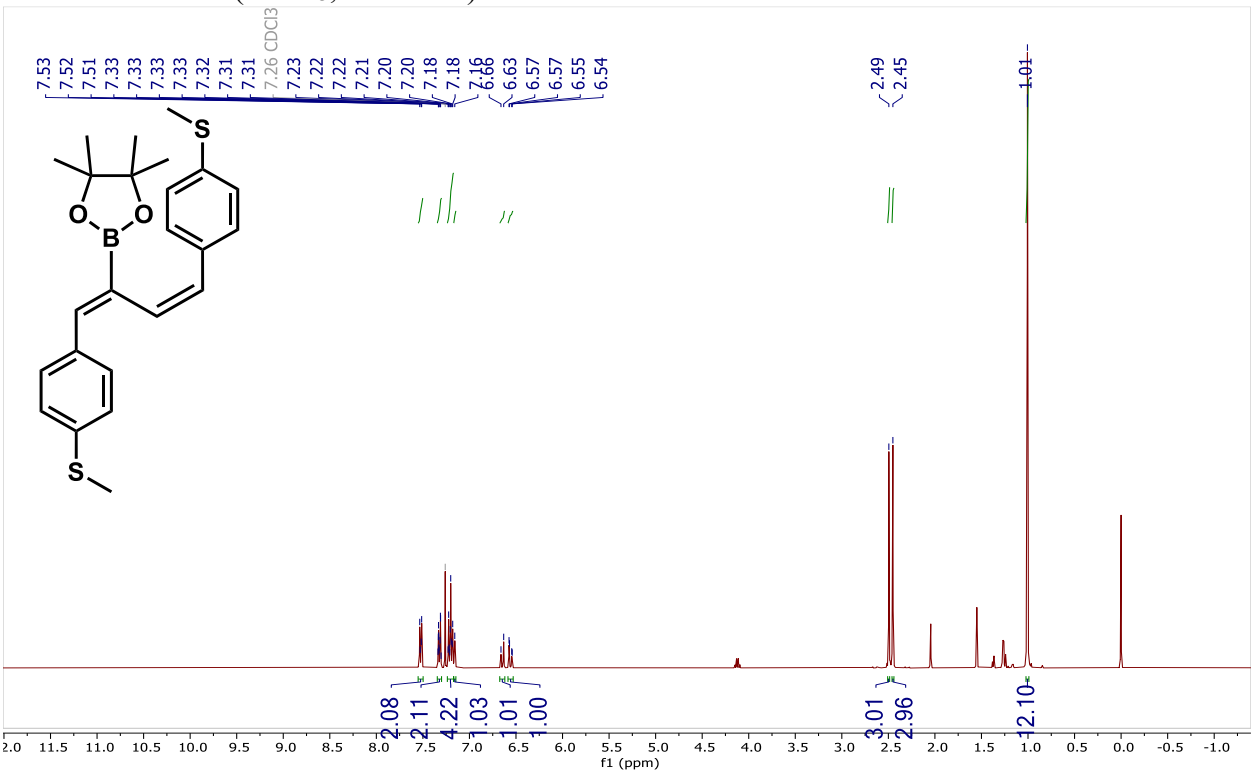

^{13}C NMR of **1.59i** ($CDCl_3$, 101 MHz)

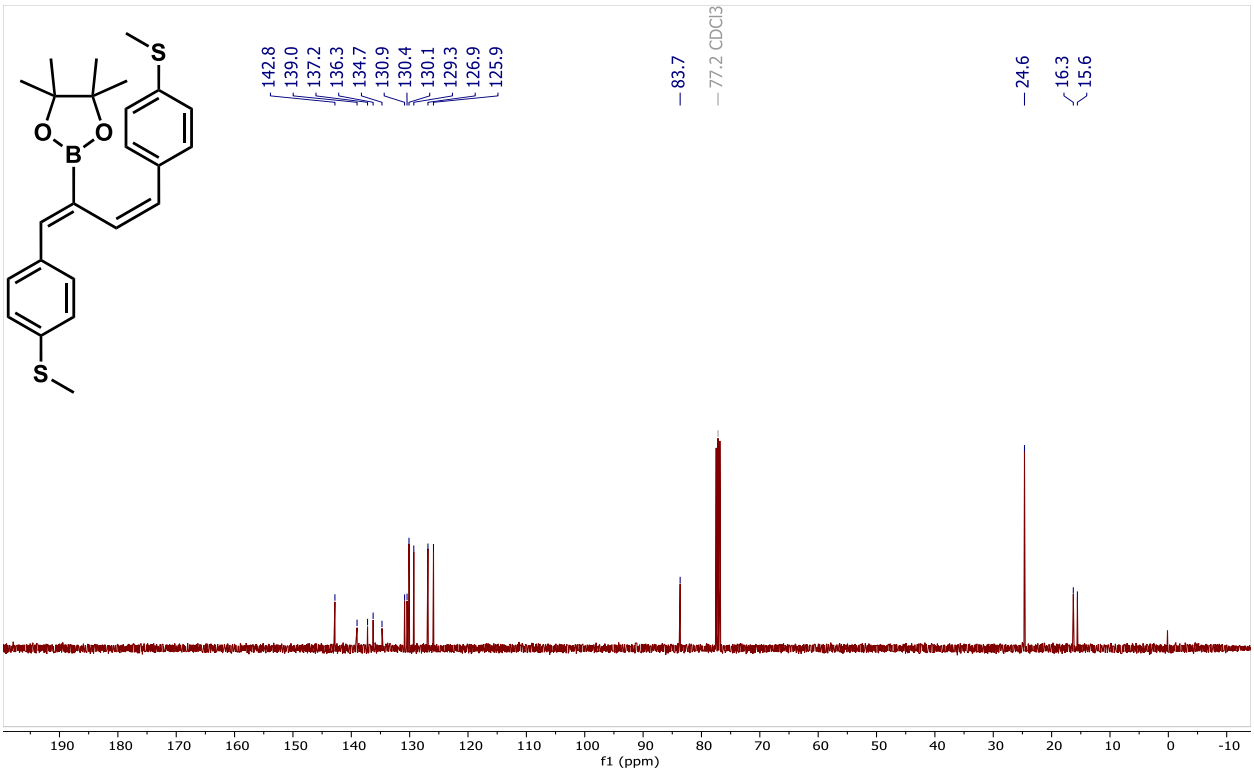

^{11}B NMR of **1.59i** ($CDCl_3$, 128 MHz)

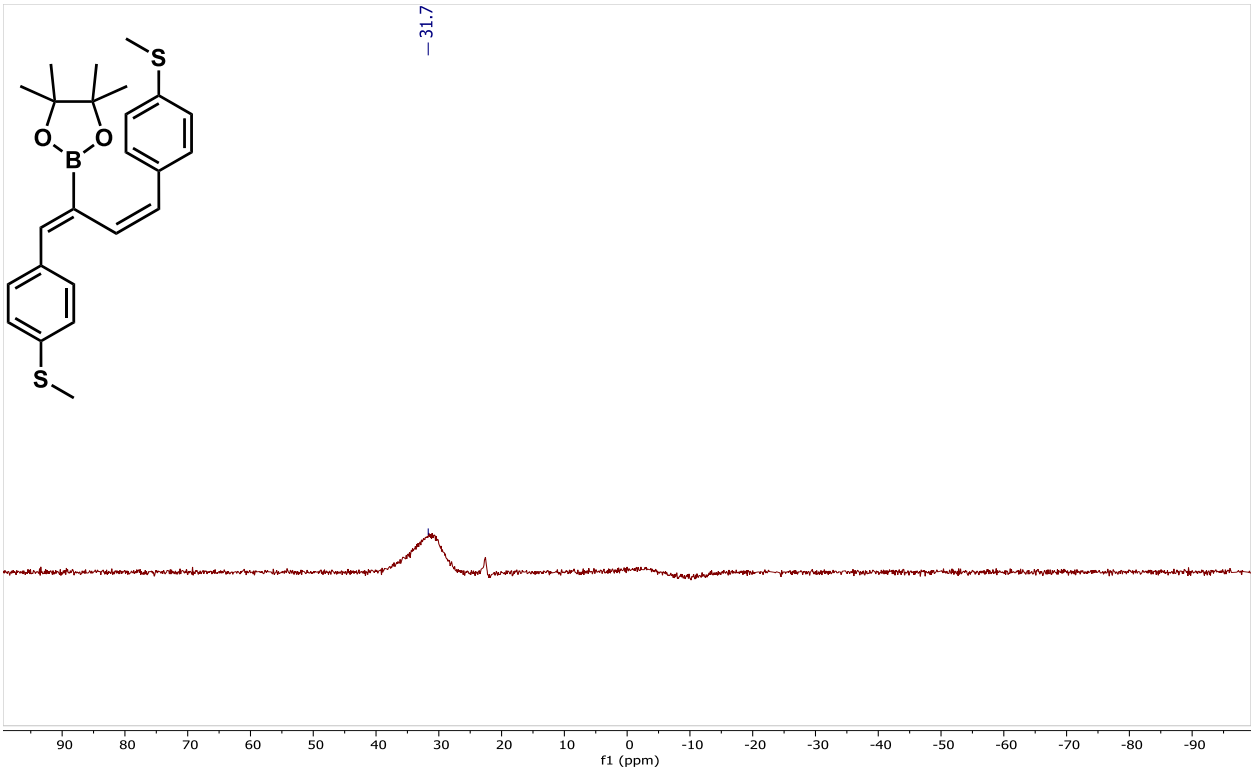

^{1}H NMR of **1.59j** ($CDCl_3$, 400 MHz)

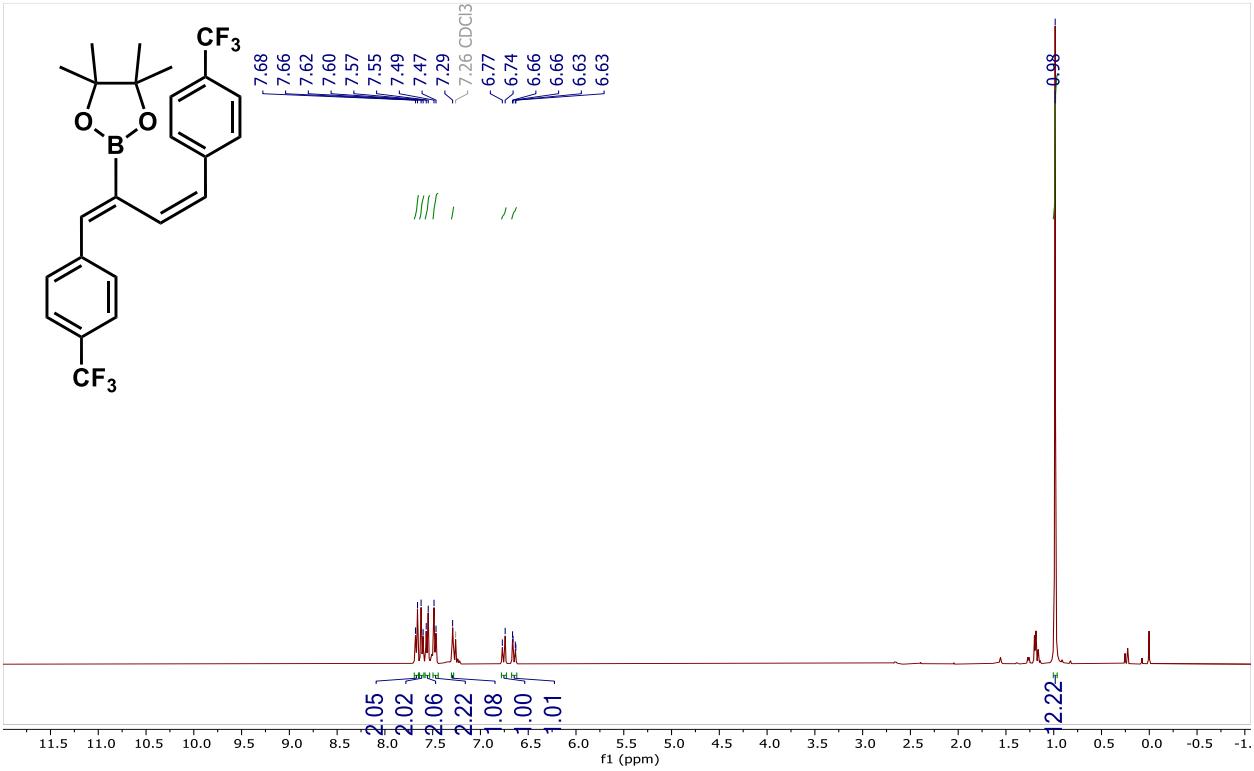

^{13}C NMR of **1.59j** ($CDCl_3$, 101 MHz)

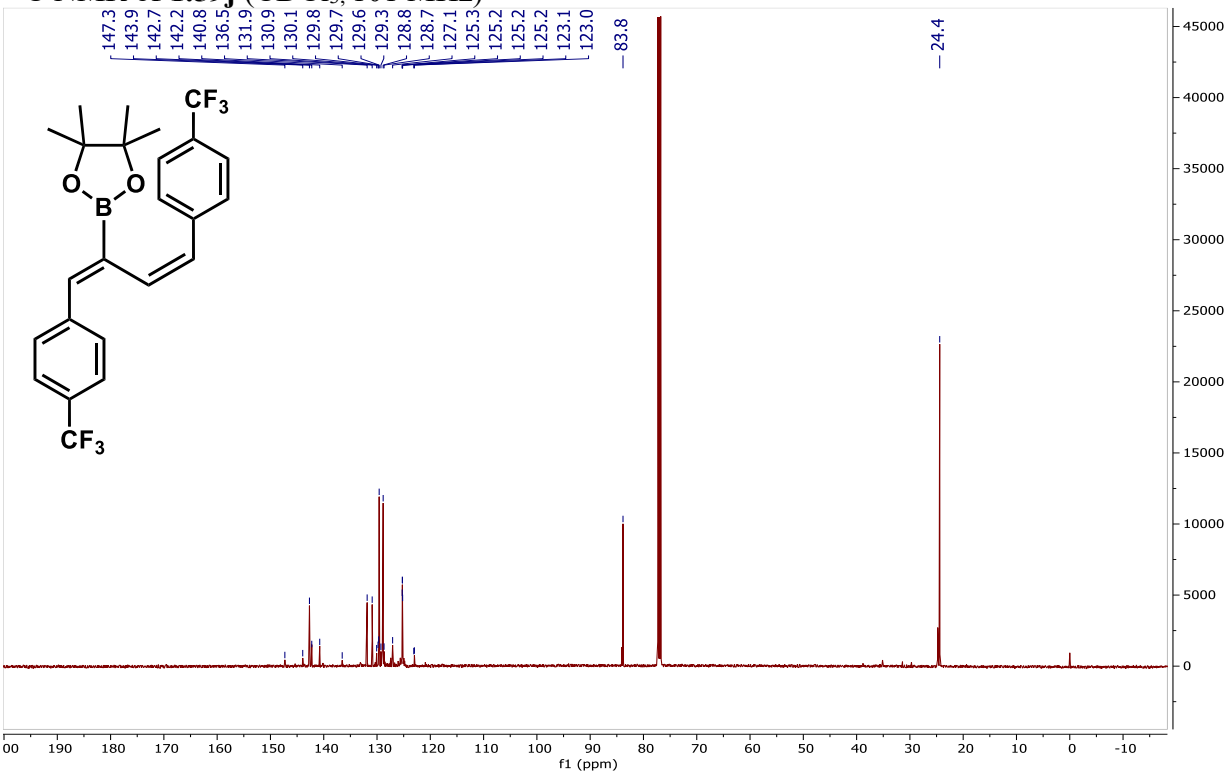

^{11}B NMR of **1.59j** ($CDCl_3$, 128 MHz)

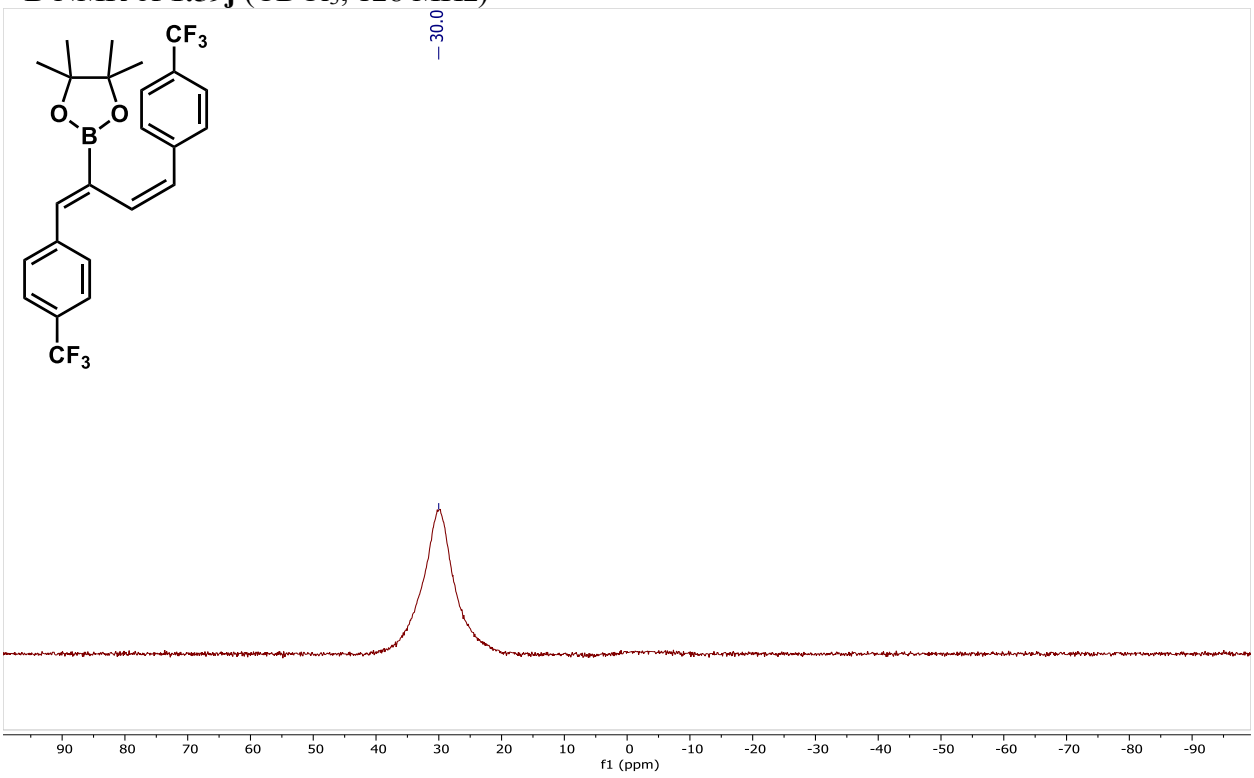

^{19}F NMR of **1.59j** ($CDCl_3$, 376 MHz)

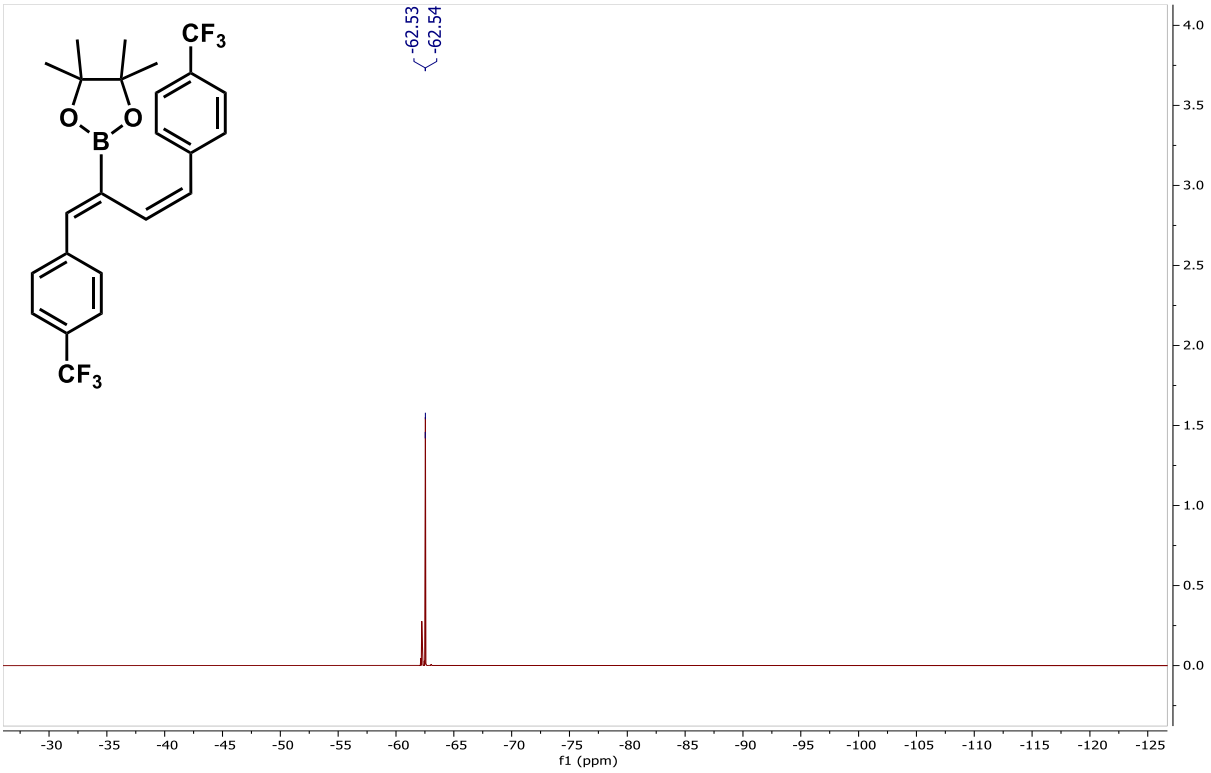

^{1}H NMR of **1.59k** ($CDCl_3$, 400 MHz)

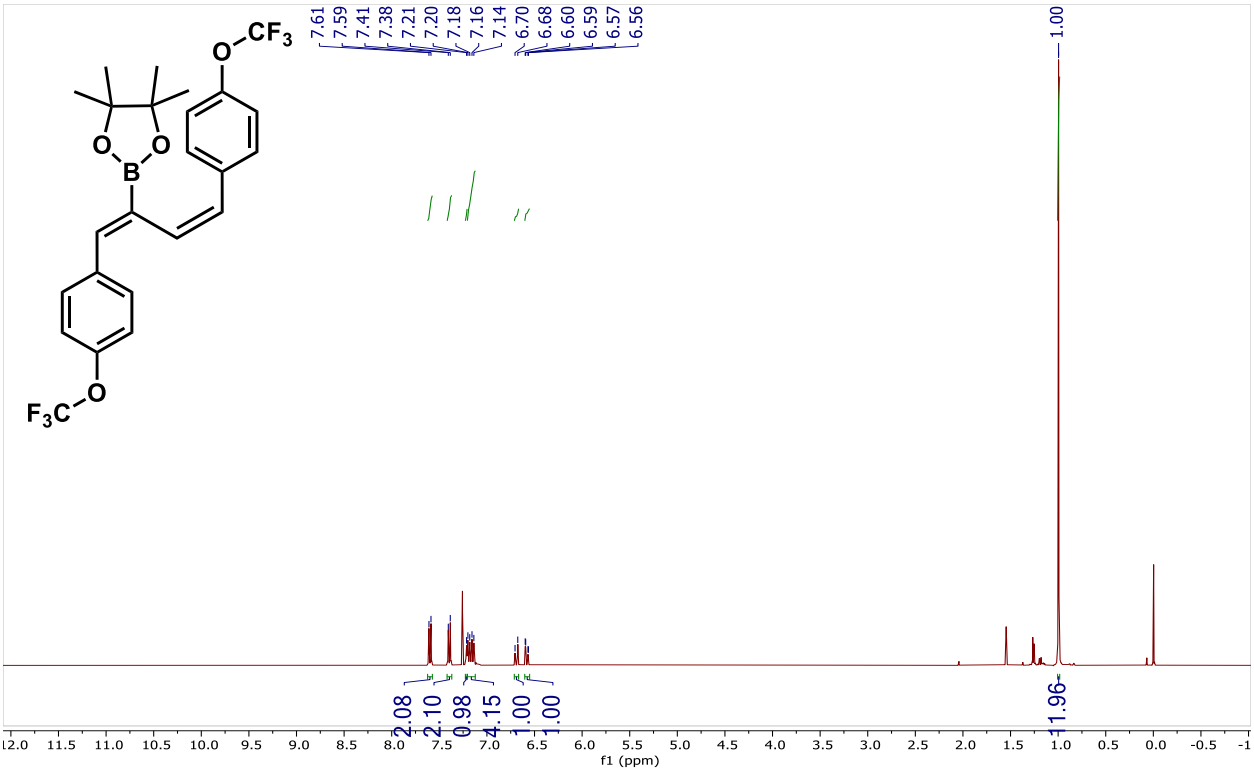

^{13}C NMR of **1.59k** ($CDCl_3$, 101 MHz)

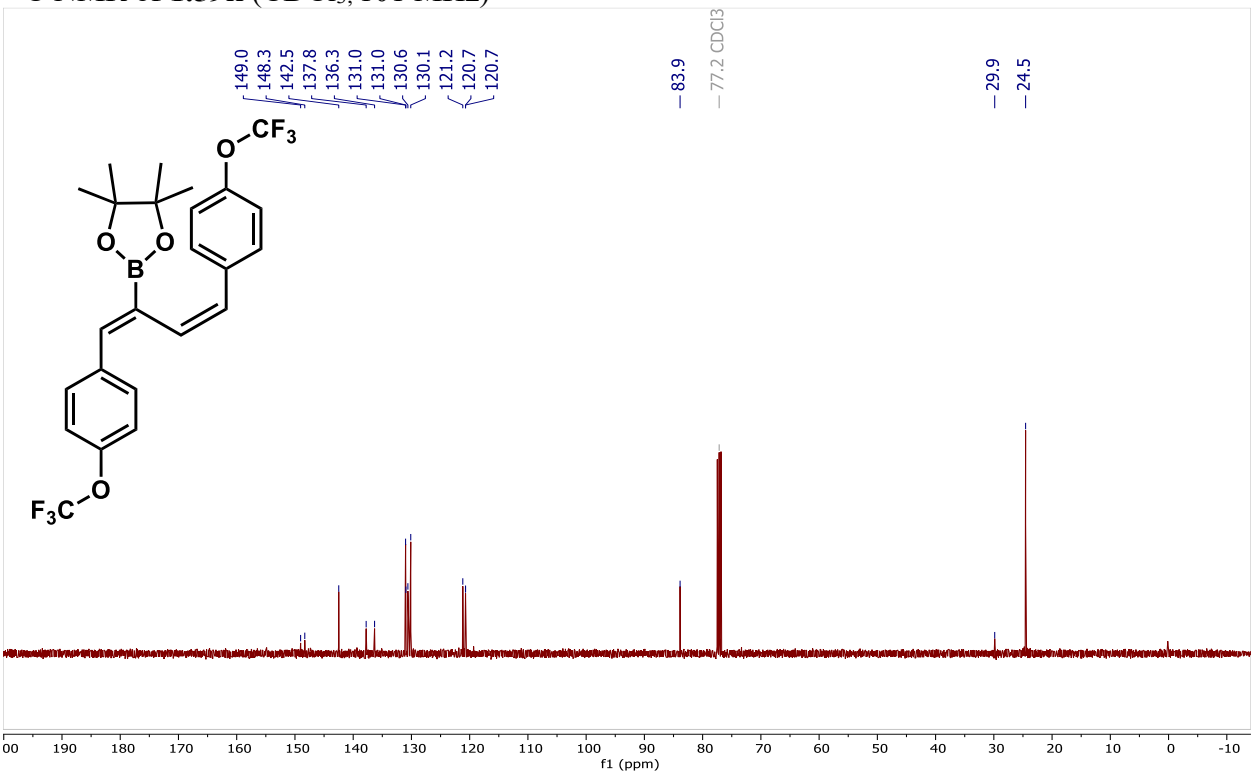

^{11}B NMR of **1.59k** ($CDCl_3$, 128 MHz)

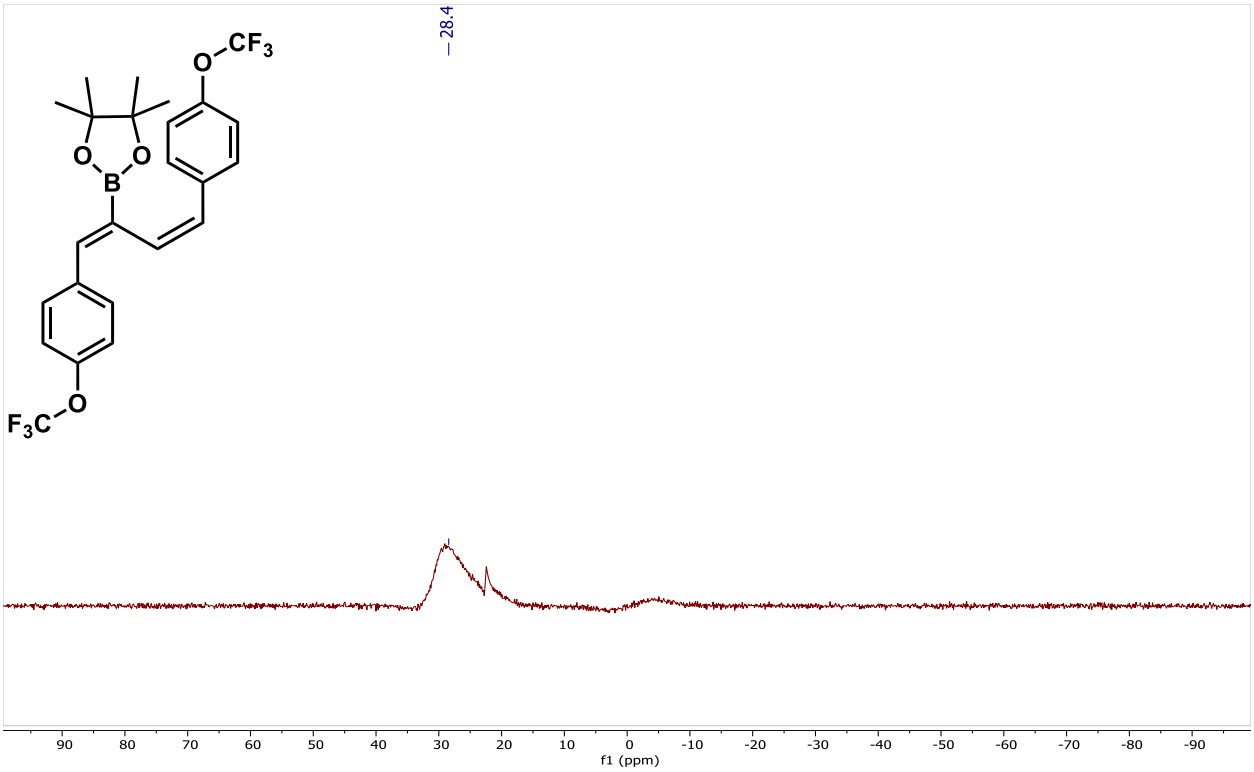

^{19}F NMR of **1.59k** ($CDCl_3$, 376 MHz)

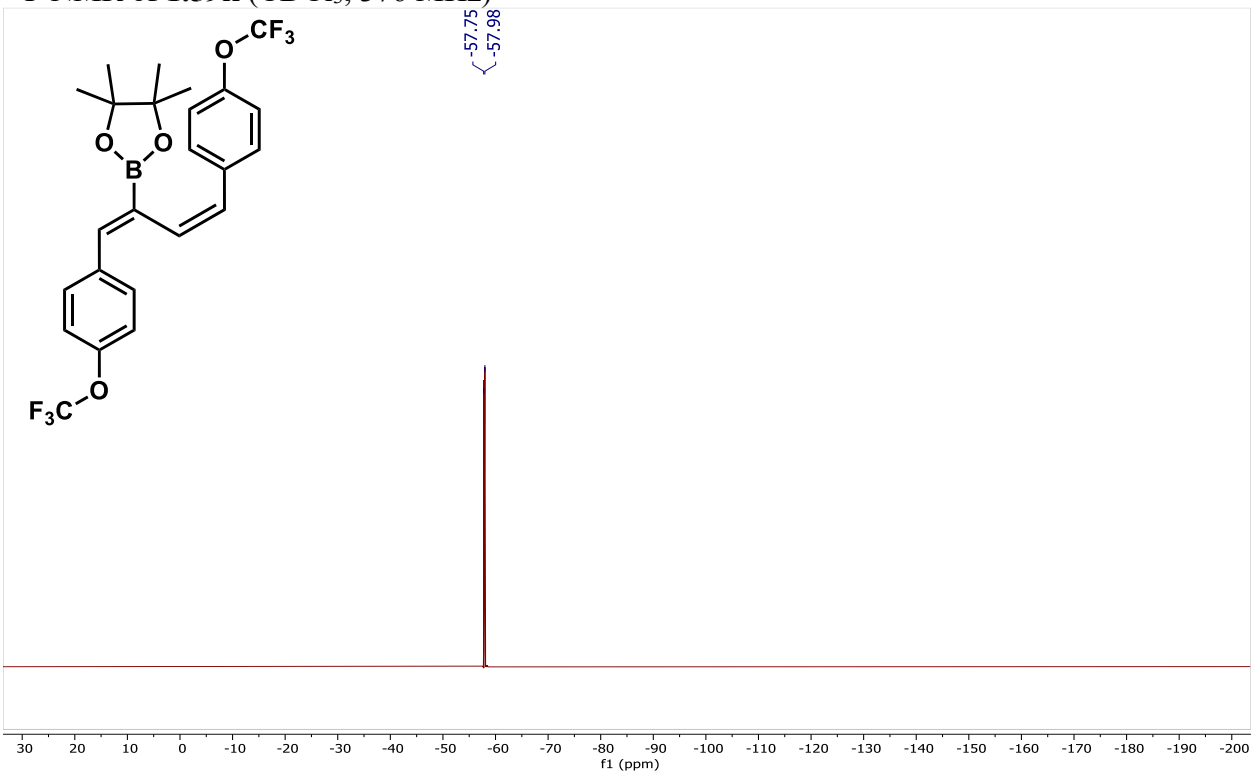

^{1}H NMR of **1.59l** ($CDCl_3$, 400 MHz)

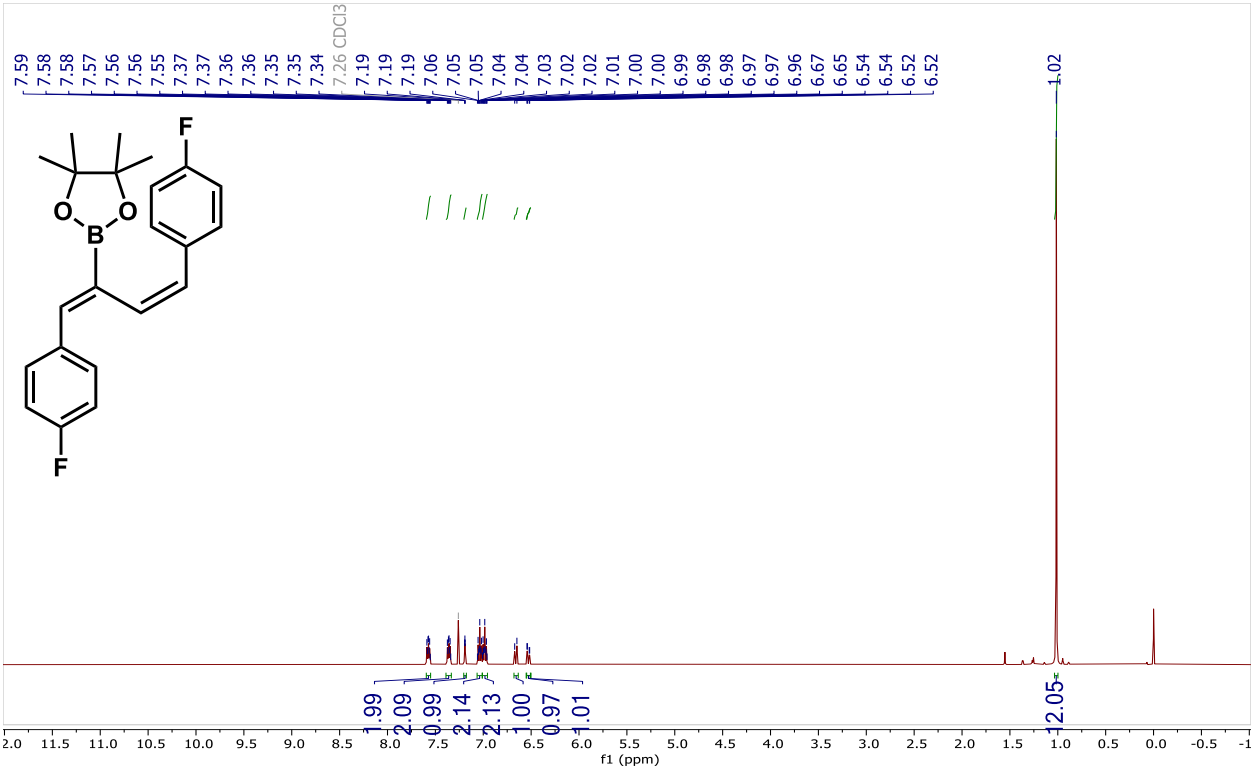

^{13}C NMR of **1.59l** ($CDCl_3$, 101 MHz)

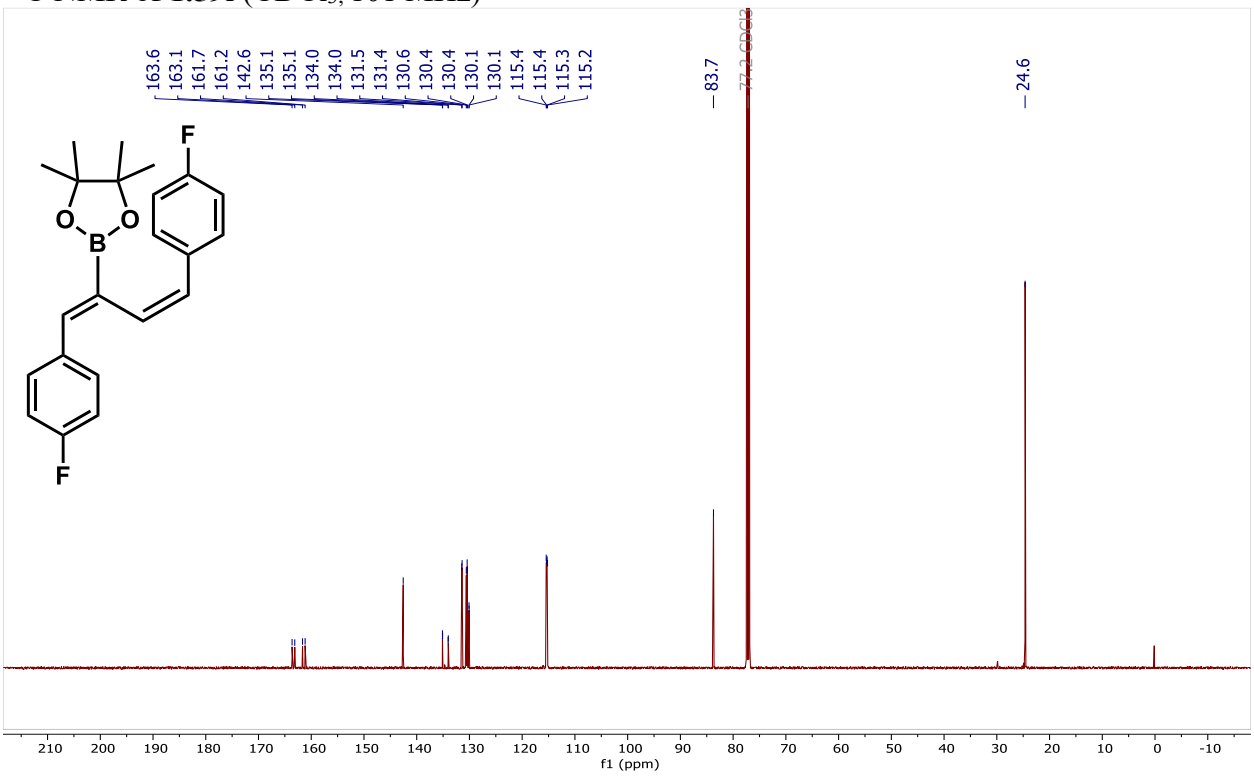

^{11}B NMR of **1.59l** ($CDCl_3$, 128 MHz)

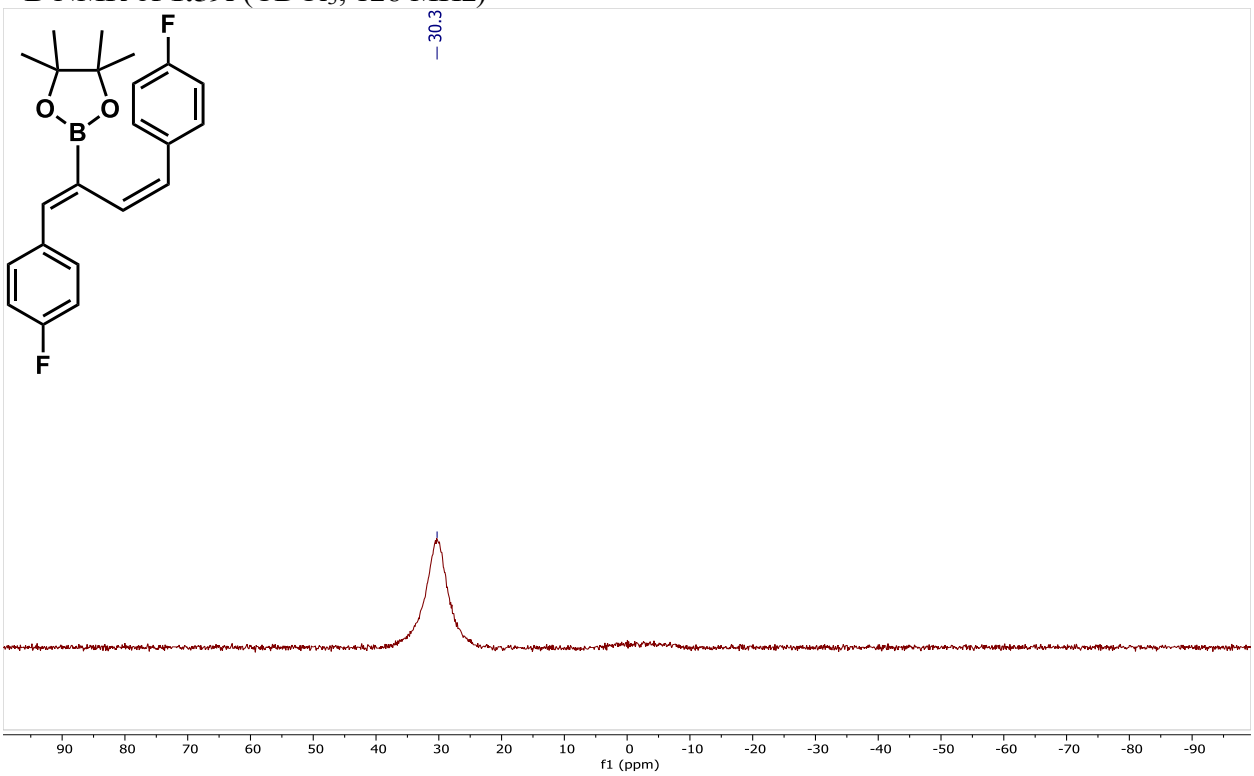

^{19}F NMR of **1.59l** ($CDCl_3$, 376 MHz)

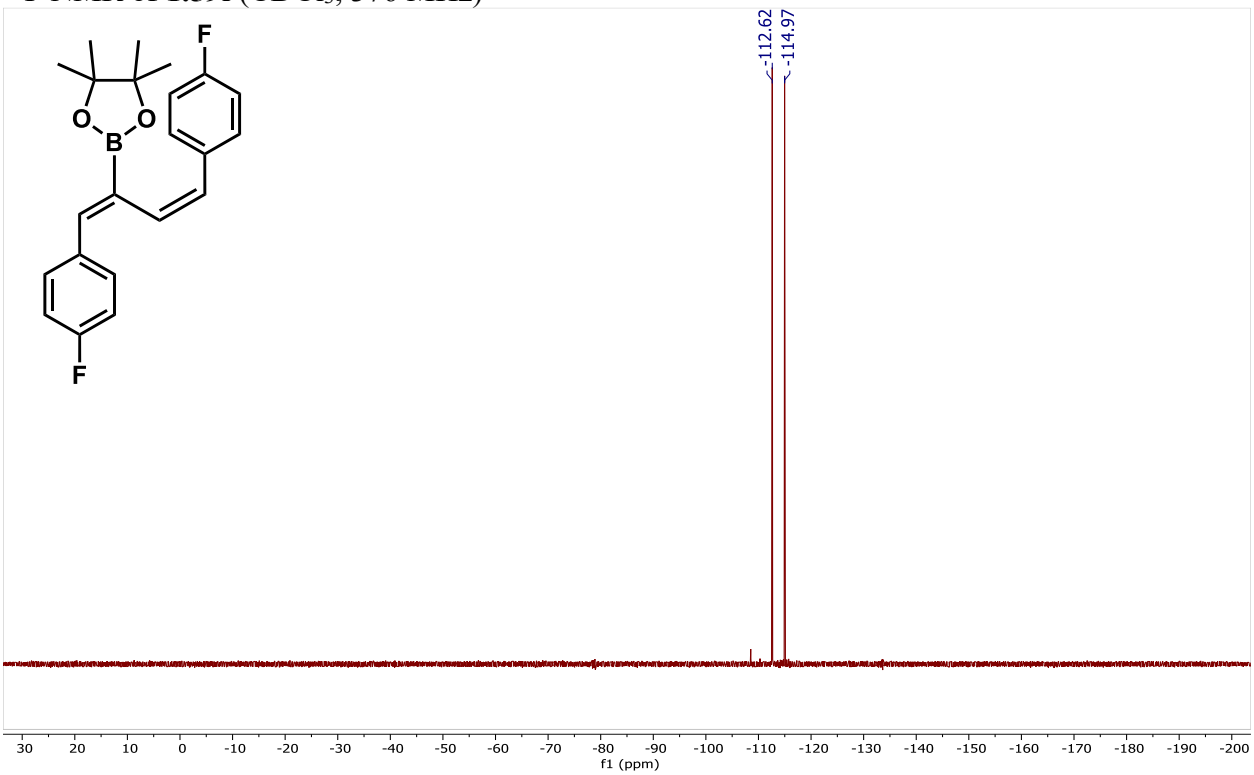

^{1}H NMR of **1.59m** ($CDCl_3$, 400 MHz)

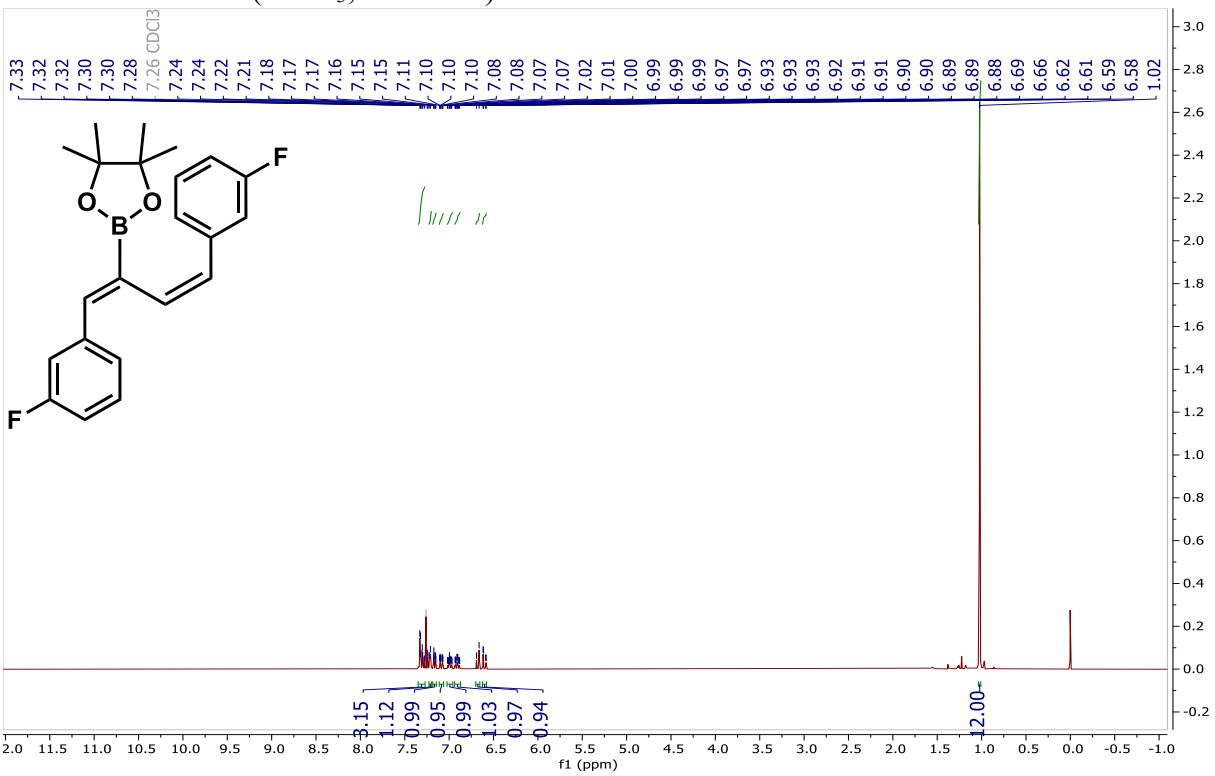

^{13}C NMR of **1.59m** ($CDCl_3$, 101 MHz)

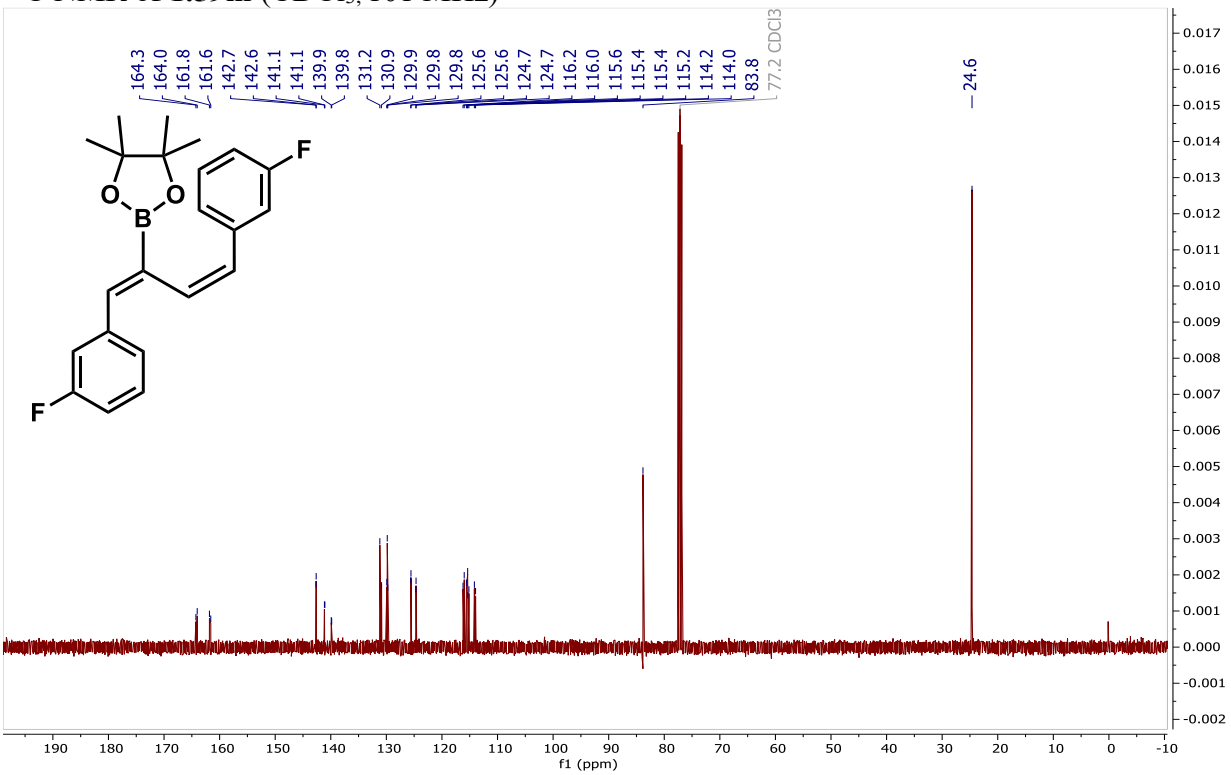

^{11}B NMR of **1.59m** ($CDCl_3$, 128 MHz)

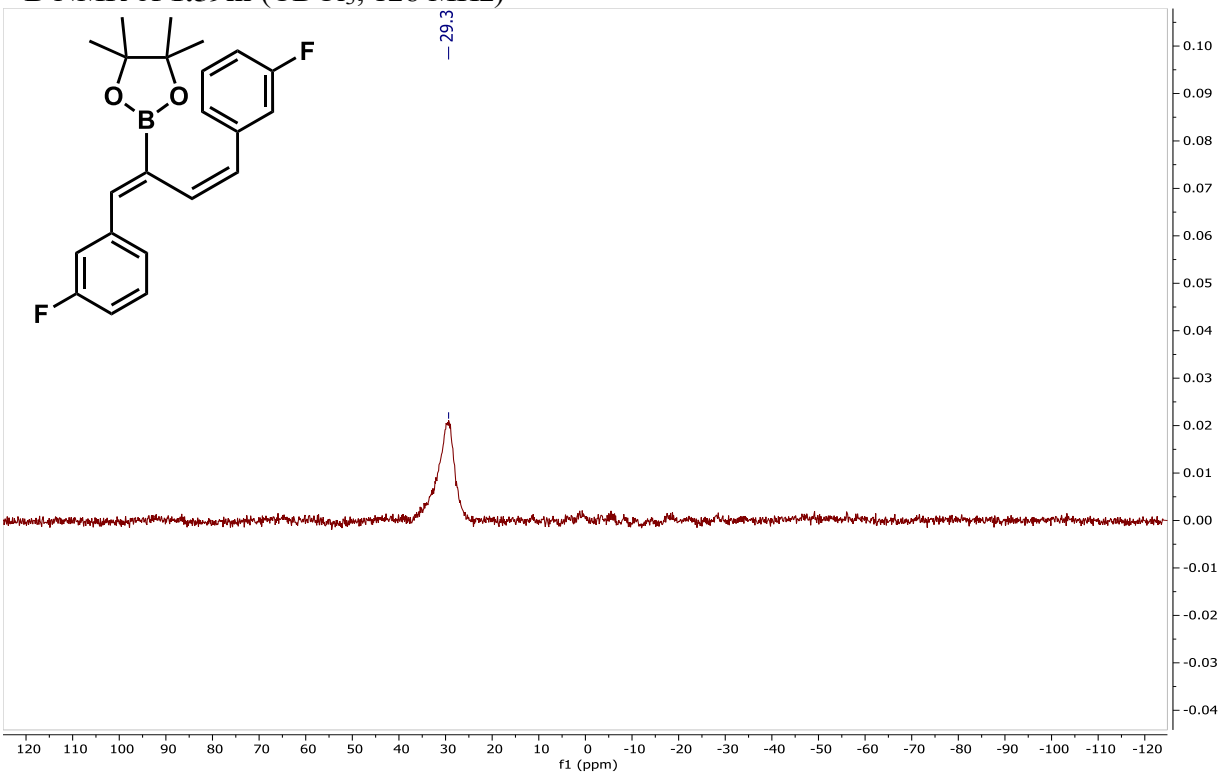

^{19}F NMR of **1.59m** ($CDCl_3$, 376 MHz)

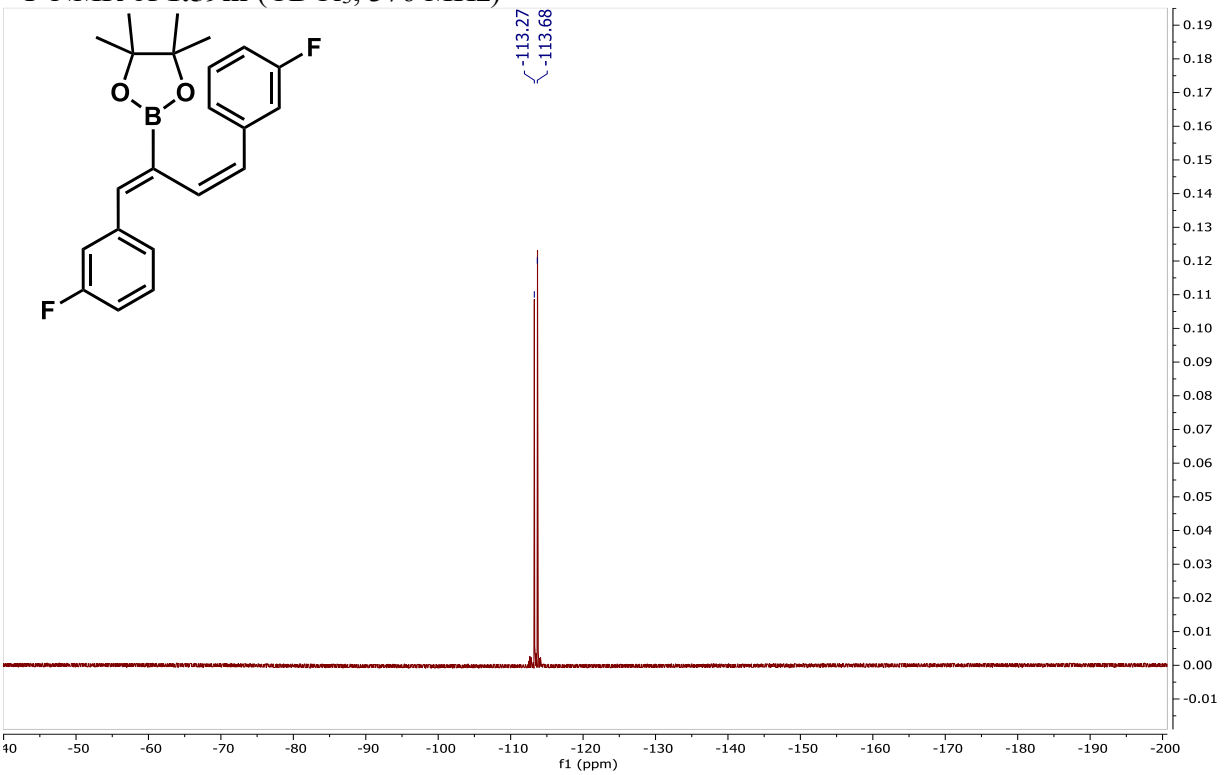

^{1}H NMR of **1.59n** ($CDCl_3$, 400 MHz)

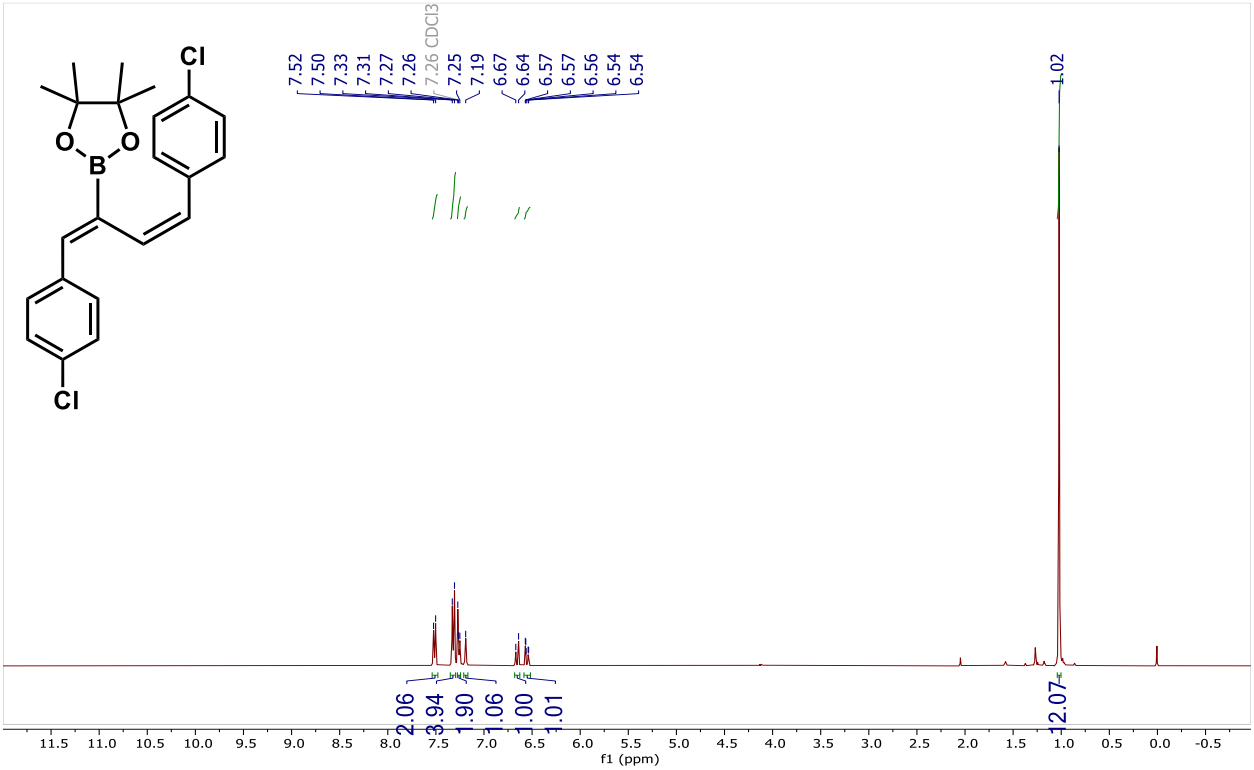

^{13}C NMR of **1.59n** ($CDCl_3$, 101 MHz)

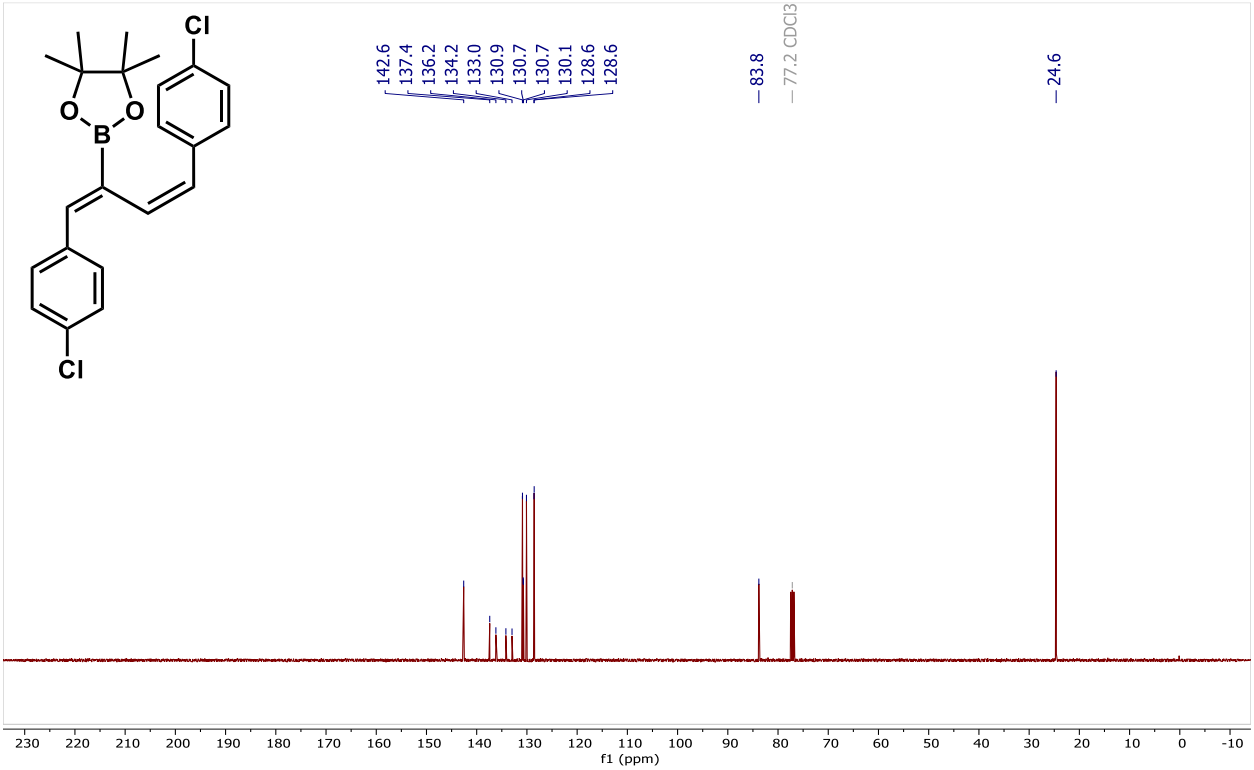

^{11}B NMR of **1.59n** ($CDCl_3$, 128 MHz)

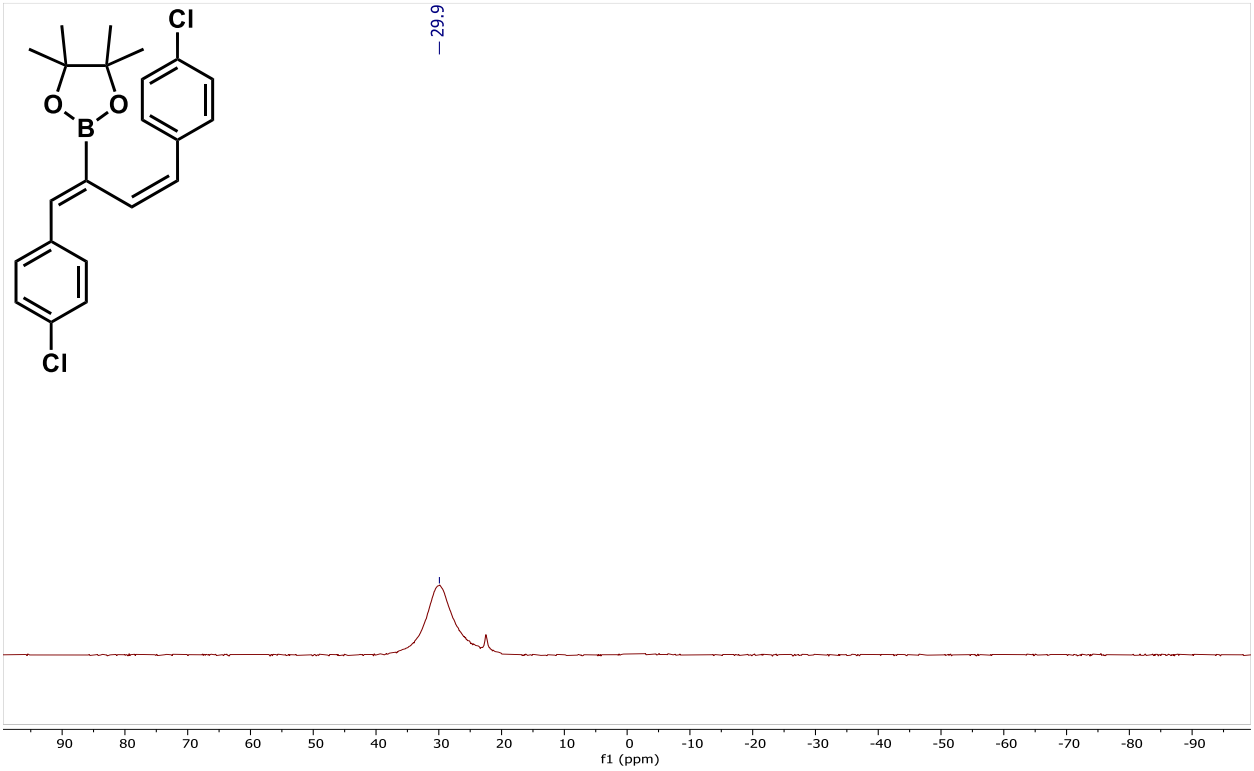

^{1}H NMR of **1.59o** ($CDCl_3$, 400 MHz)

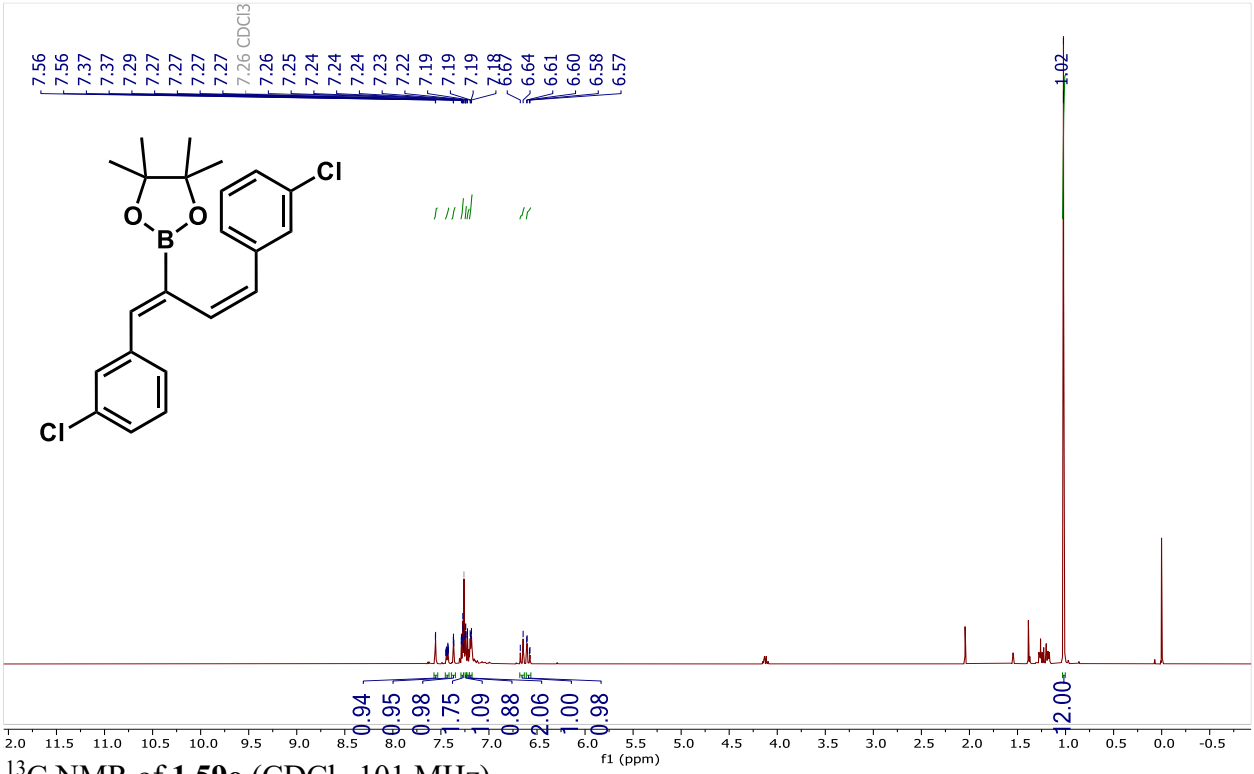

^{13}C NMR of **1.59o** ($CDCl_3$, 101 MHz)

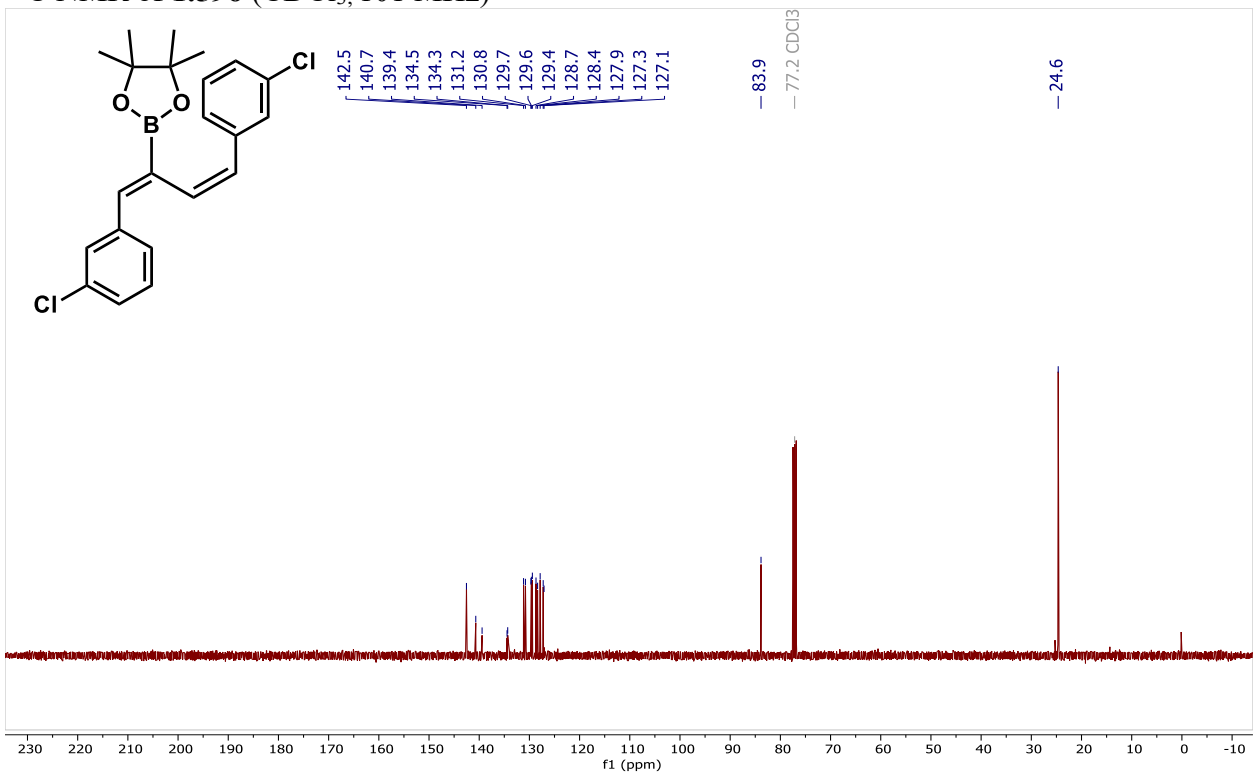

^{11}B NMR of **1.59o** ($CDCl_3$, 128 MHz)

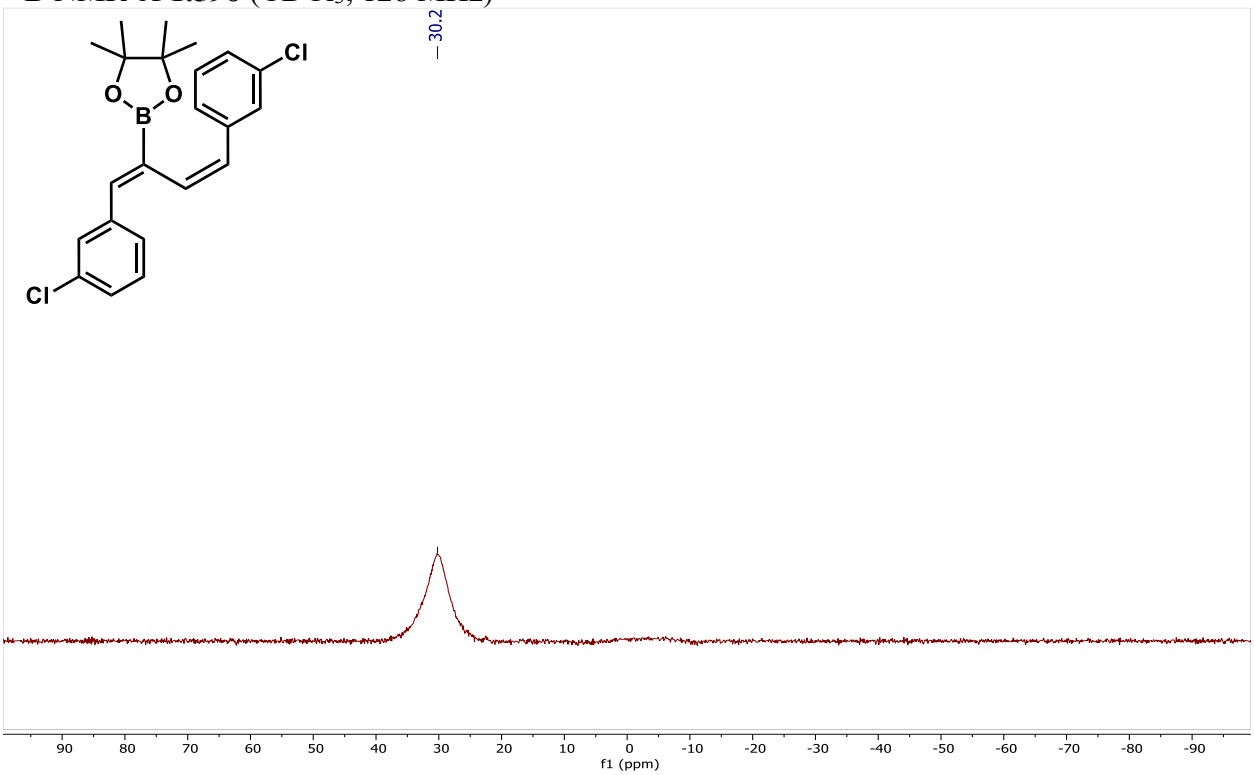

^{1}H NMR of **1.59p** ($CDCl_3$, 400 MHz)

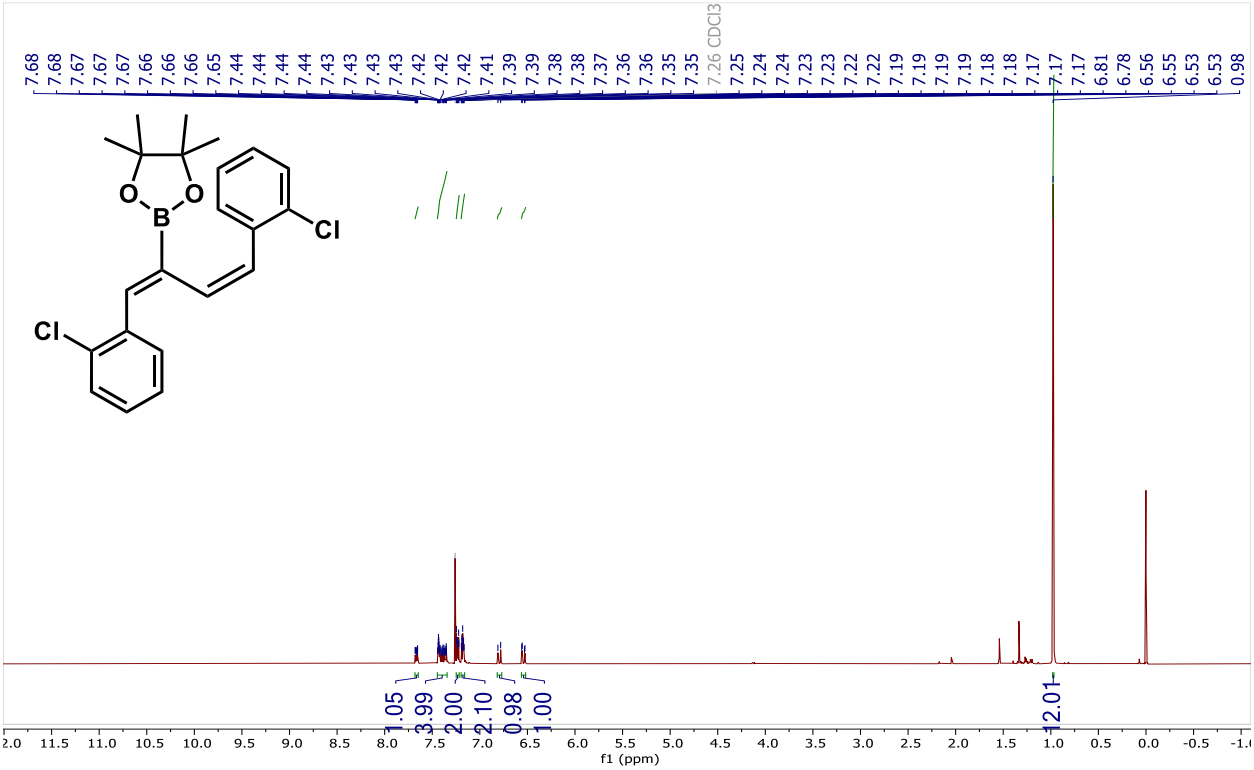

^{13}C NMR of **1.59p** ($CDCl_3$, 101 MHz)

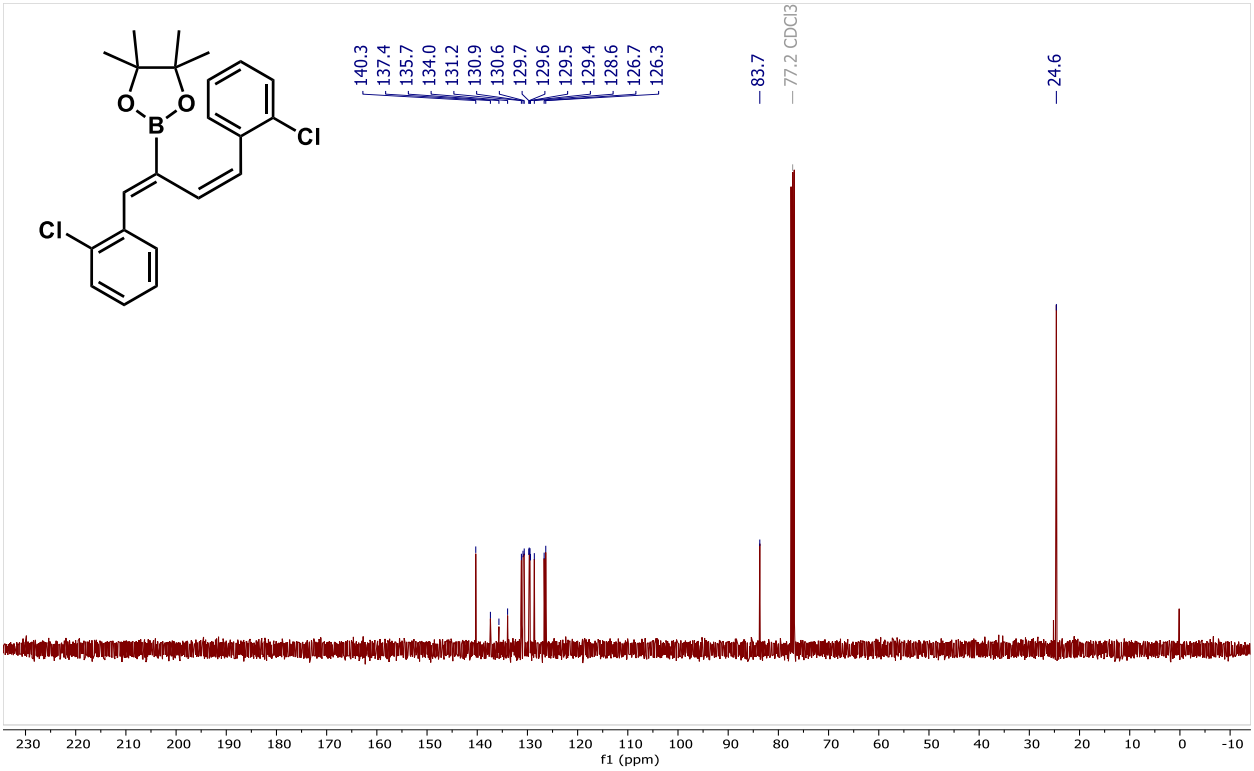

^{11}B NMR of **1.59p** ($CDCl_3$, 128 MHz)

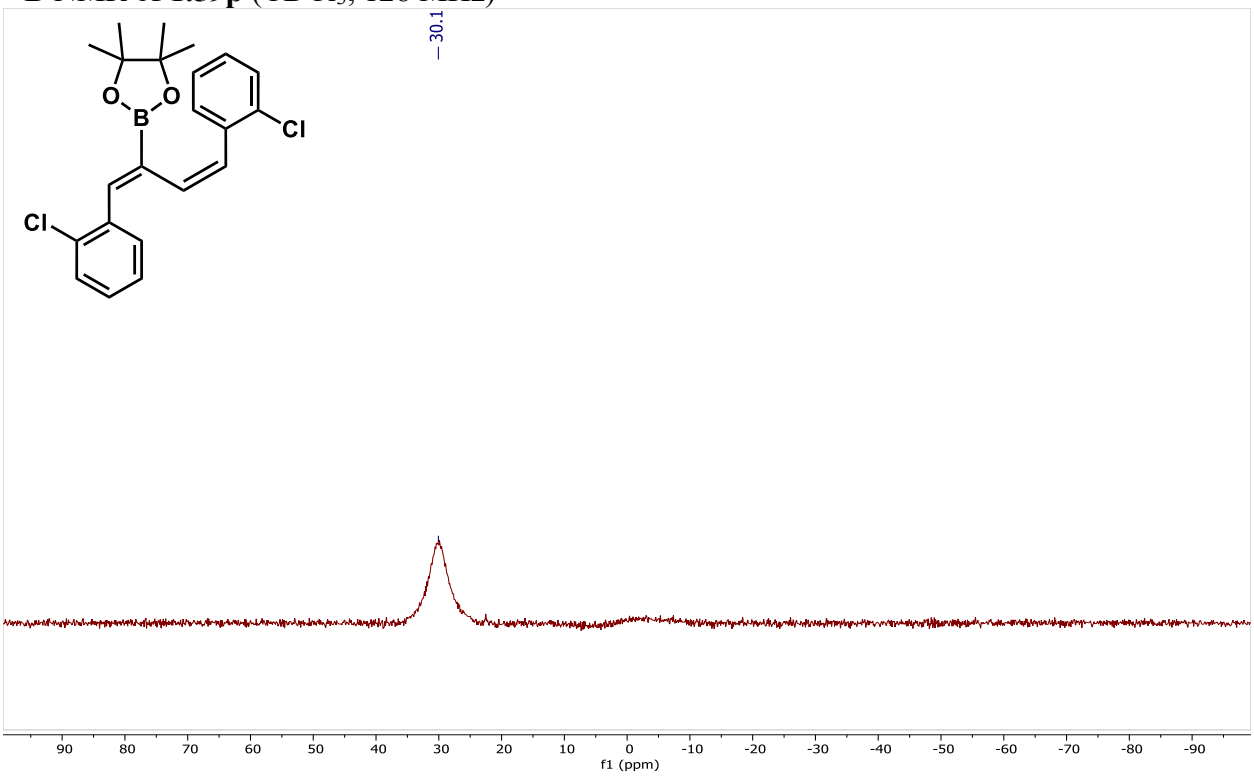

^{1}H NMR of **1.59q** ($CDCl_3$, 400 MHz)

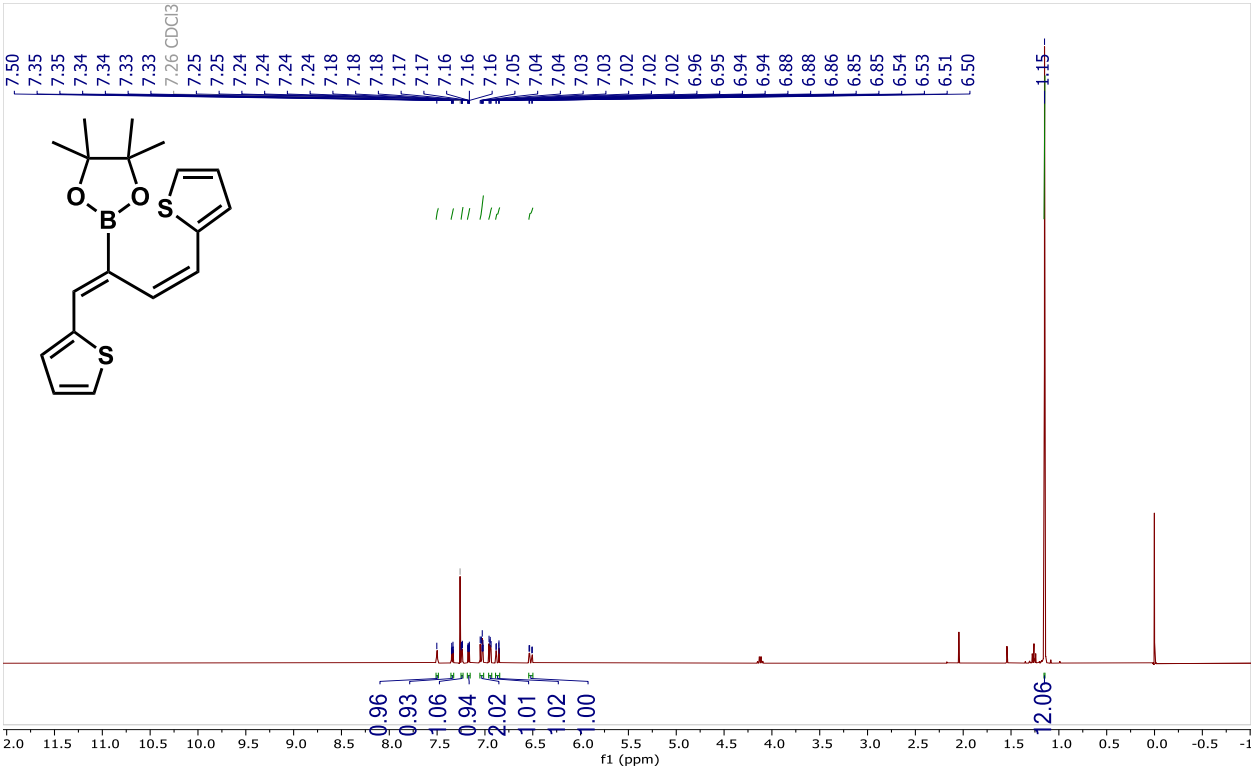

^{13}C NMR of **1.59q** ($CDCl_3$, 101 MHz)

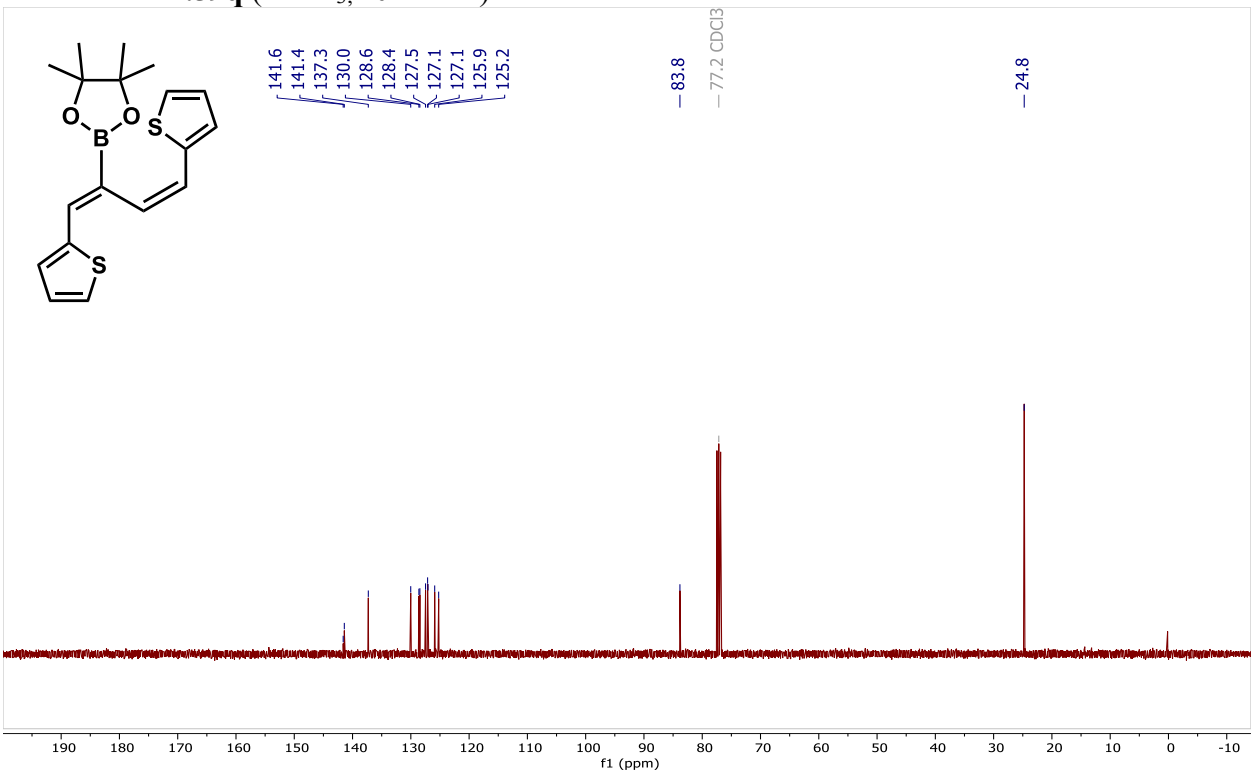

^{11}B NMR of **1.59q** ($CDCl_3$, 128 MHz)

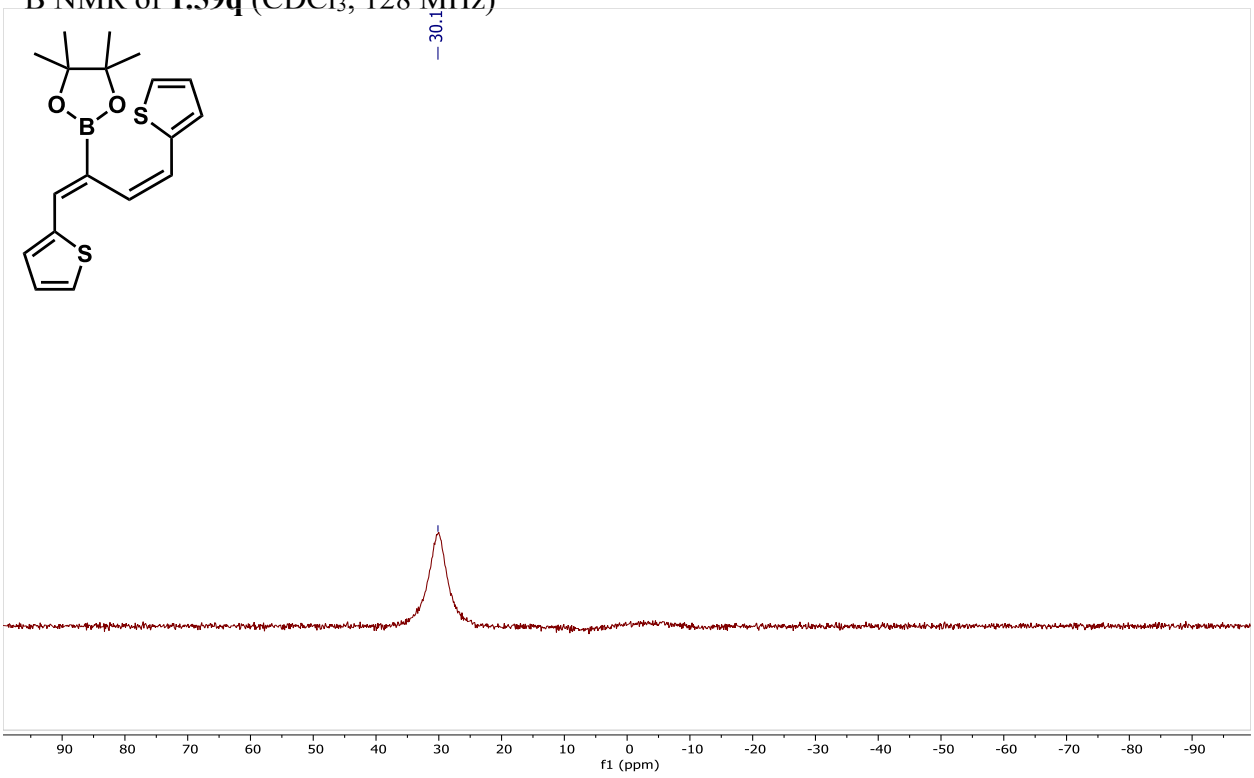

^{1}H NMR of **1.59r** ($CDCl_3$, 400 MHz)

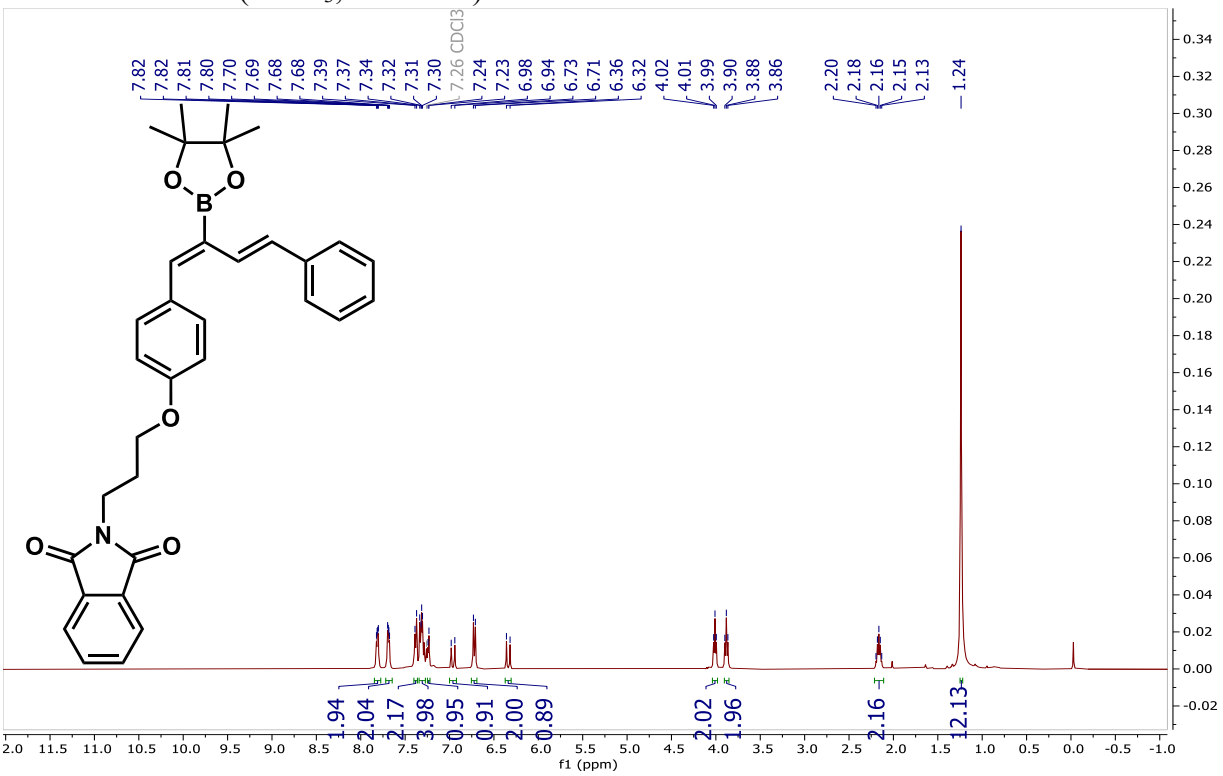

^{13}C NMR of **1.59r** ($CDCl_3$, 101 MHz)

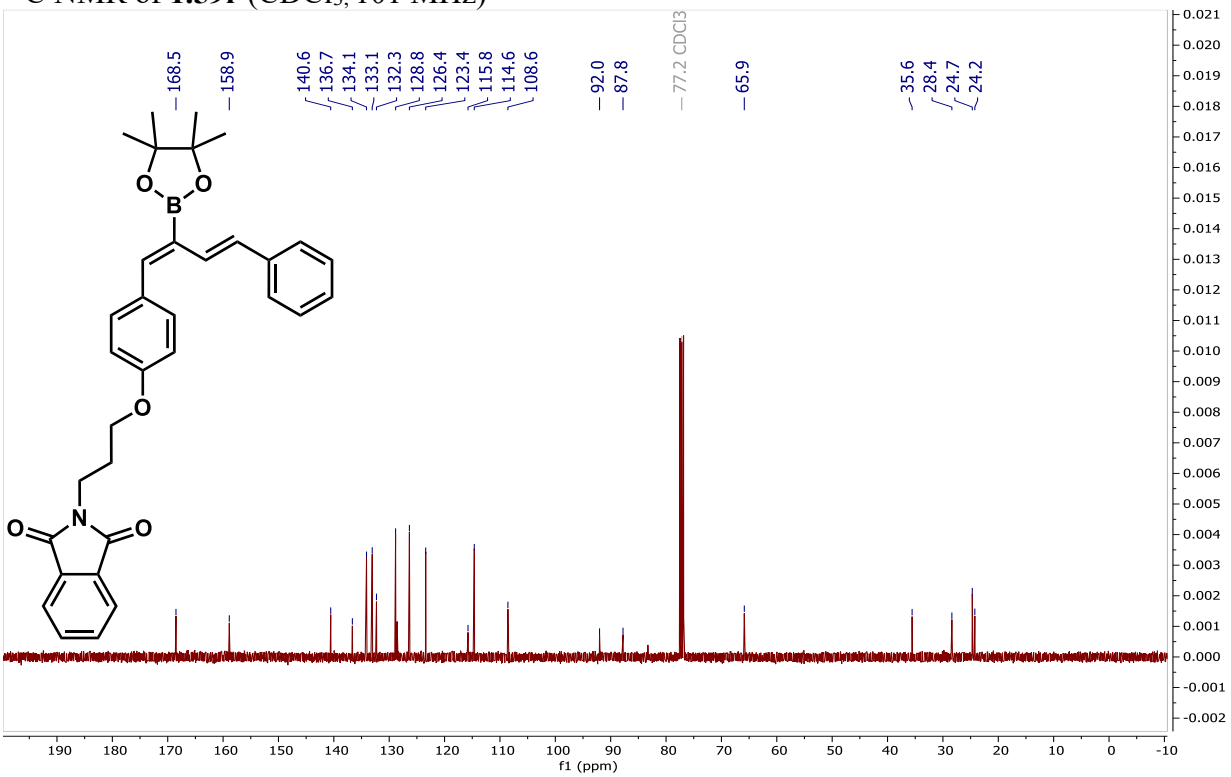

^{11}B NMR of **1.59r** ($CDCl_3$, 128 MHz)

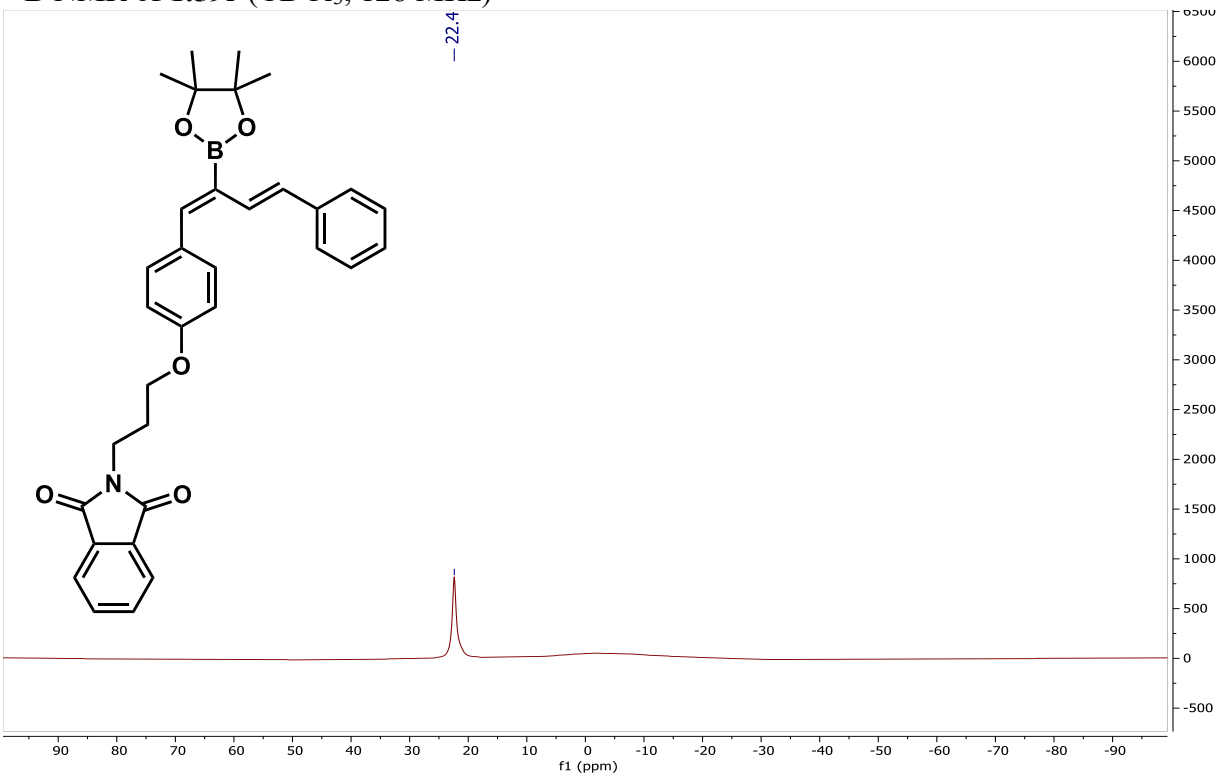

^{1}H NMR of **1.59s** ($CDCl_3$, 400 MHz)

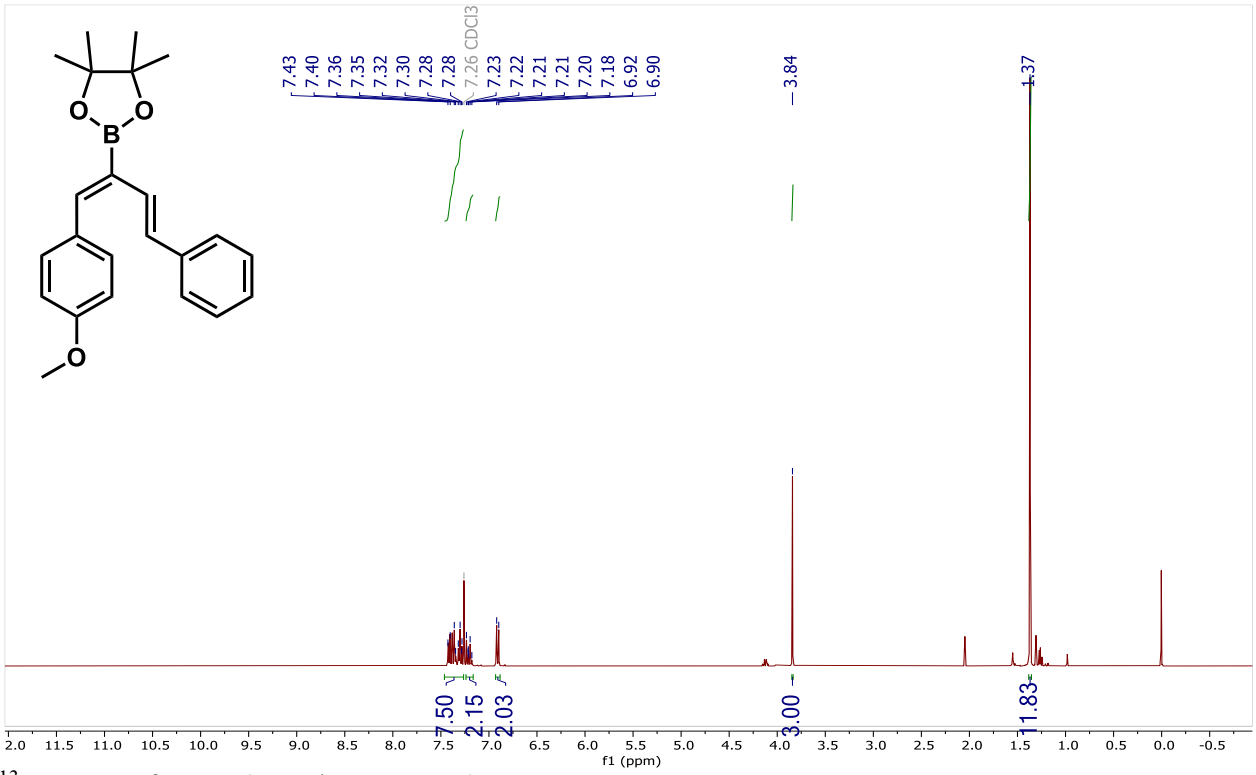

^{13}C NMR of **1.59s** ($CDCl_3$, 101 MHz)

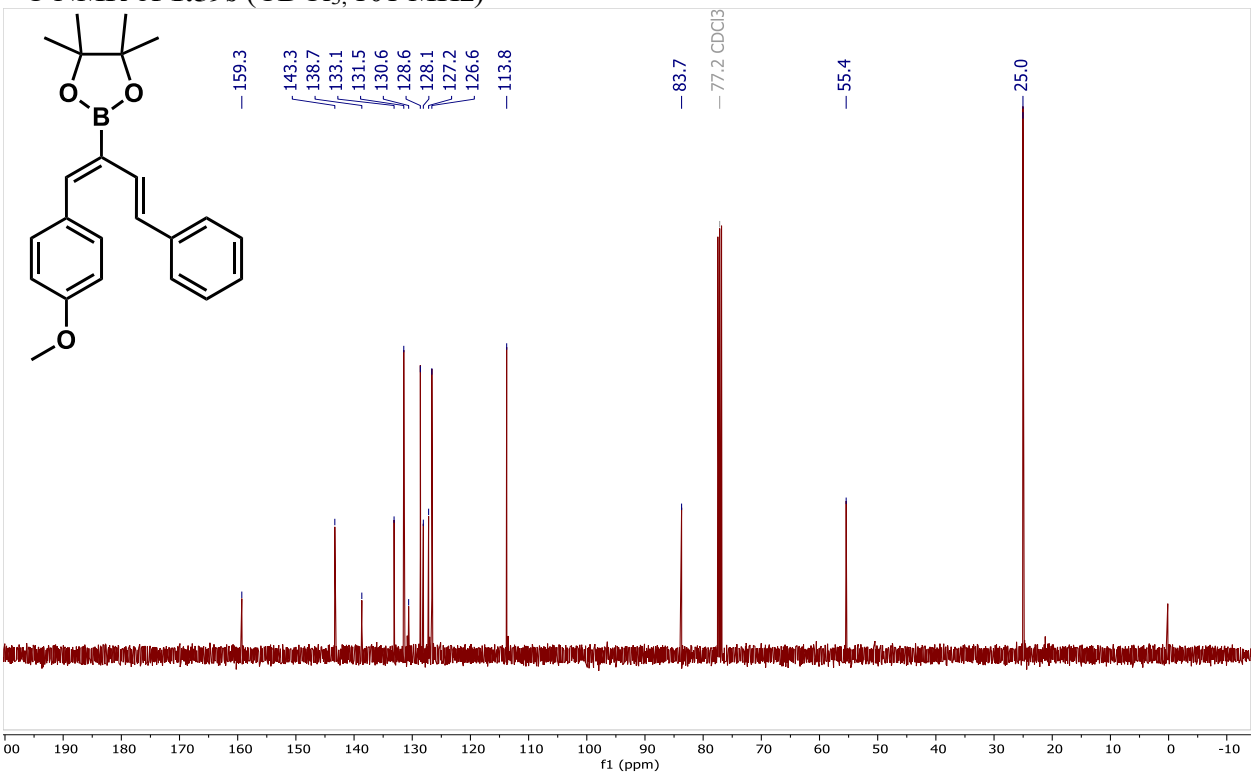

^{11}B NMR of **1.59s** ($CDCl_3$, 128 MHz)

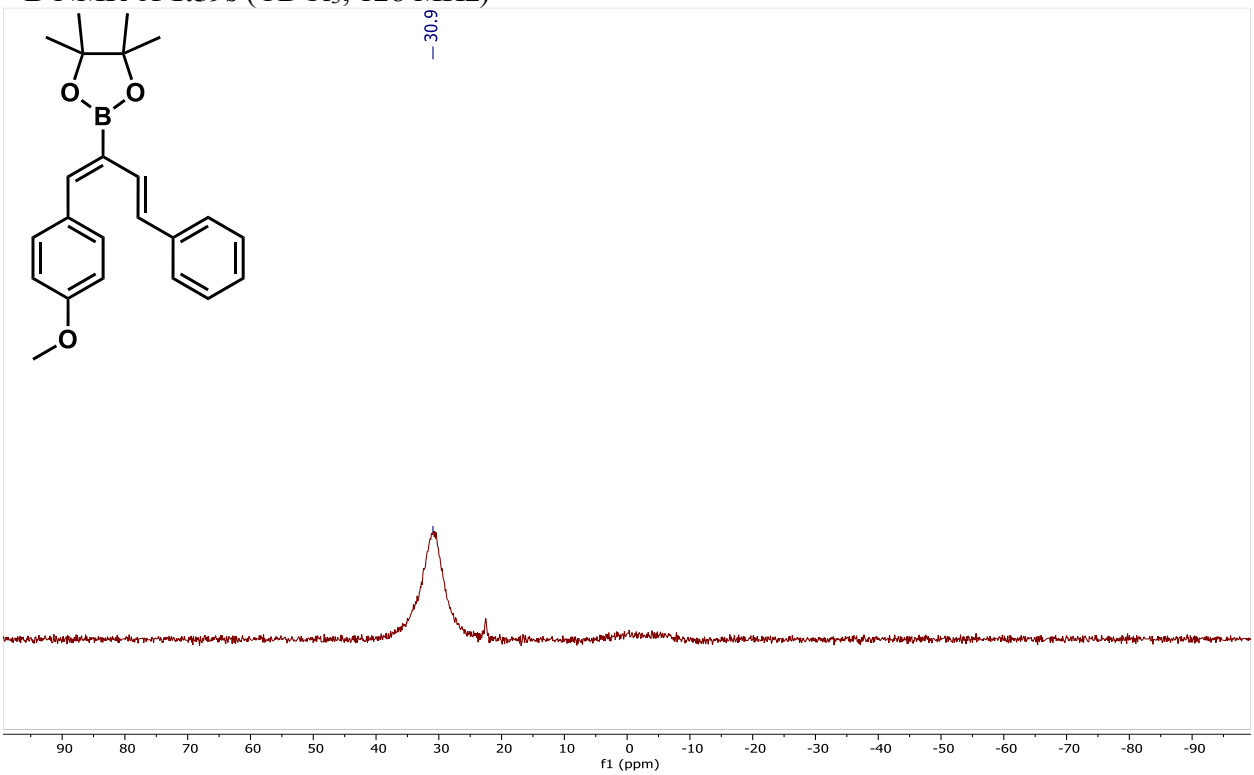

^{1}H NMR of **1.59t** ($CDCl_3$, 400 MHz)

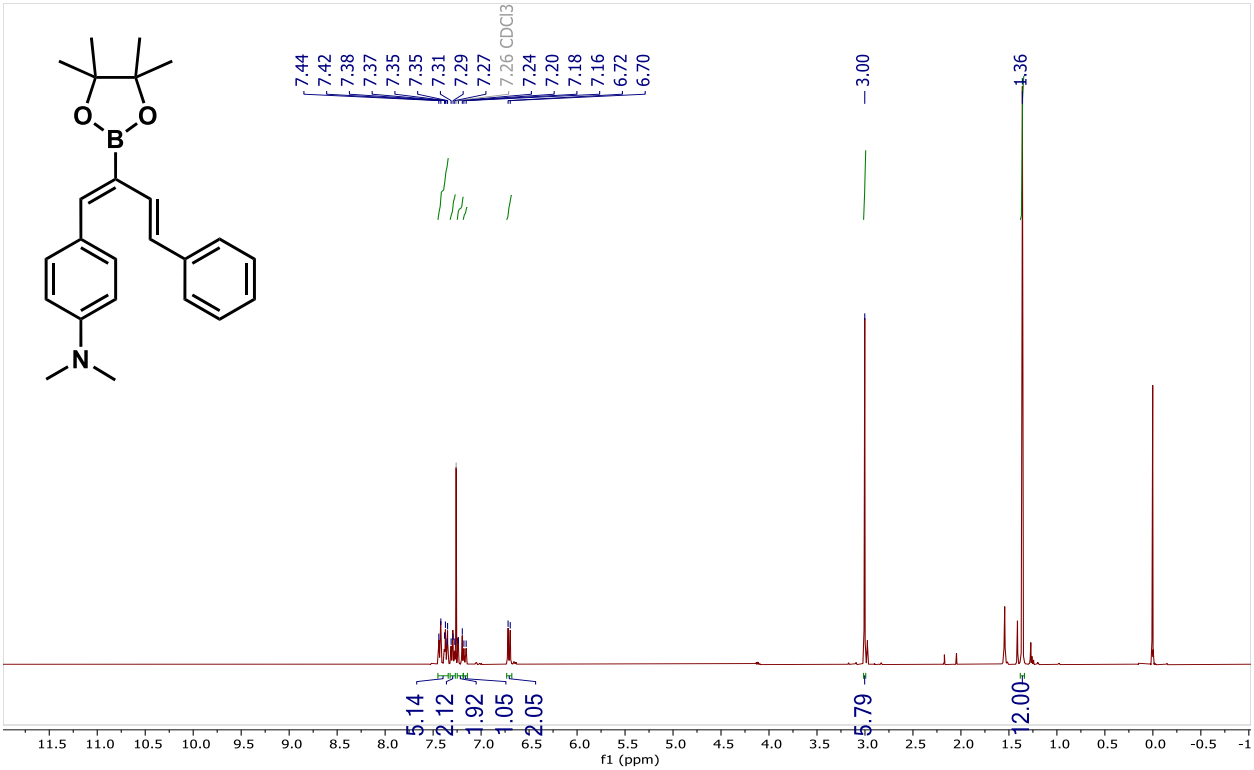

^{13}C NMR of **1.59t** ($CDCl_3$, 101 MHz)

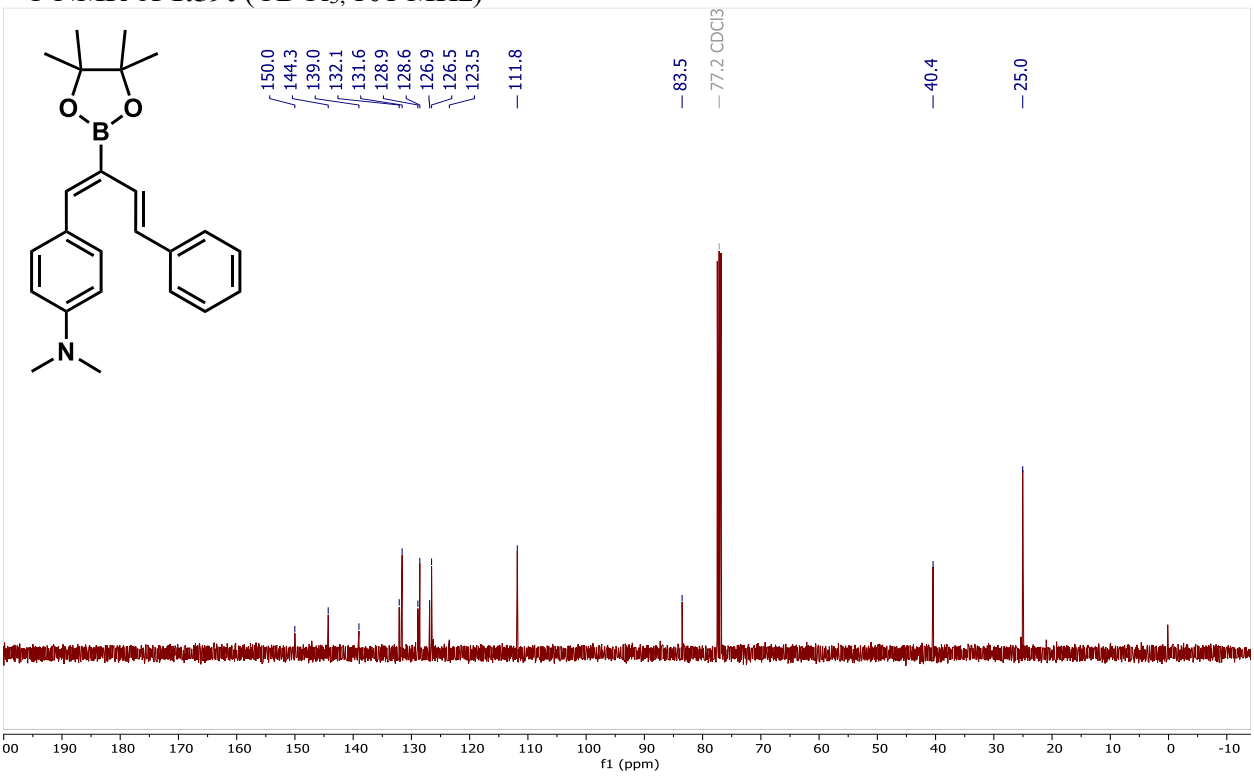

^{11}B NMR of **1.59t** ($CDCl_3$, 128 MHz)

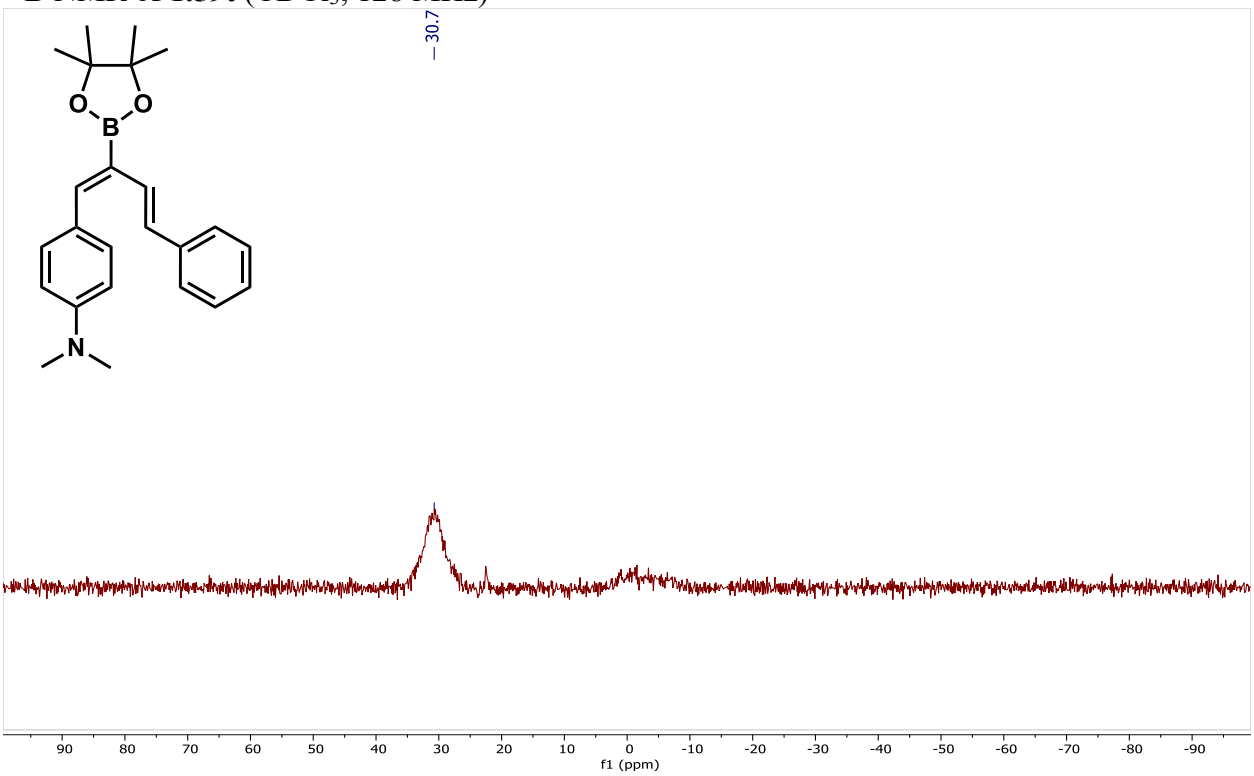

^{1}H NMR of **1.59u** ($CDCl_3$, 400 MHz)

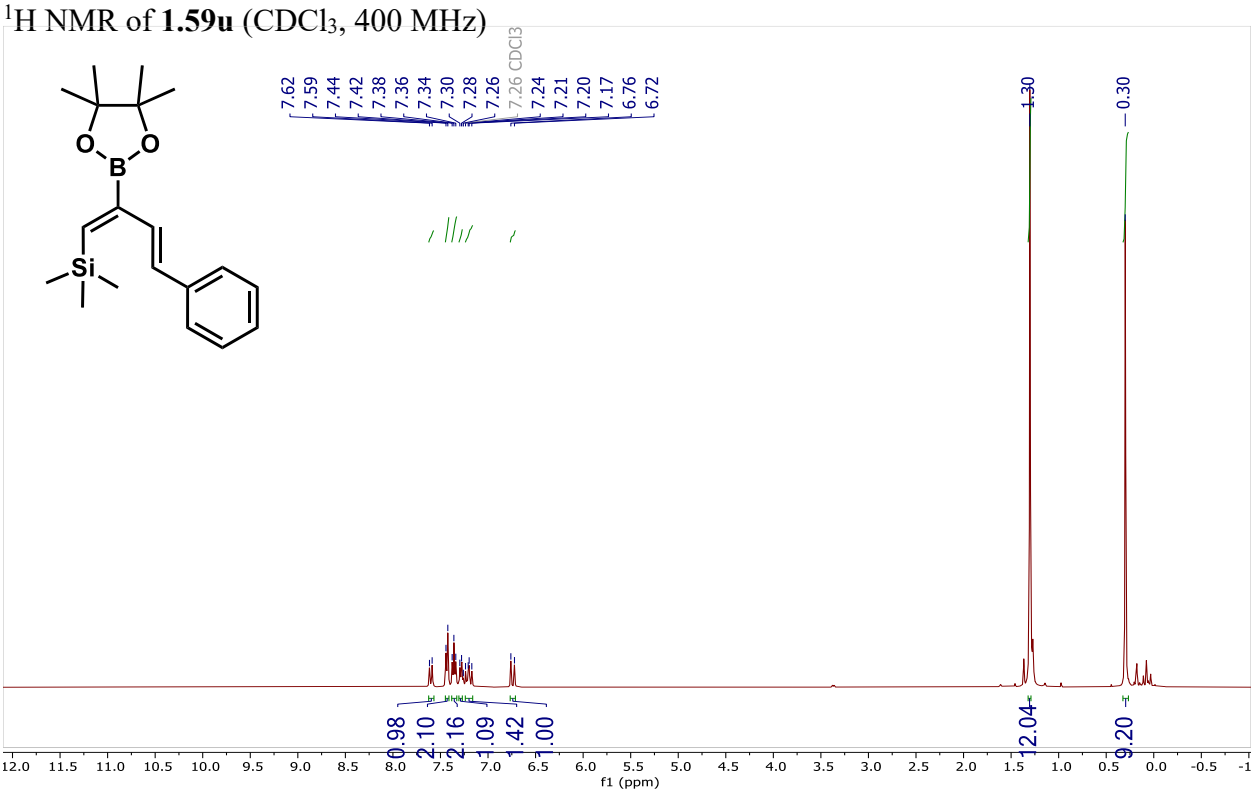

^{13}C NMR of **1.59u** ($CDCl_3$, 101 MHz)

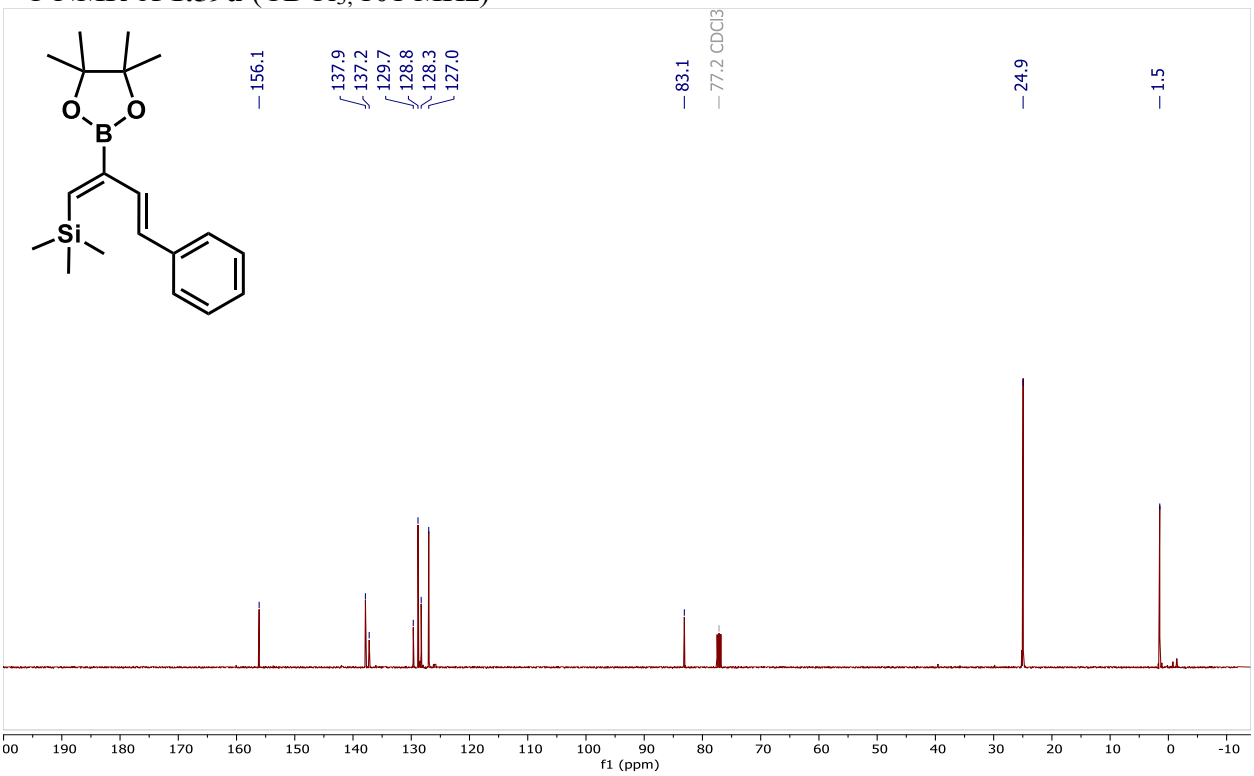

^{11}B NMR of **1.59u** ($CDCl_3$, 128 MHz)

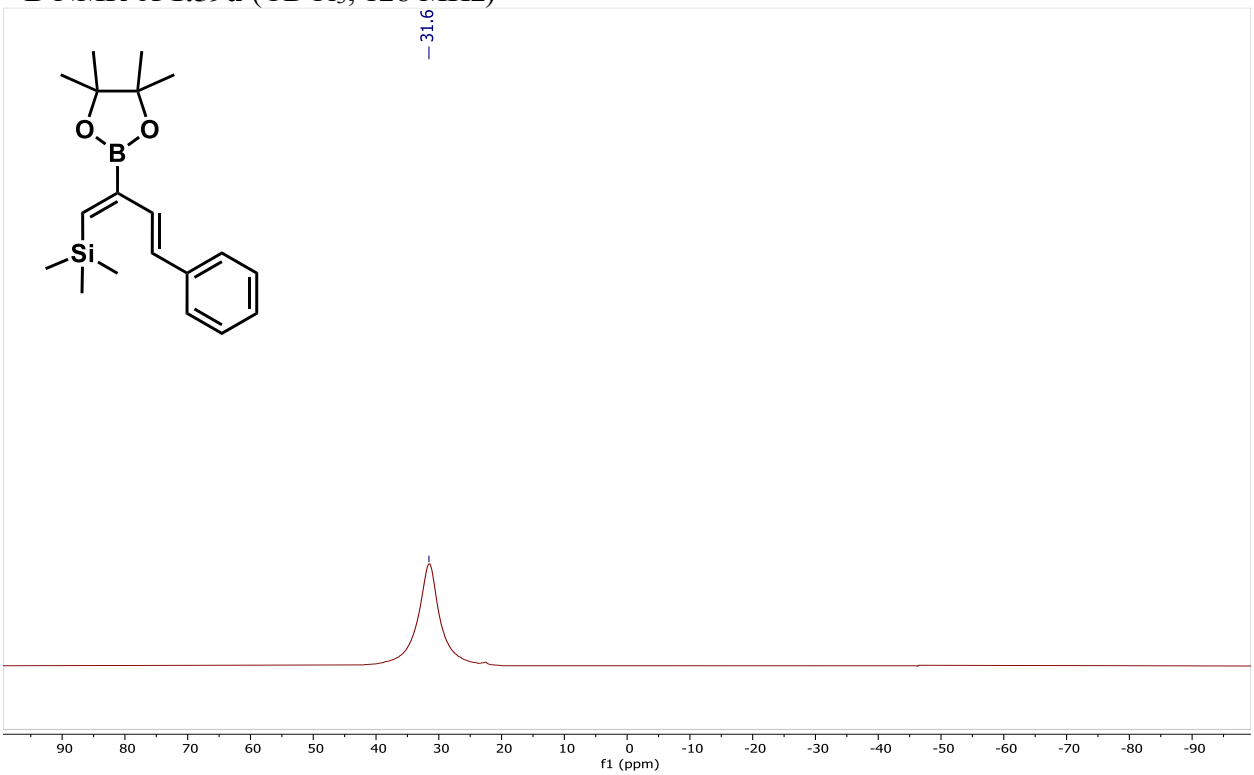

^{1}H NMR of **1.59v** ($CDCl_3$, 400 MHz)

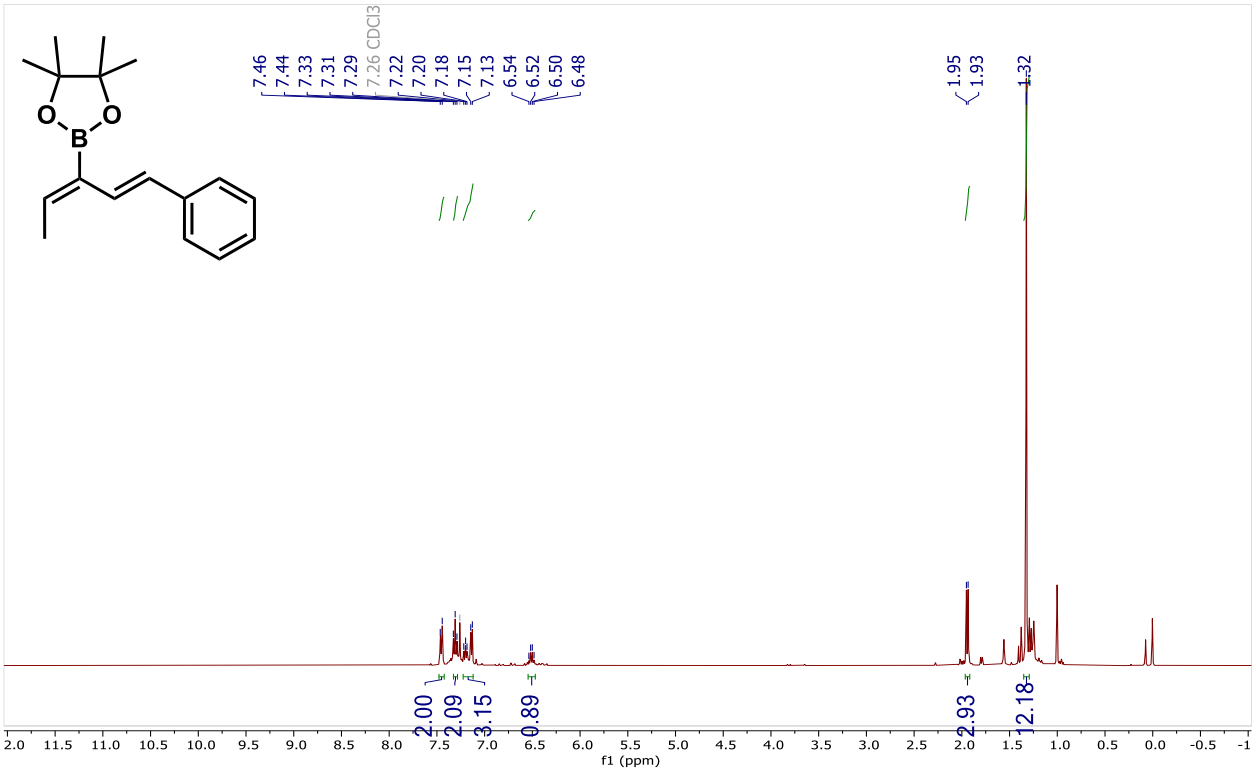

^{13}C NMR of **1.59v** ($CDCl_3$, 101 MHz)

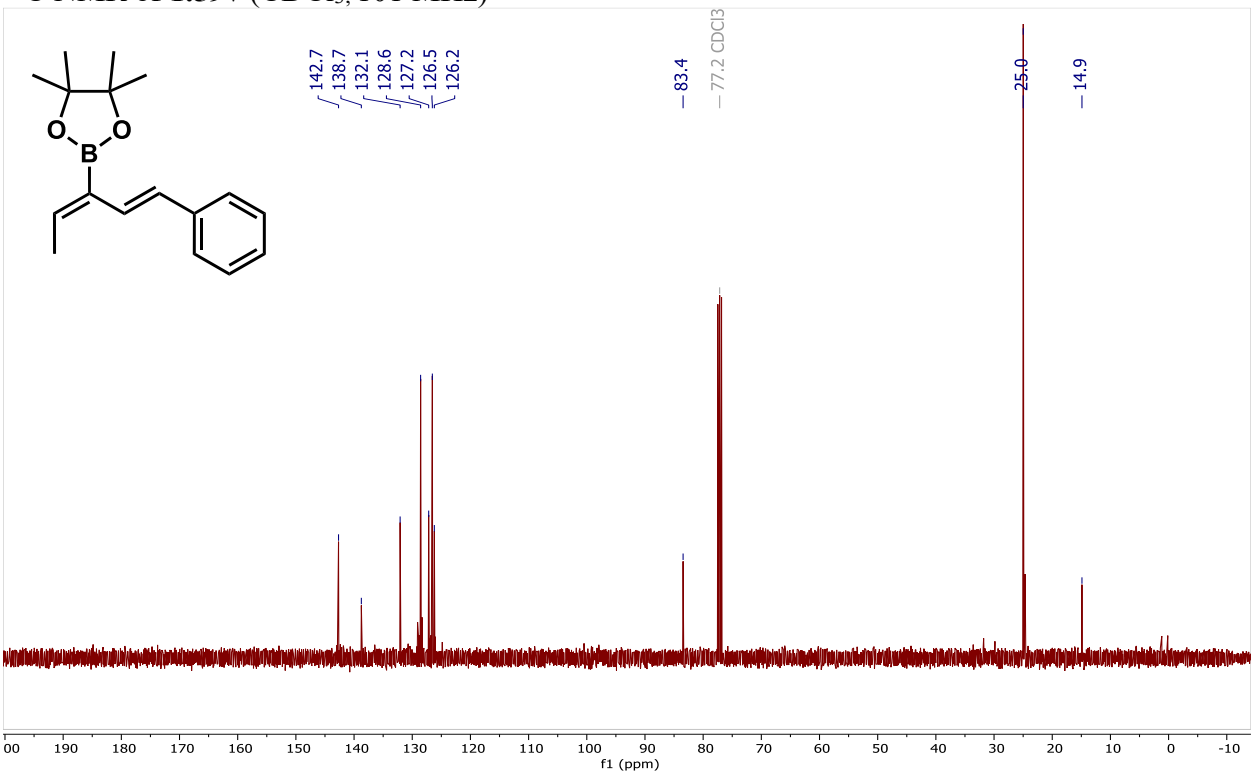

^{11}B NMR of **1.59v** ($CDCl_3$, 128 MHz)

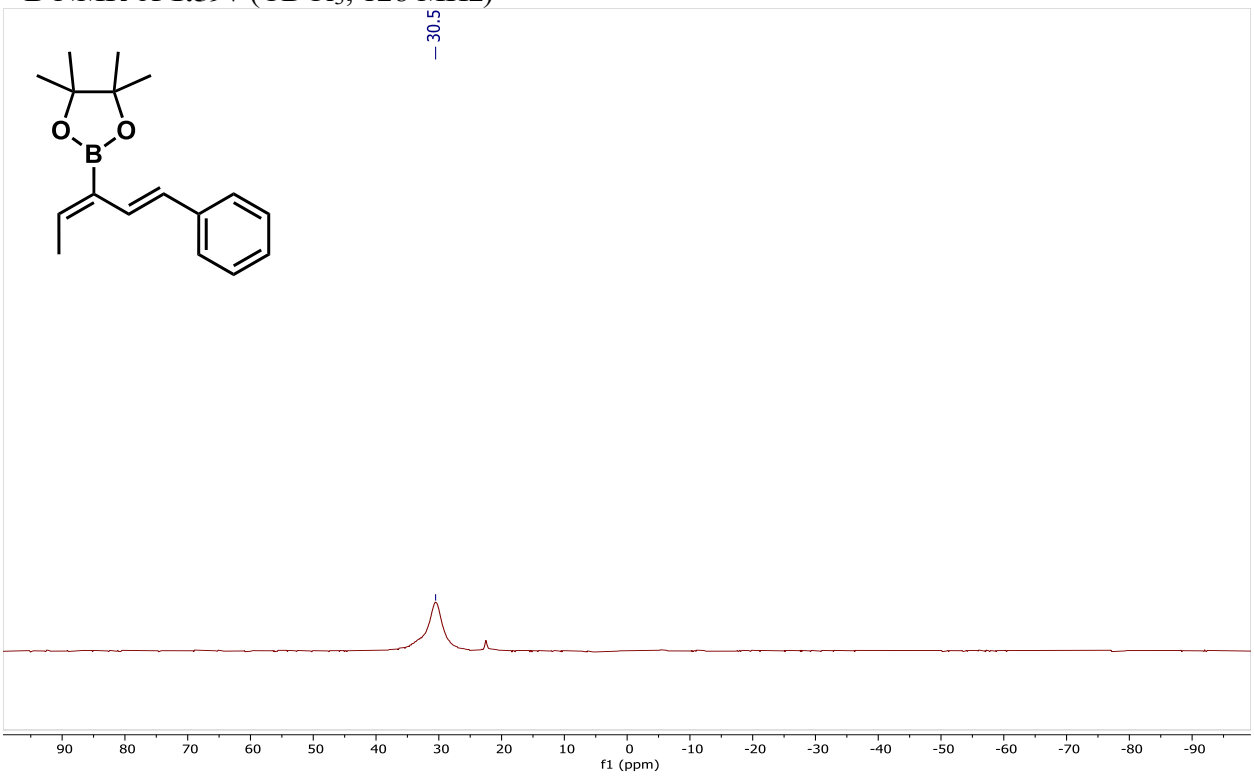

^{1}H NMR of **1.59w** ($CDCl_3$, 400 MHz)

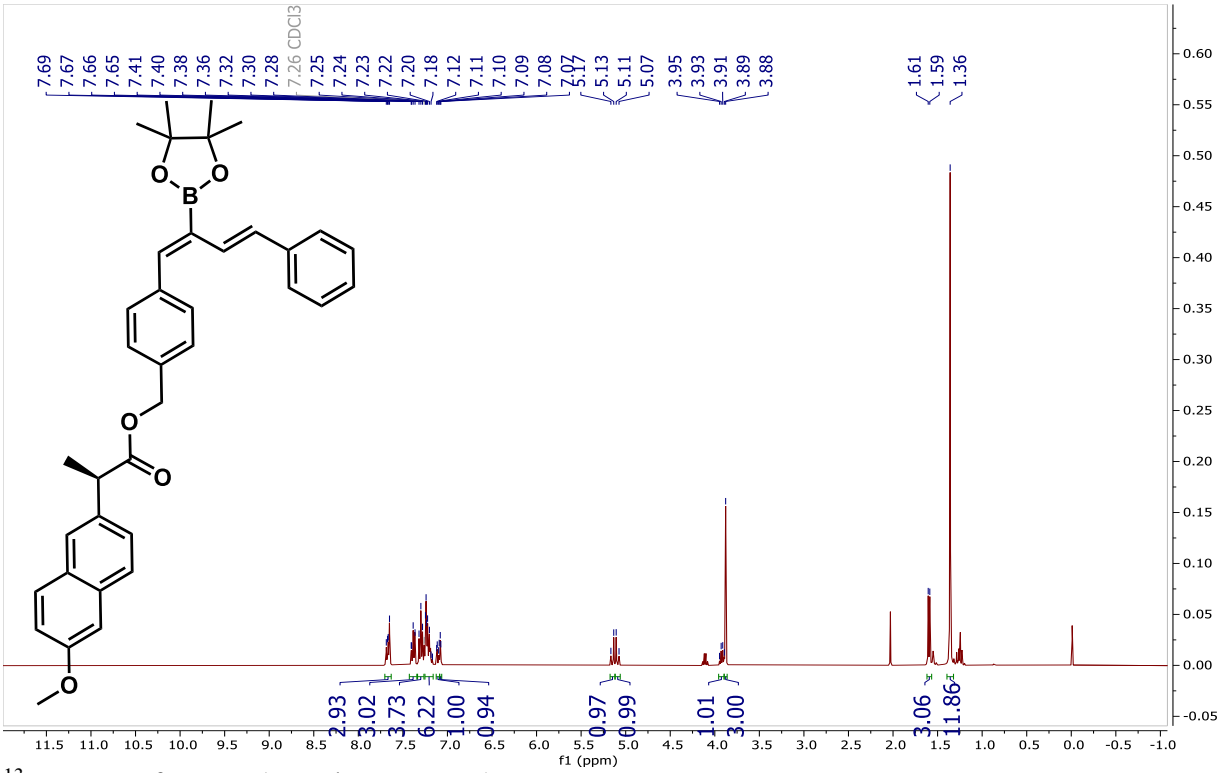

^{13}C NMR of **1.59w** ($CDCl_3$, 101 MHz)

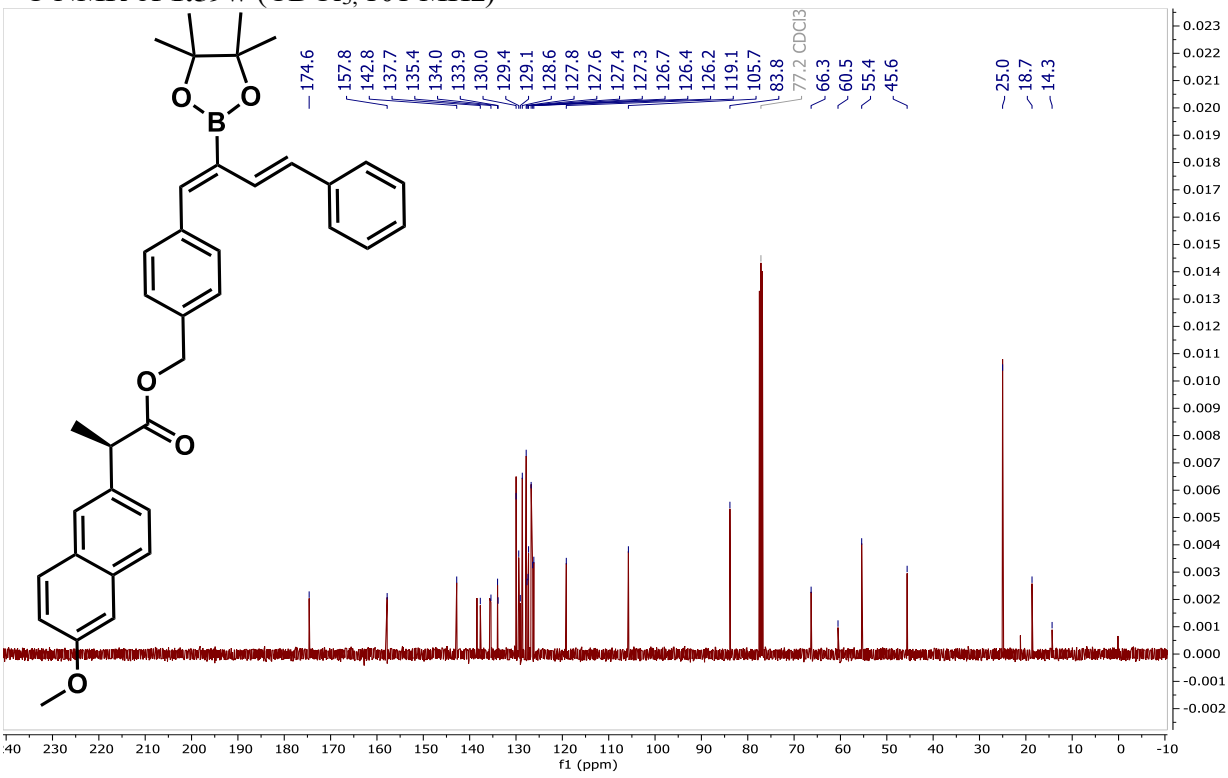

^{11}B NMR of **1.59w** ($CDCl_3$, 128 MHz)

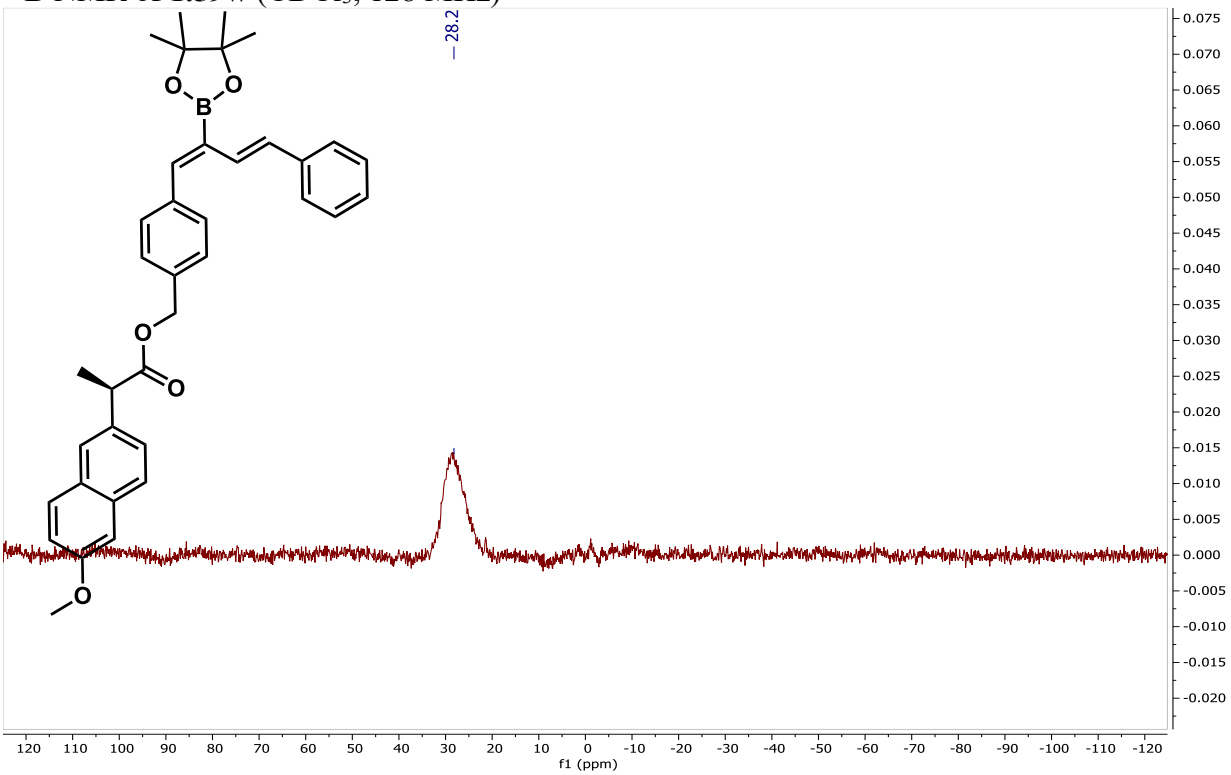

^{1}H NMR of **1.59x** ($CDCl_3$, 400 MHz)

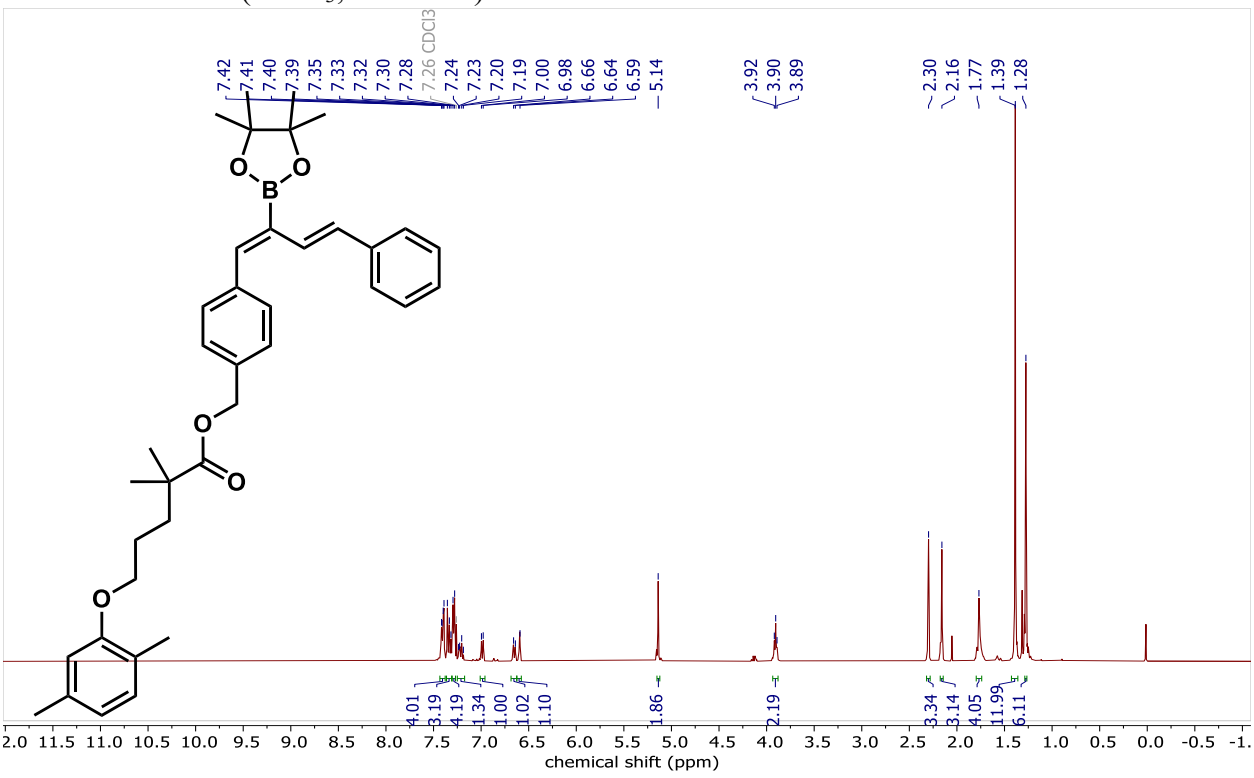

^{13}C NMR of **1.59x** ($CDCl_3$, 101 MHz)

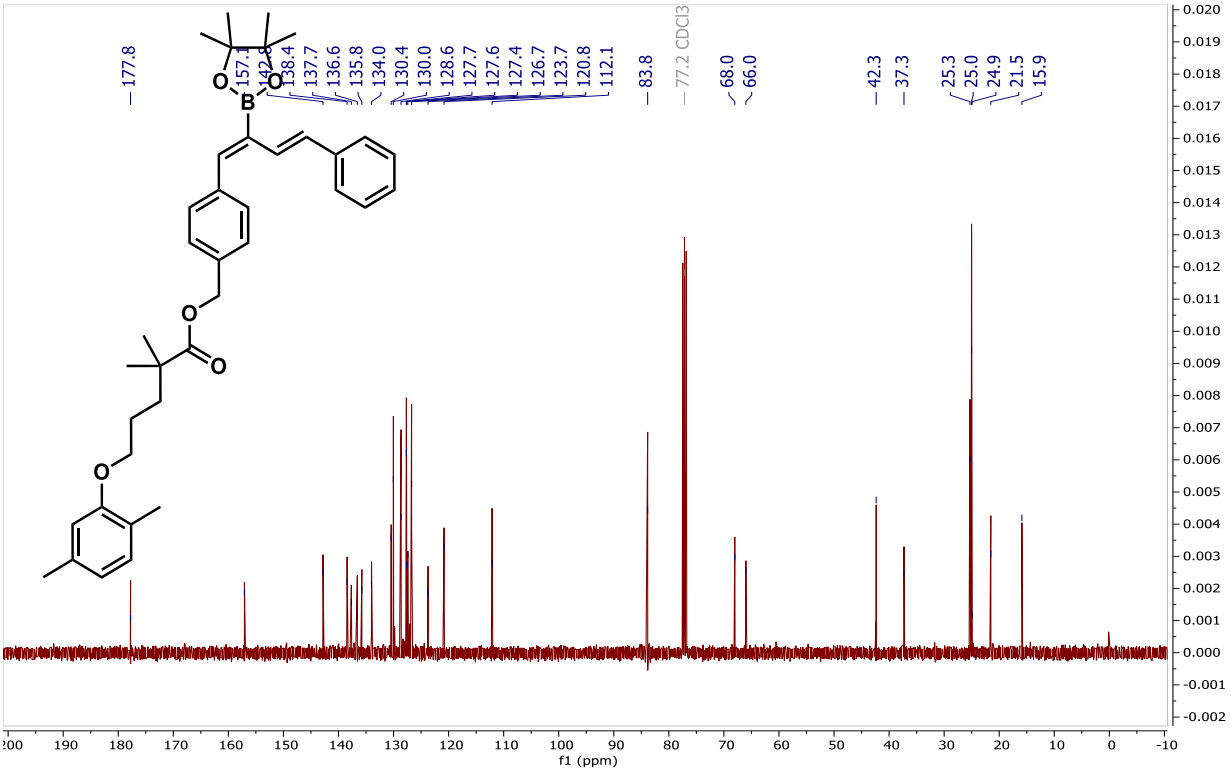

^{11}B NMR of **2x** ($CDCl_3$, 128 MHz)

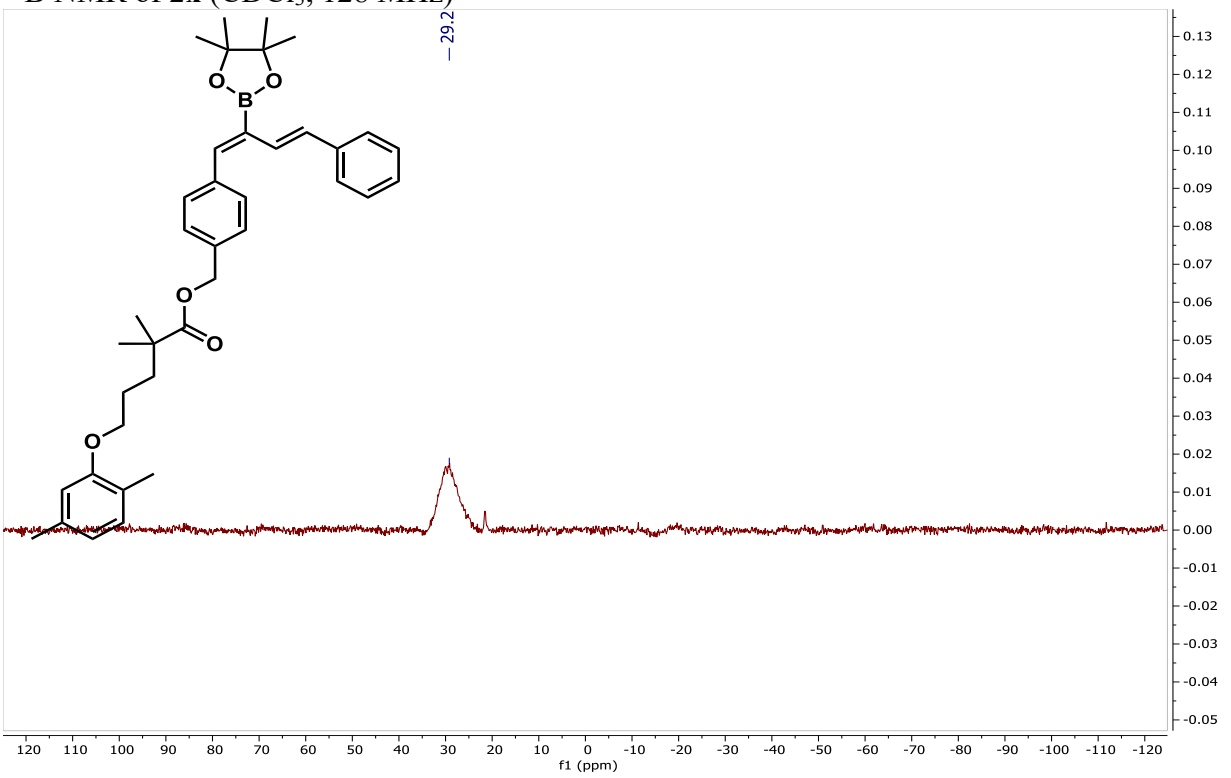

^{1}H NMR of **1.60** ($CDCl_3$, 400 MHz)

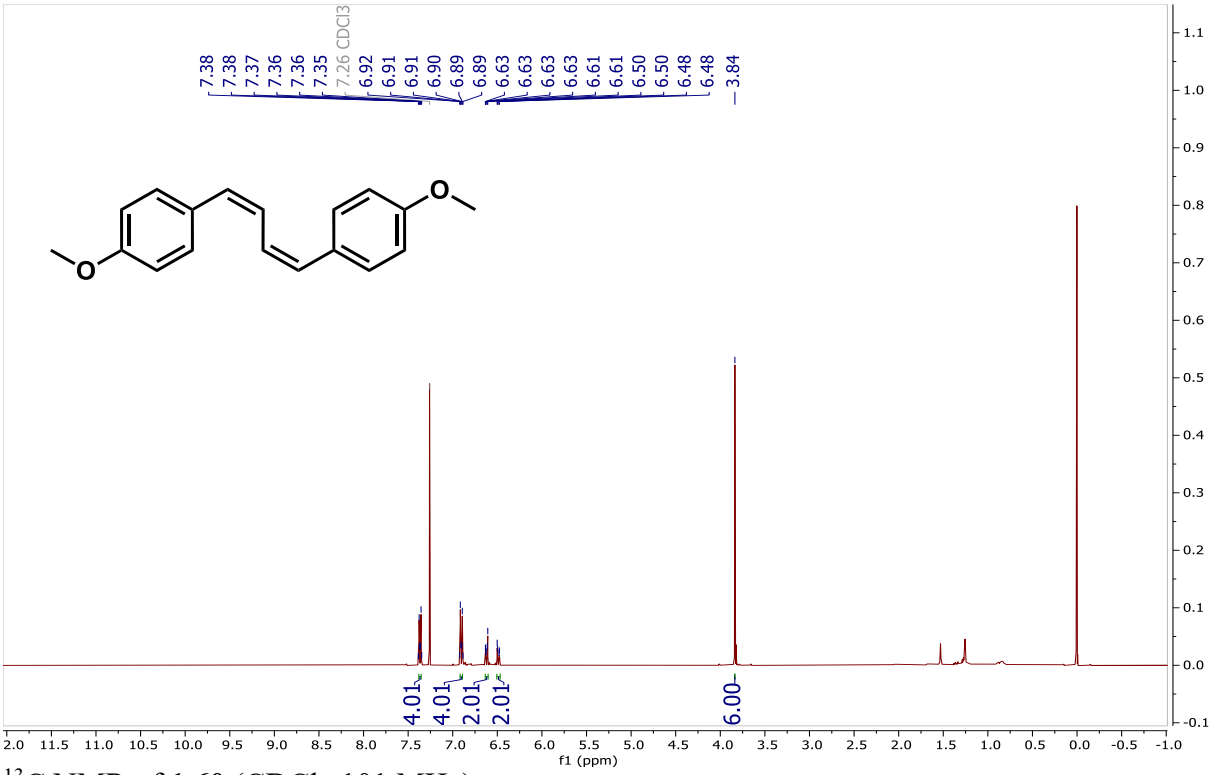

^{13}C NMR of **1.60** ($CDCl_3$, 101 MHz)

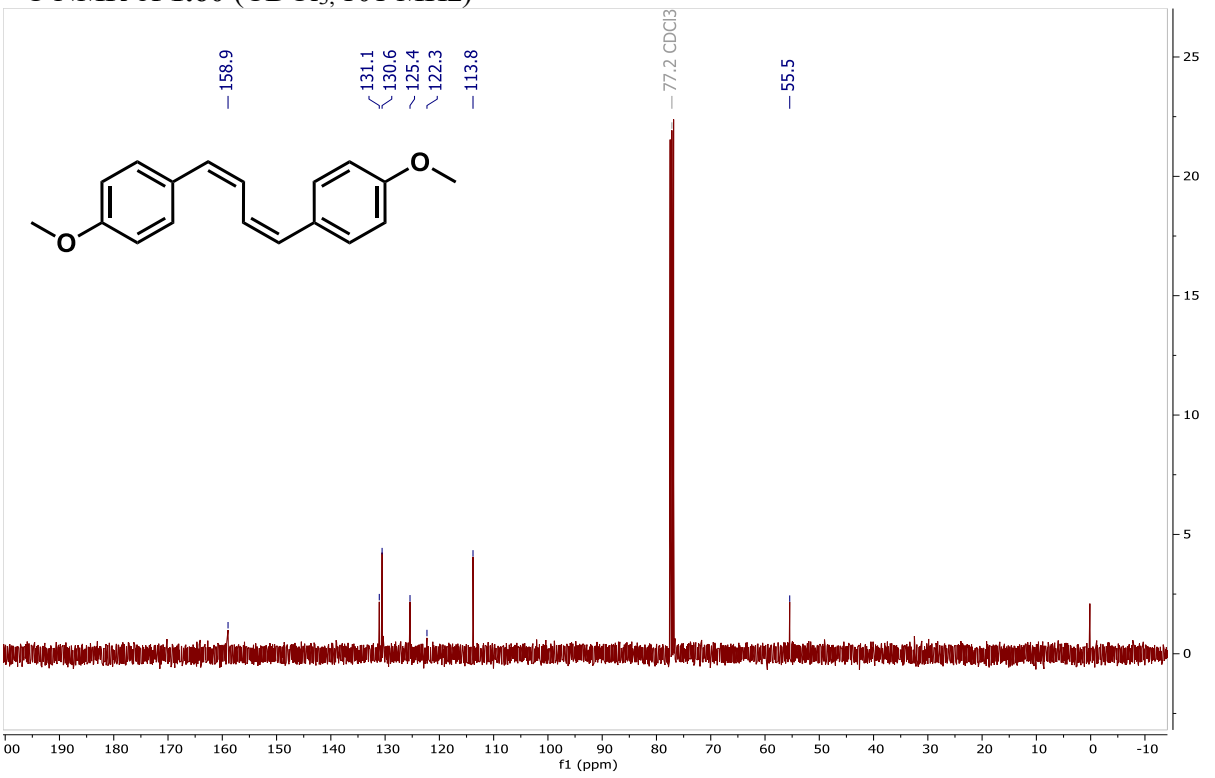

^{1}H NMR of **1.61** ($CDCl_3$, 500 MHz)

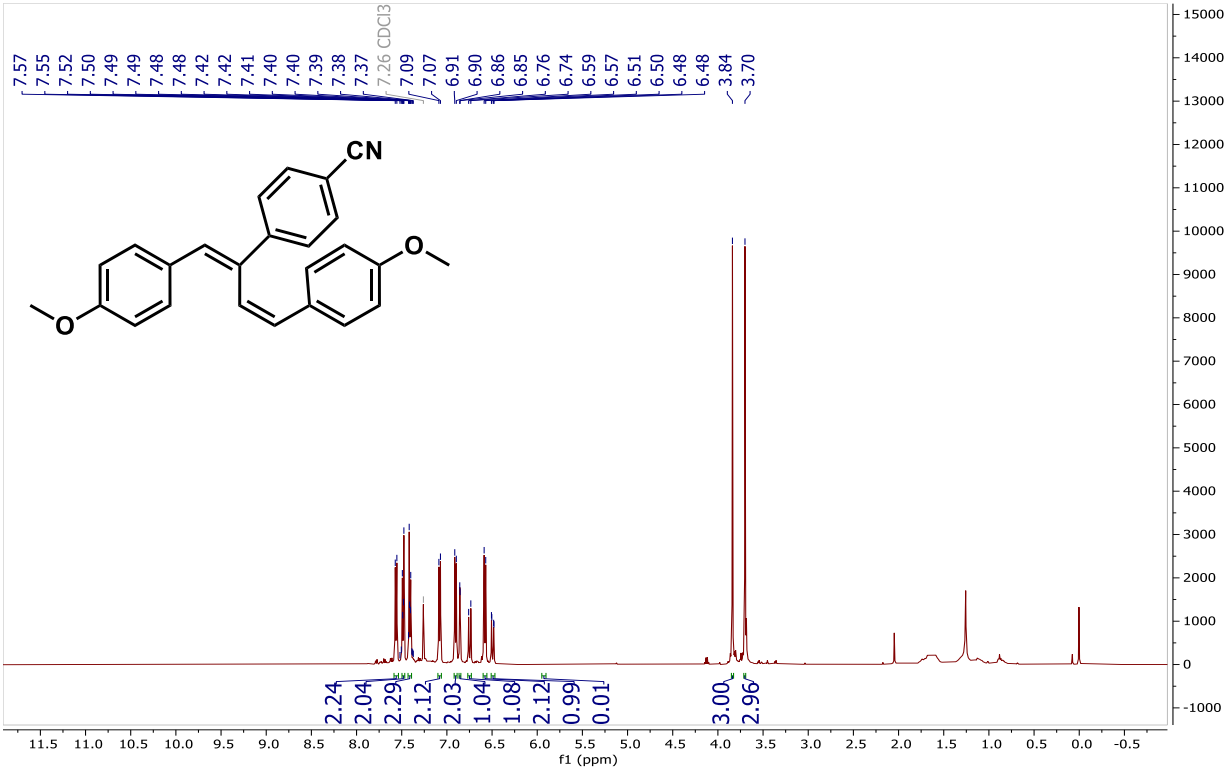

^{13}C NMR of **1.61** ($CDCl_3$, 126 MHz)

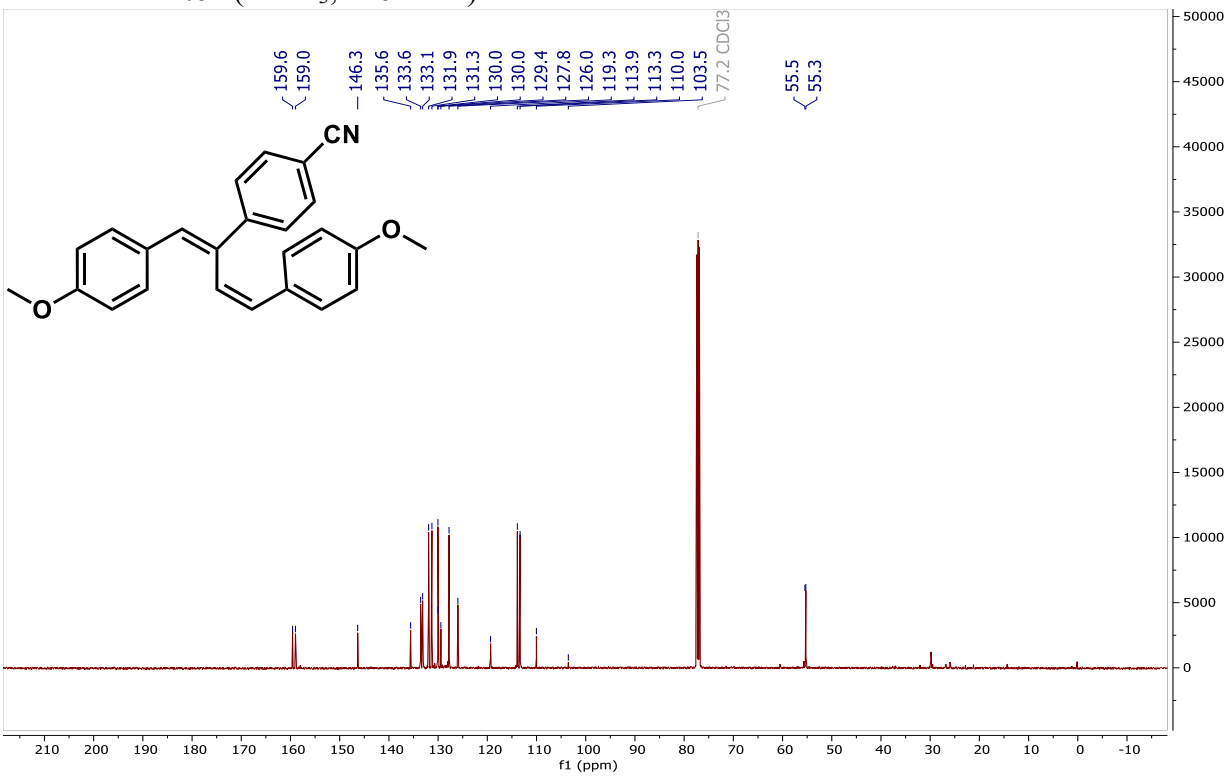

^{1}H NMR of **1.62** ($CDCl_3$, 400 MHz)

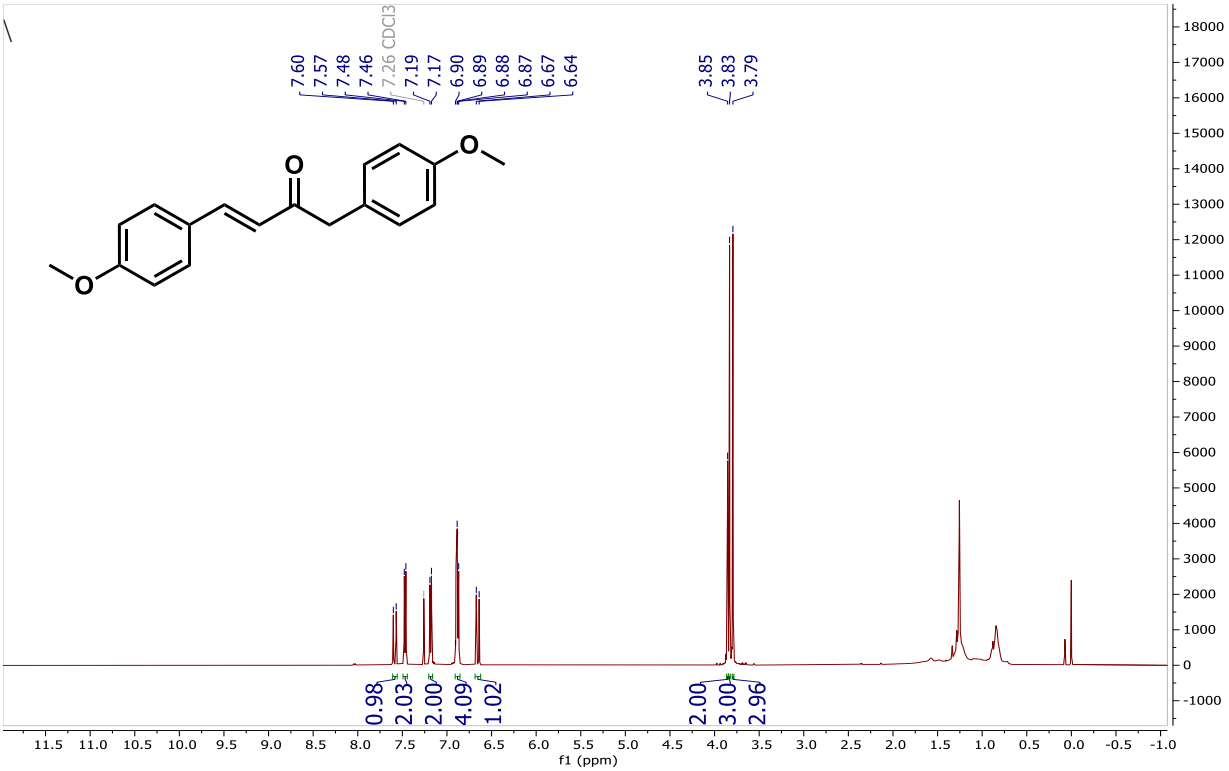

^{13}C NMR of **1.62** ($CDCl_3$, 101 MHz)

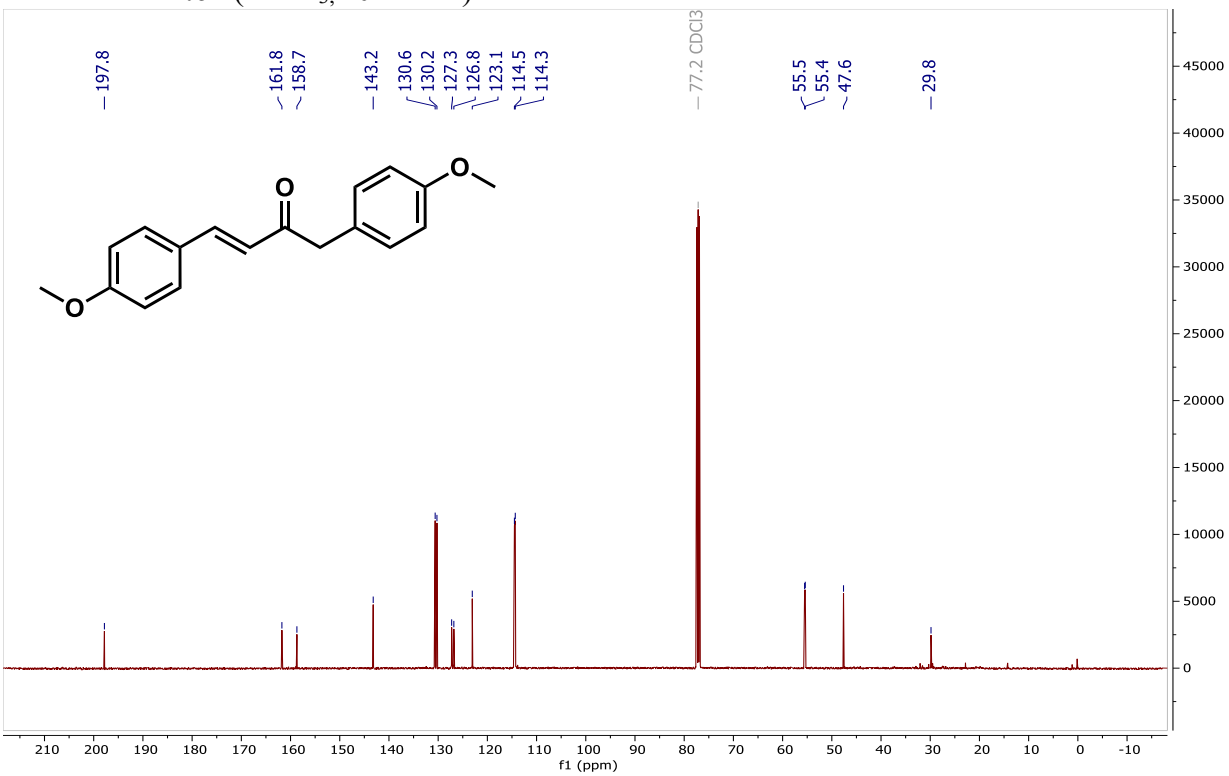

^{1}H NMR of **1.63** ($CDCl_3$, 500 MHz)

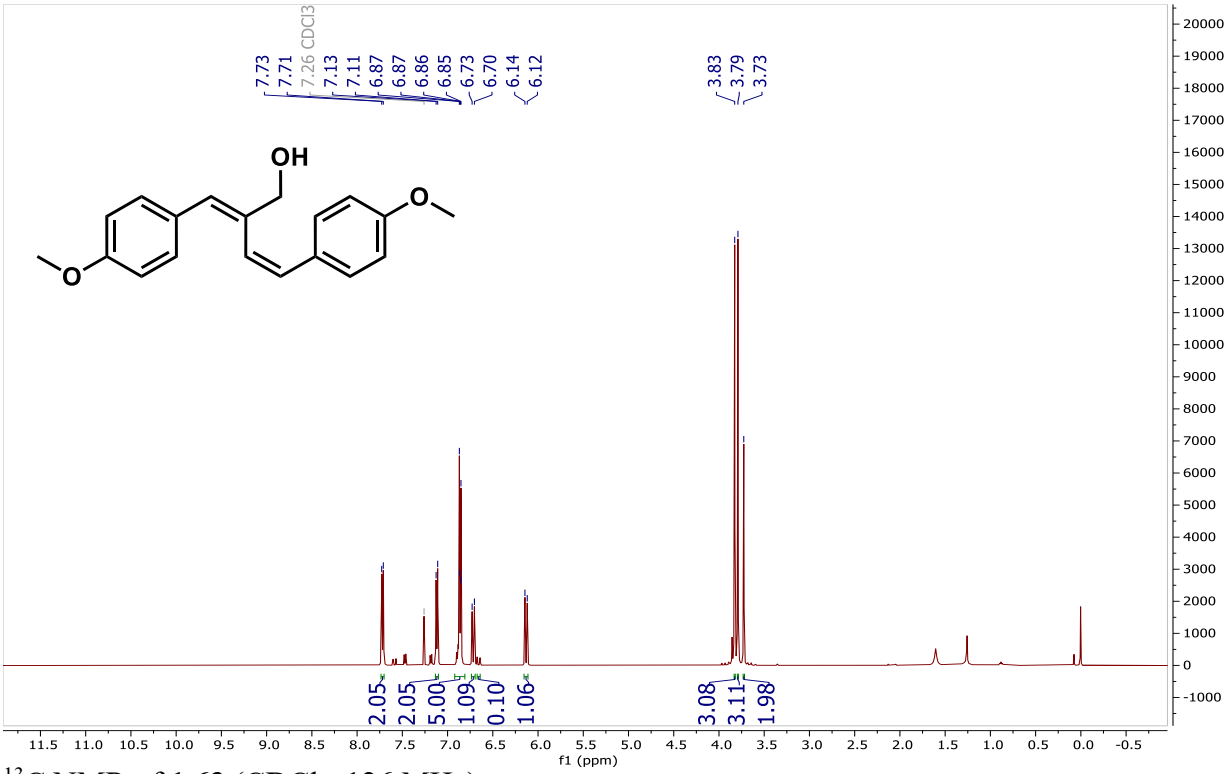

^{13}C NMR of **1.63** ($CDCl_3$, 126 MHz)

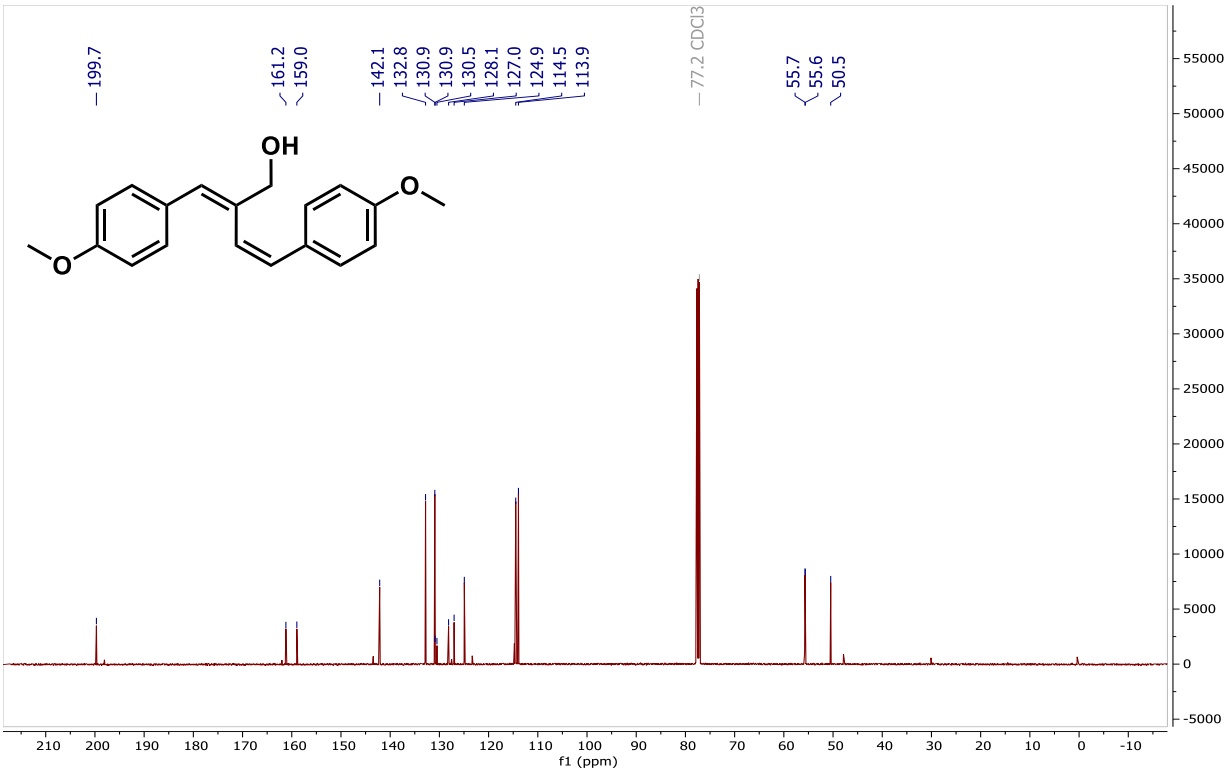

Hidden Borane Catalysis Experiment Crude ^{11}B NMR ($CDCl_3$, 128 Hz)

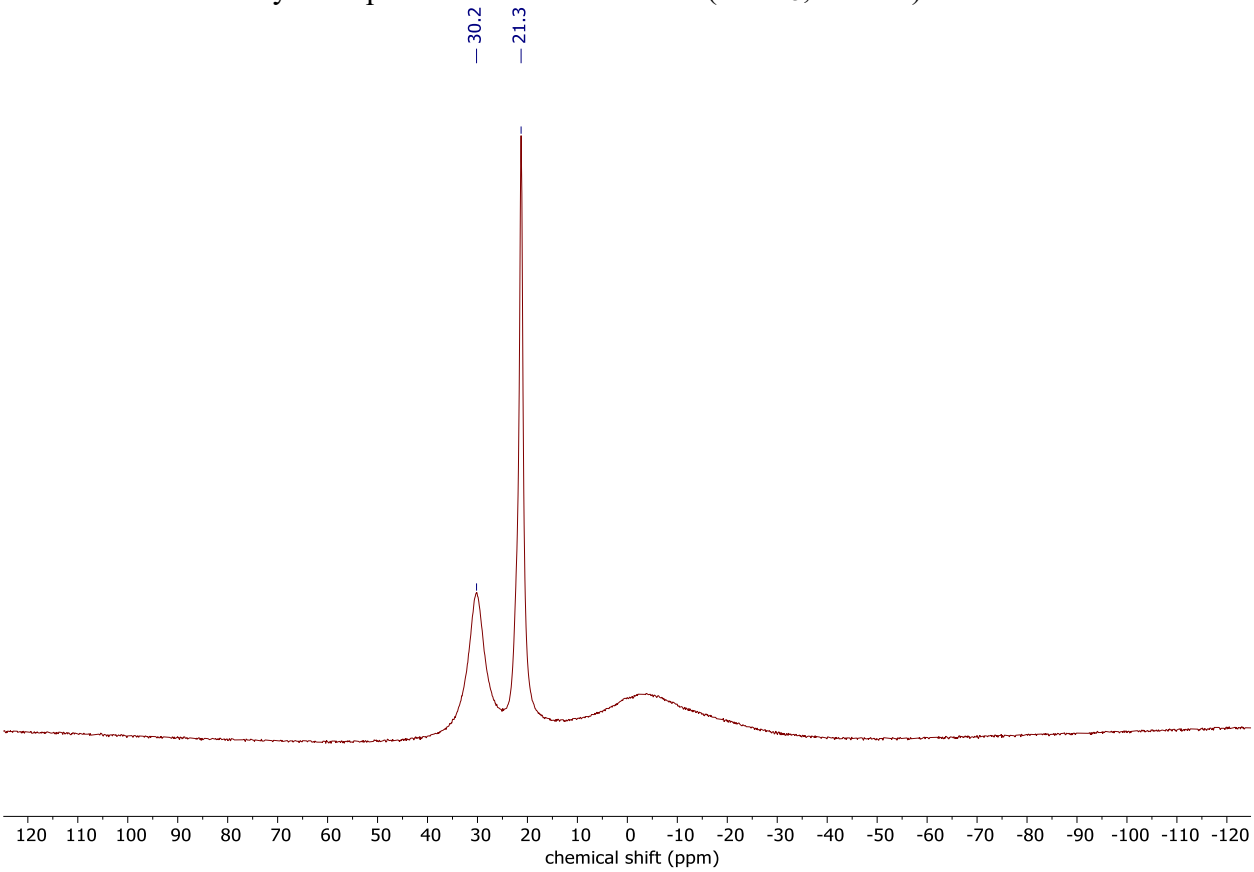

NMR spectra of α,β-dehydroamino acids for Chapter 3

^{1}H NMR **3.47a** (400 MHz) in $CDCl_3$

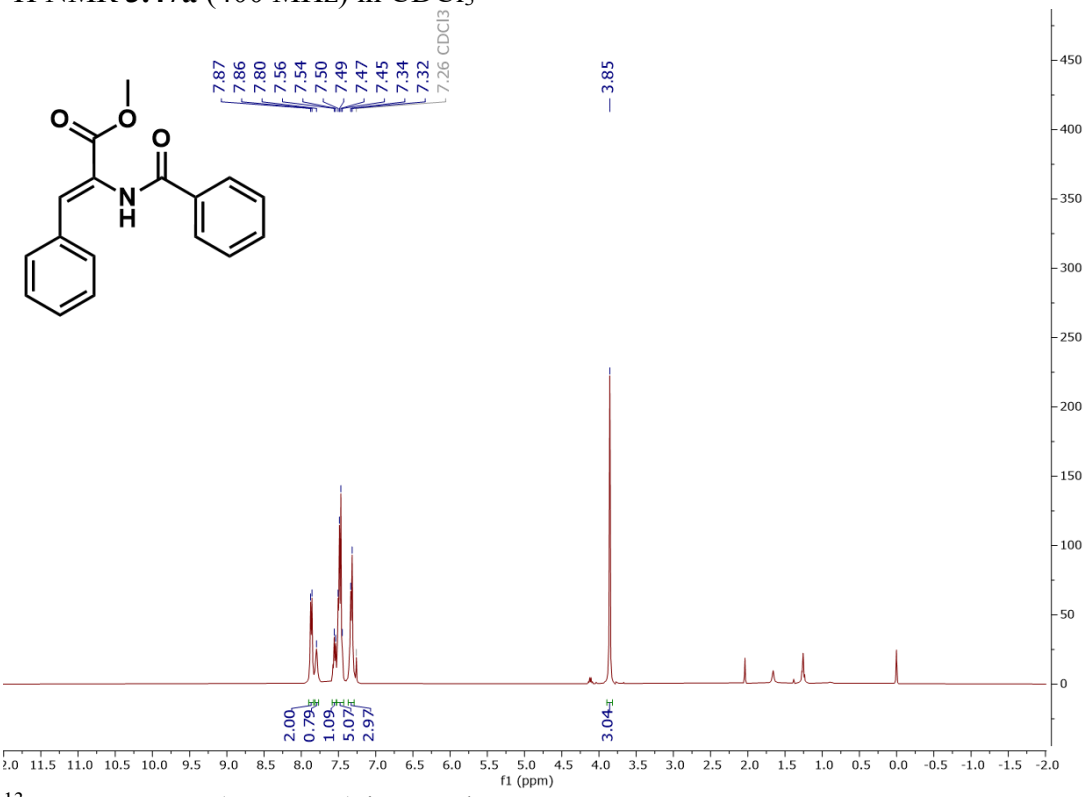

^{13}C NMR **3.47a** (101 MHz) in $CDCl_3$

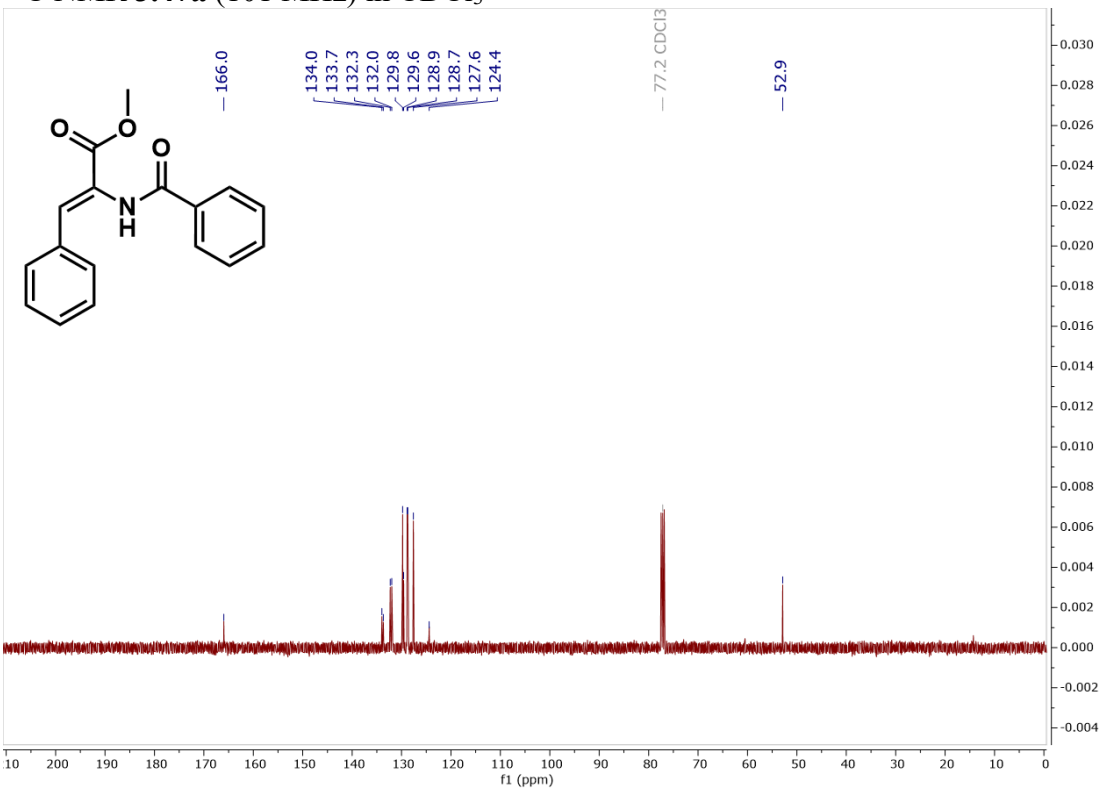

^{1}H NMR of (*E*)- **3.47a (**400 MHz) in $CDCl_3$

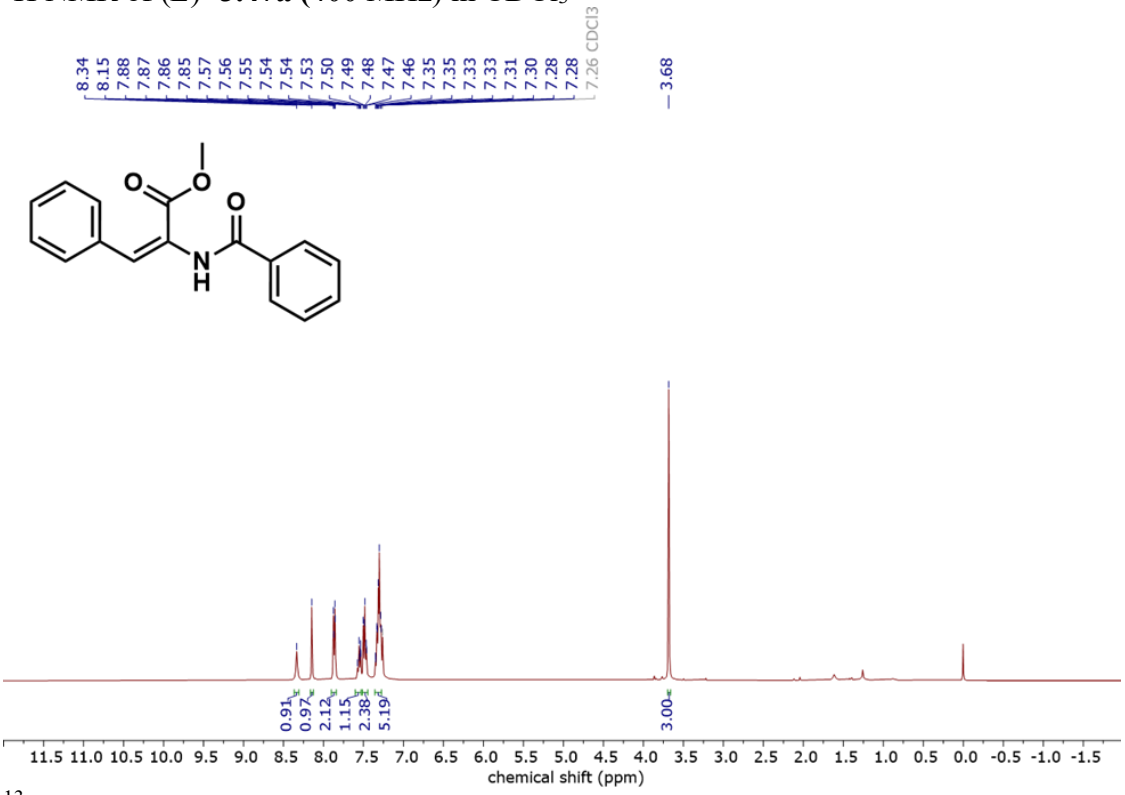

^{13}C NMR of (*E*)- **3.47a (**126 MHz) in $CDCl_3$

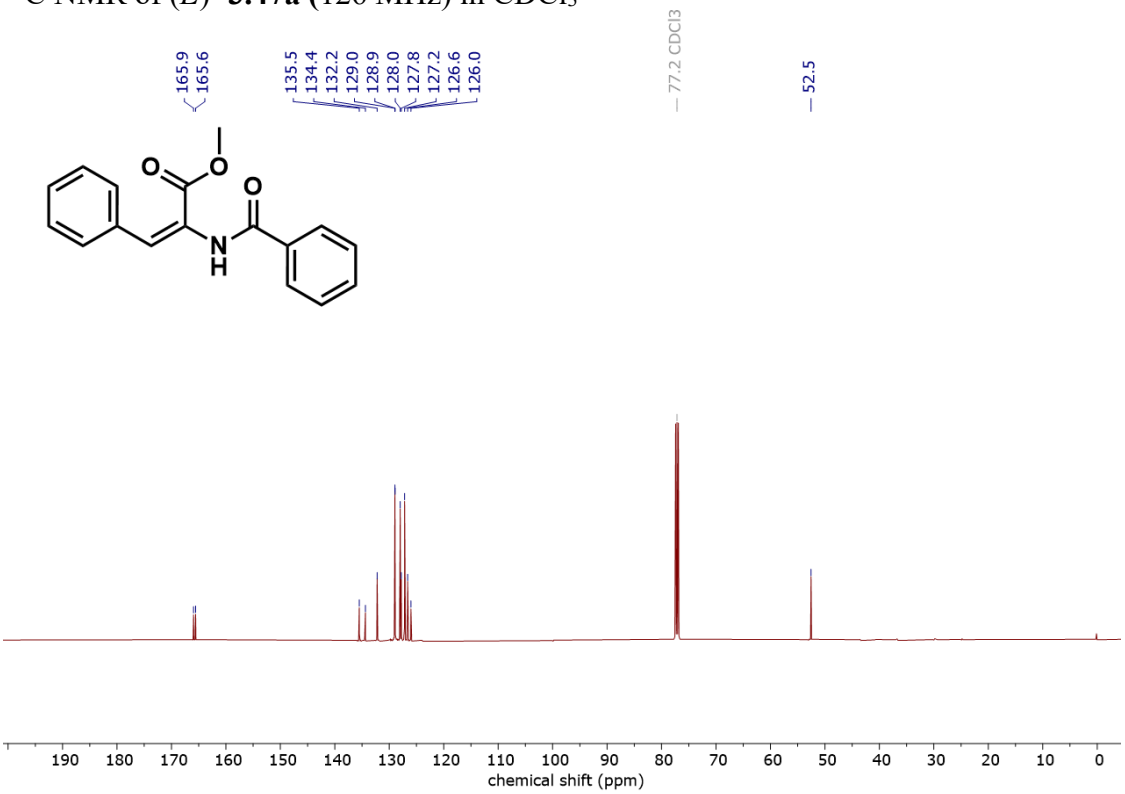

^{1}H NMR **3.47b** (400 MHz) in $CDCl_3$

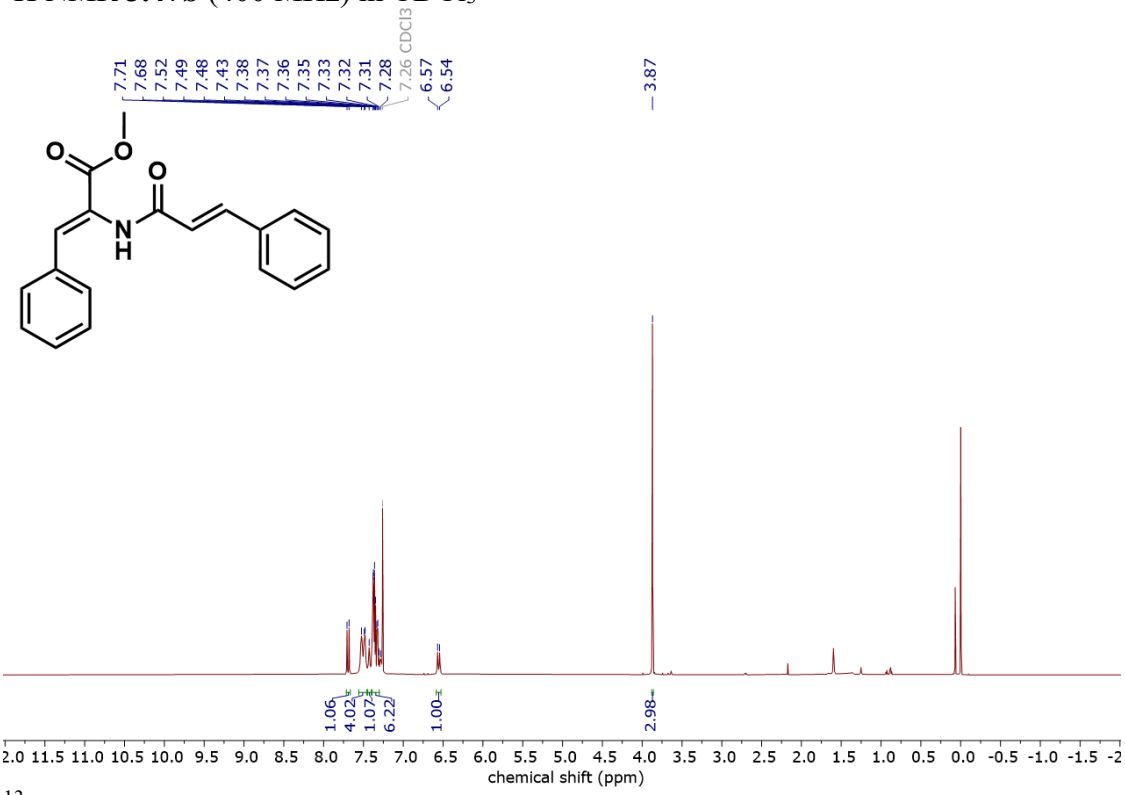

^{13}C NMR **3.47b** (101 MHz) in $CDCl_3$

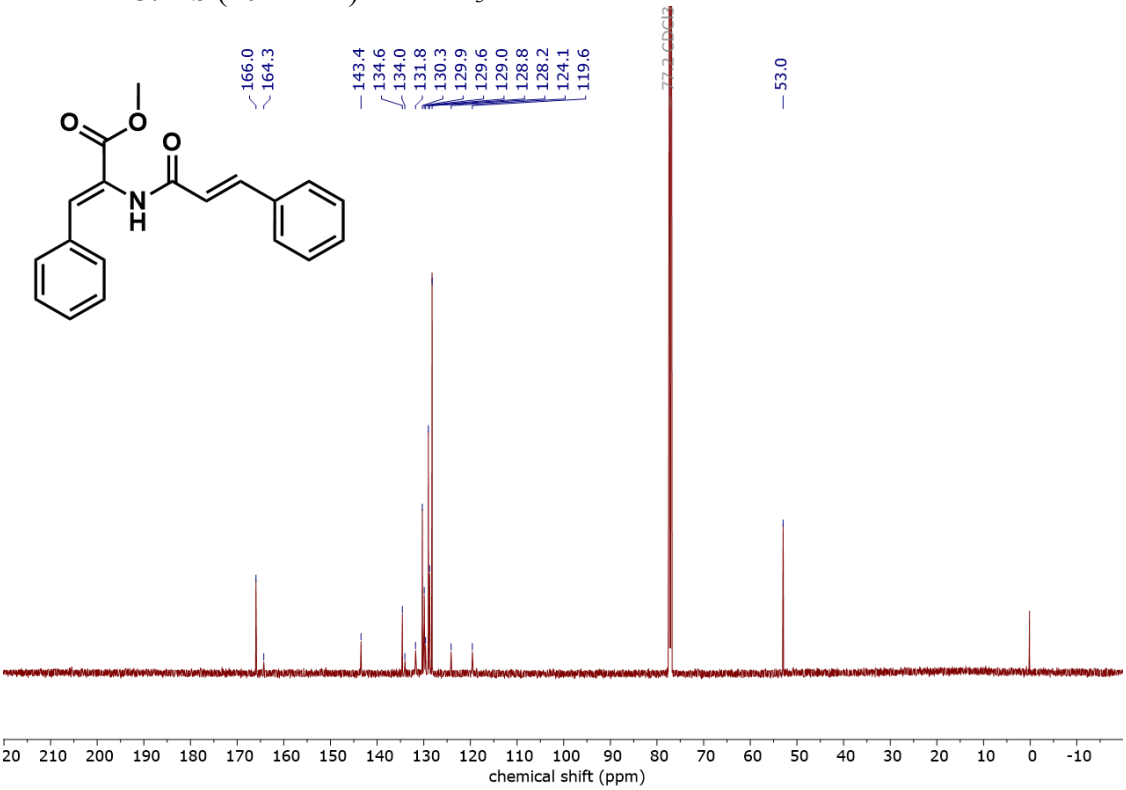

^{1}H NMR **3.47c** (500 Mz) in $CDCl_3$

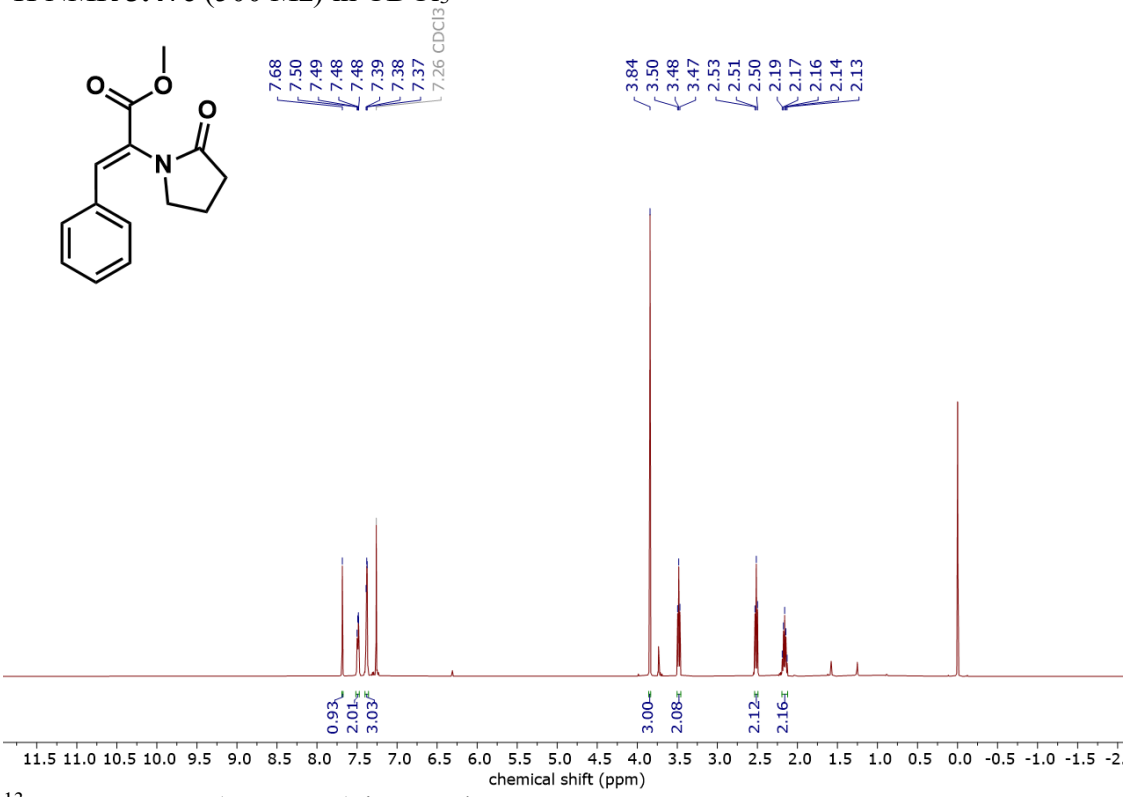

^{13}C NMR **3.47c** (126 MHz) in $CDCl_3$

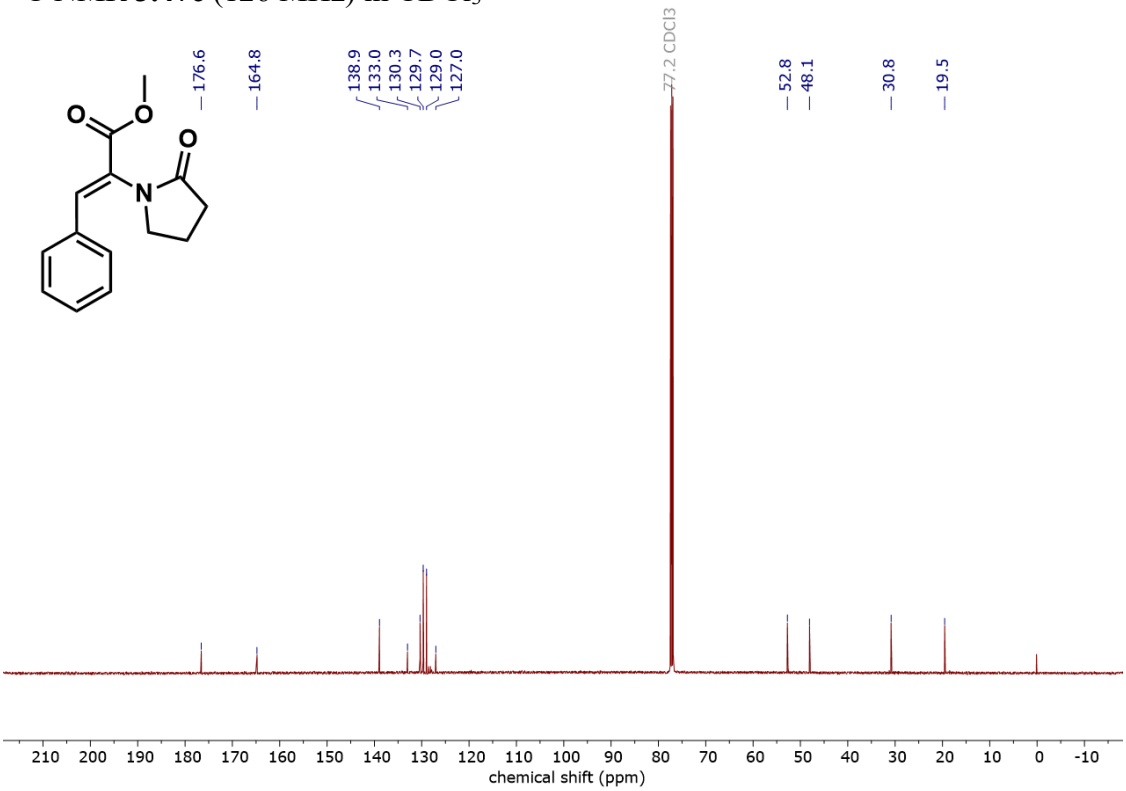

^{1}H NMR **3.47d** (500 MHz) in $CDCl_3$

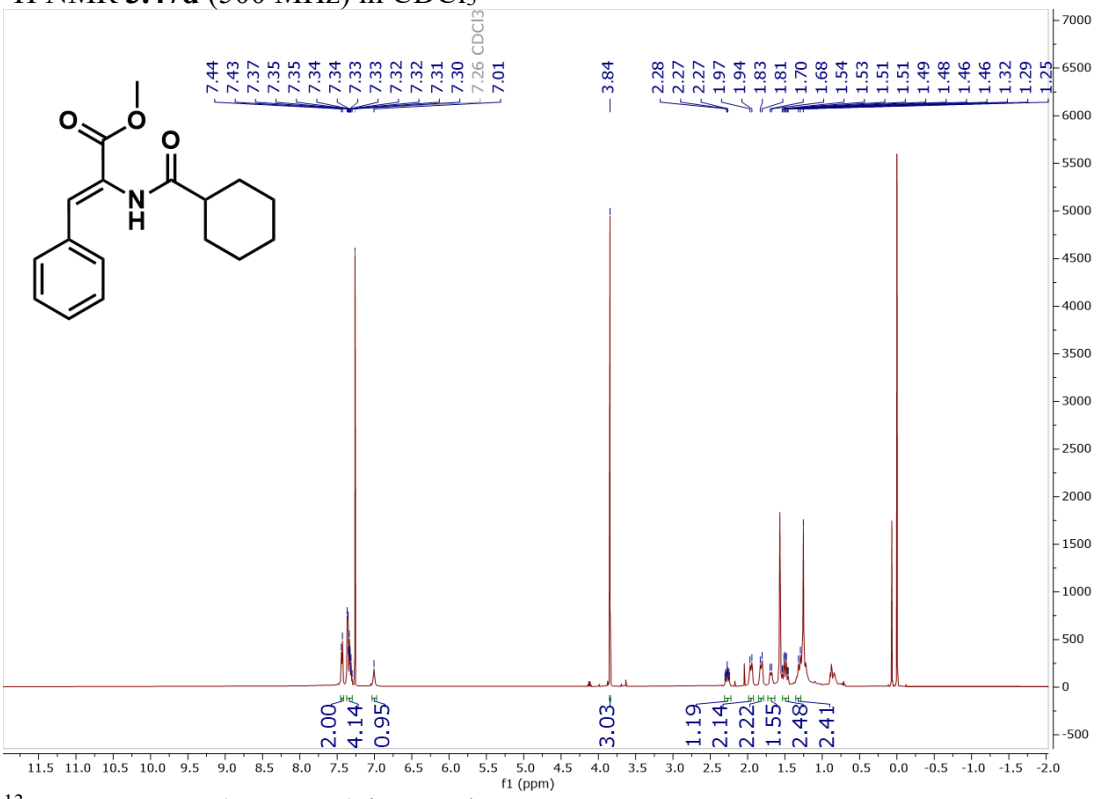

^{13}C NMR **3.47d** (126 MHz) in $CDCl_3$

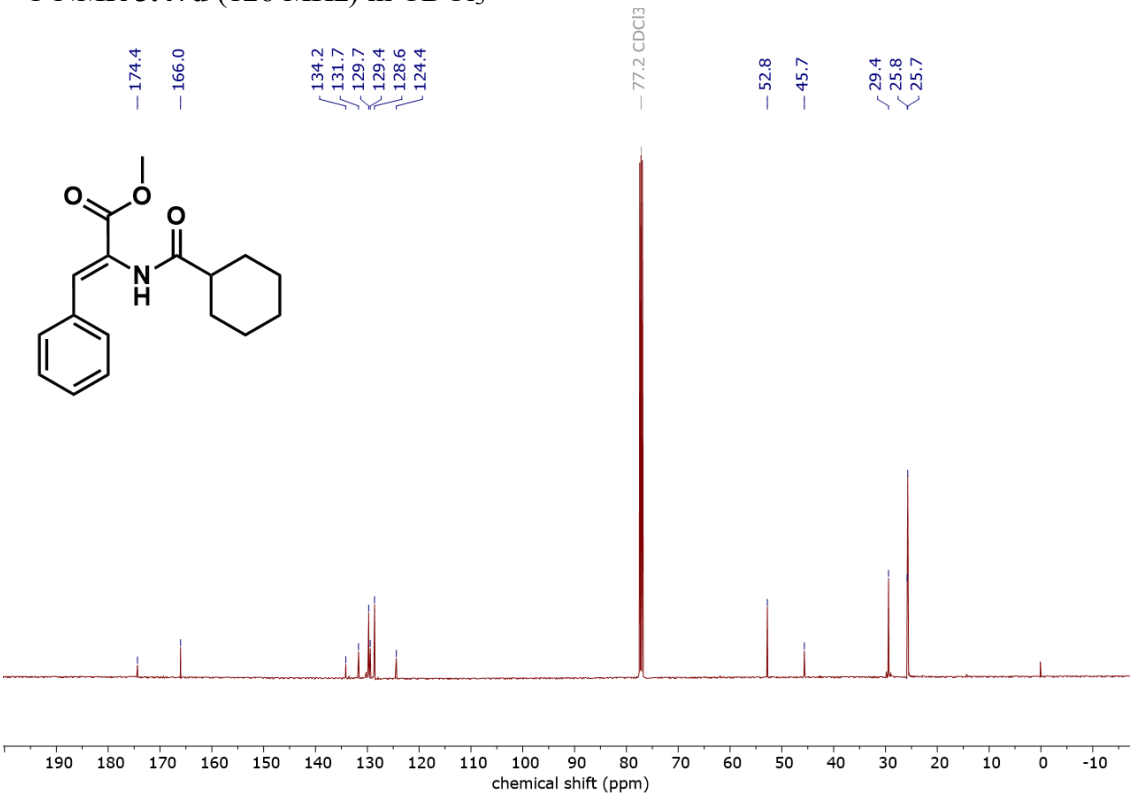

^{1}H NMR **3.47e** (600 MHz) in $CDCl_3$

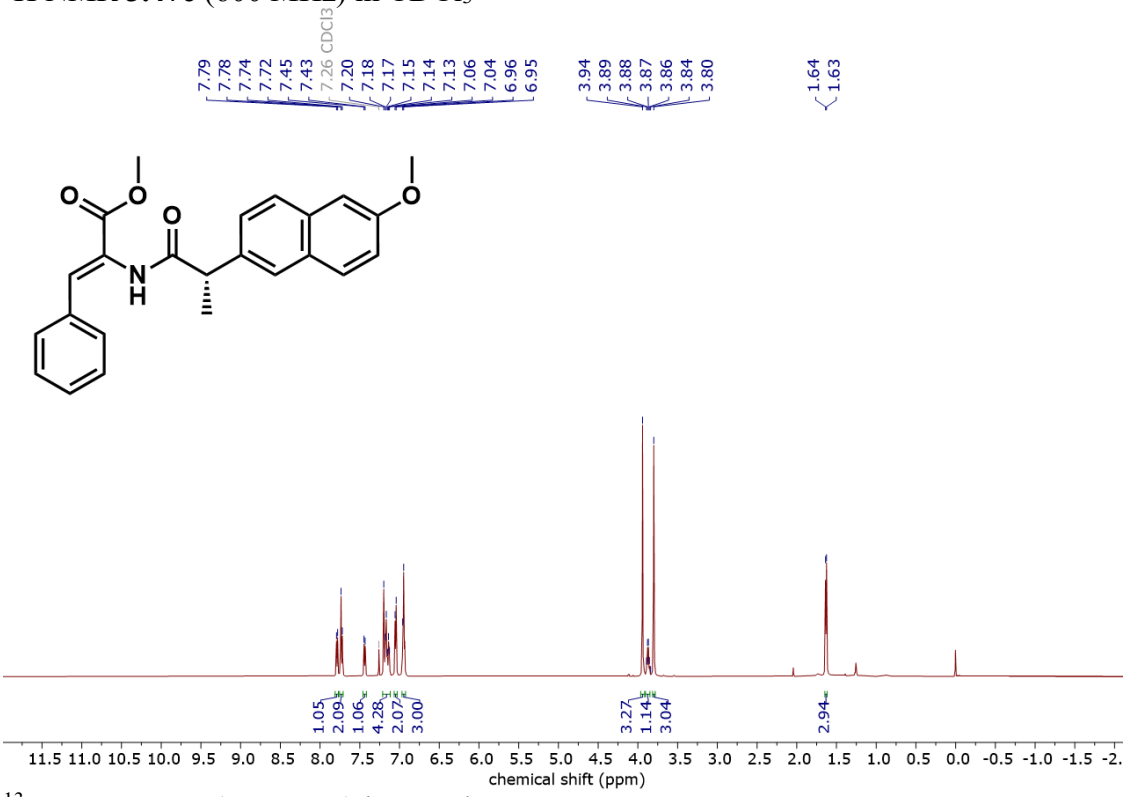

^{13}C NMR **3.47e** (151 MHz) in $CDCl_3$

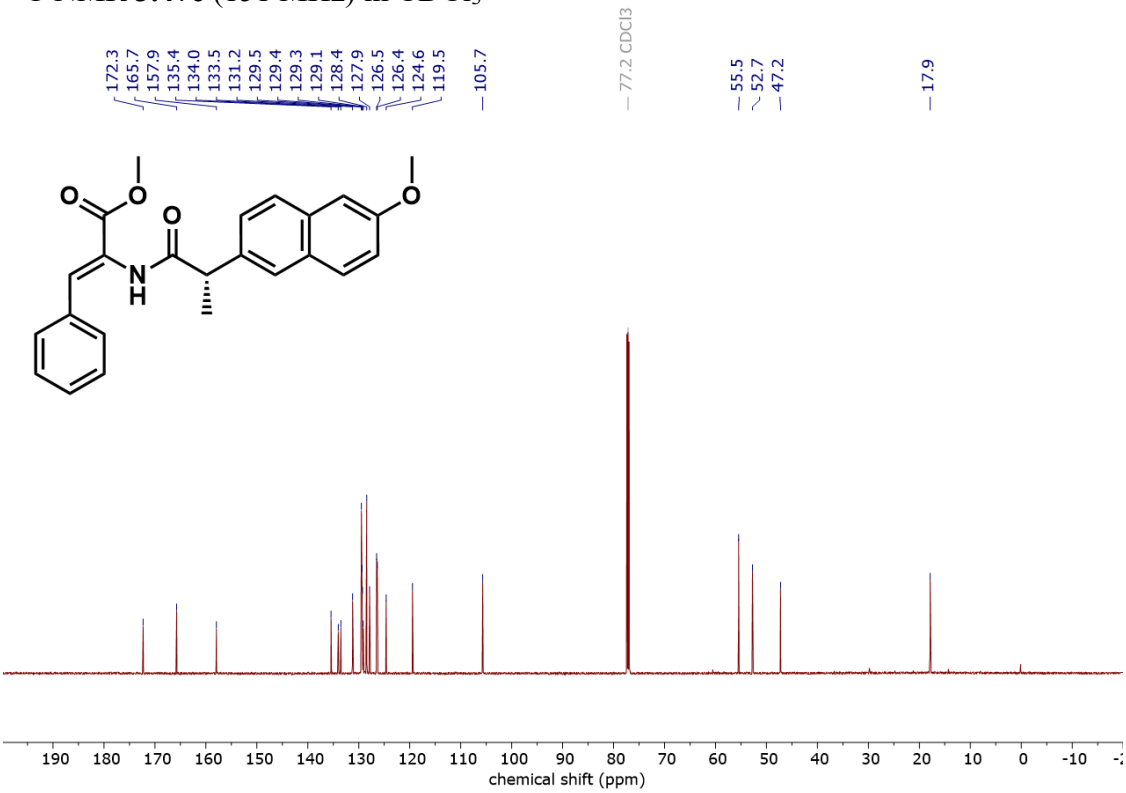

^{1}H NMR **3.47f** (400 MHz) in $CDCl_3$

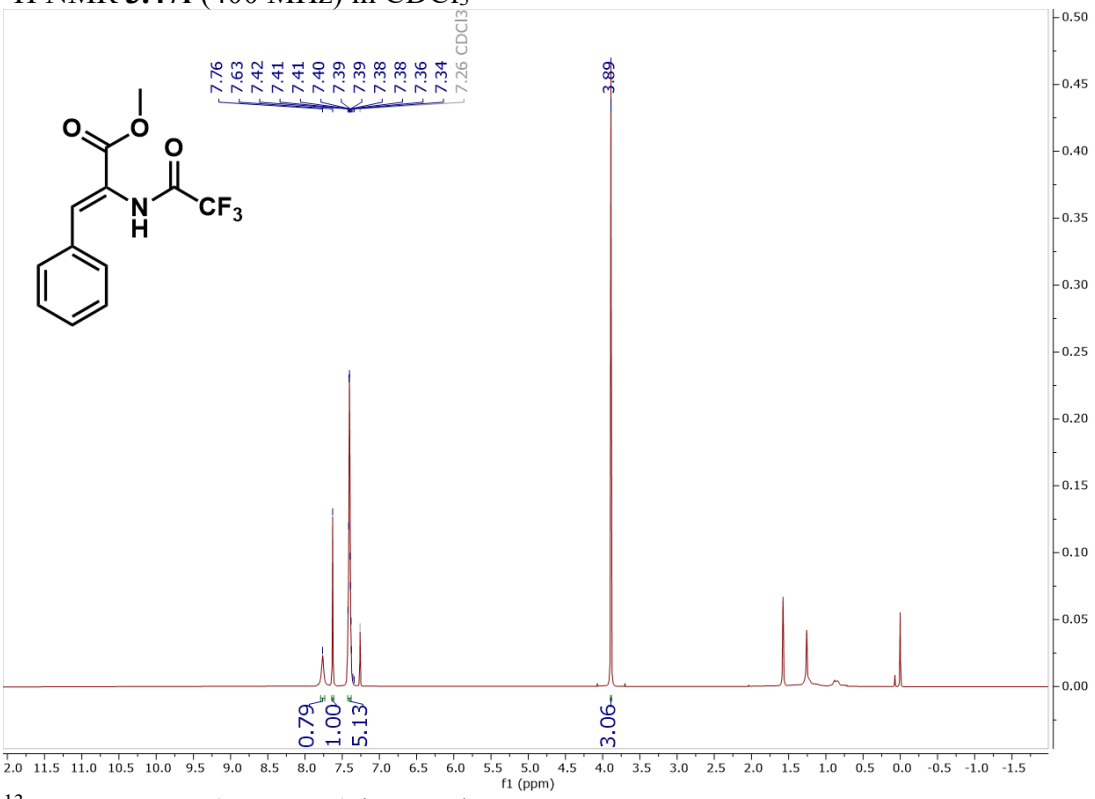

^{13}C NMR **3.47f** (126 MHz) in $CDCl_3$

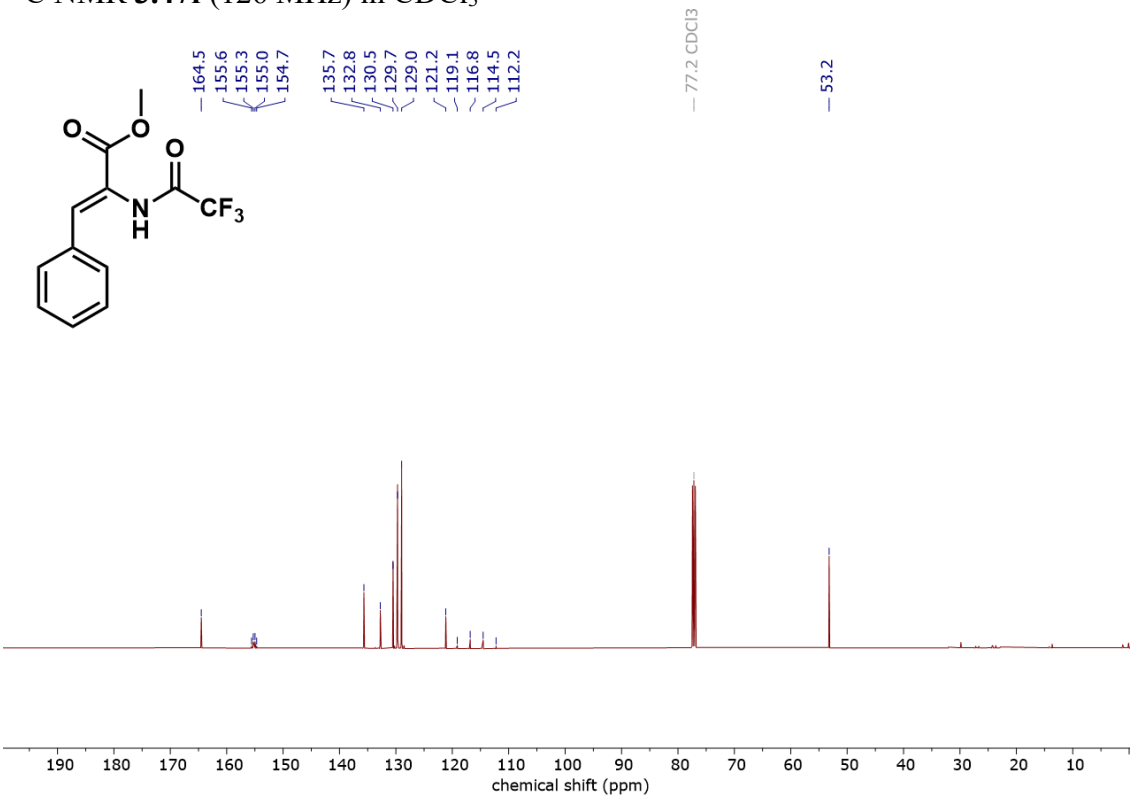

^{19}F NMR **3.47f** (376 MHz) in $CDCl_3$

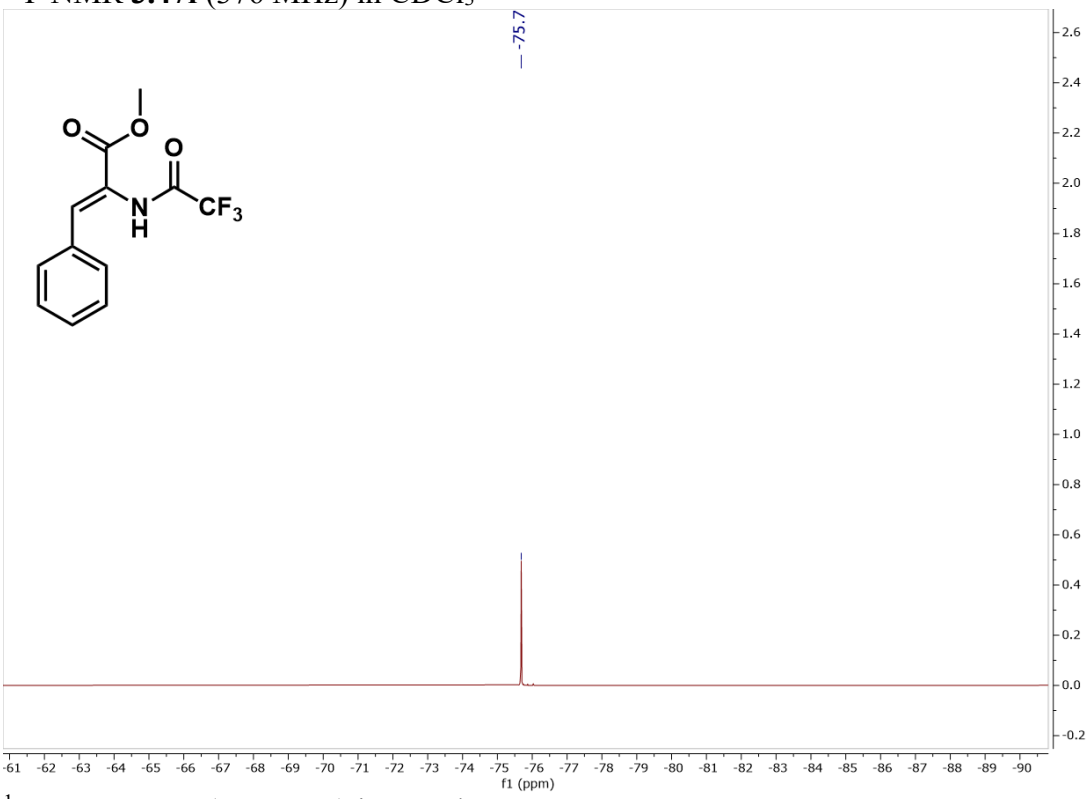

^{1}H NMR **3.47g** (400 MHz) in $CDCl_3$

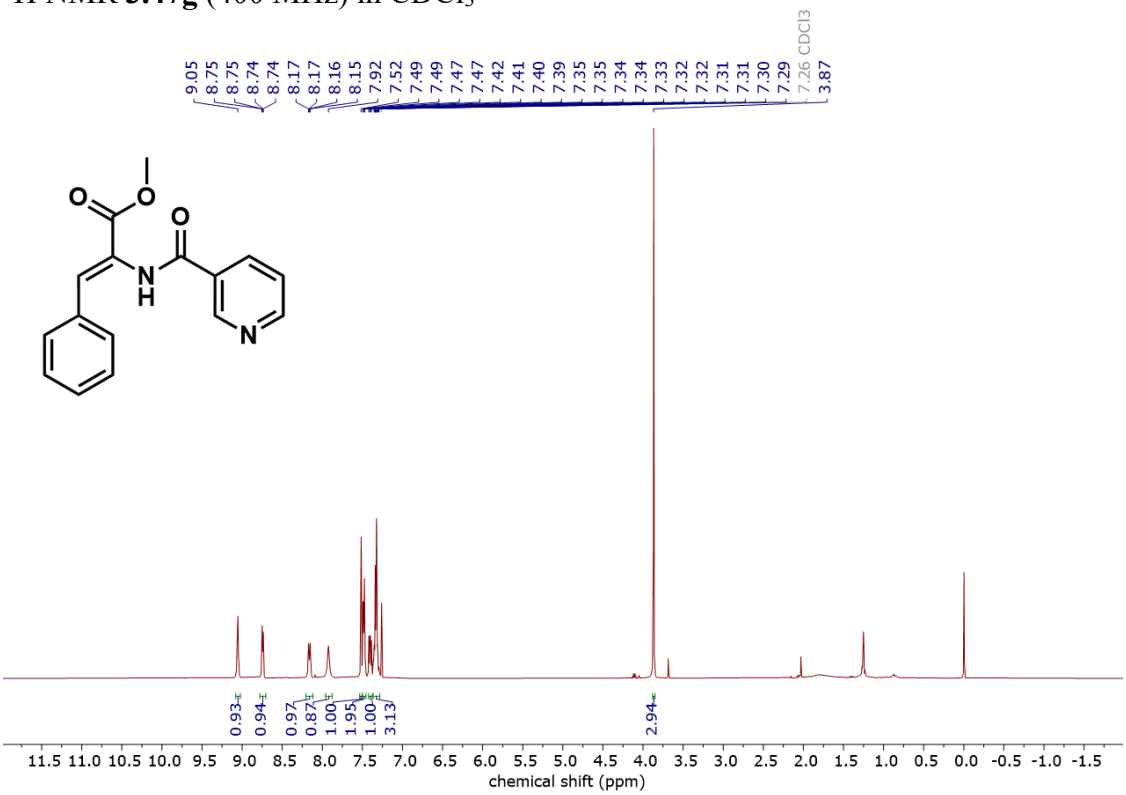

^{13}C NMR of **3.47g** (101 MHz) in $CDCl_3$

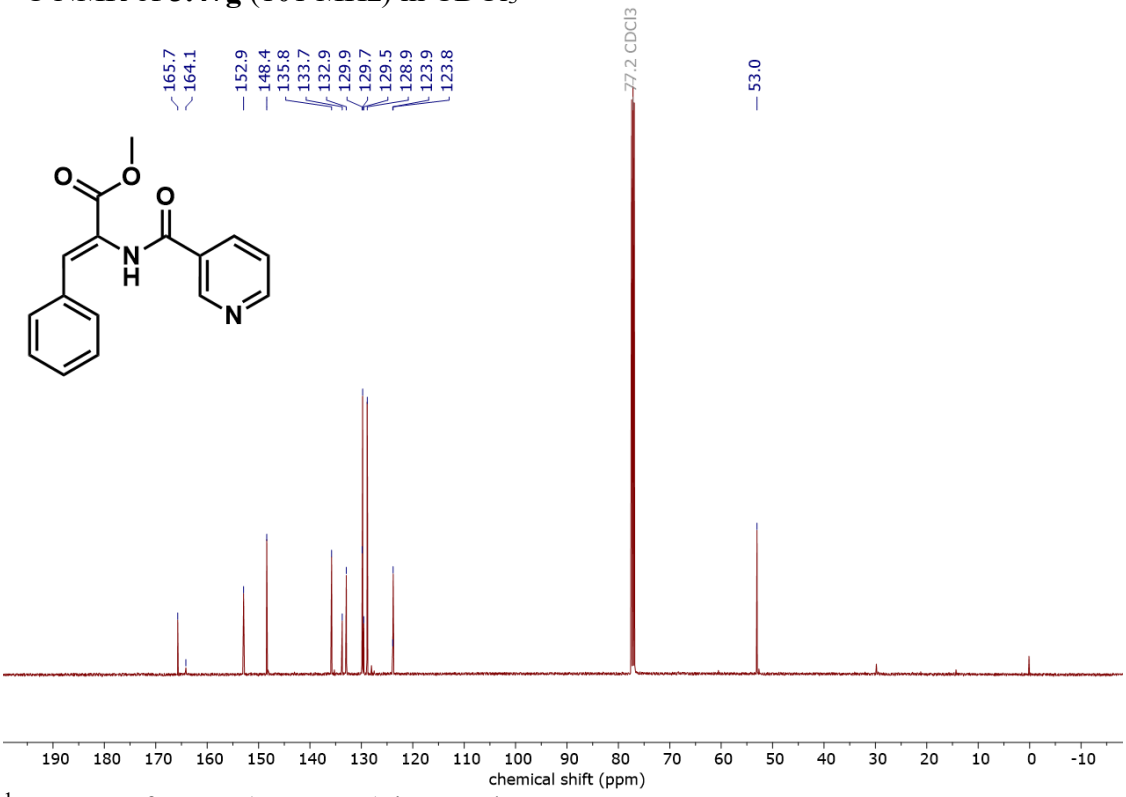

^{1}H NMR of **3.47h** (400 MHz) in $CDCl_3$

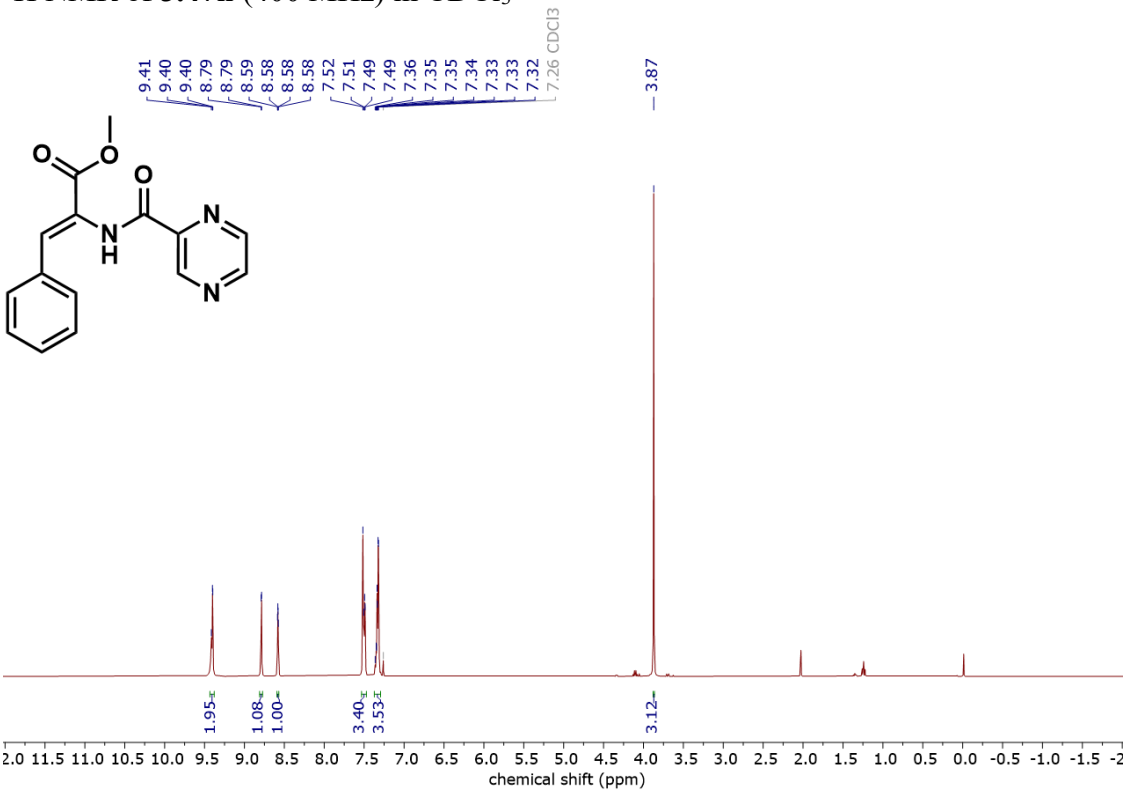

^{13}C NMR of **3.47h** (101 MHz) in $CDCl_3$

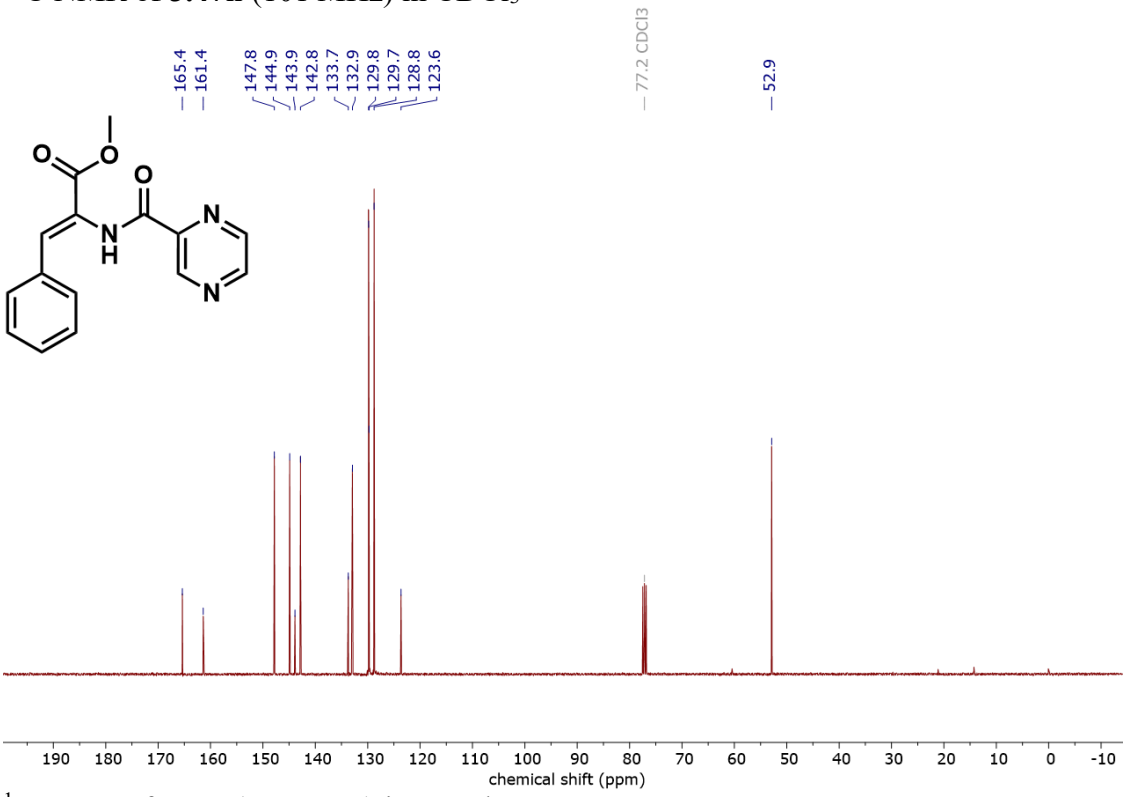

^{1}H NMR of **3.47i** (400 MHz) in $CDCl_3$

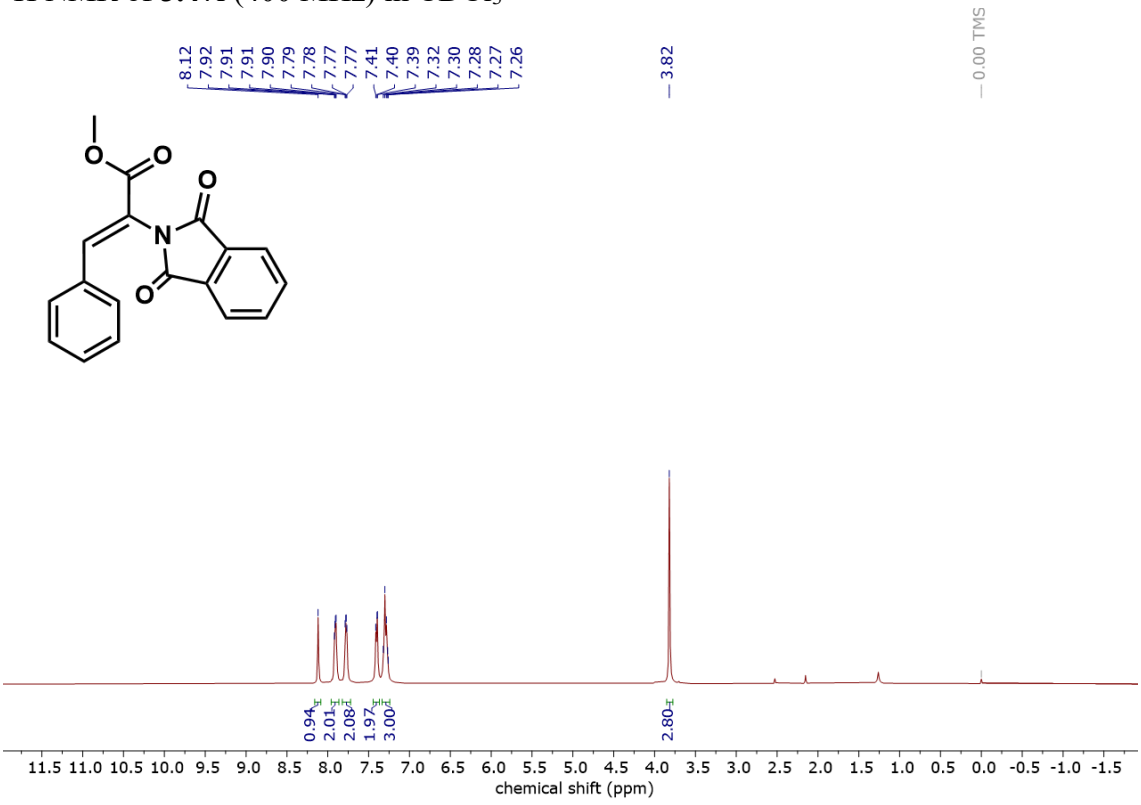

^{13}C NMR of **3.47i** (151 MHz) in $CDCl_3$

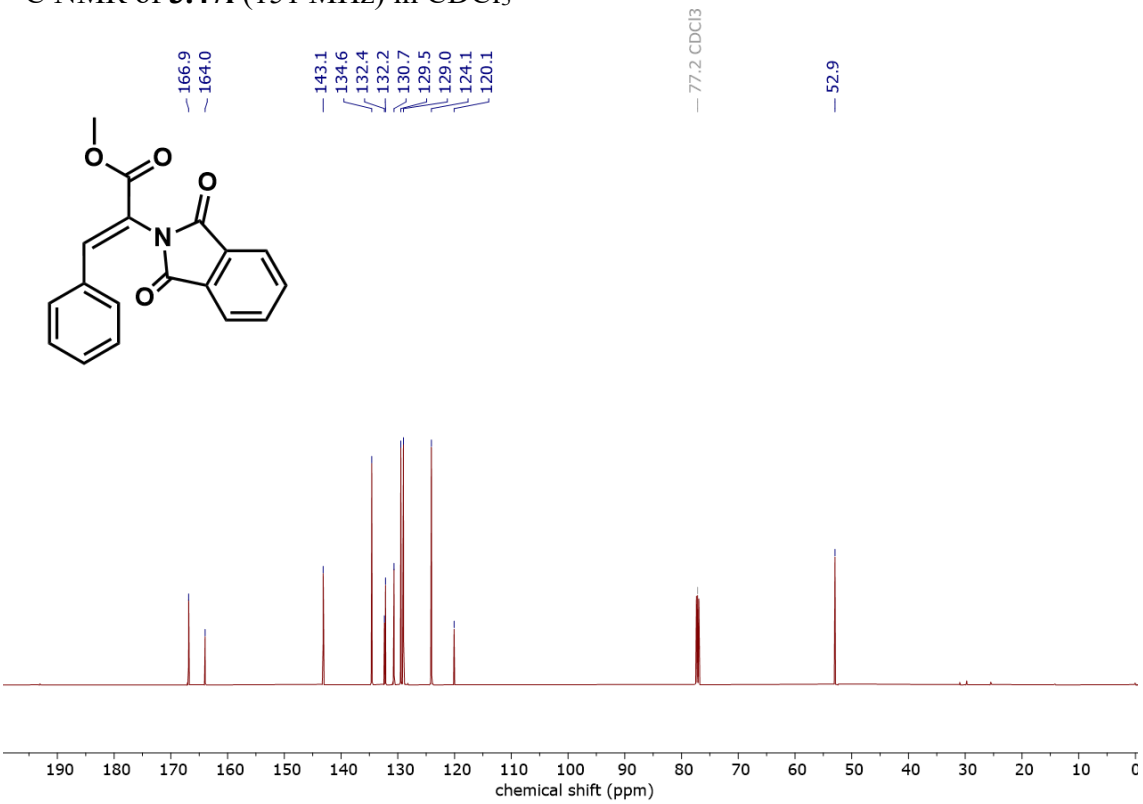

^{1}H NMR of **3.47j** (600 MHz) in $CDCl_3$

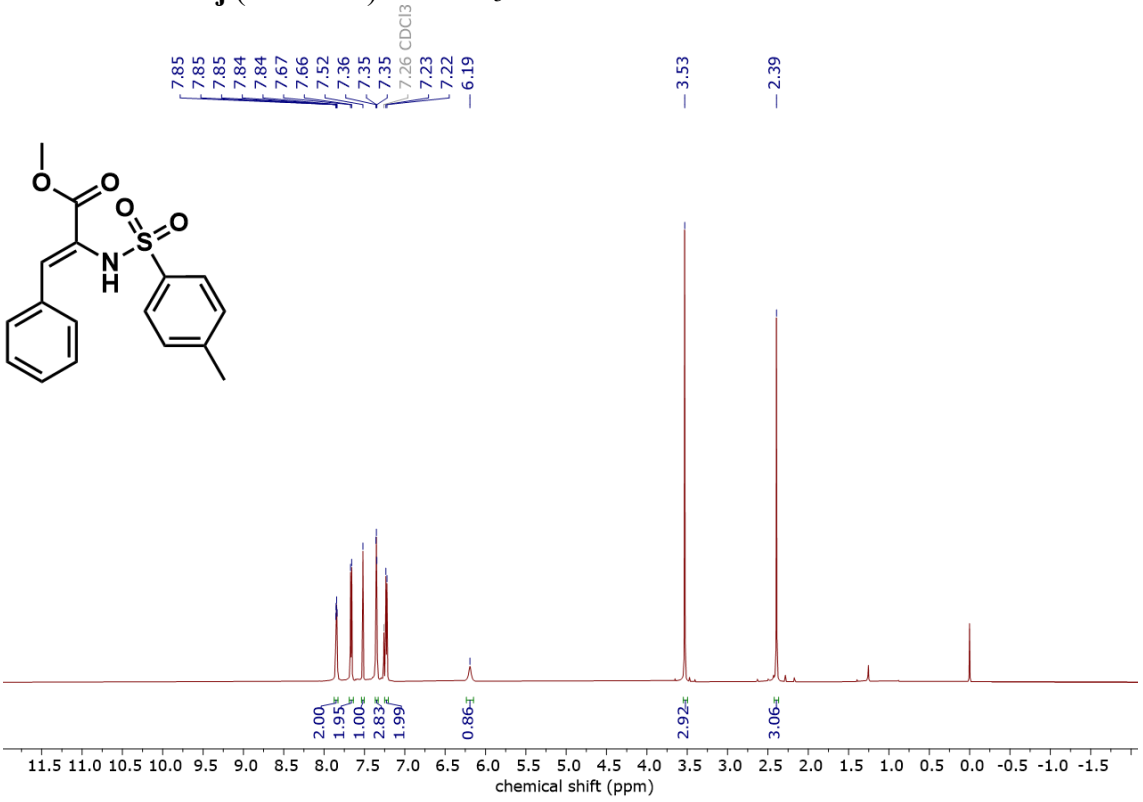

^{13}C NMR of **3.47j** (151 MHz) in $CDCl_3$

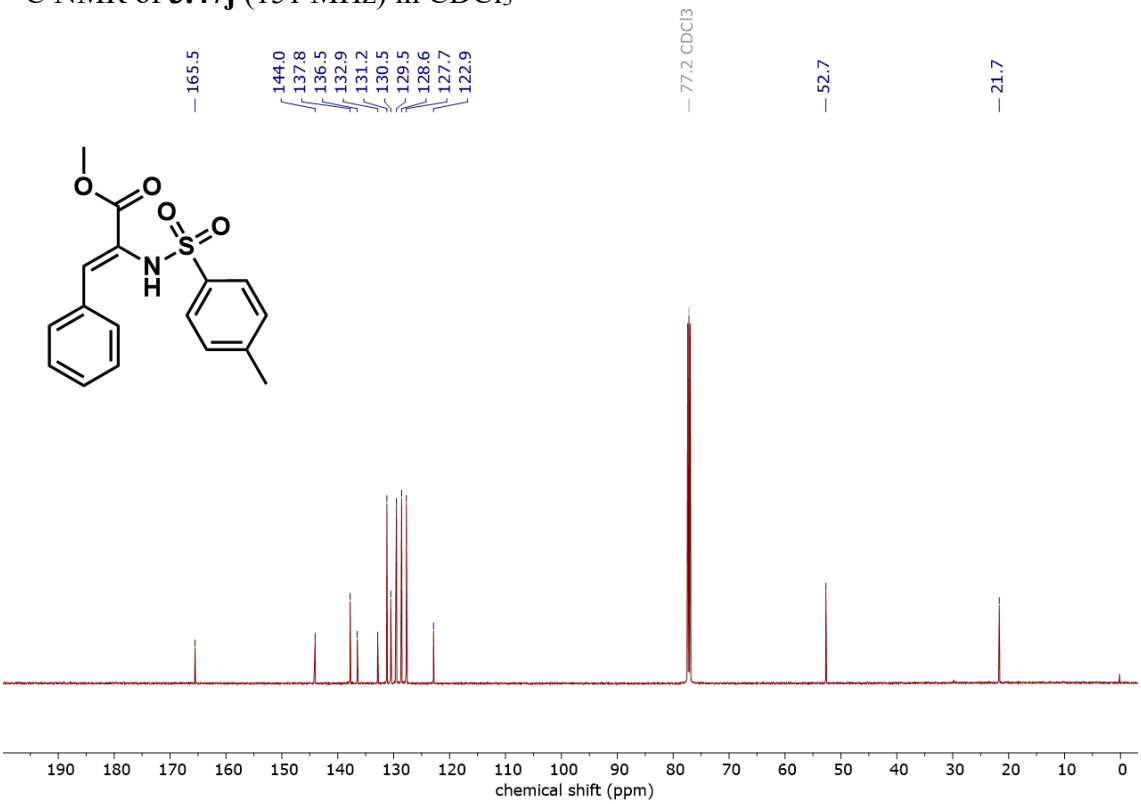

^{1}H NMR of **3.47k** (400 MHz) in $CDCl_3$

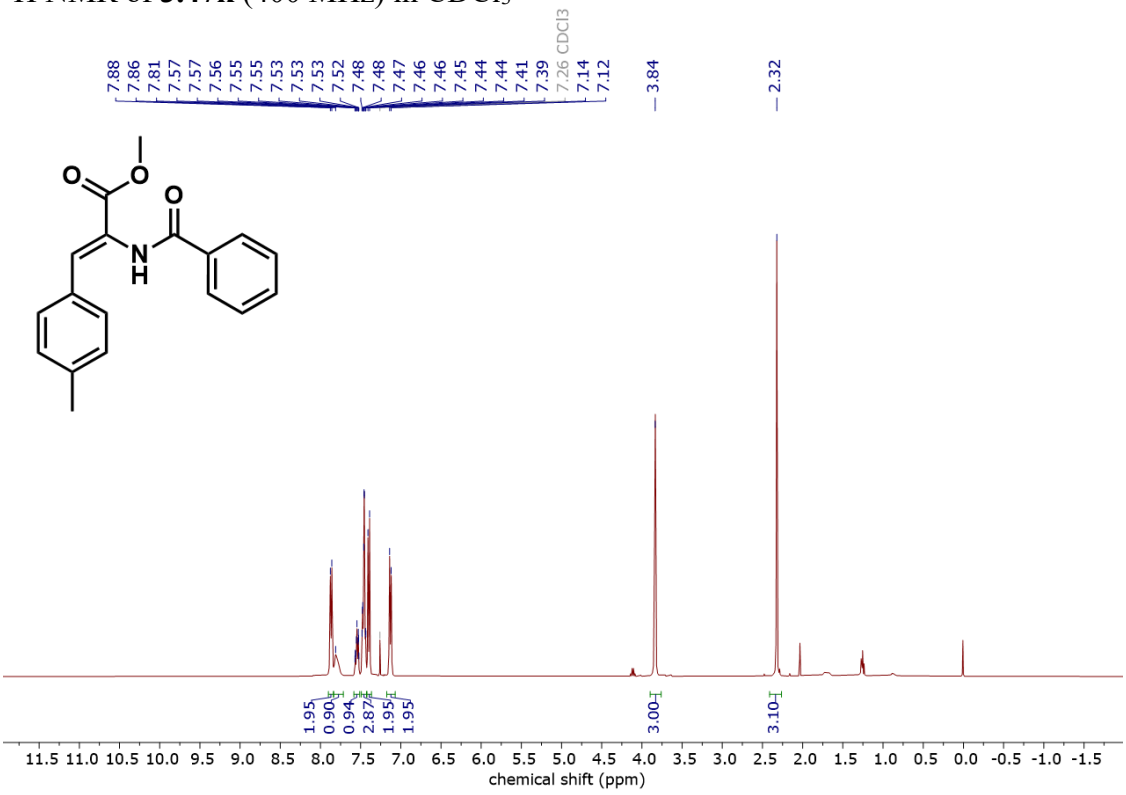

^{13}C NMR of **3.47k**(101 MHz) in $CDCl_3$

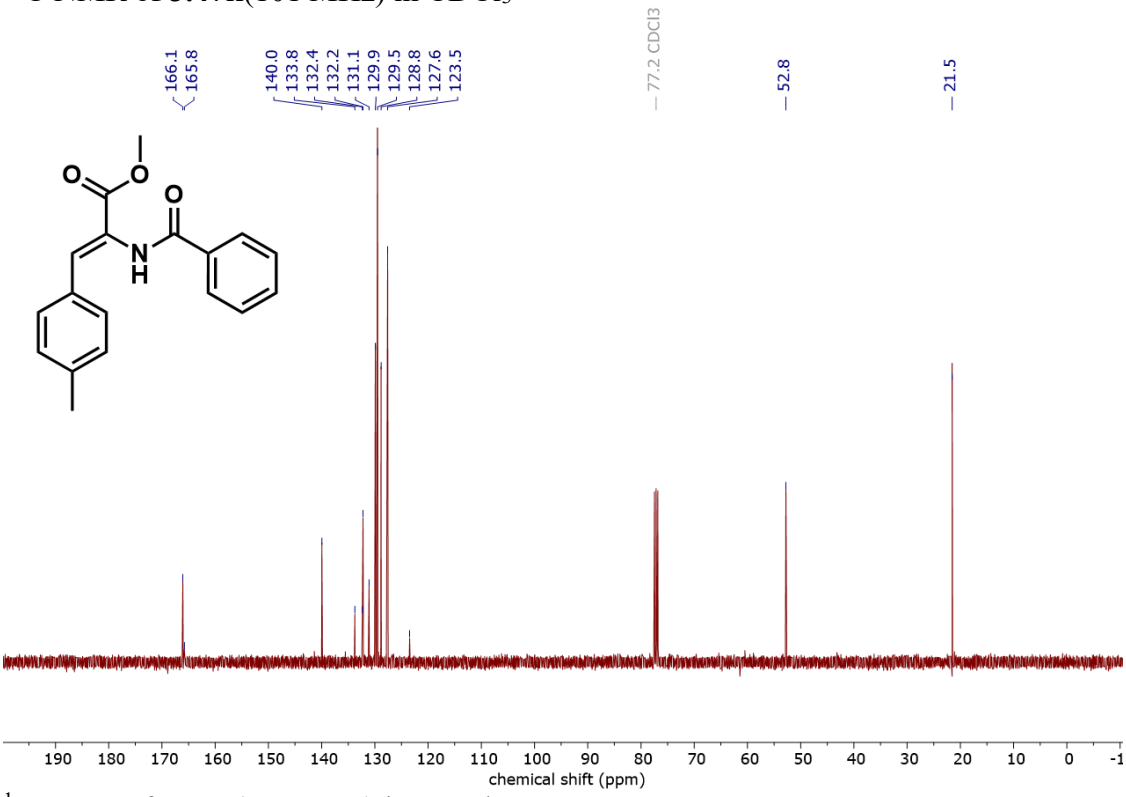

^{1}H NMR of **3.47l** (400 MHz) in $CDCl_3$

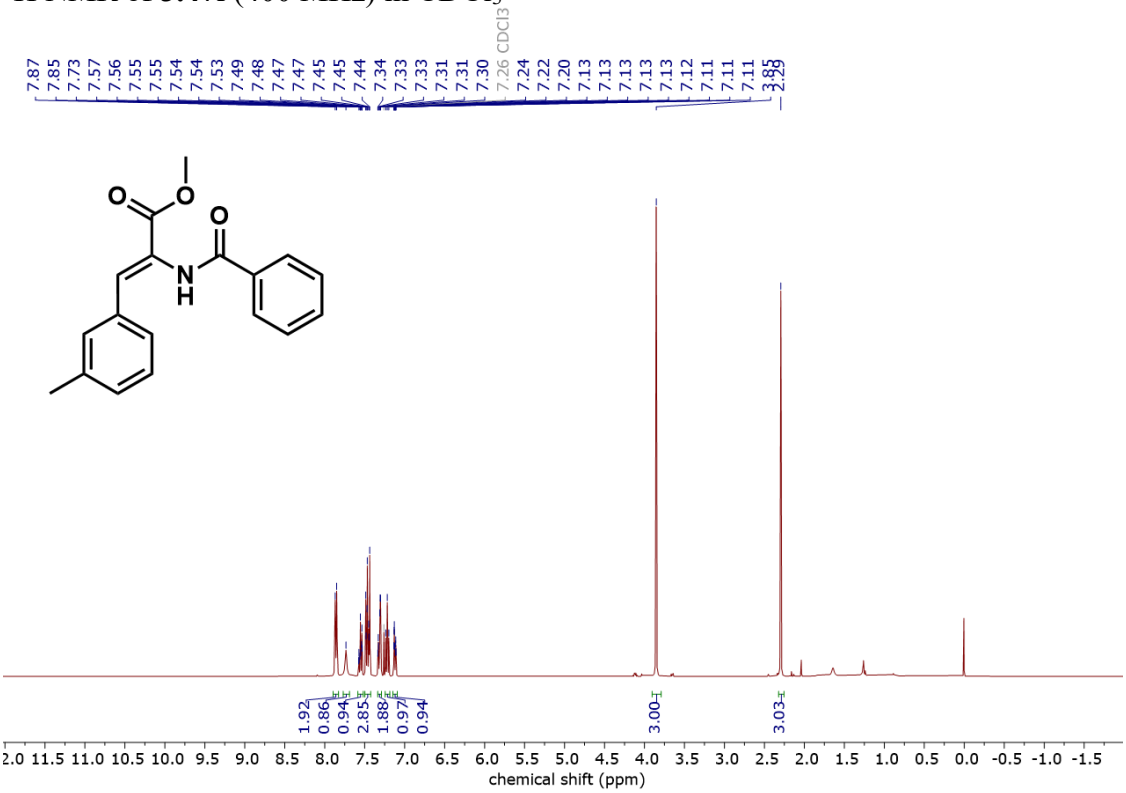

^{13}C NMR of **3.47l** (101MHz) in $CDCl_3$

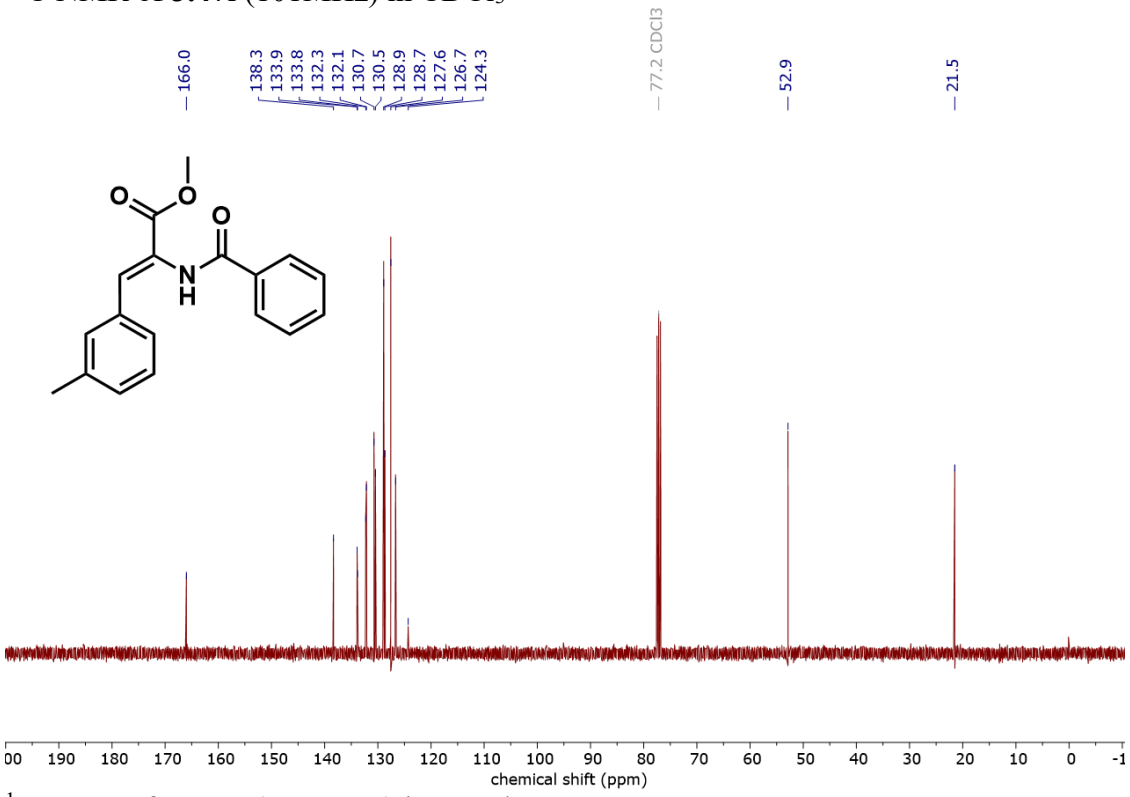

^{1}H NMR of **3.47m** (400 MHz) in $CDCl_3$

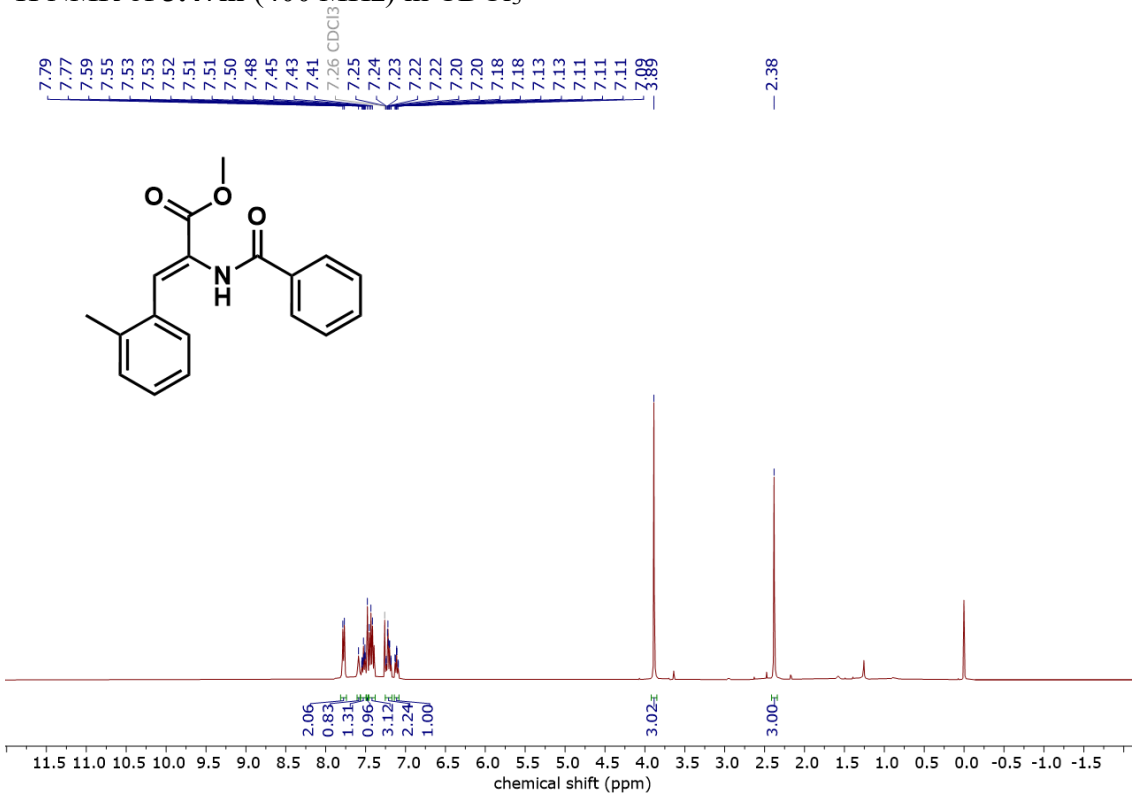

^{13}C NMR of **3.47m** (101 MHz) in $CDCl_3$

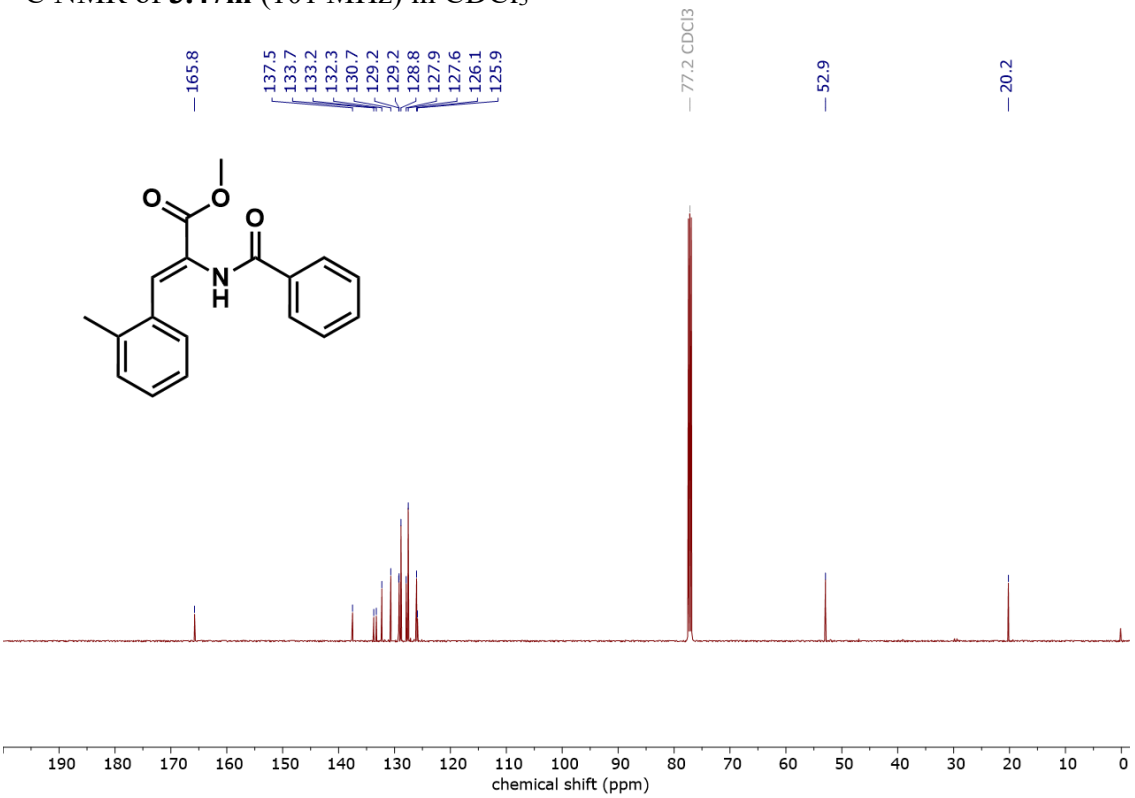

^{1}H NMR of **3.47n** (400 MHz) in $CDCl_3$

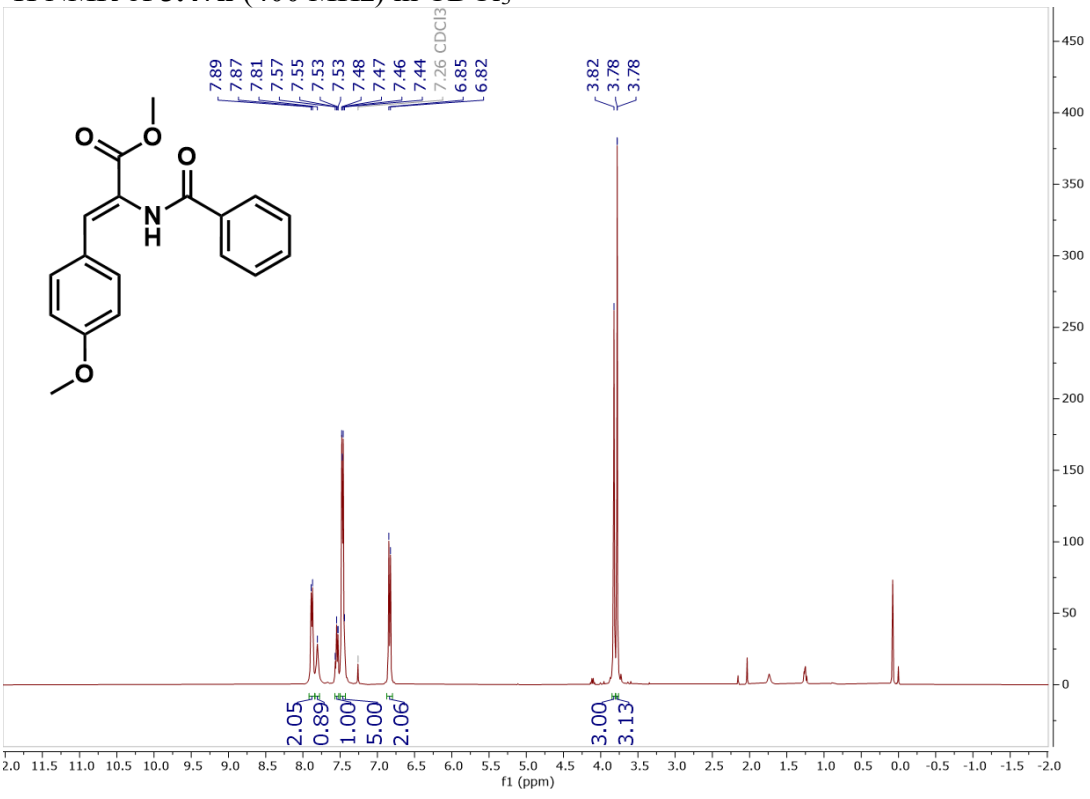

^{13}C NMR of **3.47n** (101 MHz) in $CDCl_3$

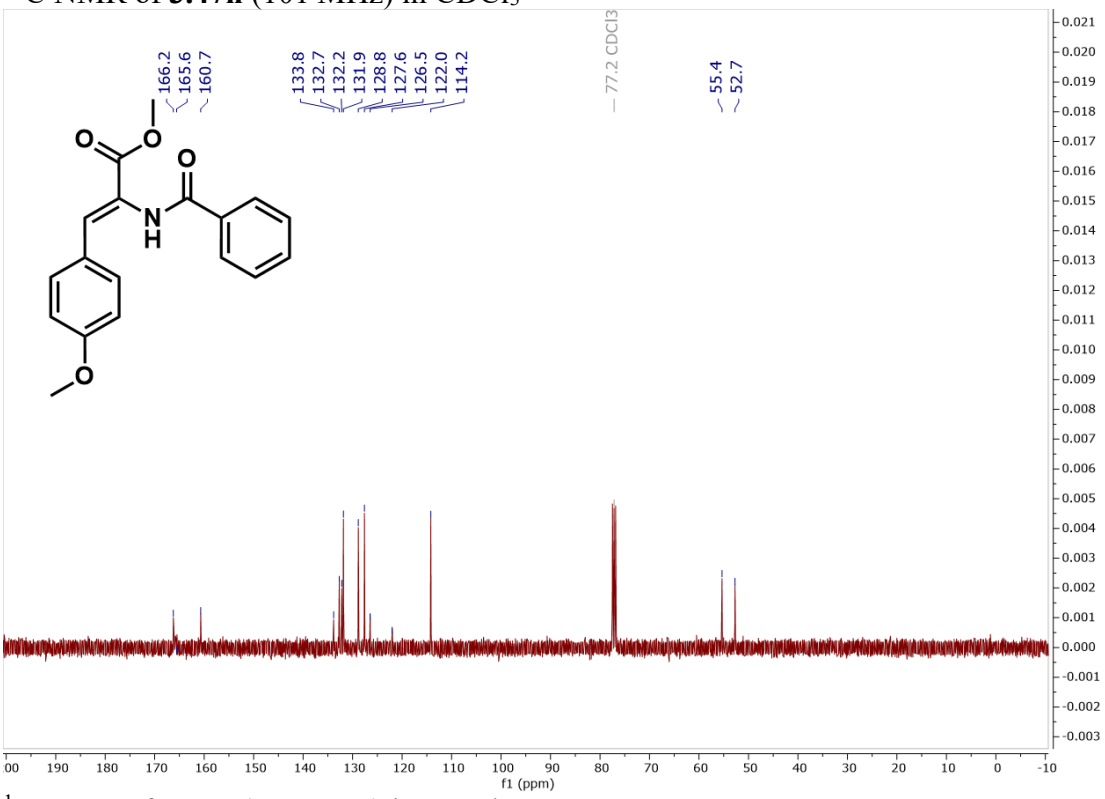

^{1}H NMR of **3.47o** (400 MHz) in $CDCl_3$

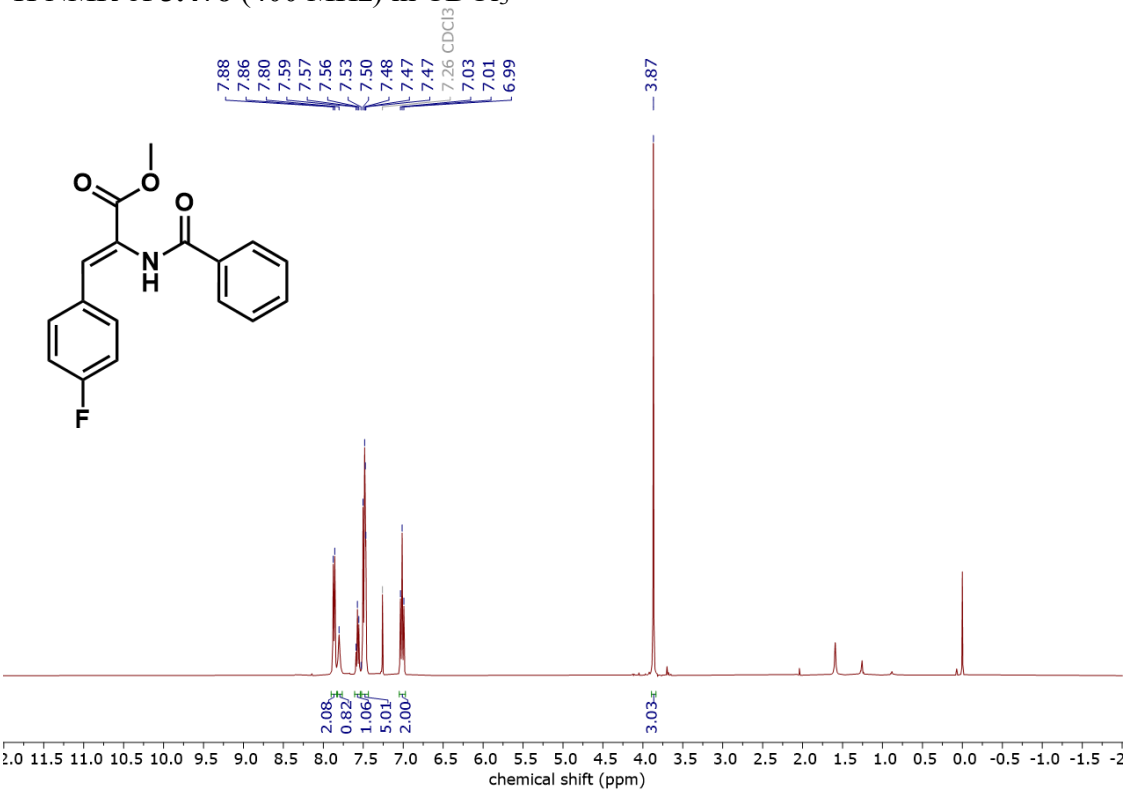

^{13}C NMR of **3.47o** (101 MHz) in $CDCl_3$

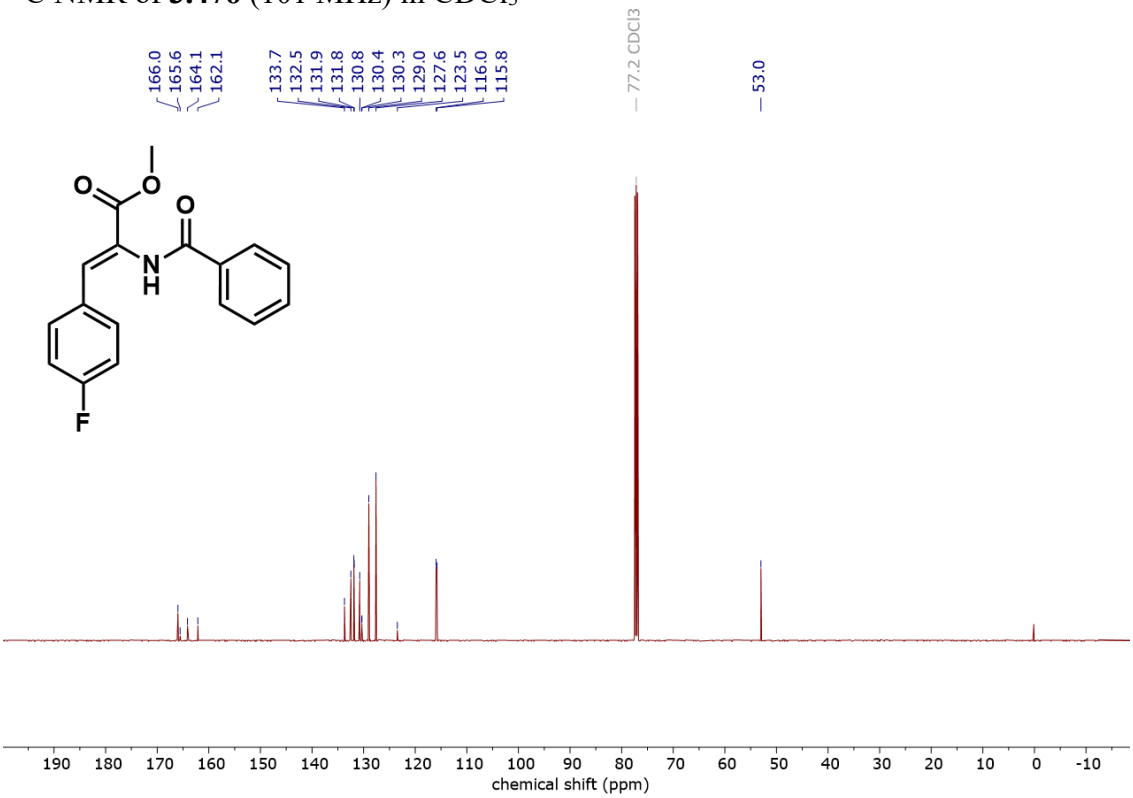

^{19}F NMR of **3.47o** (376 MHz) in $CDCl_3$

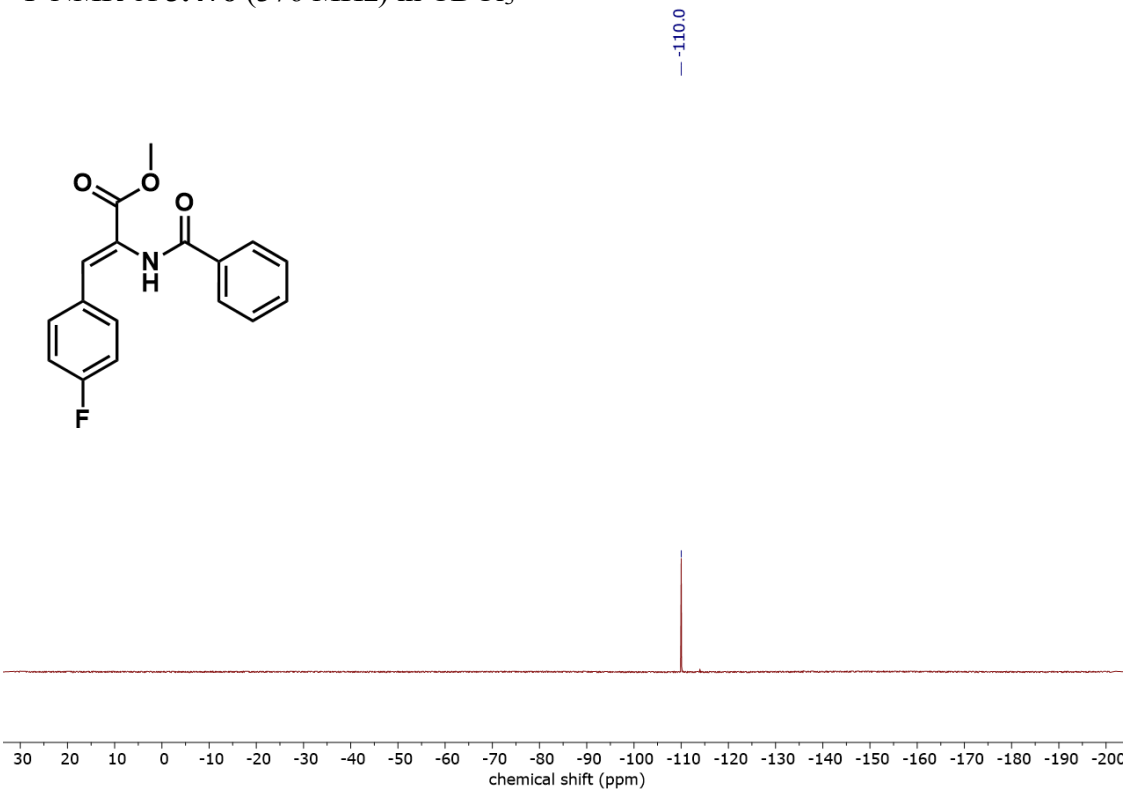

^{1}H NMR of **3.47p** (400 MHz) in $CDCl_3$

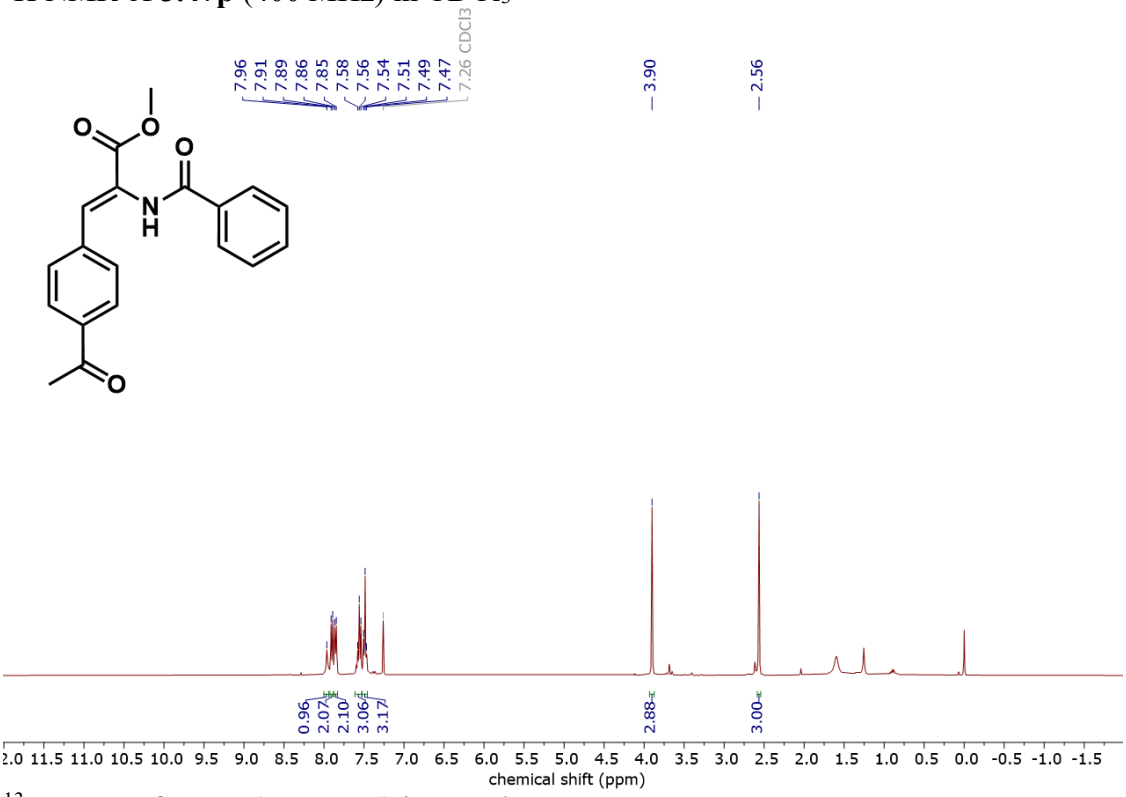

^{13}C NMR of **3.47p** (101 MHz) in $CDCl_3$

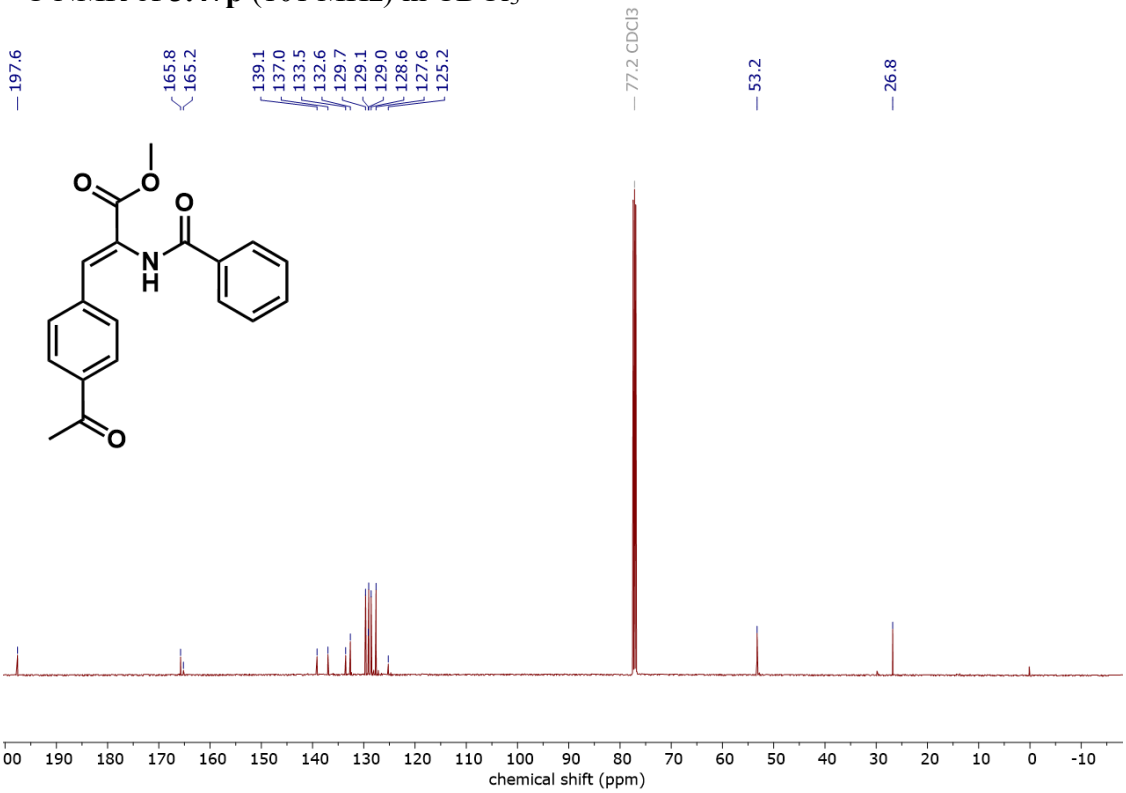

^{1}H NMR of **3.47q** (400 MHz) in $CDCl_3$

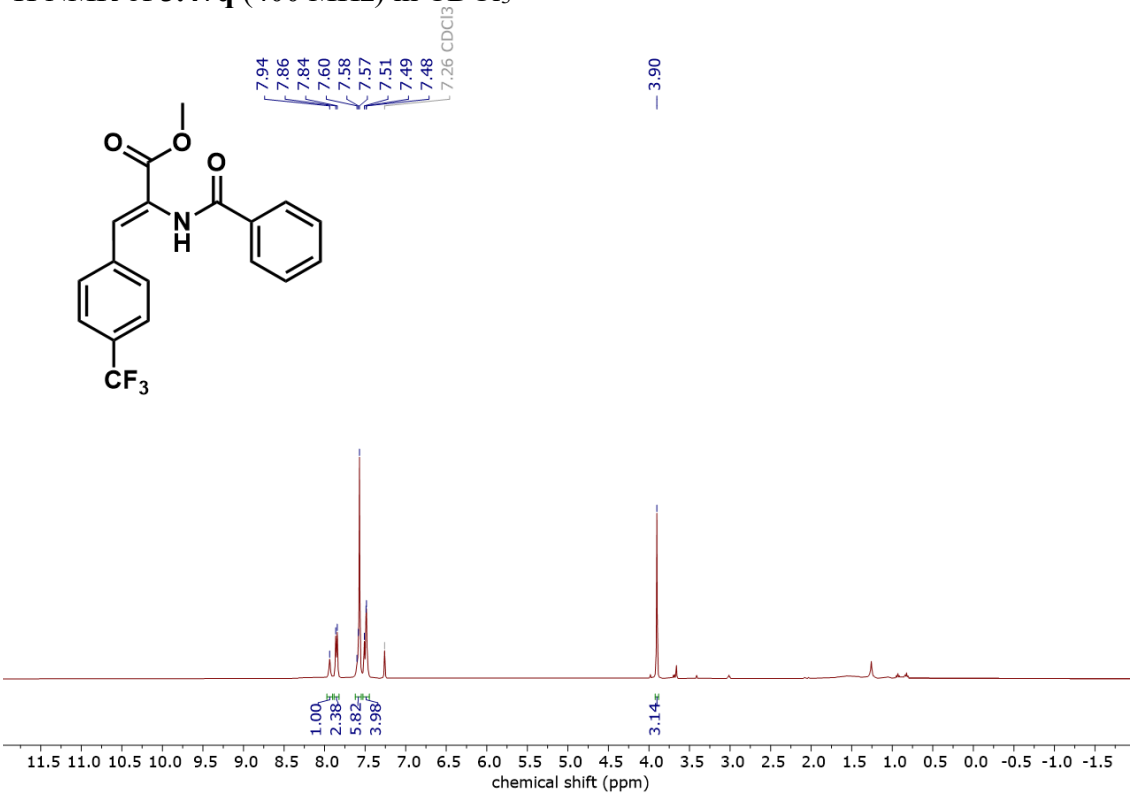

^{13}C NMR of **3.47q** (126 MHz) in $CDCl_3$

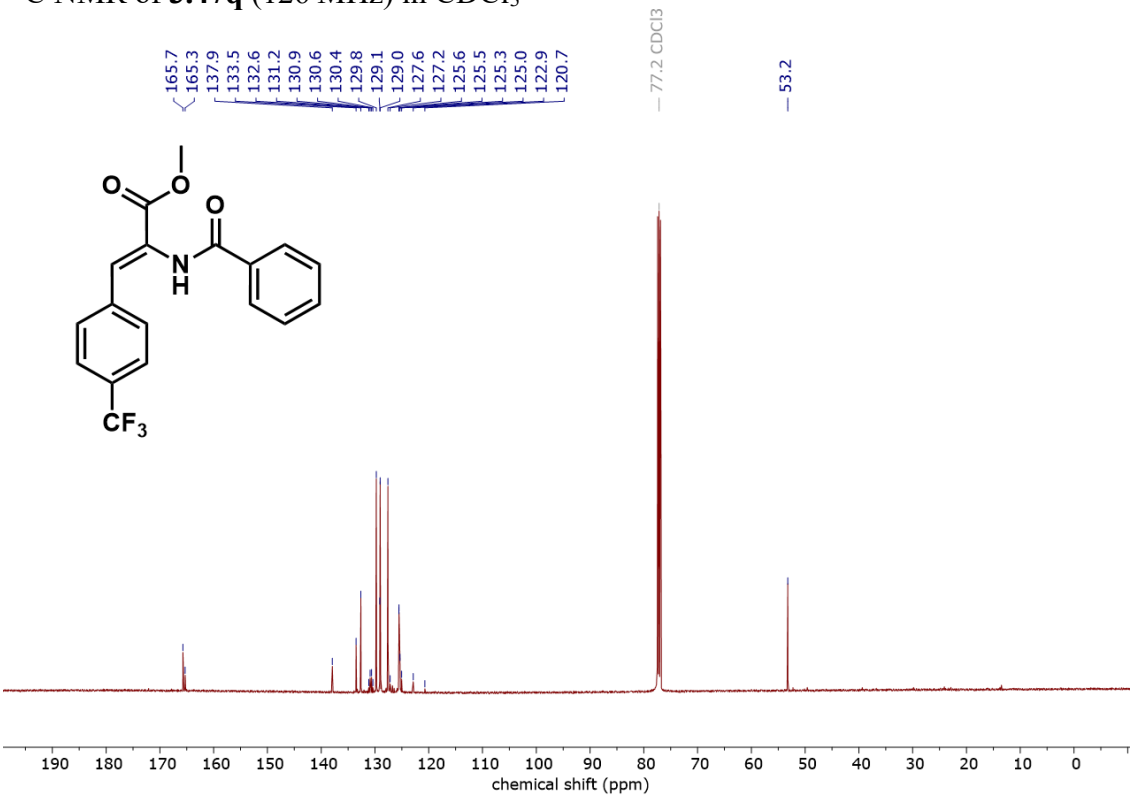

^{19}F NMR of **3.47q** (376 MHz) in $CDCl_3$

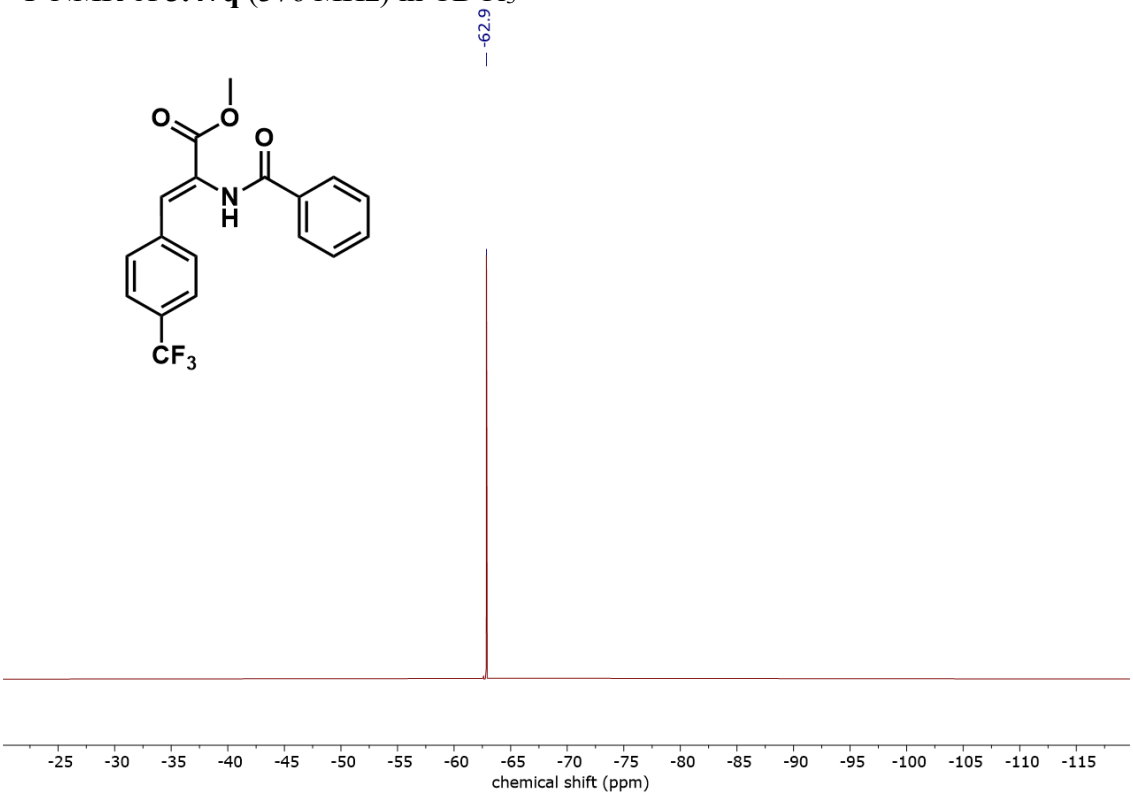

^{1}H NMR of **3.47r** (400 MHz) in $CDCl_3$

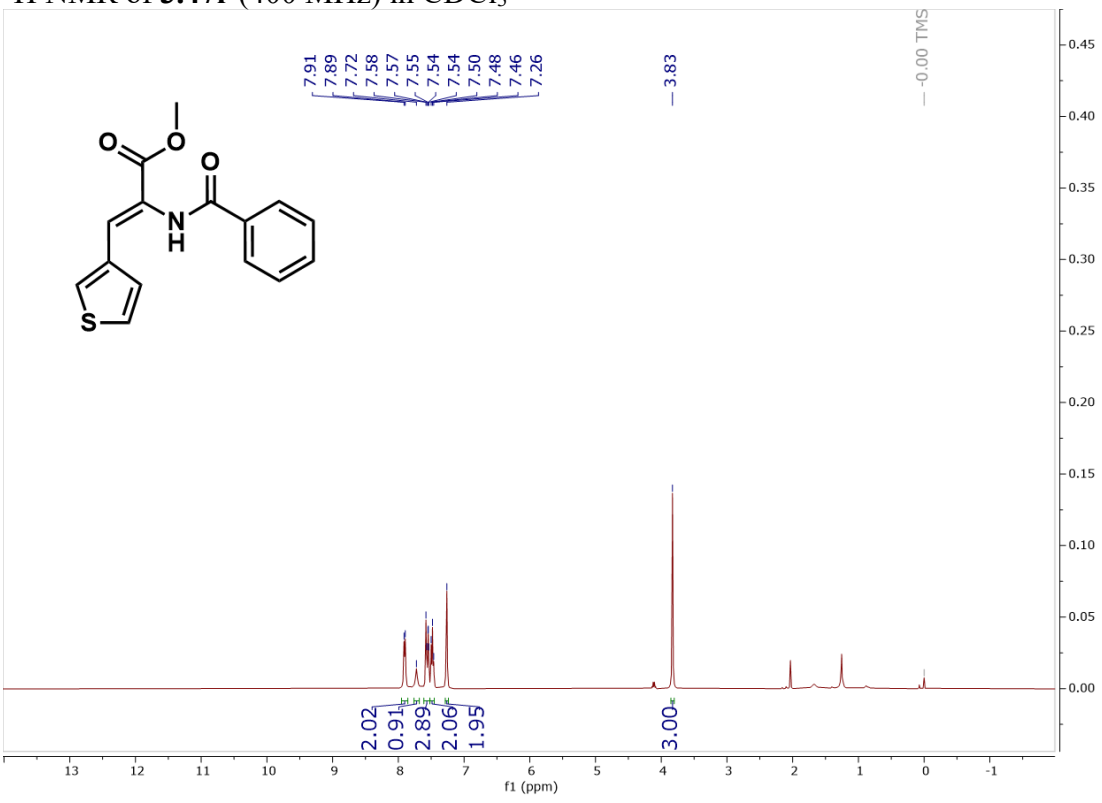

^{13}C NMR of **3.47r** (126 MHz) in $CDCl_3$

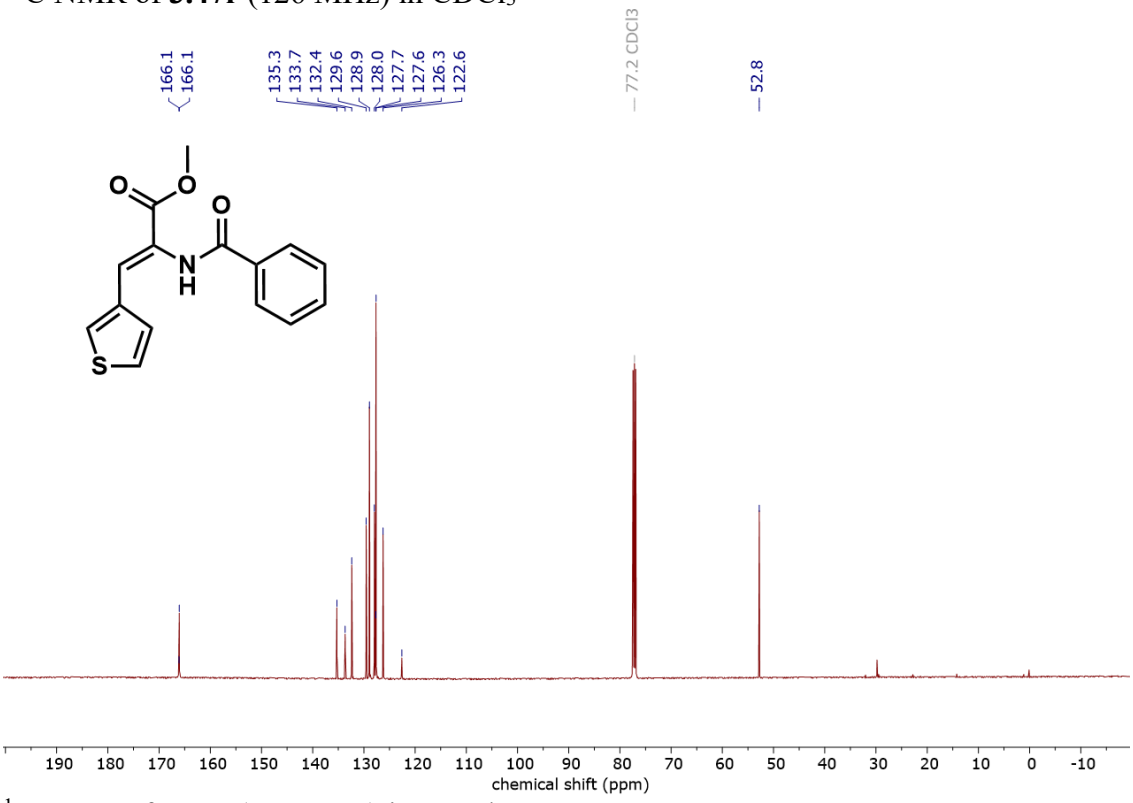

^{1}H NMR of **3.47s** (500 MHz) in $CDCl_3$

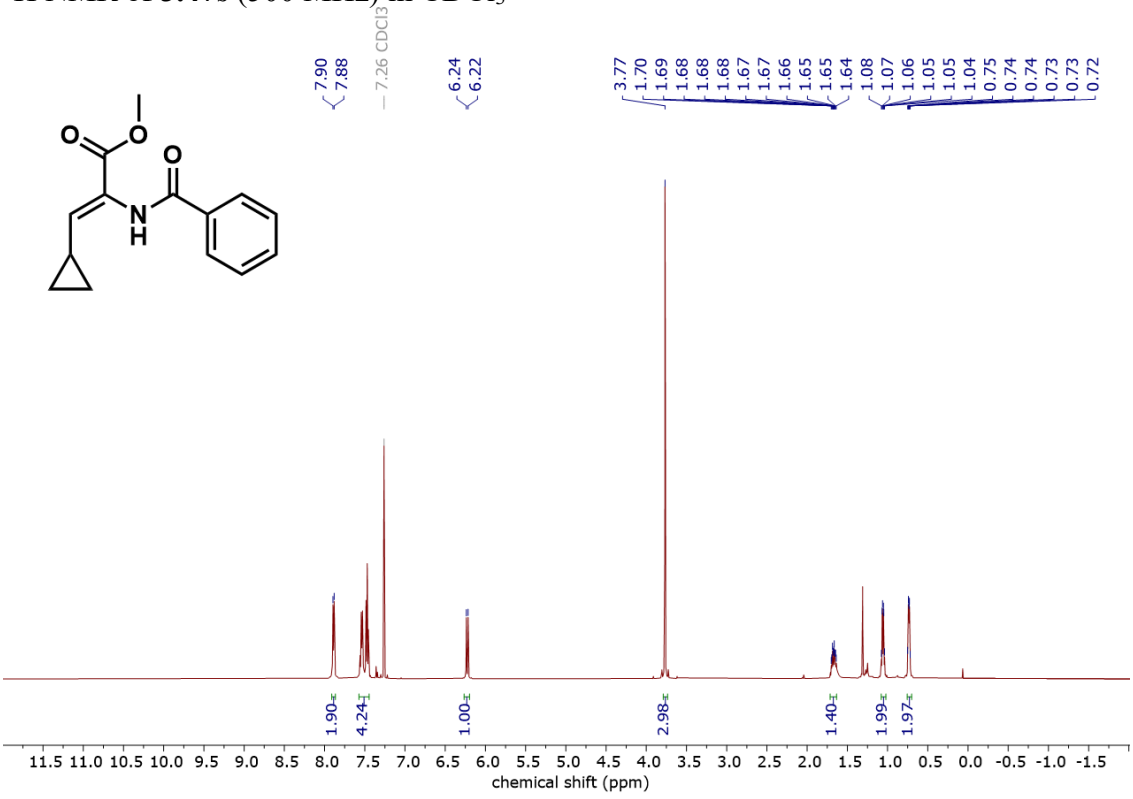

^{13}C NMR of **3.47s** (126 MHz) in $CDCl_3$

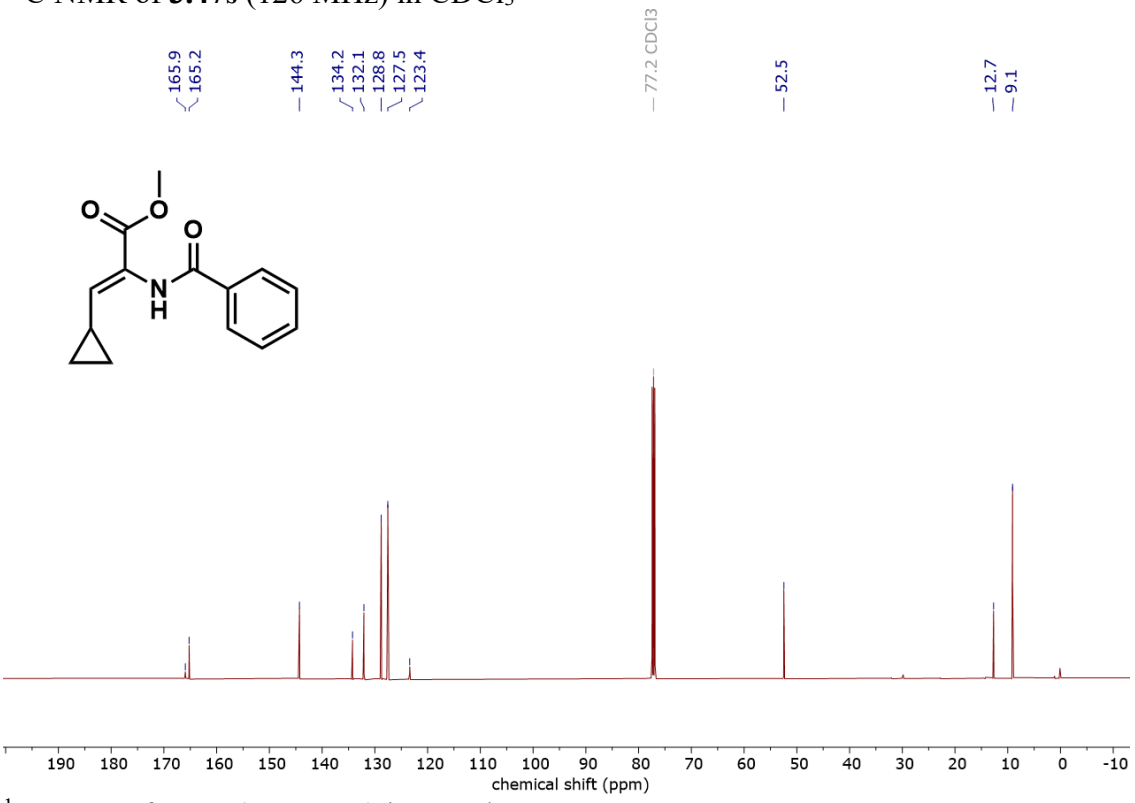

^{1}H NMR of **3.47t** (400 MHz) in $CDCl_3$

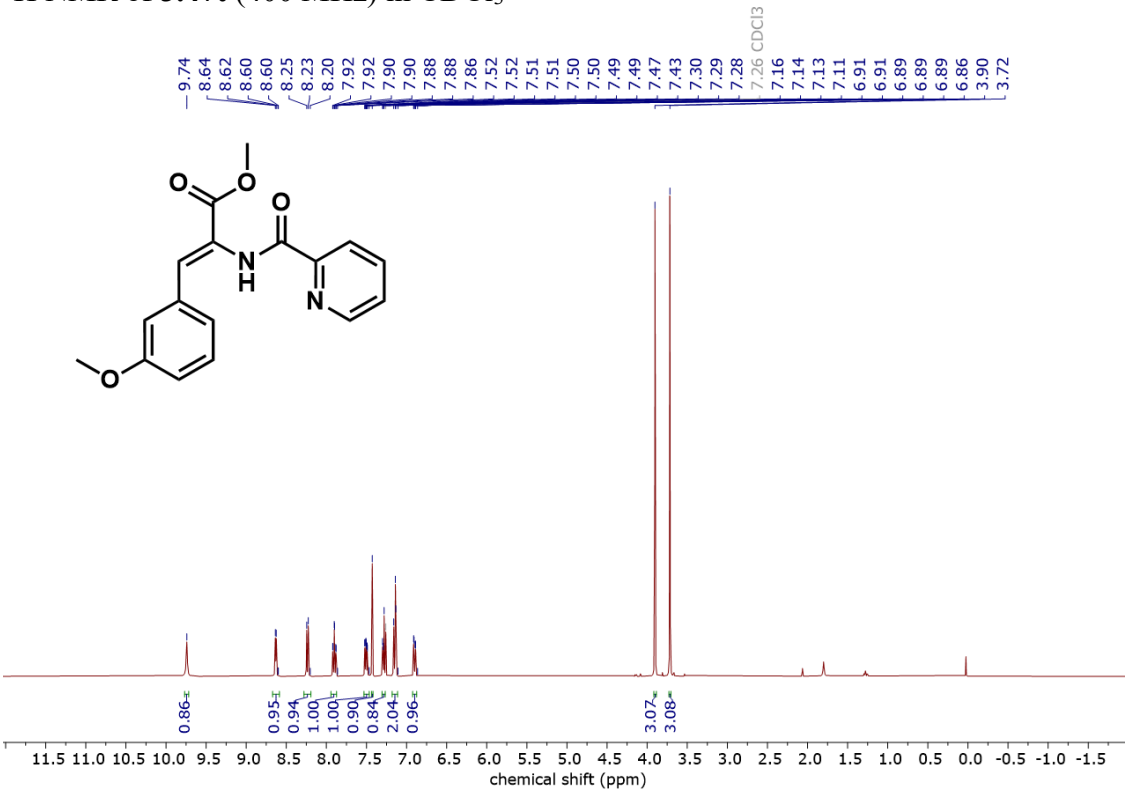

^{13}C NMR of **3.47t** (101 MHz) in $CDCl_3$

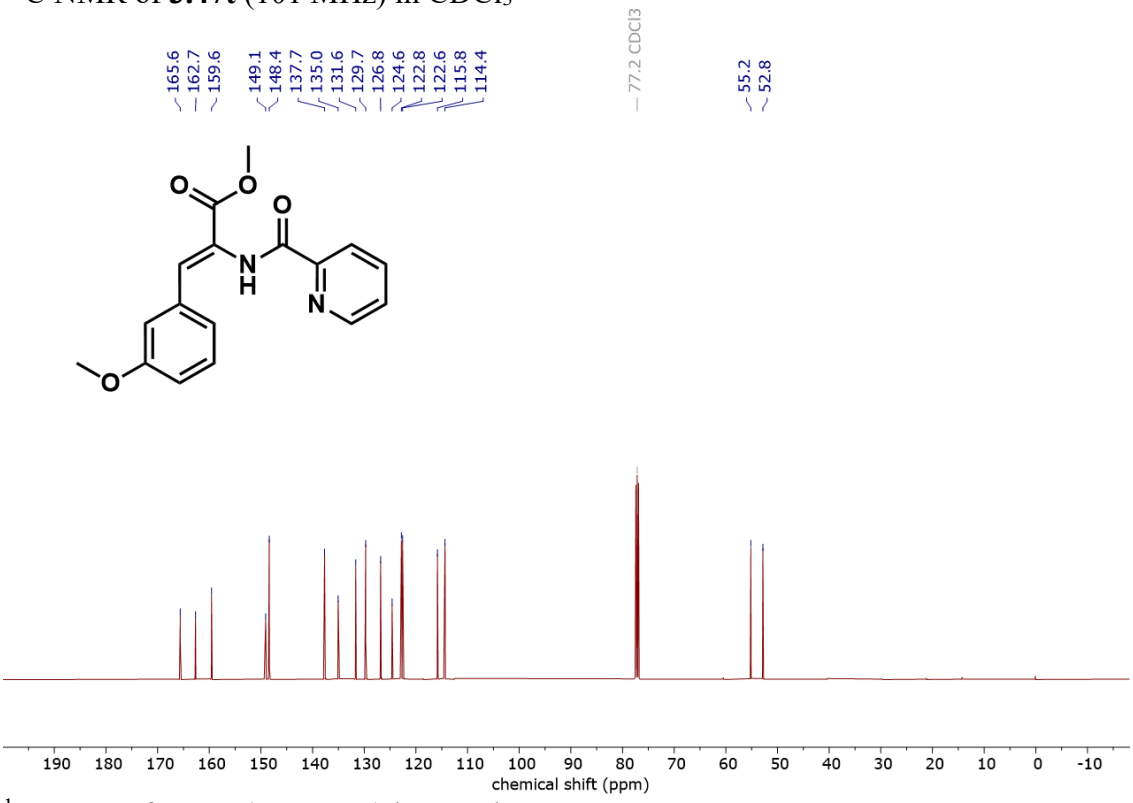

^{1}H NMR of **3.47u** (400 MHz) in $CDCl_3$

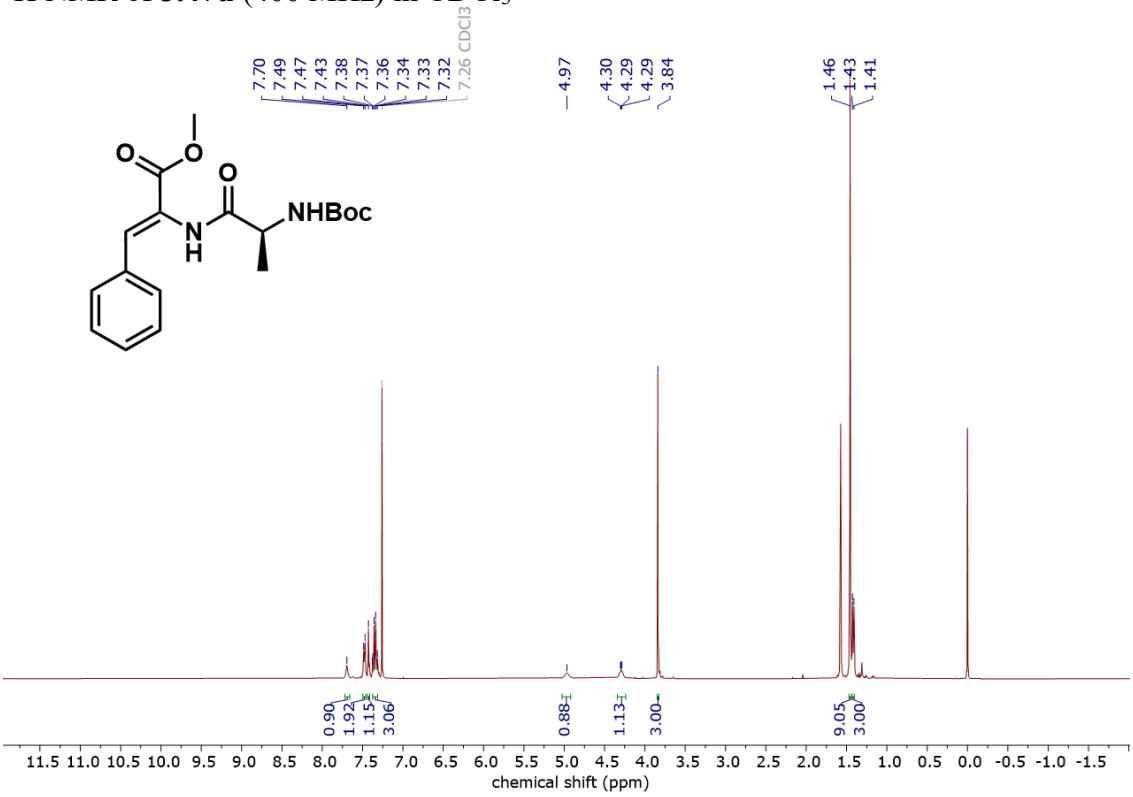

^{13}C NMR of **3.47u** (101 MHz) in $CDCl_3$

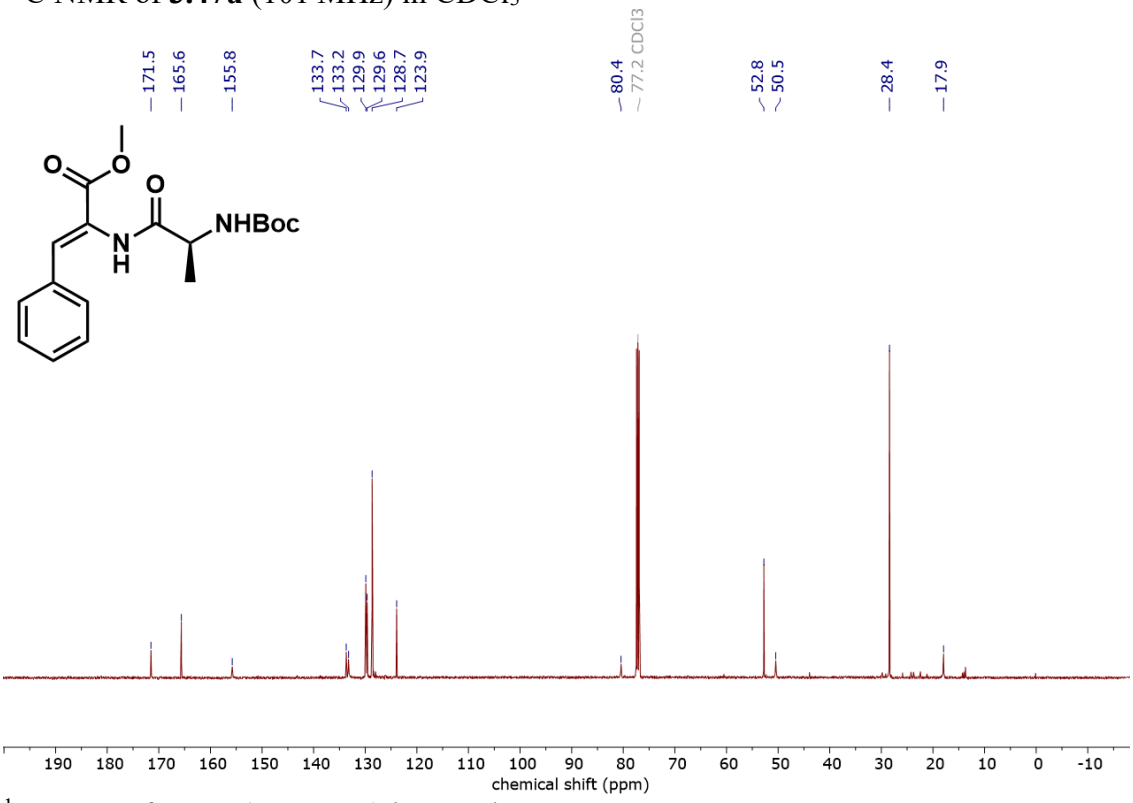

^{1}H NMR of **3.47v** (400 MHz) in $CDCl_3$

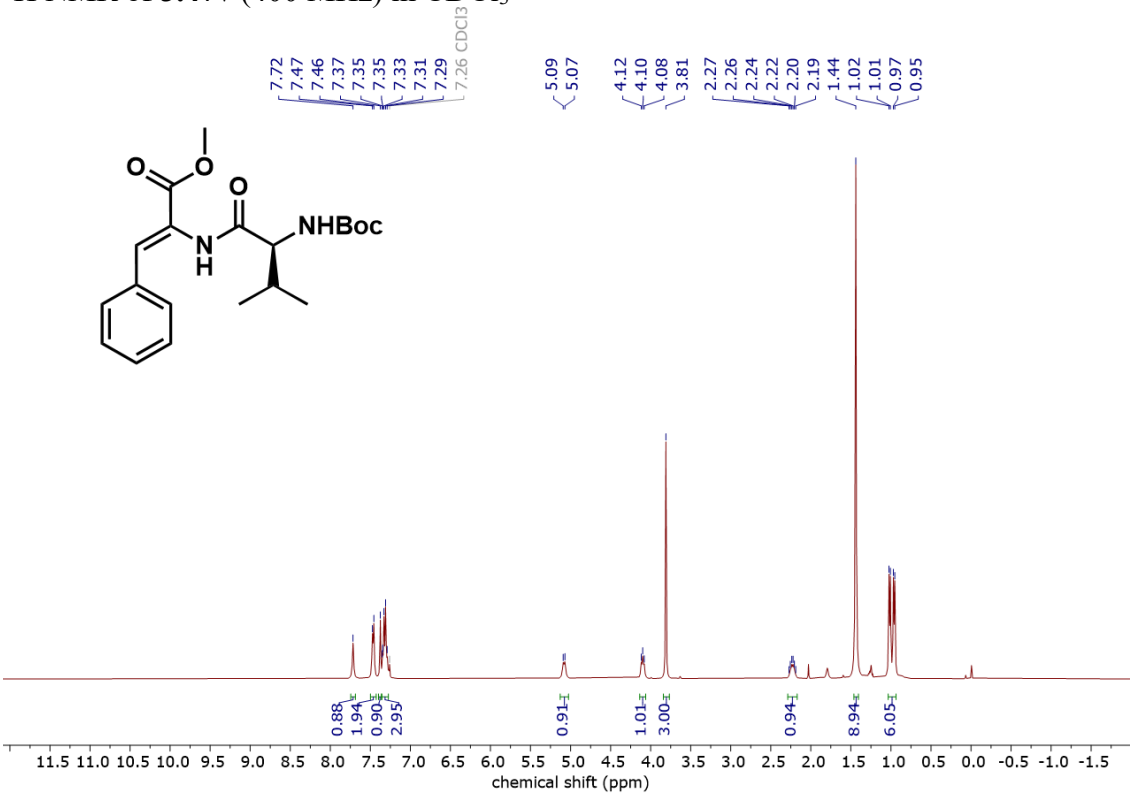

^{13}C NMR of **3.47v** (101 MHz) in $CDCl_3$

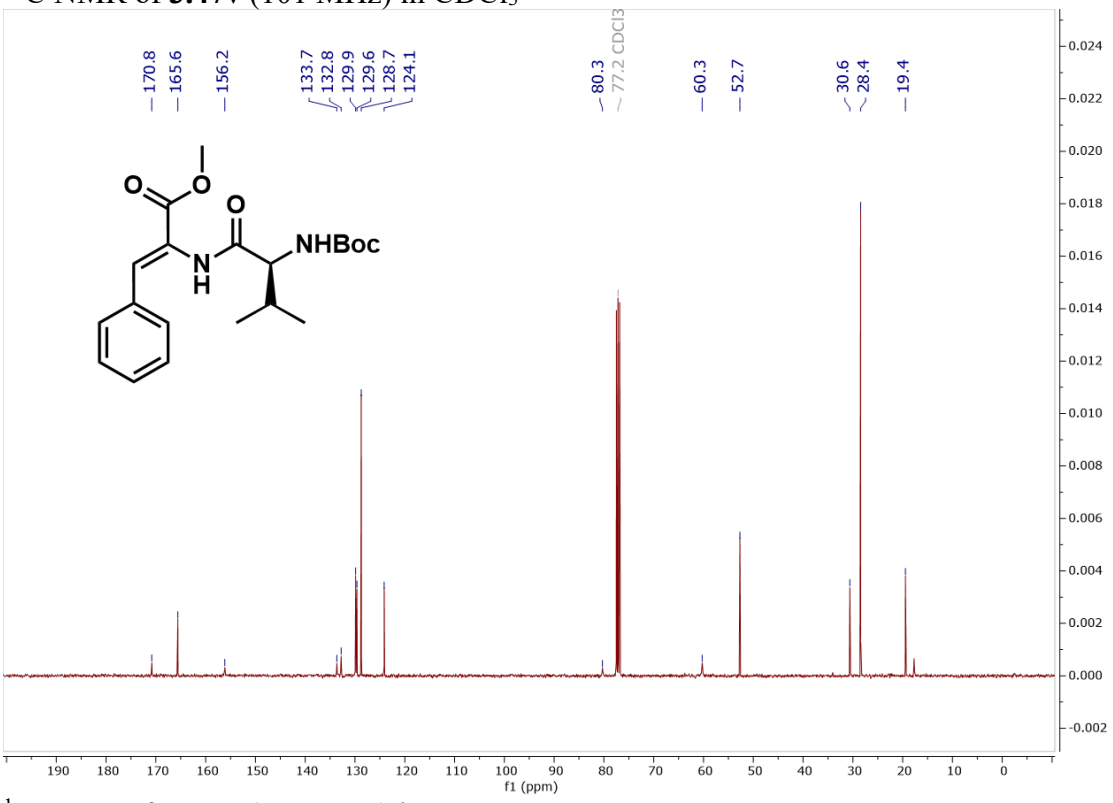

^{1}H NMR of **3.47w** (400 MHz) in CD_3OD

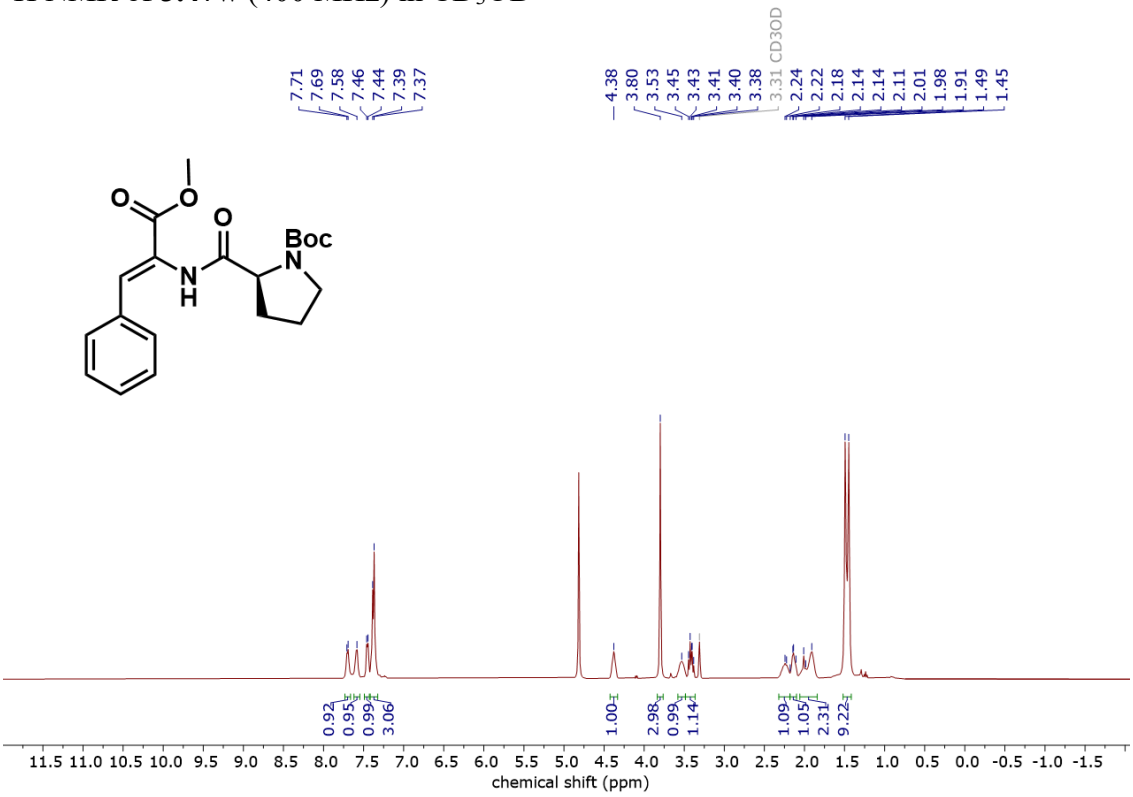

^{13}C NMR of **3.47w** (101 MHz) in CD_3OD

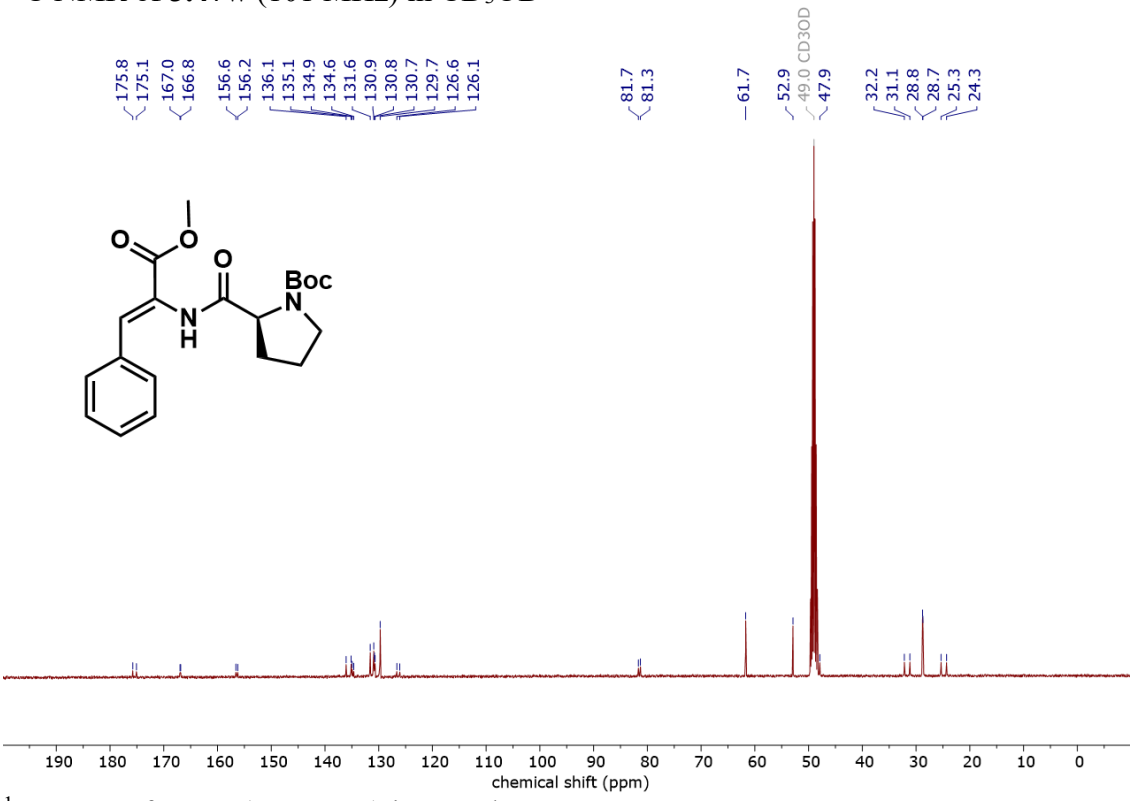

^{1}H NMR of **3.47x** (500 MHz) in $CDCl_3$

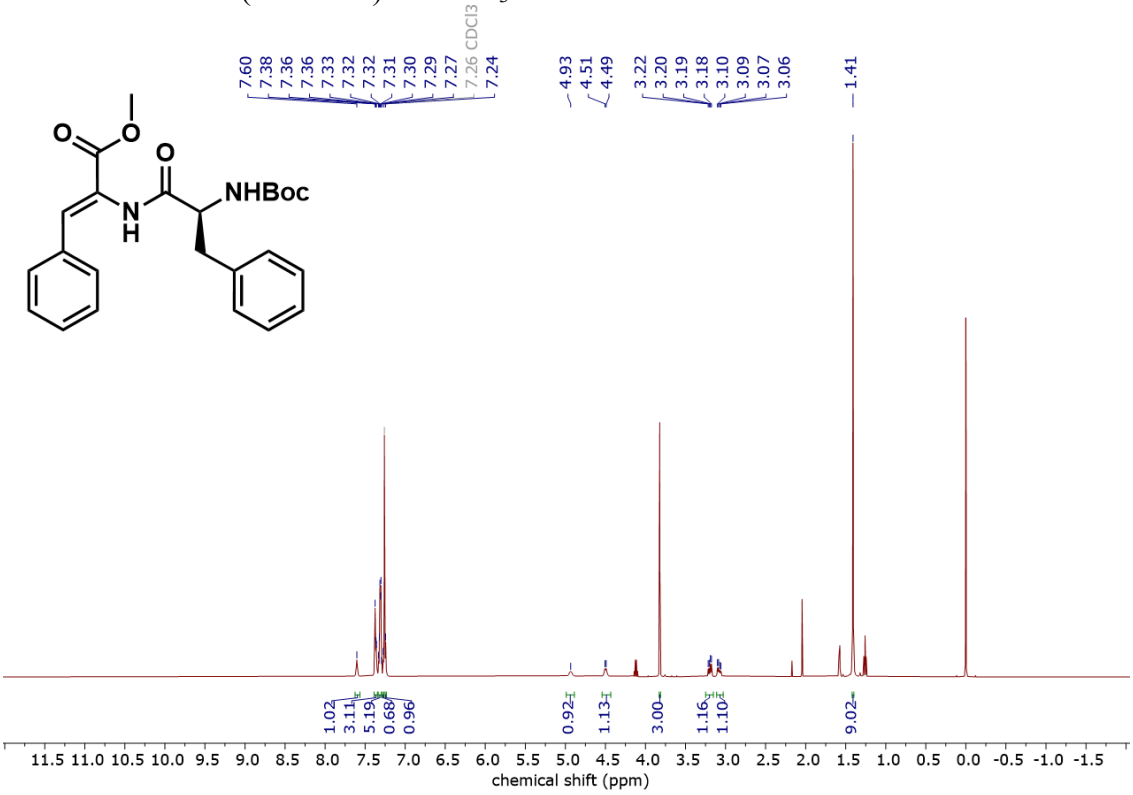

^{13}C NMR of **3.47x** (126 MHz) in $CDCl_3$

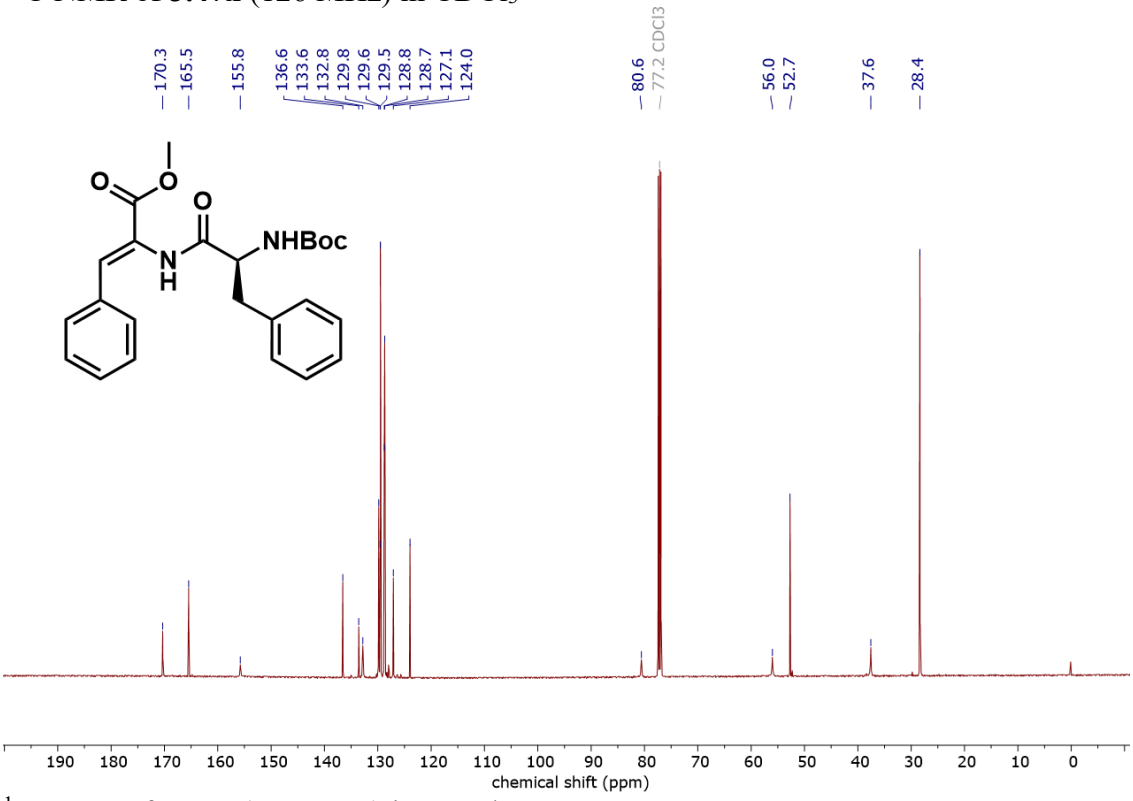

^{1}H NMR of **3.47y** (400 MHz) in $CDCl_3$

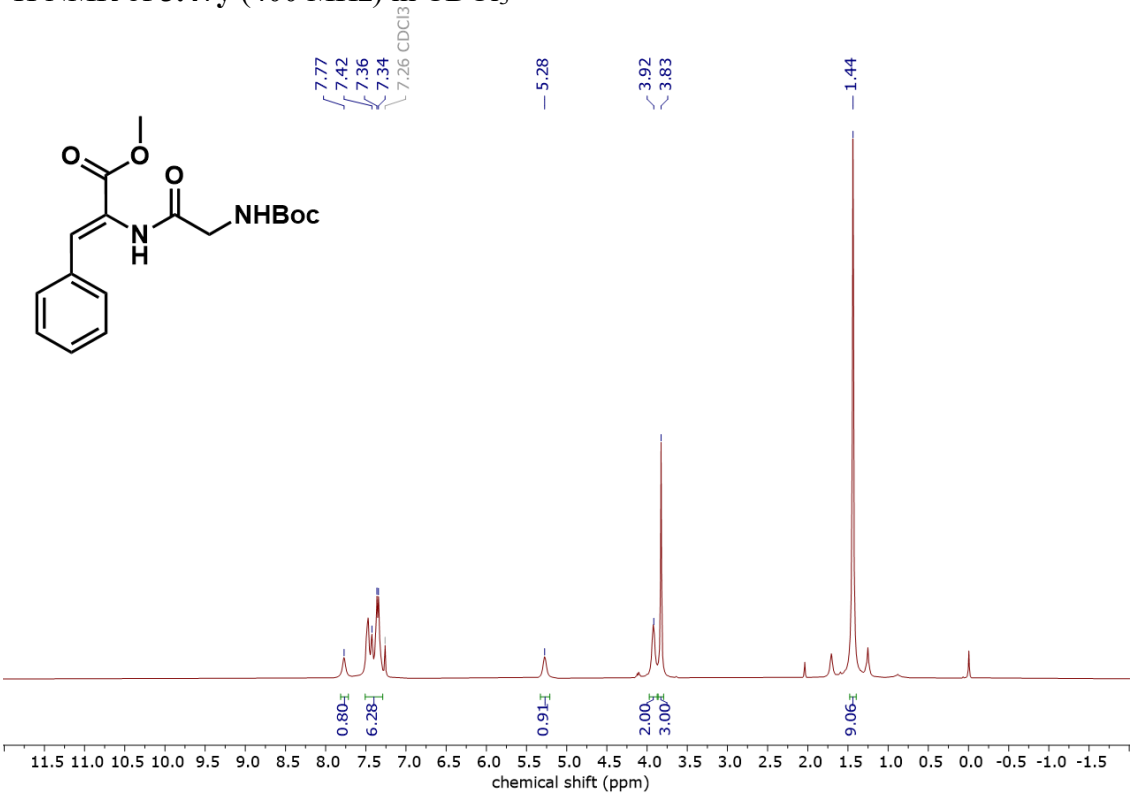

^{13}C NMR of **3.47y** (151 MHz) in $CDCl_3$

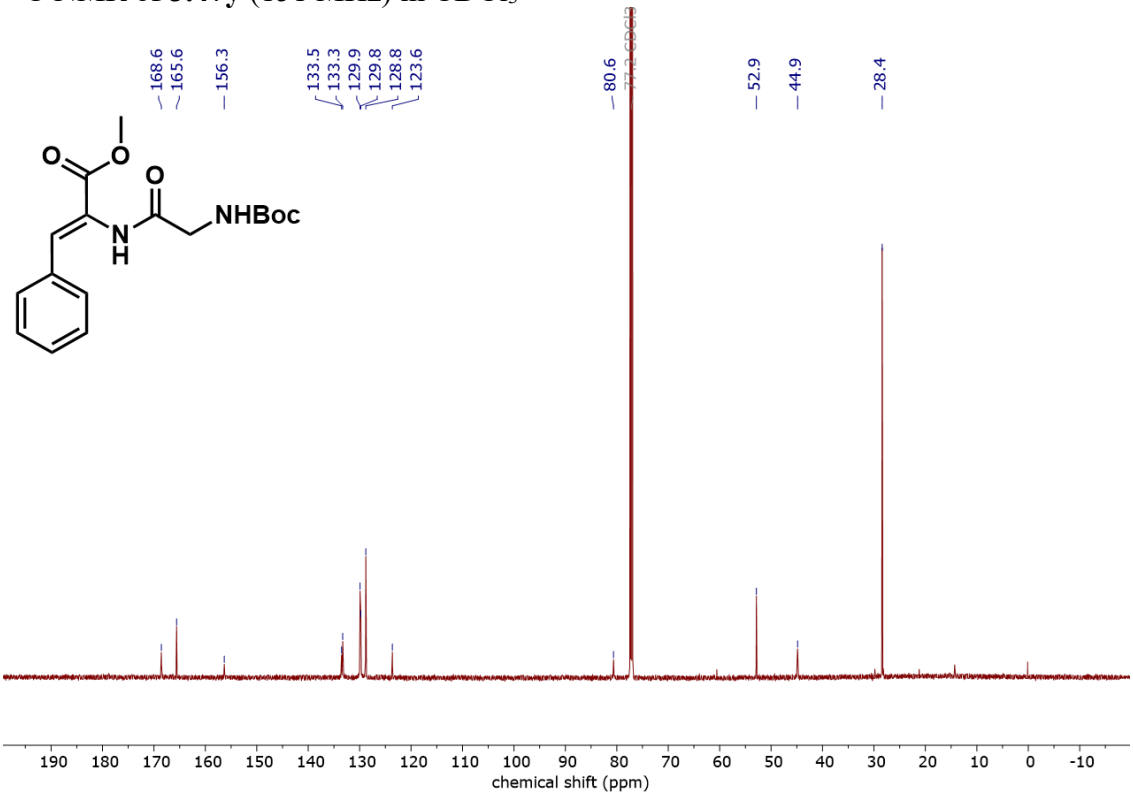

^{1}H NMR of **3.47z** (400 MHz) in CD_3OD

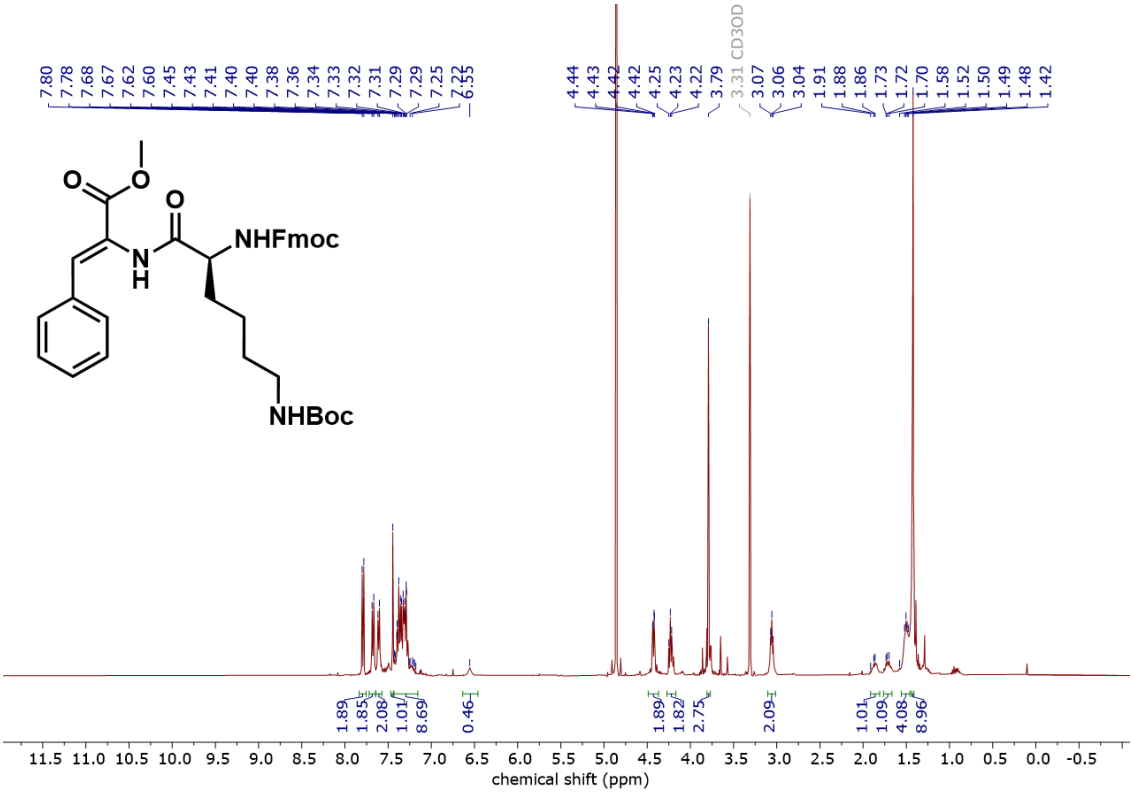

^{13}C NMR of **3.47z** (126 MHz) in $CDCl_3$

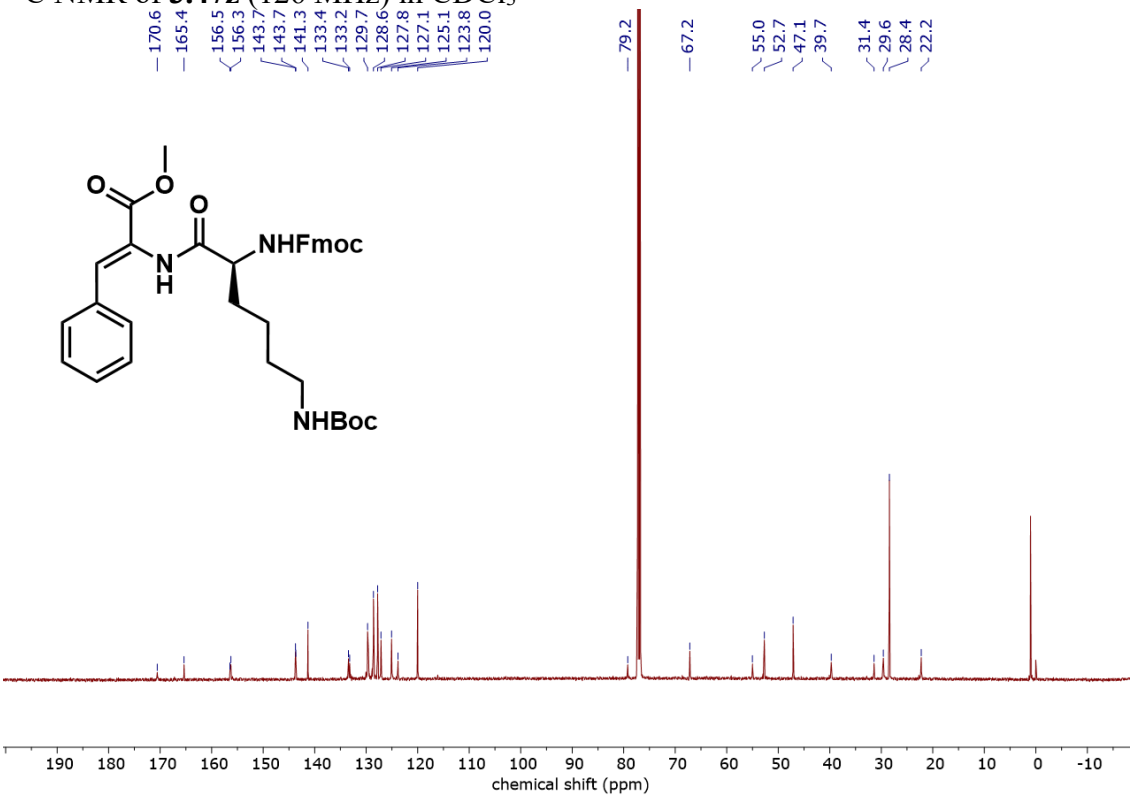

^{1}H NMR of **3.47aa** (400 MHz) in CD_3OD

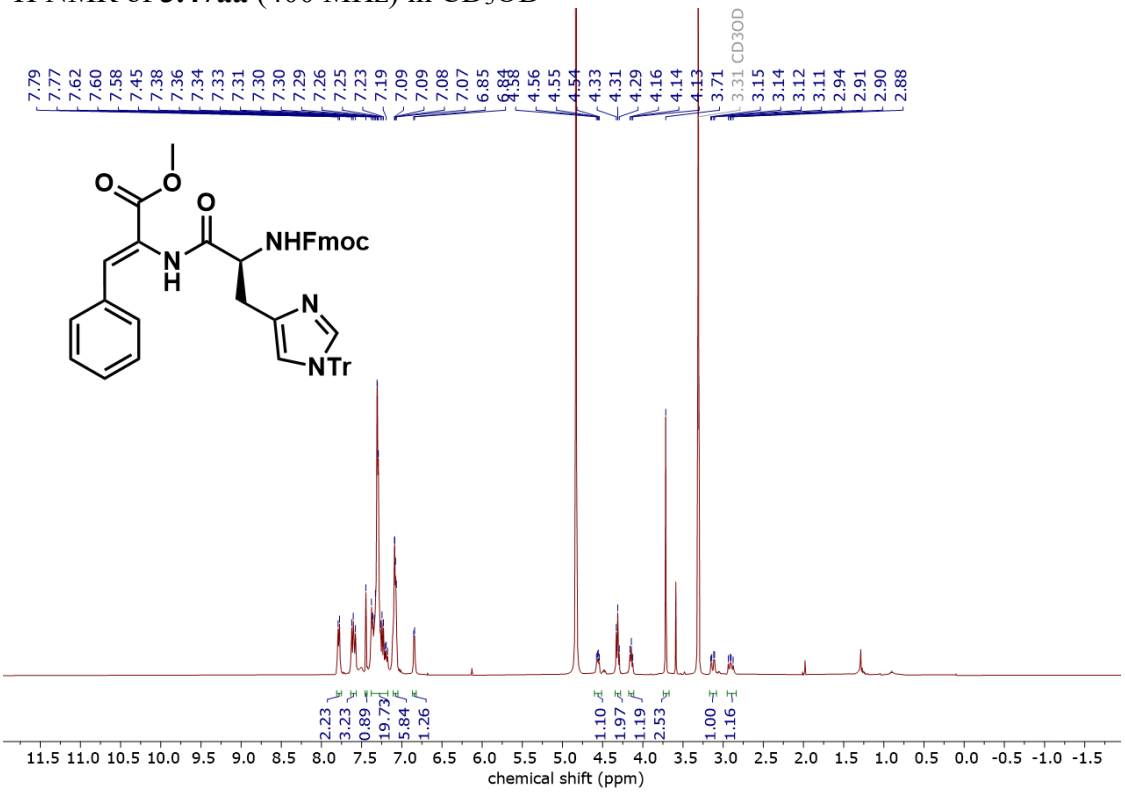

^{13}C NMR of **3.47aa** (126 MHz) in CD_3OD

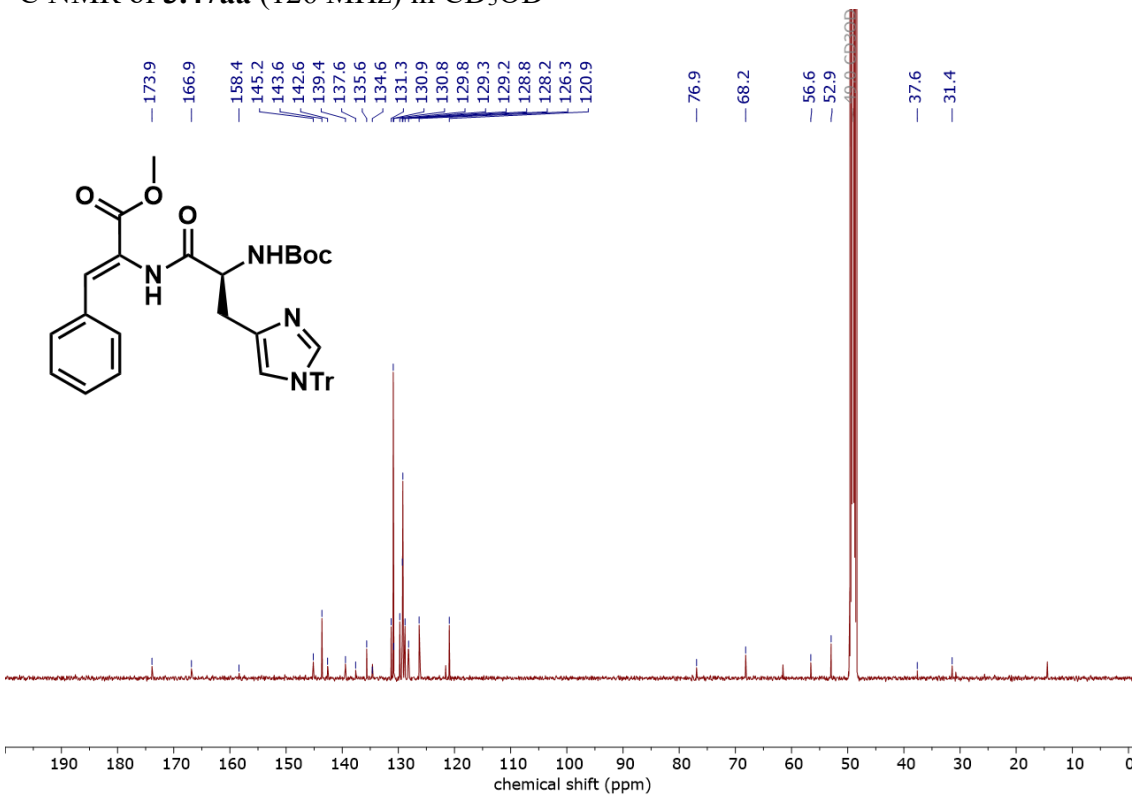

^{1}H NMR of **3.47ab** (500 MHz) in $CDCl_3$

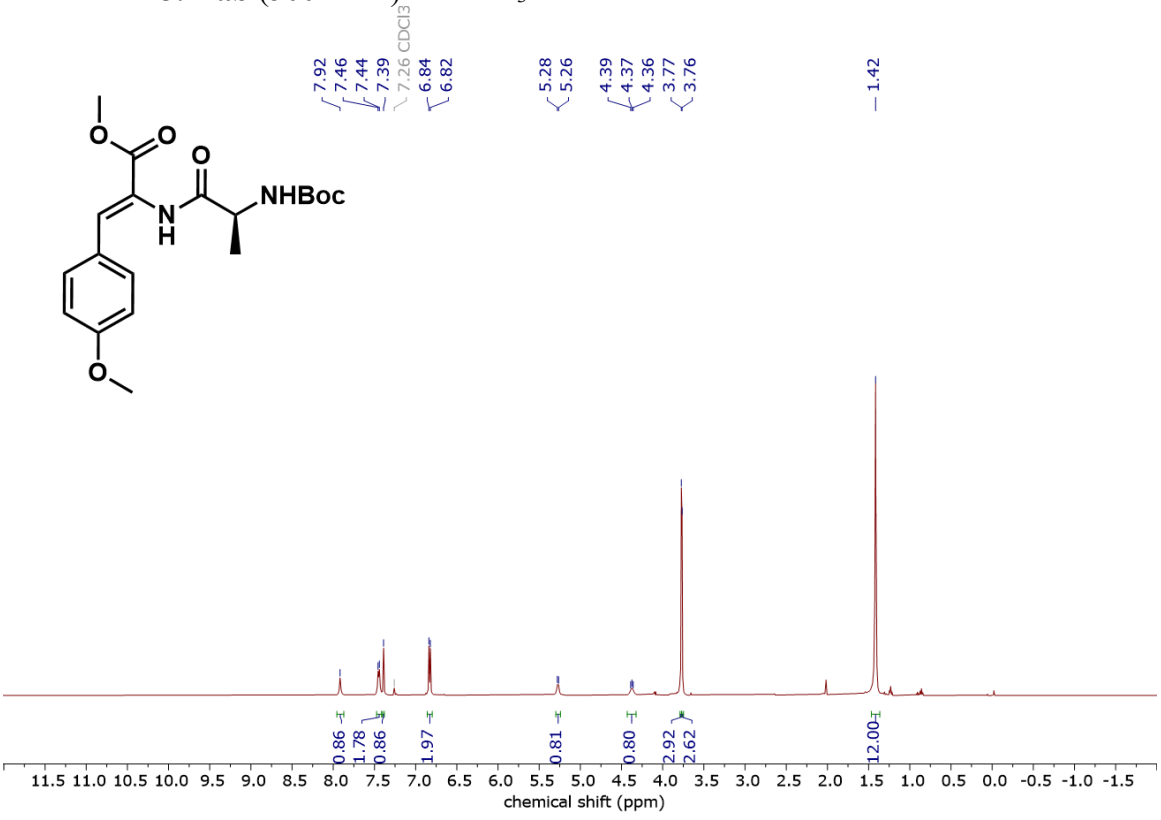

^{13}C NMR of **3.47ab** (126 MHz) in $CDCl_3$

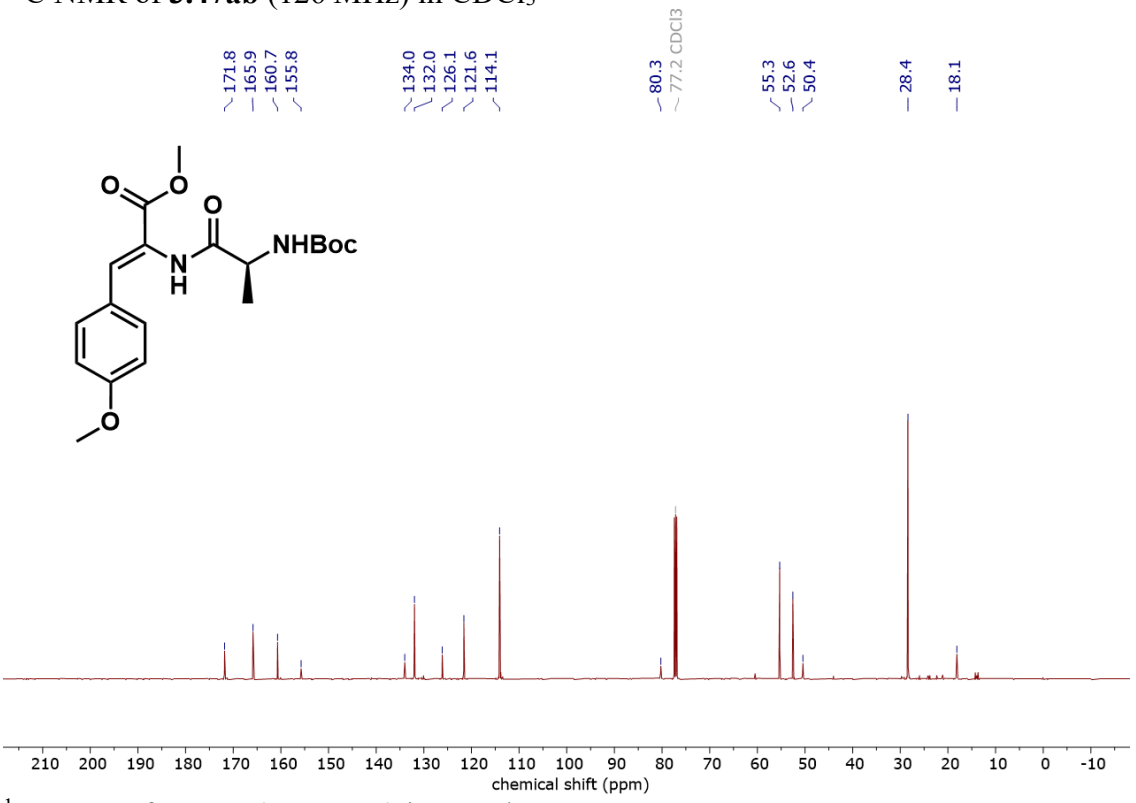

^{1}H NMR of **3.47ac** (400 MHz) in $CDCl_3$

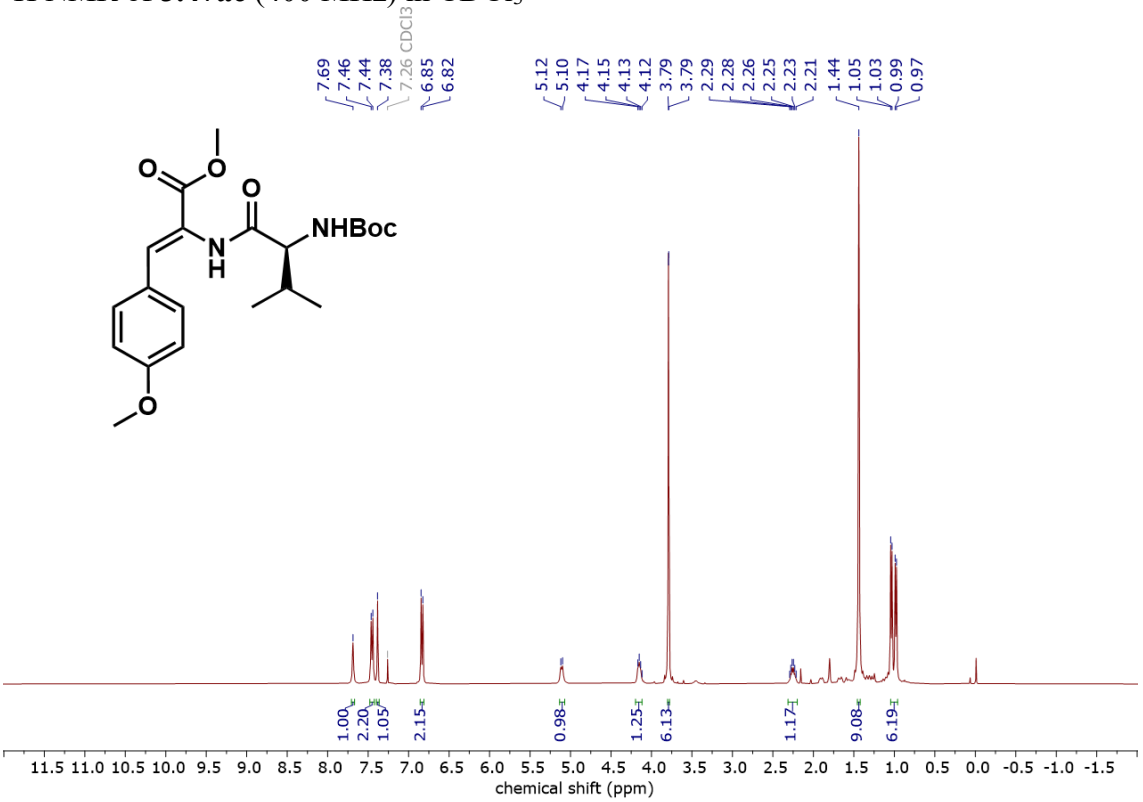

^{13}C NMR of **3.47ac** (101 MHz) in $CDCl_3$

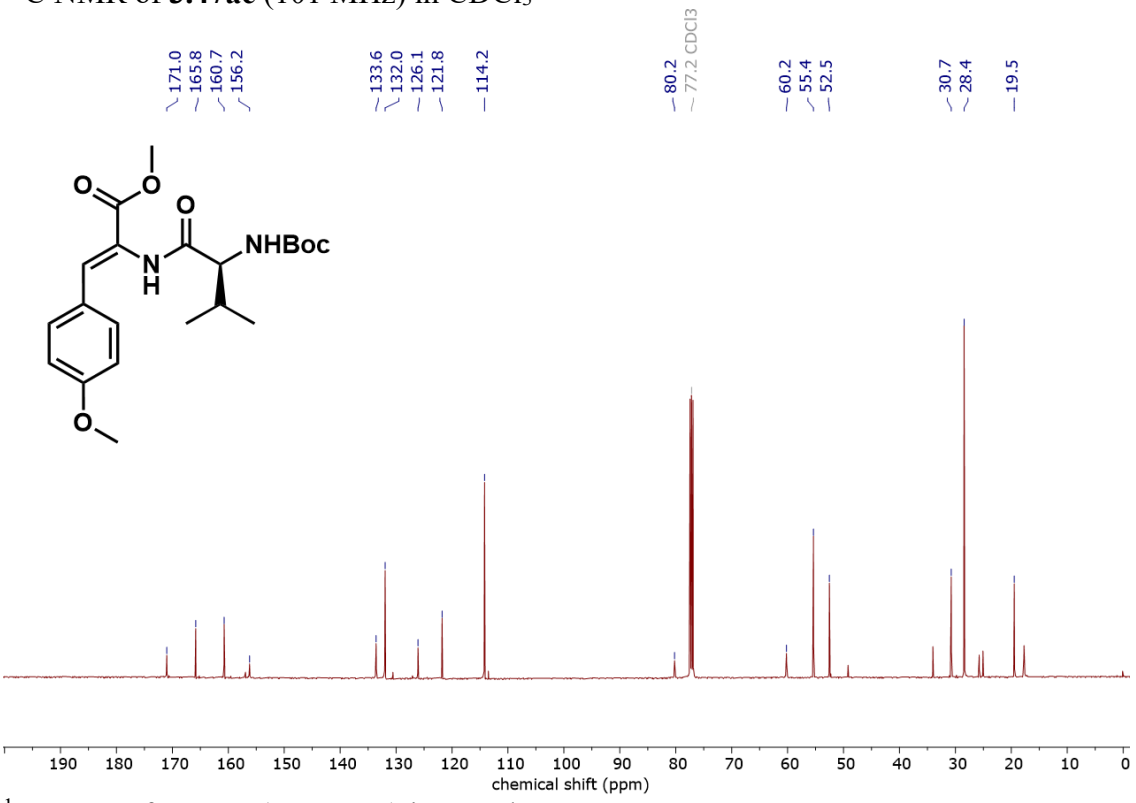

^{1}H NMR of **3.47ad** (400 MHz) in $CDCl_3$

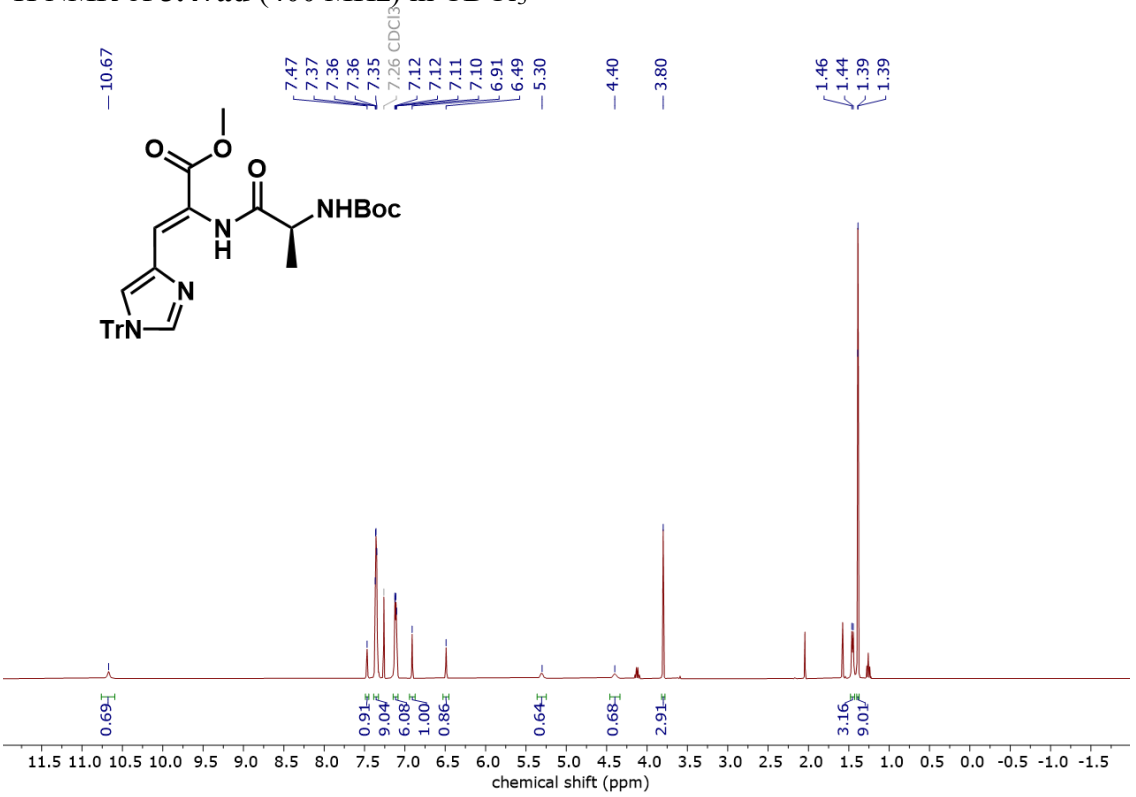

^{13}C NMR of **3.47ad** (126 MHz) in $CDCl_3$

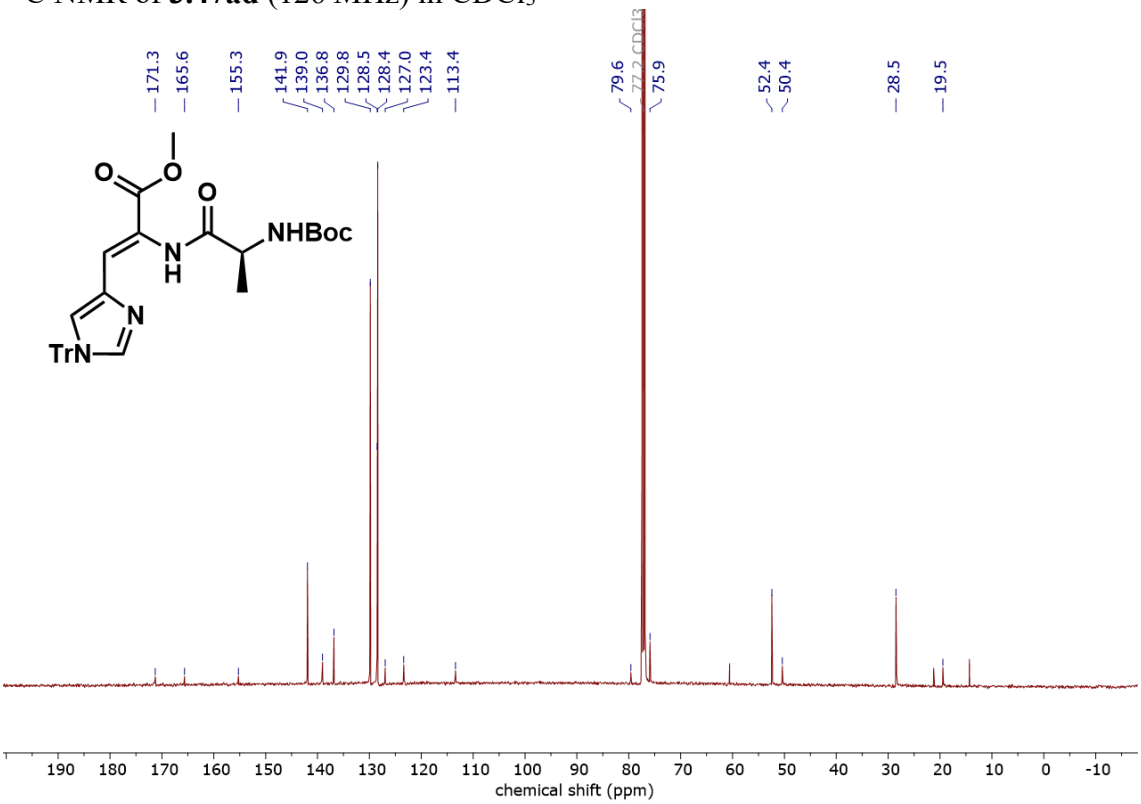

^{1}H NMR of **3.47ae** (400 MHz) in $CDCl_3$

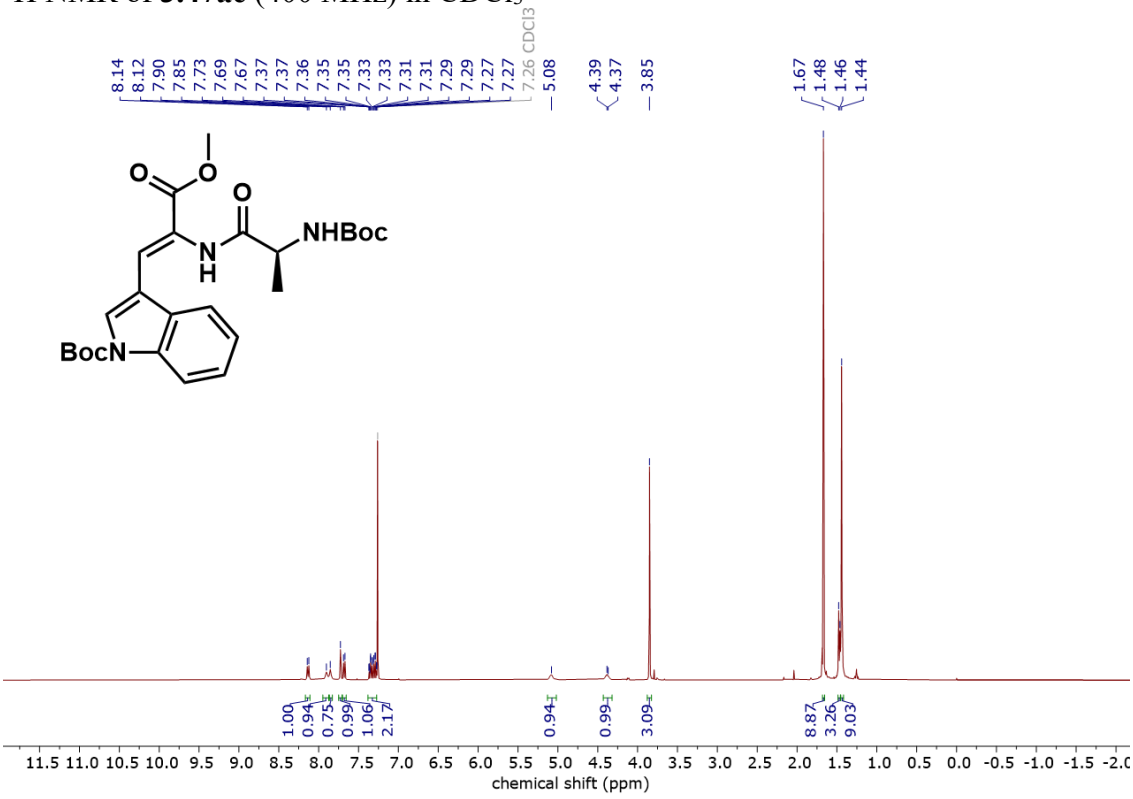

^{13}C NMR of **3.47ae** (101 MHz) in $CDCl_3$

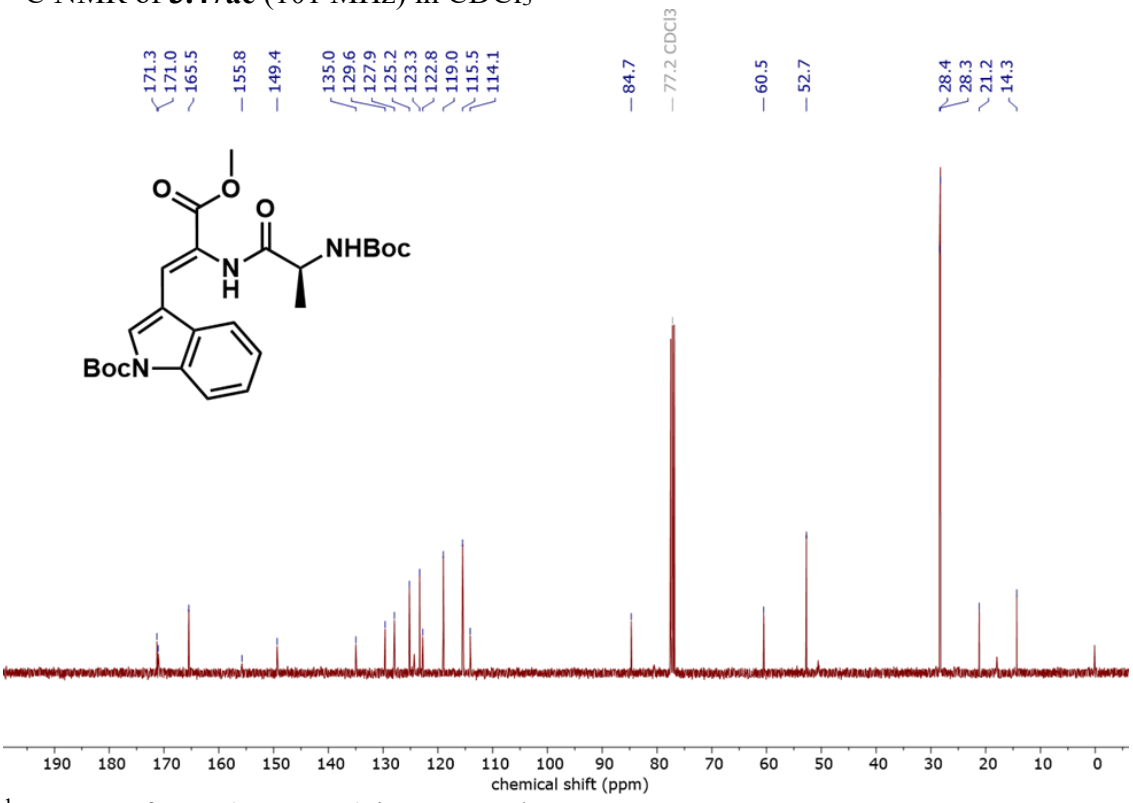

^{1}H NMR of **3.48** (400 MHz) in DMSO-d_6

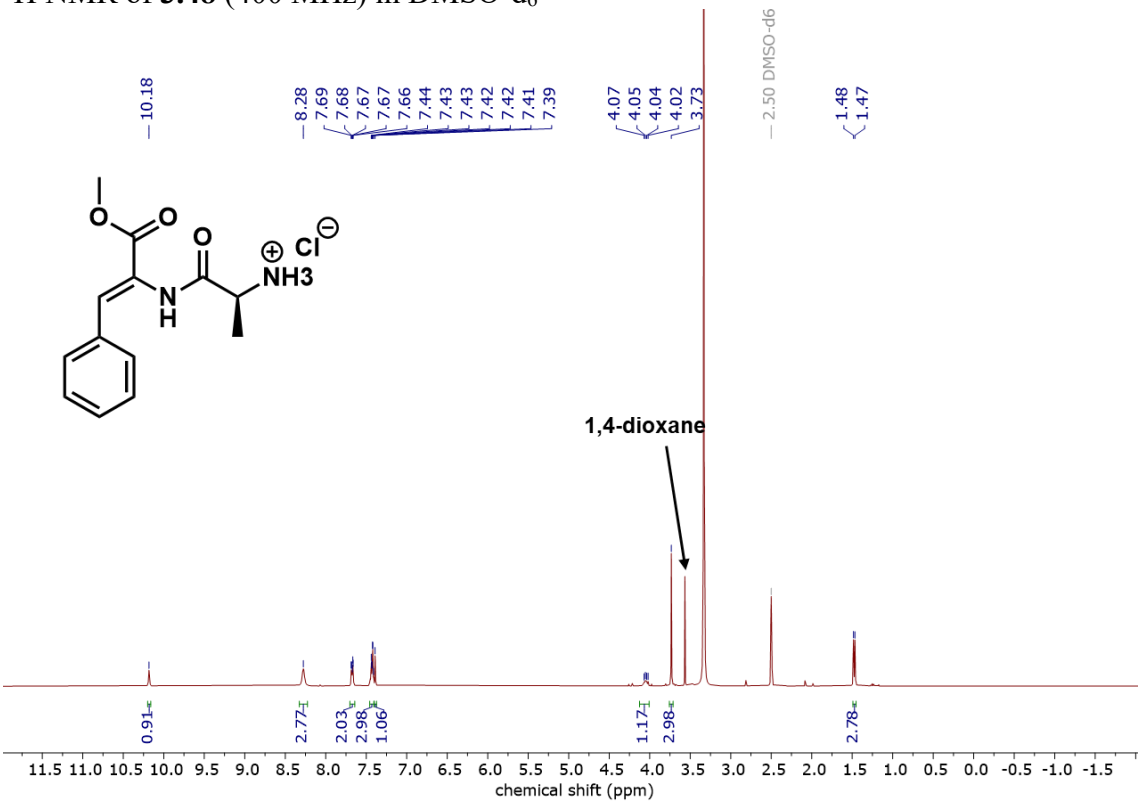

^{13}C NMR of **3.48** (126 MHz) in DMSO-d$_6$

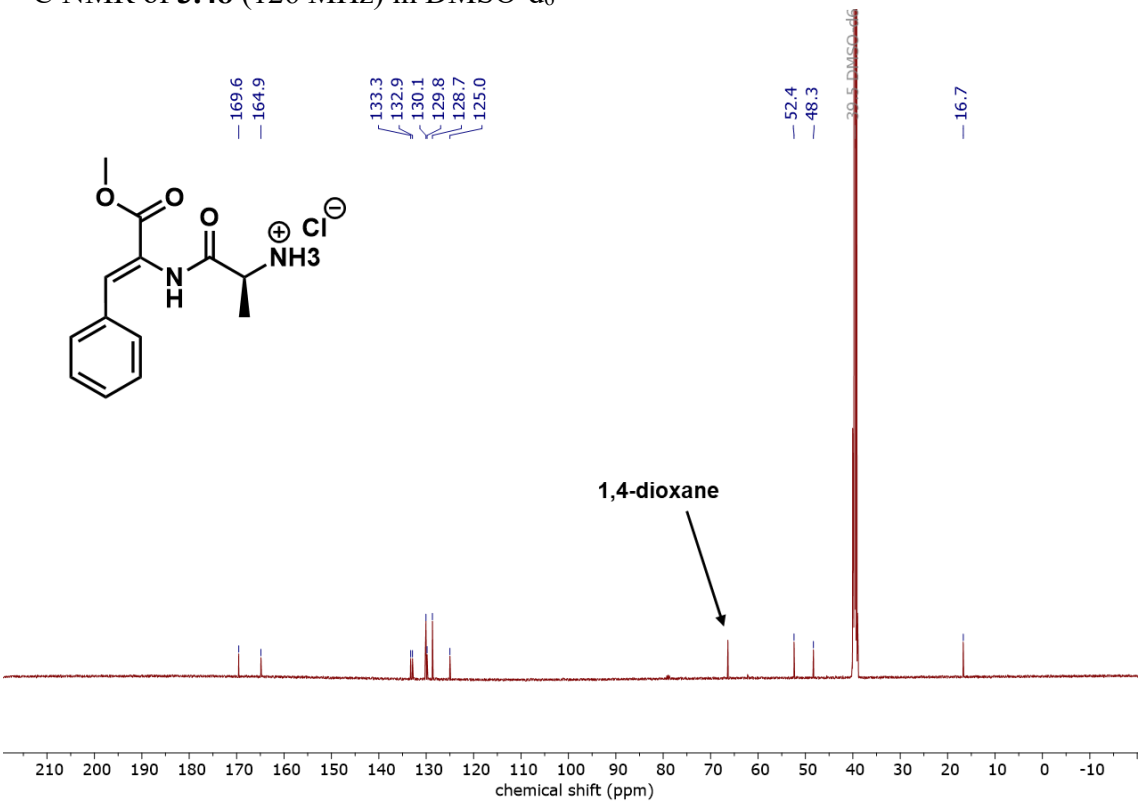

^{1}H NMR of **3.49** (400 MHz) in CDCl$_3$

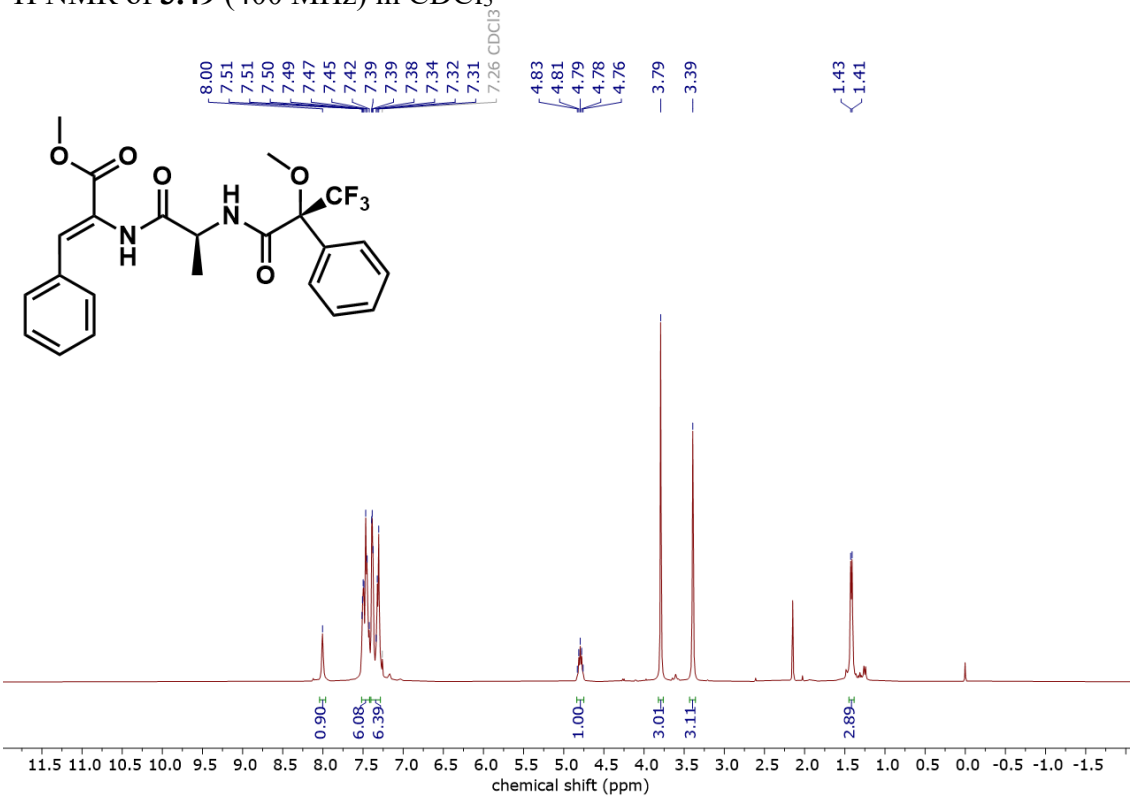

^{13}C NMR of **3.49** (126 MHz) in $CDCl_3$

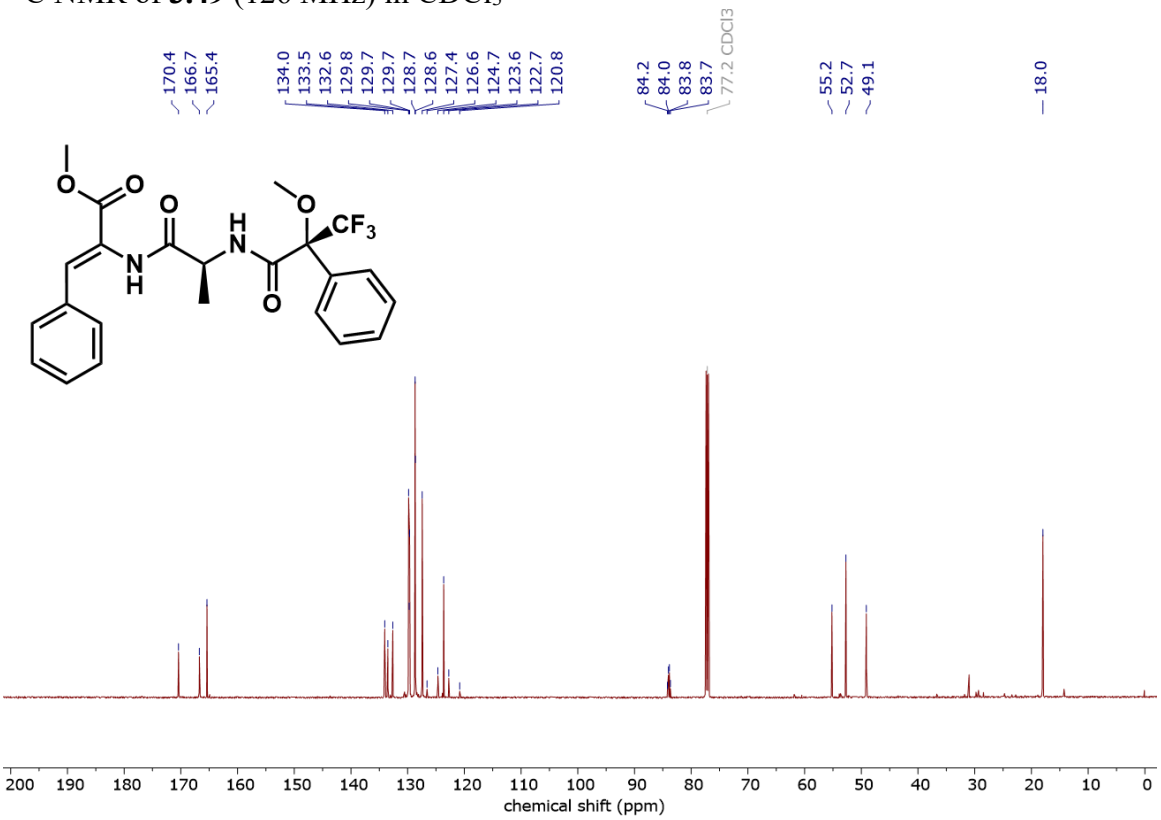

^{19}F NMR of **3.49** (376 MHz) in $CDCl_3$

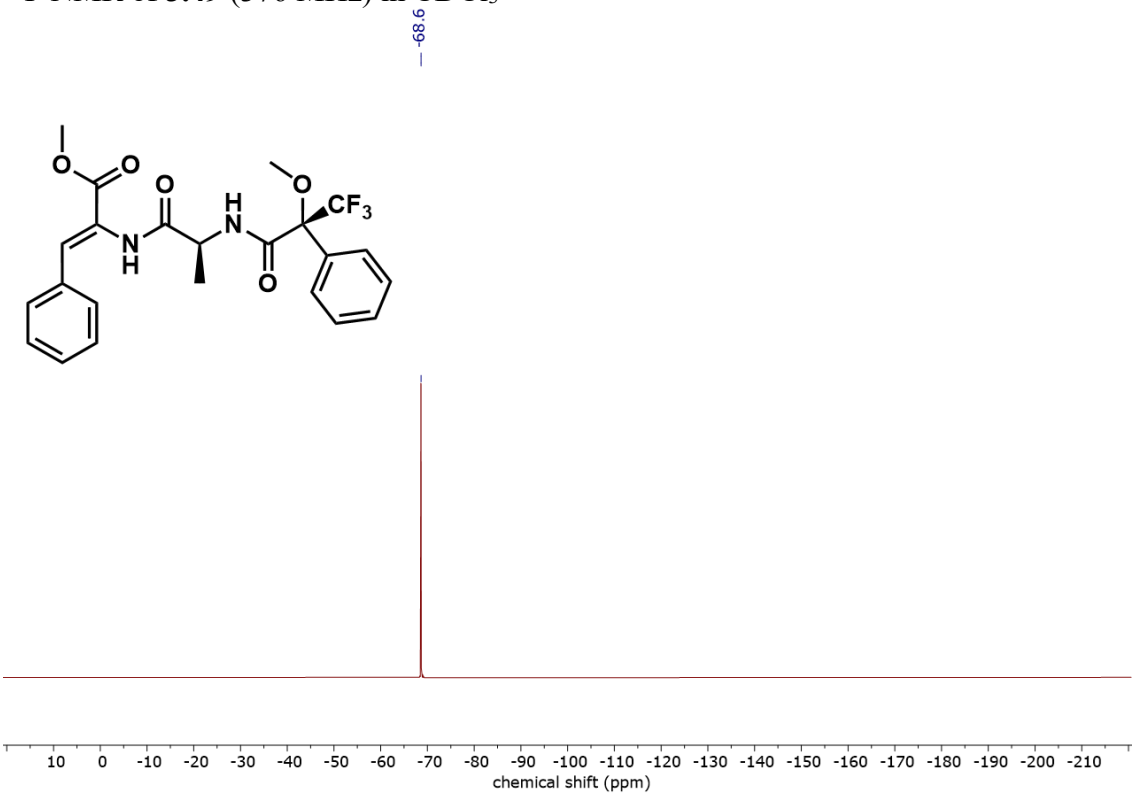

^{1}H NMR of **3.50** (400 MHz) in DMSO-d_6

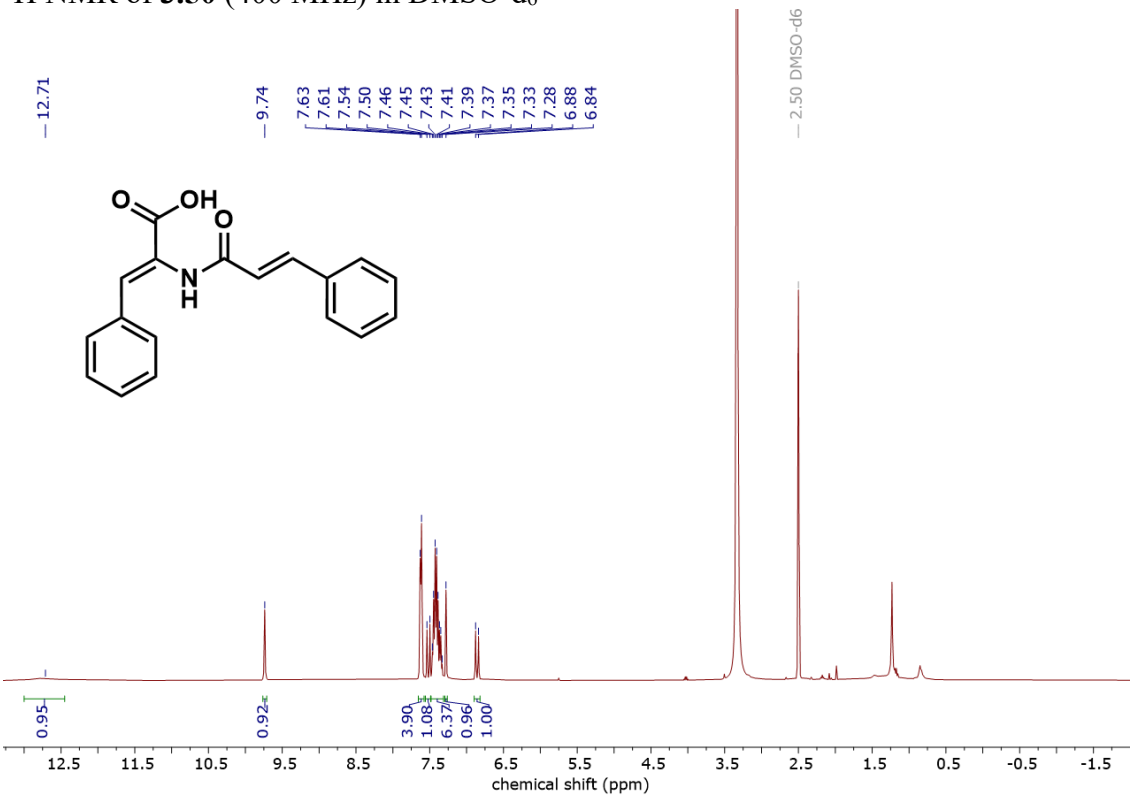

^{13}C NMR of **3.50** (101 MHz) in DMSO-d_6

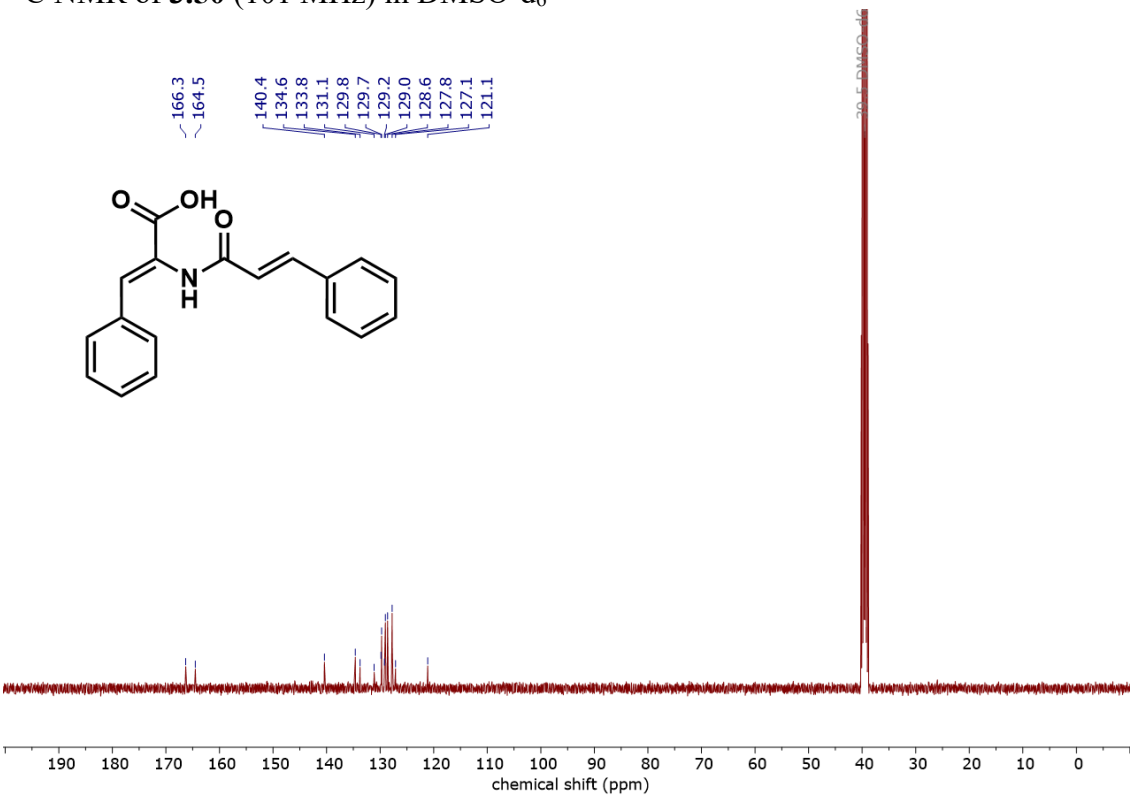

^{1}H NMR of Scutianene M (400 MHz) in DMSO-d_6

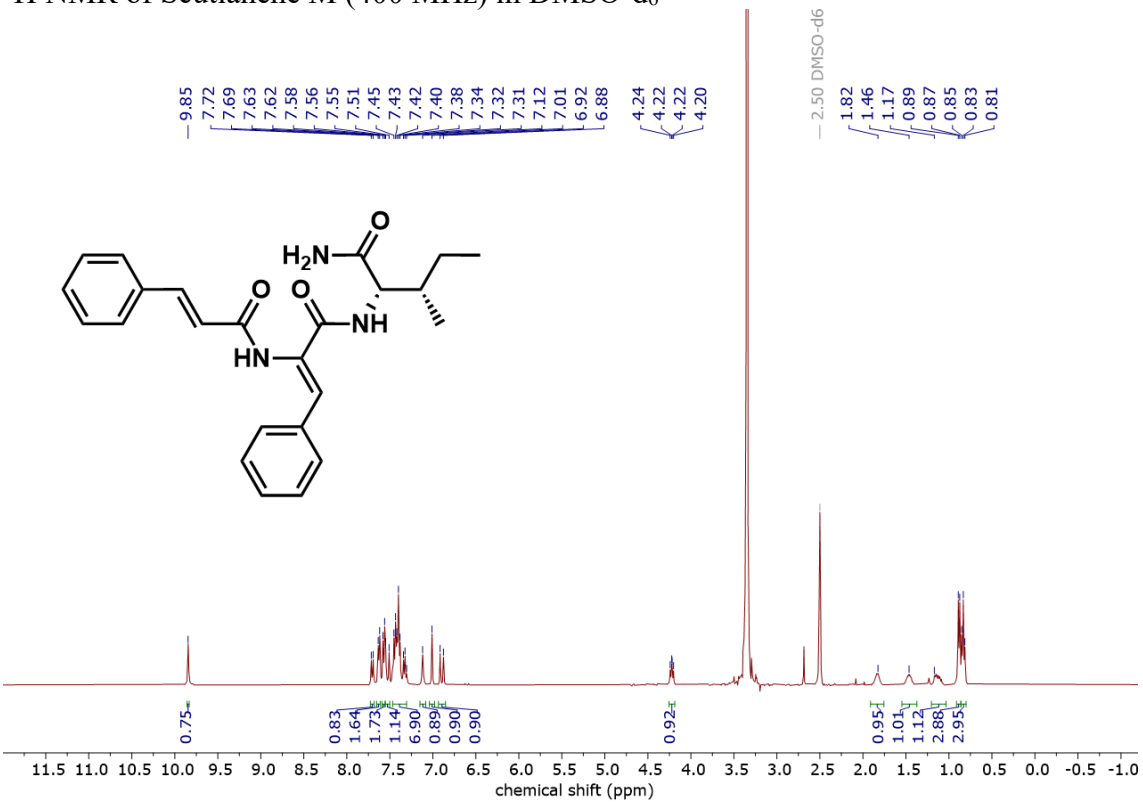

^{13}C NMR of Scutianene M (126 MHz) in DMSO-d_6

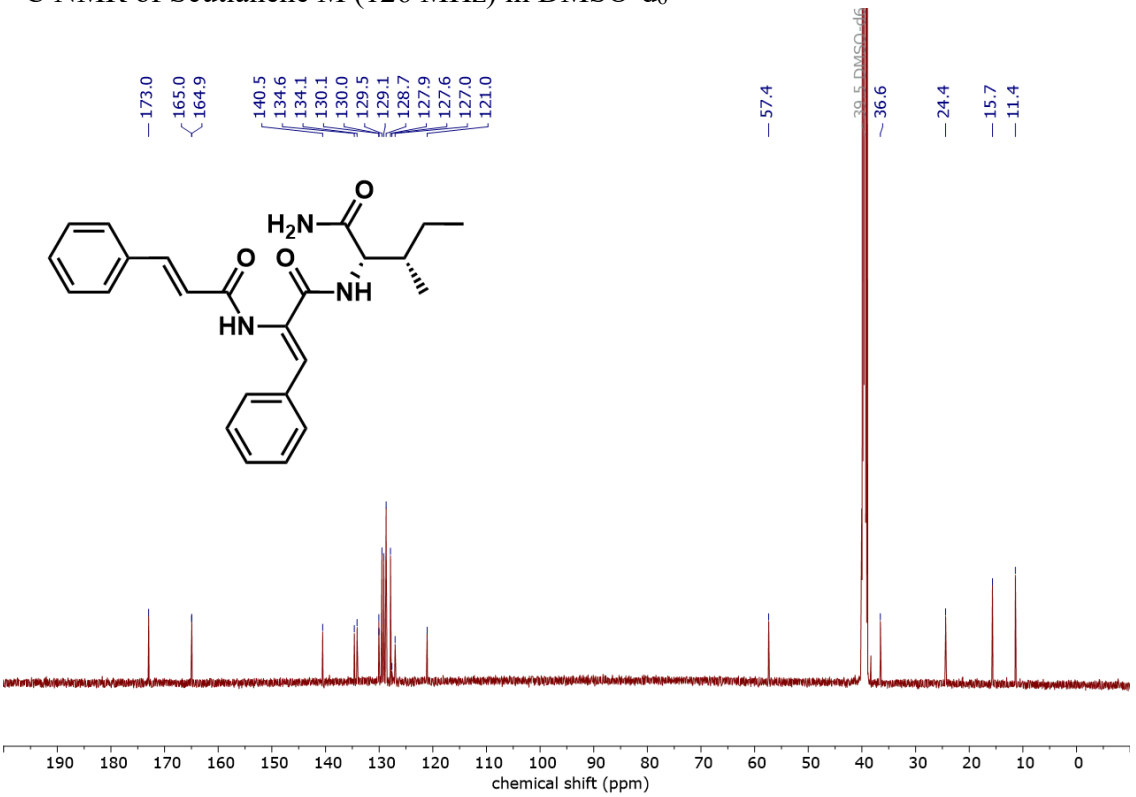

^{1}H NMR of **3.52** (600 MHz) in DMSO-d_6

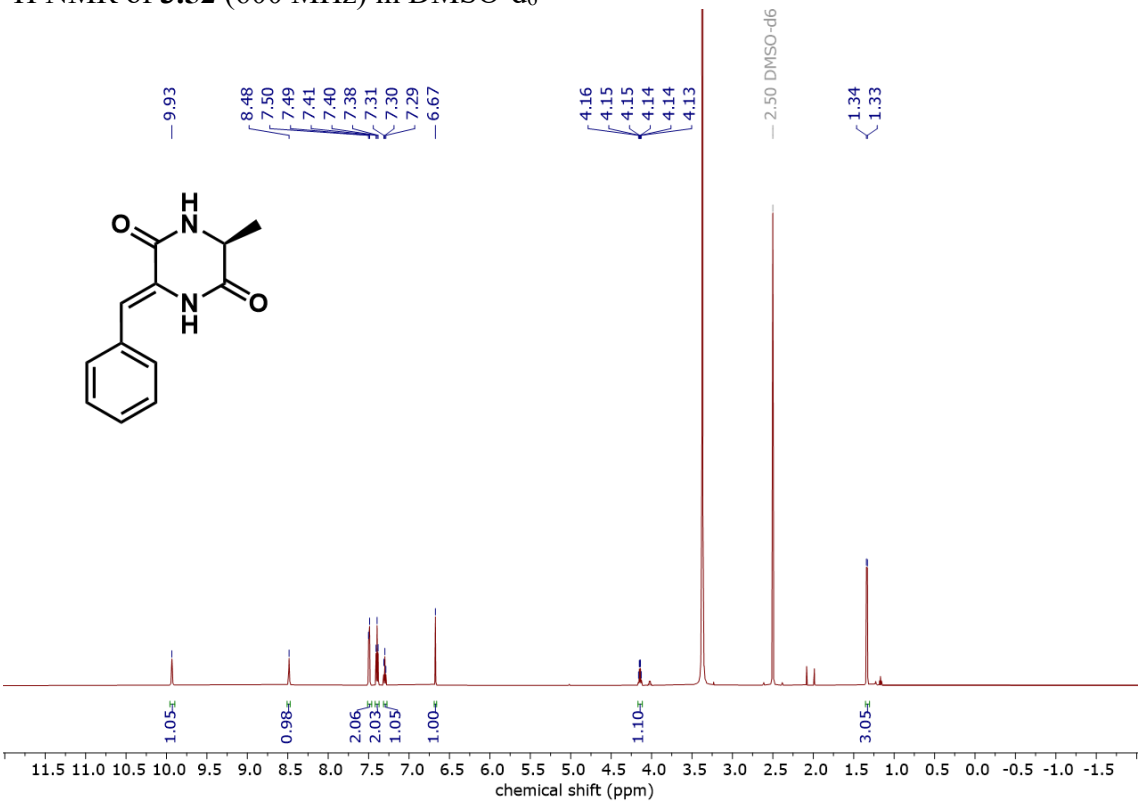

^{13}C NMR of **3.52** (151 MHz) in DMSO-d_6